

Metabolomics and metabolism of traditional chinese medicine, volume II

Edited by

Xijun Wang and Haitao Lu

Published in

Frontiers in Pharmacology



FRONTIERS EBOOK COPYRIGHT STATEMENT

The copyright in the text of individual articles in this ebook is the property of their respective authors or their respective institutions or funders. The copyright in graphics and images within each article may be subject to copyright of other parties. In both cases this is subject to a license granted to Frontiers.

The compilation of articles constituting this ebook is the property of Frontiers.

Each article within this ebook, and the ebook itself, are published under the most recent version of the Creative Commons CC-BY licence. The version current at the date of publication of this ebook is CC-BY 4.0. If the CC-BY licence is updated, the licence granted by Frontiers is automatically updated to the new version.

When exercising any right under the CC-BY licence, Frontiers must be attributed as the original publisher of the article or ebook, as applicable.

Authors have the responsibility of ensuring that any graphics or other materials which are the property of others may be included in the CC-BY licence, but this should be checked before relying on the CC-BY licence to reproduce those materials. Any copyright notices relating to those materials must be complied with.

Copyright and source acknowledgement notices may not be removed and must be displayed in any copy, derivative work or partial copy which includes the elements in question.

All copyright, and all rights therein, are protected by national and international copyright laws. The above represents a summary only. For further information please read Frontiers' Conditions for Website Use and Copyright Statement, and the applicable CC-BY licence.

ISSN 1664-8714
ISBN 978-2-83251-173-2
DOI 10.3389/978-2-83251-173-2

About Frontiers

Frontiers is more than just an open access publisher of scholarly articles: it is a pioneering approach to the world of academia, radically improving the way scholarly research is managed. The grand vision of Frontiers is a world where all people have an equal opportunity to seek, share and generate knowledge. Frontiers provides immediate and permanent online open access to all its publications, but this alone is not enough to realize our grand goals.

Frontiers journal series

The Frontiers journal series is a multi-tier and interdisciplinary set of open-access, online journals, promising a paradigm shift from the current review, selection and dissemination processes in academic publishing. All Frontiers journals are driven by researchers for researchers; therefore, they constitute a service to the scholarly community. At the same time, the *Frontiers journal series* operates on a revolutionary invention, the tiered publishing system, initially addressing specific communities of scholars, and gradually climbing up to broader public understanding, thus serving the interests of the lay society, too.

Dedication to quality

Each Frontiers article is a landmark of the highest quality, thanks to genuinely collaborative interactions between authors and review editors, who include some of the world's best academicians. Research must be certified by peers before entering a stream of knowledge that may eventually reach the public - and shape society; therefore, Frontiers only applies the most rigorous and unbiased reviews. Frontiers revolutionizes research publishing by freely delivering the most outstanding research, evaluated with no bias from both the academic and social point of view. By applying the most advanced information technologies, Frontiers is catapulting scholarly publishing into a new generation.

What are Frontiers Research Topics?

Frontiers Research Topics are very popular trademarks of the *Frontiers journals series*: they are collections of at least ten articles, all centered on a particular subject. With their unique mix of varied contributions from Original Research to Review Articles, Frontiers Research Topics unify the most influential researchers, the latest key findings and historical advances in a hot research area.

Find out more on how to host your own Frontiers Research Topic or contribute to one as an author by contacting the Frontiers editorial office: frontiersin.org/about/contact

Metabolomics and metabolism of traditional chinese medicine, volume II

Topic editors

Xijun Wang — Heilongjiang University of Chinese Medicine, China

Haitao Lu — Shanghai Jiao Tong University, China

Citation

Wang, X., Lu, H., eds. (2023). *Metabolomics and metabolism of traditional chinese medicine, volume II*. Lausanne: Frontiers Media SA.

doi: 10.3389/978-2-83251-173-2

Table of contents

- 05 **Metabolomics Analysis Coupled With UPLC/MS on Therapeutic Effect of Jigucuo Capsule Against Dampness-Heat Jaundice Syndrome**
Yanmei He, Mengli Zhang, Taiping Li, Zhien Tan, Aihua Zhang, Min Ou, Danna Huang, Fangfang Wu and Xijun Wang
- 16 **Chemical Stability of a Chinese Herbal Spirit Using LC-MS-Based Metabolomics and Accelerated Tests**
Yan Hu, Zhe Wang, Jiayue Liu, Wen Yang, Qiang Yang, Yuan-Cai Liu, Qiu-Yun You, Xiao-Jia Chen and Jian-Bo Wan
- 27 **Protective Mechanism of Gandou Decoction in a Copper-Laden Hepatolenticular Degeneration Model: *In Vitro* Pharmacology and Cell Metabolomics**
Fengxia Yin, Mengnan Nian, Na Wang, Hongfei Wu, Huan Wu, Wenchen Zhao, Shijian Cao, Peng Wu and An Zhou
- 50 **Integrated Metabolomics and Network Pharmacology Analysis Immunomodulatory Mechanisms of Qifenggubiao Granules**
Bindan Guo, Wenting Dong, Jinhai Huo, Guodong Sun, Zhiwei Qin, Xiaodong Liu, Bihai Zhang and Weiming Wang
- 66 **Dissecting the Regulation of Arachidonic Acid Metabolites by *Uncaria rhynchophylla* (Miq.) Miq. in Spontaneously Hypertensive Rats and the Predictive Target sEH in the Anti-Hypertensive Effect Based on Metabolomics and Molecular Docking**
Lei Gao, Xinqin Kong, Wenyong Wu, Zijin Feng, Haijuan Zhi, Zijia Zhang, Huali Long, Min Lei, Jinjun Hou, Wanying Wu and De-an Guo
- 78 **Multi-Omics Integration Analysis Identifies Lipid Disorder of a Non-Alcoholic Fatty Liver Disease (NAFLD) Mouse Model Improved by Zexie–Baizhu Decoction**
Yuhan Cao, Jingying Shi, Luyao Song, Junjiu Xu, Henglei Lu, Jianhua Sun, Jinjun Hou, Jing Chen, Wanying Wu and Likun Gong
- 93 **The Role and Mechanisms of Traditional Chinese Medicine for Airway Inflammation and Remodeling in Asthma: Overview and Progress**
Bo-wen Zhou, Hua-man Liu and Xin-hua Jia
- 109 **A UPLC-Q-TOF-MS-Based Metabolomics Approach to Screen out Active Components in Prepared Rhubarb for Its Activity on Noxious Heat Blood Stasis Syndrome**
Hui Zhu, Yu Duan, Kunming Qin, Junjie Jin, Xiao Liu and Baochang Cai
- 121 **Proteomics and Metabolomics Unveil *Codonopsis pilosula* (Franch.) Nannf. Ameliorates Gastric Precancerous Lesions via Regulating Energy Metabolism**
Rupu He, Ruyun Ma, Zheng Jin, Yanning Zhu, Fude Yang, Fangdi Hu and Jianye Dai

- 133 ***Pinelliae rhizoma* alleviated acute lung injury induced by lipopolysaccharide via suppressing endoplasmic reticulum stress-mediated NLRP3 inflammasome**
Ning-ning Wang, Xian-xie Zhang, Pan Shen, Cong-shu Huang, Hui-fang Deng, Lei Zhou, Lan-xin Yue, Bao-ying Shen, Wei Zhou and Yue Gao
- 151 ***Tripterygium wilfordii* glycosides ameliorates collagen-induced arthritis and aberrant lipid metabolism in rats**
Yitian Zhu, Luyun Zhang, Xiafeng Zhang, Dehong Wu, Leiming Chen, Changfeng Hu, Chengping Wen and Jia Zhou
- 163 **Revealing the mechanism of raw and vinegar-processed *Curcuma aromatica* Salisb. [Zingiberaceae] regulates primary dysmenorrhea in rats via integrated metabolomics**
Lianlin Su, Huangjin Tong, Jiuba Zhang, Min Hao, Chenghao Fei, De Ji, Wei Gu, Zhenhua Bian, Chunqin Mao and Tulin Lu
- 179 **Identification of key pharmacodynamic markers of American ginseng against heart failure based on metabolomics and zebrafish model**
Rong Dong, Yougang Zhang, Shanjun Chen, Huan Wang, Kaiqing Hu, Huanxin Zhao, Qingping Tian, Kewu Zeng, Songsong Wang and Liwen Han



Metabolomics Analysis Coupled With UPLC/MS on Therapeutic Effect of Jigucuo Capsule Against Dampness-Heat Jaundice Syndrome

Yanmei He^{1,2†}, Mengli Zhang^{1†}, Taiping Li^{1,2}, Zhien Tan¹, Aihua Zhang², Min Ou¹, Danna Huang¹, Fangfang Wu^{1*} and Xijun Wang^{1,2*}

¹National Engineering Laboratory for the Development of Southwestern Endangered Medicinal Materials, Guangxi Botanical Garden of Medicinal Plants, Nanning, China, ²National Chinmedomics Research Center, National TCM Key Laboratory of Serum Pharmacochimistry, Chinmedomics Research Center of State Administration of TCM, Laboratory of Metabolomics, Department of Pharmaceutical Analysis, Heilongjiang University of Chinese Medicine, Harbin, China

OPEN ACCESS

Edited by:

Fengguo Xu,
China Pharmaceutical University,
China

Reviewed by:

Wei Zhang,
Macau University of Science and
Technology, Macao SAR, China
Jianping Chen,
Shenzhen Traditional Chinese
Medicine Hospital, China
Xiaofei Chen,
Second Military Medical University,
China

*Correspondence:

Fangfang Wu
wfftn@163.com
Xijun Wang
xijunw@sina.com

[†]These authors have contributed
equally to this work

Specialty section:

This article was submitted to
Ethnopharmacology,
a section of the journal
Frontiers in Pharmacology

Received: 25 November 2021

Accepted: 10 January 2022

Published: 28 January 2022

Citation:

He Y, Zhang M, Li T, Tan Z, Zhang A,
Ou M, Huang D, Wu F and Wang X
(2022) Metabolomics Analysis
Coupled With UPLC/MS on
Therapeutic Effect of Jigucuo Capsule
Against Dampness-Heat
Jaundice Syndrome.
Front. Pharmacol. 13:822193.
doi: 10.3389/fphar.2022.822193

Dampness-heat Jaundice Syndrome (DHJS) is a complex Chinese medicine syndrome, while Jigucuo capsule (JGCC) is an effective compound preparation of Chinese medicine for the treatment of DHJS about liver and gallbladder, but its mechanism is not clear yet. The purpose of this study is to clarify the pathogenesis of DHJS and the treatment mechanism of JGCC. We used ultra-high performance liquid chromatography/mass spectrometry (UPLC/MS) combined with pattern recognition, accompanied the advanced software and online database for the urine metabolomics of rats. The potential biomarkers disturbing metabolism were identified and the metabolic pathway was analyzed. We investigated the callback of biomarkers after treatment with JGCC. Finally, A total of 25 potential urine biomarkers were identified, including Arachidonic acid, Phenylpyruvic acid, L-Urobilin and so on, and 14 related metabolic pathways were disturbed. After treatment with JGCC, the clinical biochemical indexes and histopathological were significantly improved, and the disturbed biomarkers were also obviously adjusted. It is proved that JGCC has remarkable effect on the treatment of DHJS.

Keywords: metabolomics, ultra-high performance liquid chromatography/mass spectrometry, dampness-heat jaundice syndrome, metabolite, jigucuo capsule

INTRODUCTION

Traditional Chinese medicine (TCM) has a long history in the treatment and prevention of diseases (Sun et al., 2018a). Since the outbreak of COVID-19, it has shown the superiority in treating diseases, gaining the international attention to TCM more and more. However, the fuzziness of Chinese medicine syndrome and the complexity of prescriptions have greatly restricted the pace of TCM realizing international modernization (Zhang et al., 2019a). With the rise of metabolomics and its application in the field of TCM, the interpretation for the effective mechanism of Chinese medicine and the precise diagnosis and accurate treatment of clinical syndromes have been effectively solved, and a set of exclusive research methods belonging to TCM have been formed-Chinmedomics. Our team used metabolomics to characterize the metabolic profile and related biomarkers of the heart-qi deficiency syndrome, and revealed the effectiveness of Wenxin formula in treating the heart-qi

deficiency syndrome and the material basis of the pharmacodynamics (Wang et al., 2013); basing on the metabolomics technology evaluated the overall effect of Kaixin San in preventing and treating Alzheimer's disease and identified related biomarkers and metabolic pathways (Chu et al., 2016); using metabolomics to develop Yinchenhao Decoction for the treatment effectiveness of DHJS, and then discover and determine the effective material basis and potential effect targets (Sun et al., 2019a). After more than 10 years of development, the metabolomics research of TCM has achieved remarkable results. Characterizing the overall effect evaluation of TCM/prescriptions from the metabolic profile of diseases/syndromes may change TCM from empirical treatment to modernization with standard and scientific methods (Sun et al., 2014; Qiu et al., 2017; Liu et al., 2018).

DHJS is a common disease in the classification of jaundice from the perspective of TCM theory, also known as Yang Huang syndrome. It was first seen in treatise on febrile diseases, which is one of the jaundice syndromes of hepatobiliary diseases. The manifestations are fever and thirst, the body and eyes are bright yellow as orange, the color of urine is as dark as strong tea, with loss of appetite, nausea and vomiting, difficult defecation, abdominal distension and pain, red tongue and greasy fur and so on (Chen et al., 2014). JGCC is composed of eight botanical drugs such as *Abrus melanospermus* subsp. *melanospermus* [Fabaceae; *Abri herba*], *Artemisia capillaris* Thunb [Asteraceae; *Artemisiae scopariae herba*], *Gardenia jasminoides* J. Ellis [Rubiaceae; *Gardeniae fructus*], *Panax notoginseng* (Burkill) F.H.Chen [Araliaceae; *Notoginseng radix et rhizoma*], *Paeonia lactiflora* Pall [Paeoniaceae; *Paeoniae radix alba*], *Origanum vulgare* L. [Lamiaceae; *Herba origani*], *Ziziphus jujuba* Mill [Rhamnaceae; *Jujubae fructus*], *Lycium barbarum* L [Solanaceae; *Lycii fructus*] and two animal materials. It has the effects of soothing the liver and gallbladder, clearing away heat and detoxification. JGCC is a good medicine for the treatment of hepatitis and cholecystitis (Zhao et al., 2009) and contains a large number of chemical components such as alkaloids, flavonoids, terpenes and organic acids. In the early stage, we have systematically studied the chemical components of JGCC, and 144 compounds have been identified (Li et al., 2021a). JGCC used in this study is a commercial drug. Before leaving the factory, strict quality control is carried out according to the enterprise standard, including character description, thin layer chromatography identification with *Artemisia capillaris* Thunb [Asteraceae; *Artemisiae scopariae herba*] is used as the control drug and the moisture content shall not exceed 7%. The quality control is effectively guaranteed, but the quantitative control of chemical components is not carried out. Corresponding research should be carried out to make up for deficiencies. We applied the advanced UPLC-G2Si-HDMS instrument system, combined with the metabolomics strategy, to explore the disturbed metabolic markers and pathways, determine the pathogenesis of DHJS (Sun et al., 2018b). We also analyzed the therapeutic effect of JGCC on DHJS from the perspective of metabolites and clarified the treatment mechanism. The results provided a basis for the establishment of quantitative standard of JGCC.

MATERIALS AND METHODS

Instrument

Acquity ultra high performance liquid chromatograph (Waters, United States); Synapt™ G2Si High definition mass spectrometer (HDMS) (Waters, United States); Sorvall ST-8R high speed freezing centrifuge (Thermo Fisher, United States); GL6231-1SCN electronic analytical balance (Sartorius Scientific instrument Co., Ltd.); Hitachi 3100 automatic biochemical analyzer (Nanning Precision Instrument Co., Ltd.); Tecan infinite M200 pro multifunctional microplate reader (Switzerland); DHG-9140A electric constant temperature blast drying oven (Shanghai Qixin Scientific Instrument Co., Ltd.); SB-800DT ultrasonic cleaning machine (Ningbo Xinzhi Biotechnology Co., Ltd.); Vortex-6 vortex instrument (Macao slinberg Instrument Manufacturing Co., Ltd.); RVC2-18CD plus vacuum concentrator (Beijing gaodetong Technology Co., Ltd.).

Drugs and Reagents

Chromatographic grade methanol, acetonitrile and formic acid (Thermo Fisher company); Distilled water (Guangzhou Watsons Food and Beverage Co., Ltd.); α -Naphthalene isothiocyanate (ANIT) (Shanghai Chaoyan Biotechnology Co., Ltd.); ethanol (Sinopharm Chemical Reagent Co., Ltd.); *Zingiber officinale* Roscoe [Zingiberaceae; *Zingiberis rhizoma*] (Guangxi Xianzhu TCM Technology Co., Ltd.) was authenticated by Prof. Xi-jun Wang of the Pharmacognosy Department, Heilongjiang University of Chinese Medicine; Normal saline (Guangxi Yuyuan Pharmaceutical Co., Ltd.); JGCC (Guangxi Yulin Pharmaceutical Group Co., Ltd.); Olive oil (Beijing Hualian Supermarket); Paraformaldehyde (Beijing Labgic Technology Co., Ltd.); Pentobarbital sodium (Beijing boatuoda Co., Ltd.); Sodium formate (Sigma, United States); Leucine enkephalin (waters, United States). Assay kit for Alanine aminotransferase (ALT), Aspartate aminotransferase (AST), Alkaline phosphatase (ALP), Total bile acid (TBA), Superoxide dismutase (SOD), Prealbumin (PA) purchased from Zhongsheng Beikong Biotechnology Co., Ltd., the kit for Total bilirubin (T-Bili) and Direct bilirubin (D-Bili) obtained from Shanghai Lanpai Biotechnology Co., Ltd.

Experimental Animal

SD rats (SPF grade), male, weighing 180 ± 20 g; feeding environment (temperature: $24 \pm 2^\circ\text{C}$, humidity: 65–75%), purchased from Guangxi Medical University. 12 h are the cycle of alternating light and dark, drinking and eating freely, and the experiment begins after a week of adaptation. Animal license number is SYXK (Gui) 2020–0014.

Preparation of Modeling Solution

300 g of *Zingiber officinale* Roscoe [Zingiberaceae; *Zingiberis rhizoma*] was weighed, soaked in 3,000 ml distilled water for 1 h, heated to boil and then with slow fire for 1 h, filtered and added 3,000 ml distilled water to the drug residue, the above operation was repeated twice, the filtrate of three times was collected and concentrated to 3,000 ml, and the 0.013 g/ml

Zingiber officinale Roscoe [Zingiberaceae; *Zingiberis rhizoma*] modeling solution was prepared by taking appropriate amount of concentrated solution and adding water. An appropriate amount of absolute ethanol was taken, distilled water was added and shaken well to prepare a 12.5% (V/V) ethanol modeling solution. Weighed 130.0 and 90.0 mg of ANIT powder, added 50 ml of olive oil, mixed well, and dissolved by ultrasound to prepare ANIT modeling solutions with concentrations of 2.6 and 1.8 mg/ml.

Animal Grouping and Administration

24 preconditioned adult male SD rats were randomly divided into three groups with eight rats in each group: blank control group, model control group and JGCC group. The rats of the model and JGCC group were given *Zingiber officinale* Roscoe [Zingiberaceae; *Zingiberis rhizoma*] solution according to the dose of 0.7 ml/200 g in the morning and 12.5% ethanol solution in the afternoon according to the dose of 1.0 ml/100 g for 14 days; ANIT olive oil solution was given at the doses of 10.4 and 7 mg/kg on the 15th and 16th days respectively, and the blank control group was given the same volume of distilled water and olive oil. From the 17th day, the JGCC group was given JGCC solution (dissolved in distilled water) at the dose of 2.16 g/kg, while the blank control group and model control group were given equal volume of distilled water, successive administration 14 days.

Collection and Processing of Biological Samples

One hour after the last administration in the morning of the 30th day, the rats were anesthetized with 2% pentobarbital sodium. Blood samples were collected from the abdominal aorta, and the fresh blood was centrifuged after 30 min (4°C, 4,000 rpm, 15 min), the supernatant was stored in the refrigerator at -80°C. After collecting the blood, the rat liver was immediately removed, the residual blood was washed with normal saline, and fixed in 4% paraformaldehyde solution for histopathological observation. Meanwhile, the urine of rats at night for 12 h was collected on days 0, 14, 16, 23, 30. The fresh urine was centrifuged (4°C, 4,000 rpm, 15 min) and the supernatant was stored in the refrigerator at -80°C.

Data Acquisition

Chromatographic Condition

The mobile phase is gradient eluted with 0.1% formic acid water (A) and 0.1% formic acid acetonitrile solution. The elution procedures is 0–3 min, 99–90%A; 3–5 min, 90–80%A; 5–8.5 min, 80–60%A; 8.5–9.5 min, 60–1%A; 9.5–11.5 min, 1–1%A; 11.5–12 min, 1–99%A; 12–14 min, 99–99%A. Chromatographic column: Waters ACQUITY UPLC® HSS T3 (2.1 mm × 100 mm, 1.8 μm); Column temperature: 40°C; Sample room temperature: 10°C; Flow rate: 0.4 ml/min; Injection volume: 2 μl; The effluent from the chromatograph is directly injected into the mass spectrometer without shunt for positive and negative ion scanning analysis.

Mass Spectrum Condition

Electronic spray ionization (ESI) source; Capillary voltage 2,000 V; Taper hole voltage 40 V; Ion source temperature 105°C; Desolvation gas temperature 400°C; Taper hole gas flow rate 50 L/h; Desolvation gas flow 800 L/h; High collision energy 20–30 V; Low collision energy 6 V. The accurate mass determination was determined by using the solvent of leucine-enkephalin ($[M + H]^+ = 556.2771$ $[M-H]^- = 554.2615$) as the locking mass solution. Full scanning in MS^E mode is adopted, and the mass scanning range is $m/z = 50$ –1,500 Da.

Preparation of Sample Solution

The rat urine sample was thawed at room temperature. The original concentration of rat urine was mixed with distilled water at 1:4, vortex for 10 s, centrifuged (4°C, 13,000 rpm for 10 min) and the supernatant was taken for UPLC-G2Si-HDMS analysis. At the same time, 10 μl of urine collected from the blank group, model group and JGCC group on days 0, 14, 16, 23, and 30 respectively were mixed and shaken to get the quality control samples for reference in the whole collection process.

Data Statistics and Analysis

Import all original data into Progenesis QI software (Waters). After the software automatically identifies peaks and reduces dimensionality, it takes the voluntarily selected optimal sample data as a reference, and the other samples are matched with it for peak alignment, the matching degree must be greater than 80%, and then carry out experimental grouping and set the extraction conditions such as retention time for peak extraction and deconvolution. At the same time, the Human Metabolome database (HMDB) was selected for compound identification. Finally, the matrix containing retention time, M/Z and normalized peak area was output. After the above data processing of peak picking, dimensionality reduction, peak extraction and identification, unsupervised principal component analysis (PCA) is performed on each group of data by using nested ezinfo 3.0 module, score plot reflecting the clustering degree of each group was obtained. The urine metabolic profile data of model group and blank control group were analyzed by orthogonal partial least squares discriminant analysis (OPLS-DA), the VIP plot reflecting the contribution of variables was obtained, and the variable ions with VIP > 1.0 and inter group *t*-test $p < 0.05$ were selected as the set of potential biomarkers; Furthermore, the biomarkers of dampness-heat jaundice rats were determined by further structural identification using secondary mass spectrometry information combined with HMDB (<https://hmdb.ca/>), KEGG and other omics databases. The associated metabolic pathway of endogenous biomarkers was constructed by MetPA database (Xiong et al., 2021). The callback degree of biomarkers in JGCC group was observed, and the biomarkers with significant callback were selected as effective biomarkers to evaluate the therapeutic effect of JGCC on rats with dampness-heat jaundice.

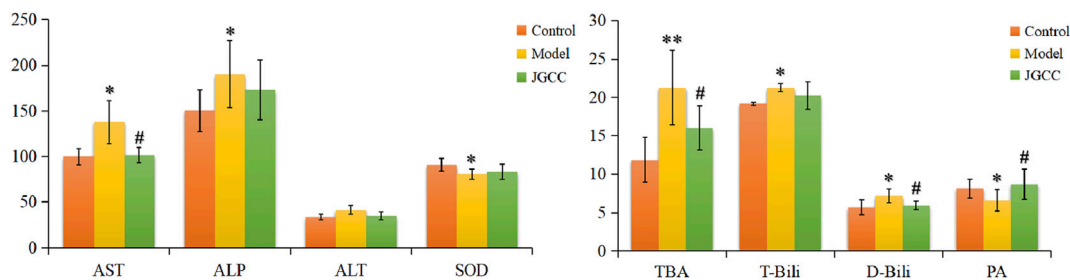


FIGURE 1 | Biochemical indexes analysis of the therapeutic effects of JGCC against DHJS. * $p < 0.05$, ** $p < 0.01$ vs Control, # $p < 0.05$, ## $p < 0.01$ vs Model. The corresponding parameters are represented to the supplementary table S1.

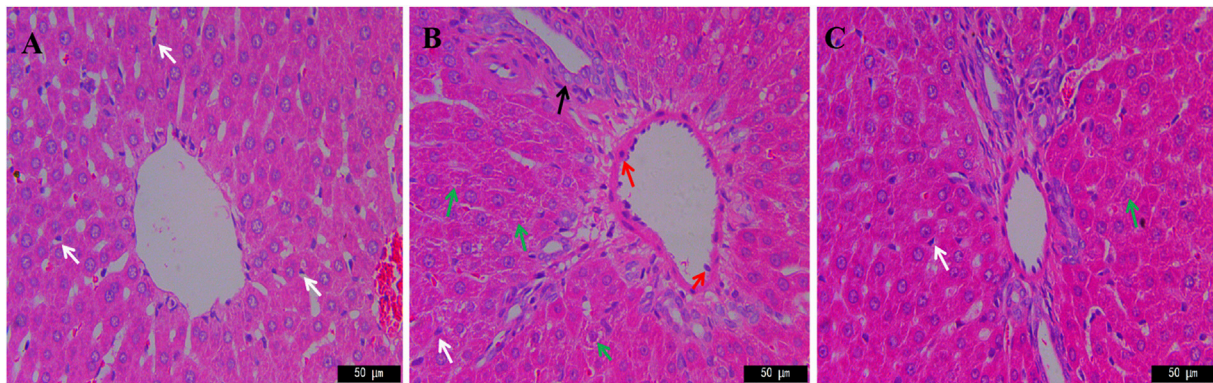


FIGURE 2 | HE staining in the therapeutic effect of JGCC against DHJS with microscope ($\times 400$). (A) Control; (B) Model; (C) JGCC. white arrows: kupffer cells; red arrows: inflammatory cells; green arrows: hepatocyte necrosis; black arrows: swelling of vascular endothelial cells.

RESULT

Clinical Biochemical Indexes

According to the instruction of the kit, the content of clinical biochemical indexes in serum of rats in each group were measured, including liver function indexes AST, ALT, PA, liver oxidation index SOD, bile function indexes ALP, TBA, T-Bili, D-Bili. The results are shown in **Figure 1** and **Supplementary Table S1**. Compared with the control group, TBA in the model group increases extremely ($p < 0.01$), AST, ALP, T-Bili and D-Bili all have a significant upward ($p < 0.05$), ALT has an increase trend, SOD and PA decrease prominently ($p < 0.05$). T-Bili and D-Bili are common clinical diagnostic indicators of jaundice, which can directly reflect the occurrence of obstructive jaundice; The above results show that the model group had severe cholestasis and obvious liver injury, indicating that the dampness-heat jaundice model was successfully established (Sun et al., 2019a; Fang et al., 2020). Compared with the model group, JGCC group has a tendency to adjust all the indexes, and there are visible differences in AST, TBA, D-Bili and PA ($p < 0.05$), which proves that JGCC has a good therapeutic effect on liver injury in rats with DHJS.

Histopathology

Liver HE staining results of rats in each group are shown in **Figure 2**. The liver cells of the blank group are tightly arranged with complete structure. There is no inflammatory cell aggregation around the interlobular veins. Kupffer cells are scattered among hepatocytes and refer to phagocytes located in the hepatic sinuses, which can clear foreign antigens, antigen-antibody complexes and cell debris in the blood, and are the guardians of the human body. Compared with the blank group, the hepatic cells in the model group were disorganized, with edema around the portal area, degeneration and necrosis of hepatic cells, nucleolysis, and decrease of kupffer cells, suggesting that the model of dampness-heat jaundice was successfully prepared (Fang et al., 2020). Compared with the model group, the liver cells of JGCC group are arranged neatly, the degree of necrosis is weaker than that of the model group, the number of kupffer cells is similar to that of the blank group, and the liver injury is significantly improved.

Metabolic Profile and Biomarkers

The clinical biochemical indexes and histopathological results show that the rat model of dampness-heat jaundice was

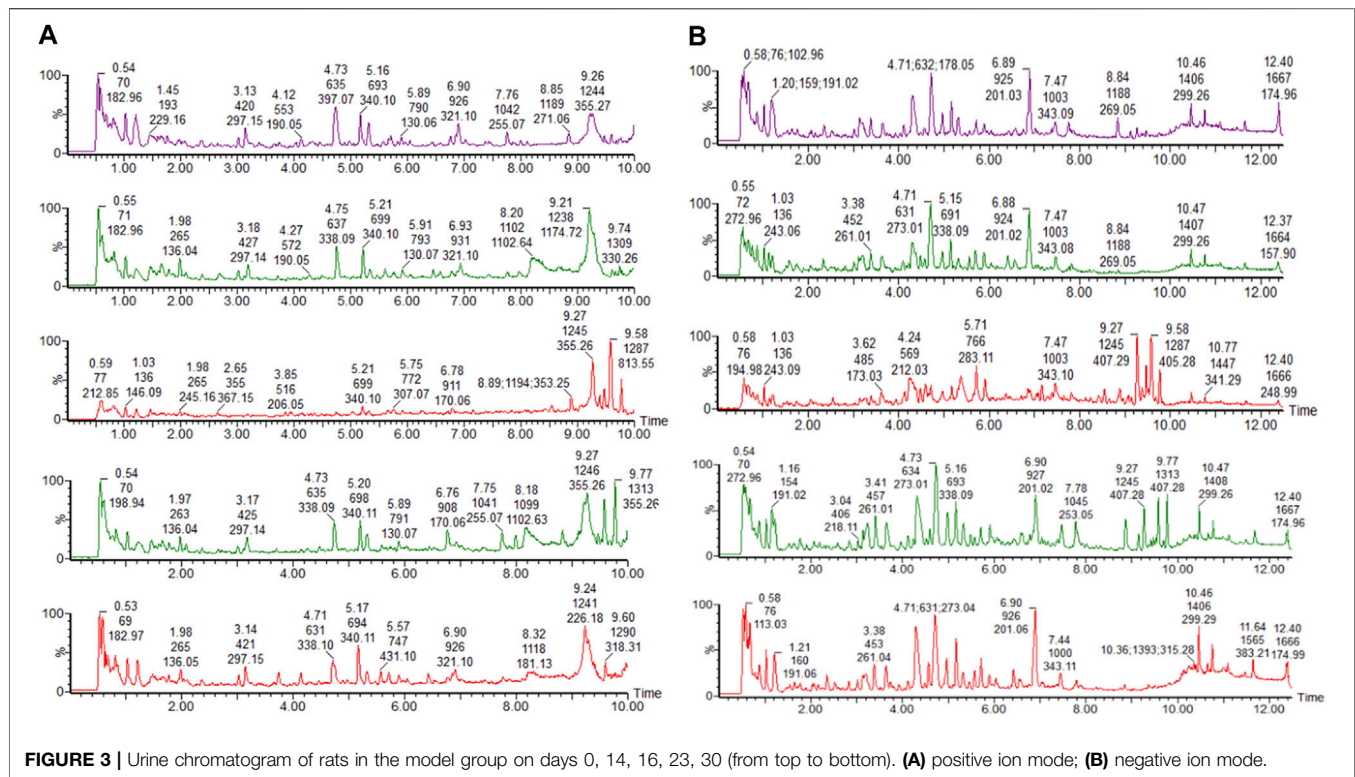


FIGURE 3 | Urine chromatogram of rats in the model group on days 0, 14, 16, 23, 30 (from top to bottom). **(A)** positive ion mode; **(B)** negative ion mode.

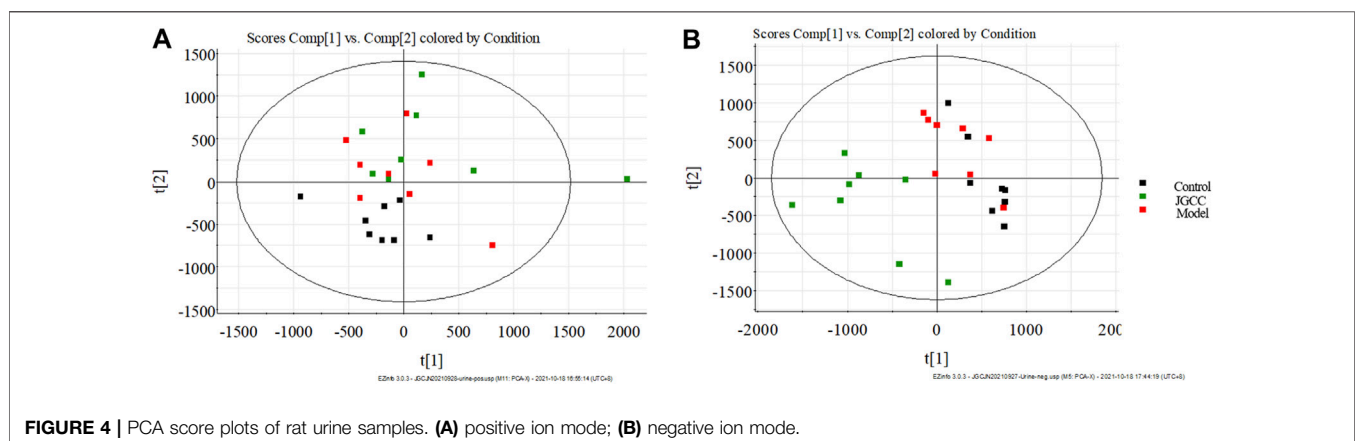


FIGURE 4 | PCA score plots of rat urine samples. **(A)** positive ion mode; **(B)** negative ion mode.

successfully established with the combined solution of *Zingiber officinale* Roscoe [Zingiberaceae; *Zingiberis rhizoma*], ethanol and ANIT. Urine TIC chromatogram showed that the urine metabolic profile of model group rats changed obviously, as is shown in **Figure 3**. The urine data was collected with UPLC-G2Si-HMDS on the 30th day and analyzed by Progenesis QI software. After standardized treatment, the score plot of PCA analysis is shown in **Figure 4**. It can be seen from the figure that the blank group and the model group are separated from each other, indicating that the metabolic network in the model group has changed. In the negative ion mode, the JGCC group is significantly far away from the model group, indicating that there is a difference between the JGCC group and the model

group; In the positive ion mode, it is seen that the JGCC group is between the blank group and the model group, suggesting that JGCC can delay the pathological process of dampness-heat jaundice rats to a certain extent. Since PCA analysis is an unsupervised mode and belongs to exploratory analysis, and metabolomics data is extremely complex, simple unsupervised analysis could not well distinguish the group differences between samples, we continue to use supervised analysis.

The urine data of the model group and the blank group were further analyzed by the supervised OPLS-DA method. The farther away from the origin of the VIP Scatter plot, the greater contribution rate of ions. The variable ions with VIP>1 and *t*-test *p* < 0.05 were selected as potential biomarkers for

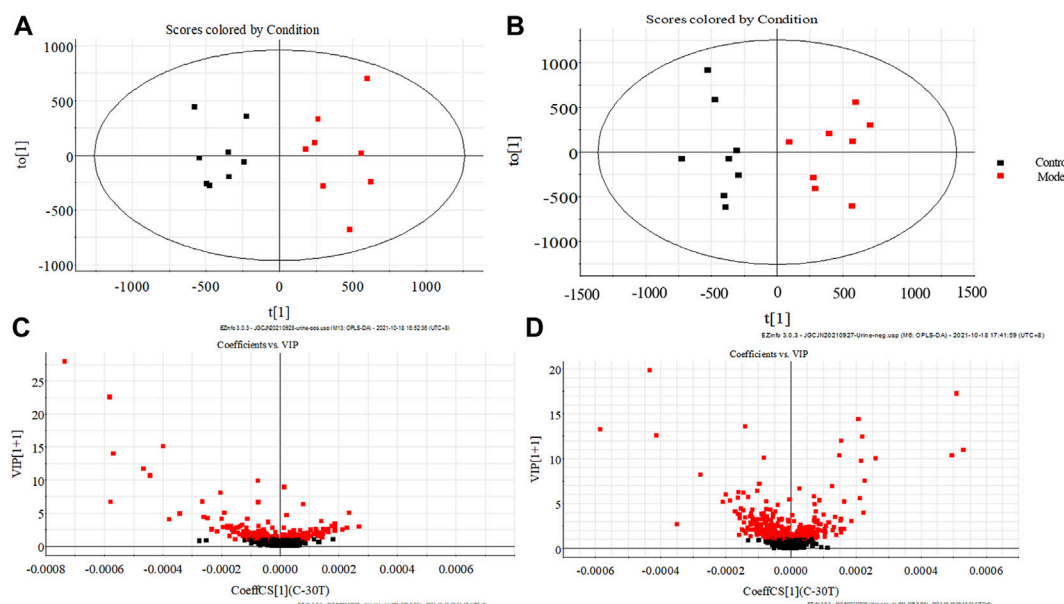


FIGURE 5 | OPLS-DA score plots of rat urine in control group and model group (A) positive ion pattern; (B) negative ion pattern. VIP scatter plots of rat urine in control group and model group. (C) positive ion pattern; (D) negative ion pattern.

structural identification, 25 potential biomarkers of dampness-heat jaundice rats were identified, See **Figure 5** and **Supplementary Table S2**. These potential biomarkers disturbed the normal metabolism of dampness-heat jaundice rats and led to metabolic abnormalities. 25 biomarkers were significantly different between the model group and the blank group, while 19 biomarkers in the JGCC group were callback and 9 of them showed significantly, among them, Tryptophanol, Glucosamine, Urocanic acid, *trans*-Dodec-2-enoic acid, *L*-Urobilin, Pyridoxal, Dodecanoic acid, Adrenochrome, and Arachidonic acid could all return to the same level as the blank group. It is indicated that JGCC can prominently inhibit the metabolic disorder of rats with dampness-heat jaundice and has obvious therapeutic effect, as shown in **Figure 6** and **Supplementary Table S3**.

Metabolic Pathway Analysis

The metabolic pathways related to biomarkers were constructed by using MetPA online database, we constructed 14 metabolic pathways, including phenylalanine, tyrosine and tryptophan biosynthesis, arachidonic acid metabolism, tryptophan metabolism, vitamin B6 metabolism, phenylalanine metabolism, histidine metabolism, pentose and glucuronate interconversions, citrate cycle, glyoxylate and dicarboxylate metabolism, biosynthesis of unsaturated fatty acids, amino sugar and nucleotide sugar metabolism, arginine and proline metabolism, fatty acid biosynthesis and steroid hormone biosynthesis, as shown in **Figure 7** and **Figure 8**. The results show that endogenous metabolites interfere with the metabolic pathways related to DHJS; among them, vitamin B6 metabolism, arachidonic acid metabolism, phenylalanine metabolism, pentose and glucuronate interconversions, histidine metabolism, citrate

cycle, glyoxylate and dicarboxylate metabolism, steroid hormone biosynthesis have a greater effect on metabolic disorder in rats with dampness-heat jaundice.

DISCUSSION

Due to the changes of health mode and disease spectrum, a single traditional clinical biochemical index can no longer meet the diagnosis of complex system diseases in today's society (Wang et al., 2012), especially TCM syndromes, such as DHJS, is the process of complex pathological changes of the body in the hot and humid environment, mainly involving the liver and other organs. In recent years, the emerging metabolomics technology can use specific biomarkers to represent complex TCM syndromes, and the markers are in an important position of relevant metabolic pathways have an irreplaceable position. UPLC/MS is a mature and effective detection method for compounds. It ionizes samples into gaseous ion mixtures and separates them according to their *m/z*. Commonly used ion sources are Electron impact ionization (EI), ESI, Atmospheric pressure chemical ionization (APCI) and so on; Which is mainly used for the analysis of macromolecular organic compounds with high polarity, thermal instability and difficult volatilization, or compounds that are difficult to be analyzed by gas chromatography mass spectrometry. At present, the liquid chromatography electrospray ionization mass spectrometry system has been widely used in high-throughput drug analysis. It can improve analytical speed, selectivity, sensitivity and reliability. About 80% of the compounds can be detected by mass spectrometry after chromatographic separation; It is also possible to identify the metabolic components in

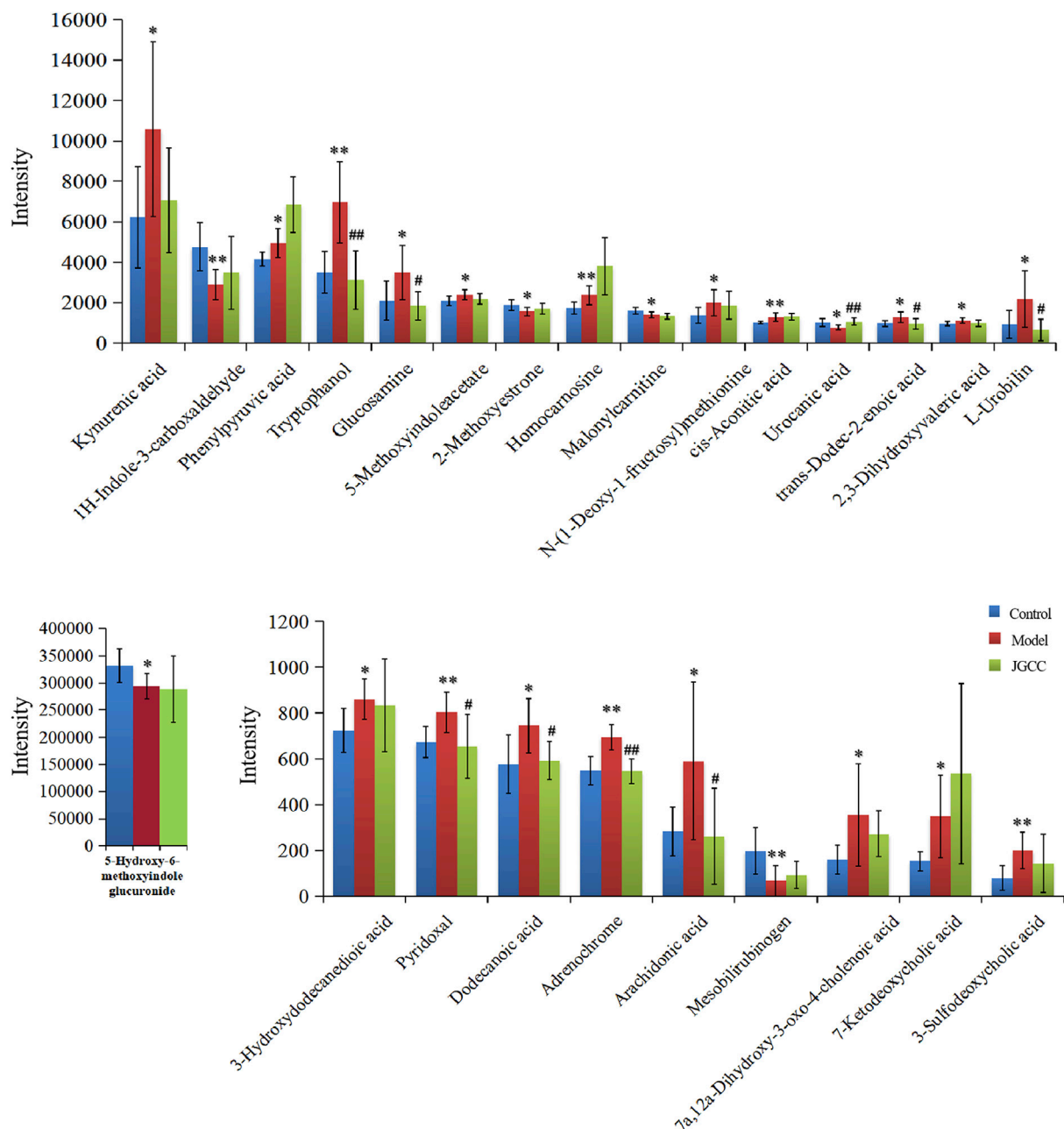


FIGURE 6 | Relative expression intensity of potential biomarkers in control, model and JGCC group. * $p < 0.05$, ** $p < 0.01$ vs Control; # $p < 0.05$, ## $p < 0.01$ vs Model.

biological samples and detect endogenous metabolic markers associated with disease occurrence in vivo. For example, Postmenopausal osteoporosis (PMOP) is a common clinical disease in postmenopausal women, UPLC/MS method was used to identify serum metabolites, and finally 16 potential biomarkers were identified, which is helpful to clarify the pathological mechanism of PMOP rats (Zhang et al., 2019b); The researchers used ultra-high performance liquid chromatography-quadrupole time of flight-tandem mass spectrometry to screen 33 metabolites related to alcoholic liver

injury (ALD) for clarifying the pathogenesis of ALD (Qiu et al., 2020); Coronary heart disease (CHD) is a relatively complex disease, there is no effective method for early diagnosis and prevention, The metabolomics technology based on UPLC-HDMS can clarify the metabolic spectrum, biomarkers and related metabolic pathways of CHD model. The researchers eventually determined 25 biomarkers and 9 related metabolic pathways associated with CHD (Sun et al., 2019b). Therefore, the combination of UPLC/MS and metabolomics technology can comprehensively understand TCM syndromes from the

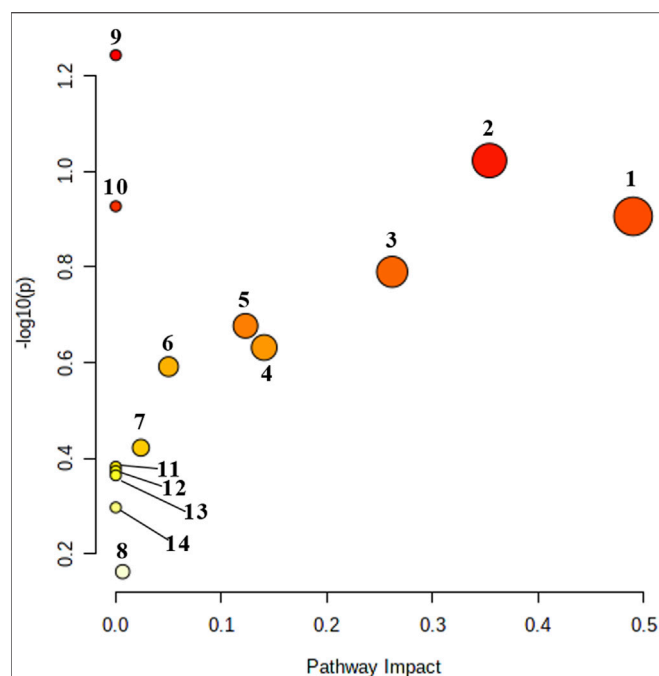


FIGURE 7 | Urine metabolic pathway analysis results. 1: Vitamin B6 metabolism; 2: Arachidonic acid metabolism; 3: Phenylalanine metabolism; 4: Pentose and glucuronate interconversions; 5: Histidine metabolism; 6: Citrate cycle; 7: Glyoxylate and dicarboxylate metabolism; 8: Steroid biosynthesis; 9: Phenylalanine, tyrosine and tryptophan biosynthesis; 10: Tryptophan metabolism; 11: Biosynthesis of unsaturated fatty acids; 12: Amino sugar and nucleotide sugar metabolism; 13: Arginine and proline metabolism; 14: Fatty acid biosynthesis.

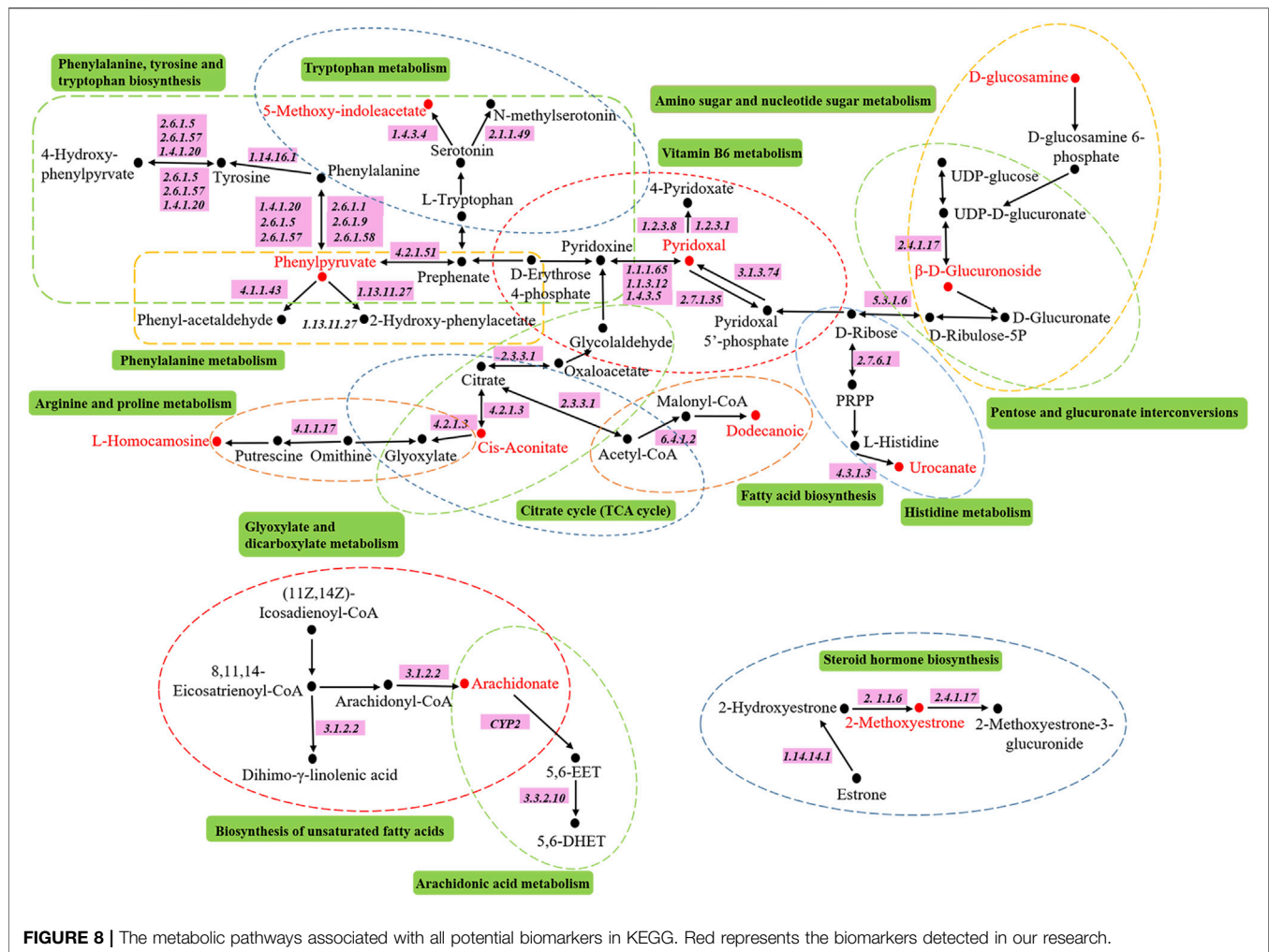
perspective of multi-level and multi-target, and then thoroughly understand the mechanism of TCM in the treatment of diseases (Fang et al., 2016).

Ethanol was used to produce wet background, *Zingiber officinale* Roscoe [Zingiberaceae; *Zingiberis rhizoma*] was used to produce heat background, and combined with ANIT was used to prepare the rat model of dampness-heat jaundice in this study, which was evaluated by classical diagnostic indexes. At the same time, the histopathological examination of the liver preliminarily showed that the rats with dampness-heat jaundice were successfully prepared, and the liver injury was significantly improved after treatment with JGCC. This modeling method has been very mature, adopted by many scholars and recognized by the majority of researchers (Fang et al., 2016; Fang et al., 2020; Liu et al., 2018; Sun et al., 2019a; Xiong et al., 2021). The therapeutic dose of JGCC was calculated according to the daily dose of 85.71 mg/kg for human. In the pretreatment experiment, we carried out the rat pharmacodynamic test of low, medium and high doses of JGCC. The doses were 0.54, 1.08, and 2.16 g/kg respectively, which were calculated according to 1, 2 and 4 times of the equivalent dose of human administration; Through the improvement of biochemical indexes and liver histopathology, it was found that the therapeutic effect of high-dose group was better than that of low and medium dose groups. Therefore, the dosage of the treatment group we chose

2.16 g/kg. On this basis, advanced UPLC-G2Si-HDMS technology combined with pattern recognition method was used to identify the phenotype of DHJS, and 25 key urine metabolites were identified as potential biomarkers, which play an important role in the regulation of metabolic network.

Studies have shown that one of the important pathways involved in severe liver injury in the pathogenesis of DHJS is the pentose and glucuronate interconversions (Zhang et al., 2016a; Fang et al., 2016; Sun et al., 2018b; Liu et al., 2018; Sun et al., 2019a). In the liver, glucuronic acid combines with lipophilic poisons through glycosidic bonds to form hydrophilic substances that are excreted from the body in the bile or kidney. This process can be used to evaluate the detoxification ability of the liver. Uridine diphosphate glucose produced during glucose metabolism is further oxidized to uridine diphosphate glucuronate (UDPGA), under the catalysis of uridine diphosphate glucuronosyltransferase 1A1 (UGT1A1, EC2.4.1.17), UDPGA can combine glucose with hydroxyl or amino of toxic substances, so as to increase water solubility and facilitate the excretion of toxic substances. Bilirubin is produced by red blood cells. When red blood cells age, lipophilic indirect bilirubin will be released and enter liver tissue with blood circulation and be converted into direct bilirubin with high hydro-soluble under the action of glucuronic acid, which is excreted from the body (Roche and Kobos., 2004). UGT1A1 is an important metabolic enzyme, which can not only catalyze the glucuronidation of drugs, poisons, steroids and thyroid hormones, promote the biosynthesis of glucosides in the brain, but also participate in the synthesis of endogenous compounds such as bilirubin, bile acids and short chain fatty acids (Rowland et al., 2013). Through focusing analysis, it is found that UGT1A1 is the only bilirubin metabolic enzyme located the upstream of D-glucuronic acid in the metabolic pathway of pentose and glucuronate interconversions. Indirect bilirubin must be transformed into direct bilirubin through UGT1A1 (Memon et al., 2016). It combines with Y protein and Z protein to produce highly water-soluble bilirubin-Y protein and bilirubin-Z protein, which are dissolved in bile and then excreted from the body. Therefore, any error of pentose and glucuronate interconversions will lead to an increase in the assay of bilirubin in serum, and the obvious clinical manifestations is that skin and mucosa are as yellow as orange (Fang et al., 2020). It is found that 5-Hydroxy-6-methoxyindole glucuronide is a product of UDPGA under the action of UGT1A1. In our study, we found that the 5-Hydroxy-6-methoxyindole glucuronide content in the urine of model rats was significantly lower than blank group, which proves that the metabolism of model rats is abnormal, resulting in the disorder of the pentose and glucuronate interconversions, further leading to the occurrence of dampness-heat jaundice.

Arachidonic acid is a ω -6 polyunsaturated fatty acids mainly exists on the cell membrane in the form of phospholipids and plays an important biological role in the liver (Li et al., 2021b; Zhao et al., 2021). The metabolites of arachidonic acid, as lipid mediators, play an important role in regulating the physiological function and pathology of the liver, such as prostaglandin E2, prostacyclin, thromboxane A2 and leukotriene C4. When liver injury occurs,



macrophages gather in the liver and activate, resulting in the release of a large number of arachidonic acid metabolites, such as toxic prostaglandins, leukotrienes, TXs, free radicals and tumor necrosis factor- α , these toxic substances directly lead to the damage of hepatocytes (Chen et al., 2011; Sun et al., 2018a; Sztolsztener et al., 2020). Arachidonic acid, as an important inflammatory lipid mediator, regulates oxidative stress in hepatocyte mitochondria through three metabolic pathways of cyclooxygenase, lipoxygenase and cytochrome P450, resulting in the oxidation of a large number of fatty acids and the formation of lipid peroxides, the deposition of collagen in the liver, aggravating the injury of hepatocytes and the activation of hepatic stellate cells, and finally accelerating the injury of hepatocytes (Sacerdoti et al., 2003; Tallima, 2021). In our study, the content of arachidonic acid in the urine of model group was dramatically higher than blank control group. It proves that the metabolism of arachidonic acid is abnormal, and its metabolic pathway is disordered; a large number of inflammatory cell infiltration can be found in the pathological tissue section, which further supports the abnormal metabolism of arachidonic acid. After the treatment of JGCC, the content of arachidonic acid in rat urine was significantly reduced and returned to the blank group, proving that the JGCC has a obvious therapeutic effect.

The liver is the main metabolic site of phenylalanine. Under normal circumstances, phenylalanine in the body is mainly metabolized to tyrosine with the catalysis of enzymes (Tessari et al., 2010). When the liver has pathological changes, phenylalanine metabolism is disordered, resulting in abnormal metabolism, which leads to generate phenylpyruvic acid and phenylacetic acid by transamination with the blood circulation entering the systemic circulation, the clinical manifestation is called phenyl ketonuria (Liu et al., 2018; Fang et al., 2016). Due to the increase of phenylalanine and ketones in the blood, some hepatocytes are damaged and substances in hepatocytes are released into the blood, including aspartate aminotransferase (AST). AST is an essential substance for the metabolic transformation of phenylalanine and phenylpyruvic acid, and it is also one of the gold indexes reflecting liver function in clinic. Phenylpyruvic acid is a direct metabolite of phenylalanine, and its amount is closely related to tyrosinemia. The increase of phenylpyruvic acid content in urine reflects the abnormal metabolism of phenylalanine, suggesting that intracellular tyrosine aminotransferase causes hepatocyte injury and tyrosinemia (Zhang et al., 2016b; Sanaei Dashti and Sedigheh Hamzavi, 2019). Therefore, tyrosinemia and abnormal

metabolism of AST can promote the occurrence of jaundice syndrome. In this study, the content of phenylpyruvic acid in urine of rats with dampness-heat jaundice was significantly higher than blank group, suggesting that phenylalanine metabolism is abnormal and its metabolic pathway is disturbed. This result is proved by the significant increase of clinical biochemical index AST. The content of AST decreased prominently and was pulled back to the level of blank group with the treatment of JGCC.

Vitamin B6 is a nitrogen-containing compound, mainly in three natural forms: pyridoxal, pyridoxol, pyridoxamine and their phosphoric acid derivatives such as Pyridoxal-5-phosphate (PLP), pyridoxol-5-phosphate (PNP), pyridoxamine -5-phosphate (PMP), which are abundant in the liver. The liver is an active tissue for vitamin B6 metabolism. Vitamin B6, a component of some coenzymes in human body, is involved in various metabolic reactions, especially the metabolism of amino acids. It is closely related to nearly hundred enzyme reactions, including the metabolism of all amino acids, such as heme metabolism and tryptophan metabolism, as well as the biosynthesis of some neuromedians and DNA (Mitchell et al., 1976; Bitetto et al., 2011). Relevant studies have shown that AST requires PLP as a coenzyme to express its activity. Patients with liver disease have abnormal PLP regulation. Therefore, aberrant metabolism of vitamin B6 will directly lead to disordered operation of relevant metabolic network in the body, and ultimately result in the occurrence of jaundice. In our study, the content of pyridoxal in the urine of rats with dampness-heat jaundice was significantly higher than that of the blank group, which proved that the metabolism of vitamin B6 in the model group was abnormal and caused the appearance of dampness-heat jaundice. After treatment with JGCC, the content of pyridoxal in urine returned to the normal level.

CONCLUSION

In this study, we established a rat model of DHJS according to the basic theory of TCM. The success of model preparation was preliminarily proved by classical clinical biochemical indexes and liver histopathology. On this basis, 25 urine biomarkers of rats with dampness-heat jaundice were successfully identified by advanced UPLC-G2Si-HDMS technology combined with metabolomics. These markers are considered as possible drug targets, and 14 related metabolic pathways are determined. After treatment with JGCC, the disordered metabolic pathways are regulated successfully. Meanwhile, we have carried out a detailed biological elaboration on several major pathways with high impact value in metabolic pathways, and combined with the analysis of related metabolites in urine, the pathogenesis of

dampness-heat jaundice and the therapeutic mechanism of JGCC have been clarified. It is proved that urine metabolomics is a favorable tool for in-depth study of TCM syndromes, and provides a promising strategy for JGCC in the treatment of DHJS.

DATA AVAILABILITY STATEMENT

The original contributions presented in the study are included in the article/**Supplementary Material**, further inquiries can be directed to the corresponding authors.

ETHICS STATEMENT

The animal study was reviewed and approved by the Animal Welfare and Research Ethics Committee of Guangxi Botanical Garden of Medicinal Plants.

AUTHOR CONTRIBUTIONS

XW conceived and designed the experiment. FW and AZ, guided the experiment. TL, MZ, and ZT fed animals and carried out experiment. YH collected and analyzed the data, YH completed the writing and modification of the paper. FW directed the revision of the article. All authors read and approved the final manuscript.

FUNDING

This work was supported by Guangxi Key Research and Development Program (AB20159029), Guangxi Natural Science Foundation Program (2018JJB140057), Scientific and Technology Development Program of Guangxi (AD18126013), the 'Ba Gui Scholars' program of Guangxi, the Science and Technology Innovation Team Project of Guangxi Botanical Garden of Medicinal Plants (2019001), and the Central Government Guides Local Science and Technology Development Fund Projects (ZY21195044).

SUPPLEMENTARY MATERIAL

The Supplementary Material for this article can be found online at: <https://www.frontiersin.org/articles/10.3389/fphar.2022.822193/full#supplementary-material>

REFERENCES

- Bitetto, D., Fattovich, G., Fabris, C., Ceriani, E., Falletti, E., Fornasiere, E., et al. (2011). Complementary Role of Vitamin D Deficiency and the interleukin-28B

- Rs12979860 C/T Polymorphism in Predicting Antiviral Response in Chronic Hepatitis C. *Hepatology* 53 (4), 1118–1126. doi:10.1002/hep.24201
Chen, J., Liu, D., Bai, Q., Song, J., Guan, J., Gao, J., et al. (2011). Celecoxib Attenuates Liver Steatosis and Inflammation in Non-alcoholic Steatohepatitis Induced by High-Fat Diet in Rats. *Mol. Med. Rep.* 4, 811–816. doi:10.3892/mmr.2011.501

- Chen, Y., Jiang, T. H., Ru, W. Z., Mao, A. W., and Liu, Y. (2014). Objective Tongue Inspection on 142 Liver Cancer Patients with Damp-Heat Syndrome. *Chin. J. Integr. Med.* 20, 585–590. doi:10.1007/s11655-014-1756-z
- Chu, H., Zhang, A., Han, Y., Lu, S., Kong, L., Han, J., et al. (2016). Metabolomics Approach to Explore the Effects of Kai-Xin-San on Alzheimer's Disease Using UPLC/ESI-Q-TOF Mass Spectrometry. *J. Chromatogr. B Analyt. Technol. Biomed. Life Sci.* 1015–1016, 50–61. doi:10.1016/j.jchromb.2016.02.007
- Fang, H., Zhang, A., Yu, J., Wang, L., Liu, C., Zhou, X., et al. (2016). Insight into the Metabolic Mechanism of Scoparone on Biomarkers for Inhibiting Yanghuang Syndrome. *Sci. Rep.* 6, 37519. doi:10.1038/srep37519
- Fang, H., Zhang, A., Zhou, X., Yu, J., Song, Q., and Wang, X. (2020). High-throughput Metabolomics Reveals the Perturbed Metabolic Pathways and Biomarkers of Yang Huang Syndrome as Potential Targets for Evaluating the Therapeutic Effects and Mechanism of Geniposide. *Front. Med.* 14, 651–663. doi:10.1007/s11684-019-0709-5
- Li, T., Zhang, M., Tan, Z., Miao, J., He, Y., Zhang, A., et al. (2021a). Rapid Characterization of the Constituents in Jigucuo Capsule Using Ultra High Performance Liquid Chromatography with Quadrupole Time-Of-Flight Mass Spectrometry. *J. Sep. Sci.* in press. doi:10.1002/jssc.202100664
- Li, S., Su, W., Zhang, X. Y., and Guan, Y. F. (2021b). Arachidonic Acid Metabolism and Steady-State Regulation of Hepatic Glucose and Lipid Metabolism. *J. Physiol.* 73, 657–664. doi:10.13294/j.aps.2021.0052
- Liu, X.-y., Zhang, A.-h., Zhang, H., Li, M.-x., Song, Q., Su, J., et al. (2018). Serum Metabolomics Strategy for Understanding the Therapeutic Effects of Yin-Chen-Hao-Tang against Yanghuang Syndrome. *RSC Adv.* 8, 7403–7413. doi:10.1039/c7ra11048k
- Memon, N., Weinberger, B. I., Hegyi, T., and Aleksunes, L. M. (2016). Inherited Disorders of Bilirubin Clearance. *Pediatr. Res.* 79, 378–386. doi:10.1038/pr.2015.247
- Mitchell, D., Wagner, C., Stone, W. J., Wilkinson, G. R., and Schenker, S. (1976). Abnormal Regulation of Plasma Pyridoxal 5'-phosphate in Patients with Liver Disease. *Gastroenterology* 71 (6), 1043–1049. doi:10.1016/s0016-5085(76)80056-x
- Qiu, S., Zhang, A., Zhang, T., Sun, H., Guan, Y., Yan, G., et al. (2017). Dissect New Mechanistic Insights for Geniposide Efficacy on the Hepatoprotection Using Multionics Approach. *Oncotarget* 8, 108760–108770. doi:10.18632/oncotarget.21897
- Qiu, S., Zhang, A.-h., Guan, Y., Sun, H., Zhang, T.-l., Han, Y., et al. (2020). Functional Metabolomics Using UPLC-Q/TOF-MS Combined with Ingenuity Pathway Analysis as a Promising Strategy for Evaluating the Efficacy and Discovering Amino Acid Metabolism as a Potential Therapeutic Mechanism-Related Target for Geniposide against Alcoholic Liver Disease. *RSC Adv.* 10 (5), 2677–2690. doi:10.1039/c9ra09305b
- Roche, S. P., and Kobos, R. (2004). Jaundice in the Adult Patient. *Am. Fam. Physician* 69, 299–304. doi:10.1016/S0095-4543(03)00123-4
- Rowland, A., Miners, J. O., and Mackenzie, P. I. (2013). The UDP-Glucuronosyltransferases: Their Role in Drug Metabolism and Detoxification. *Int. J. Biochem. Cell Biol.* 45, 1121–1132. doi:10.1016/j.biocel.2013.02.019
- Sacerdoti, D., Gatta, A., and McGiff, J. C. (2003). Role of Cytochrome P450-dependent Arachidonic Acid Metabolites in Liver Physiology and Pathophysiology. *Prostaglandins Other Lipid Mediat* 72, 51–71. doi:10.1016/s1098-8823(03)00077-7
- Sanaei Dashti, A., and Sedigheh Hamzavi, S. (2019). Tyrosinemia Presenting with Multiple Hepatic Lesions and Splenomegaly. *J. Clin. Gastroenterol.* 53, 76–77. doi:10.1097/MCG.0000000000000744
- Sun, H., Zhang, A. H., Zou, D. X., Sun, W. J., Wu, X. H., and Wang, X. J. (2014). Metabolomics Coupled with Pattern Recognition and Pathway Analysis on Potential Biomarkers in Liver Injury and Hepatoprotective Effects of Yinchenhao. *Appl. Biochem. Biotechnol.* 173, 857–869. doi:10.1007/s12010-014-0903-5
- Sun, H., Yang, L., Li, M. X., Fang, H., Zhang, A. H., Song, Q., et al. (2018a). UPLC-G2Si-HDMS Untargeted Metabolomics for Identification of Metabolic Targets of Yin-Chen-Hao-Tang Used as a Therapeutic Agent of Dampness-Heat Jaundice Syndrome. *J. Chromatogr. B Analyt. Technol. Biomed. Life Sci.* 1081–1082, 41–50. doi:10.1016/j.jchromb.2018.02.035
- Sun, H., Zhang, A.-h., Song, Q., Fang, H., Liu, X.-y., Yang, L., et al. (2018b). Functional Metabolomics Discover Pentose and Glucuronate Interconversion Pathways as Promising Targets for Yang Huang Syndrome Treatment with Yinchenhao. *RSC Adv.* 8, 36831–36839. doi:10.1039/c8ra06553e
- Sun, H., Zhang, A. H., Yang, L., Li, M. X., Fang, H., Xie, J., et al. (2019a). High-throughput Chinmedomics Strategy for Discovering the Quality-Markers and Potential Targets for Yinchenhao Decoction. *Phytomedicine* 54, 328–338. doi:10.1016/j.phymed.2018.04.015
- Sun, H., Zhang, A.-h., Li, X.-n., Zhang, K.-m., Yan, G.-l., Han, Y., et al. (2019b). Exploring Potential Biomarkers of Coronary Heart Disease Treated by Jing Zhi Guan Xin Pian Using High-Throughput Metabolomics. *RSC Adv.* 9 (20), 11420–11432. doi:10.1039/c8ra10557j
- Sztolsztener, K., Chabowski, A., Harasim-Symbor, E., Bielawiec, P., and Konstantynowicz Nowicka, K. (2020). Arachidonic Acid as an Early Indicator of Inflammation during Non-alcoholic Fatty Liver Disease Development. *Biomolecules* 10 (8), 1133. doi:10.3390/biom10081133
- Tallima, H. (2021). Clarification of Arachidonic Acid Metabolic Pathway Intricacies. *ACS omega* 6, 15559–15563. doi:10.1021/acsomega.1c01952
- Tessari, P., Vettore, M., Million, R., Puricelli, L., and Orlando, R. (2010). Effect of Liver Cirrhosis on Phenylalanine and Tyrosine Metabolism. *Curr. Opin. Clin. Nutr. Metab. Care* 13, 81–86. doi:10.1097/MCO.0b013e32833833af
- Wang, X. J., Zhang, A. H., Han, Y., Wang, P., Sun, H., Song, G., et al. (2012). Urine Metabolomics Analysis for Biomarker Discovery and Detection of Jaundice Syndrome in Patients with Liver Disease. *Mol. Cell. Proteomics* 11, 370–380. doi:10.1074/mcp.M111.016006
- Wang, X., Wang, Q., Zhang, A., Zhang, F., Zhang, H., Sun, H., et al. (2013). Metabolomics Study of Intervention Effects of Wen-Xin-Formula Using Ultra High-Performance Liquid Chromatography/mass Spectrometry Coupled with Pattern Recognition Approach. *J. Pharm. Biomed. Anal.* 74, 22–30. doi:10.1016/j.jpba.2012.10.009
- Xiong, H., Zhang, A.-H., Guo, Y.-J., Zhou, X.-H., Sun, H., Yang, L., et al. (2021). A Clinical and Animal Experiment Integrated Platform for Small-Molecule Screening Reveals Potential Targets of Bioactive Compounds from a Herbal Prescription Based on the Therapeutic Efficacy of Yinchenhao Tang for Jaundice Syndrome. *Engineering* 7 (9), 1293–1305. doi:10.1016/j.eng.2020.12.016
- Zhang, A., Yan, G., Zhou, X., Wang, Y., Han, Y., Guan, Y., et al. (2016a). High Resolution Metabolomics Technology Reveals Widespread Pathway Changes of Alcoholic Liver Disease. *Mol. Biosyst.* 12, 262–273. doi:10.1039/c5mb00603a
- Zhang, T., Zhang, A., Qiu, S., Sun, H., Han, Y., Guan, Y., et al. (2016b). High-throughput Metabolomics Approach Reveals New Mechanistic Insights for Drug Response of Phenotypes of Geniposide towards Alcohol-Induced Liver Injury by Using Liquid Chromatography Coupled to High Resolution Mass Spectrometry. *Mol. Biosyst.* 13, 73–82. doi:10.1039/c6mb00742b
- Zhang, A.-H., Sun, H., Yan, G.-L., Han, Y., Zhao, Q.-Q., and Wang, X.-J. (2019a). Chinmedomics: A Powerful Approach Integrating Metabolomics with Serum Pharmacochimistry to Evaluate the Efficacy of Traditional Chinese Medicine. *Engineering* 5, 60–68. doi:10.1016/j.eng.2018.11.008
- Zhang, A. H., Ma, Z. M., Sun, H., Zhang, Y., Liu, J. H., Wu, F. F., et al. (2019b). High-Throughput Metabolomics Evaluate the Efficacy of Total Lignans from Acanthopanax Senticosus Stem against Ovariectomized Osteoporosis Rat. *Front. Pharmacol.* 10 (553), 553. doi:10.3389/fphar.2019.00553
- Zhao, G., Yang, W. Q., Liu, L., Li, Y. P., and Li, L. M. (2021). Research Progress on Arachidonic Acid CYP450 Metabolism and Non-alcoholic Fatty Liver and Exercise Intervention. *Life Sci.* 33, 989–996. doi:10.13376/j.cbls/2021108
- Zhao, P., Ye, Z. W., He, D. X., Pan, L., and Lin, J. (2009). Study on the Protective Effect of Jigucuo Capsule on Hepatic Fibrosis in Rats. *Chin. J. Exp. prescription* 15, 99–101. doi:10.13422/j.cnki.syfx.2009.10.038

Conflict of Interest: The authors declare that the research was conducted in the absence of any commercial or financial relationships that could be construed as a potential conflict of interest.

Publisher's Note: All claims expressed in this article are solely those of the authors and do not necessarily represent those of their affiliated organizations, or those of the publisher, the editors and the reviewers. Any product that may be evaluated in this article, or claim that may be made by its manufacturer, is not guaranteed or endorsed by the publisher.

Copyright © 2022 He, Zhang, Li, Tan, Zhang, Ou, Huang, Wu and Wang. This is an open-access article distributed under the terms of the Creative Commons Attribution License (CC BY). The use, distribution or reproduction in other forums is permitted, provided the original author(s) and the copyright owner(s) are credited and that the original publication in this journal is cited, in accordance with accepted academic practice. No use, distribution or reproduction is permitted which does not comply with these terms.



Chemical Stability of a Chinese Herbal Spirit Using LC-MS-Based Metabolomics and Accelerated Tests

Yan Hu^{1,2†}, Zhe Wang^{3†}, Jiayue Liu³, Wen Yang³, Qiang Yang³, Yuan-Cai Liu³, Qiu-Yun You⁴, Xiao-Jia Chen^{1*} and Jian-Bo Wan^{1*}

¹State Key Laboratory of Quality Research in Chinese Medicine, Institute of Chinese Medical Sciences, University of Macau, Macao, China, ²State Key Laboratory Breeding Base of Systematic Research, Development and Utilization of Chinese Medicine Resources, School of Pharmacy, Chengdu University of Traditional Chinese Medicine, Chengdu, China, ³Hubei Provincial Key Laboratory for Quality and Safety of Traditional Chinese Medicine Health Food, Jing Brand Co., Ltd, Wuhan, China, ⁴Pharmacy School, Hubei University of Chinese Medicine, Wuhan, China

OPEN ACCESS

Edited by:

Haitao Lu,
Shanghai Jiao Tong University, China

Reviewed by:

Jun Xu,
Hong Kong Baptist University, Hong
Kong SAR, China
Zhe-Sheng Chen,
St. John's University, United States

*Correspondence:

Xiao-Jia Chen
xiaojiachen@um.edu.mo
Jian-Bo Wan
jbowan@um.edu.mo

[†]These authors have contributed
equally to this work

Specialty section:

This article was submitted to
Ethnopharmacology,
a section of the journal
Frontiers in Pharmacology

Received: 19 January 2022

Accepted: 18 February 2022

Published: 07 March 2022

Citation:

Hu Y, Wang Z, Liu J, Yang W, Yang Q,
Liu Y-C, You Q-Y, Chen X-J and
Wan J-B (2022) Chemical Stability of a
Chinese Herbal Spirit Using LC-MS-
Based Metabolomics and
Accelerated Tests.
Front. Pharmacol. 13:857706.
doi: 10.3389/fphar.2022.857706

As a prevalent medicinal liquor among Chinese people, a type of Chinese herbal spirit from Jing Brand Co., Ltd (CHS-J) is a newly developed health beverage with the health functions of anti-fatigue and immune enhancement. The researchers from the enterprise found that the contents of several components in CHS-J samples have been significantly decreasing during the stated storage period, as detected by the HPLC-UV method, which would make a great challenge for quality control of CHS-J. Furthermore, the chemical stability of CHS-J during the storage period is greatly challenged affected, especially in the environment of high temperature and light exposure. To systematically reveal the unstable components and promote the quality control of CHS-J, the chemical stability of CHS-J during the shelving storage period was characterized by the UPLC/Q-TOFMS-based metabolomics approach. First, the targeted and untargeted metabolomics approaches discovered the significantly changed components in CHS-J samples produced in different years. Furthermore, the accelerated tests of newly produced CHS samples and several authorized standards were conducted to validate the above results and elucidate the possible mechanisms underlying these chemical changes. Moreover, these chemical changes during the storage period had little influence on the anti-fatigue effect of CHS-J samples. These findings will offer new insight into the understanding of the chemical stability of CHS-J and will facilitate the quality control of CHS-J.

Keywords: chinese herbal spirit, metabolomics, accelerated test, quality control, anti-fatigue

INTRODUCTION

Chinese herbal spirit (CHS) is an alcoholic beverage in which several precious herbs are commonly immersed. CHS has become increasingly popular among Chinese people in past decades due to its nourishing and tonic activities. A type of CHS from Jing Brand Co., Ltd (CHS-J) is a newly developed health beverage, which is brewed by modern bioengineering technology with a faint-scented Xiaoqu liquor and the extracts of several Chinese herbal medicines, such as *Astragalus membranaceus* (Fisch.) Bge. [Fabaceae; Astragali Radix], *Epimedium brevicornu* Maxim [Berberidaceae, Epimedium Folium], *Cistanche deserticola* Ma [Orobanchaceae; Cistanches Herba], *Lycium barbarum* L. [Solanaceae; Lycii Fructus], and *Curculigo orchioidea* Gaertn. [Hypoxidaceae; Curculiginis Rhizoma] (Liu et al., 2018). These herbal medicines are carefully composited under the guidance

of traditional Chinese medicine theory, and several of them are edible Chinese Medicines and used as foods. CHS-J has been shown to exert anti-inflammation (Feng et al., 2013), health-care functions of immune enhancement (Liu et al., 2018), and anti-fatigue (Liu et al., 2018). CHS-J contained enormous and complex components with great structural diversity and a wide range of concentration distribution, including flavonoids, saponins, alkaloids, phenylethanoids, coumarins, anthraquinones, and volatile oil, etc. (Hu et al., 2021), which were blended in 35% (v/v) of the base liquor. Thus, the chemical stability of CHS-J during the storage period is greatly challenged, especially in the environment of high temperature and light exposure. The researchers from the enterprise found that the contents of several components in CHS-J have significantly been decreasing during the storage period, as detected by the HPLC-UV method, which would make a great challenge for quality control of CHS. Moreover, whether these changes during the storage period influence the function of CHS-J (such as the anti-fatigue effects) remains unclear.

As an emerging omics platform, metabolomics allows to comprehensively characterize entire small molecules (M.W. < 1000 Da) in the biological system and their dynamic changes in response to internal and external factors (Wan et al., 2013). Metabolomics emphasizes the whole system rather than individual parts, and this feature is in accordance with the natural characteristics of Chinese Medicines, such as the holistic and dynamic nature (Wang et al., 2011a). In the past years, the metabolomics approach has been widely employed for quality evaluation and discrimination of Chinese Medicines (Chan et al., 2007; Lee et al., 2009; Toh et al., 2010; Wang et al., 2011b; Sun and Chen, 2011; Xiang et al., 2011; Kim et al., 2012; Yang et al., 2012). It has also been used to monitor the changes in both chemical components and their concentrations in a given Chinese medicine that is derived from various species (Lee et al., 2009; Xiang et al., 2011), different geographical areas (Sun and Chen, 2011), processing methods (Chan et al., 2007; Toh et al., 2010), and growing years (Yang et al., 2012). Thus, metabolomics offers a promising approach for the in-depth understanding of the chemical stability of CHS-J during the shelving storage period. Ultra-high performance liquid chromatography/quadrupole time-of-flight mass spectrometry (UHPLC/Q-TOFMS) is the most popular and desirable analytical platform for mapping the chemical components in the biological sample due to its high throughput, high sensitivity, and depth of coverage (Xia et al., 2020). Therefore, in the current study, the chemical stability of CHS-J during the shelving storage period was characterized by the UPLC/Q-TOFMS-based metabolomics approach. First, the significantly changed components in CHS-J samples produced in different years were discovered by targeted and untargeted metabolomics approaches. Second, the accelerated tests of newly-produced CHS samples and authorized standards were conducted to validate the above results and elucidate the possible mechanisms underlying these chemical changes.

Furthermore, the anti-fatigue effects of CHS-J samples with different storage periods was also conducted and compared.

MATERIALS AND METHODS

Materials and Chemicals

CHS-J specimens produced by five different years, i.e., 2014, 2015, 2016, 2018, and 2020 ($n = 20$) and 35% (v/v) of base liquor of CHS-J were kindly provided by Jing brand Co. Ltd (Hubei, China), and the company declined to disclose the detailed information, such as the amount of each herb and the extraction procedure, as a trade secret. All specimens were stored at room temperature and light-protected environment at the Institute of Chinese Medical Sciences, University of Macau, Macao. Thirteen reference compounds, including Z-ligustilide, Baohuoside I, Sagittatoside B, Epimedin B, Echinacoside, 2''-O-rhamnosyl Icariside II and Magnoflorine, were purchased from Baoji herbest Bio-Tech Co. Ltd (Shaanxi, China). Their purities were over 98%, as detected by HPLC-UV. Acetonitrile (HPLC-grade) and formic acid (HPLC-grade) were obtained from Merck (Darmstadt, Germany) and Aladdin Industrial Inc. (Shanghai, China), respectively. Deionized water was prepared by a Millipore Milli-Q water purification system (Bedford, MA, United States). A drying and heating oven (ED260 model, BINDER GmbH, Tuttlingen, Germany) and constant climate chambers (KBF 240 model, BINDER GmbH) were used in temperature-accelerated and light-accelerated tests, respectively.

Sample Preparation

Approximate 1 ml of CHS-J samples was mixed with the equivalent volume of acetonitrile. The solution was vortexed for 1 min and then centrifuged at 4°C (14,800 rpm, 20 min). The supernatant was filtered through a 0.22 μ m polytetrafluoroethylene filter (Millipore, Bedford, MA, United States) prior to the UHPLC-MS analysis. An equal volume (10 μ l) of each CHS-J sample was mixed to generate a pooled QC sample, which offers a representative "mean" sample consisting of all analytes. The QC sample was analyzed 6 times at the beginning and end of the sequence, and then every 10 tested CHS-J samples to evaluate the system stability and method reproducibility.

Untargeted Metabolomics Analysis

After sample preparation, CHS-J samples were analyzed by UHPLC-Q-TOFMS. Chromatographic separation was conducted on a Waters ACQUITY UPLC BEH C_{18} column (100 \times 2.1 mm, 1.7 μ m) with column temperature at 35°C. The analytes were subjected to gradient elution chromatography with a mobile phase composed of 0.1% formic acid (v/v) in water (phase A) and 0.1% formic acid (v/v) in acetonitrile (phase B). The solvent gradient elution program was used as follows with the flow rate of 0.3 ml min⁻¹: linear gradient from 5 to 40% B (0–15 min), 40–70% B (15–18 min), 70–100% B (18–20 min); isocratic 100% B (20–22 min), 100–5% B (22–22.1 min), 5% B (22.1–25 min). The sample injection

volume was 2 μ l, and the autosampler temperature was maintained at 4°C. The electrospray ionization (ESI) source with MS^E continuum acquisition mode was adopted to collect mass spectra in positive and negative ion modes. The key MS parameters were set as follows: MS range, m/z 50 to m/z 1200; capillary voltage, +3.0 kV in ESI+ and -2.5 kV in ESI-; cone voltage (CV), 40 V; cone gas flow, 50 L h⁻¹; desolvation gas flow, 600 L h⁻¹; source temperature, 100 °C; desolvation temperature, 250 °C. A lock-mass calibrant of leucine-enkephalin (200 ng/ml) was continuously infused at flow-rate of 50 μ l/min via a lock spray interface, generating the reference ions ($[M+H]^+ = 556.2771$, $[M-H]^- = 554.2615$) for mass correction during the analysis.

Targeted Metabolomics Analysis

To determine the levels of seven changed compounds highlighted in untargeted metabolomics, including Z-ligustilide, baohuoside I, sagittatoside B, epimedin B, echinacoside, 2''-O-rhamnosyl icaricide II and magnoflorine, an ACQUITYTM UPLC system coupled with a Xevo TQD triple-quadrupole tandem mass spectrometry (QQQ-MS/MS, Waters Co., Manchester, United Kingdom) were used to quantitatively determine these components in CHS-J samples. Chromatographic separation was achieved on the identical BEH C₁₈ column using the same mobile phases. The flow-rate was set at 0.3 ml min⁻¹ with the following solvent gradient: 5–40% B (0–12 min), 40–100% B (12–16 min), 100% B (16–18 min), and the re-equilibrated by 5% B for 3 min. Data acquisition was conducted on a Xevo TQD QQQ-MS equipped with an ESI using multiple reaction monitoring (MRM) mode. MS was operated in the positive mode to obtain satisfactory MS response for seven investigated analytes. The optimized MS parameters were depicted as follows: capillary voltage, +3.5 kV; source temperature, 140°C; desolvation gas flow and temperature, 650 L h⁻¹, and 350°C; cone flow, 50 L h⁻¹. The ion transitions, cone voltage (CV), and collision energy (CE) for each compound were optimized and shown in **Supplementary Table S1**.

Accelerated Tests of CHS-J Sample and Reference Standards

The chemical difference in CHS-J samples produced in different years might be attributed to the unstable components and the chemical variation of herbal medicines used in different years. To further confirm the instability of components in CHS-J sample during storage, the accelerated tests of the newly produced CHS-J (the year 2020) were conducted. In the temperature-accelerated tests, 100 ml of CHS-J samples ($n = 8$) were placed in clean glass bottles with airtight rubber seal flip caps and maintained at constant 60 \pm 2°C and shield from light. 0.5 ml of liquor from each bottle was collected every 2 weeks and continuously collected for 8 weeks. In light-accelerated tests, 100 ml of CHS-J samples ($n = 8$) were exposed at the light (5500 \pm 500 Lux, 50% R.H., 25°C), 0.5 ml of liquor was collected every

3 until 12 weeks. All collected liquor samples were stored at –80°C until analysis.

To reveal the potential degradation pathways, the selected reference standards were also subjected to temperature-accelerated and light-accelerated tests as described above. The reference standards were accurately weighed and dissolved in 35% (v/v) of base liquor individually at the final concentration of 20 μ g ml⁻¹ with 3 replicates. 0.5 ml of solution from each bottle was collected weekly. All collected samples were stored at –80°C until UHPLC-Q-TOFMS analysis.

Anti-Fatigue Study

Animal treatment

After 7-day acclimatization, a total of 60 male Kunming mice were randomly divided into the following three groups ($n = 20$ per group): control group (normal saline); 2014-year group (15 ml/kg/days CHS-J samples produced in 2014); 2020-year group (15 ml/kg/days CHS-J samples produced in 2020). Each mouse was orally administered with the CHS-J samples for 14 consecutive days. The health status of the mice was observed each day. According to the Technical standards for testing and assessment of health food (2003 edition), the exhaustive swimming time, hepatic glycogen level, muscle glycogen level, blood lactic acid level, urea nitrogen level, and lactic dehydrogenase level were tested to estimate the anti-fatigue effects (Ministry of Health of the People's Republic of China, 2003).

Exhaustive Swimming Test

In brief, after 30 min of last intragastric administration, a lead sheath, weighing 5% of the mouse's body weight, was tied to the root of the mouse tail. Four tempered glass pools (50 \times 40 \times 40 cm) were filled with water to a depth of 30 cm. The mice (10/group) were dropped into the water. The swimming time (from dropping into the water to sinking underwater for over 10 s) was recorded. The water temperature was 25 \pm 1°C.

Determination of Hepatic Glycogen Level and Muscle Glycogen Level

The mice (20/group) were killed by cervical vertebral dislocation, and their liver and muscle tissues were extracted for further analysis. Since glycogen in the liver tissues is unstable and loses activity quickly *in vivo*; thus, 100 mg of liver tissue from each mouse was weighed, cleaned using normal saline, dried with filter paper, and then diluted in lye immediately. The anthrone colorimetric method was adapted to estimate the quantity of hepatic glycogen and muscle glycogen.

Determination of Blood Lactic Acid Level, Urea Nitrogen Level, and Lactic Dehydrogenase Level

The mice (20/group) were forced to swim in pools for 90 min without weight loading. After a 60-min resting period, blood was sampled from eyes and collected in tubes containing heparin. Plasma samples were collected by centrifugation for 10 min at 3,800 rpm. The blood lactic acid levels were measured using blood lactic acid assay kits, and the concentrations of urea nitrogen were analyzed using urea

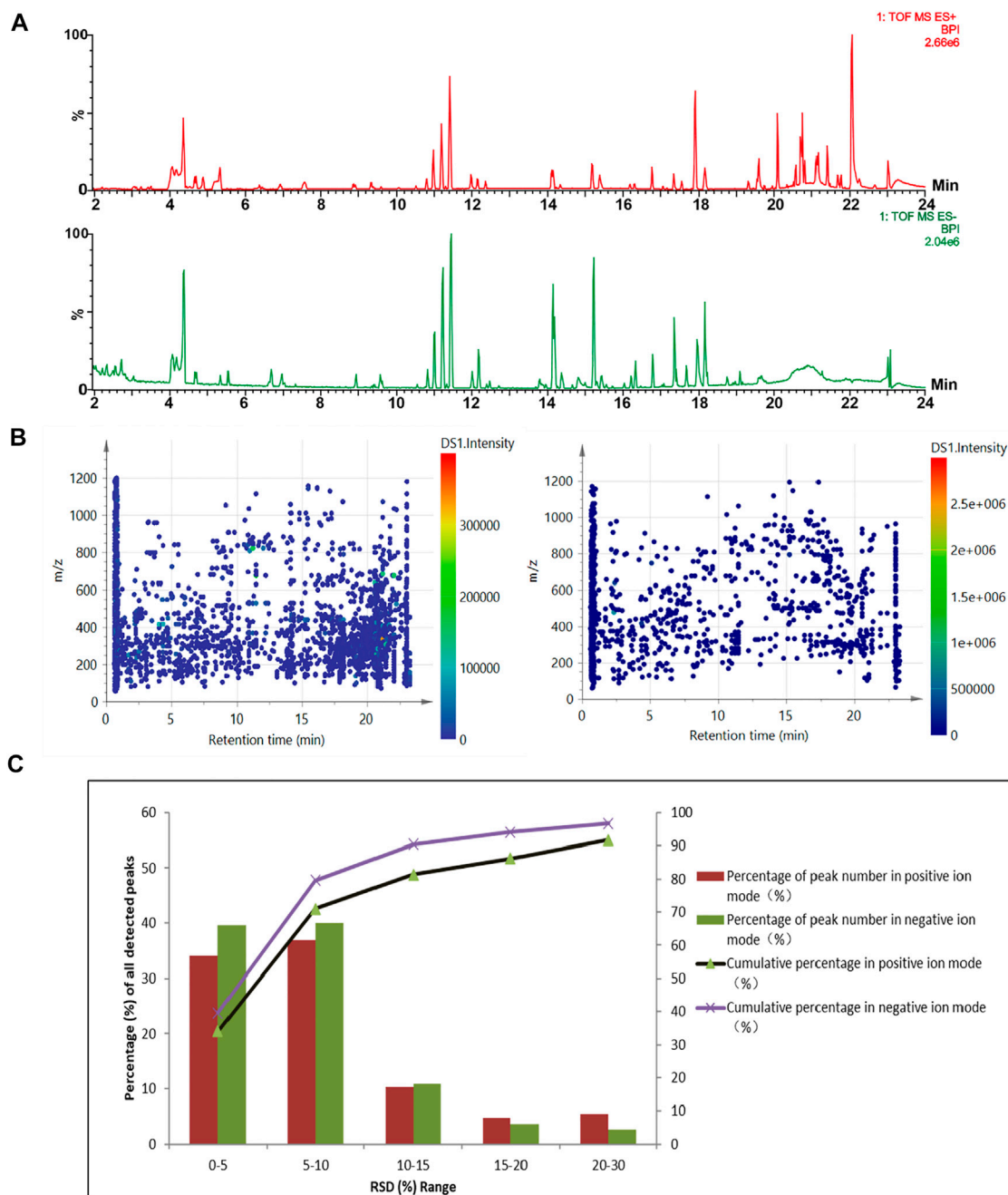


FIGURE 1 | (A) Representative base-peak ion (BPI) chromatograms of QC samples detected in the positive (up) and negative (down) ion modes. **(B)** The distribution of the detected ions. **(C)** RSD (%) distribution of the detected peaks in the QC sample.

assay kits. The lactic dehydrogenase activity in plasma was measured by the automatic biochemical analyzer.

STATISTICAL ANALYSIS

The data acquired in UHPLC-Q-TOFMS analysis were processed by Progenesis QI software (Nonlinear Dynamics, Newcastle, United Kingdom) for peak picking and alignment.

The processed data were subsequently analyzed by SIMCA-P software (version 14.1, Umetrics, Umeå, Sweden) for multivariate statistical analysis. The contents and relative peak areas of investigated analytes were analyzed by GraphPad Prism (version 6.0, San Diego, CA, United States) to visualize the variation in different groups. The levels of analytes were expressed as the mean \pm standard deviation (S.D.), and a *p*-value of less than 0.05 was considered statistically significant.

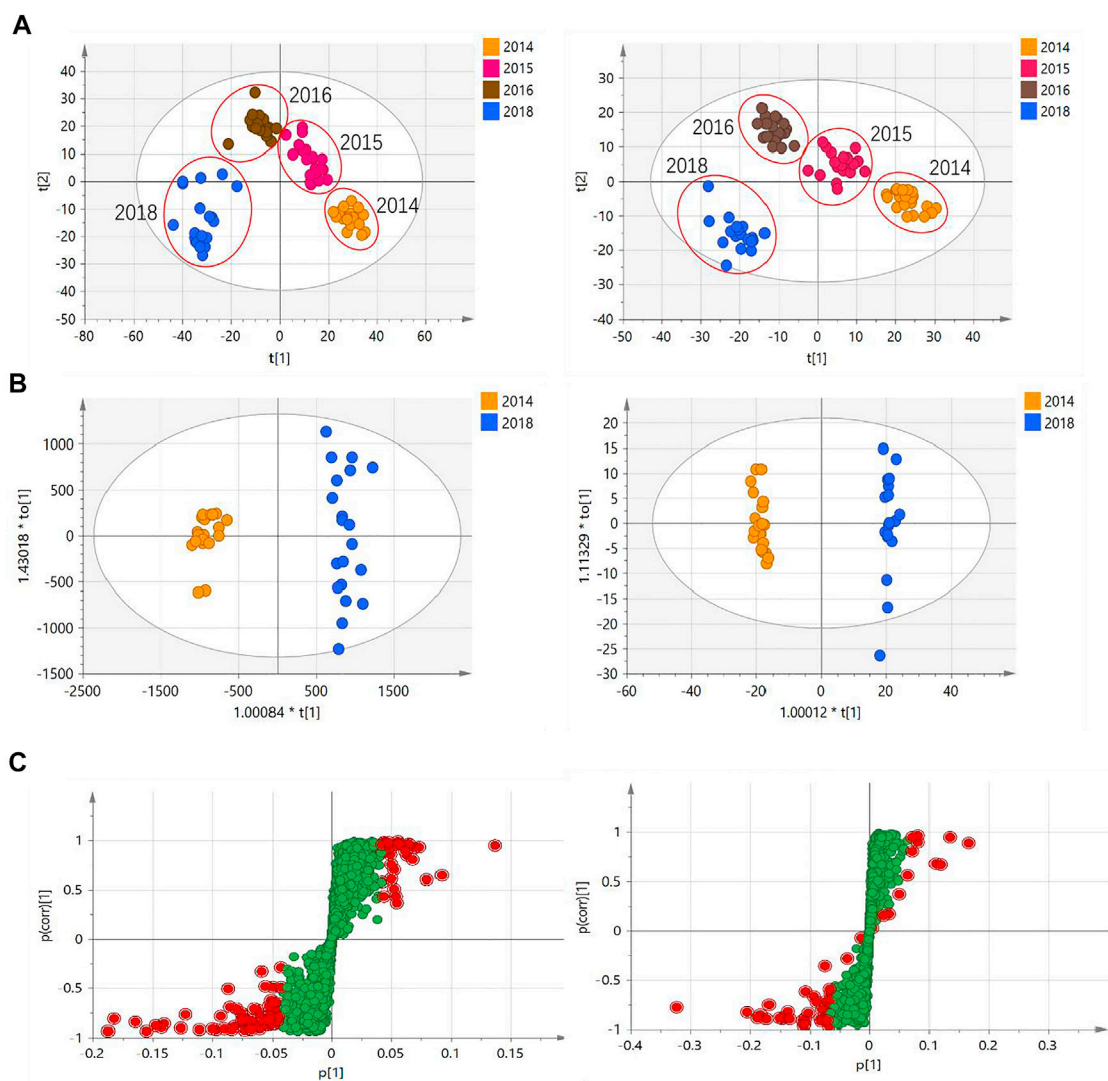


FIGURE 2 | (A) PLS-DA score plots of CHS-J samples with different production years in positive (left) and negative (right) ion modes. **(B)** OPLS-DA score plots and **(C)** their S-plots of CHS-J samples produced in 2014 and 2018 detected in positive (left) and negative (right) ion modes.

RESULTS AND DISCUSSION

Method Validation of UPLC/Q-TOFMS

Due to containing several herbal extracts and the base liqueur, the CHS-J is a highly complex matrix consisting of numerous organic compounds with a wide range of concentrations. Under the optimized chromatographic and MS conditions, the major components in CHS-J were well separated and detected in both positive and negative ion modes. The representative base peak intensity (BPI) chromatograms of the QC sample are illustrated in **Figure 1A**. A pooled QC sample was used for the method validation of UHPLC/Q-TOFMS. The raw data acquired was pre-treated using Progenesis QI for peak picking and alignment. After “80% rule” processing, 2775 and 1143 variables were generated from the QC samples detected in positive and negative ion modes, respectively. These ions are

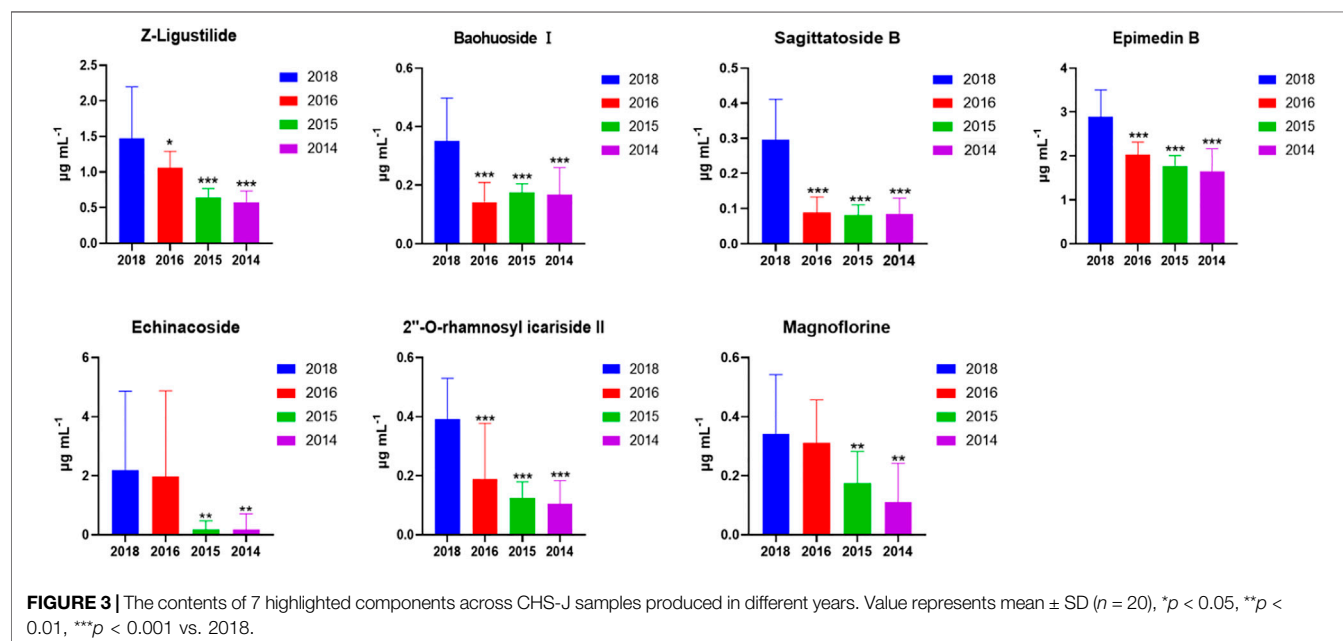
fairly evenly distributed in whole chromatograms (**Figure 1B**). Furthermore, the relative standard deviation (RSD) distribution of these ions in QC samples was commonly used to evaluate the stability and reproducibility of untargeted metabolomics analysis. As shown in **Figure 1C**, 91.7 and 96.8% of the variables with RSD less than 30% were observed in positive and negative ion modes, respectively, along with 71.2 and 79.9% of the ions with RSD $\leq 10\%$, which demonstrated the excellent stability and reliability of the UPLC/Q-TOFMS method for untargeted metabolomics.

Metabolomics Analysis of CHS-J Samples With Different Storage Years

To characterize the chemical differences across CHS-J samples with different storage years, CHS-J samples produced by 2014, 2015, 2016, and 2018 were used for

TABLE 1 | Identifications of the highlighted ions which were validated by reference standards.

| RT (min) | Formula | [M + H] ⁺ / [M - H] ⁻ | Measured mass | Exact mass | Error (ppm) | MS/MS | Compound | Tendency ^a |
|----------|---|--|---------------|------------|-------------|--|------------------------------|-----------------------|
| 4.91 | C ₂₀ H ₂₄ NO ₄ | [M + H] ⁺ | 342.1714 | 342.1705 | 2.63 | 297.1131, 271.0854, 265.0898, 189.0550, 127.0382, 109.0280 | Magnoflorine | ↓ |
| 5.55 | C ₃₅ H ₄₆ O ₂₀ | [M - H] ⁻ | 785.2534 | 785.2504 | 3.82 | 623.2162, 161.0267 | Echinacoside | ↓ |
| 11.01 | C ₃₈ H ₄₈ O ₁₉ | [M + H] ⁺ | 809.2809 | 809.2868 | -7.29 | 677.2504, 531.1844, 369.1310, 313.0676 | Epimedin B | ↓ |
| 16.23 | C ₃₂ H ₃₈ O ₁₄ | [M + H] ⁺ | 647.2301 | 647.2340 | -6.03 | 369.1310, 313.0676 | Sagittatoside B | ↓ |
| 16.35 | C ₃₃ H ₄₀ O ₁₄ | [M + H] ⁺ | 661.2514 | 661.2496 | 2.72 | 515.1921, 369.1310, 313.0676 | 2''-O-rhamnosyl Icariside II | ↓ |
| 16.80 | C ₂₇ H ₃₀ O ₁₀ | [M + H] ⁺ | 515.1921 | 515.1917 | 0.78 | 369.1310, 313.0676 | Baohuoside I | ↓ |
| 17.92 | C ₁₂ H ₁₄ O ₂ | [M + H] ⁺ | 191.1069 | 191.1072 | -1.57 | 173.0959, 145.1019, 115.0564, 105.0679, 91.0563 | Z-ligustilide | ↓ |

^aCHS-J, produced in the year 2014 vs. 2018.

untargeted metabolomics analysis. After data preprocessing, the partial least squares discriminant analysis (PLS-DA), a supervised multivariate data analysis, was constructed. Sevenfold cross-validation was conducted to validate the quality of the PLS-DA model. The parameters R^2 and Q^2 represent the interpretability of the variable and the model's predictability, respectively. The cumulative values of R^2X , R^2Y , and Q^2 were close to the optimal value of 1.0, indicating the established models with excellent predictive capability and fitness (Wan et al., 2013). As depicted in **Figure 2A**, all tested CHS-J samples from four different production years were clustered in PLS-DA score plots in both positive ($R^2X = 0.596$, $R^2Y = 0.964$, $Q^2 = 0.943$) and negative ($R^2X = 0.702$, $R^2Y = 0.98$, $Q^2 = 0.963$) ion modes, indicating the significant differences in the chemical profile of CHS-J samples produced in the different years. To reveal the discrepant components contributing most to the group separation, the differentiated compounds were picked by S-plot derived from the OPLS-DA model constructed by CHS-J samples produced

between the year 2014 and year 2018 (**Figures 2B,C**). Variables with variable importance in the projection (VIP) > 2 were tentatively highlighted to be important for discrimination (**Figures 2B,C**). The variables were further filtered by $p < 0.05$ and fold-change $FC > 2$. As a result, 39 and 14 variables were highlighted in positive and negative ion modes, respectively. The structures were tentatively assigned by an in-house database and further validated by their reference standards. Finally, 7 compounds were accurately identified, as shown in **Table 1**. The intensity tendency of these compounds in CHS-J samples with different storage years was analyzed, and most of the identified compounds had a gradually decreasing trend along with the increasing storage years (data not shown).

To confirm the findings from untargeted metabolomics, these seven highlighted components in CHS-J samples produced in different years were quantitatively determined by UHPLC-QQQ-MS/MS in multiple reaction monitoring (MRM) mode as described previously (Hu et al., 2021). As shown in **Figure 3**,

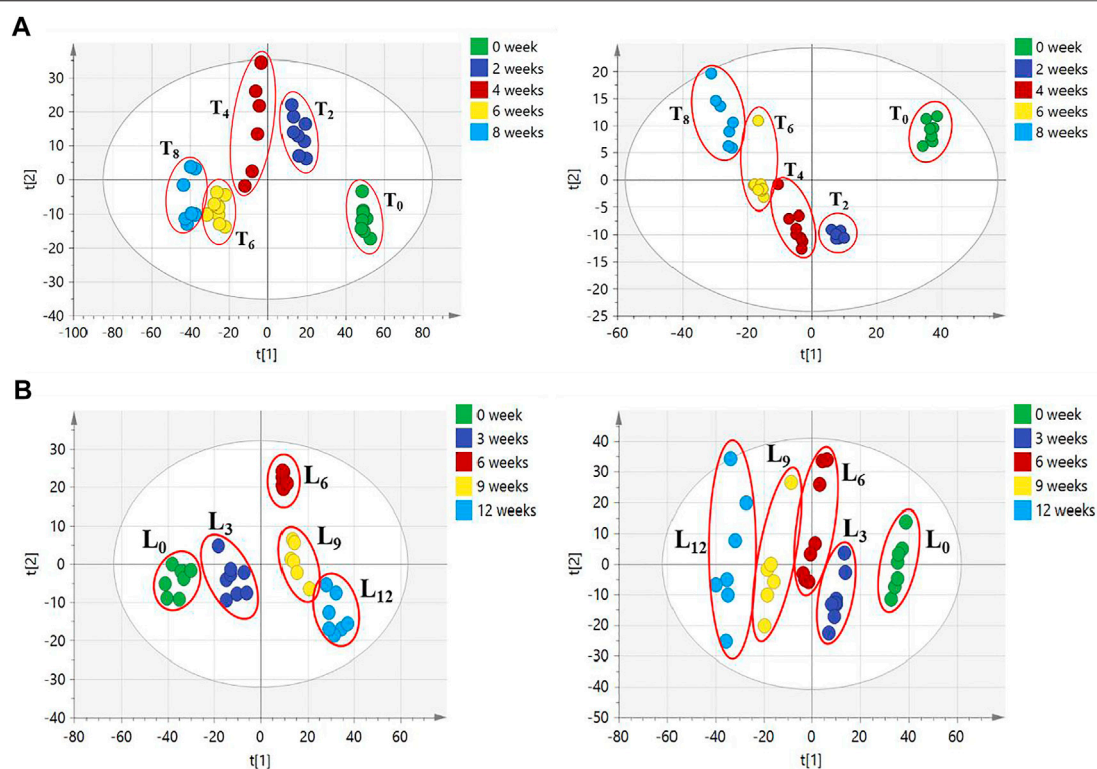


FIGURE 4 | PCA score plots of CHS-J samples in (A) temperature- and (B) light-accelerated tests detected in positive (left) and negative (right) ion modes.

the concentrations of seven highlighted components across CHS-J samples produced in 2018 were higher than those in tested samples produced in other years, except that no significant difference in the levels of echinacoside or magnoflorine between samples 2018 and 2016.

Metabolomics Analysis of CHS-J Samples in Accelerated Tests

The difference in these compound levels in CHS-J samples produced in different years might be attributed to the instability of components and the chemical variation of herbal

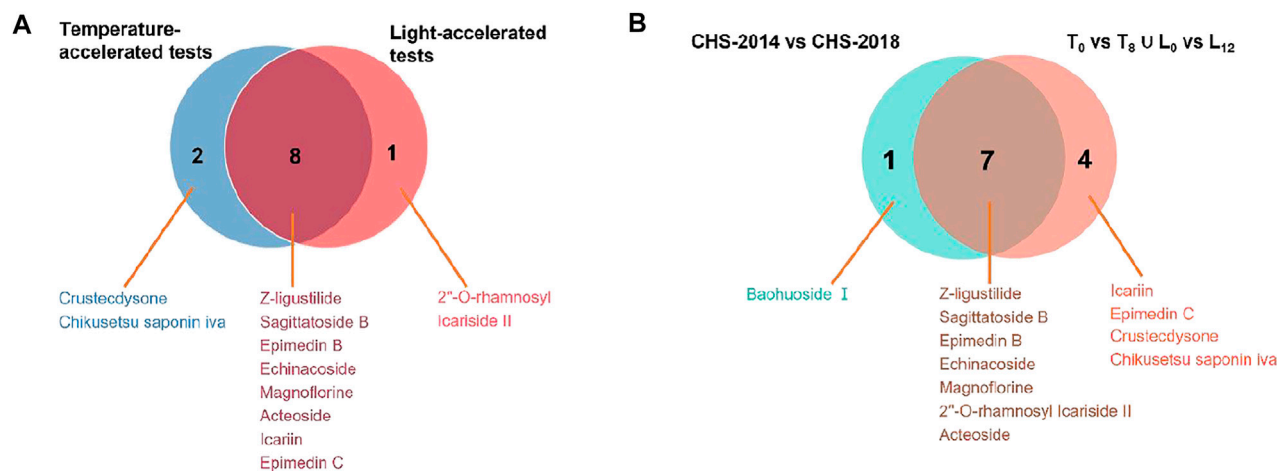


FIGURE 5 | Venn diagrams show the common compounds of (A) temperature-accelerated and light-accelerated groups and (B) accelerated tests and CHS-J samples produced in different production years.

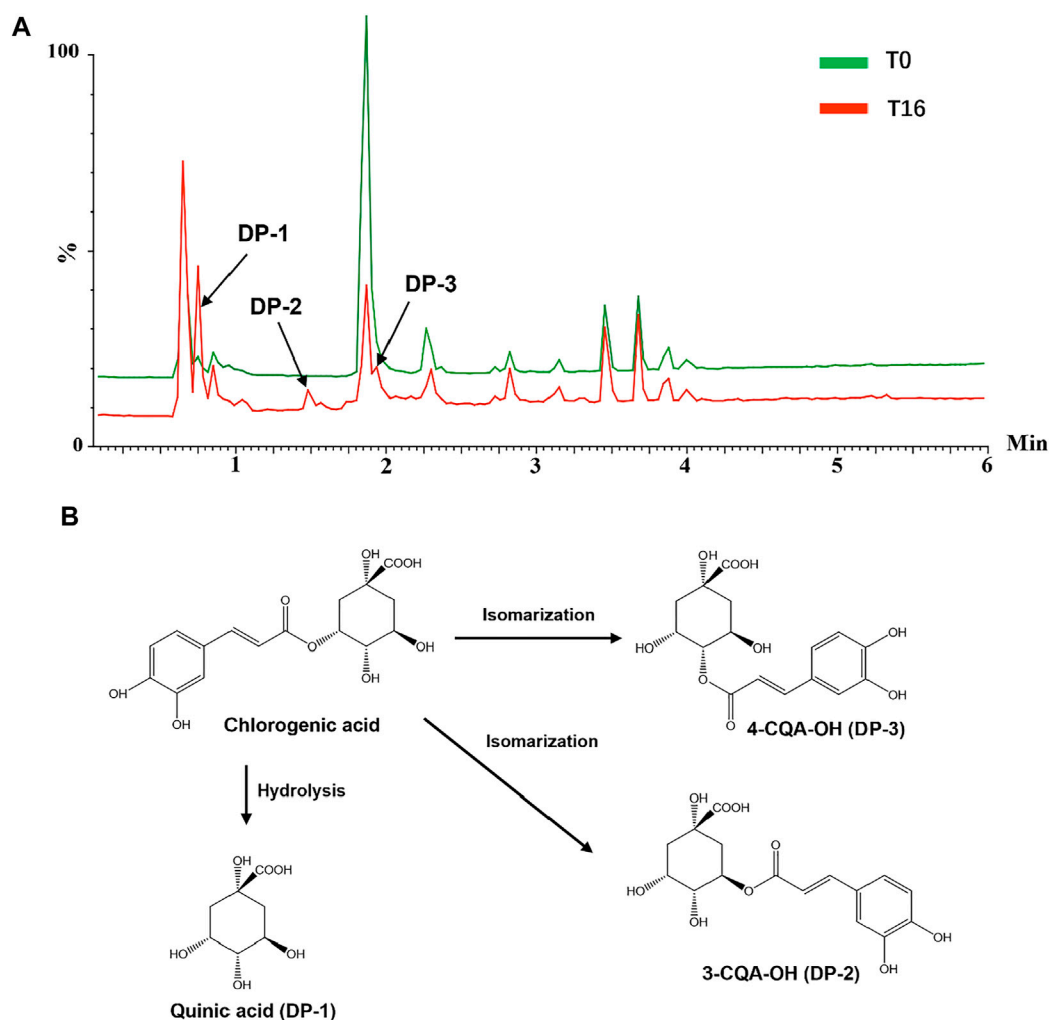


FIGURE 6 | (A) TIC of chlorogenic acid dissolved in base liquor before (T_0) and after 16 weeks (T_{16}) in temperature-accelerated tests. **(B)** Proposed degradation mechanism of chlorogenic acid in base liquor under high-temperature exposure.

TABLE 2 | Effects of CHS-J samples produced in 2014 and 2020 on exhaustive swimming time, hepatic glycogen, muscle glycogen, blood lactic acid, urea nitrogen, and lactic dehydrogenase levels in mice ($n = 10$, mean \pm SD), * $p < 0.05$, ** $p < 0.01$ vs. control group, $\blacktriangle p < 0.05$ vs. 2014.

| Group | Exhaustive swimming time (min) | Hepatic glycogen (mg/g) | Muscle glycogen (mg/g) | Blood lactic acid (mmol/L) | Urea nitrogen (mmol/L) | Lactic dehydrogenase (U/L) |
|--------------|--------------------------------|-------------------------|------------------------|------------------------------------|------------------------|--------------------------------------|
| Control | 13.20 \pm 2.53 | 6.55 \pm 4.56 | 0.66 \pm 0.42 | 5.82 \pm 1.01 | 8.35 \pm 1.29 | 447.49 \pm 64.77 |
| CHS-J (2014) | 24.90 \pm 3.93** | 22.11 \pm 8.18** | 1.68 \pm 0.65** | 2.03 \pm 0.46** | 3.70 \pm 0.92** | 605.10 \pm 90.09** |
| CHS-J (2020) | 22.20 \pm 3.08** | 18.64 \pm 8.26** | 1.30 \pm 0.49* | 3.18 \pm 1.19** \blacktriangle | 4.12 \pm 0.44** | 523.51 \pm 86.09* \blacktriangle |

medicines used in different years. To further confirm the instability of components in CHS-J sample, the accelerated tests of the newly produced CHS-J (the year 2020) were conducted. The CHS-J samples were continuously collected for 8 and 12 weeks in temperature-accelerated and light-accelerated tests, respectively. The samples were collected every 2 weeks (T_0 , T_2 , T_4 , T_6 , T_8) in temperature-accelerated tests and every 3 weeks (L_0 , L_3 , L_6 , L_9 , L_{12}) in light-accelerated tests were analyzed by the

developed UHPLC-Q-TOFMS. To visualize the chemical profile across groups, the principal component analysis (PCA), an unsupervised data analysis, was conducted. As shown in **Figure 4A**, all observations were located in the Hotelling T² (0.95) ellipse, PCA score plots derived from both positive ($R^2X = 0.727$, $Q^2 = 0.633$) and negative ($R^2X = 0.899$, $Q^2 = 0.729$) ion modes exhibited tight clusters of CHS-J samples from each time point in temperature-accelerated tests and discrimination across

groups. Importantly, the longer treatment by high temperature, the farther the cluster of CHS-J samples departs from untreated CHS-J group (T_0), indicating the more remarkable changes in the component profile of CHS-J samples along with an increasing treatment time. Similar results were observed in the light-accelerated tests (**Figure 4B**). To reveal the components contributing most to the group separation, the supervised OPLS-DA of temperature- (T_0 vs. T_8) and light-accelerated group (L_0 vs. L_{12}) were further constructed. The variables with $VIP > 2$ and $p < 0.05$ were highlighted as important components for the discrimination. As a result, 10 out of 48 and 9 out of 54 differential variables were identified by their reference standards in temperature- (**Supplementary Table S2**) and light- (**Supplementary Table S3**) accelerated groups, respectively. Among them, 8 compounds, including Z-ligustilide, echinacoside, magnoflorine, sagittatoside B, epimedin B, icariin, acteoside, and epimedin C, were common features between temperature- and light-accelerated tests (**Figure 5A**), indicating that these compounds might be sensitive to both temperature and light. While crustecdysone and chikusetsu saponin iva were thermosensitive components, 2''-O-rhamnosyl Icariside II was photosensitive (**Figure 5A**). Furthermore, a Venn diagram for CHS-J samples produced by different years and accelerated test datasets show 7 common features (**Figure 5B**), which indicated that the instability of these components might largely contribute to the differences in CHS-J samples with different storage periods.

Accelerated Tests of Reference Standards

To further investigate the possible mechanisms underlying these chemical changes, accelerated tests of several reference standards were conducted. The individual reference standards with severe degradation, including chlorogenic acid, echinacoside, baohuoside I, 2''-O-rhamnosyl icaric acid II, Z-ligustilide dissolved in 35% (v/v) of base liquor were subjected to temperature-accelerated or light-accelerated tests, respectively. The solution before and after accelerated tests were analyzed by a UPLC/Q-TOFMS. The degradation products derived from these reference standards exposed to temperature and light were tentatively assigned by matching their MS and MS/MS data with that of the literatures (Xie et al., 2011; Dawidowicz and Typek, 2010; Zanoelo and Benincá, 2009; Zuo et al., 2013; Yan et al., 2018) and summarized in **Supplementary Table S3**. Taking chlorogenic acid as an example, the total ion chromatogram (TIC) of chlorogenic acid alcohol base solution (T_0) and chlorogenic acid alcohol base solution after 16 weeks (T_{16}) in temperature-accelerated tests was shown in **Figure 6A**. Chlorogenic acid was degraded seriously when exposed to high temperatures, and several new products were generated. A newly generated degradation peak at $RT = 0.75$ min in chlorogenic acid solution after 16 weeks of high-temperature treatment was identified as quinic acid. The presence of quinic acid in alcohol base solution is not surprising because chlorogenic acid is an ester comprised of caffeic and quinic acids. However, caffeic acid was not found in this solution. Two new induced peaks at $RT = 1.48$ and 1.94 min were identified as 3-O-caffeoylquinic acid and 4-O-caffeoylquinic acid, respectively. The proposed degradation

mechanism was speculated and illustrated in **Figure 6B**. In the presence of hydroxide ion $[OH]^-$, the nucleophile on the neighboring hydroxyl group of the quinic acid ring attacked the carbonyl carbon of 5-O-caffeoylquinic acid, which resulted in the internal transesterification of trans-5-caffeoylquinic acid. The caffeoyl moiety transferred from the C5- position to the 4- and 3-positions via ortho-cyclic ester intermediate structures, which further hydrolyzed into esters (Zanoelo and Benincá, 2009; Dawidowicz and Typek, 2010; Xie et al., 2011). But it is difficult to distinguish the two compounds due to their similar MS and MS/MS pattern. Furthermore, chlorogenic acid was also degraded seriously when exposed to light, and its degradation products mainly are the hydroxylated chlorogenic acids (**Supplementary Figure S1**). Our data indicated that the degradation mechanism of most compounds was hydrolysis and isomerization, which is related to the ethyl alcohol-water environment of CHS-J, while high temperature and light accelerated these degradation processes with varying degrees.

Anti-Fatigue Effects of CHS-J Samples Produced in 2014 and 2020

Compared to the control group, the exhaustive swimming time, hepatic glycogen level, muscle glycogen level, blood lactic acid level, urea nitrogen level, and lactic dehydrogenase level in both CHS-J samples produced in 2014 and 2020 groups showed a significant difference ($p < 0.01$), except hepatic glycogen and lactic dehydrogenase in CHS-J samples produced in 2020 group ($p < 0.05$), indicating that storage period had little influence on the anti-fatigue effect of CHS-J samples (**Table 2**). Moreover, compared with CHS-J samples produced in the 2020 group, CHS-J samples produced in the 2014 group had a decreased blood lactic acid and a higher level of lactic dehydrogenase. However, for the exhaustive swimming time, hepatic glycogen level, muscle glycogen level, and urea nitrogen level, there were no significant differences in these four anti-fatigue indexes between CHS-J samples produced in the 2014 group and 2020 group. Collectively, the chemical changes during the storage period had little influence on the anti-fatigue effect of CHS-J samples.

CONCLUSION

In this study, the targeted and untargeted metabolomics were integrated to reveal the changed components in different production years of CHS-J. Moreover, accelerated tests were performed to validate the findings in the metabolomics study and explore the stability of compounds in CHS-J. The results demonstrated that some components in CHS-J were changed with the increasing years of storage, and most of them gradually decreased over the duration. The accelerated tests revealed that these changes might be attributed to the chemical degradation of components in CHS-J when exposed to high temperatures or light. Moreover, these changes during the storage period had little influence on the anti-fatigue effect of CHS-J. These findings will offer new insight into understanding the stability of components and anti-fatigue effect in CHS-J and will facilitate the quality control of CHS-J. Meanwhile, the current study indicates that metabolomics is an efficient approach to comprehensively characterize TCM quality in a complex matrix.

DATA AVAILABILITY STATEMENT

The original contributions presented in the study are included in the article/**Supplementary Material**, further inquiries can be directed to the corresponding authors.

ETHICS STATEMENT

The animal study was reviewed and approved by the Institutional Animal Care and Use Committee of Hubei University of Chinese Medicine.

AUTHOR CONTRIBUTIONS

J-BW and ZW conceived and designed the experiments; YH performed the experiment and prepared the manuscript; FX and X-JC analyzed the data; WY and Y-CL revised the manuscript;

J-BW and X-JC, finalized the manuscript. All authors read and approved the final manuscript.

FUNDING

The work was financially supported by grants from Enterprise Cooperation Project (CP/003/2018), and the Science and Technology Development Fund, Macau SAR (File no. 0034/2019/A1).

SUPPLEMENTARY MATERIAL

The Supplementary Material for this article can be found online at: <https://www.frontiersin.org/articles/10.3389/fphar.2022.857706/full#supplementary-material>

REFERENCES

- Chan, E. C., Yap, S. L., Lau, A. J., Leow, P. C., Toh, D. F., and Koh, H. L. (2007). Ultra-performance Liquid Chromatography/time-Of-Flight Mass Spectrometry Based Metabolomics of Raw and Steamed Panax Notoginseng. *Rapid Commun. Mass. Spectrom.* 21, 519–528. doi:10.1002/rcm.2864
- Dawidowicz, A. L., and Typek, R. (2010). Thermal Stability of 5-O-Caffeoylquinic Acid in Aqueous Solutions at Different Heating Conditions. *J. Agric. Food Chem.* 58, 12578–12584. doi:10.1021/jf103373t
- Feng, S., Shan, Y., Lu, S., Liu, Y., and He, G. (2013). The Anti-inflammatory Effect of Moderate Drinking. *Liquor-mak. Sci. Tech.*, 121–124. doi:10.13746/j.njkj.2013.07.005
- Hu, Y., Wang, Z., Xia, F., Yang, W., Liu, Y.-C., and Wan, J.-B. (2021). Simultaneous Quantification of Bioactive Components in Chinese Herbal Spirits by Ultra-high Performance Liquid Chromatography Coupled to Triple-Quadrupole Mass Spectrometry (UHPLC-QQQ-MS/MS). *Chin. Med.* 16, 26. doi:10.1186/s13020-021-00435-0
- Kim, N., Kim, K., Lee, D., Shin, Y. S., Bang, K. H., Cha, S. W., et al. (2012). Nontargeted Metabolomics Approach for Age Differentiation and Structure Interpretation of Age-dependent Key Constituents in Hairy Roots of Panax Ginseng. *J. Nat. Prod.* 75, 1777–1784. doi:10.1021/np300499p
- Lee, E. J., Shaykhtudinov, R., Weljie, A. M., Vogel, H. J., Facchini, P. J., Park, S. U., et al. (2009). Quality Assessment of Ginseng by (1)H NMR Metabolite Fingerprinting and Profiling Analysis. *J. Agric. Food Chem.* 57, 7513–7522. doi:10.1021/jf901675y
- Liu, S. H., Li, H. J., Sun, X. Z., Wang, L., Liu, Y. C., Wan, C. P., et al. (2018). Analysis of Volatile Flavoring Compounds in Jinjiu Liquor by GC-MS. *Liquor-mak. Sci. Tech.*, 80–86. doi:10.13746/j.njkj.2017329
- Ministry of Health of the People's Republic of China (2003). Edition. *China National Health Inspection*. Beijing: Technical standards for testing & assessment of health food.
- Sun, J., and Chen, P. (2011). Differentiation of Panax Quinquifolius Grown in the USA and China Using LC/MS-based Chromatographic Fingerprinting and Chemometric Approaches. *Anal. Bioanal. Chem.* 399, 1877–1889. doi:10.1007/s00216-010-4586-7
- Toh, D. F., New, L. S., Koh, H. L., and Chan, E. C. (2010). Ultra-high Performance Liquid Chromatography/time-Of-Flight Mass Spectrometry (UHPLC/TOFMS) for Time-dependent Profiling of Raw and Steamed Panax Notoginseng. *J. Pharm. Biomed. Anal.* 52, 43–50. doi:10.1016/j.jpba.2009.12.005
- Wan, J. B., Bai, X., Cai, X. J., Rao, Y., Wang, Y. S., and Wang, Y. T. (2013). Chemical Differentiation of Da-Cheng-Qi-Tang, a Chinese Medicine Formula, Prepared by Traditional and Modern Decoction Methods Using UPLC/Q-TOFMS-based Metabolomics Approach. *J. Pharm. Biomed. Anal.* 83, 34–42. doi:10.1016/j.jpba.2013.04.019
- Wang, X., Sun, H., Zhang, A., Sun, W., Wang, P., and Wang, Z. (2011). Potential Role of Metabolomics Approaches in the Area of Traditional Chinese Medicine: as Pillars of the Bridge between Chinese and Western Medicine. *J. Pharm. Biomed. Anal.* 55, 859–868. doi:10.1016/j.jpba.2011.01.042
- Wang, X., Sun, H., Zhang, A., Wang, P., and Han, Y. (2011). Ultra-performance Liquid Chromatography Coupled to Mass Spectrometry as a Sensitive and Powerful Technology for Metabolomic Studies. *J. Sep. Sci.* 34, 3451–3459. doi:10.1002/jssc.201100333
- Xia, F., Liu, C., and Wan, J. B. (2020). Characterization of the Cold and Hot Natures of Raw and Processed Rehmanniae Radix by Integrated Metabolomics and Network Pharmacology. *Phytomedicine* 74, 153071. doi:10.1016/j.phymed.2019.153071
- Xiang, Z., Wang, X. Q., Cai, X. J., and Zeng, S. (2011). Metabolomics Study on Quality Control and Discrimination of Three Curcuma Species Based on Gas Chromatograph-Mass Spectrometry. *Phytochem. Anal.* 22, 411–418. doi:10.1002/pca.1296
- Xie, C., Yu, K., Zhong, D., Yuan, T., Ye, F., Jarrell, J. A., et al. (2011). Investigation of Isomeric Transformations of Chlorogenic Acid in Buffers and Biological Matrixes by Ultra-performance Liquid Chromatography Coupled with Hybrid Quadrupole/ion Mobility/orthogonal Acceleration Time-Of-Flight Mass Spectrometry. *J. Agric. Food Chem.* 59, 11078–11087. doi:10.1021/jf203104k
- Yan, Y., Liu, T. X., Bi, D., Liu, W. J., Song, Q. Q., Li, J., et al. (2018). Transformation Pathways in Methanol of Echinacoside, a Principal Effective Ingredient of Cistanches Herba. *Zhongguo Zhong Yao Za Zhi* 43, 2321–2325. doi:10.19540/j.cnki.cjcmm.20180309.001
- Yang, S. O., Shin, Y. S., Hyun, S. H., Cho, S., Bang, K. H., Lee, D., et al. (2012). NMR-based Metabolic Profiling and Differentiation of Ginseng Roots According to Cultivation Ages. *J. Pharm. Biomed. Anal.* 58, 19–26. doi:10.1016/j.jpba.2011.09.016
- Zanoelo, E. F., and Benincá, C. (2009). Chemical Kinetics of 5-O-Caffeoylquinic Acid in Superheated Steam: Effect of Isomerization on Mate (*Ilex Paraguariensis*) Manufacturing. *J. Agric. Food Chem.* 57, 11564–11569. doi:10.1021/jf903388a
- Zuo, A. H., Cheng, M. C., Zhuo, R. J., Wang, L., and Xiao, H. B. (2013). Structure Elucidation of Degradation Products of Z-Ligustilide by UPLC-QTOF-MS and NMR Spectroscopy. *Yao Xue Xue Bao* 48, 911–916. doi:10.16438/j.0513-4870.2013.06.008

Conflict of Interest: ZW, JL, WY, QY, and Y-CL was employed by the company Jing Brand Co.Ltd.

The remaining authors declare that the research was conducted in the absence of any commercial or financial relationships that could be construed as a potential conflict of interest.

Publisher's Note: All claims expressed in this article are solely those of the authors and do not necessarily represent those of their affiliated organizations, or those of the publisher, the editors and the reviewers. Any product that may be evaluated in

this article, or claim that may be made by its manufacturer, is not guaranteed or endorsed by the publisher.

Copyright © 2022 Hu, Wang, Liu, Yang, Yang, Liu, You, Chen and Wan. This is an open-access article distributed under the terms of the Creative Commons Attribution License (CC BY). The use, distribution or reproduction in other forums is permitted, provided the original author(s) and the copyright owner(s) are credited and that the original publication in this journal is cited, in accordance with accepted academic practice. No use, distribution or reproduction is permitted which does not comply with these terms.



Protective Mechanism of Gandou Decoction in a Copper-Laden Hepatolenticular Degeneration Model: *In Vitro* Pharmacology and Cell Metabolomics

OPEN ACCESS

Edited by:

Xijun Wang,
Heilongjiang University of Chinese
Medicine, China

Reviewed by:

Tingting Zhou,
Second Military Medical University,
China
Aihua Zhang,
Heilongjiang University of Chinese
Medicine, China

*Correspondence:

Hongfei Wu
wuhongfei@ahcm.edu.cn
An Zhou
anzhou@ahcm.edu.cn

[†]These authors have contributed
equally to this work and share first
authorship

Specialty section:

This article was submitted to
Ethnopharmacology,
a section of the journal
Frontiers in Pharmacology

Received: 05 January 2022

Accepted: 17 February 2022

Published: 23 March 2022

Citation:

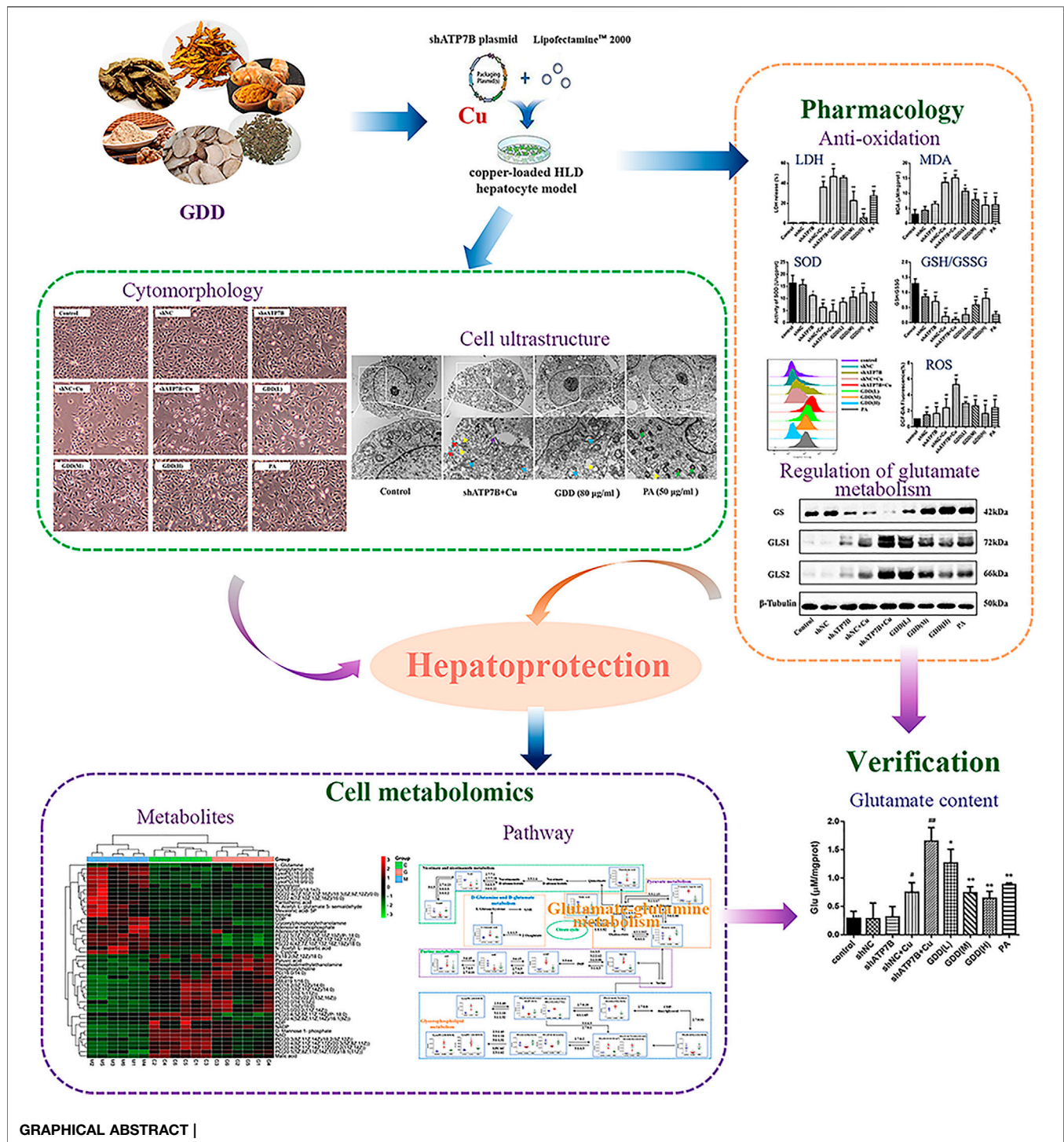
Yin F, Nian M, Wang N, Wu H, Wu H,
Zhao W, Cao S, Wu P and Zhou A
(2022) Protective Mechanism of
Gandou Decoction in a Copper-Laden
Hepatolenticular Degeneration Model:
In Vitro Pharmacology and
Cell Metabolomics.
Front. Pharmacol. 13:848897.
doi: 10.3389/fphar.2022.848897

Fengxia Yin^{1†}, Mengnan Nian^{1†}, Na Wang¹, Hongfei Wu^{2,3*}, Huan Wu^{2,3}, Wenchen Zhao⁴,
Shijian Cao⁵, Peng Wu³ and An Zhou^{1,3*}

¹The Experimental Research Center, Anhui University of Chinese Medicine, Hefei, China, ²School of Pharmacy, Anhui University of Chinese Medicine, Hefei, China, ³Anhui Province Key Laboratory of Research and Development of Chinese Medicine, Anhui Province Key Laboratory of Chinese Medicinal Formula, Hefei, China, ⁴Department of Pharmaceutical Sciences, School of Pharmacy, University of Pittsburgh, Pittsburgh, PA, United States, ⁵The First Affiliated Hospital of Anhui University of Chinese Medicine, Hefei, China

Gandou decoction (GDD) is a classic prescription for the treatment of hepatolenticular degeneration (HLD) in China; however, the liver-protecting mechanism of this prescription needs further evaluation. In the present study, we explored the protective mechanisms of GDD in a copper-laden HLD model using integrated pharmacology and cellular metabolomics *in vitro*. The results revealed that GDD could significantly promote copper excretion in copper-laden HLD model cells and improve the ultrastructural changes in hepatocytes. In addition, GDD could decrease the extent of lipid peroxidation, levels of reactive oxygen species, and the release rate of lactate dehydrogenase while increasing the activity of superoxide dismutase and the ratio of glutathione to oxidized glutathione in the copper-laden HLD model cells. On conducting statistical analysis of significant metabolic changes, 47 biomarkers and 30 related metabolic pathways were screened as pharmacological reactions induced by GDD in HLD model cells. D-glutamate and D-glutamine metabolic pathways showed the highest importance and significance among the 30 metabolic pathways, and the differential expression levels of the glutamine synthetase (GS) and the renal type and liver type GLS (GLS1 and GLS2) proteins were verified by Western blotting. Collectively, our data established the underlying mechanism of GDD therapy, such as the promotion of copper excretion and improvement in oxidative stress by regulating the expressions of GS, GLS1, and GLS2 protein to protect hepatocytes from injury.

Keywords: gandou decoction, copper-laden HLD hepatocyte model, hepatolenticular degeneration, cell metabolomics, pharmacology



1 INTRODUCTION

Hepatolenticular degeneration (HLD), also known as Wilson's disease (WD), is a genetic copper overload disease caused by inactivating mutations in the copper transporter P-type ATPase gene (ATP7B) (Ala et al., 2007). Disease-causing mutations of ATP7B lead to impaired intracellular copper

trafficking and consequent high copper accumulation in tissues, especially in the liver (Tanzi et al., 1993; Terada et al., 1998). Owing to the deposition of copper in the liver, the most typical disorders of HLD patients include hepatic diseases such as asymptomatic hepatomegaly, hepatic damage, liver fibrosis, cirrhosis, progressive systemic sclerosis, and liver failure (Bandmann et al., 2015). Like few other genetic and

metabolic disorders, HLD can effectively be maintained with pharmacological agents. The most useful and direct clinical treatment for HLD is copper chelation therapy using copper-chelating agents, e.g., D-penicillamine, trientine, tetrathiomolybdate, and dimercaptosuccinic acid, which can promote the elimination of copper. Unfortunately, copper-chelating agents usually have multiple toxic adverse effects, including immunologically induced lesions, renal toxicity, and poor compliance, which consequently result in failure of treatment (Hedera, 2017; Liu et al., 2017). Therefore, more effective and less toxic medications are desperately needed for the treatment of HLD.

Gandou decoction (GDD) is a classic compound prescription in traditional Chinese medicine (TCM) and is composed of six Chinese medicinal herbs: *Rheum palmatum* L. (Chinese name: Dahuang), *Coptis chinensis* Franch. (Chinese name: Huanglian), *Curcuma longa* L. (Chinese name: Jianghuang), *Lysimachia christinae* Hance (Chinese name: Jinqiancao), *Alisma orientale* (Sam.) Juzep. (Chinese name: Zexie), and *Panax notoginseng* (Burk.) F. H. Chen (Chinese name: Sanqi) in fixed proportions. In China, GDD has widely been used as an effective clinical therapeutic agent against HLD for decades. Previous clinical studies have demonstrated that GDD can not only significantly promote the excretion of copper and markedly improve the clinical manifestations of HLD patients but also exhibit significant liver protection (Xue et al., 2007; Wang et al., 2012; Xu et al., 2012). Given the great clinical therapeutic effects and high safety of GDD, it has been recommended for the clinical treatment of HLD patients as a basic prescription. In our previous study, we have revealed the chemical profile and the metabolites of GDD *in vitro* and *in vivo* based on ultra-performance liquid chromatography/quadrupole time-of-flight mass spectrometry (UPLC-Q-TOF-MS^E). In total, 96 chemical constituents, including protostane triterpenoids, flavonoids, triterpenoid saponins, tannins, curcuminoids, and anthraquinones, have been identified in GDD (Xu et al., 2019). Based on these results, we further identified prototypes and metabolites of GDD in the serum, liver, and urine after oral administration to normal and copper-laden rats (an animal model of HLD) (Xu et al., 2020; Zhang et al., 2020). Meanwhile, we found that GDD could reduce copper accumulation (Cheng et al., 2018), regulate metabolic profile (Xu et al., 2021), and alleviate hepatic injury by inhibiting oxidative stress in HLD model rats (Wang et al., 2020). Taken together, GDD could effectively treat HLD with several benefits. However, the biological mechanism and significance for these effects were still not clear and needed further study.

Metabolomics focuses on subtle changes in metabolites (relative molecular mass less than 1,000) in complex biological systems (such as cells, tissues, or organisms) and is applied to investigate disease pathogenesis, evaluate the therapeutic effects, and discover potential biological mechanisms (Yang et al., 2019). Cell metabolomics, an important embranchment of metabolomics, is capable of directly revealing the pathological changes and pathogenesis of the disease at a metabolic level. Compared with the tissues or organisms, cell metabolomics has obvious advantages such as lower costs, better stability and

reproducibility, fewer ethical issues, among others (Chrysanthopoulos et al., 2010; Cuperlović-Culf et al., 2010). In the past few years, cell metabolomics has been used for revealing the therapeutic mechanisms underlying the use of herbs alone or TCM formulae in diseases (Sun et al., 2018; Zhang et al., 2019; Ma et al., 2020). The major analytical techniques in metabolomics are nuclear magnetic resonance (NMR) spectroscopy, gas chromatography-mass spectrometry (GC-MS), capillary electrophoresis-mass spectrometry (CE-MS), and liquid chromatography-mass spectrometry (LC-MS). UPLC-Q-TOF/MS quickly became the preferred tool in cell metabolomics studies for its high resolution, high sensitivity, good reproducibility, and less sample requirement (Wu et al., 2020). The conventional reverse-phase (RP) column commonly used in UPLC-Q-TOF/MS mainly focuses on the middle and nonpolar metabolites. In contrast, the hydrophilic interaction liquid chromatography (HILIC) column is ideal for the analysis of polar metabolites. Therefore, a combination of RPLC and HILIC may be able to ensure maximum coverage in metabolomics (González-Ruiz et al., 2017).

Pieces of evidence from clinical and animal studies show that GDD has good therapeutic action against HLD. In this report, the rat liver-derived cell line BRL-3A was used to clarify the protective effect and metabolism mechanism of GDD. First, the ATP7B short-hairpin RNA (shRNA) plasmid transient transfection technique was used to damage BRL-3A cells, establishing an HLD hepatocyte injury model. The cytoprotective effect of GDD was then evaluated by detecting the changes in intracellular copper levels. Second, oxidative stress-related indicators, including superoxide dismutase (SOD), lipid peroxidation (MDA), glutathione (GSH) to oxidized glutathione (GSSH) level, and reactive oxygen species (ROS) level, were determined. Moreover, the ultrastructure of hepatocytes was observed under a transmission electron microscope (TEM). Third, the cellular untargeted metabolomics method based on UPLC-Q-TOF/MS was used to identify the biomarkers for exploring the potential mechanism of GDD in HLD at a cellular level. Finally, on this basis, enzymes in the critical metabolic pathways were verified by Western blotting.

2 MATERIALS AND METHODS

2.1. Reagents and Chemicals

RPMT1640 was purchased from Corning (Manassas, United States). Fetal bovine serum (FBS) was purchased from Hyclone (Logan, United States). Trypsin digestion solution was purchased from Beyotime Biotechnology (Shanghai, China). Penicillin-streptomycin solution was obtained from Service Biotechnology (Wuhan, China). Furthermore, 3-(4,5-dimethylthiazol-2-yl)-2,5-diphenyl-tetrazolium bromide (MTT) was purchased from BioFroxx (Einhausen, Germany). shRNA plasmid vector kit was purchased from GenePharma Co. Ltd. (Shanghai, China). Lipofiter (batch number: 20201202) was purchased from Shanghai Hanheng Biotechnology Co., Ltd.

Phosphate buffer saline (PBS) was purchased from Suobao Biotechnology Co., Ltd. (Shanghai, China). Lipid oxidation (MDA) detection kit, total superoxide dismutase (T-SOD) activity test kit, reactive oxygen species (ROS) detection kit, glutathione (GSH) and oxidized glutathione (GSSH) detection kit, Bradford protein concentration determination kit, and lactate dehydrogenase (LDH) cytotoxicity test kit were all purchased from Beyotime Biotechnology Co., Ltd. (Shanghai, China). Glutamate (Glu) content detection kits were obtained from Solarbio Science and Technology Co., Ltd. (Beijing, China). A rabbit monoclonal antibody, GLS1, was purchased from Abcam (Cambridge, United Kingdom). Mouse anti- β -tubulin monoclonal antibody, HRP-labeled goat anti-mouse IgG, and HRP-labeled goat anti-rabbit IgG were all purchased from Zhongshan Jinqiao Biological Technology Co., Ltd. (Beijing, China). ECL hypersensitive photoluminescence solution was purchased from Affinity Biologicals (Cincinnati, United States). The six herbs of *R. palmatum* L. (Batch number: 20180106), *C. chinensis* Franch. (Batch number: 20180101), *C. longa* L. (Batch number: 20180120), *L. christinae* Hance (Batch number: 20180113), *A. orientale* (Sam.) Juzep. (Batch number: 20180107), and *P. notoginseng* (Burk.) F. H. Chen (Batch number: 20180109) were purchased from Beijing Tongrentang Pharmacy Co., Ltd. (Hefei, China) and identified by Professor Rongchun Han, an expert from Traditional Chinese Pharmacology of the Anhui University of Chinese Medicine. All herbs had been deposited at the Herbarium of the Anhui University of Chinese Medicine, Hefei, China (Herbarium code: ACM, voucher numbers: 18,056, 18,031, 18,059, 18,070, 18,052, and 18,067). The details of drug materials are provided in **Supplementary Table S1**.

2.2 Preparation of Gandou Decoction

According to the prescription, a mixture of *R. palmatum* L. (10 g), *C. chinensis* Franch. (10 g), *C. longa* L. (10 g), *L. christinae* Hance (12 g), *A. orientale* (Sam.) Juzep. (12 g), and *P. notoginseng* (Burk.) F. H. Chen (1.5 g) was crushed using a high-speed pulverizer. After mixing, eightfold in water was added to extract and reflux for an hour each; this was repeated two times. The filtrate was strained and combined, then evaporated to a certain volume, and vacuum freeze-dried into a powder (15.3% yield). The quality of GDD was evaluated by measuring the contents of curcumin (16.45 mg/g), chrysophanol (6.69 mg/g), rhein (7.15 mg/g), physcion (4.41 mg/g), emodin (3.63 mg/g), aloe-emodin (3.16 mg/g), quercetin (3.44 mg/g), and kaempferide (1.99 mg/g) via high-performance liquid chromatography method, according to our previous research (Wang et al., 2020).

2.3 Cell Culture

The BRL-3A cells (ATCC: CRL-1442) were acquired from the Shanghai cell bank of the Chinese Academy of Sciences. The cells were cultured in RPMI-1640 medium with 10% FBS and 1% penicillin-streptomycin at 37°C in a 5% CO₂ atmosphere. Passaging was conducted every 2–3 days, and the cells in the logarithmic growth phase were selected for the following experiments.

2.4 Establishment of Copper-Laden Hepatolenticular Degeneration Hepatocyte Injury Model Induced by CuSO₄

In this study, screening was performed by 4',6-diamidino-2-phenylindole (DAPI) staining method, real-time polymerase chain reaction (qPCR), and Western blotting (**Supplementary Information S1.1**). The method of RNA interference was used to establish the HLD hepatocyte model. The plasmid transfection group of shATP7B-4 with the strongest gene interference effect was chosen for the study of the copper-laden HLD hepatocyte injury model (**Supplementary Information 2.1**).

Subsequently, the copper-laden HLD hepatocyte injury model was established by CuSO₄ induction, which simulates the copper-overload phenomenon of HLD patients. Approximately 5×10^3 /100 μ l BRL-3A cells were seeded in a 96-well plate. After being transfected with shATP7B plasmid for 48 h, CuSO₄ (0, 100, 200, 300, 400, 500, and 600 μ M) was added with 5% FBS, and the cells were incubated for 12, 24, 36, and 48 h. At the same time, the control group and the shNC group were used as the controls, and six repeating holes were set up in each concentration. The cells in each group were incubated with 10- μ l MTT solution (5 mg/ml) for 4 h at 37°C. The supernatant was discarded, and 150- μ l DMSO was added to dissolve formazan. The optical density (OD) values were measured at 490 nm, and the cell viability (CV) (%) was calculated from the mean OD values of the six wells according to the following formula: $CV (\%) = (OD_{\text{Test}} - OD_{\text{Blank control}}) / (OD_{\text{Control}} - OD_{\text{Blank control}}) \times 100\%$.

2.5 Evaluation of the Protective Effect of Gandou Decoction on Copper-Laden Hepatolenticular Degeneration Hepatocyte

Approximately 5×10^3 HLD hepatocytes/100- μ l solution were seeded in a 96-well plate, and various concentrations on GDD (10, 20, 40, 80, 160, and 320 μ g/ml) were added. The follow-up operation was the same as that mentioned in **Section 2.4**. Subsequently, the CV (%) was calculated, viability above 90% indicated a safe concentration.

After administering the low, medium, and high doses of GDD (20, 40, and 80 μ g/ml) and a dose of penicillamine (PA) (50 μ g/ml), the experiment was divided into nine groups: control group, shNC group, shATP7B group, shNC + Cu group, shATP7B + Cu group, low, medium, and high GDD group, and PA group. The CV (%) was then calculated, as mentioned before.

2.6 Study on the Effect of Copper Excretion on Gandou Decoction in Copper-Laden Hepatolenticular Degeneration Hepatocytes

2.6.1 Observation of Cu²⁺ Fluorescence Intensity in Cells

Under a fluorescence microscope (Olympus CKX41, Olympus Corp., Japan), the fluorescence intensity of intracellular copper (Duan et al., 2019), which indicated the intracellular copper level, was observed using the PP-Cu fluorescence probe. The

cells were divided into nine groups following the same steps mentioned in **Section 2.5**. The culture medium was absorbed, and then, PP-Cu fluorescent probe (0.5 μM) was added to each well. After incubation for 1 h, the supernatant was discarded. This was followed by washing two times with PBS, and the fluorescence intensity of intracellular Cu^{2+} was observed under a fluorescence microscope using the green light excitation channel. Three visual fields were randomly selected for each group.

2.6.2 Measurement of Cu^{2+} Content in Copper-Laden Hepatolenticular Degeneration Hepatocytes

Cells were collected and washed with PBS twice. Then, the cells were resuspended in PBS, crushed by ultrasonic waves in an ice bath, and centrifuged (4°C, 12,000 rpm) for 20 min. The supernatant (cytoplasm) of the cells was then obtained. The intracellular Cu^{2+} content was measured by Bradford protein quantification and atomic absorption spectrometry (AAS) (Thermo Corp., United States) (Liu et al., 2016). The ratio between copper and protein (nanogram per milligram) in each group was calculated as actual intracellular Cu^{2+} , and the experiment was repeated three times.

2.7 Protective Effect of Gandou Decoction on Copper-Laden Hepatolenticular Degeneration Hepatocytes

2.7.1 Morphological Observation

An inverted microscope was used to observe the morphological changes in nine groups of cells. After transfection for 48 h, different concentrations (20, 40, and 80 $\mu\text{g}/\text{ml}$) of GDD and PA were administered to cells in the corresponding groups and maintained for 6 h; the solution was then incubated in CuSO_4 (300 μM) for 24 h. The cell morphology in each group was observed under an inverted microscope and photographed.

2.7.2 Observation of Cell Ultrastructure

The cells were digested with 0.25% trypsin and centrifuged (4°C, 1,000 rpm) for 3 min to make a single-cell suspension. The suspension was stained with uranyl acetate and led citrate after fixation, dehydration, embedding, solidification, and sectioning, and then observed and photographed under a TEM.

2.7.3 Measurement of Lipid Peroxidation, Total Superoxide Dismutase, Reactive Oxygen Species, Glutathione and Oxidized Glutathione, and Lactate Dehydrogenase

Ultrasonic pulverization was performed, followed by centrifugation for 10 min. Subsequently, the cell supernatant was collected in each group, and the levels of MAD and GSH/GSSH, as well as the activities of SOD, and the release of LDH were determined according to the instructions of the respective kits. In addition, the ROS content of the cells was determined using a fluorescence probe. Cells in each group were incubated with the dichlorodihydrofluorescein (DCFH-DA) probe (10 μM)

for 20 min at 37°C, blending every 3–5 min. The cells were washed with serum-free medium three times, and the fluorescence intensity was detected by flow cytometry (excitation wavelength: 488 nm; emission wavelength: 525 nm).

2.8 Metabolite Extraction

The cells in the shNC group, shATP7B + Cu group, and (high-dose) GDD group were selected for the metabolomic study. Liquid-liquid extraction (Ivanisevic et al., 2013; Cuykx et al., 2017) was performed to extract metabolites from cells in each group. The extractant of methanol-ethyl acetate-water (2:2:1) was used to extract intracellular metabolites in each group. The cell Petri dish in each group was taken out and rinsed once with PBS (3 ml). Following this, methanol/water (2:1; 800 μl) was added, and the solution was frozen and thawed quickly three times (10 min at 25°C for 1 min under liquid nitrogen). The cells were then crushed using an ultrasonic cell disrupter (instrument parameters: working 5 s, interval 5 s, power 30%, working times: 4). Subsequently, 400- μl ethyl acetate was added, and the mixture was whirled for 30 s (repeated six times) after incubating in a cold-water bath for 5 min. It was then centrifuged at 13,000 g for 30 min at 4°C; the supernatant was extracted into a 1.5-ml EP tube and incubated at -80°C for 6–8 h. After delamination, two parts of the liquid were transferred into a new 1.5-ml EP tube (after layered, the top layer was used for RPLC-Q-TOF/MS analysis, and the bottom layer was used for HILIC-Q-TOF/MS analysis). The liquid was then blown dry with nitrogen and redissolved with 200 μl of the mobile phase. This was followed by centrifugation at 13,000 \times g/min under 4°C; the supernatant (100 μl) was placed in an injection vial. Meanwhile, quality control (QC) samples were prepared by mixing aliquots of 20 μl of shNC, shATP7B + Cu, and (high-dose) GDD group samples as described earlier.

2.9 Cellular Metabolomics Experiments

The cellular metabolomics study was conducted using the UPLC system (ACQUITY, WATERS, Milford, United States) coupled with a Xevo G2-XS Q-TOF/MS detector (ACQUITY, WATERS, United States). All samples were evaluated on an ACQUITY UPLC@HILIC column (2.1 mm \times 100 mm, 1.7 μm) or an ACQUITY UPLC@BEH C_{18} column (2.1 mm \times 100 mm, 1.7 μm). These two columns have used the separations under the following condition: column temperature, 38°C; sample room temperature, 4°C; flow rate, 0.2 ml/min, and injection volume, 1 μl . The mobile phase of the C_{18} column separation system consists of 0.1% formic acid aqueous solution (A) and 0.1% formic acid-acetonitrile (B), and the elution gradient of it was as follows: 5–12% A for 0–2.5 min, 12% A for 2.5–5 min, 12–32% A for 5–10 min, 32–29% for 10–11 min, 29–5% for 11–12 min, and 5% A for 12–15 min. For HILIC column separation, the mobile phase A was water and B was acetonitrile/isopropanol (5:2); both solvents contained 5-mM ammonium acetate and 0.1% formic acid. The elution gradient was set as follows: 0–2 min, 35–82% B; 2–9 min, 82–90% B; 9–14 min, 90–90% B; 14–15 min, 90–35% B; and 15–17 min, 35% B. QC samples were randomly distributed in the measured sample sequence.

In the Q-TOF/MS analysis part, optimal conditions for mass spectrometry were as follows: electrospray ionization (ESI) was

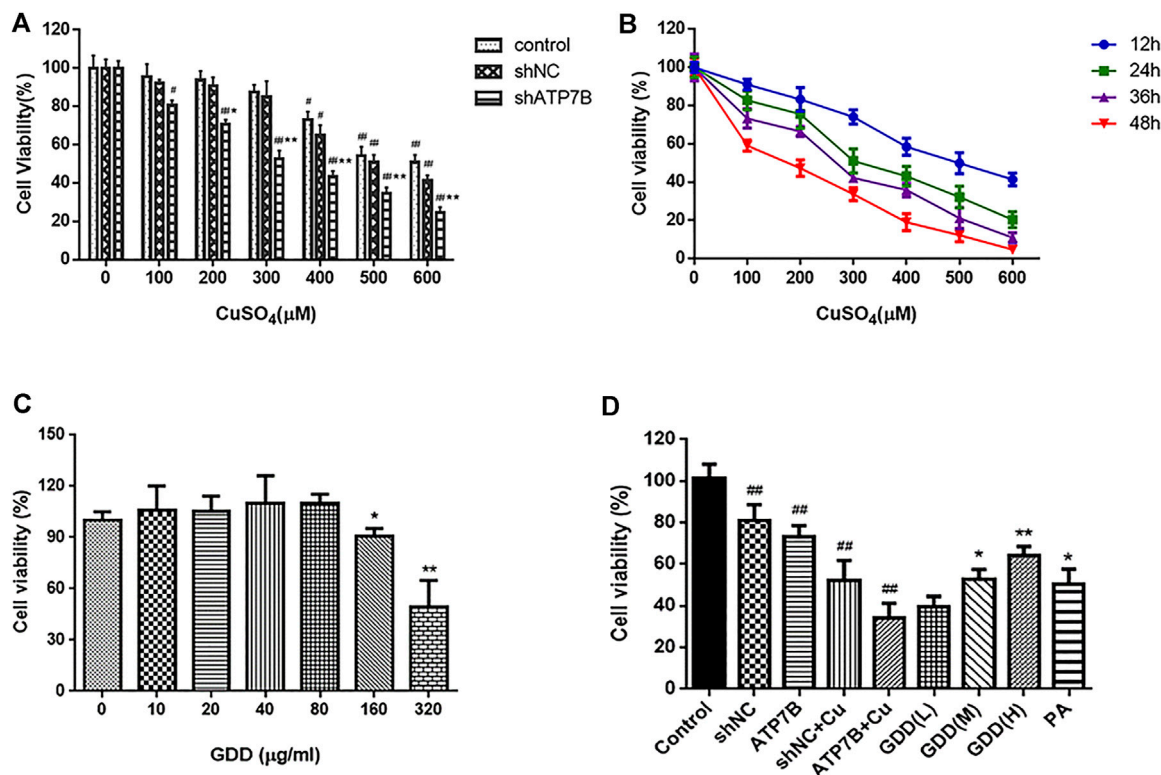


FIGURE 1 | (A) Cell viability in control, shNC, and shATP7B transfected after 24-h incubation with different concentrations CuSO_4 ($\bar{x} \pm s, n = 6$). $^{\#}p < 0.05$, $^{##}p < 0.01$ compared with corresponding blank group without CuSO_4 treatment; $^*p < 0.05$, $^{**}p < 0.01$ compared between shNC and shATP7B groups at same copper concentration; **(B)** dose and time-effect curves of shATP7B transfected cell viability after incubation with CuSO_4 ($\bar{x} \pm s, n = 6$); **(C)** cell viability after 24 h treated by GDD ranging from 0 to 320 $\mu\text{g/ml}$ (0, 10, 20, 40, 80, 160, and 320 $\mu\text{g/ml}$) ($\bar{x} \pm s, n = 6$). $^*p < 0.05$, $^{**}p < 0.01$ compared with control group; **(D)** cell viability in copper-laden HLD hepatocytes before and after GDD treatment ($\bar{x} \pm s, n = 6$). $^*p < 0.05$, $^{**}p < 0.01$ compared with shATP7B + Cu group.

used to produce ions; the temperatures of ion source were 120°C (+)/110°C (−), and the gas temperature was 350°C; the capillary voltage was 2.5kV/−2.0 kV; the gas flow rate was 600 L/h; the low collision energy was 6 V, and the high collision energy was 20–40 V; the mass range was 50–1200 Da. In the process of data acquisition, 200 ng/ml leucine enkephalin was used for real-time correction in the positive model (m/z 556.2771) and negative model (m/z 554.2615).

In addition, the QC sample was used for methodological investigations; it was injected six times continuously according to the experimental conditions mentioned earlier to investigate the precision of the instrument. Meanwhile, the QC sample was inserted into the injection sequence; that is, one QC sample was inserted between every four samples to investigate the stability of the sample (within 24 h after sample treatment). One ion peak was randomly selected in each column and each ion mode (Xu et al., 2021), and the relative standard deviation (RSD) of the ion peak area and retention time were calculated.

2.10 Data Processing and Multivariate Statistical Analyses

All experiments were repeated three times, and results are expressed as mean \pm standard deviation. One-way analysis

of variance (ANOVA) was performed by statistical inference using SPSS17.0 statistical software. For homogeneity of variance, the least significant difference (LSD) test was performed for multiple comparisons between groups, whereas the uneven variance was evaluated using Dunnett's T3 test. A difference of $p < 0.05$ or $p < 0.01$ was considered statistically significant.

For metabolomics analysis, cell markers were studied using the Pregenic QI V 2.0 software and EZinfo 3.0 software, and the original data of UPLC-Q-TOF/MS were imported into the QI software for data processing (including baseline filtering, peak recognition, correction of retention time, and normalization). The filtered datasets were imported into EZinfo 3.0 software for multivariate statistical analysis. This software included unsupervised principal component analysis (PCA), which compared the differences among the shNC group, shATP7B + Cu group, and GDD group; it also observed the stability of the whole analysis process and supervised orthogonal partial least square discriminant analysis (OPLS-DA), which was used to screen metabolites with large metabolic differences among groups. The OPLS-DA model was verified by ANOVA of cross-validated residuals (CV-ANOVA). Differential variables are screened according to variable weight value (VIP) > 1.0 .

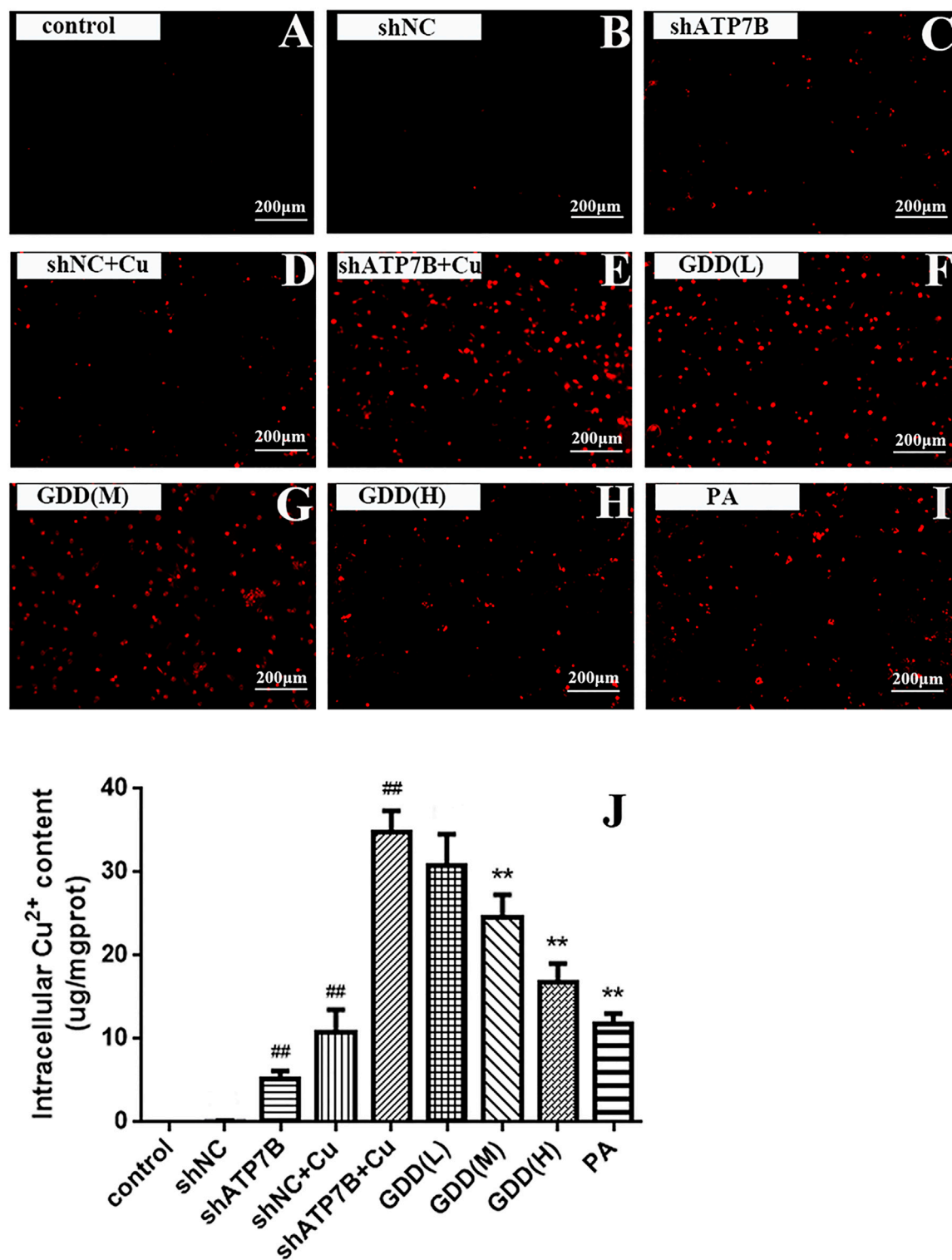


FIGURE 2 | (A–I) Cu^{2+} fluorescence intensity of copper-laden HLD hepatocytes treated with GDD by fluorescence microscope (magnification = $\times 100$); **(J)** effect of GDD on content of Cu^{2+} in copper-laden HLD hepatocytes ($\bar{x} \pm s, n = 6$). # $p < 0.05$, ## $p < 0.01$ compared with control group; * $p < 0.05$, ** $p < 0.01$ compared with shATP7B + Cu group.

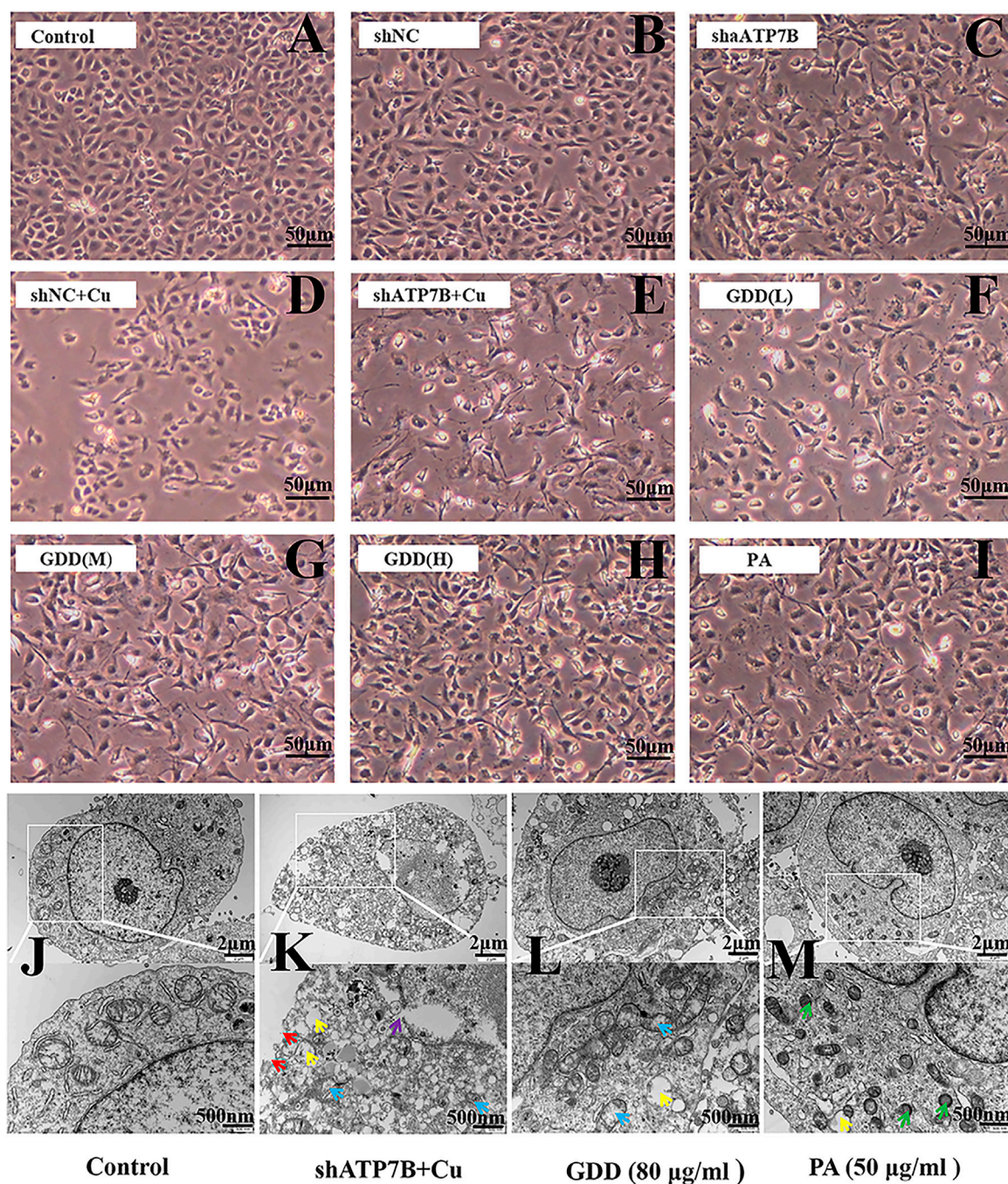


FIGURE 3 | (A–I) Morphological changes of copper-laden HLD hepatocytes treated with GDD by inverted microscope ($\times 200$); **(J–M)** ultrastructure of copper-laden HLD hepatocytes observed by transmission electron microscope ($\times 10,000$ or $\times 25,000$) (red arrow: cell membrane rupture; yellow arrow: mitochondrial vacuolation; purple arrow: nuclear membrane rupture; blue arrow: mitochondrial cristal rupture; green arrow: mitochondrial shrinkage).

2.11 Construction and Analysis of Metabolites and Metabolic Pathway

Accurate m/z obtained by multivariate statistical analysis was matched with the metabolites in the online database: Human Metabolomics database (HMDB) (which satisfies ± 10 PPM).

After evaluating the retention time and excimer ion information under low collision energy of mass spectrometry data, the ion fragments with high collision energy were compared with the HMDB (<http://www.hmdb.ca/>), which helped obtain potential metabolite biomarkers. Subsequently, normalized peak areas of

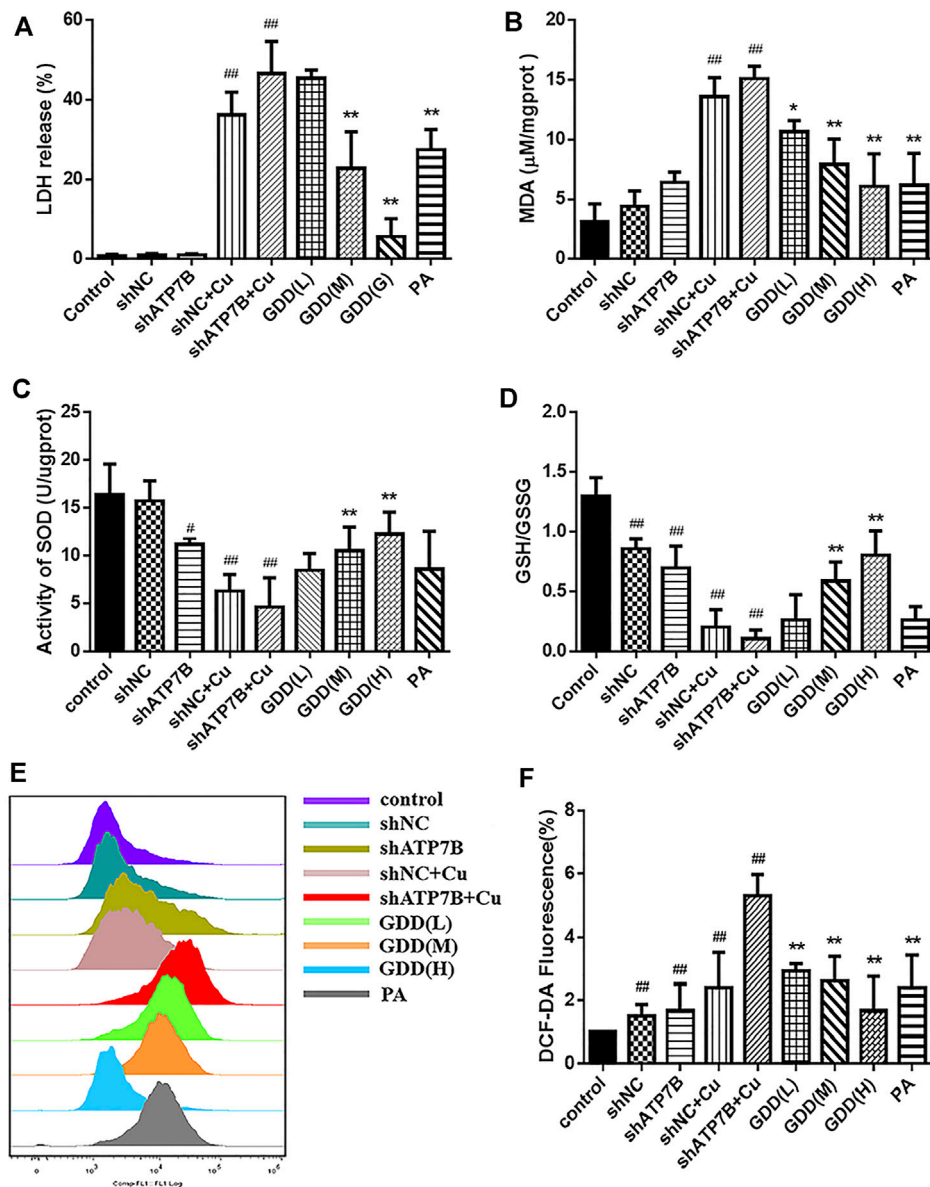


FIGURE 4 | Effects of MDA (A), LDH release (B), SOD (C), GSH/GSSG (D), and ROS (E, F) levels in copper-laden HLD hepatocytes ($\bar{x} \pm s, n = 3$). # $p < 0.05$, ## $p < 0.01$ compared with control group; * $p < 0.05$, ** $p < 0.01$ compared with shATP7B + Cu group.

potential metabolite biomarkers in each group were used to represent the relative content of corresponding metabolites in each group, and the differences in metabolites in each group were verified by one-way ANOVA. Finally, data information was imported into MetaboAnalyst 5.0 software, and the metabolic pathway was analyzed combined with the Kyoto Encyclopedia of Genes and Genomes database (<http://www.kegg.jp/>).

2.12 Western Blotting

The cells in each group were treated according to the method mentioned in Section 2.7.3. According to the instructions

mentioned in the glutamate content detection kit, the level of glutamate in the cells was detected. Protein content was determined using the BCA protein detection kit. The loading buffer was added in equal amounts to the proteins. After sodium dodecyl sulfate (SDS)-polyacrylamide gel electrophoresis (PAGE), transfer membrane and sealing, the membrane and the antibody (GS: 1:1,000, GLS1: 1:500, and GLS2: 1:1,000) were incubated overnight at 4°C. Subsequently, goat anti-rabbit and goat anti-mouse antibodies were added at an appropriate dilution (diluted ratio: 1:15,000). Grayscale scanning and quantitative analysis were conducted using the Alphaview software.

3 RESULTS

3.1 Effects of CuSO₄ on Viability of shATP7B-Transfected Cells

As shown in **Figure 1A**, results showed that the cell survival rate in the shATP7B group was lower than that in other groups. Subsequently, shATP7B-transfected cells were incubated with CuSO₄ solution ranging in concentration from 0 to 600 μ M (0, 100, 200, 300, 400, 500, and 600 μ M) for 12, 24, 36, and 48 h, and their MTT assays (**Figure 1B**) indicated that with an increase in copper concentration (the range of 100–600 μ M CuSO₄) and incubation time, the cell survival rate showed a certain dose- and time-dependent decrease. The IC₅₀ value for CuSO₄ was estimated to be 300 μ M at 24 h, which was selected as an optimum modeling condition of copper-laden HLD hepatocytes.

3.2 Effect of Gandou Decoction on the Viability of Copper-Laden Hepatolenticular Degeneration Hepatocytes

The results of the MTT assay showed (**Figure 1C**) that GDD had no toxicity toward HLD hepatocytes in concentrations ranging from 10 to 80 μ g/ml, which was considered a safe concentration range. Accordingly, concentrations of 20, 40, and 80 μ g/ml GDD were selected for the low-, medium-, and high-dose groups, respectively, in the follow-up study. Similarly, the optimal dose of PA was determined to be 50 μ g/ml.

The results for the HLD hepatocyte model experiments are shown in **Figure 1D**. The cell viabilities in the shNC group, shATP7B group, shNC + Cu group, and shATP7B + Cu group were $81.20 \pm 7.47\%$, $52.12 \pm 9.76\%$, $73.08 \pm 5.62\%$, and $34.19 \pm 7.14\%$ respectively. Compared with the shATP7B + Cu group, the groups with medium- and high-dose GDD treatment and penicillamine pretreatment showed an increased cell survival rate to varying degrees, and the cell viabilities in these groups were $53.00 \pm 5.44\%$, $64.21 \pm 4.40\%$, and $50.42 \pm 7.19\%$, respectively. These results show that GDD has a strong protective effect on injured copper-laden HLD hepatocytes.

3.3 Excretion of Copper Promoted by Gandou Decoction in Copper-Laden Hepatolenticular Degeneration Hepatocytes

3.3.1 Fluorescence Intensity of Cu²⁺ in Copper-Laden Hepatolenticular Degeneration Hepatocytes Affected by Gandou Decoction

As shown in **Figures 2A–I**, there was almost no red fluorescence in the cells in the control group, implying the little content of copper in these cells. After incubation with CuSO₄, the weak red fluorescence in the shNC and shATP7B groups significantly increased, indicating an increase in intracellular Cu²⁺ content. Compared with the shNC + Cu group, the shATP7B + Cu group showed sparsely stained cells and stronger intensity of red fluorescence. However, after intervention with low, medium, and high doses of GDD and PA in the shATP7B + Cu group,

the fluorescence intensity of copper decreased. The number of stained cells increased, especially in cells treated with high doses of GDD and PA. These results show that GDD could effectively inhibit the accumulation of copper and reduce its level in copper-laden HLD hepatocytes.

3.3.2 Effect of Gandou Decoction on Cu²⁺ Content of Copper-Laden Hepatolenticular Degeneration Hepatocytes

The results of AAS determination showed that GDD has an effect on expelling copper. As shown in **Figure 2J**, the content of Cu²⁺ in the control group, shNC group, and shATP7B group was low, but that in the shATP7B + Cu group was significantly increased ($p < 0.01$), which indicated the accumulation of Cu²⁺ in copper-laden HLD hepatocytes. The copper content in cells treated with GDD and PA, especially high-dose GDD, was significantly lower than that in the shATP7B + Cu group ($p < 0.05$, $p < 0.01$).

3.4 Protective Effect of Gandou Decoction on Copper-Laden Hepatolenticular Degeneration Hepatocytes

Inverted microscope observation indicated that GDD could reduce injury in copper-laden HLD hepatocytes in different degrees. As shown in **Figure 3A**, in the control group, the cells showed a uniform flat or polygonal shape, adherent growth, complete cell membrane, and high density. After shATP7B transfection, the cell structure deteriorated, the cell membrane was sunken, and some cells were divided into fragments. Further through modeling by CuSO₄, the number of cells significantly decreased, the number of suspended cells increased, cell membrane ruptured, cells shrunk, and cell damage intensified, indicating that CuSO₄ can significantly inhibit cell growth (**Figures 3B–E**). However, after intervention with different concentrations of GDD and PA (**Figures 3F–I**), the cell status and degree of death improved. The number of viable cells increased compared with that in the shATP7B + Cu group.

Further evaluation of the changes of cell ultrastructure showed intact cell shape, round nucleus, complete and smooth nuclear membrane, various organelles in the cytoplasm, and lots of mitochondria in the control group (**Figure 3J–M**); even mitochondrial crista could be clearly seen. Compared with the control group, the shATP7B + Cu group showed a ruptured cell and nuclear membrane, disappeared nucleolus, decreased mitochondria number, blurred ridgeline of mitochondria, and obvious vacuolation. The structure of hepatocytes in GDD and PA groups was normal, with improvement in the blurred cristae and vacuolization of mitochondria.

3.5 Measurement of Biochemical Indices in Copper-Laden Hepatolenticular Degeneration Hepatocytes

The results showed that the level of MDA in the shATP7B + Cu group was significantly higher than that in the control group (**Figure 4B**, $p < 0.05$), and intracellular MDA levels were

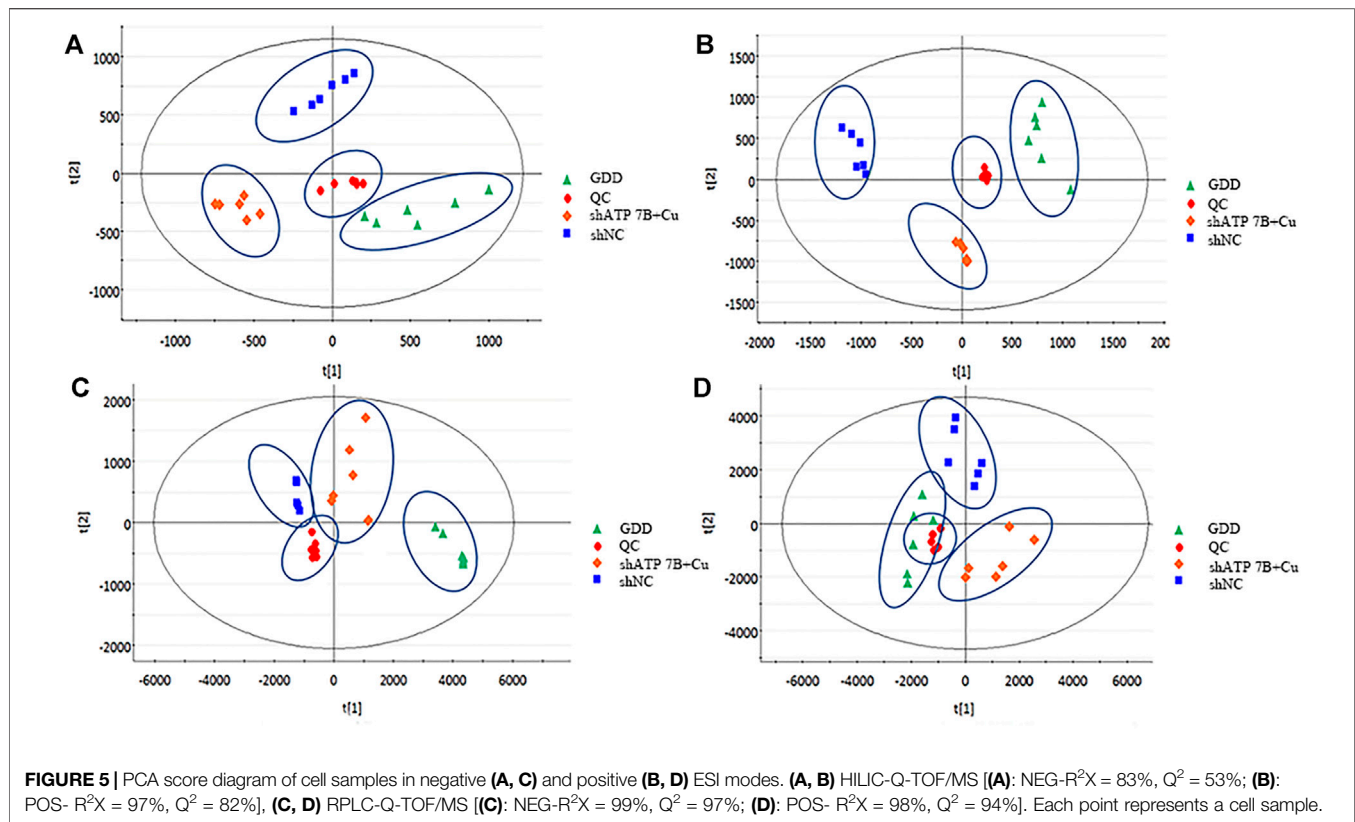


FIGURE 5 | PCA score diagram of cell samples in negative (A, C) and positive (B, D) ESI modes. (A, B) HILIC-Q-TOF/MS [(A): NEG-R²X = 83%, Q² = 53%; (B): POS- R²X = 97%, Q² = 82%], (C, D) RPLC-Q-TOF/MS [(C): NEG-R²X = 99%, Q² = 97%; (D): POS- R²X = 98%, Q² = 94%]. Each point represents a cell sample.

effectively decreased after treatment with different doses of GDD and PA ($p < 0.05$). LDH is a relatively stable enzyme released outside the cell because of the destruction of the cell membrane structure, and it was regarded as an essential indicator of cell membrane integrity status. Compared with the control group (Figure 4A), the shATP7B + Cu group showed significantly increased LDH release. However, medium and high doses of GDD and PA could effectively reduce LDH release in HLD hepatocytes ($p < 0.01$). SOD, as the central defensive antioxidant enzyme in cells, directly participates in the decomposition of ROS in the body, reducing hepatocyte injury. The results of SOD detection showed that SOD activity in the shATP7B + Cu group was significantly lower than that in the control group (Figure 4C, $p < 0.01$). In contrast, the decrease in SOD activity was attenuated by medium- and high-dose GDD treatment ($p < 0.01$). As an antioxidant molecule, GSH plays an important role in intracellular redox balance, which is an important indicator of intracellular homeostasis. The results (Figure 4D) showed that after incubation with 300- μ M CuSO₄, GSH/GSSG levels in the shNC + Cu group and shATP7B + Cu group were only one-sixth and one-twelfth of the control group, respectively, indicating that the GSH in cells was almost completely suppressed. However, the medium- and high-dose GDD groups significantly inhibited the decrease in GSH/GSSG levels ($p < 0.01$). In addition, a DCFH-DA fluorescence probe was used to determine the content of ROS in cells. The results suggested that the

fluorescence intensity in HLD hepatocytes significantly increased after CuSO₄ induction for 24 h, indicating that CuSO₄ promoted the release of ROS in cells ($p < 0.01$), and the fluorescence intensity-dependent reduction of DCF was caused by the pre-protection of the low, medium, and high doses of GDD. This indicated that GDD could reduce intracellular ROS. These results suggest that GDD has a significant protective effect against abnormal changes in copper-laden HLD hepatocytes (Figures 4E,F).

3.6 Multivariate Statistical Analysis

Combining the HILIC column and C₁₈ column results, the total ion chromatograms (TICs) in the shNC group, shATP7B + Cu group, and GDD group were obtained with the full scan mode of dual ESI via UPLC-Q-TOF/MS analysis. The high reproducibility of the QC data demonstrated that the instrument is stable and the metabolomics analysis method is reliable (Supplementary Information S2.2). As shown in Supplementary Figure S2 and Supplementary Figure S3, there are differences in the metabolic profiles of samples between different groups in the positive and negative ion modes.

The data were analyzed by the pattern recognition method to reveal the differences among the three groups under positive and negative ion modes. Given that in unsupervised multivariate analysis, PCA can truly reflect the clustering of samples, on processing data by PCA, it was found that there were differences among the shNC group, shATP7B + Cu group, and GDD group under negative and positive modes (Figure 5).

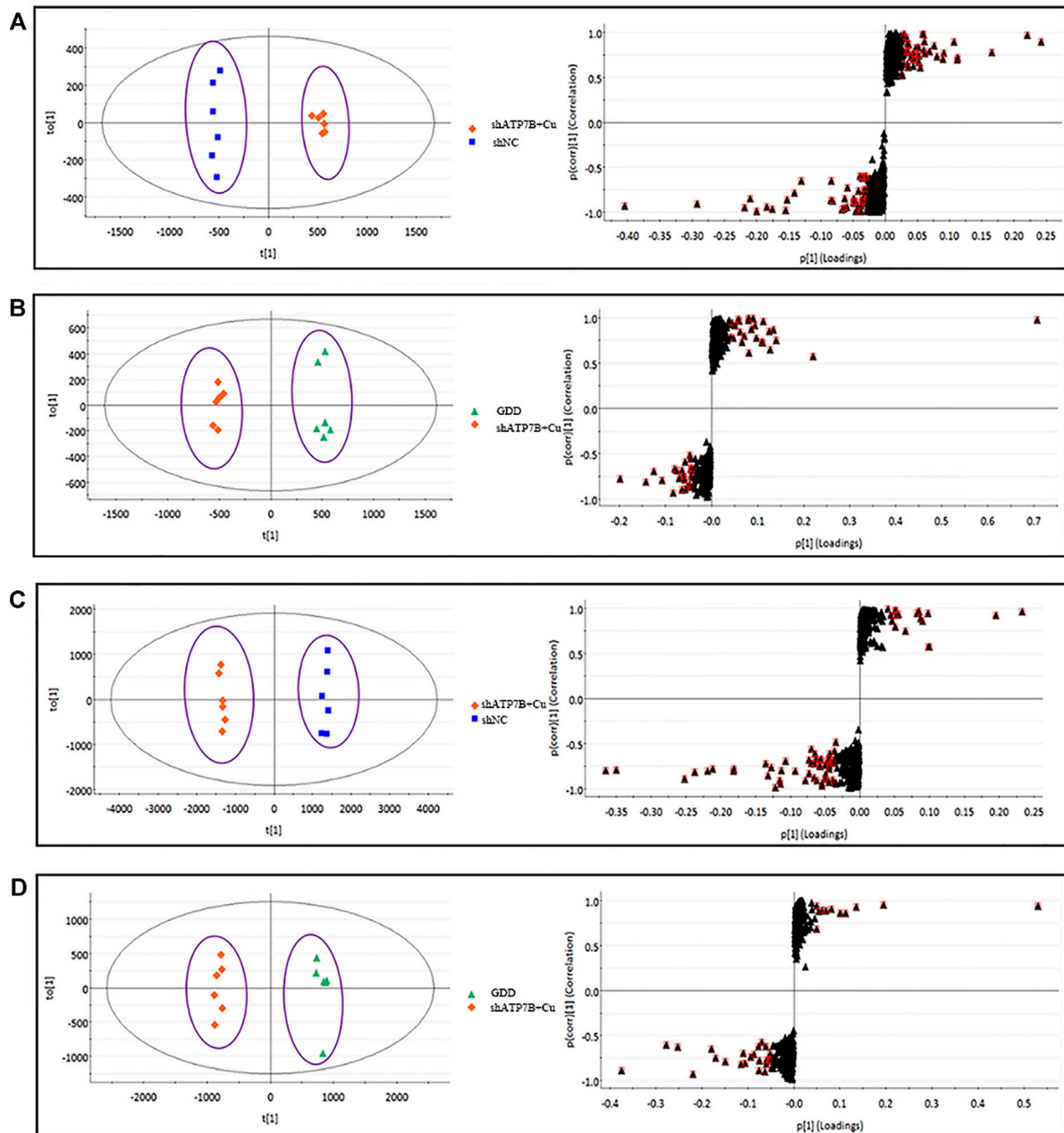


FIGURE 6 | (shNC group, shATP7B + Cu group, and GDD group) OPLS-DA score and its corresponding S-plot for differential analysis between different groups of cell samples in HILIC-Q-TOF/MS negative and positive ESI mode. [(A). NEG- $R^2Y = 1$, $Q^2 = 99\%$; (B). NEG- $R^2Y = 99\%$, $Q^2 = 98\%$; (C). POS- $R^2Y = 1$, $Q^2 = 98\%$; (D). POS- $R^2Y = 99\%$, $Q^2 = 96\%$].

For further tracking the specific changes among the three groups, the supervised multivariate OPLS-DA method was used to analyze the variables. The OPLS-DA score map and S-plot diagram in the positive and negative ion modes were obtained, respectively (Figure 6 and Figure 7). The OPLS-DA diagram showed that the shNC and shATP7B + Cu groups were distributed on both sides of $t[1]$ in the OPLS-DA score map, indicating a significant difference in metabolites between the

two groups. The S-plot diagram directly showed different metabolites. When the variable is far from the origin, the VIP value is higher, and the contribution to the separation between the two groups is larger. In the figures, the variables with VIP values >1 circled in red boxes are the potential biomarkers between the two groups. The differences in metabolites in all groups were also observed more intuitively using a hierarchical clustering heatmap (Figure 8A). In the

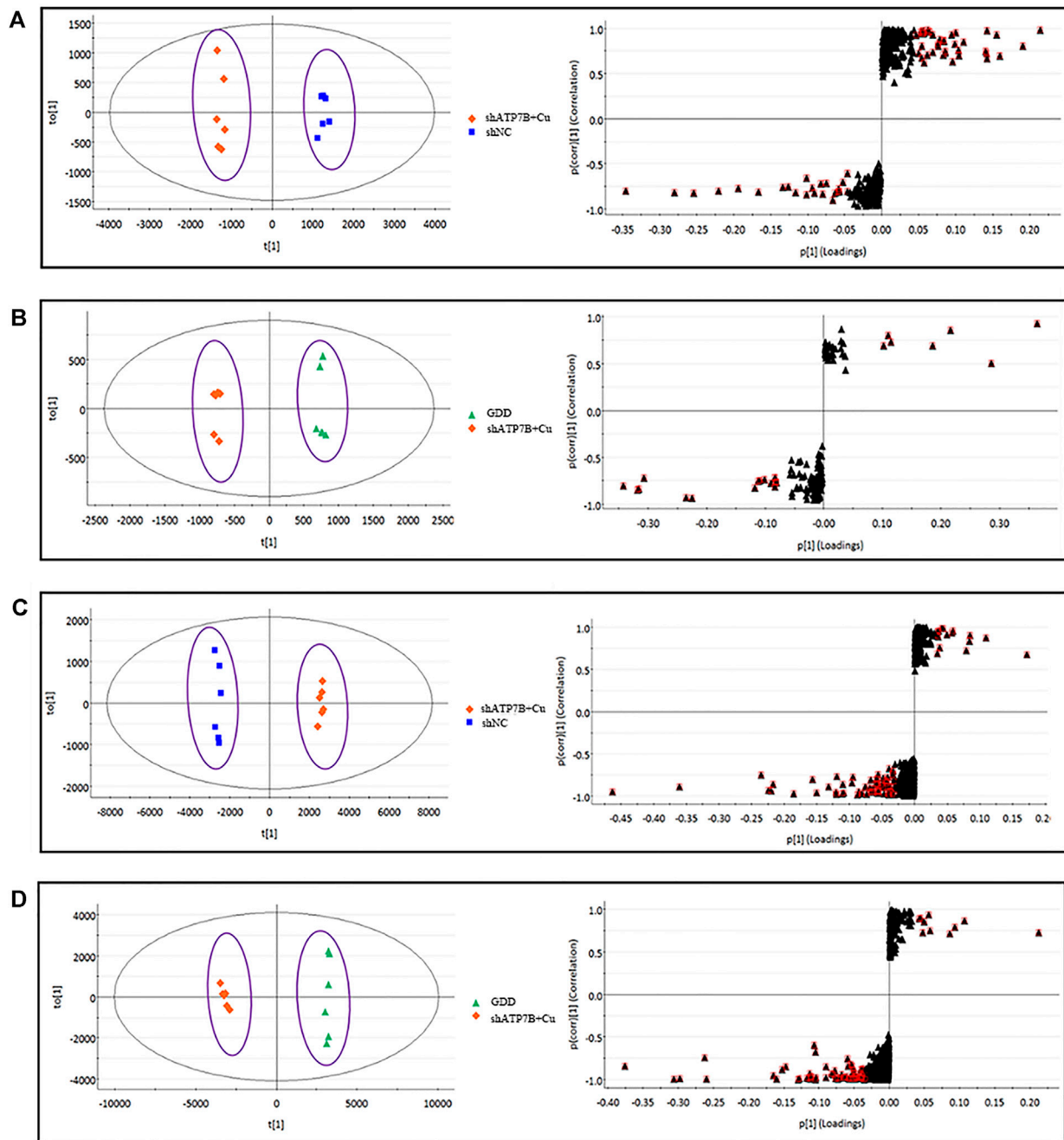
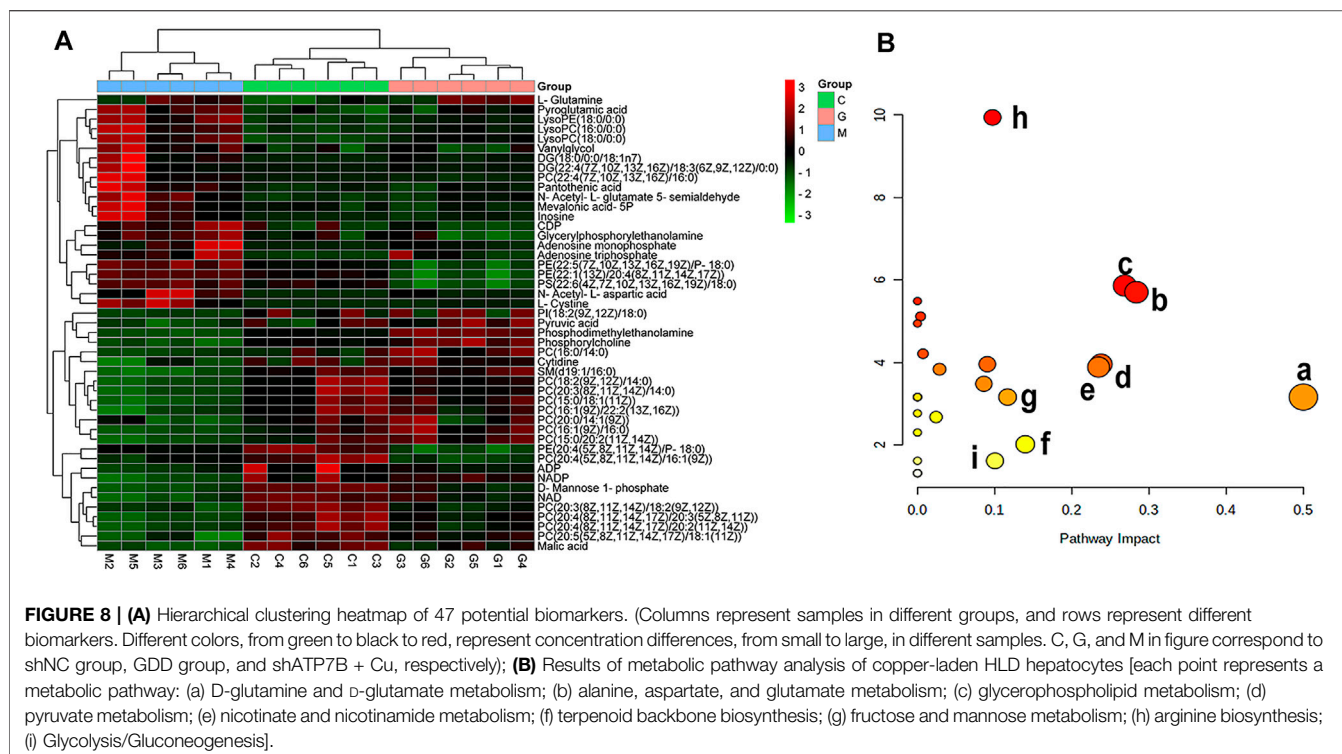


FIGURE 7 | (shNC group, shATP7B + Cu group, and GDD group) OPLS-DA score and its corresponding S-plot for differential analysis between different groups of cell samples in RPLC-Q-TOF/MS negative and positive ESI mode. **(A)**. NEG- $R^2Y = 99\%$, $Q^2 = 97\%$; **(B)**. NEG- $R^2Y = 99\%$, $Q^2 = 99\%$; **(C)**. POS- $R^2Y = 1$, $Q^2 = 99\%$; **(D)**. POS- $R^2Y = 1$, $Q^2 = 99\%$.

figure, the biomarker concentrations in the shATP7B + Cu group significantly differed from those in the shNC group and the GDD group, whereas there was no significant difference in the concentration of biomarkers between the GDD group and the shNC group, indicating that after GDD administration, the cell metabolic pattern reverses to normal or close to normal levels.

3.7 Metabolite Identification

The metabolites of each group under the two separate systems of HILIC and C_{18} were statistically analyzed by ANOVA. The metabolites with a VIP value >1 were obtained by selecting the different substances and combining them with the S-plot diagram. Subsequently, the metabolites with a VIP value >1 were screened by HMDB and secondary fragmentation analysis of MS,



and the fragment information under high and low collision energy was further matched to verify the chemical structure of the metabolites.

For the metabolites isolated by the HILIC column, the 22 differential metabolites were determined in the shATP7B + Cu group (Table 1), with 13 metabolites increasing and nine metabolites decreasing in concentration. After GDD treatment, levels of pyroglutamic acid, N-acetyl-L-aspartic acid, vanylglycol, L-glutamic acid, glycerylphosphorylethanolamine, pantothenic acid, mevalonic acid-5P, CDP, ATP, N-acetyl-L-glutamate 5-semialdehyde, L-cystine, inosine, malic acid, pyruvic acid, phosphodimethylethanolamine, cytidine, D-mannose 1-phosphate, AMP, ADP, NAD, NADP, and phosphorylcholine (Supplementary Figure S4 and Supplementary Figure S5) were markedly altered in copper-laden HLD hepatocytes. As mentioned earlier, the results of identification under the C_{18} separation system are as shown in Table 2. A total of 25 metabolites related to copper-laden HLD hepatocytes were obtained, with decreased levels of 17 metabolites and increased levels of eight metabolites (Supplementary Figure S6 and Supplementary Figure S7). The results indicated that these metabolites in hepatocytes are the potential biomarkers of the intervention effects of GDD and may be associated with the GDD mechanism of action.

3.8 Analysis of Metabolic Pathway

The 47 biomarkers were screened using two chromatographic columns mentioned earlier, and their normalized peak area was imported into Metaboanalyst 5.0 software for metabolic pathway enrichment and analysis. The results showed that 30 metabolic

pathways were affected in copper-laden HLD hepatocytes (Figure 8B), including glutamate–glutamine metabolism (a); alanine, aspartic acid, and glutamate metabolism (b); glycerol phospholipid metabolism (c); pyruvate metabolism (d); nicotinic acid and nicotinamide metabolism (e); terpene skeleton biosynthesis (f); fructose and mannose metabolism (g); arginine biosynthesis (h); and glycolysis/gluconeogenesis (i). Among these, the glutamate–glutamine metabolic pathway has the most significant influence, with an influence value of 0.5, which is an important metabolic pathway. The KEGG database and the related references were used to further explore the role of differential metabolites.

3.9 Effect of Gandou Decoction on Glutamate Level in Copper-Laden Hepatocellular Degeneration Hepatocytes

Glutamate is an important biomarker of GDD correcting copper-laden HLD hepatocyte metabolic disorder, and therefore, further quantitative analysis of glutamate is necessary for HLD hepatocytes. As shown in Figure 9A, the glutamate content in the shATP7B + Cu group significantly increased ($p < 0.01$). After low-, medium-, and high-dose GDD and PA treatments, the glutamate content in HLD hepatocytes significantly decreased ($p < 0.05$ or $p < 0.01$), suggesting that the glutamate verification results were consistent with the metabolomic results.

In the physiological state, the synthesis, decomposition, uptake, and reabsorption of glutamate is a process of dynamic

TABLE 1 | Potential biomarkers in copper-laden HLD hepatocytes detected by HILIC-Q-TOF/MS and their variation tendency (NEG and POS).

| No | Features (tR-m/z) | Cal. m/z | Delta m/z (ppm) | VIP | | Metabolite identification | Formula | Ion form | Fragment ions | Trend | |
|----|-------------------|----------|-----------------|--------------------------------|---------------------------|-------------------------------------|---|-------------------------|------------------------------|-------|-----|
| | | | | C ^a /M ^b | VIP a M/G ^c | | | | | M/C | G/M |
| 1 | 1.84_128.0349 | 128.0353 | 3.1 | 7.92 | 5.16 | Pyroglutamic acid | C ₅ H ₇ NO ₃ | M-H | 126.7031 | ↑ | ↓ |
| 2 | 1.85_133.0132 | 133.0142 | 7.5 | 5.21 | 2.55 | Malic acid | C ₄ H ₆ O ₅ | M-H | 115.0065 | ↓ | ↑ |
| 3 | 1.09_133.0135 | 133.0142 | 5.3 | 2.81 | 3.29 | Pyruvic acid | C ₃ H ₄ O ₃ | M + FA-H | 87.0082 | ↓ | ↑ |
| 4 | 5.24_168.0428 | 168.0431 | 1.8 | 1.55 | 2.13 | Phosphodimethylethanolamine | C ₄ H ₁₂ NO ₄ P | M-H | 96.9607, 78.9591 | ↓ | ↑ |
| 5 | 1.55_174.0399 | 174.0408 | 5.2 | 4.70 | 3.33 | N-Acetyl-L-aspartic acid | C ₆ H ₉ NO ₅ | M-H | 130.0463, 88.0421 | ↑ | ↓ |
| 6 | 1.04_183.0665 | 183.0663 | 1.1 | 1.19 | 1.14 | Varylglycol | C ₉ H ₁₂ O ₄ | M-H | 153.0552, 121.0281 | ↑ | ↑ |
| 7 | 1.07_192.0487 | 192.0508 | 0 | 2.00 | 1.50 | L-Glutamic acid | C ₅ H ₉ NO ₄ | M + FA-H | 127.9222, 123.9017, 74.0032 | ↑ | ↓ |
| 8 | 4.55_214.0485 | 214.0485 | 0 | 1.92 | 1.90 | Glycerolphosphorylethanolamine | C ₅ H ₁₄ NO ₆ P | M-H | 168.9919, 96.9587, 78.9578 | ↑ | ↓ |
| 9 | 1.68_218.1020 | 218.1034 | 6.4 | 2.29 | 1.83 | Pantothenic acid | C ₉ H ₁₇ NO ₅ | M-H | 146.0817, 128.0600, 88.0399 | ↑ | ↓ |
| 10 | 5.28_242.0803 | 242.0782 | 8.7 | 3.62 | 3.56 | Cytidine | C ₉ H ₁₃ N ₃ O ₅ | M-H | 168.0435, 112.9812 | ↓ | ↑ |
| 11 | 5.11_259.0226 | 259.0224 | 0.8 | 6.76 | 2.13 | D-Mannose 1-phosphate | C ₆ H ₁₃ O ₉ P | M-H | 229.0061, 96.9607, 78.9578 | ↓ | ↑ |
| 12 | 5.35_273.0380 | 273.0380 | 0 | 1.82 | 1.56 | Mevalonic acid-5P | C ₆ H ₁₃ O ₇ P | M + FA-H | 96.9587, 78.9578 | ↑ | ↓ |
| 13 | 4.91_346.0555 | 346.0558 | 0.9 | 1.73 | 1.22 | AMP | C ₁₀ H ₁₄ N ₅ O ₇ P | M-H | 134.0459, 96.9667, 78.9578 | ↑ | ↓ |
| 14 | 7.19_402.0094 | 402.0109 | 3.7 | 1.56 | 1.97 | CDP | C ₉ H ₁₅ N ₃ O ₁₁ P ₂ | M-H | 173.9330, 158.9236, 96.9667 | ↑ | ↓ |
| 15 | 8.13_426.0220 | 426.0220 | 0 | 7.58 | 3.35 | ADP | C ₁₀ H ₁₅ N ₅ O ₁₀ P ₂ | M-H | 426.0193, 158.9236 | ↓ | ↑ |
| 16 | 9.55_505.9878 | 505.9885 | 1.4 | 2.54 | 1.23 | ATP | C ₁₀ H ₁₆ N ₅ O ₁₃ P ₃ | M-H | 408.0143, 238.8838, 176.9303 | ↑ | ↓ |
| 17 | 5.70_662.1057 | 662.1018 | 5.9 | 5.94 | 2.90 | NAD | C ₂₁ H ₂₇ N ₇ O ₁₄ P ₂ | M-H | 425.9982, 78.9596 | ↓ | ↑ |
| 18 | 7.91_742.0680 | 742.0680 | 0 | 1.13 | 1.02 | NADP | C ₂₁ H ₂₈ N ₇ O ₁₇ P ₃ | M-H | 96.9687, 78.9578 | ↓ | ↑ |
| 19 | 1.01_138.0551 | 138.0561 | 7.2 | 1.23 | 1.28 | N-Acetyl-L-glutamate 5-semialdehyde | C ₇ H ₁₁ NO ₄ | M + H-2H ₂ O | 138.0564, 130.0691 | ↑ | ↓ |
| 20 | 5.23_184.0754 | 184.0739 | 8.1 | 2.39 | 4.55 | Phosphorylcholine | C ₅ H ₁₅ NO ₄ P | M + H | 124.9771, 98.9858, 84.0804 | ↓ | ↑ |
| 21 | 4.60_241.0339 | 241.0346 | 2.9 | 2.13 | 2.69 | L-Cystine | C ₆ H ₁₂ N ₂ O ₄ S ₂ | M + H | 177.0340, 149.0213, 122.0281 | ↑ | ↓ |
| 22 | 2.56_291.0716 | 291.070 | 5.5 | 2.51 | 1.82 | Inosine | C ₁₀ H ₁₂ N ₄ O ₅ | M + Na | 133.0792 | ↑ | ↓ |

^aC means shNC, group.^bM means shATP7B + Cu group.^cG means GDD, group.

Change of potential biomarkers in copper-laden HLD, hepatocytes among groups were statistically analyzed by multivariate statistical analysis and ANOVA. Significant changed biomarkers were flagged with (↓) content decreased and (↑) content increased. p-values were calculated by Student's t-test (threshold < 0.05).

equilibrium. Glutamine synthetase (GS) and glutaminase (GLS) are critical enzymes in the glutamate biosynthesis pathway. GLS can further be divided into renal-type GLS (GLS1) and liver-type GLS (GLS2). Western blotting experiments were conducted to verify GS, GLS1, and GLS2. The results (**Figure 9B**) showed that compared with the control group, the shATP7B + Cu group showed a significantly decreased protein expression of GS ($p < 0.01$). In contrast, it was highly expressed in the medium- and high-dose GDD groups. Furthermore, the protein expressions of GLS1 and GLS2 increased significantly in the shATP7B + Cu group and decreased in a dose-dependent manner after intervention with different doses of GDD. All results showed that the corrective effect of GDD on glutamate levels in copper-laden HLD hepatocytes was associated with the upregulation of GS protein expression and downregulation of GLS1 and GLS2 protein expression.

4 DISCUSSION

As an effective therapeutic prescription for treating HLD, GDD was reported to have copper removal and hepatoprotective effects against HLD in clinical trials and *in vitro* studies (Hu et al., 2002; Yang and Cheng, 2002; Xue et al., 2007; Li et al., 2013). However, the biological mechanism underlying the basis for these effects remain unknown. In the present investigation, using RNA interference technology, shATP7B RNA was transiently transfected into BRL-3A rat hepatocytes, and a hepatocyte model similar to the pathological HLD was successfully constructed to evaluate the underlying GDD mechanism. BRL-3A cells, which are normal rat hepatogenic cell line cells, are widely used in the study of various liver diseases *in vitro* (Yang et al., 2020), including studies on hepatocyte proliferation, post-hepatectomy regeneration (Chang et al., 2017), hepatotoxicity

TABLE 2 | Potential biomarkers in copper-laden HLD hepatocytes detected by RPLC-Q-TOF/MS and their variation tendency (NEG and POS).

| No | Features (t_R - m/z) | Cal. m/z | Delta m/ z (ppm) | VIP | | Metabolite identification | Formula | Ion form | Fragment ions | Trend | |
|----|-------------------------------|-------------|------------------------|------------------------------------|----------------------|---|---|---------------------------|---------------------------------|---------|---------|
| | | | | C ^a / M ^b | M/ G ^c | | | | | M/ C | G/ M |
| 1 | 14.93_750.5472 | 750.5443 | 3.9 | 1.62 | 1.45 | PE [20:4 (5Z,8Z,11Z,14Z)/P-18:0] | C ₄₃ H ₇₆ NO ₇ P | M-H | 303.2314 | ↓ | ↑ |
| 2 | 14.84_776.5684 | 776.5684 | 0 | 2.18 | 1.51 | PE [22:5 (7Z,10Z,13Z,16Z,19Z)/P-18:0] | C ₄₅ H ₈₀ NO ₇ P | M-H | 462.2978, 331.2635 | ↑ | ↓ |
| 3 | 14.55_834.5309 | 834.5291 | 2.2 | 1.03 | 1.05 | PS[22:6 [4Z,7Z,10Z,13Z,16Z,19Z]/18:0] | C ₄₆ H ₇₈ NO ₁₀ P | M-H | 327.2201, 283.2606 | ↑ | ↓ |
| 4 | 11.30_861.5532 | 861.5499 | 3.8 | 4.17 | 2.40 | PI[18:2 (9Z,12Z)/18:0] | C ₄₅ H ₈₃ O ₁₃ P | M-H | 581.3096, 283.2606, 241.0166 | ↓ | ↑ |
| 5 | 10.84_866.5963 | 866.5917 | 5.3 | 7.92 | 5.16 | PE [22:1 (13Z)/20:4 (8Z,11Z,14Z,17Z)] | C ₅ H ₇ NO ₃ | M-H | 303.2349 | ↑ | ↓ |
| 6 | 4.14_482.3258 | 482.3241 | 3.5 | 1.39 | 1.14 | LysoPE (18:0/0:0) | C ₂₃ H ₄₈ NO ₇ P | M + H | 341.3078, 323.2951 | ↑ | ↓ |
| 7 | 3.35_496.3415 | 496.3398 | 3.4 | 2.34 | 1.81 | LysoPC(16:0/0:0) | C ₂₄ H ₅₀ NO ₇ P | M + H | 184.0744 | ↑ | ↓ |
| 8 | 4.03_524.3730 | 524.3711 | 3.6 | 2.16 | 1.52 | LysoPC(18:0/0:0) | C ₂₆ H ₅₄ NO ₇ P | M + H | 184.0744 | ↑ | ↓ |
| 9 | 11.38_605.5479 | 605.5509 | 5.0 | 1.06 | 1.26 | DG (18:0/0:0/18:1n7) | C ₃₉ H ₇₄ O ₅ | M + H-H ₂ O | 605.5486, 323.2933 | ↑ | ↓ |
| 10 | 11.89_667.5217 | 667.5272 | 8.2 | 1.28 | 1.18 | DG [22:4 (7Z,10Z,13Z,16Z)/18:3 (6Z,9Z,12Z)/0:0] | C ₄₁ H ₇₂ O ₅ | M + Na | 667.5309, 335.2493 | ↑ | ↓ |
| 11 | 11.21_706.5393 | 706.5381 | 1.7 | 2.44 | 3.58 | PC(16:0/14:0) | C ₃₈ H ₇₆ NO ₈ P | M + H | 184.0744 | ↓ | ↑ |
| 12 | 12.60_717.5894 | 717.5905 | 1.5 | 1.86 | 1.76 | SM(d19:1/16:0) | C ₄₀ H ₈₁ N ₂ O ₆ P | M + H | - | ↓ | ↑ |
| 13 | 9.44_730.5400 | 730.5381 | 2.6 | 2.49 | 2.19 | PC[18:2 (9Z,12Z)/14:0] | C ₄₀ H ₇₆ NO ₈ P | M + H | 184.0744 | ↓ | ↑ |
| 14 | 11.26_732.5525 | 732.5538 | 1.8 | 5.51 | 6.96 | PC[16:1 (9Z)/16:0] | C ₄₀ H ₇₆ NO ₈ P | M + H | 549.4932, 494.3158, 184.0744 | ↓ | ↑ |
| 15 | 12.60_746.5686 | 746.5694 | 1.1 | 3.71 | 3.31 | PC[15:0/18:1 (11Z)] | C ₄₁ H ₈₀ NO ₈ P | M + H | 184.0744 | ↓ | ↑ |
| 16 | 9.91_756.5547 | 756.5538 | 1.2 | 1.91 | 1.47 | PC[20:3 (8Z,11Z,14Z)/14:0] | C ₄₂ H ₇₈ NO ₈ P | M + H | 363.2894, 184.0744 | ↓ | ↑ |
| 17 | 14.08_760.5851 | 760.5851 | 0 | 7.59 | 6.59 | PC[20:0/14:1 (9Z)] | C ₄₂ H ₈₂ NO ₈ P | M + H | 571.5199, 227.2030, 166.0644 | ↓ | ↑ |
| 18 | 12.58_772.5808 | 772.5851 | 5.6 | 2.91 | 3.54 | PC[15:0/20:2 (11Z,14Z)] | C ₄₃ H ₈₂ NO ₈ P | M + H | 184.0744 | ↓ | ↑ |
| 19 | 9.50_780.5561 | 780.5538 | 2.9 | 3.10 | 1.42 | PC[20:4 (5Z,8Z,11Z,14Z)/16:1 (9Z)] | C ₄₄ H ₇₈ NO ₈ P | M + H | 184.0744 | ↓ | ↑ |
| 20 | 9.50_806.5717 | 806.5694 | 2.9 | 2.96 | 1.97 | PC[20:5 (5Z,8Z,11Z,14Z,17Z)/18:1 (11Z)] | C ₄₆ H ₈₀ NO ₈ P | M + H | 323.2900, 247.2437, 184.0744 | ↓ | ↑ |
| 21 | 10.89_808.5849 | 808.5849 | 0 | 5.03 | 5.33 | PC[20:3 (8Z,11Z,14Z)/18:2 (9Z,12Z)] | C ₄₆ H ₈₂ NO ₈ P | M + H | 623.4977, 321.2749, 184.0744 | ↓ | ↑ |
| 22 | 9.94_810.5989 | 810.6007 | 2.2 | 3.39 | 6.93 | PC[22:4 (7Z,10Z,13Z,16Z)/16:0] | C ₄₆ H ₈₄ NO ₈ P | M + H | 627.5403, 184.0744 | ↓ | ↑ |
| 23 | 14.42_812.6144 | 812.6164 | 2.5 | 1.46 | 1.13 | PC[16:1 (9Z)/22:2 (13Z,16Z)] | C ₄₆ H ₈₆ NO ₈ P | M + H | 627.5352, 184.0744 | ↓ | ↑ |
| 24 | 10.18_832.5857 | 832.5851 | 0.7 | 3.85 | 2.32 | PC[20:4 (8Z,11Z,14Z,17Z)/20:3 (5Z,8Z,11Z)] | C ₄₈ H ₈₂ NO ₈ P | M + H | 184.0744 | ↓ | ↑ |
| 25 | 10.82_834.6011 | 834.6011 | 0 | 3.12 | 1.32 | PC[20:4 (8Z,11Z,14Z,17Z)/20:2 (11Z,14Z)] | C ₄₈ H ₈₄ NO ₈ P | M + H | 184.0744 | ↓ | ↑ |

^aC means shNC group.^bM means shATP7B + Cu group.^cG means GDD group.

Change of potential biomarkers in copper-laden HLD, hepatocytes among groups were statistically analyzed by multivariate statistical analysis and ANOVA. Significant changed biomarkers were flagged with (↓) content decreased and (↑) content increased. p-values were calculated by Student's t-test (threshold < 0.05).

(Liu et al., 2021), liver function (Hu et al., 2020), oxidative stress (Li et al., 2018), and inflammation (Luo et al., 2021). It was reported that some researchers chose tumor (HepG2 cells) and normal liver cells (BRL-3A cell) to explore the survival time of and cell proliferation in patients with liver cancer (Ye et al., 2019). Another study revealed the regulatory mechanism of acetic acid (AcOH) with regard to liver lipid metabolism in BRL-3A cells (Li et al., 2018). In these studies, the BRL-3A cells were often used to construct a pathological model *in vitro*. Therefore, in our study, an *in vitro* model of HLD was constructed using BRL-3A cells. Subsequently, the HLD cell model was verified *via* RT-PCR and Western blotting, which showed that the levels of ATP7B mRNA and protein in plasmid transfection groups were significantly lower than those in control and shNC groups (Supplementary Figures S1G–L).

As the primary pathological organ in HLD, pathological changes in the liver are caused by mutations in the ATP7B gene and copper metabolism disorder. Therefore, 300-μM CuSO₄ was selected as the optimum modeling concentration for copper-laden HLD hepatocytes through cytotoxicity assays (Figures 1A,B). After this, GDD extract at a concentration of 80 μg/ml showed a strong protective effect on the injury in copper-laden HLD hepatocytes in cell viability evaluation (Figures 1C,D). The study of cell morphology showed that the number of adherent cells significantly increased, and the cell morphology improved in the groups with GDD and PA treatment (Figures 3A–I). In addition, in agreement with the results of PA, GDD could promote the excretion of excessive Cu²⁺ and reduce the accumulation of Cu²⁺ in copper-laden HLD hepatocytes (Figures 2A–J). Thus, GDD may be chelating

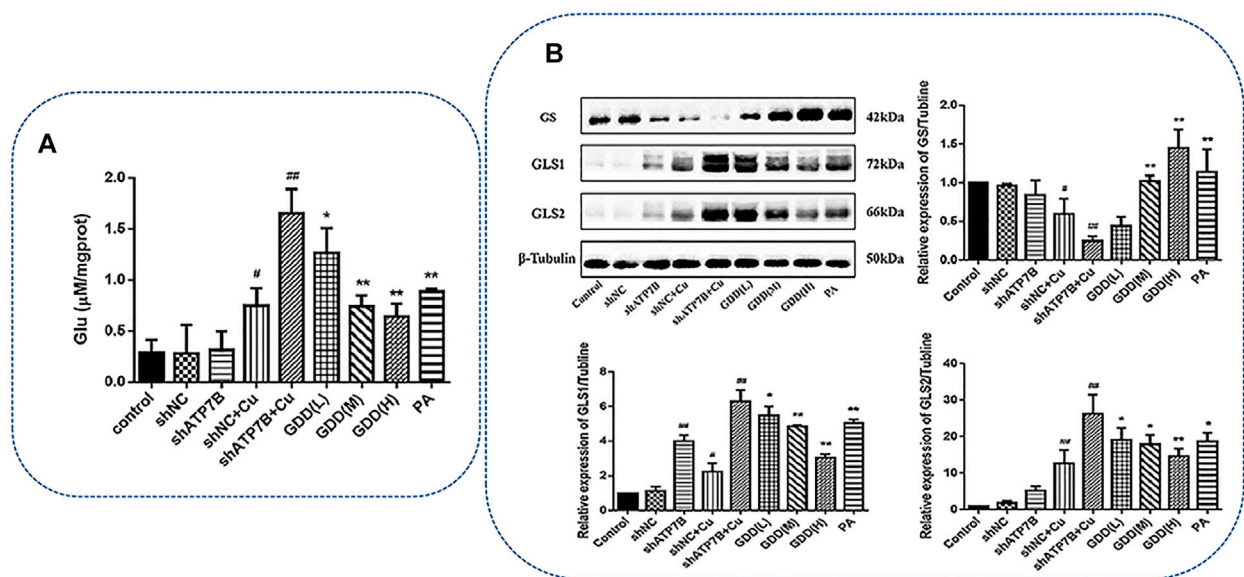


FIGURE 9 | (A) Effect of GDD on content of glutamate in copper-laden HLD hepatocytes ($\bar{x} \pm s, n = 3$) $^{\#}p < 0.05$, $^{##}p < 0.01$ compared with control group; $^{*}p < 0.05$, $^{**}p < 0.01$ compared with shATP7B + Cu group; **(B)** effects of GDD on GS, GLS1, and GLS2 expression in copper-laden HLD hepatocytes.

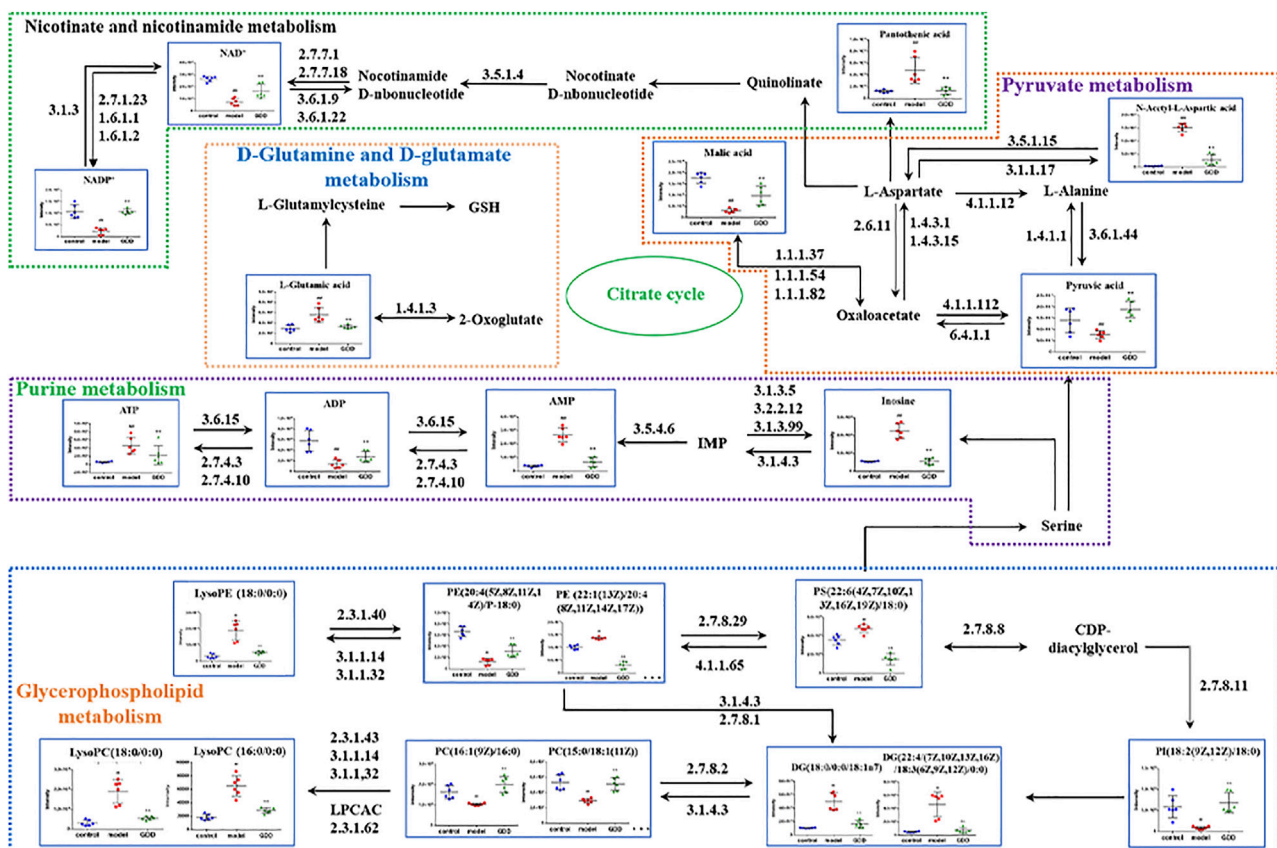


FIGURE 10 | Metabolic network diagram of potential biomarkers in copper-laden HLD hepatocytes by GDD.

with Cu^{2+} to reduce the toxicity of Cu^{2+} in hepatocytes and reduces the damage caused by copper-load to HLD hepatocytes.

It is well known that intracellular copper overload can generate the hydroxyl radicals in a Fenton reaction and promote oxidative stress, thereby causing cell injury (Boveris et al., 2012; Valko et al., 2016). Excess-free copper can also promote the generation of ROS in rat liver after acute and chronic exposure to the metal (Jiménez and Speisky, 2000). Intracellular accumulation of copper can also cause an increase in MDA content and LDH release and a decline in GSH/GSSG ratio in the cytosol, further altering mitochondrial morphology and aggravating cell damage (Jiménez et al., 2002; Mladenovic et al., 2014; Musacco-Sebio et al., 2014). SOD activity, MDA content, LDH release, and GSH/GSSG ratio are very important indices, which can reflect the capability of antioxidation (Kumar et al., 2016). The current study revealed that copper exposure significantly enhances ROS production and reduces ROS decomposition in the shATP7B + Cu group; MDA content and LDH release were also significantly increased in this group compared with the control, shNC, and shATP7B groups. In contrast, SOD activity and GSH/GSSG ratio were decreased after increasing copper loads. In addition, GDD could attenuate the oxidative stress induced by copper administration by increasing the SOD activity and GSH/GSSG ratio and decreasing ROS content, MDA content, and LDH release. The results demonstrated that GDD could effectively protect BRL-3A cells from copper-induced hepatic oxidative stress (**Figure 4**). Further study of the morphological and ultrastructural changes indicated that GDD could reduce injury in copper-laden HLD hepatocytes to varying degrees and has obvious protective effects (**Figure 3**).

To further explore the mechanism of GDD in HLD, cell metabolomics analysis was performed to study the functional metabolites of GDD in the copper-laden HLD hepatocytes. Metabolomic studies found that 47 biomarkers and 30 metabolic pathways are closely linked to the therapeutic effect of GDD on HLD, mainly including D-glutamine and D-glutamate metabolism; alanine, aspartic acid, and glutamic acid metabolism; and glycerophospholipid metabolism. The specific metabolic pathway is shown in **Figure 10**.

Glutamate is an important amino acid for organisms to maintain a normal physiological function. Glutamate participates in many metabolic processes such as amino acid and sugars metabolism and plays an important role in maintaining nitrogen balance in organisms (Kimball and Jefferson, 2006; Nie et al., 2018). GS and GLS are key enzymes in the glutamate biosynthesis pathway. GS catalyzes glutamate and ammonia to synthesize glutamine in the mammalian liver, which is the main energy source for tumor cells. In mouse and human livers, GS is limited to hepatocytes around hepatic venules. Changes in GS activity are associated with severe hepatic and neurodegenerative diseases, and the absence or malformation of GS can lead to death (Wasfy and Shams Eldeen, 2015; Moreira et al., 2017). GLS exists in mammalian cells in two isozymes, GLS1 (kidney type) and GLS2 (liver type) (Aledo et al., 2000). Some studies have reported that GLS2 is

converted to GLS1 in the process of hepatocellular carcinogenesis, and GLS1 was involved in the migration and invasion of hepatocellular carcinoma cells (Zhang et al., 2016). Both GLS1 and GLS2 regulate the antioxidant defense function of cells by increasing the level of GSH and decreasing the level of ROS, protecting cells from oxidative stress. Silencing the expression of GLS1 or inhibiting the activity of GLS1 can disturb this redox homeostasis (Chen et al., 2017; Li et al., 2019) of cancer cells. By evaluating the expression levels of GS, GLS1, and GLS2, the homeostasis of glutamate synthesis and metabolism in the body was measured. Once the homeostasis of glutamate synthesis and metabolism is destroyed, it will cause metabolic disorder, resulting in excessive accumulation of glutamate and consequent toxic effects (McKenna, 2007; Pang et al., 2020). The results showed that the glutamate level in copper-laden HLD hepatocytes was significantly higher than that in the shNC cells. An abnormal increase in glutamate activates the signaling pathway of downstream ROS, causing oxidative damage, and can eventually lead to the death of hepatocytes (Banday and Lejon, 2017). After GDD therapy, glutamate levels in cells tended to be normal, indicating that the protective effect of GDD on HLD may be associated with glutamate metabolism.

Glycerophospholipids are the most abundant phospholipids in organisms. Glycerophospholipids are a major component of the cell and organelle membrane. Furthermore, abnormal metabolism of the glycerophospholipid phosphatidylcholine (PC) is often closely associated with cancer, stroke, and neurodegenerative diseases, and its mechanism is relevant to the increase in stability and integrity of biofilms, reducing the cellular inflammatory response and oxidative stress (Janko et al., 2013). PC, as a substrate for phosphatidylserine (PS) synthesis, participates in acute inflammation (Su et al., 2013). Lysophosphatidylcholine (LPC) is a strong pro-inflammatory regulatory factor, which can stimulate phospholipase A2 through two signaling pathways, and leads to the release of arachidonic acid. Therefore, an irrepressible increase in the level of hemolytic phosphate choline may cause an inflammatory response and then lead to immune damage (Siskind, 2005). Phosphatidylethanolamine (PE) is associated with sustaining the normal structure and function of cells and is closely correlated with the growth, proliferation, and differentiation of cells; it is also an inducer of cellular apoptosis (Zhao and Wang, 2020). Its further hydrolysis will produce lysophosphatidylethanolamine (LPE) (Vance and Tasseva, 2013).

In this study, the metabolism of glycerophospholipid in copper-laden HLD hepatocytes was significantly altered. The level of intracellular phospholipid choline significantly decreased after CuSO_4 treatment, whereas the levels of PC, LPE, PE, and PS increased. Changes in these endogenous metabolites suggest that CuSO_4 can cause a disorder in glycerol phospholipid metabolism, consequently causing liver injury. In the GDD group, these altered metabolites showed varying degrees of callback trend, further indicating that GDD may improve the glycerophosphate metabolism disorder induced by CuSO_4 .

The primary metabolites associated with pyruvate metabolism identified in this study were pyruvate and malate. Pyruvate is the final product of glycolysis and is transported as the main fuel to the mitochondria. It drives ATP production through various biosynthesis pathways, including oxidative phosphorylation and cross-citric acid cycle, and plays an important role in energy metabolism. At the same time, pyruvate can effectively clear free radicals away in the body and play an antioxidant effect (Kao and Fink, 2010). Modern pharmacological studies have shown that pyruvic acid can alleviate organ damage (in organs such as the liver, heart, lung, kidney, and brain) mediated by redox reactions (Gray et al., 2014; Yang et al., 2016). As an intermediate of the tricarboxylic acid cycle, malate is a momentous organic acid produced in the process of cellular metabolism, which improves not only the ability of oxidative phosphorylation and energy metabolism but also the metabolism and antioxidation of liver tissues (Wu et al., 2007; Hikosaka et al., 2021). After CuSO₄ induction, the contents of pyruvate and malate in the shATP7B + Cu group were decreased compared with the shNC group. It is indicated that CuSO₄ may destroy the stability of the tricarboxylic acid cycle by affecting intermediate products, causing a disturbance in energy metabolism, and subsequently resulting in damage to hepatocytes. After GDD treatment, pyruvate and malate in cells tended to return to control-like levels, suggesting that the protective effect of GDD on copper-laden HLD hepatocytes may be associated with the regulation of energy metabolism.

In addition, nicotinamide adenine dinucleotide (NAD⁺) and its reduced form (NADH) and nicotinamide adenine dinucleotide phosphate (NADP⁺) and its reduced form (NADPH) are considered to be regulators of glycolysis and mitochondrial oxidative phosphorylation. Studies have shown that increasing NAD⁺ concentrations and increased levels of NAD⁺-dependent enzymes can treat certain metabolic disorders, such as obesity, alcoholic liver disease (Ding et al., 2017; Wang et al., 2018), and even hepatocellular carcinoma (Tummala et al., 2014). Deficiencies or imbalances in cellular NAD(H) and NADP(H) levels perturbed cellular redox state and metabolic homeostasis, leading to redox stress, energy stress, and ultimately diseased states (Ying, 2008; Huang et al., 2018). Compared with the shNC cells, copper-laden HLD hepatocytes showed significantly decreased levels of NAD⁺ and NADP⁺, whereas GDD-treated cells showed an increase in the levels of both metabolites. When cells are under oxidative stress, the AMP/ATP ratio increases (Emerling et al., 2009; Rato et al., 2014). However, studies have also found that during acute inflammation, intracellular ATP levels were abnormally elevated (Bodin and Burnstock, 1998). In this study, the level of ATP in copper-laden HLD hepatocytes increased, whereas the levels of AMP and ADP decreased, which may be because AMP and ADP were converted into ATP under cellular stress. After GDD intervention, the content of related metabolites tended to normal levels. Thus, it can be seen that high copper stimulation can lead to energy metabolism disorders in copper-laden HLD hepatocytes, and GDD may play a protective role by regulating energy metabolism.

In general, we studied the therapeutic mechanism of GDD in copper-laden HLD hepatocytes through cell metabolomics analysis and found 47 biomarkers that can provide new therapeutic targets for the prevention and treatment of HLD. We further provide references in the research of target pathways.

5 CONCLUSION

In this research, a copper-laden HLD hepatocyte model was established based on molecular biology techniques, and the mechanism of GDD in copper-laden HLD hepatocytes was investigated by a combination of pharmacological and cellular metabolomics analyses. The regulatory effect of GDD on glutamate–glutamine metabolism, glycerolipid metabolism, pyruvate metabolism, and other pathways at a metabolic level improved copper-laden HLD hepatocyte metabolism disorders and led to hepatocyte protection. Furthermore, GDD modulated the abnormal biosynthesis of glutamate, an important marker for GDD to correct copper-laden HLD hepatocyte metabolism disorders, by inhibiting GS and activating GLS. These findings provide a new strategy for exploring the protective effect of GDD on copper-laden HLD hepatocytes and provide a new therapeutic target for the prevention and treatment of HLD.

DATA AVAILABILITY STATEMENT

The original contributions presented in the study are included in the article/**Supplementary Material**, further inquiries can be directed to the corresponding authors.

AUTHOR CONTRIBUTIONS

AZ, FY, MN, and NW: conceptualization, methodology, validation, review, and editing. HFW, HW, WZ, SC, and PW: formal analysis, visualization, supervision, and resources. All authors interpreted the results and critically revised the manuscript for the scientific content. All authors approved the final version of the article.

FUNDING

This study was supported by the National Natural Science Foundation of China (nos. 81872976 and 82074385), Key Project of the National Science Fund of Anhui Province (no. KJ2021ZD0061), and Exploratory research project of Anhui University of Chinese Medicine (project no. 2020ZD04).

SUPPLEMENTARY MATERIAL

The Supplementary Material for this article can be found online at: <https://www.frontiersin.org/articles/10.3389/fphar.2022.848897/full#supplementary-material>

REFERENCES

- Ala, A., Walker, A. P., Ashkan, K., Dooley, J. S., and Schilsky, M. L. (2007). Wilson's Disease. *Lancet* 369 (9559), 397–408. doi:10.1016/S0140-6736(07)60196-2
- Aledo, J. C., Gómez-Fabre, P. M., Olalla, L., and Márquez, J. (2000). Identification of Two Human Glutaminase Loci and Tissue-specific Expression of the Two Related Genes. *Mamm. Genome* 11 (12), 1107–1110. doi:10.1007/s003350010190
- Banday, V. S., and Lejon, K. (2017). Elevated Systemic Glutamic Acid Level in the Non-obese Diabetic Mouse Is Idd Linked and Induces Beta Cell Apoptosis. *Immunology* 150 (2), 162–171. doi:10.1111/imm.12674
- Bandmann, O., Weiss, K. H., and Kaler, S. G. (2015). Wilson's Disease and Other Neurological Copper Disorders. *Lancet Neurol.* 14 (1), 103–113. doi:10.1016/S1474-4422(14)70190-5
- Bodin, P., and Burnstock, G. (1998). Increased Release of ATP from Endothelial Cells during Acute Inflammation. *Inflamm. Res.* 47 (8), 351–354. doi:10.1007/s000110050341
- Boveris, A., Musacco-Sebio, R., Ferrarotti, N., Saporito-Magriñá, C., Torti, H., Massot, F., et al. (2012). The Acute Toxicity of Iron and Copper: Biomolecule Oxidation and Oxidative Damage in Rat Liver. *J. Inorg. Biochem.* 116, 63–69. doi:10.1016/j.jinorgbio.2012.07.004
- Chang, C., Zhao, W., Luo, Y., Xi, L., Chen, S., Zhao, C., et al. (2017). Serine Peptidase Inhibitor Kazal Type I (SPINK1) Promotes BRL-3A Cell Proliferation via P38, ERK, and JNK Pathways. *Cell Biochem. Funct.* 35 (6), 339–348. doi:10.1002/cbf.3288
- Chen, G. Y., Chao, H. C., Liao, H. W., Tsai, I. L., and Kuo, C. H. (2017). Rapid Quantification of Glutaminase 2 (GLS2)-Related Metabolites by HILIC-MS/MS. *Anal. Biochem.* 539, 39–44. doi:10.1016/j.ab.2017.10.002
- Cheng, M., Wu, H., Wu, H., Liu, X., and Zhou, A. (2018). Metabolic Profiling of Copper-Laden Hepatolenticular Degeneration Model Rats and the Interventional Effects of Gandou Decoction Using UPLC-Q-TOF/MS. *J. Pharm. Biomed. Anal.* 164, 187–195. doi:10.1016/j.jpba.2018.10.041
- Chrysanthopoulos, P. K., Goudar, C. T., and Klapa, M. I. (2010). Metabolomics for High-Resolution Monitoring of the Cellular Physiological State in Cell Culture Engineering. *Metab. Eng.* 12 (3), 212–222. doi:10.1016/j.ymben.2009.11.001
- Cuperlović-Cul, M., Barnett, D. A., Cul, A. S., and Chute, I. (2010). Cell Culture Metabolomics: Applications and Future Directions. *Drug Discov. Today* 15 (15–16), 610–621. doi:10.1016/j.drudis.2010.06.012
- Cuykx, M., Negreira, N., Beirnaert, C., Van den Eede, N., Rodrigues, R., Vanhaecke, T., et al. (2017). Tailored Liquid Chromatography-Mass Spectrometry Analysis Improves the Coverage of the Intracellular Metabolome of HepaRG Cells. *J. Chromatogr. A* 1487, 168–178. doi:10.1016/j.chroma.2017.01.050
- Ding, R. B., Bao, J., and Deng, C. X. (2017). Emerging Roles of SIRT1 in Fatty Liver Diseases. *Int. J. Biol. Sci.* 13 (7), 852–867. doi:10.7150/ijbs.19370
- Duan, G., Zhang, G., Yuan, S., Ji, R., Zhang, L., and Ge, Y. (2019). A Pyrazolo[1,5-A] Pyridine-Based Ratiometric Fluorescent Probe for Sensing Cu²⁺ in Cell. *Spectrochim. Acta A. Mol. Biomol. Spectrosc.* 219, 173–178. doi:10.1016/j.saa.2019.04.057
- Emerling, B. M., Weinberg, F., Snyder, C., Burgess, Z., Mutlu, G. M., Viollet, B., et al. (2009). Hypoxic Activation of AMPK Is Dependent on Mitochondrial ROS but Independent of an Increase in AMP/ATP Ratio. *Free Radic. Biol. Med.* 46 (10), 1386–1391. doi:10.1016/j.freeradbiomed.2009.02.019
- González-Ruiz, V., Pezzatti, J., Roux, A., Stoppini, L., Boccard, J., and Rudaz, S. (2017). Unravelling the Effects of Multiple Experimental Factors in Metabolomics, Analysis of Human Neural Cells with Hydrophilic Interaction Liquid Chromatography Hyphenated to High Resolution Mass Spectrometry. *J. Chromatogr. A* 1527, 53–60. doi:10.1016/j.chroma.2017.10.055
- Gray, L. R., Tompkins, S. C., and Taylor, E. B. (2014). Regulation of Pyruvate Metabolism and Human Disease. *Cell Mol Life Sci.* 71 (14), 2577–2604. doi:10.1007/s00018-013-1539-2
- Hedera, P. (2017). Update on the Clinical Management of Wilson's Disease. *Appl. Clin. Genet.* 10, 9–19. doi:10.2147/TACG.S79121
- Hikosaka, K., Yaku, K., Okabe, K., and Nakagawa, T. (2021). Implications of NAD Metabolism in Pathophysiology and Therapeutics for Neurodegenerative Diseases. *Nutr. Neurosci.* 24 (5), 371–383. doi:10.1080/1028415X.2019.1637504
- Hu, W.-B., Yang, R.-M., Ren, M.-s., and Yang, G.-e. (2002). Observation of the Clinical Therapeutic Effect of Gandou Tablet I on Hepatolenticular Degeneration. *Cjim* 8 (1), 7–10. doi:10.1007/BF02934609
- Hu, X., Zhou, C., He, G., Cheng, Y., Pan, M., and Gao, Y. (2020). Inhibition of Frizzled-2 by Small Interfering RNA Protects Rat Hepatic BRL-3A Cells against Cytotoxicity and Apoptosis Induced by Hypoxia/Reoxygenation. *Gastroenterol. Hepatol.* 43 (3), 107–116. doi:10.1016/j.gastrohep.2019.02.006
- Huang, Q., Sun, M., Li, M., Zhang, D., Han, F., Wu, J. C., et al. (2018). Combination of NAD⁺ and NADPH Offers Greater Neuroprotection in Ischemic Stroke Models by Relieving Metabolic Stress. *Mol. Neurobiol.* 55 (7), 6063–6075. doi:10.1007/s12035-017-0809-7
- Ivanisevic, J., Zhu, Z. J., Plate, L., Tautenhahn, R., Chen, S., O'Brien, P. J., et al. (2013). Toward 'omic Scale Metabolite Profiling: a Dual Separation-Mass Spectrometry Approach for Coverage of Lipid and central Carbon Metabolism. *Anal. Chem.* 85 (14), 6876–6884. doi:10.1021/ac401140h
- Janko, C., Jeremic, I., Biermann, M., Chaurio, R., Schorn, C., Muñoz, L. E., et al. (2013). Cooperative Binding of Annexin A5 to Phosphatidylserine on Apoptotic Cell Membranes. *Phys. Biol.* 10 (6), 065006. doi:10.1088/1478-3975/10/6/065006
- Jiménez, I., and Speisky, H. (2000). Effects of Copper Ions on the Free Radical-Scavenging Properties of Reduced Glutathione: Implications of a Complex Formation. *J. Trace Elem. Med. Biol.* 14 (3), 161–167. doi:10.1016/S0946-672X(00)80005-X
- Jiménez, I., Aracena, P., Letelier, M. E., Navarro, P., and Speisky, H. (2002). Chronic Exposure of HepG2 Cells to Excess Copper Results in Depletion of Glutathione and Induction of Metallothionein. *Toxicol. Vitro* 16 (2), 167–175. doi:10.1016/S0887-2333(01)00117-5
- Kao, K. K., and Fink, M. P. (2010). The Biochemical Basis for the Anti-inflammatory and Cytoprotective Actions of Ethyl Pyruvate and Related Compounds. *Biochem. Pharmacol.* 80 (2), 151–159. doi:10.1016/j.bcp.2010.03.007
- Kimball, S. R., and Jefferson, L. S. (2006). Signaling Pathways and Molecular Mechanisms through Which Branched-Chain Amino Acids Mediate Translational Control of Protein Synthesis. *J. Nutr.* 136 (1 Suppl. 1), 227S–31S. doi:10.1093/jn/136.1.227S
- Kumar, V., Kalita, J., Bora, H. K., and Misra, U. K. (2016). Relationship of Antioxidant and Oxidative Stress Markers in Different Organs Following Copper Toxicity in a Rat Model. *Toxicol. Appl. Pharmacol.* 293, 37–43. doi:10.1016/j.taap.2016.01.007
- Li, W. J., Wang, J. F., and Wang, X. P. (2013). Wilson's Disease: Update on Integrated Chinese and Western Medicine. *Chin. J. Integr. Med.* 19 (3), 233–240. doi:10.1007/s11655-012-1089-8
- Li, L., He, M., Xiao, H., Liu, X., Wang, K., and Zhang, Y. (2018a). Acetic Acid Influences BRL-3A Cell Lipid Metabolism via the AMPK Signalling Pathway. *Cell Physiol Biochem* 45 (5), 2021–2030. doi:10.1159/000487980
- Li, L., Zhao, J., Ge, C., Yu, L., and Ma, H. (2018b). Dehydroepiandrosterone Rehabilitate BRL-3A Cells Oxidative Stress Damage Induced by Hydrogen Peroxide. *J. Cel Physiol* 233 (8), 6262–6272. doi:10.1002/jcp.26458
- Li, B., Cao, Y., Meng, G., Qian, L., Xu, T., Yan, C., et al. (2019). Targeting Glutaminase 1 Attenuates Stemness Properties in Hepatocellular Carcinoma by Increasing Reactive Oxygen Species and Suppressing Wnt/beta-Catenin Pathway. *EBioMedicine* 39, 239–254. doi:10.1016/j.ebiom.2018.11.063
- Liu, L. L., Tang, Q. Q., and Zhu, Y. C. (2016). Effect of Mini Ad-ATP7B-GFP on the Copper Metabolism of Skin Fibroblasts of Wilson's Disease Patients. *Chin. J. Neurol.* 49 (2), 102–107. (In Chinese).
- Liu, J., Luan, J., Zhou, X., Cui, Y., and Han, J. (2017). Epidemiology, Diagnosis, and Treatment of Wilson's Disease. *Intractable Rare Dis. Res.* 6 (4), 249–255. doi:10.5582/irdr.2017.01057
- Liu, H., Lai, W., Liu, X., Yang, H., Fang, Y., Tian, L., et al. (2021). Exposure to Copper Oxide Nanoparticles Triggers Oxidative Stress and Endoplasmic Reticulum (ER)-stress Induced Toxicology and Apoptosis in Male Rat Liver and BRL-3A Cell. *J. Hazard. Mater.* 401, 123349. doi:10.1016/j.jhazmat.2020.123349
- Luo, W., Li, L., Xu, W., Zhang, J., and Xu, J. (2021). Toxic Effects of Docosahexaenoic Acid Treatment in the Rat Liver BRL-3A Cell. *Toxics* 9 (5), 112. doi:10.3390/toxics9050112

- Ma, S., Wang, F., Zhang, C., Wang, X., Wang, X., and Yu, Z. (2020). Cell Metabolomics to Study the Function Mechanism of *Cyperus Rotundus* L. On Triple-Negative Breast Cancer Cells. *BMC Complement. Med. Ther.* 20 (1), 262. doi:10.1186/s12906-020-02981-w
- McKenna, M. C. (2007). The Glutamate-Glutamine Cycle Is Not Stoichiometric: Fates of Glutamate in Brain. *J. Neurosci. Res.* 85 (15), 3347–3358. doi:10.1002/jnr.21444
- Mladenovic, J., Paunovic, M., Matic, M., Knezevic, V., Ognjanovic, B., Stajin, A., et al. (2014). Copper-induced Changes of Lipid Peroxidation and Hemato-Biochemical Parameters in Rat Blood: Protective Role of Flavonoids. *Arch. Biol. Sci. Belgra* 66 (3), 1271–1279. doi:10.2298/ABS1403271M
- Moreira, C., Ramos, M. J., and Fernandes, P. A. (2017). Clarifying the Catalytic Mechanism of Human Glutamine Synthetase: a QM/MM Study. *J. Phys. Chem. B* 121 (26), 6313–6320. doi:10.1021/acs.jpbc.7b02543
- Musacco-Sebio, R., Saporito-Magriñá, C., Semprine, J., Torti, H., Ferrarotti, N., Castro-Parodi, M., et al. (2014). Rat Liver Antioxidant Response to Iron and Copper Overloads. *J. Inorg. Biochem.* 137, 94–100. doi:10.1016/j.jinorgbio.2014.04.014
- Nie, C., He, T., Zhang, W., Zhang, G., and Ma, X. (2018). Branched Chain Amino Acids: Beyond Nutrition Metabolism. *Int. J. Mol. Sci.* 19 (4), 954. doi:10.3390/ijms19040954
- Pang, Y. Y., Zhou, Y. Z., Song, J., Du, G. H., and Qin, X. M. (2020). Anti-aging Effect of *Scutellaria Baicalensis* Georgi Leaves Based on ^1H NMR Serum and Liver Metabolomics. *Acta Pharm. Sin* 55 (1), 74–82. (In Chinese). doi:10.16438/j.0513-4870.2019-0377
- Rato, L., Duarte, A. I., Tomás, G. D., Santos, M. S., Moreira, P. I., Socorro, S., et al. (2014). Pre-diabetes Alters Testicular PGC1- α /SIRT3 axis Modulating Mitochondrial Bioenergetics and Oxidative Stress. *Biochim. Biophys. Acta* 1837 (3), 335–344. doi:10.1016/j.bbabi.2013.12.008
- Siskind, L. J. (2005). Mitochondrial Ceramide and the Induction of Apoptosis. *J. Bioenerg. Biomembr.* 37 (3), 143–153. doi:10.1007/s10863-005-6567-7
- Su, X., Wang, H., Zhu, L., Zhao, J., Pan, H., and Ji, X. (2013). Ethyl Pyruvate Ameliorates Intracerebral Hemorrhage-Induced Brain Injury through Anti-cell Death and Anti-inflammatory Mechanisms. *Neuroscience* 245, 99–108. doi:10.1016/j.neuroscience.2013.04.032
- Sun, H., Zhang, A. H., Liu, S. B., Qiu, S., Li, X. N., Zhang, T. L., et al. (2018). Cell Metabolomics Identify Regulatory Pathways and Targets of Magnoline against Prostate Cancer. *J. Chromatogr. B Anal. Technol. Biomed. Life Sci.* 1102–1103, 143–151. doi:10.1016/j.jchromb.2018.10.017
- Tanzi, R. E., Petrukhin, K., Chernov, I., Pellequer, J. L., Wasco, W., Ross, B., et al. (1993). The Wilson Disease Gene Is a Copper Transporting ATPase with Homology to the Menkes Disease Gene. *Nat. Genet.* 5 (4), 344–350. doi:10.1038/ng1293-344
- Terada, K., Schilsky, M. L., Miura, N., and Sugiyama, T. (1998). ATP7B (WND) Protein. *Int. J. Biochem. Cel Biol.* 30 (10), 1063–1067. doi:10.1016/s1357-2725(98)00073-9
- Tummala, K. S., Gomes, A. L., Yilmaz, M., Graña, O., Bakiri, L., Ruppen, I., et al. (2014). Inhibition of de novo NAD(+) Synthesis by Oncogenic URI Causes Liver Tumorigenesis through DNA Damage. *Cancer cell* 26 (6), 826–839. doi:10.1016/j.ccell.2014.10.002
- Valko, M., Jomova, K., Rhodes, C. J., Kuča, K., and Musilek, K. (2016). Redox- and Non-Redox-metal-induced Formation of Free Radicals and Their Role in Human Disease. *Arch. Toxicol.* 90 (1), 1–37. doi:10.1007/s00204-015-1579-5
- Vance, J. E., and Tasseva, G. (2013). Formation and Function of Phosphatidylserine and Phosphatidylethanolamine in Mammalian Cells. *Biochim. Biophys. Acta* 1831 (3), 543–554. doi:10.1016/j.bbalip.2012.08.016
- Wang, Y., Xie, C. L., Fu, D. L., Lu, L., Lin, Y., Dong, Q. Q., et al. (2012). Clinical Efficacy and Safety of Chinese Herbal Medicine for Wilson's Disease: a Systematic Review of 9 Randomized Controlled Trials. *Complement. Ther. Med.* 20 (3), 143–154. doi:10.1016/j.ctim.2011.12.004
- Wang, S., Wan, T., Ye, M., Qiu, Y., Pei, L., Jiang, R., et al. (2018). Nicotinamide Riboside Attenuates Alcohol Induced Liver Injuries via Activation of SirT1/PGC-1 α /Mitochondrial Biosynthesis Pathway. *Redox Biol.* 17, 89–98. doi:10.1016/j.redox.2018.04.006
- Wang, N., Cheng, M., Zhang, X., Wu, H., Wu, H., Cao, S., et al. (2020). Gandou Decoction Decreases Copper Levels and Alleviates Hepatic Injury in Copper-Laden Hepatolenticular Degeneration Model Rats. *Front. Pharmacol.* 11, 582390. doi:10.3389/fphar.2020.582390
- Wasfy, R. E., and Shams Eldeen, A. A. (2015). Roles of Combined Glypican-3 and Glutamine Synthetase in Differential Diagnosis of Hepatocellular Lesions. *Asian Pac. J. Cancer Prev.* 16 (11), 4769–4775. doi:10.7314/apjcp.2015.16.11.4769
- Wu, J. L., Wu, Q. P., and Zhang, J. M. (2007). Effects of L-Malate on Activities of Transferases in Different Tissues of Aged Rats. *Food Sci.* 28 (10), 507–510. (In Chinese).
- Wu, H., Wang, L., Zhan, X., Wang, B., Wu, J., and Zhou, A. (2020). A UPLC-Q-TOF/MS-based Plasma Metabolomics Approach Reveals the Mechanism of Compound Kushen Injection-Based Intervention against Non-small Cell Lung Cancer in Lewis Tumor-Bearing Mice. *Phytomedicine* 76, 153259. doi:10.1016/j.phymed.2020.153259
- Xu, G. C., Chen, H. Z., Zhang, J., Fang, X., Li, J., Ge, Q., et al. (2012). Observation of Gandou Decoction in Increasing 24h Urinary Copper Excretion and Improvement in the Treatment of Hepatolenticular Degeneration. *Clin. J. Tradit. Chin. Med.* 24 (11), 1055–1057. (In Chinese). doi:10.16448/j.cjctm.2012.11.041
- Xu, L., Liu, Y., Wu, H., Wu, H., Liu, X., and Zhou, A. (2019). Rapid Identification of Chemical Profile in Gandou Decoction by UPLC-Q-TOF-MSE Coupled with Novel Informatics UNIFI Platform. *J. Pharm. Anal.* 10 (1), 35–48. doi:10.1016/j.jpah.2019.05.003
- Xu, L., Liu, Y., Wu, H., and Zhou, A. (2020). Rapid Identification of Absorbed Components and Metabolites of Gandou Decoction in Rat Plasma and Liver by UPLC-Q-TOF-MSE. *J. Chromatogr. B Anal. Technol. Biomed. Life Sci.* 1137, 121934. doi:10.1016/j.jchromb.2019.121934
- Xu, R., Liang, J., Cheng, M., Wu, H., Wu, H., Cao, S., et al. (2021). Liver and Urine Metabolomics Reveal the Protective Effect of Gandou Decoction in Copper-Laden Hepatolenticular Degeneration Model Rats. *J. Chromatogr. B* 1179, 122844. doi:10.1016/j.jchromb.2021.122844
- Xue, B. C., Yang, R. M., Hu, J. Y., Han, Y. Z., and Wang, J. H. (2007). Effect of Gandou Decoction IV Combined with Short-Term Decoppering Therapy with Sodium Dimercapto-Sulphonate on Serum Indexes of Hepatic Fibrosis in Patients with Wilson's Disease. *Zhongguo Zhong Xi Yi Jie He Za Zhi* 27 (9), 785–788. (In Chinese).
- Yang, R. M., and Cheng, N. (2002). Observation on Short-Term Effect and Follow-Up of Integrative Medicine in Treating 198 Patients with Hepatolenticular Degeneration. *Chin. J. Integr. Tradit. West. Med.* 22 (9), 657–659. (In Chinese). doi:10.1007/bf02934410
- Yang, R., Zhu, S., and Tonnessen, T. I. (2016). Ethyl Pyruvate Is a Novel Anti-inflammatory Agent to Treat Multiple Inflammatory Organ Injuries. *J. Inflamm. (Lond)* 13, 37. doi:10.1186/s12950-016-0144-1
- Yang, Q., Zhang, A.-h., Miao, J.-h., Sun, H., Han, Y., Yan, G.-l., et al. (2019). Metabolomics Biotechnology, Applications, and Future Trends: a Systematic Review. *RSC Adv.* 9, 37245–37257. doi:10.1039/C9RA06697G
- Yang, W., Liu, R., Xia, C., Chen, Y., Dong, Z., Huang, B., et al. (2020). Effects of Different Fatty Acids on BRL3A Rat Liver Cell Damage. *J. Cel Physiol* 235 (9), 6246–6256. doi:10.1002/jcp.29553
- Ye, B., Yin, L., Wang, Q., and Xu, C. (2019). ACC1 Is Overexpressed in Liver Cancers and Contributes to the Proliferation of Human Hepatoma Hep G2 Cells and the Rat Liver Cell Line BRL 3A. *Mol. Med. Rep.* 19 (5), 3431–3440. doi:10.3892/mmr.2019.9994
- Ying, W. (2008). NAD $^+$ /NADH and NADP $^+$ /NADPH in Cellular Functions and Cell Death: Regulation and Biological Consequences. *Antioxid. Redox Signal.* 10 (2), 179–206. doi:10.1089/ars.2007.1672
- Zhang, C., Liu, J., Zhao, Y., Yue, X., Zhu, Y., Wang, X., et al. (2016). Glutaminase 2 Is a Novel Negative Regulator of Small GTPase Rac1 and Mediates P53 Function in Suppressing Metastasis. *eLife* 5, e10727. doi:10.7554/eLife.10727
- Zhang, M., Liu, Y., Liu, M., Liu, B., Li, N., Dong, X., et al. (2019). UHPLC-QTOF/MS-based Metabolomics Investigation for the Protective Mechanism of Danshen in Alzheimer's Disease Cell Model Induced by A β 1-42. *Metabolomics* 15 (2), 13. doi:10.1007/s11306-019-1473-x
- Zhang, X. Y., Liu, Y., Wu, H., Cao, S. J., Wu, P., and Zhou, A. (2020). Identification of Major Bioactive Components and Metabolites of Gandou Decoction in Rat Urine by an Integrative Approach Based on UPLC-Q-TOF-MS E Coupled with Xenometabolomics Analytical Platform. *Acta Pharm. Sin* 55 (5), 217–224. (In Chinese). doi:10.16438/j.0513-4870.2019-0796

Zhao, H., and Wang, T. (2020). PE Homeostasis Rebalanced through Mitochondria-ER Lipid Exchange Prevents Retinal Degeneration in *Drosophila*. *Plos Genet.* 16 (10), e1009070. doi:10.1371/journal.pgen.1009070

Conflict of Interest: The authors declare that the research was conducted in the absence of any commercial or financial relationships that could be construed as a potential conflict of interest.

Publisher's Note: All claims expressed in this article are solely those of the authors and do not necessarily represent those of their affiliated organizations or those of

the publisher, the editors, and the reviewers. Any product that may be evaluated in this article, or claim that may be made by its manufacturer, is not guaranteed or endorsed by the publisher.

Copyright © 2022 Yin, Nian, Wang, Wu, Wu, Zhao, Cao, Wu and Zhou. This is an open-access article distributed under the terms of the Creative Commons Attribution License (CC BY). The use, distribution or reproduction in other forums is permitted, provided the original author(s) and the copyright owner(s) are credited and that the original publication in this journal is cited, in accordance with accepted academic practice. No use, distribution or reproduction is permitted which does not comply with these terms.

GLOSSARY

AAS atomic absorption spectrometry

ANOVA one-way analysis of variance

BPI Base Peak Intensity

Cu²⁺ copper ion

CV cell viability

DAPI 4' 6-diamidino-2-phenylindole

DCFH-DA dichlorodihydrofluorescein

GDD Gandou decoction

GLS glutaminase

GS glutamine synthetase

GSH glutathione

GSSH oxidized glutathione

HILIC hydrophilic interaction liquid chromatography

HLD hepatolenticular degeneration

HRP horseradish peroxidase

LDH lactate dehydrogenase

LSD least significant difference

MDA Lipid peroxidation

MTT 3-[4,5dimethyl(thiozol-2-yl)]-2,5-diphenyltetradinmbromide

NC negative control

OD optical density

OPLS-DA orthogonal partial least square discriminant analysis

PA penicillamine

PAGE polyacrylamide gel electrophoresis

PCA principal component analysis

QC quality control

qPCR Real-Time PCR

ROS reactive oxygen species

RP reversed-phase

SDS sodium dodecyl sulfate

shRNA short hairpin RNA

SOD superoxide dismutase

TCM traditional Chinese medicine

TEM transmission electron microscope

UPLC-Q-TOF/MS Ultra-performance liquid chromatography quadrupole time of flight mass spectrometry

VIP variable important in the projection



Integrated Metabolomics and Network Pharmacology Analysis Immunomodulatory Mechanisms of Qifenggubiao Granules

Bindan Guo[†], Wenting Dong[†], Jinhai Huo, Guodong Sun, Zhiwei Qin, Xiaodong Liu, Bihai Zhang* and Weiming Wang*

Institute of Chinese Materia Medica, Heilongjiang Academy of Chinese Medicine Sciences, Harbin, China

OPEN ACCESS

Edited by:

Xijun Wang,
Heilongjiang University of Chinese
Medicine, China

Reviewed by:

Xianju Huang,
South-Central University for
Nationalities, China
Aihua Zhang,
Heilongjiang University of Chinese
Medicine, China

*Correspondence:

Bihai Zhang
laotou421@126.com
Weiming Wang
zyjy@163.com

[†]These authors have contributed
equally to this work

Specialty section:

This article was submitted to
Ethnopharmacology,
a section of the journal
Frontiers in Pharmacology

Received: 03 December 2021

Accepted: 07 March 2022

Published: 05 April 2022

Citation:

Guo B, Dong W, Huo J, Sun G, Qin Z,
Liu X, Zhang B and Wang W (2022)
Integrated Metabolomics and Network
Pharmacology Analysis
Immunomodulatory Mechanisms of
Qifenggubiao Granules.
Front. Pharmacol. 13:828175.
doi: 10.3389/fphar.2022.828175

Background: Qifenggubiao granules (QFGBG) is a new Chinese medicine independently developed by Heilongjiang Academy of Traditional Chinese Medicine, which combines the essence of Yupingfeng powder and Shengmai yin (invention patent number: CN1325098C, approval number: Sinopharm Zhunzi B20020410), and has been included in the 2020 edition of Chinese Pharmacopoeia. It has remarkable pharmacodynamic results and conclusive clinical effects in the treatment of allergic rhinitis, chronic cough and other diseases. Previous pharmacological studies have shown that it has immunomodulatory effect, but its immunomodulatory mechanism is still unclear.

Methods: In this study, cyclophosphamide (CTX) was used to establish the immune hypofunction model in mice, and the weight change, index of immune organs in spleen and thymus, pathological sections of immune organs and inflammatory factors were used to evaluate the model. Based on the metabolic biomarkers obtained by metabolomics technology, the potential targets of Qifeng Gubiao Granule immunomodulation were obtained by integrating the targets of blood components, metabolites and diseases through network pharmacology. Meanwhile, GO enrichment analysis and KEGG pathway analysis were carried out on the potential targets.

Results: QFGBG can increase body weight and organ index, and recover immune organ damage caused by CP. Metabolomics identified 13 metabolites with significant changes, among which the level of phospholipid (PC) metabolites decreased significantly in the model group. Sphingosine -1- phosphate, 1- palmitoyl phosphatidylcholine [LysoPC (16: 0/0:0)] and other metabolites were significantly increased in the model group, and 98 targets of Qifeng's external immune regulation were obtained by intersecting 629 component targets, 202 metabolite targets and 1916 disease targets. KEGG pathway analysis obtained 233 related metabolic pathways, and the top 20 metabolic pathways mainly involved IL-17 signaling pathway, TNF signaling pathway, Sphingolipid signaling pathway, and so on.

Conclusion: QFGBG may act on AKT1, IL6, MAPK3, PTGS2, CASP3, MAPK1, ESR1, PPARG, HSP90AA1, PPARG and other targets, acting through Sphingolipid signaling

pathway and signaling pathway. Combined with pharmacodynamic evaluation, the immunomodulatory effect of QFGBG was confirmed, and the immunomodulatory mechanism of QFGBG with multiple targets and multiple pathways was preliminarily clarified.

Keywords: Qifenggubiao granules, metabonomics, network pharmacology, cyclophosphamide, immunosuppression

INTRODUCTION

Qifenggubiao granules (QFGBG) is a new Chinese medicine independently developed by Heilongjiang Academy of Traditional Chinese Medicine (invention patent number: CN 1325098C, approval number: Sinopharm Zhunzi B20020410), which is included in Chinese Pharmacopoeia in 2020 edition, and is composed of six medicinal herbs: *Astragalus mongholicus* Bunge (Fabaceae), *Eleutherococcus senticosus* (Rupr. & Maxim.) Maxim (Araliaceae), *Atractylodes macrocephala* Koidz (Asteraceae), *Saposhnikovia divaricata* (Turcz. ex Ledeb.) Schischk (Apiaceae), *Ophiopogon japonicus* (Thunb.) Ker Gawl (Asparagaceae), and *Schisandra chinensis* (Turcz.) Baill (Schisandraceae), with a ration of 6:3:2:2:2:1. It combines the essence of Yupingfeng powder and Shengmai Yin, and replaces *Panax ginseng* C.A.Mey (Araliaceae) with Heilongjiang genuine medicinal material *Eleutherococcus senticosus* (Rupr. & Maxim.) Maxim (Araliaceae), which has the effects of tonifying lung and kidney and invigorating spleen, and is included in the 2020 edition of Chinese Pharmacopoeia (Edited by National Pharma, 2015). It mainly contains flavonoids, organic acids, polysaccharides and other components, all of which have immunoregulatory effects (Dandan et al., 2020; Ran et al., 2020), Modern pharmacological studies preliminarily show that it can improve the body immunity through improve the phagocytic function of macrophages and increase the formation rate of erythrocyte C_{3b} receptor garland (Weiming and Shuming, 2005), and restore the immune balance of allergic rhinitis (AR) rats (Tianshuai et al., 2021), but its immune regulation mechanism has not been reported yet.

In order to study the immunomodulatory mechanism of QFGBG, cyclophosphamide (CTX) was used to establish a mouse model of hyp immunity. CP is an alkylating agent, which can destroy immune cells, interfere with the proliferation and differentiation of T and B cells, reduce the number of normal T and B cells, and inhibit cellular and humoral immune responses (Xie et al., 2015). Because of its strong immunosuppressive effect on immune-related cells (Yunbo, 2013), the immunosuppressive mouse model induced by CP has been used as a valuable tool to detect the good immunoprotective efficacy of natural compounds (Kim et al., 1211; Yoo et al., 2020).

Metabonomics studies the human body as a complete system, which has the characteristics of wholeness, dynamics, non-trauma, close to physiology, etc. It is very similar to the principle of wholeness and dynamics of traditional Chinese medicine, and provides a new and powerful technical means for traditional Chinese medicine research (Shan et al., 2015).

Network pharmacology is based on the interaction between “disease-gene-target-drug,” and constructs the related network from the perspective of biological system, explores the pathogenesis and course development of diseases, and reveals the interaction between various targets of drugs in the body, which is beneficial to the multi-level exploration of the action mechanism of active compounds of traditional Chinese medicine (Bing et al., 2017). The research methods of metabonomics and network pharmacology based on the holistic view are consistent with the systematic view advocated by traditional Chinese medicine research, so they are especially suitable for studying the action mechanism of complex systems of traditional Chinese medicine (Li et al., 2021).

This study will combine metabonomics and network pharmacology methods, metabonomics identifies potential biomarkers, and at the same time, network pharmacology is used to find biomarker targets and correlate component targets and disease targets, Narrow the target range of QFGBG immunomodulation, and provide technical support for the follow-up research.

MATERIALS AND METHODS

Experimental Instruments and Reagents

QFGBG (Produced by Pharmaceutical Factory of Heilongjiang Institute of Traditional Chinese Medicine, batch number: 07210501, which meets the standards on pages 979–980 of Chinese Pharmacopoeia I, 2020), Cyclophosphamide injection (jiangsu hengrui Pharmaceutical Co., Ltd.; batch number: 20092225), Levamisole hydrochloride tablets (Renhetang Pharmaceutical Co., Ltd.; batch number: 201001), Watsons water, Formic acid (Fisher Company), Acetonitrile and methanol (Merck, Germany), UltraSYBR One Step RT-qPCR Kit (CW0659, CoWin Biosciences, China), themouse serum IL-4 (EK0405), IFN- γ (EK0375) ELISA kit (Boster, China), Mouse ACTB Endogenous Reference Genes Primers, 10 μ M (B661302-0001, Sangon Biotech, China).

Nitrogen generator (Hangzhou Dacker, DFNW-5LB), Cryogenic centrifuge (Thermofisher, 17R), Upright white photo microscope (Nikon Japan, Eclipse Ci-L), Scanning software (3 dhistech Hungary, CaseViewer2.4), Panoramic slice scanner (3DHISTECH Hungary, PANNORAMIC, DESK/MIDI/250/1000), Ultra-high performance liquid chromatograph (AB Sciex ExionLC AD, United States), Mass spectrometer (AB SCIEX Triple-TOFTM 5600+, United States), Infinite M200 PRO (Tecan, Switzerland), Bioer Line gene 9600 fluorescence Quantitative PCR instrument (Hangzhou Bioeri, China).

Animal Experiment

There are 90 male ICR mice (about 26 g) with animal certificate number SCXK (Liao) 2020-0001, which are provided by Liaoning Changsheng Biotechnology Co., Ltd. The study was conducted strictly according to the ethical guidelines for using experimental animals in Heilongjiang province, guided and approved by the animal ethics committee of the academy of traditional Chinese medicine of Heilongjiang province [(2011)93]. Adaptive feeding for 7 days, ICR mice were randomly divided into 6 groups, with 15 mice in each group, they are normal control (NC), model control (MC), QFGBG low-dose(L), QFGBG medium-dose(M), QFGBG high-dose(H) and positive control levamisole hydrochloride (PC). NC group administered normal saline as well as MC, low-dose group administered QFGBG (13 g/kg), medium-dose group administered QFGBG (26 g/kg), and high-dose group administered QFGBG (52 g/kg). positive control administered levamisole hydrochloride (25 mg/kg). On the 8th day, mice in each group except the blank group were injected with CP 80 mg/kg intraperitoneally for three consecutive days, From the 11 days, each group was given corresponding doses of drugs, 15 consecutive days.

Mice in each group fasted for 12 h after the last administration time, The mice were weighed before modeling and after the experiment, and the weight changes of mice in each group were measured. and whole blood was collected, Approximately 1 mL of whole blood was collected, The serum was obtained through centrifuged at 3000 rpm and 4°C for 15 min, the spleen and thymus of each group of mice were collected and weighed, And then fixed with 4% neutral formaldehyde. The liver tissue was washed and frozen.

Pharmacodynamic Evaluation

The fixed spleen and thymus organs were washed with distilled water and dehydrated with ethanol gradient. Xylene was transparently treated twice, soaked in wax, and embedded in a paraffin embedding machine. The embedded tissue was fixed on a microtome for sectioning and placed on a clean carrier. On the glass slides, the slides are dried in a 60°C constant temperature oven, and then dewaxed, HE stained, dehydrated, and finally sealed with neutral gum.

Biochemical Index Detection

After the mouse serum was thawed, it was centrifuged at 3000 rpm for 10 min. The supernatant was taken for ELISA detection, and a microplate reader was used for detection.

Metabonomics Sample Preparation

Serum samples were thawed at 4°C before preparation. 100 µL serum samples were diluted with 300 µL methanol (precooled at 4°C), swirl at 2500 rpm for 1.5 min, Centrifuge at 4°C and 13000 rpm for 10 min blow dry the supernatant with nitrogen, and freeze at -80°C. Before running on the machine, 150 µL of 80% methanol (precooled at 4°C) was re-dissolved, and centrifuged at 4°C 13000 rpm at 4°C for 10 min. The supernatant was taken and put into the inner liner tube, and the liquid was sampled. 10 µL of serum was drawn from all samples, which were mixed and used as QC samples. QC

samples were tested every 5 samples to evaluate the stability of the system.

UPLC-Q-TOF-MS Conditions

The Waters Acquity UPLC BEH C18 column (100 mm × 2.1 mm, 1.7 µm), aquityupl-cbeh C18 vanguard pre-column (100 mm × 2.1 mm, 1.7 µm), the column temperature is 35°C, and the mobile phase is 0.1% formic acid solution (A) -0.1% formic acid acetonitrile (B). 2–5 min, 60–40% B, 5–11 min, 30–70% B, 11–13 min, 10–90% B, 13–14 min, 100% B, 14.1–17 min, 95–5% B.

ESI ion source is used, ionization mode is positive and negative ion mode, ion source voltage is 5500 V, ion source temperature is 550°C, cracking voltage is 80 V, collision energy is 40 V, CES is 20 eV, atomizing gas is N₂, auxiliary gas and atomizing auxiliary gas are both 55 PSI, air curtain gas is 35 PSI, and scanning range of sub-ions is 80–1600 Da. Eight peaks with IDA response value exceeding 100 cps were set for secondary mass spectrometry scanning, and the scanning range of Product-Ion was 80–1600 Da, and dynamic background subtraction was started. The data acquisition software is Analyst TF 1.6 software, and the image processing system is Peakview 2.0.

ESI ion source is used, ionization mode is positive and negative ion mode, ion source voltage is 5500 V, ion source temperature is 550°C, cracking voltage is 80 V, collision energy is 40 V, CES is 20 eV, atomizing gas is N₂, auxiliary gas and atomizing auxiliary gas are both 55 PSI, air curtain gas is 35 PSI, and scanning range of sub-ions is 80–1600 Da. Eight peaks with IDA response value exceeding 100 cps were set for secondary mass spectrometry scanning, and the scanning range of Product-Ion was 80–1600 Da, and dynamic background subtraction was started. The data acquisition software is Analyst TF 1.6 software, and the image processing system is Peakview 2.0.

Network Pharmacology Research

Blood Components and Disease Target Prediction

Enter the SMILE format of blood component (Dandan et al., 2021) into Swiss target prediction database (<http://www.swisstargetprediction.ch/>). The target of the final composition is obtained after removing the duplicate target from the Database. The Online Mendelian Inheritance in Man (OMIM, <https://omim.org/>), The TTD (<http://db.idrblab.net/ttd/>), the database (TTD, <http://db.idrblab.net/ttd/>), Drug and Target Database (<https://go.drugbank.com/>), DisGeNET Database (<https://www.disgenet.org/>) were used to search for the immune dysregulation-related targets. Enter the target points of components into Cytoscape 3.8.2 to construct the network visualization diagram of “medicinal materials-components-targets”.

Prediction of Differential Metabolite Targets

Based on metabolomics, the obtained differential metabolites were input into HMDB database to obtain the SMILE format of substances and input into Swiss Target Prediction database to obtain metabolite targets. Enter the target into Cytoscape 3.8.2 to construct the “metabolite-target” network diagram.

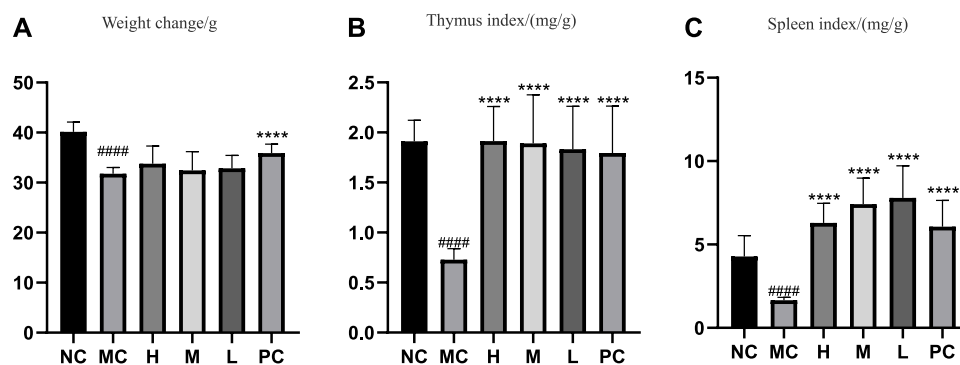


FIGURE 1 | (A) Effects of QGGBG and CP on the weight change of ICR mouse. **(B)** Effects of QGGBG and CP on thymus index of ICR mouse. **(C)** Effects of QGGBG and CP on spleen index of ICR mouse.

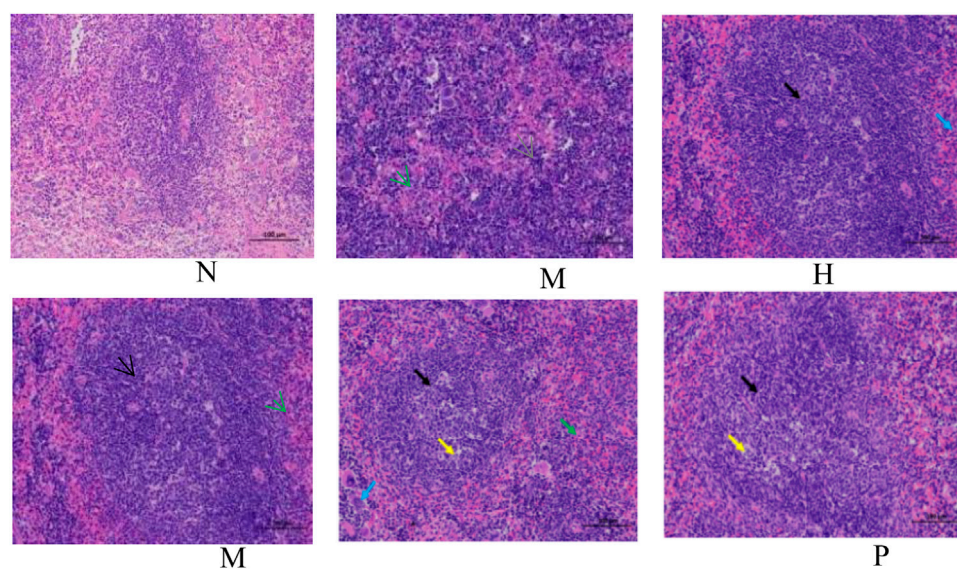


FIGURE 2 | Effects of QGGBG on the spleen tissues in the HE stained histopathological images. (200 \times , the black arrow represents the expansion of germinal center, the yellow arrow represents nuclear fragmentation, the green arrow represents neutrophil infiltration, the blue arrow represents a small increase in the number of multinucleated giant cells, and the gray arrow represents extramedullary hematopoiesis).

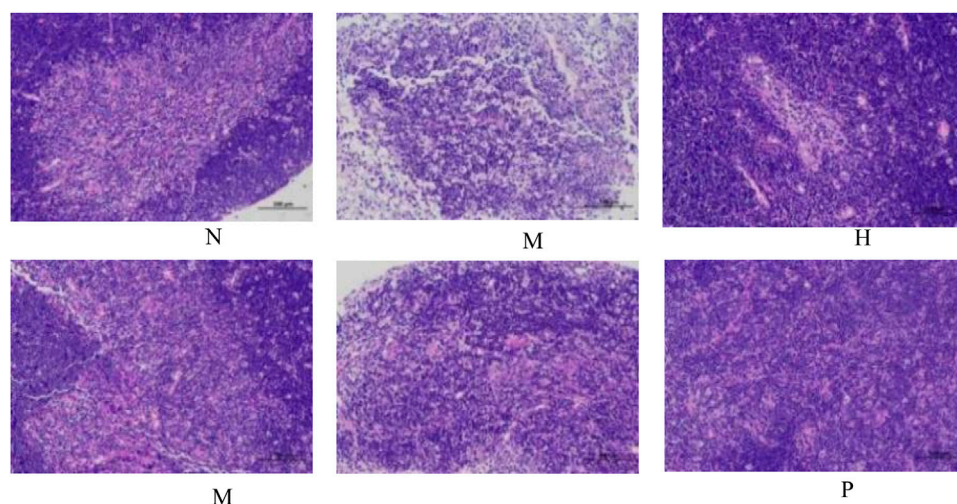


FIGURE 3 | Effects of QGGBG on the thymus tissues in the HE stained histopathological images. (200 \times).

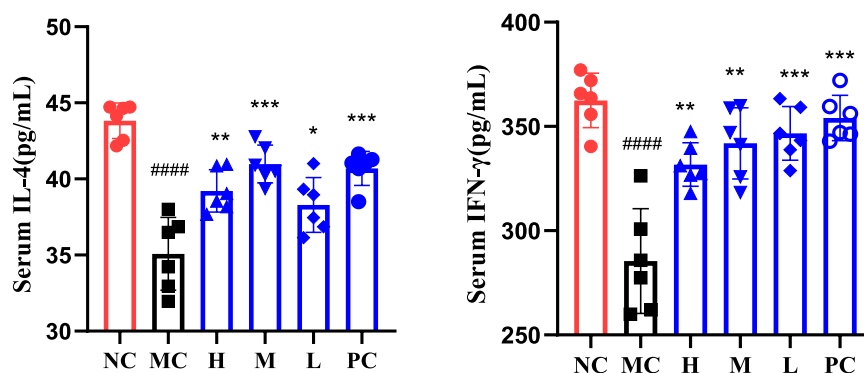


FIGURE 4 | Serum IL-4 and IFN- γ expression levels. The significant difference was calculated using analysis of variance, # p -values of NC vs. MC, #### $p < 0.0001$, ### $p < 0.001$, ## $p < 0.01$, # $p < 0.05$, * p -values compared with MC, **** $p < 0.0001$, *** $p < 0.001$, ** $p < 0.01$, * $p < 0.05$.

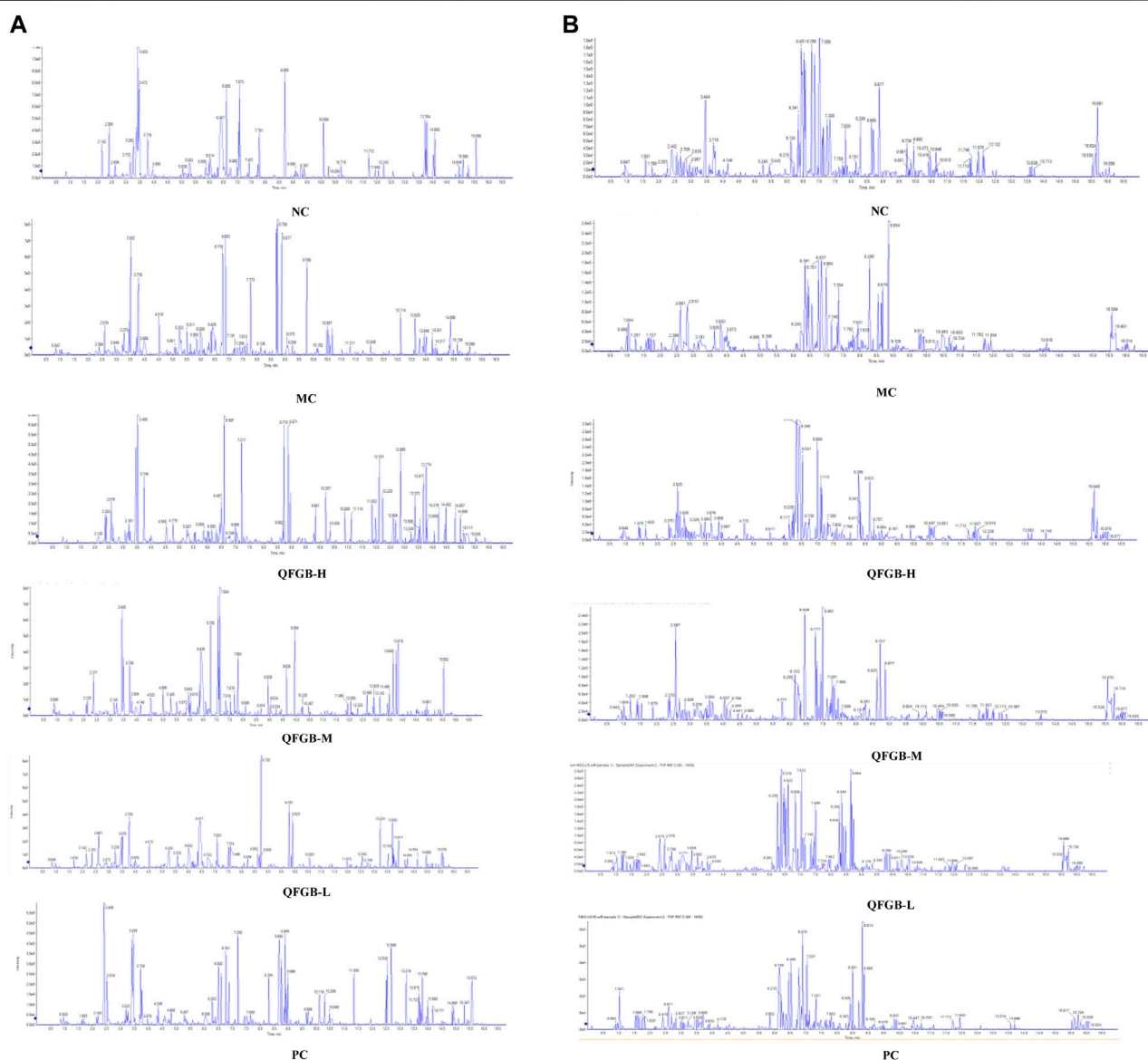
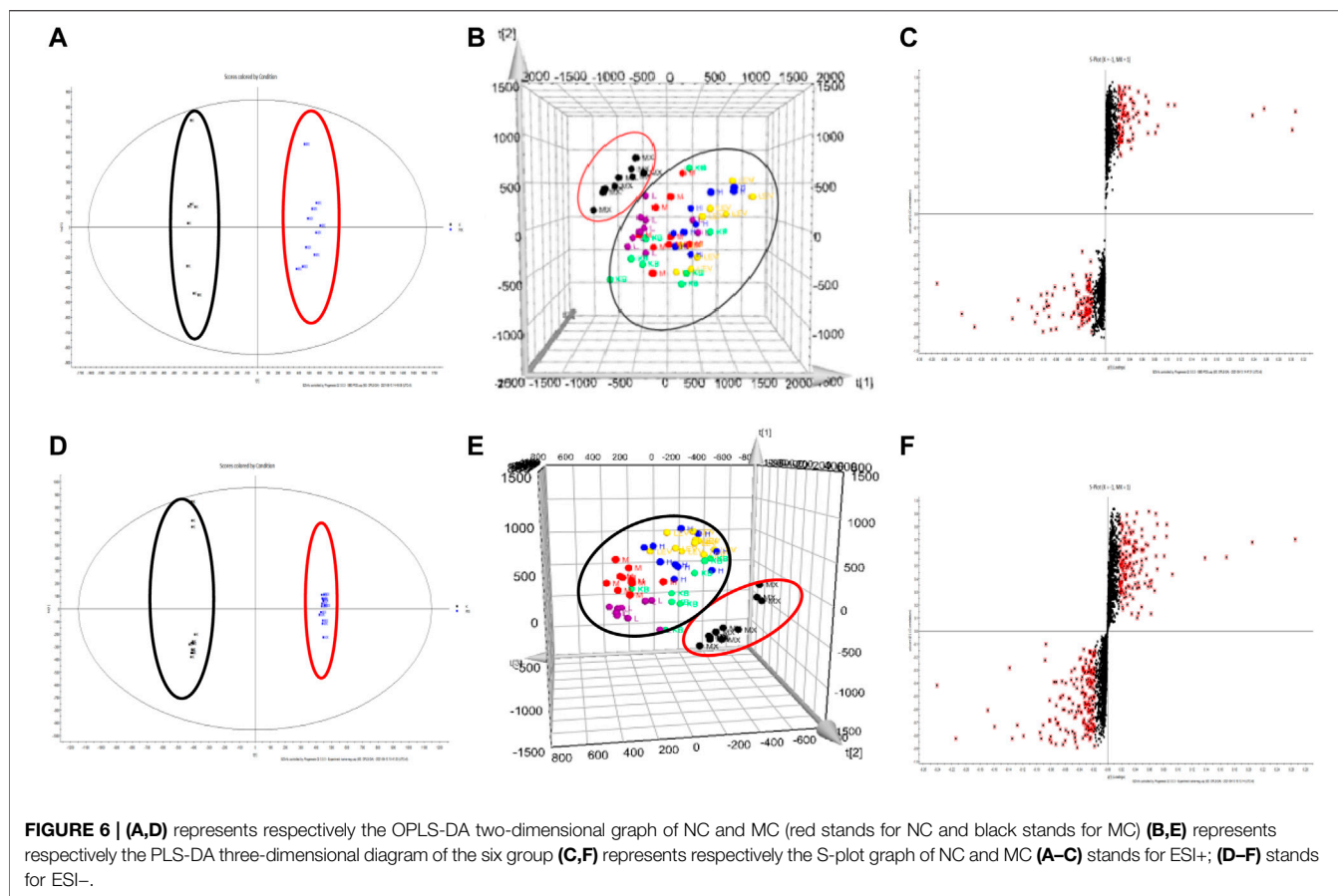


FIGURE 5 | The TIC of six group. (A) ESI+; (B) ESI-.



Construction of Immune Regulation Network Diagram

The component target, disease target and metabolite target were input into Venny 2.1 software to obtain the intersection target, and the PPI network diagram was obtained by importing the intersection target into String (<https://string-db.org/>) website. Furthermore, the nodes in the network are ranked according to the Degree by using the CytoHubba plug-in of Cytoscape 3.8.2, and the top 10 targets are selected as potential targets.

Analysis of Related Channels

The intersection targets were input into Metaspase (<http://metaspase.org/>) website for GO and KEGG analysis, with $p < 0.05$. GO function analysis is mainly used to describe the functions of gene products, including biological process (BP), cell composition (CC) and molecular function (MF). KEGG is used to analyze the possible action pathway of the target and to explore the mechanism of immune enhancement of QFGBG.

Data Processing

The data collected by UPLC-Q-TOF-MS were subjected to peak detection, peak alignment and normalization by Progenesis QI software, and then the data were imported into EZinfo software

for analysis. According to the variable importance projection (VIP) value of OPLS/PLS-DA model, $VIP > 1$, $p < 0.05$ was selected to find the differential metabolites.

GraphPad Prism version 8.0.2 software was used for all statistical analysis. All data are expressed as average \pm standard deviation ($\bar{X} \pm SD$) and the difference between the two groups was compared by t test, and the p value < 0.05 showed statistical significance.

RESULTS

Pharmacodynamic Evaluation

The change in body weight and organ index is shown in **Figure 1A**. It can be seen that the weight of the model group is obviously reduced compared with that of the blank group ($p < 0.001$), and all of them recovered after administration, and PC had the most obvious recovery effect ($p < 0.001$). The index changes of thymus and spleen are shown in **Figures 1B,C**, the spleen and thymus of the model group all showed significant atrophy, which is significant difference with the blank group ($p < 0.001$), and both showed significant recovery after administration ($p < 0.001$). HE staining of spleen and thymus is shown in **Figures 2, 3**. In the model group, the number of spleen nodules decreased significantly, extramedullary hematopoiesis was found in the red

TABLE 1 | Potential biomarkers of immunedys regulation.

| No. | Retention time (min) | m/z | HMDB ID | Molecular formula | MS/MS | Mass error (ppm) | Metabolites | VIP | Trend | Adducts |
|-----|----------------------|-------------|-----------|-------------------|---|------------------|--|---------|-------|---------------|
| 1 | 7.047116667 | 496.3391024 | HMDB10382 | C24H50NO7P | 496.3398;478.3292;184.0733;166.0628;104.1070 | -1.339657256 | LysoPC(16:0) | 12.8004 | ↑## | M + H |
| 2 | 5.29415 | 302.304604 | HMDB00269 | C18H39NO2 | 302.3042;284.2948;106.0863;88.0757;57.0699 | -2.495755536 | Sphinganine | 2.1454 | ↑#### | M + H |
| 3 | 3.150766667 | 585.270166 | HMDB00054 | C33H36N4O6 | 585.2708;568.2443;550.2337;412.1867;285.1234;267.1129 | -1.019001737 | Bilirubin | 1.48879 | ↑## | M + H |
| 4 | 1.8212 | 218.1374324 | HMDB00824 | C10H19NO4 | 218.1387;159.0652;144.1020;57.0335 | -5.766686337 | Propionylcarnitine | 1.02012 | ↓### | M + H |
| 5 | 0.94125 | 203.0512566 | HMDB00122 | C6H12O6 | 203.0526;145.0496;85.0285;57.0335 | -7.509597353 | D-Glucose | 1.04127 | ↓### | M + Na |
| 6 | 11.71848333 | 784.58456 | HMDB08040 | C44H82NO8P | 784.5851;725.4991;601.5191;184.0733;60.0808 | -0.665788027 | PC(18:0/18:3(6Z,9Z,12Z)) | 12.9616 | ↓#### | M + H |
| 7 | 8.697666667 | 1047.737099 | HMDB10561 | C69H100O6 | 1047.7238;525.3614;524.3672;184.0730 | -4.013308875 | Triacylglycerol | 7.96941 | ↑### | M + Na |
| 8 | 15.53698333 | 830.5678648 | HMDB08156 | C48H80NO8P | 852.5514/830.5524;771.4960;669.4853;184.0733;86.0965 | -1.888676062 | PC(18:2(9Z,12Z)/22:6(4Z,7Z,10Z,13Z,16Z,19Z)) | 2.45112 | ↓#### | M + H, M + Na |
| 9 | 5.851483333 | 380.2554225 | HMDB00277 | C18H38NO5P | 380.2561;364.2611;284.2948;264.2686;120.9661 | -1.618790293 | Sphingosine-1-phosphate | 1.62037 | ↑#### | M + H, M + Na |
| 10 | 1.737733333 | 103.0406311 | HMDB00008 | C4H8O3 | 103.0437;73.0325;59.0502;57.0346; | 5.415183325 | 2-Hydroxybutyric acid | 1.01357 | ↑#### | M – H |
| 11 | 1.524233333 | 191.0193906 | HMDB00094 | C6H8O7 | 191.0197;173.0091;154.9986;129.0193;115.0036;72.9931 | -1.747673614 | Citric acid | 2.2793 | ↓## | M – H |
| 12 | 9.435466667 | 277.2173996 | HMDB01388 | C18H30O2 | 277.2183;259.2067;233.2274;182.1312;71.0138 | 0.344590538 | Alpha-Linolenic acid | 2.19489 | ↑### | M – H |
| 13 | 10.47606667 | 279.2334667 | HMDB00673 | C18H32O2 | 279.2329;261.2224;205.1962;149.0972;83.0502 | 1.830270977 | Linoleic acid | 5.2674 | ↑#### | M – H |

^aChange trends compared with the normal. The levels of differential metabolites were marked with downregulated (↓) and upregulated (↑).

Notes: #p-values of NC vs. MC, ####p < 0.0001, ###p < 0.001, ##p < 0.01.

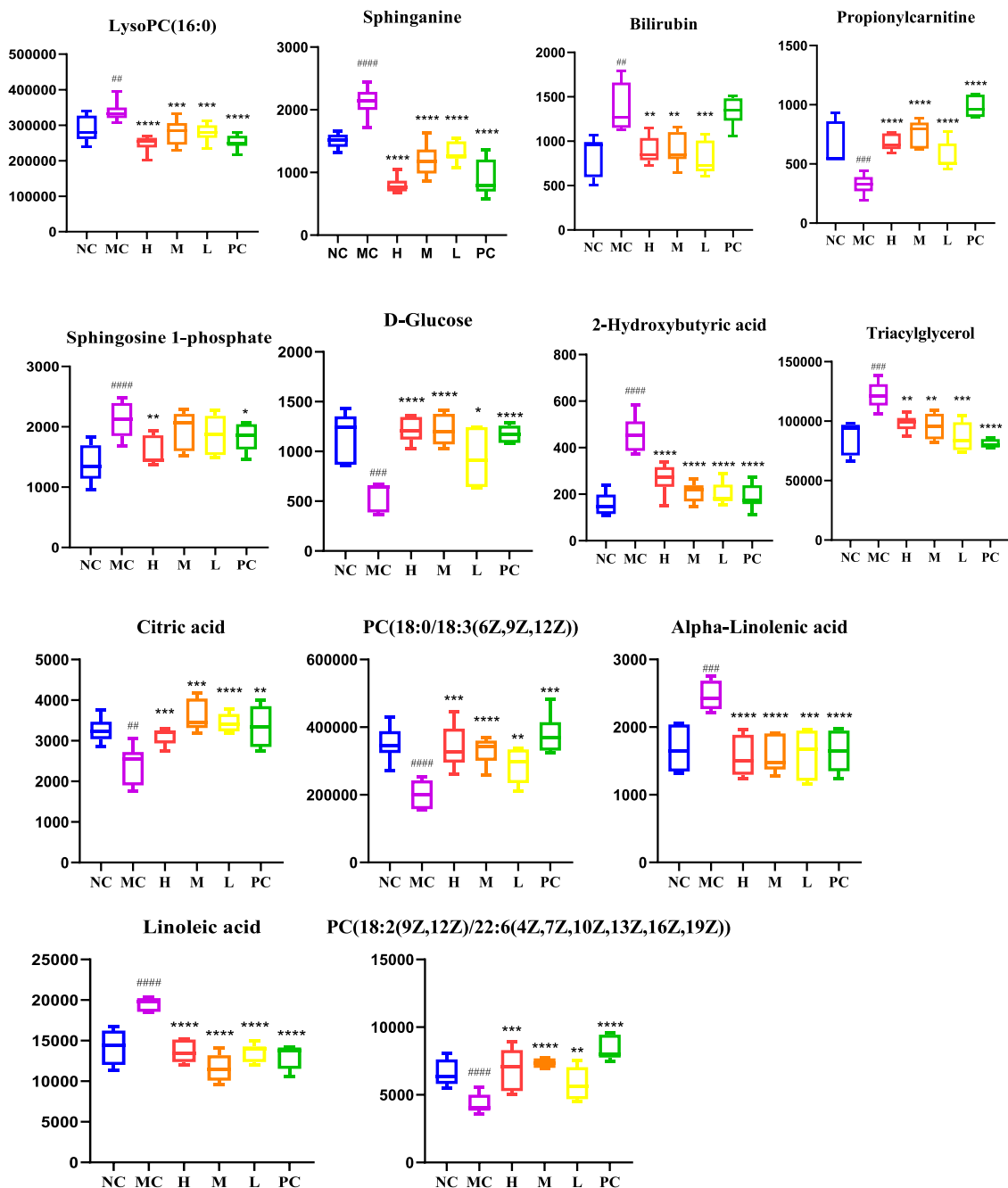
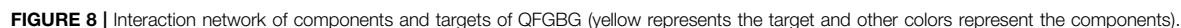


FIGURE 7 | Changes in levels of the potential biomarkers in the six groups. # p -values compared with MC; #### $p < 0.0001$, ### $p < 0.001$, ## $p < 0.01$, * p -values compared with MC, **** $p < 0.0001$, *** $p < 0.001$, ** $p < 0.01$, * $p < 0.05$.

pulp (black arrow), neutrophil infiltration was rare (green arrow), and the germinal center was enlarged in the blank group (black arrow), which indicated that inflammatory reaction occurred, and lymphoid tissue produced protective response to the body, after administration, the number of spleen nodules basically recovered, neutrophil infiltration (green arrow), a small amount of nuclear fragmentation (yellow arrow) and a small increase in the number of multinucleated giant cells (gray arrow)

were rare, and there was no significant difference between the rest and the blank group. Thymic cells were sparse, and the boundaries between cortex and medulla were blurred, indicating that immune organs were damaged. After administration, all patients were adjusted back, and there was no significant difference among the groups. Thymus and spleen are important immune organs of the body. The size of thymus index can reflect the immune status of the body. From the above



Using IFN- γ , IL-4 as evaluation indicators **Figure 4.** T lymphocytes play an important role in the body's immunity, among which CD4 + T cells can be expressed on the surface of helper T cells (Th), which can be divided into Th1 cells and Th2 cells, among which Th1 cells mainly secrete cytokines such as IL-2 and IFN- γ , and their levels can reflect the degree of inflammation damage, while Th2 cells mainly secrete cytokines such as IL-4 and IL-10, which are closely related to the progress and chronic diseases (Borish and Rosenwasser, 1996; Hirata et al., 2001; Wynn Thomas, 2015). IFN- γ is a cytokine with various biological activities produced by activated T lymphocytes, and it is an important immunomodulatory factor *in vivo* (Manjunatha et al., 2012), On the one hand, it can resist virus, inhibit virus

UPLC-Q-TOF/MS was used to analyze the metabolomics of serum samples from six groups of mice. The TIC diagram is shown in **Figure 5**. There is no obvious difference in each group

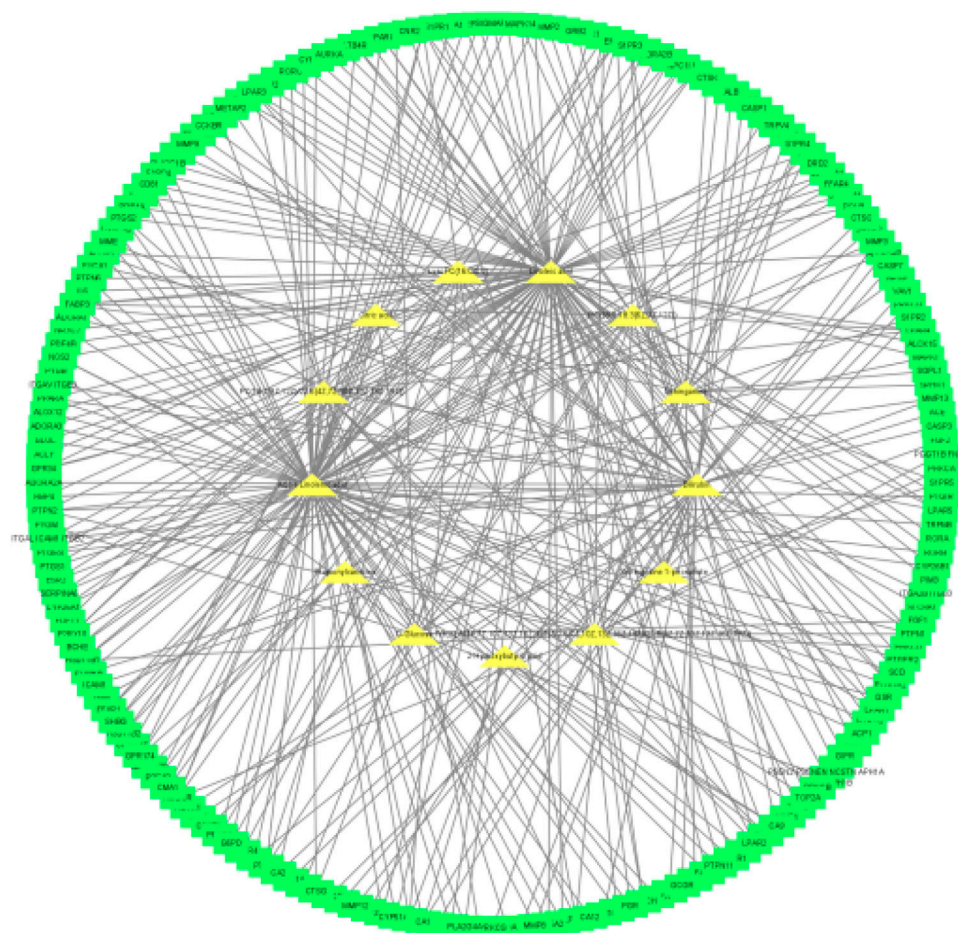


FIGURE 9 | Interaction network of components metabolite and targets of QFGBG (Green squares represent targets, and yellow triangles represent metabolites).

from TIC diagram, which needs further analysis. The results of metabolomics analysis of each group are shown in **Figure 6**. From blank and model OPLS-DA two-dimensional diagrams (**Figures 6A,D**), it can be seen that the clustering of the two groups clearly indicates that PC causes the changes of metabolites in mice, and the metabolites of each group approach the blank after administration (**Figures 6B,E**), which indicates that QFGBG has a callback effect on the changes of metabolites caused by CP.

3.3.2 Determination and Analysis of Significant Differences

In order to identify the potential biomarkers of QFGBG playing an immunomodulatory role from thousands of variables, the variables were uniformly extracted with $p < 0.05$ and $VIP > 1$ as parameters in combination with S-Plot (**Figures 6C,F**) and OPLS-DA diagrams and matched with HMDB (<http://www.hmdb.ca>) online database, and finally 13 differential markers were determined (**Table 1**). Mainly lipids (glycerophospholipids, sphingolipids, glycerides) and some fatty acid metabolites (linoleic acid, α -linolenic acid), in which the levels of phospholipids (PC), glucose and citric acid metabolites were significantly reduced in the model

group; Sphingosine -1- phosphate, 1- palmitoyl phosphatidylcholine [LysoPC(16:0/0:0)], bilirubin, linoleic acid and other metabolites increased in the model group, and QFGBG could adjust the contents of these metabolites. Taking the abundance of 13 biomarkers as ordinate and groups as abscissa, we can clearly see the differences among groups (**Figure 7**).

Network Pharmacology Results

Prediction of Target Points of Blood Components of Qifenggubiao Granules

A total of 33 blood components and 629 component targets were identified, and the target points were input into the software of Cytoscape3.8.2 to obtain the “component-target” (**Figure 8**). As shown in the **Figure 8**, yellow represents the target and other colors represent the components.

3.4.2 Prediction of Metabolite Targets of Qifenggubiao Granules

A total of 13 metabolic biomarkers and 202 metabolite targets were identified, and the “metabolite-target” is shown in

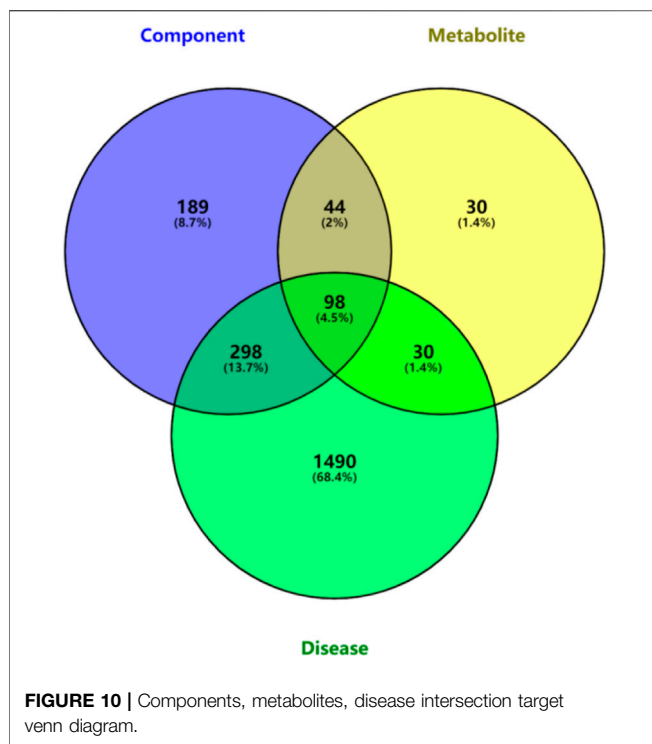


(Figure 9). Among them, yellow triangles represent metabolites and green rectangles represent targets.

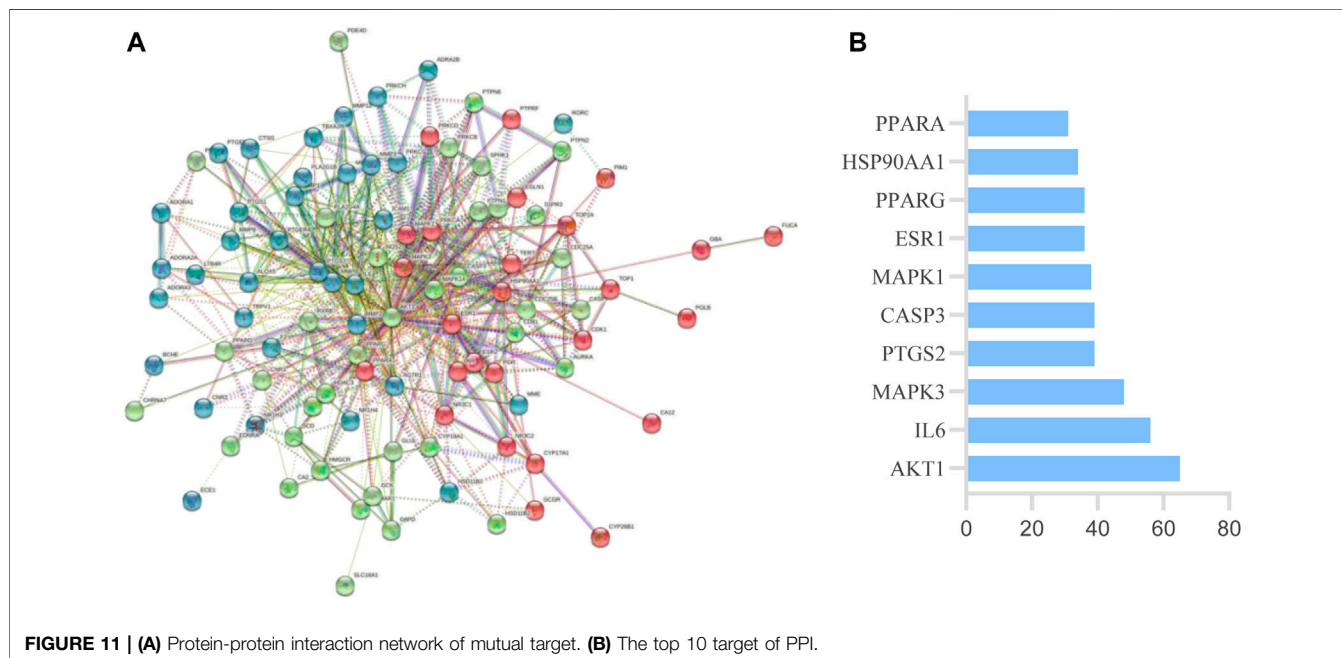
Analysis of Immune Regulation Target Protein Network of Qifenggubiao Granules

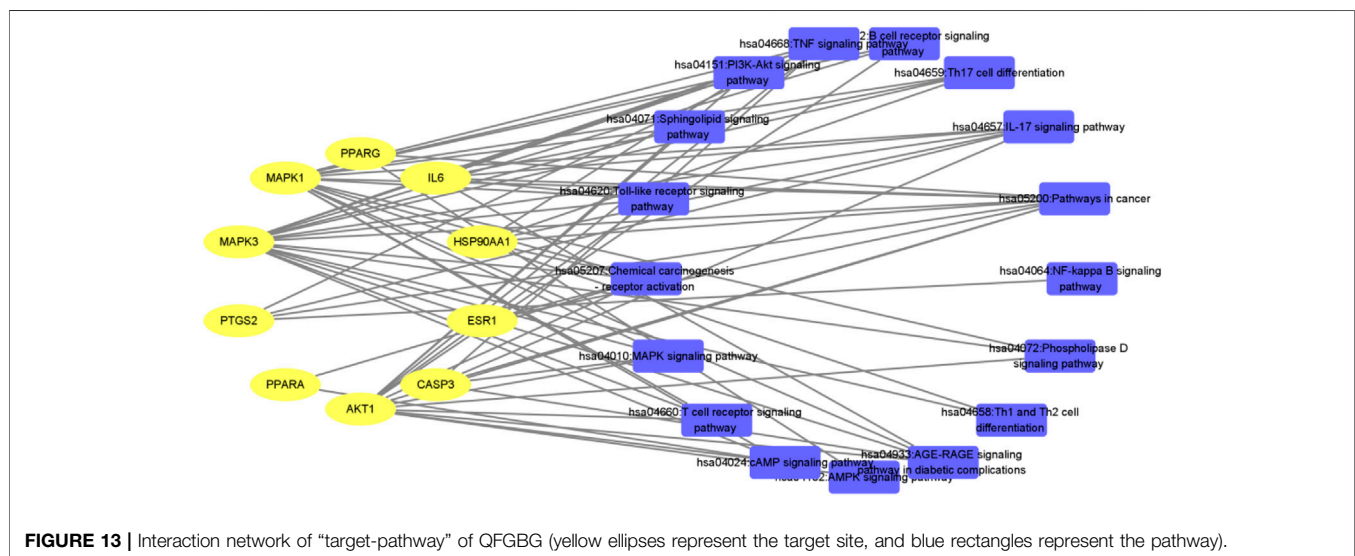
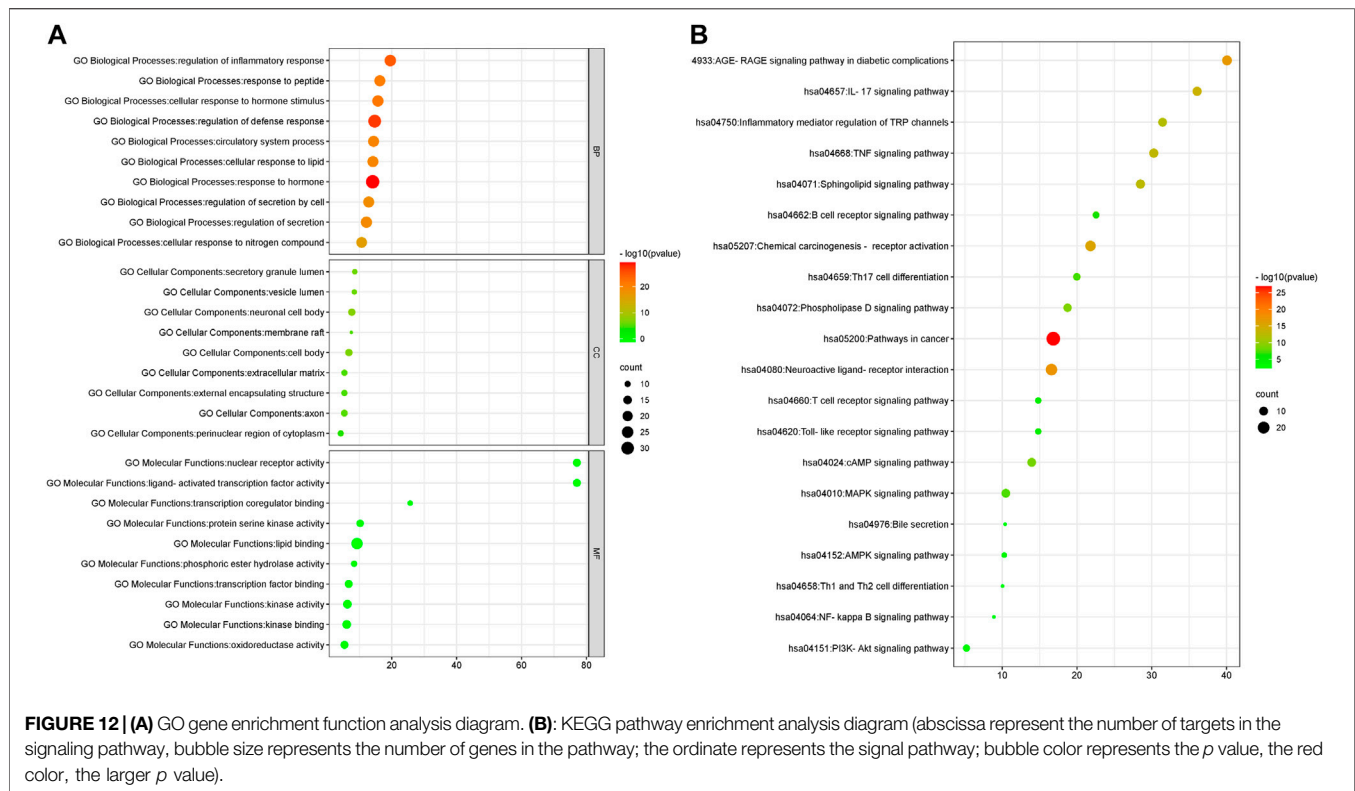
A total of 135 intersection targets were obtained from 629 component targets, 202 metabolite targets and 1916 disease targets of QFGBG, and 98 (Figure 10) intersection targets were

input into String database to construct PPI network diagram, as shown in (Figure 11A). The minimum required interaction score is 0.4, the PPI network graph has 98 nodes and 634 edges, and the average degree of nodes is 12.9. Each node represents a protein, and the connection between nodes represents the interaction between protein. The common target may be related to the immune regulation mechanism of QFGBG. The network diagram of protein interaction is helpful to understand the functional relationship between protein more intuitively. Entering intersection targets into Cytoscape. First, the targets whose degree is greater than the mean (12.9) in the network are screened. On this basis, the first 10 nodes whose degree is greater than the mean degree (degree >24.4857142857143) are defined as the core targets (Figure 11B).

GO Enrichment Analysis and KEGG Pathway Analysis

To further reveal the immune regulation mechanism of QFGBG, we used Metscape database to analyze GO enrichment and KEGG pathway of the above 98 targets. GO analysis mainly includes three parts, biological process (BP), cellular component (CC), and molecular function (MF). GO analysis showed that BP included 1139 enrichment results, including regulation of defense response, regulation of inflammatory response, regulation of secretion. CC includes 76 enrichment results, mainly involving neuronal cell body, external encapsulating structure, cell body, and secretory granule lumen. The MF includes 108 enrichment results, including lipid binding, nuclear receptor activity, protein kinase activity etc. The enrichment results are sorted according to *p* value. The online analysis platform (<http://www.bioinformatics.com.cn>) is used to draw the top 10 analysis results of three parts, as shown in (Figure 12A). 233 pathways were obtained by analysis of KEGG gene annotation functional analysis. These pathways mainly include Sphingolipid signaling pathway, Inflammatory mediator regulation of trpchannels, MAPK





signaling pathway etc. The results of visual analysis of the top 20 pathways are shown in (Figure 12B).

DISCUSSION

Immunity is a physiological function of the human body. The human body relies on this function to identify “self” and “non-

self" components, thus destroying and rejecting antigens entering the human body or damaged cells and tumor cells produced by itself, so as to maintain human health. The immune system mainly has three functions: defense, stabilization, and surveillance. Once these functions are out of balance, pathological reactions will occur. Inflammation is a manifestation of immune response to infection or injury, and is the result of activation of innate and/or acquired immune

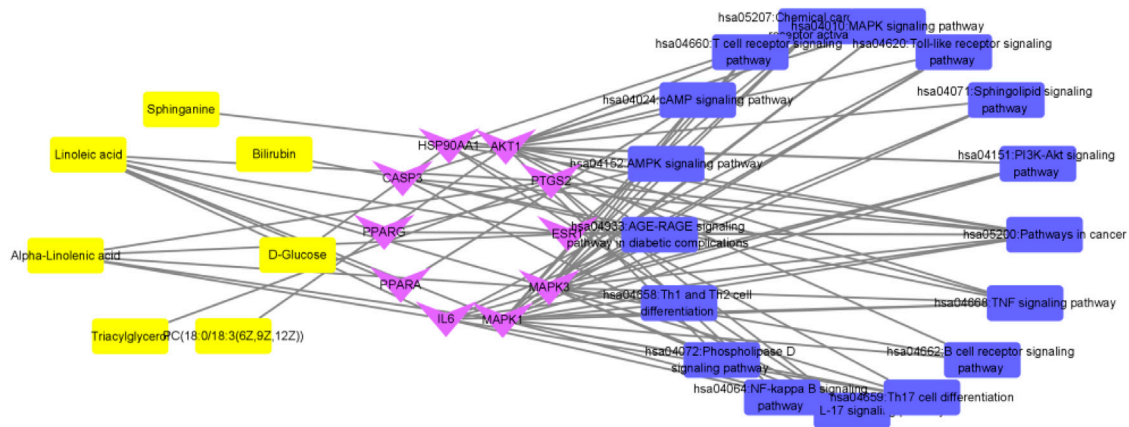


FIGURE 14 | Interaction network of “metabolite-target-pathway” of QFGBG (yellow represents metabolites, purple represents targets, and blue represents pathways).

response (June 2017), that is, inflammation is a manifestation of initiation and activation of immune response (June 2019). Immunoregulation involves multi-target and multi-pathway, which is a complex mechanism of interaction between immune cells, immune molecules, immune organs, and other systems (such as neuroendocrine system, etc.). Traditional Chinese medicine has complex components, and there is synergistic effect among multiple components, metabonomics, and network pharmacology are based on the balance of system biology and biological network. Starting from the overall model, they can improve or adjust the balance of biological network by adjusting signal pathways in multiple ways to improve the curative effect of drugs (Qi, 2018), which is more in line with the holistic view and systematization of traditional Chinese medicine. The results showed that QFGBG could reverse the damage of immune organs caused by CTX and increase the levels of IL-4 and IFN- γ in serum, Metabonomics analysis shows that QFGBG can increase the level of phospholipid (PC) metabolites and reduce the contents of sphingosine, sphingosine -1- phosphate, triglyceride, and other metabolites. Furthermore, 98 possible immunomodulatory targets of Qifeng solid surface can be obtained by network pharmacological analysis. AKT1, IL6, MAPK3, PTGS2, CASP3, MAPK1, ESR1, PPARG, HSP90AA1, and PPARG are the key targets of immune regulation. The KEGG pathway analysis of potential targets shows that QFGBG may play an immunomodulatory role through inflammatory pathways such as inflammatory mediator regulation of Trp channels, Sphingolipid signaling pathway, and MAPK signaling pathway. The key targets obtained from network pharmacology are enriched into the same or different metabolic pathways, and then the levels of various metabolites are regulated to regulate the whole organism. See **Figures 13, 14** for the specific visualization diagrams of “target-pathway” and “target-metabolite-pathway,” respectively.

Sphingolipid Signaling Pathway

Studies have shown that cyclophosphamide can cause liver injury (Huanying, 2019). Liver plays a key role in metabolism, biosynthesis, secretion, and detoxification. In recent years, it has been found that sphingolipid metabolism is involved in the occurrence and development of liver diseases. Sphinganine is not only an important component of cell membrane structure, but also an inactive precursor in sphingolipid metabolism and an important effector molecule in cell signal transduction (Jiuli et al., 2011). Tumor necrosis factor (TNF- α) is most related to the pathological damage process of liver, which can affect the proliferation, growth, inflammation, regeneration, and apoptosis of liver cells (Shaoyuan et al., 2015). TNF- α can activate the activities of sphingosine kinase 1 and sphingosine kinase 2 (SPHKs), which in turn catalyzes the phosphorylation of Sphinganine to produce S1P (Yanhong et al., 2019). However, high concentration of S1P can mediate the internalization of S1P receptors (S1PRs) and reduce the outward migration of lymphocytes in the immune system, thus achieving the immunosuppressive effect (Yoshihiko et al., 2016), the contents of sphingosine and S1P in the model group increased significantly ($p < 0.001$), which indicated that Sphinganine might be phosphorylated to S1P by SPHKs catalysis, and then play an immunosuppressive role. After administration, the content of each group increased. It shows that QFGBG can play an immunomodulatory role by reducing the contents of Sphinganine and S1P through sphingolipid signaling pathway.

Mitogen-Activated Protein Kinases Signaling Pathway

Mitogen-activated protein kinases (MAPKs) are a kind of serine/threonine protein kinases, which widely exist in mammalian cells. MAPK pathway is an important way to

transfer extracellular signals into cells and cause cell biological reactions (such as cell proliferation, differentiation, transformation, and apoptosis, etc) (Yanwu, 2016), which mainly includes three cascade reactions. Extracellular signal-regulated protein kinase (ERK) pathway, c-jun N-terminal kinase (JNK) pathway and p38 MAPK pathway, the activation of which can promote the production of inflammatory cytokines and aggravate inflammatory reaction (Seger and Krebs, 1995). Modern pharmacological studies have shown that MAPK is closely related to liver diseases, respiratory diseases and other diseases (Jinchuan et al., 2022; Zhihua et al., 2020; Tianyi et al., 2021). Studies have shown that reducing ERK, p38 MAPK mRNA expression and p-ERK and p-p38 MAPK expression in rat lung tissue can improve airway inflammation in asthmatic rats (Feng et al., 2018). Dephosphorylation of p38 MAPK can not only alleviate excessive lung inflammation induced by macrophage and PMNs recruitment, but also inhibit macrophage from non-inflammatory apoptosis to inflammation (Li et al., 2018). Phosphatidylcholine (PC) is not only an important component of biofilm system in eukaryotes, but also a signal molecule of cell signal transduction (Exton, 1994). Changes in PC content and structure can lead to abnormal enzyme activity, receptor function and membrane permeability, thus affecting metabolism and function of organisms (Caiyun, 2008). Lysophosphatidylcholine (LysoPC) is one of the metabolites of mammalian phospholipids and the hydrolysis product of phospholipase A2 of phosphatidylcholine, which is widely involved in many physiological and pathological processes including inflammatory reactions (Sedlis et al., 1993). When the biofilm is damaged, MAPK, as an important cell conduction pathway, will inevitably be affected. In the experiment, the content of PC in CP group decreased significantly, and LysoPC increased, indicating that its biofilm was damaged. After administration, the contents of PC and LysoPC in each group were adjusted back to different degrees, indicating that QFGBG can regulate the content of downstream PC through MAPK, and then play an immunomodulatory role.

Inflammatory Mediator Regulation of Transient Receptor Potential Channels

Inflammation plays an important role in many kinds of diseases, which mainly refers to various inflammatory diseases caused by complex reactions caused by tissue injury or pathogen infection (Xin et al., 2019). TRP channel is a kind of ion channel, which can be activated by heat, and TRPV1 ~ 4 are typical thermosensitive transient receptor potential channels (Holzer, 2011). They will be stimulated by exogenous or endogenous substances, and produce various neuropeptides, which will lead to neurogenic inflammation such as local tissue vasodilation and increased permeability, inflammatory cell exudation, mucosal congestion and edema, and bronchoconstriction (Grace et al., 2014). And the high expression of TRPA1/TRPV1 plays an important role in the pathogenesis of chronic cough (Bonvini et al., 2015; Bonvini

and Belvisi, 2017; Xinyang and Shunan, 2014). This is consistent with the clinical direction of QFGBG, and on the other hand, it is explained that QFGBG may play a role in the treatment of chronic cough through TRP channel.

CONCLUSION

Network pharmacology provides key technical support for revealing the scientific connotation of traditional Chinese medicine compound, discovering drug targets and guiding the research and development of new traditional Chinese medicine drugs (Wenxia et al., 2012). Traditional network pharmacology studies mostly combine chemical components and disease targets to study traditional Chinese medicine. From the perspective of system level and biological network as a whole, it analyzes the law of molecular association between drugs and therapeutic objects (World Traditional Chinese, 2021). The entry of traditional Chinese medicine into the blood may be the material basis of its efficacy (Chunlu et al., 2020). Metabolites are considered to be the most intuitive reflection of physiological and pathological conditions of organism, and subtle changes of gene expression and protein expression will be amplified on metabolites (XiJun, 2015), and key metabolites can provide reference for disease phenotype (Xiongjian et al., 2021). Metabonomics, through the judgment and further analysis of metabolites, finally gets a whole result (Weiwei et al., 2011). Metabonomics explores the regulatory mechanism of gene function, providing reliable basis for drug treatment or disease pathogenesis. Network pharmacology reveals the pathogenesis of complex diseases and the therapeutic mechanism of drugs from the system level, which are integrated and complementary to each other (Wang, 2020). And the immune regulation mechanism of QFGBG was studied from gene level and metabolite level. In this study, we found that CP caused immunosuppression in mice. QFGBG can improve the organ index of mice in each group, repair the pathological damage caused by CP and play an immunomodulatory role. According to the results of network pharmacology and metabonomics, QFGBG may act on AKT1, IL6, MAPK3, PTGS2, CASP3, MAPK1, ESR1, PPARG, HSP90AA1, PPARG, etc. Through Sphingolipid signaling pathway, MAPK signaling pathway, inflammatory mediator regulation of trp channels further regulate the content of metabolites such as PC, LysoPC, Sphinganine, etc. and play an immunomodulatory role. The above results indicate that QFGBG plays a multi-target, multi-channel, multi-level, and multi-faceted role in immune regulation.

DATA AVAILABILITY STATEMENT

The original contributions presented in the study are included in the article/Supplementary Material, further inquiries can be directed to the corresponding authors.

ETHICS STATEMENT

The animal study was reviewed and approved by The study was conducted strictly according to the ethical guidelines for using experimental animals in Heilongjiang province, guided and approved by the animal ethics committee of the academy of traditional Chinese medicine of Heilongjiang province [(2011)93].

AUTHOR CONTRIBUTIONS

WW and BZ designed and supervised the study. BG and WD performed the experiments and wrote the manuscript. JH, GS,

ZQ and XL participated in analyzing the data. All authors have read and approved the final manuscript.

FUNDING

The research is supported by natural science foundation of Heilongjiang province (LH 2020H10); Contract of Heilongjiang Province Key R&D Plan Project (GA21C016); Research project of traditional Chinese medicine of Heilongjiang province (ZHY2020-043); Contract for guiding projects of key R&D plan in Heilongjiang Province (GZ202110056).

REFERENCES

- Bing, L., Fei, H., and Zhong, W. (2017). Consideration of Clinical Value of Prescriptions Under the Background of Multi-Omics Network [J]. *Chinese Journal of Traditional Chinese Medicine* 42 (05), 848–851. doi:10.19540/j.cnki.cjcmm.20170103.001
- Bonvini, S. J., and Belvisi, M. G. (2017). Cough and Airway Disease: The Role of Ion Channels. *Pulm. Pharmacol. Ther.* 47, 21–28. doi:10.1016/j.pupt.2017.06.009
- Bonvini, S. J., Birrell, M. A., Smith, J. A., and Belvisi, M. G. (2015). Targeting TRP Channels for Chronic Cough: from Bench to Bedside. *Naunyn Schmiedeberg's Arch. Pharmacol.* 388, 401–420. doi:10.1007/s00210-014-1082-1
- Borish, L., and Rosenwasser, L. J. (1996). Update on Cytokines. *J. Allergy Clin. Immunol.* 97 (3), 719–734. doi:10.1016/s0091-6749(96)80146-1
- Caiyun, W. (2008). *Study on the Regulatory Effect of Taurocholic Acid on Immune Cell Function in Mice*. Hohhot: Inner Mongolia Agricultural University.
- Chunlu, Z., Jing, W., and Yuhang, Q. (2020). Study on Serum Pharmacokinetics of Duliang Wan. *Chin. J. Mod. Appl. Pharm.* 37 (04), 443–446. doi:10.13748/j.cnki.issn1007-7693.2020.04.011
- Dandan, Z., Wenfeng, W., Jinhai, H., and Weiming, W. (2021). Study on Serum Pharmacokinetics of Qifeng Gubiao Granules Based on UPLC-Q-TOF-MS Technology. *Chin. Herbal Med.* 52 (03), 643–652. doi:10.7501/j.issn.0253-2670.2021.03.006
- Dandan, Z., Wenfeng, W., Jinhai, H., and Weiming, W. (2020). UPLC-Q-TOF-MS Analysis of Chemical Constituents of Qifeng Gubiao Granules. *Chin. Med.* 42 (06), 1649–1657. doi:10.3969/j.issn.1001-1528.2020.06.052
- Edited by National Pharmacopoeia Commission (2015). *Pharmacopoeia of the People's Republic of China (2020 Edition, Part I)*. Beijing: Chemical Industry Press.
- Exton, J. H. (1994). Phosphatidylcholine Breakdown and Signal Transduction. *Biochim. Biophys. Acta (BBA) - Lipids Lipid Metab.* 1212 (1), 26–42. doi:10.1016/0005-2760(94)90186-4
- Feng, X., Hanyan, X., and Shufen, Z. (2018). Effects of Chaipu Decoction on Airway Inflammation and ERK/p38MAPK Signaling Pathway in Asthmatic Rats. *Chinese J. Exp. traditional Med. formulae* 24 (02), 104–109. doi:10.13422/j.cnki.syfjx.2018020104
- Grace, M. S., Baxter, M., Dubuis, E., Birrell, M. A., and Belvisi, M. G. (2014). Transient Receptor Potential (TRP) Channels in the Airway: Role in Airway Disease. *Br. J. Pharmacol.* 171, 2593–2607. doi:10.1111/bph.12538
- Hirata, M., Kage, M., Hara, T., Yoneda, Y., Zhang, M., and Fukuma, T. (2001). Schistosoma Japonicum Egg Granuloma Formation in the Interleukin-4 or Interferon-Gamma Deficient Host. *Parasite Immunol.* 23 (6), 271–280. doi:10.1046/j.1365-3024.2001.00382.x
- Holzer, P. (2011). Transient Receptor Potential (TRP) Channels as Drug Targets for Diseases of the Digestive System. *Pharmacol. Ther.* 131, 142–170. doi:10.1016/j.pharmthera.2011.03.006
- Huanying, Y. (2019). *Study on the Protective Effect of Dendrobium Huoshanense on Liver and Immune System Damage Induced by Cyclophosphamide in Mice*. Zhenjiang: Jiangsu University.
- Jinchuan, X., Renyuan, C., and Jing, Y. (2022). Effect of Baicalin on LPS-Induced Acute Lung Injury in Rats Through p38 MAPK/NLRP3 Pathway [J]. *Chinese Journal of Experimental Traditional Medical Formulae* 28 (2), 79–86. doi:10.13422/j.cnki.syfjx.20220104
- Jiuli, S., Huizhen, L., and Ping, G. (2011). Research Progress of Sphingolipid Metabolism and Related Diseases. *Biotechnology* 21 (05), 93–97. doi:10.3969/j.issn.1004-311X.2011.05.137
- Jun, L. (2019). Correctly Understand the Relationship Among Immunity, Inflammation and Metabolism of Persistent Inflammation-Immunosuppression-Catabolic Syndrome. *Chin. Electron. J. Crit. Med. (online edition)* 5 (04), 302–306.
- Jun, L. (2017). Correctly Understand the Relationship between Immune Dysfunction and Inflammation in Critically Ill Patients. *Chin. J. Med.* 97 (7), 483–486.
- Kim, S.-Y., Shin, J.-S., Chung, K.-S., Han, H.-S., Lee, H.-H., Lee, J.-H., et al. Immunostimulatory Effects of Live Lactobacillus Sakei K040706 on the CYP-Induced Immunosuppression Mouse Model. *Nutrients* 12 (11), 3573. doi:10.3390/nu12113573
- Li, D., Ren, W., Jiang, Z., and Zhu, L. (2018). Regulation of the NLRP3 Inflammasome and Macrophage Pyroptosis by the P38 MAPK Signaling Pathway in a Mouse Model of Acute Lung Injury. *Mol. Med. Rep.* 18 (18), 4399–4409. doi:10.3892/mmr.2018.9427
- Li, M., Gao, Y., Yue, X., Zhang, B., Zhou, H., Yuan, C., et al. (2021). Integrated Metabolomics and Network Pharmacology Approach to Reveal Immunomodulatory Mechanisms of Yupingfeng Granules. *J. Pharm. Biomed. Anal.* 194, 113660. doi:10.1016/j.jpba.2020.113660
- Manjunatha, A. M., Xu, S. L., Andrew, F., and Xiang, J. (2012). CD4 + Th2 Cells Function Alike Effector Tr1 and Th1 Cells through the Deletion of a Single Cytokine IL-6 and IL-10 Gene. *Molecul Immunol.* 51, 143–149.
- Panpan, F., Xuemei, L., and Xiaobao, J. (2014). Progress in Pharmacological Research of Interferon [J]. *Journal of Guangdong Pharmaceutical University* 30 (6), 780–783.
- Qi, M. (2018). *Treatment Effects of Pulsatilla Decoction in Dampness-Heat Diarrhea by Metabolomics and Network Pharmacology Approach*. Lanzhou: Gansu Agricultural University.
- Ran, C., Tingting, W., Kailing, L., Ruifeng, S., Jie, S., and jingzai, Z. (2020). Characteristics and Application of Immunomodulatory and Antiviral Chinese Medicine. *Chin. herbal Med.* 51 (06), 1412–1426.
- Sedlis, S. P., Hom, M., Sequeira, J. M., and Esposito, R. (1993). Lysophosphatidylcholine Accumulation in Ischemichumanmyo-Cardium. *J. Lab. Clin. Med.* 121 (1), 111–117.
- Seger, R., and Krebs, E. G. (1995). The MAPK Signaling cascade. *FASEB j.* 9 (9), 726–735. doi:10.1096/fasebj.9.9.7601337
- Shan, Z., Pengcheng, W., and Jian, F. (2015). Metabonomics Technology and its Application in Traditional Chinese Medicine Research. *Chin. Herbal Med.* 46 (05), 756–765.
- Shaoyuan, W., Jinlan, Z., and Dan, Z. (2015). Recent Advances in Study of Sphingolipids on Liver Diseases. *J. Pharm.* 50 (12), 1551–1558.
- Tianshuai, Z., Kun, D., and Weiming, W. (2021). Effect of Qifenggubiao Granule on the Immune Balance of Th1/Th2/Th17 Cells in Rats with Allergic Rhinitis. *Chin. Med. Sci. Tech.* 28 (06), 880–883.
- Tianyi, L., Demin, L., and Siyi, C. (2021). Regulation of Glucocorticoid Receptor by p38MAPK Signaling Pathway in 20 Diseases of Respiratory System. *Med. Rev.* 27 (04), 625–630.

- Wang, X. (2020). *Study on the Mechanism of Lingguizhugan Decoction in the Treatment of Heart Failure Based on Network Pharmacology and Metabolomics*. Shijiazhuang: Hebei Medical University.
- Weiming, W., and Shuming, Z. (2005). Experimental Study on the Effect of Qifeng Gubiao Granule on Immune Function in Mice. *Heilongjiang Traditional Chin. Med.* 34 (2), 37–39.
- Weiwei, Z., Wentao, X., and Li, W. (2011). Metabonomics Research Technology and its Application. *Biotechnol. Bull.* 12, 57–64.
- Wenxia, Z., Xiaorui, C., and Yongxiang, Z. (2012). Network Pharmacology: a new Idea of Understanding Drugs and Discovering Drugs [J]. *Chinese Journal of Pharmacology and Toxicology* 26 (01), 4–9. doi:10.3867/j.issn.1000-3002.2012.01.002
- World Traditional Chinese Medicine (2021). Guide to Network Pharmacology Evaluation Methods. *World Traditional Chin. Med.* 16 (04), 527–532.
- Wynn Thomas, A. (2015). Type 2 Cytokines: Mechanisms and Therapeutic Strategies.[J]. *Nat. Rev. Immunol.* 15, 271–282. doi:10.1038/nri3831
- Xijun, W. (2015). Systematic Methodology of Basic Research on Pharmacodynamic Substances of Traditional Chinese medicine — Metabonomics of TCM Prescription and Syndrome [J]. *Chinese Journal of Traditional Chinese Medicine* 40 (01), 13–17. doi:10.4268/cjcmm.20150103
- Xie, J., Yu, Q., Nie, S., Fan, S., Xiong, T., and Xie, M. (2015). Effects of *Lactobacillus Plantarum* NCU116 on Intestine Mucosal Immunity in Immunosuppressed Mice. *J. Agric. Food Chem.* 63 (51), 10914–10920. doi:10.1021/acs.jafc.5b04757
- Xin, Y., Yahui, L., and Lailai, L. (2019). Study on the Anti-inflammatory Effect of Volatile Oil from *Desmodium Styracifolium* Based on TRP Channel. *Chin. Herbal Med.* 50 (01), 134–141.
- Xinyang, S., and Shunan, Z. (2014). Overview of Research Progress of Traditional Chinese and Western Medicine on Chronic Cough [J]. *World Journal of Traditional Chinese Medicine* 9 (08), 974–977. doi:10.3969/j.issn.1673-7202.2014.08.002
- Xiongjian, G., Shengwen, L., and Guangli, Y. (2021). The Neuroprotective effect of Geniposide on Chronic Alcoholism Rats Based on Metabonomics [J]. *Chinese Journal of Experimental Traditional Medical Formulae* 1–12. doi:10.13422/j.cnki.syfjx.20220348
- Yanhong, B., Hong, W., and Minghui, S. (2019). The Role of Sphingosine 1-Phosphate and its Signaling Pathway in Inflammation-Related Diseases. *Chin. Pharmacol. Bull.* 35 (08), 1041–1046.
- Yanwu, H. (2016). *Effects and Mechanisms of Icarin against Atherosclerosis via MAPK Signaling Pathway*. Changchun: Jilin University.
- Yoo, J. H., Lee, Y. S., Ku, S., and Lee, H. J. (2020). Phellinus Baumii Enhances the Immune Response in Cyclophosphamide-Induced Immunosuppressed Mice. *Nutr. Res.* 75, 15–31. doi:10.1016/j.nutres.2019.12.005
- Yoshihiko, K., Kazuo, K., and Koichiro, T. (2016). Blockade of Sphingosine 1-Phosphate Receptor 2 Signaling Attenuates High-Fat Diet-Induced Adipocyte Hypertrophy and Systemic Glucose Intolerance in Mice.[J]. *Endocrinology* 157, 1839–51. doi:10.1210/en.2015-1768
- Yunbo, Z. (2013). Effect of Cyclophosphamide on Immune System. *Anhui Agric. Sci.* 41 (30), 12040–12042.
- Zhihua, D., Guiliu, H., and Xiaoshan, Q. (2020). Research Progress of the Relationship between p38MAPK Signaling Pathway and Liver Diseases. *Med. Rev.* 26 (22), 4395–4403.

Conflict of Interest: The authors declare that the research was conducted in the absence of any commercial or financial relationships that could be construed as a potential conflict of interest.

Publisher's Note: All claims expressed in this article are solely those of the authors and do not necessarily represent those of their affiliated organizations, or those of the publisher, the editors and the reviewers. Any product that may be evaluated in this article, or claim that may be made by its manufacturer, is not guaranteed or endorsed by the publisher.

Copyright © 2022 Guo, Dong, Huo, Sun, Qin, Liu, Zhang and Wang. This is an open-access article distributed under the terms of the Creative Commons Attribution License (CC BY). The use, distribution or reproduction in other forums is permitted, provided the original author(s) and the copyright owner(s) are credited and that the original publication in this journal is cited, in accordance with accepted academic practice. No use, distribution or reproduction is permitted which does not comply with these terms.



Dissecting the Regulation of Arachidonic Acid Metabolites by *Uncaria rhynchophylla* (Miq). Miq. in Spontaneously Hypertensive Rats and the Predictive Target sEH in the Anti-Hypertensive Effect Based on Metabolomics and Molecular Docking

OPEN ACCESS

Edited by:

Xijun Wang,
Heilongjiang University of Chinese
Medicine, China

Reviewed by:

Wai San Cheang,
University of Macau, China
Masashi Tawa,
Osaka Medical and Pharmaceutical
University, Japan

*Correspondence:

Jinjun Hou
jinjun_hou@simm.ac.cn
Wanying Wu
wanyingwu@simm.ac.cn

[†]These authors have contributed
equally to this work and share first
authorship

Specialty section:

This article was submitted to
Ethnopharmacology,
a section of the journal
Frontiers in Pharmacology

Received: 31 March 2022

Accepted: 16 May 2022

Published: 30 May 2022

Citation:

Gao L, Kong X, Wu W, Feng Z, Zhi H,
Zhang Z, Long H, Lei M, Hou J, Wu W
and Guo D-a (2022) Dissecting the
Regulation of Arachidonic Acid
Metabolites by *Uncaria rhynchophylla*
(Miq). Miq. in Spontaneously
Hypertensive Rats and the Predictive
Target sEH in the Anti-Hypertensive
Effect Based on Metabolomics and
Molecular Docking.
Front. Pharmacol. 13:909631.
doi: 10.3389/fphar.2022.909631

Lei Gao^{1,2†}, Xinqin Kong^{1,2†}, Wenyong Wu^{1,3}, Zijin Feng¹, Haijuan Zhi¹, Zijia Zhang¹,
Huali Long¹, Min Lei¹, Jinjun Hou^{1*}, Wanying Wu^{1,2*} and De-an Guo^{1,2}

¹National Engineering Laboratory for TCM Standardization Technology, Shanghai Institute of Materia Medica, Chinese Academy of Sciences, Shanghai, China, ²University of Chinese Academy of Sciences, Beijing, China, ³School of Chinese Materia Medica, Nanjing University of Chinese Medicine, Nanjing, China

Uncaria rhynchophylla (Miq). Miq. (UR), as a traditional Chinese medicine, was employed in treating hypertension as a safe and effective therapy. The pharmacological properties of UR have characteristics of multiple biological targets and multiple functional pathways. Hypertension is related to impaired metabolic homeostasis and is especially associated with the abnormal regulation of arachidonic acid metabolites, the classical cardiovascular active compounds. This study aimed to examine the anti-hypertensive effect of UR extract (URE) and its regulating role in differential metabolic pathways. The results showed that daily administration of URE at a dose of 4 g crude drug/kg orally could exert hypotensive effects on spontaneously hypertensive rats (SHRs) for 8 weeks. Non-targeted metabolomics analysis of the plasma samples suggested that the anti-hypertension effect of URE in SHRs was associated with the reorganization of the perturbed metabolic network, such as the pathways of glycerophospholipid metabolism, linoleic acid metabolism, and arachidonic acid metabolism. For the targeted metabolomics, twenty-eight arachidonic acid metabolites in SHRs were quantitatively analyzed for the first time based on ultra-high performance liquid chromatography-tandem mass spectrometry method after URE administration. URE restored the functions of these cardiovascular active compounds and rebalanced the dynamics of arachidonic acid metabolic flux. Among them, the inhibition of soluble epoxide hydrolase (sEH) enzyme activity and up-regulation of vasodilators epoxyeicosatrienoic acids (EETs) were identified as contributors to the anti-hypertension effect of URE on SHRs, and sEH represented an attractive and promising drug-binding target of URE. With the molecular docking approach, 13 potential anti-hypertension ingredients as well as sEH inhibitors were discovered, which were worthy of further investigation and verification in future studies.

Keywords: *Uncaria*, anti-hypertensive, arachidonic acid metabolites, sEH = soluble epoxide hydrolase, EETS, metabolomics, molecular docking, indole alkaloids

1 INTRODUCTION

U. rhynchophylla (Miq.) Miq. (UR), a traditional Chinese medicine (TCM), has been used for centuries to treat cardiovascular diseases, especially hypertension. The extracted chemical components from *Uncaria* mainly include indole alkaloids, which have been demonstrated as the bioactive constituents (Qin et al., 2021). Recent research indicates that UR extract (URE) also has other pharmacological effects, including sedation, anti-Alzheimer's disease, anti-drug addiction (Liang et al., 2020).

Hypertension is a prevalent chronic disease and a major risk factor for cardiovascular-related morbidity and mortality (Forouzanfar et al., 2017). Since the pathogenesis of hypertension is often associated with dyslipidemia, inflammation, and oxidative stress, hypertension is considered to be a metabolic disorder (Yang and Lao, 2019). Clinical studies have established an association between serum metabolite profiles and blood pressure in hypertensive patients (Arnett and Claas, 2018; Nikolic et al., 2014) and thus the use of metabolomic approaches and techniques in hypertension has attracted increasing interest in biomarker discovery and disease diagnoses. Metabolomic studies are being used to identify small metabolites that can be considered potential biomarkers of inflammation, oxidative stress, and other cardiovascular health conditions (Currie and Delles, 2017). In clinical studies and animal models, particularly in spontaneously hypertensive rats (SHRs), changes in several metabolites were closely associated with hypertension (Aa et al., 2010; Akira et al., 2012; Akira et al., 2013).

Recent studies showed that arachidonic acid (AA) and its metabolites have a crucial role in the pathobiology of hypertension (Zhou et al., 2021). AA is an essential fatty acid that is metabolized by cyclooxygenase (COX), cytochrome P450 (CYP) enzymes, and lipid oxygenase (LOX) pathways to regulate cardiovascular function. The CYP metabolites epoxyeicosatrienoic acids (EETs) are metabolized by soluble epoxide hydrolase (sEH) to the corresponding dihydroxyeicosatrienoic acids (Das, 2018). EETs are potent endothelium-derived vasodilators, particularly in the coronaries. Enhancing the synthesis of vascular EETs or inhibiting the degradation of the EETs may represent a new therapeutic approach for cardiovascular diseases (Campbell et al., 2017). Inhibition of sEH lowered blood pressure in SHRs (Jung et al., 2005; Huang et al., 2007; Xiao et al., 2010), and sEH inhibitors are also under clinical trials for treating hypertension (Yang et al., 2017).

Previous studies have shown that *Uncaria* extracts could effectively lower systolic blood pressure (SBP) in SHRs and modulate the metabolic profiles. Ana Liu et al. found the anti-hypertensive effects were associated with lipid metabolism (dihydroceramide, ceramide, PC, LysoPC, and TXA₂), vitamin and amino acids metabolism (nicotinamide riboside, 5-HTP) (Liu et al., 2018). Feng et al., (2019) identified six biomarkers in the urine over a 6-months treatment period. Despite these findings, the detailed mechanism underlying the anti-hypertensive effect of URE is unclear, and the regulation of

arachidonic acid metabolites by URE has not been previously studied, which restricts more application of UR.

This study explored the anti-hypertension effect and underlying pharmacological mechanisms of URE in an SHR rat model. Initially, the effects of URE on the metabolic network of the plasma were analyzed using non-targeted metabolomics. AA metabolites, significantly altered after URE treatment, were then quantified using the ultra-high performance liquid chromatography-tandem mass spectrometry (UHPLC-MS) method to further investigate their regulation. Finally, molecular docking was used to elucidate mechanisms of action and discover the potential active compounds.

2 MATERIALS AND METHODS

2.1 Chemicals and Reagents

Plant material of UR was kindly provided by Dr. Huiqin Pan. The voucher specimens were deposited at the herbarium of the Shanghai Institute of Materia Medica. The authentication was based on the botanical traits recorded in the Chinese Flora (<http://frps.iplant.cn/frps/Uncaria>). 1 kg of UR samples was ground and passed through the No. 2 sieve (850 µm), with a passing rate of more than 80%. The powder was extracted twice by refluxing with boiling water (1:15, w/v) for 20 min each time. The combined solution obtained was concentrated under reduced pressure and lyophilized using a freezing vacuum dryer. The extract was analyzed using LC-HRMS to establish the compounds present. The corresponding chromatographic fingerprinting was published in a previous study of our lab since the same preparation method was used (Feng et al., 2019).

19-hydroxyeicosatetraenoic acid (19-HETE), 20-hydroxyeicosatetraenoic acid (20-HETE), 18-hydroxyeicosatetraenoic acid (18-HETE), 17-hydroxyeicosatetraenoic acid (17-HETE), 16-hydroxyeicosatetraenoic acid (16-HETE), 11-hydroxyeicosatetraenoic acid (11-HETE), 12-hydroxyeicosatetraenoic acid (12-HETE), 9-hydroxyeicosatetraenoic acid (9-HETE), 8-hydroxyeicosatetraenoic acid (8-HETE), 5-hydroxyeicosatetraenoic acid (5-HETE), 15-hydroxyeicosatetraenoic acid (15-HETE), thromboxane-B2 (TXB₂), prostaglandin F2α (PGF₂α), prostaglandin D2 (PGD₂), prostaglandin E1 (PGE₁), prostaglandin E2 (PGE₂), prostaglandin I2 (PGI₂), leukotriene-E4 (LTE₄), leukotriene-B4 (LTB₄), 20-carboxy-leukotriene-B4 (20-carboxy-LTB₄), 6-trans-leukotriene-B4 (6-trans-LTB₄), 11.12-epoxyeicosatrienoic acid (11.12-EET), 8.9-epoxyeicosatrienoic acid (8.9-EET), 5.6-epoxyeicosatrienoic acid (5.6-EET), 14.15-epoxyeicosatrienoic acid (14.15-EET), 11.12-dihydroxy eicosatrienoic acid (11.12-DHET), 8.9-dihydroxy eicosatrienoic acid (8.9-DHET), 5.6-dihydroxy eicosatrienoic acid (5.6-DHET), 14.15-dihydroxy eicosatrienoic acid (14.15-DHET), 11.12-dihydroxy eicosatrienoic acid-d₁₁ (11.12-DHET-d₁₁), 5-hydroxyeicosatetraenoic acid-d₈ (5-HETE-d₈), leukotriene-B₄-d₄ (LTB₄-d₄), prostaglandin E₂-d₄ (PGE₂-d₄), and thromboxane-B₂-d₄ (TXB₂-d₄) were purchased from Cayman Chemicals (Ann Arbor, MI, United States). Deuterated compounds (11.12-DHET-d₁₁, 5-HETE-d₈, LTB₄-d₄, and PGE₂-d₄) were used as internal standards (IS) for quantification.

HPLC-grade acetonitrile and isopropanol were acquired from Merck KGaA (Merck, Darmstadt, Germany) and acetic acid from

Sigma-Aldrich (St. Louis, MO, United States) was used as the mobile phase. Formic acid and ethyl acetate were purchased from Sigma-Aldrich (St. Louis, MO, United States) and used as solvents for sample extraction. Deionized water (18.2 MΩ cm at 25°C) was prepared using a Millipore Alpha-Q water purification system (Millipore, Bedford, United States).

2.2 Animals and Drug Administration

The animal studies were carried out after approval of the protocol by the Animal Ethics Committee of Shanghai Institute of Materia Medica (Shanghai, China). The protocol number was 2017-10-GDA-47. Male SHR and normotensive control Wistar Kyoto rats (WKYs) at 10 weeks old were purchased from Wei Tong Li Hua Animal Center (Beijing, China). Rats were housed individually in metabolic cages in a standard animal laboratory with a 12-h light/dark cycle. Water and standard rat chow were available *ad libitum*, and the rats were acclimated to the facilities and environment for 2 weeks before the experiments were initiated.

The SHR rats were then randomly divided into three groups. The following preparations were administered to the rats based on the groups to which they were assigned: vehicle (deionized water) or agents suspended in the vehicle, including captopril (CAP) at 30 mg/kg (ig per day), URE at 4.00 g/kg (measured as the quantity of crude material administered ig per day, the dose was calculated as human dose 12 g/60 kg/day). The Wistar rats were defined as the normotensive control group and given the same intervention as the SHR group. All animals were given the gastric infusion once at the same time of day for a continuous period of 8 weeks.

2.3 Measurement of Blood Pressure and Heart Rate

Blood pressure was measured using a rat non-invasive tail artery blood pressure meter (SHANGHAI ALCOTT BIOTECH CO., LTD., China). The instrument was turned on and preheated for 20 min before measurement, and the pressure signal was calibrated. The rat was fixed in the fixation box, and the rat's tail was inserted into the tail cannula to access the pulse receptor. Turn on the heating blanket under the rat and start to detect the change of pulse wave. After a stable pulse wave appeared, the blood pressure of the rat was measured by clicking the measurement button. The sphygmomanometer could record the systolic and diastolic blood pressure and heart rate of the rat simultaneously.

After the rats were acclimatized in the animal room for 1 week, all rats were trained to measure blood pressure to minimize interference with the measurement data during normal blood pressure measurement due to rat discomfort. Five sets of valid data were measured for each rat, and the average of the remaining data after excluding the highest and lowest values was taken as the result of the current measurement. All rats were measured once before dosing and used as a basis for grouping.

2.4 Sample Preparation

Under isoflurane anesthesia, blood was collected from abdominal aorta in sodium heparin anticoagulation tubes until rat death. Each blood sample was centrifuged at 4,000 rpm for 10 min at 4°C. The

supernatant was transferred into clean 1.5 ml centrifuge tubes and frozen at -80°C until UHPLC/MS analysis was performed.

To a 300 µl aliquot of each sample, 1.5 µl of IS solution-(LTB₄-d₄, PGE₂-d₄, 11.12-DHET-d₁₁, 5-HETE-d₈ and TXB₂-d₄ at 500 ng/ml) and 900 µl of ethyl acetate (containing 0.025% formic acid) were added, and the samples were vortexed by vortex-mixing for 3 min. After centrifugation (4°C, 4,000 rpm) for 10 min, the 800 µl of supernatants were pooled and evaporated under nitrogen. The residue was reconstituted with methanol: water 50 µl (1:1, v/v) and 5 µl of the supernatant was injected into the UPLC-QQQ-MS system for analysis.

2.5 Chromatography and Mass Spectrometry Conditions

Chromatographic separation was performed on Agilent 6495 Triple Quadrupole (QQQ) LC/MS system with Agilent Jet Stream Technology (AJST) enhanced electrospray source (UHPLC-QQQ-MS) (Agilent Technologies, United States). The analytical column was a Waters ACQUITY UPLC BEH C18 (1.7 µm, 2.1 × 100 mm). The mobile phase was comprised of solvent A: 100% H₂O (0.1% acetic acid) and solvent B: 10% isopropanol +90% acetonitrile, with gradient elution as follows: 90%–65% A at 0–3.5 min, 65%–60% A at 3.5–5.5 min, 60%–58% A at 5.5–7 min, 58%–50% A at 7–9 min, 50%–35% A at 9–15 min, 35%–25% A at 15–17 min, 25%–15% A at 17–18.5 min, 15%–5% A at 18.5–19.5 min, 5% A at 19.5–21 min, 5%–90% A at 21–22.5 min, and 90% A at 22.5–27 min. The flow rate was kept at 0.30 ml/min. The temperatures of the autosampler and column were kept at 4 and 40°C, respectively. The injection volume of all samples was set at 5.0 µl.

The mass spectrometric analysis was done in the negative ion mode (AJST-ESI⁻). The product ions and optimal collision energies of all the compounds were selected with MassHunter Optimizer software (B.09). The ESI source parameters were optimized with MassHunter Source and iFunnel Optimizer software (B.09). The AJST-ESI⁻ conditions were finally set as follows: capillary voltage, 3,500 V; drying gas flow 14 L/min at a temperature of 200°C; nebulizer gas flow 35 psi. All the compounds were detected in dynamic multiple reaction monitoring (MRM) mode with optimized transitions and collision energies. Samples were analyzed randomly for unbiased measurement with a deuterated reference solution as internal standards to ensure accuracy and reproducibility.

2.6 Data Processing and Pattern Recognition Analysis

The plasma samples were analyzed and manipulated using MassHunter software (Agilent Technologies, Inc., United States). MassHunter Optimizer 2.0 optimization software was used to automatically optimize mass spectrometry parameters, ion pairs, and collision voltages for each analyte to be analyzed. Qualitative data were analyzed using QQQ Qualitative analysis (version B.06.00., Agilent Technologies, Inc., United States); quantitative data were analyzed using QQQ Quantitative Analysis (version B.03.02., Agilent Technologies, Inc., United States). Before chemometric analysis, the

missing values for each sample class were treated using the 80% rule. The data were introduced to SIMCA-P V14.0 (Umetrics, Sweden, Stockholm) for orthogonal partial least squares discriminant analysis (OPLS-DA). The quality of the models was evaluated with the relevant R^2 and Q^2 . Statistical significance of blood pressure, heart rate and plasma samples were analyzed using one-way analysis of variance (ANOVA) with the Tukey HSD test for post hoc analysis, implemented in GraphPad Prism 9.0 (<https://www.graphpad.com/scientific-software/prism/>).

2.7 Identification of Differential Endogenous Metabolites and Metabolic Pathway Analysis

For identification of differential endogenous metabolites, the accurate MS fragments with the metabolites were searched in One-MAP (One-step Metabolomics, Dalian ChemDataSolution Information Technology Co. Ltd., Dalian, China) and online free databases such as the Human Metabolome Database (<http://www.hmdb.ca/>), Metlin (<http://metlin.scripps.edu/>), and KEGG (<http://www.genome.jp/kegg/pathway.html>). Pathway analysis was performed by MetaboAnalyst 5.0 (<https://www.metaboanalyst.ca/>), which is a useful web-based tool for pathway analysis and visualization of metabolomics.

2.8 Molecular Docking

Simulation of the binding of alkaloid monomers to the metabolic enzyme sEH of EETs was carried out based on the molecular docking software SwissDock. Firstly, the structural formulae of corynoxine, corynoxine B, geissoschizine methylether, uncarine B, isomitraphylline, isorhynchophylline, rhynchophylline, isocorynoxine, mitraphylline, hirsutine, corynoxine, hirsutine, and uncarine A were drawn using Chemdraw 3D software to establish the 3D structures of the ligands, which were energy-optimized and saved in .mol2 format for subsequent docking analysis. Secondly, the X-ray crystal structures of sEH were downloaded from the RCSB Protein Data. The X-ray crystal structure of sEH (PDB No. 1EK2) was downloaded from the RCSB Protein Data Bank (<http://www.rcsb.org>) at a resolution of 3 Å. The X-ray crystal structure was analyzed to identify reasonable binding sites and binding pockets that could be used to define the target site and determine the rationality of the docking conformation. SwissDock was used for fast docking to generate different conformational orientations and to obtain electrostatic and van der Waals interactions between the ligand molecule and the binding site, from which the FullFitness (kcal/mol) and Estimated ΔG (kcal/mol) scores and the 3D conformations of the corresponding protein-small-molecule docking complexes are shown. Finally, the mapping was analyzed using LigPlus.

3 RESULTS AND DISCUSSION

3.1 The Effect of URE on Blood Pressure and Heart Rate

In this experiment, systolic blood pressure (SBP), diastolic blood pressure (DBP), and heart rate (HR) were measured to assess the

anti-hypertension effect of URE over 8 weeks of intragastric administration. In contrast to blood pressure measurements under anesthesia, the non-invasive tail artery sphygmomanometry used in this study, performed in a conscious state of the rats, was able to exclude changes in blood pressure caused by anesthetic drugs.

The effects of long-term URE treatment on blood pressure and HR in SHR were shown in **Figure 1**. The SBP, DBP, and HR of the control group (WKY) remained stable during the 8-weeks time course. The SBP and DBP in the model group (SHR) increased slowly throughout the experiment and eventually remained above 180 and 140 mmHg, a typical trend of blood pressure in SHRs - a slow increment in blood pressure with the age increase. Blood pressure and HR were measured at the second, fourth, and eighth weeks after treatment with CAP and URE, respectively. The SBP and DBP in the CAP and URE groups decreased rapidly after 2 weeks of administration and then remained relatively stable. After 8 weeks of treatment, the SBP and DBP of the CAP and URE groups were significantly lower than those of the SHR model group ($p < 0.0001$). In conclusion, in terms of the effects on SBP and DBP, the URE group showed the same trend as the CAP, and there was no significant difference between the two groups.

As for the effects on HR, the CAP group fluctuated dramatically and was the same as that of the model group at the end of 8 weeks of administration, whereas the URE group decreased slowly during the dosing period. This phenomenon may, to some extent, indicate the difference in the anti-hypertensive mechanism between URE and CAP. CAP was an angiotensin-converting enzyme inhibitor (ACEI), which reduced blood pressure without reflex tachycardia and compensatory change in heart rate. The perturbation of heart rate by URE might be attributed to its characteristics of multiple biological targets and functional pathways, but this effect was not significant and more data were needed in future studies.

3.2 Non-Targeted Metabolomics Pattern Analysis

To obtain the global profile of metabolites in the plasma of different experimental groups, the non-targeted metabolomics analysis was performed with UHPLC-MS under optimized conditions. The OPLS-DA, a supervised method to classify groups and extract potential biomarkers, was subsequently used to investigate the specific compounds altered by the URE treatment. The corresponding score plots from the OPLS-DA showed apparent separation between the SHR and URE groups in both positive and negative ion modes, indicating a differential metabolite composition between the two groups (**Figures 2A,B**). In addition, the OPLS-DA model parameters, including $R^2(X)$, $R^2(Y)$, and Q^2 had values of 0.785, 0.944, and 0.468 in the positive ion mode, and 0.784, 0.999, and 0.825 in the negative ion mode, exhibiting good reproducibility and predictability in explaining the differences between the two groups.

Variable importance in projection (VIP) is the variable weight value of the OPLS-DA model variables and can be used to detect biologically significant differential metabolites. Fold Change (FC)

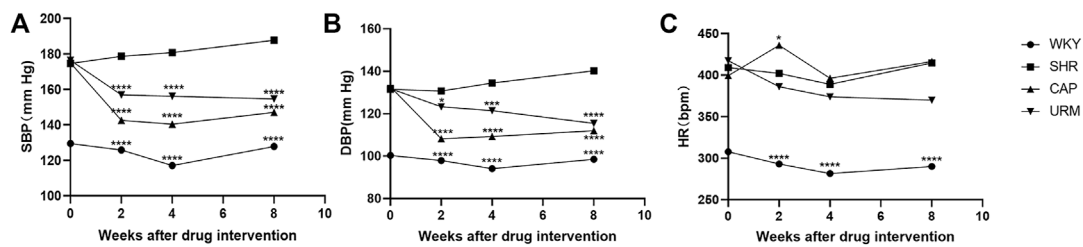


FIGURE 1 | Effect of URE on blood pressure and heart rate in spontaneously hypertensive rats. **(A)** SBP, **(B)** DBP, **(C)** HR. Values are mean \pm SD ($n = 10$). * $p < 0.05$, ** $p < 0.01$, *** $p < 0.001$, **** $p < 0.0001$ vs. SHR (one-way ANOVA with the Tukey HSD test). WKY, control group; SHR, model group; CAP, positive control group; URE, treatment group.

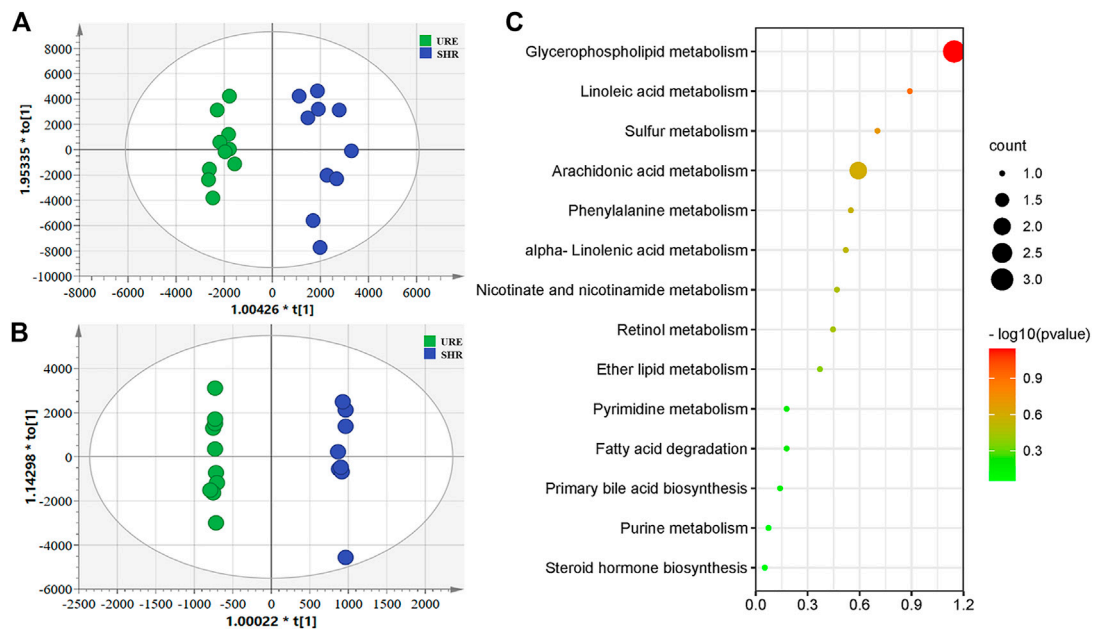


FIGURE 2 | **(A and B)** showed the OPLS-DA scores based on metabolic profiling of the URM and SHR groups, and **(C)** was the summary of differentially metabolic pathway analysis with MetaboAnalyst. **(A)** Scores plot from OPLS-DA model classifying URE and SHR groups under the positive ion mode; **(B)** Scores plot from OPLS-DA model classifying URE and SHR groups under the negative ion mode; **(C)** The differential metabolite enrichment dot bubble maps with the data of count.

is usually used to calculate the difference in expression of a metabolite between two groups. Moreover, statistical analysis is performed using a t -test to assess significant differences between the two groups. Based on $VIP > 1$, $FC > 2$, and $p < 0.05$, 573 and 539 potential differential metabolites were screened from the positive and negative ions, respectively. For further annotation, the MS^1 and MS^2 spectrum of metabolites were further analyzed in One-MAP (One-step Metabolomics, Dalian ChemDataSolution Information Technology Co. Ltd., Dalian, China). 78 and 27 metabolites were identified in the positive and negative ion modes by the MS/MS fragments, including lipids and lipid-like molecules, organic acids and derivatives, amino acids and derivatives, hormones, vitamins, and other compounds. For an in-depth understanding of the defined differential metabolites, metabolic changes were investigated based on

pathway analysis. Using MetaboAnalyst to search for differential metabolite-related pathways, there were significant changes in 14 metabolic pathways. The results showed that the regulation from URE was mainly related to the pathways of glycerophospholipid metabolism, linoleic acid metabolism, sulfur metabolism, and arachidonic acid metabolism, some of which were strongly associated with hypertension (Figure 2C).

Several metabolomic results of hypertension suggested that specific metabolites involved in the glycerophospholipid pathway had an important role in nitric oxide production as well as vascular remodeling (Jiang et al., 2015; Chu et al., 2016; Ke et al., 2018) and were even associated with the development of ischaemic hypertensive stroke (Guo et al., 2019). Linoleic acid could increase oxidative and inflammatory stresses, and abnormalities in linoleic acid metabolism was a risk factor for

the development of hypertension by directly or indirectly influencing the cardiovascular disease process (Sato et al., 2005; Feig et al., 2008) as evidenced by relevant clinical studies (Feig and Johnson, 2003; Sun et al., 2021). Selhorst et al., (2000) found that idiopathic intracranial hypertension was associated with abnormal retinol metabolism by measuring serum retinol values in normal subjects and patients with idiopathic intracranial hypertension (IIH). Bujak et al., (2016) found increased plasma levels of free fatty acids and enhanced lipolysis in patients with pulmonary arterial hypertension (PAH). In addition, metabolomic studies in SHR highlighted that various metabolites involved in phenylalanine metabolism, nicotinamide metabolism, pyrimidine metabolism, and steroid hormone biosynthesis were also associated with the development of hypertension.

Plenty of studies have demonstrated that hypertension is correlated with disturbed substance metabolism. In the current study, the URE treatment significantly altered some metabolic perturbations, which could be a crucial mechanism of its therapeutic effect. This was different from the regulatory effect of CAP on the metabolomic profile. There were few differential metabolites screened and identified in the CAP-treatment group, and only two pathways with p -value < 0.05 were obtained, including glutathione metabolism and sulfur metabolism (Supplementary Figure S3). By contrast, URE restored the functions of key metabolic pathways and thus elicited metabolic network reorganization.

3.3 Targeted Detection of Arachidonic Acid Metabolites in Plasma Samples

The aforementioned pathway enrichment results (Figure 2C) showed that the metabolism of AA, which was closely associated with hypertension, was significantly altered before and after URE treatment. AA is an important ω -6 polyunsaturated fatty acid and a precursor of several active components in the body, which plays an important role in cardiovascular diseases (Aspromonte et al., 2014; Jamieson et al., 2017; Zhang et al., 2021). In this study, a UHPLC-MS method was developed to further investigate the regulation of AA metabolites by URE. This method was sensitive, reproducible, and allowed simultaneous analysis of a range of AA metabolites without the requirement of derivatization.

The analysis was performed on an ACQUITY UPLC BEH C18 (2.1 \times 100 mm, 1.7 μ m) column. In the negative ion mode (AJS-ESI⁻), AA metabolites were ionized into deprotonated ionic substances ([M-H]⁻) (Zhang et al., 2007), which were used for EETs, HETEs, PGs, LTs, etc. as precursor ions for collision-induced decomposition (CID). The dynamic MRM method was chosen for further experiments, which was more suitable for complex samples with low levels of target analytes than the traditional time-segmented MRM method. The dynamic MRM allowed monitoring of more MRM ion pairs in a single acquisition while maintaining the high sensitivity, selectivity, and reproducibility of the chromatographic results (Dong et al., 2015). Other parameters were summarized in Table 1, including retention times for the analytes and internal standards, as well as the fragmentation voltage (Fragmentor), cell accelerator

voltage (CA), and collision energy (CE) of AA metabolites in dynamic MRM mode. The method has been fully validated, and the result was highly precise, accurate, and met the methodological requirements for quantifying *in vivo* biological samples. Validation details were shown in Supplementary Figure S1.

AA is metabolized by COX, LOX, and CYP450 enzymes to form several metabolites. The established LC-MS/MS method was used to detect the content of AA metabolites in plasma samples from rats in the WKY, SHR, and URE groups, and the results were shown in Figure 3.

3.3.1 COX Pathway

COX-1 and COX-2 convert AA to prostaglandins, prostacyclin, and thromboxanes. Prostaglandins are unsaturated fatty acids that exert various biological activities, such as inducing vasodilation and inhibiting platelet aggregation. Many studies showed that PGE₂ and PGD₂ have hypotensive activity (Smyth et al., 2009; Foudi et al., 2008; Davis et al., 2004). PGI₂ also has a similar function to prostaglandins and can be used to treat PAH (Dorris and Peebles, 2012; O'Connell et al., 2016). In contrast, thromboxane has platelet aggregation and vasoconstriction functions. As shown in Figure 3A, the plasma concentrations of PGF_{2 α} , PGE₁, PGE₂, and PGD₂ in the SHRs were significantly reduced, but all were up-regulated after URE treatment. In addition, prostacyclin showed the same characteristics of changes as prostaglandins. As classical inflammatory factors, regulation of prostaglandins was crucial to maintain homeostasis and prevent inappropriate inflammation. Inflammatory processes were important participants in the pathophysiology of hypertension, and inflammation regulation could contribute to the development of therapeutic approaches for hypertension and its complications (Savoia and Schiffrin, 2006).

3.3.2 LOX Pathway

LOXs catalyze the dioxygenation of polyunsaturated fatty acids to their corresponding hydroperoxyeicosatetraenoic acids (HPETEs), which are subsequently converted to hydroxyeicosatetraenoic acids (HETEs), leukotrienes (LTs), and lipoxins (LXs). LTs are important mediators in the development of inflammation and allergy and strongly correlated with asthma and rhinitis. Studies showed that LTB₄ contributes to PAH (Tian et al., 2014; Li et al., 2020). In this experiment, a total of three LTs were detected, as shown in Figure 3B. Compared with the control group, the concentrations of all the three compounds in the model group were significantly decreased. They could be increased after URE administration, showing a strong correlation between LTs and hypertension. The underlying molecular mechanism of this interesting correlation was unclear and needed to be studied subsequently.

3.3.3 CYP450 Pathway

CYP450 enzymes contain multiple isoforms that convert AA into different metabolites, mainly produce HETEs by ω -hydroxylase and EETs by epoxigenase. In this section, we measured various

TABLE 1 | LC-MS/MS parameters used for the analysis of AA metabolites.

| Analyte | Rt (min) | Precursor ion | Product ion | Fragmentor (V) | CA (V) | CE (V) |
|-----------------|----------|---------------|-------------|----------------|--------|--------|
| 5,6-EET | 17.69 | 319.2 | 191.3 | 380 | 5 | 8 |
| 8,9-EET | 17.50 | 319.2 | 69.21 | 380 | 5 | 13 |
| 11,12-EET | 17.29 | 319.2 | 167.1 | 380 | 5 | 12 |
| 14,15-EET | 16.75 | 319.2 | 301.1 | 380 | 5 | 8 |
| 5,6-DHET | 14.05 | 337.2 | 319.1 | 380 | 5 | 12 |
| 8,9-DHET | 13.34 | 337.2 | 127.2 | 380 | 5 | 24 |
| 11,12-DHET | 12.79 | 337.2 | 167.1 | 380 | 5 | 20 |
| 14,15-DHET | 12.23 | 337.2 | 207.1 | 380 | 5 | 16 |
| 5-HETE | 16.46 | 319.2 | 257.2 | 380 | 5 | 12 |
| 8-HETE | 15.79 | 319.2 | 301.3 | 380 | 5 | 12 |
| 9-HETE | 16.10 | 319.2 | 167.2 | 380 | 5 | 16 |
| 11-HETE | 15.50 | 319.2 | 167.2 | 380 | 5 | 16 |
| 12-HETE | 15.79 | 319.2 | 179.2 | 380 | 5 | 12 |
| 15-HETE | 15.03 | 319.2 | 301.3 | 380 | 5 | 12 |
| 16-HETE | 14.25 | 319.2 | 233.3 | 380 | 5 | 12 |
| 17-HETE | 14.13 | 319.2 | 247.2 | 380 | 5 | 12 |
| 18-HETE | 13.96 | 319.2 | 261.3 | 380 | 5 | 16 |
| 19-HETE | 13.77 | 319.2 | 301.1 | 380 | 5 | 16 |
| 20-HETE | 13.75 | 319.2 | 289.2 | 380 | 5 | 16 |
| LTB4 | 11.21 | 335.2 | 195.1 | 380 | 5 | 16 |
| 20-Carboxy-LTB4 | 5.25 | 365.2 | 347.2 | 380 | 5 | 16 |
| 6-trans-LTB4 | 10.90 | 335.2 | 195.3 | 380 | 5 | 12 |
| PGD2 | 7.46 | 351.2 | 271.2 | 380 | 5 | 16 |
| PGE1 | 7.31 | 353.2 | 317.2 | 380 | 5 | 12 |
| PGE2 | 7.14 | 351.2 | 333.2 | 380 | 5 | 8 |
| PGF2 α | 6.87 | 353.2 | 291.2 | 380 | 5 | 20 |
| PGI2 | 5.21 | 369.2 | 245.2 | 380 | 5 | 28 |
| TXB2 | 6.32 | 369.2 | 169.1 | 380 | 5 | 20 |
| 11,12-DHET-d11 | 12.71 | 348.3 | 167.2 | 380 | | 20 |
| 5-HETE-d8 | 16.36 | 327.3 | 309.2 | 380 | 5 | 12 |
| LTB4-d4 | 11.17 | 339.2 | 197.1 | 380 | 5 | 16 |
| PGE2-d4 | 7.11 | 355.2 | 319.1 | 380 | 5 | 12 |
| TXB2-d4 | 6.28 | 373.2 | 173.1 | 380 | 5 | 16 |

HETE components, and the results were shown in **Figures 3C–E**. The plasma concentrations of all the HETEs in the model group were significantly lower than those in the normal control group. Except for 17-HETE and 18-HETE, the plasma concentrations of all the other HETEs were significantly upregulated after URE treatment. As reported, 12-HETE and 15-HETE function as endothelium-derived relaxing factors (EDRFs) in arteries and contribute to vasodilation (Chawengsub et al., 2009). URE restored the functions of these vasodilating factors and rebalanced the dynamics of metabolic flux. By contrast, 20-HETE mediates contractile response through activation of Rho-kinase and sensitizes vascular SMCs to constrictors (Randriamboavonjy et al., 2003; Kizub et al., 2016). It is hypothesized that in this experiment, the changes in 20-HETE may be a mechanism of negative feedback regulation, in which sustained hypertension leads to the inhibition of 20-HETE synthesis, resulting in a decrease in its plasma concentration. After the administration of the anti-hypertensive drug, the feedback mechanism was disturbed, and the inhibition of 20-HETE synthesis was diminished so that the plasma concentration was adjusted back to the normal level.

EETs, which are metabolized by epoxygenases, have various biological effects, including anti-inflammatory, cardiovascular and metabolic disease modulation (Tacconelli and Patrignani,

2014; Lai and Chen, 2021). Their effects on hypertension are mainly vasodilative through calcium-dependent potassium channels (Campbell et al., 1996; Campbell and Falck, 2007). The plasma concentrations of EETs in SHR were significantly reduced but regulated after URE administration (**Figure 3F**). Among the four isomers, 8,9-EET had the highest plasma concentration, and 11,12-EET had the lowest. 14,15-EET in the control group showed a dramatic difference from the SHR group, and significant back-regulation was also observed after URE administration. In contrast, DHETs, as inactive hydrolysis products of EETs by the sEH enzyme, showed an opposite trend in the WKY, SHR, and URE groups (**Figure 3G**). Furthermore, the ratio of the concentration of EETs to DHETs in rat plasma was analyzed, from which we could infer sEH activity (Stefanovski et al., 2020). The results showed that EETs/DHETs in the plasma of spontaneously hypertensive rats were significantly up-regulated after URE treatment (**Figure 3H**), indicating that the hydrolytic activity of the sEH enzyme was inhibited. The above results suggested that URE may exert a hypotensive effect by inhibiting sEH enzyme activity and up-regulating the concentration of EETs. The therapeutic potential for manipulating EETs through sEH inhibitors has been well recognized for the past decade. Inhibition of sEH lowered blood pressure in SHR (Jung et al., 2005; Huang et al., 2007; Xiao et al.,

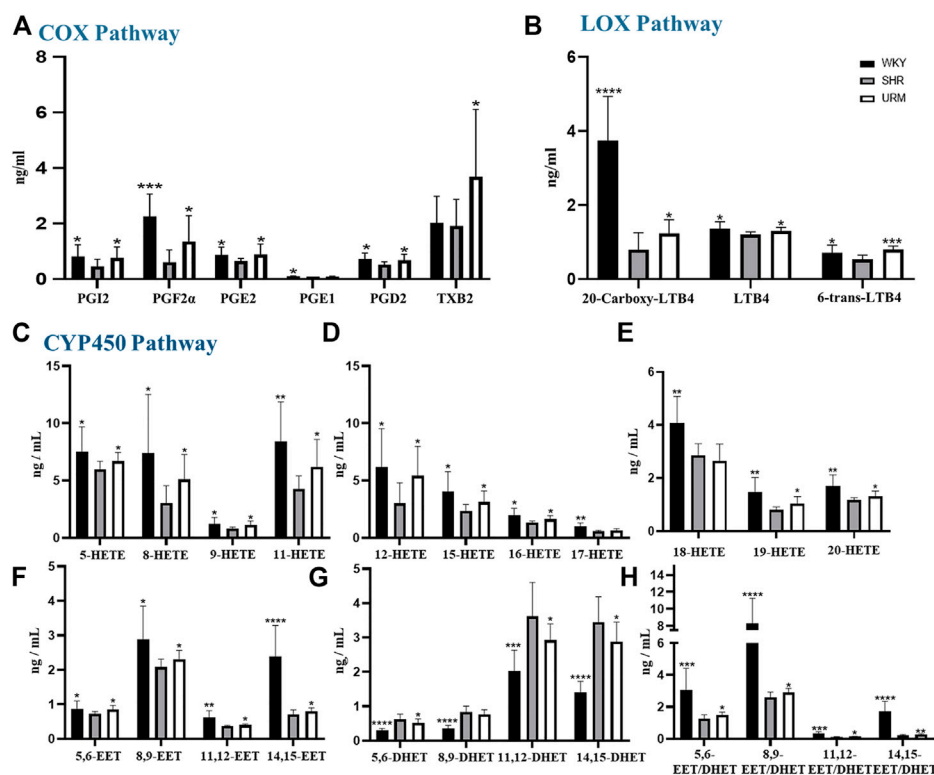


FIGURE 3 | Effects of URE on arachidonic acid metabolites concentrations in plasma of spontaneously hypertensive rats. **(A)** were the concentrations of PGs, PGI₂, and TXs in the plasma of different groups of rats, **(B)** were the concentrations of LTs; **(C–E)** were the concentrations of HETEs. **(F)** and **(G)** were the concentrations of EETs and DHETs, and **(H)** were the EET/DHET ratios. Values are mean \pm SD ($n = 8$). * $p < 0.05$, ** $p < 0.01$, *** $p < 0.001$, **** $p < 0.0001$ vs. SHR.

2010). Moreover, the biological actions of EETs had the potential to prevent complications by improving endothelial function and decreasing organ damage in cardiovascular disease (Imig, 2012). It provided a novel therapeutic approach to cardiovascular disease.

3.4 Molecular Docking Analysis for Potential Active Ingredients

Targeted metabolomics results suggested that sEH enzymes might be the potential target for the hypotensive effect of URE. Therefore, we performed the target validation using the molecular docking approach.

First, the protein-ligand crystal structure of murine sEH (PDB ID: 1EK2) was obtained from the PDB database. The receptor-ligand interactions were analyzed and displayed using the NGL protein web visualization tool, and the 3D visualization was shown in **Figure 4A**. There were multiple intermolecular interaction forces, which allowed small molecules to bind tightly to the receptor. Next, A chain was selected and analyzed using Protein-Ligand Interaction Profiler (PLIP) for key amino acid residues, intermolecular hydrophobic interactions, and hydrogen bonding interactions. The key amino acid residues were Hsp 466, Leu 441 and Tyr 408, etc. The specific results were shown in **Supplementary Tables S1, S2**.

The binding pattern of ligand 1-cyclohexyl-3-dodecyl urea (CDU) in sEH was predicted using the SwissDock program, and the binding conformation was ranked according to FullFitness (kcal/mol). The more tightly the protein was bound to the small molecule, the more energy was released and the lower the FullFitness (kcal/mol) and Estimated ΔG (kcal/mol). Therefore, the binding conformation of CDU and sEH with FullFitness of -2564.3965 kcal/mol and Estimated ΔG of -8.827662 kcal/mol was selected for the analysis. As shown in **Figure 4B**, although the binding of CDU to sEH did not form hydrogen bonding interactions, the formation of hydrophobic interactions between the carbon and oxygen atoms in the CDU and amino acid residues such as Hsp 466, Leu 441, and Tyr 408 provided strong Van der Waals forces to the molecule, allowing a tight binding between the ligand and receptor.

The structures of indole alkaloids from *Uncaria* were obtained, converted into 3D structures, and saved in.mol2 format using Chemdraw software for molecular docking after energy optimization. Among them, 13 indole alkaloids were successfully docked with sEH (**Table 2; Supplementary Table S2**), and four alkaloids with the lowest Estimated ΔG were selected for docking result analysis (**Figure 4C**). Rhynchophylline formed hydrophobic interaction forces with Trp 415 (A), Pro 312 (A), and Val280 (A). Isorhynchophylline (IR) had hydrogen bonding with Asn

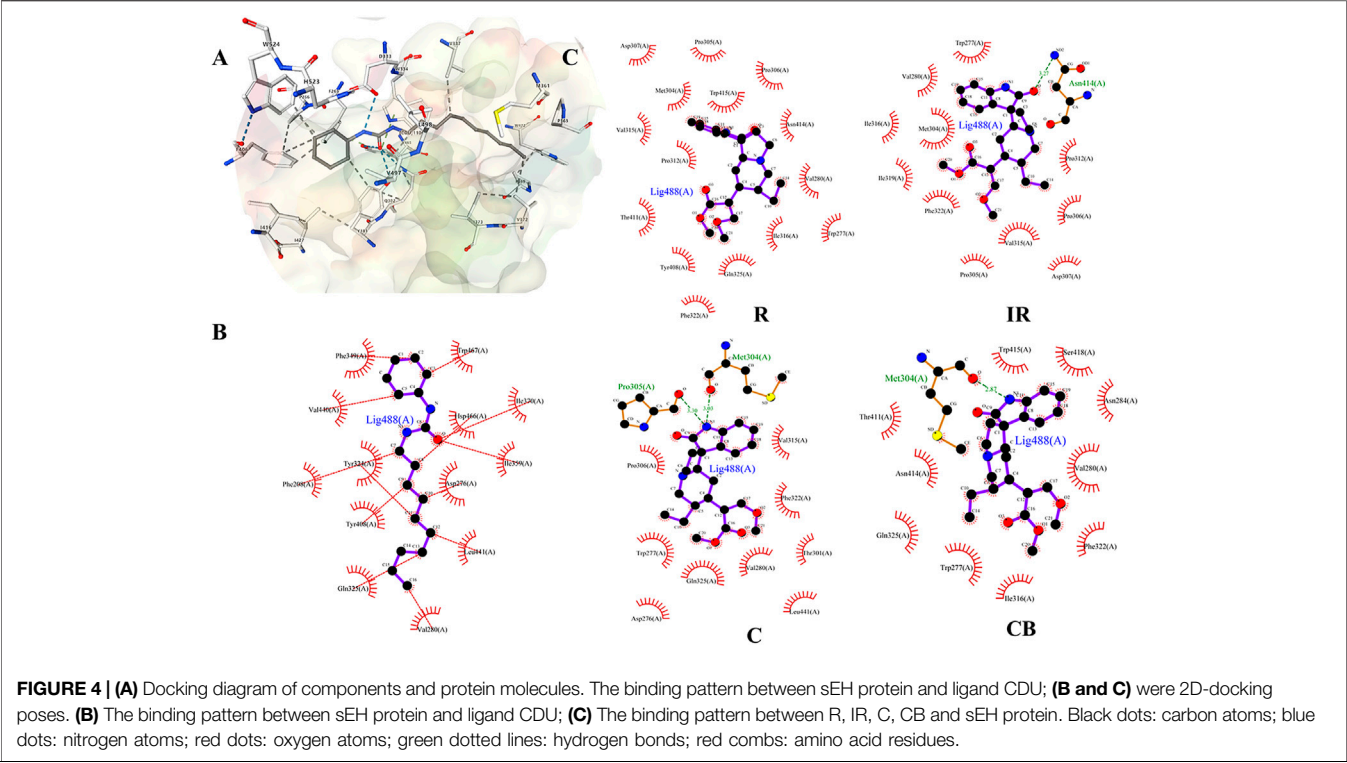


TABLE 2 | Binding energies of different alkaloids sEH protein.

| Compound | Full Fitness (kcal/mol) | Estimated ΔG (kcal/mol) |
|-----------------------------|-------------------------|-------------------------|
| CDU | −2564.3965 | −8.8276 |
| Uncarine B | −2461.5860 | −8.2986 |
| Uncarine A | −2455.6870 | −8.3054 |
| Corynoxine B | −2450.8916 | −8.6332 |
| Corynoxine | −2449.1235 | −9.0312 |
| Rhynchophylline | −2454.3022 | −8.8454 |
| Isorhynchophylline | −2446.0030 | −8.5065 |
| Corynoxine | −2443.2860 | −8.6532 |
| Isocorynoxine | −2439.0300 | −8.3091 |
| Hirsutine | −2449.8406 | −8.0997 |
| Hirsuteine | −2433.6223 | −8.0973 |
| Geissoschizine methyl ether | −2457.0188 | −7.8905 |
| Isomitraphylline | −2453.3780 | −7.6835 |
| Mitraphylline | −2451.8720 | −7.5514 |

414 (A) with an intermolecular distance of 3.27 Å and formed hydrophobic interactions with amino acid residues such as Met 304 (A) and Val 315 (A). Corynoxine (C) formed hydrogen bonds with Pro 305 (A) and Met 304 (A) and hydrophobic interactions with amino acid residues such as Trp 277 (A) and Gln 325 (A). Corynoxine B (CB) had hydrogen bonds with Met304 (A) and hydrophobic interactions with Trp 277 (A), Phe 322 (A), etc. This showed that all four alkaloids could enter the sEH binding pocket and bind stably to the amino acid residues in the pocket. Potential anti-hypertension compounds and sEH

inhibitors were discovered through the molecular docking approach.

The above results indicated that sEH might be the target protein of URE treatment, and potential anti-hypertension ingredients, as well as sEH inhibitors, were discovered through the molecular docking approach. As reported, clinical trials highlighted the promise of sEH inhibitors, such as GSK2256294, a novel sEH inhibitor, attenuated endothelial dysfunction induced by EET decrease on human resistance vessels in a clinical trial of 12 patients with COPD (Yang et al., 2017). On the whole, there was great potential in

pursuing sEH as a cardiovascular therapeutic target, and the potential sEH inhibitors in URE were worthy to be deeply explored and verified in future studies.

4 CONCLUSION

In summary, the anti-hypertension effect of URE in the SHR rat model was associated with the reorganization of the perturbed metabolic network, such as the pathway of glycerophospholipid metabolism, linoleic acid metabolism, and arachidonic acid metabolism. Twenty-eight arachidonic acid metabolites in SHR rat model were quantitatively analyzed based on UHPLC-MS method after URE administration for the first time. URE restored the functions of these vasoactive compounds and rebalanced the dynamics of arachidonic acid metabolic flux. Among them, the inhibition of sEH enzyme activity and up-regulation of vasodilators EETs were identified as contributors to the anti-hypertension effect of URE on SHRs. Using the molecular docking approach, thirteen potential anti-hypertension ingredients, as well as sEH inhibitors, were discovered from UR for further validation.

DATA AVAILABILITY STATEMENT

The datasets presented in this study can be found in online repositories. The names of the repository/repositories and accession number(s) can be found in the article/Supplementary Material.

ETHICS STATEMENT

The animal study was reviewed and approved by the Animal Ethics Committee of Shanghai Institute of Materia Medica (Shanghai, China).

REFERENCES

- Aa, J. Y., Wang, G. J., Hao, H. P., Huang, Q., Lu, Y. H., Yan, B., et al. (2010). Differential Regulations of Blood Pressure and Perturbed Metabolism by Total Ginsenosides and Conventional Antihypertensive Agents in Spontaneously Hypertensive Rats. *Acta Pharmacol. Sin.* 31 (8), 930–937. doi:10.1038/aps.2010.86
- Akira, K., Hichiya, H., Morita, M., Shimizu, A., and Mitome, H. (2013). Metabonomic Study on the Biochemical Response of Spontaneously Hypertensive Rats to Chronic Taurine Supplementation Using (1)h nmr Spectroscopic Urinalysis. *J. Pharm. Biomed. Anal.* 85, 155–161. doi:10.1016/j.jpba.2013.07.018
- Akira, K., Masu, S., Imachi, M., Mitome, H., and Hashimoto, T. (2012). A Metabonomic Study of Biochemical Changes Characteristic of Genetically Hypertensive Rats Based on (1)h nmr Spectroscopic Urinalysis. *Hypertens. Res.* 35 (4), 404–412. doi:10.1038/hr.2011.182
- Arnett, D. K., and Claas, S. A. (2018). Omics of Blood Pressure and Hypertension. *Circ. Res.* 122 (10), 1409–1419. doi:10.1161/CIRCRESAHA.118.311342
- Aspromonte, N., Monitillo, F., Puzzovivo, A., Valle, R., Caldarola, P., and Iacoviello, M. (2014). Modulation of Cardiac Cytochrome P450 in Patients with Heart Failure. *Expert Opin. Drug Metab. Toxicol.* 10 (3), 327–339. doi:10.1517/17425255.2014.872240

AUTHOR CONTRIBUTIONS

LG: Conceptualization, Methodology, Writing — review and editing, Validation, Formal analysis, Investigation, Visualization; XK: Conceptualization, Methodology, Visualization, Writing — original draft, Data curation, Formal analysis, Investigation; WeW: Methodology, Software, Validation; ZF: Methodology, Software, Validation; HZ: Conceptualization, Funding acquisition; ZZ: Resources; HL: Resources; ML: Resources; JH: Conceptualization, Methodology, Software, Validation, Writing — review and editing, Project administration, Funding acquisition; WaW: Resources, Supervision, Writing — review and editing, Project administration, Funding acquisition; D-aG: Resources, Supervision, Writing — review and editing.

FUNDING

This research was supported by grants from the National Natural Sciences Foundation of China (Grant No. 82003915).

ACKNOWLEDGMENTS

We thank Jing Huang in Waters Corporation for her cooperation and support. We thank Wei Rao, Emmanuelle Claude, Jonathan P. Willams, Mark Towers, Philippa Hart, and Yanchao Shi in Waters Corporation for the technical support.

SUPPLEMENTARY MATERIAL

The Supplementary Material for this article can be found online at: <https://www.frontiersin.org/articles/10.3389/fphar.2022.909631/full#supplementary-material>

- Bujak, R., Mateo, J., Blanco, I., Izquierdo-García, J. L., Dudzik, D., Markuszewski, M. J., et al. (2016). New Biochemical Insights into the Mechanisms of Pulmonary Arterial Hypertension in Humans. *PLoS One* 11 (8), e0160505. doi:10.1371/journal.pone.0160505
- Campbell, W. B., and Falck, J. R. (2007). Arachidonic Acid Metabolites as Endothelium-Derived Hyperpolarizing Factors. *Hypertension* 49 (3), 590–596. doi:10.1161/01.HYP.0000255173.50317.fc
- Campbell, W. B., Gebremedhin, D., Pratt, P. F., and Harder, D. R. (1996). Identification of Epoxyeicosatrienoic Acids as Endothelium-Derived Hyperpolarizing Factors. *Circ. Res.* 78 (3), 415–423. doi:10.1161/01.res.78.3.415
- Campbell, W. B., Imig, J. D., Schmitz, J. M., and Falck, J. R. (2017). Orally Active Epoxyeicosatrienoic Acid Analogs. *J. Cardiovasc. Pharmacol.* 70 (4), 211–224. doi:10.1097/FJC.0000000000000523
- Chawengsub, Y., Gauthier, K. M., and Campbell, W. B. (2009). Role of Arachidonic Acid Lipoxygenase Metabolites in the Regulation of Vascular Tone. *Am. J. Physiol. Heart Circ. Physiol.* 297 (2), H495–H507. doi:10.1152/ajpheart.00349.2009
- Chu, Y., Jiang, H., Ju, J., Li, Y., Gong, L., Wang, X., et al. (2016). A Metabolomic Study Using HPLC-TOF/MS Coupled with Ingenuity Pathway Analysis: Intervention Effects of Rhizoma Alismatis on Spontaneous Hypertensive Rats. *J. Pharm. Biomed. Anal.* 117, 446–452. doi:10.1016/j.jpba.2015.09.026
- Currie, G., and Delles, C. (2017). The Future of "Omics" in Hypertension. *Can. J. Cardiol.* 33 (5), 601–610. doi:10.1016/j.cjca.2016.11.023

- Das, U. N. (2018). Arachidonic Acid in Health and Disease with Focus on Hypertension and Diabetes Mellitus: A Review. *J. Adv. Res.* 11, 43–55. doi:10.1016/j.jare.2018.01.002
- Davis, R. J., Murdoch, C. E., Ali, M., Purbrick, S., Ravid, R., Baxter, G. S., et al. (2004). EP4 Prostanoid Receptor-Mediated Vasodilatation of Human Middle Cerebral Arteries. *Br. J. Pharmacol.* 141 (4), 580–585. doi:10.1038/sj.bjp.0705645
- Dong, Y., Yan, K., Ma, Y., Wang, S., He, G., Deng, J., et al. (2015). A Sensitive Dilute-And-Shoot Approach for the Simultaneous Screening of 71 Stimulants and 7 Metabolites in Human Urine by LC-MS-MS with Dynamic MRM. *J. Chromatogr. Sci.* 53 (9), 1528–1535. doi:10.1093/chromsci/bmv048
- Dorris, S. L., and Peebles, R. S., Jr. (2012). PGI2 as a Regulator of Inflammatory Diseases. *Mediat. Inflamm.* 2012, 926968. doi:10.1155/2012/926968
- Feig, D. I., and Johnson, R. J. (2003). Hyperuricemia in Childhood Primary Hypertension. *Hypertension* 42 (3), 247–252. doi:10.1161/01.HYP.0000085858.66548.59
- Feig, D. I., Kang, D. H., and Johnson, R. J. (2008). Uric Acid and Cardiovascular Risk. *N. Engl. J. Med.* 359 (17), 1811–1821. doi:10.1056/NEJMra0800885
- Feng, Z., Hou, J., Yu, Y., Wu, W., Deng, Y., Wang, X., et al. (2019). Dissecting the Metabolic Phenotype of the Antihypertensive Effects of Five Uncaria Species on Spontaneously Hypertensive Rats. *Front. Pharmacol.* 10, 845. doi:10.3389/fphar.2019.00845
- Forouzanfar, M. H., Liu, P., Roth, G. A., Ng, M., Biryukov, S., Marczak, L., et al. (2017). Global Burden of Hypertension and Systolic Blood Pressure of at Least 110 to 115 mm Hg, 1990–2015. *JAMA* 317 (2), 165–182. doi:10.1001/jama.2016.19043
- Foudi, N., Kotelevets, L., Louedec, L., Leséche, G., Henin, D., Chastre, E., et al. (2008). Vasorelaxation Induced by Prostaglandin E2 in Human Pulmonary Vein: Role of the EP4 Receptor Subtype. *Br. J. Pharmacol.* 154 (8), 1631–1639. doi:10.1038/bjp.2008.214
- Guo, X., Li, Z., Zhou, Y., Yu, S., Yang, H., Zheng, L., et al. (2019). Metabolic Profile for Prediction of Ischemic Stroke in Chinese Hypertensive Population. *J. Stroke Cerebrovasc. Dis.* 28 (4), 1062–1069. doi:10.1016/j.jstrokecerebrovasdis.2018.12.035
- Huang, H., Morisseau, C., Wang, J., Yang, T., Falck, J. R., Hammock, B. D., et al. (2007). Increasing or Stabilizing Renal Epoxyeicosatrienoic Acid Production Attenuates Abnormal Renal Function and Hypertension in Obese Rats. *Am. J. Physiol. Ren. Physiol.* 293 (1), F342–F349. doi:10.1152/ajprenal.00004.2007
- Imig, J. D. (2012). Epoxides and Soluble Epoxide Hydrolase in Cardiovascular Physiology. *Physiol. Rev.* 92 (1), 101–130. doi:10.1152/physrev.00021.2011
- Jamieson, K. L., Endo, T., Darwesh, A. M., Samokhvalov, V., and Seubert, J. M. (2017). Cytochrome P450-Derived Eicosanoids and Heart Function. *Pharmacol. Ther.* 179, 47–83. doi:10.1016/j.pharmthera.2017.05.005
- Jiang, H., Shen, Z., Chu, Y., Li, Y., Li, J., Wang, X., et al. (2015). Serum Metabolomics Research of the Anti-hypertensive Effects of Tengfu Jiangya Tablet on Spontaneously Hypertensive Rats. *J. Chromatogr. B Anal. Technol. Biomed. Life Sci.* 1002, 210–217. doi:10.1016/j.jchromb.2015.08.010
- Jung, O., Brandes, R. P., Kim, I. H., Schweda, F., Schmidt, R., Hammock, B. D., et al. (2005). Soluble Epoxide Hydrolase Is a Main Effector of Angiotensin II-Induced Hypertension. *Hypertension* 45 (4), 759–765. doi:10.1161/01.HYP.0000153792.29478.1d
- Ke, C., Zhu, X., Zhang, Y., and Shen, Y. (2018). Metabolomic Characterization of Hypertension and Dyslipidemia. *Metabolomics* 14 (9), 117. doi:10.1007/s11306-018-1408-y
- Kizub, I. V., Lakhkar, A., Dhagia, V., Joshi, S. R., Jiang, H., Wolin, M. S., et al. (2016). Involvement of Gap Junctions between Smooth Muscle Cells in Sustained Hypoxic Pulmonary Vasoconstriction Development: a Potential Role for 15-HETE and 20-HETE. *Am. J. Physiol. Lung Cell Mol. Physiol.* 310 (8), L772–L783. doi:10.1152/ajplung.00377.2015
- Lai, J., and Chen, C. (2021). The Role of Epoxyeicosatrienoic Acids in Cardiac Remodeling. *Front. Physiol.* 12, 642470. doi:10.3389/fphys.2021.642470
- Li, S., Zhai, C., Shi, W., Feng, W., Xie, X., Pan, Y., et al. (2020). Leukotriene B4 Induces Proliferation of Rat Pulmonary Arterial Smooth Muscle Cells via Modulating GSK-3 β / β -Catenin Pathway. *Eur. J. Pharmacol.* 867, 172823. doi:10.1016/j.ejphar.2019.172823
- Liang, J. H., Wang, C., Huo, X. K., Tian, X. G., Zhao, W. Y., Wang, X., et al. (2020). The Genus Uncaria: A Review on Phytochemical Metabolites and Biological Aspects. *Fitoterapia* 147, 104772. doi:10.1016/j.fitote.2020.104772
- Liu, A., Chu, Y. J., Wang, X., Yu, R., Jiang, H., Li, Y., et al. (2018). Serum Metabolomics Study Based on LC-MS and Antihypertensive Effect of Uncaria on Spontaneously Hypertensive Rats. *Evid. Based Complement. Altern. Med.* 2018, 9281946. doi:10.1155/2018/9281946
- Nikolic, S. B., Sharman, J. E., Adams, M. J., and Edwards, L. M. (2014). Metabolomics in Hypertension. *J. Hypertens.* 32 (6), 1159–1169. doi:10.1097/HJH.0000000000000168
- O'Connell, C., Amar, D., Boucly, A., Savale, L., Jaïs, X., Chaumais, M. C., et al. (2016). Comparative Safety and Tolerability of Prostacyclins in Pulmonary Hypertension. *Drug Saf.* 39 (4), 287–294. doi:10.1007/s40264-015-0365-x
- Qin, N., Lu, X., Liu, Y., Qiao, Y., Qu, W., Feng, F., et al. (2021). Recent Research Progress of Uncaria Spp. Based on Alkaloids: Phytochemistry, Pharmacology and Structural Chemistry. *Eur. J. Med. Chem.* 210, 112960. doi:10.1016/j.ejmech.2020.112960
- Randriamboavonjy, V., Busse, R., and Fleming, I. (2003). 20-HETE-induced Contraction of Small Coronary Arteries Depends on the Activation of Rho-Kinase. *Hypertension* 41 (3 Pt 2), 801–806. doi:10.1161/01.HYP.0000047240.33861.6B
- Sato, M., Shibata, K., Nomura, R., Kawamoto, D., Nagamine, R., and Imaizumi, K. (2005). Linoleic Acid-Rich Fats Reduce Atherosclerosis Development beyond its Oxidative and Inflammatory Stress-Increasing Effect in Apolipoprotein E-Deficient Mice in Comparison with Saturated Fatty Acid-Rich Fats. *Br. J. Nutr.* 94 (6), 896–901. doi:10.1079/bjn20051409
- Savaio, C., and Schiffrin, E. L. (2006). Inflammation in Hypertension. *Curr. Opin. Nephrol. Hypertens.* 15 (2), 152–158. doi:10.1097/01.mnh.0000203189.57513.76
- Selhorst, J. B., Kulkantrakorn, K., Corbett, J. J., Leira, E. C., and Chung, S. M. (2000). Retinol-binding Protein in Idiopathic Intracranial Hypertension (IIH). *J. Neuroophthalmol.* 20 (4), 250–252. doi:10.1097/00041327-200020040-00009
- Smyth, E. M., Grosser, T., Wang, M., Yu, Y., and FitzGerald, G. A. (2009). Prostanoids in Health and Disease. *J. Lipid Res.* 50 Suppl (Suppl. 1), S423–S428. doi:10.1194/jlr.R800094-JLR200
- Stefanovski, D., Shih, P. B., Hammock, B. D., Watanabe, R. M., and Youn, J. H. (2020). Assessment of Soluble Epoxide Hydrolase Activity *In Vivo*: A Metabolomic Approach. *Prostagl. Other Lipid Mediat* 148, 106410. doi:10.1016/j.prostaglandins.2020.106410
- Sun, J., Ding, W., Liu, X., Zhao, M., and Xi, B. (2021). Serum Metabolites of Hypertension Among Chinese Adolescents Aged 12–17 Years. *J. Hum. Hypertens.* 2021. doi:10.1038/s41371-021-00602-8
- Tacconelli, S., and Patrignani, P. (2014). Inside Epoxyeicosatrienoic Acids and Cardiovascular Disease. *Front. Pharmacol.* 5, 239. doi:10.3389/fphar.2014.00239
- Tian, W., Jiang, X., Sung, Y. K., Qian, J., Yuan, K., and Nicolls, M. R. (2014). Leukotrienes in Pulmonary Arterial Hypertension. *Immunol. Res.* 58 (2–3), 387–393. doi:10.1007/s12026-014-8492-5
- Xiao, B., Li, X., Yan, J., Yu, X., Yang, G., Xiao, X., et al. (2010). Overexpression of Cytochrome P450 Epoxygenases Prevents Development of Hypertension in Spontaneously Hypertensive Rats by Enhancing Atrial Natriuretic Peptide. *J. Pharmacol. Exp. Ther.* 334 (3), 784–794. doi:10.1124/jpet.110.167510
- Yang, L., Cheriyan, J., Gutterman, D. D., Mayer, R. J., Ament, Z., Griffin, J. L., et al. (2017). Mechanisms of Vascular Dysfunction in COPD and Effects of a Novel Soluble Epoxide Hydrolase Inhibitor in Smokers. *Chest* 151 (3), 555–563. doi:10.1016/j.chest.2016.10.058
- Yang, M., and Lao, L. (2019). Emerging Applications of Metabolomics in Traditional Chinese Medicine Treating Hypertension: Biomarkers, Pathways and More. *Front. Pharmacol.* 10, 158. doi:10.3389/fphar.2019.00158
- Zhang, J. H., Pearson, T., Matharoo-Ball, B., Ortori, C. A., Warren, A. Y., Khan, R., et al. (2007). Quantitative Profiling of Epoxyeicosatrienoic, Hydroxyeicosatetraenoic, and Dihydroxyeicosatetraenoic Acids in Human Intrauterine Tissues Using Liquid

- Chromatography/Electrospray Ionization Tandem Mass Spectrometry. *Anal. Biochem.* 365 (1), 40–51. doi:10.1016/j.ab.2007.03.001
- Zhang, T., Au Yeung, S. L., and Schooling, C. M. (2021). Associations of Arachidonic Acid Synthesis with Cardiovascular Risk Factors and Relation to Ischemic Heart Disease and Stroke: A Univariable and Multivariable Mendelian Randomization Study. *Nutrients* 13 (5), 1489. doi:10.3390/nu13051489
- Zhou, Y., Khan, H., Xiao, J., and Cheang, W. S. (2021). Effects of Arachidonic Acid Metabolites on Cardiovascular Health and Disease. *Int. J. Mol. Sci.* 22 (21), 2029. doi:10.3390/ijms222112029

Conflict of Interest: The authors declare that the research was conducted in the absence of any commercial or financial relationships that could be construed as a potential conflict of interest.

Publisher's Note: All claims expressed in this article are solely those of the authors and do not necessarily represent those of their affiliated organizations, or those of the publisher, the editors and the reviewers. Any product that may be evaluated in this article, or claim that may be made by its manufacturer, is not guaranteed or endorsed by the publisher.

Copyright © 2022 Gao, Kong, Wu, Feng, Zhi, Zhang, Long, Lei, Hou, Wu and Guo. This is an open-access article distributed under the terms of the Creative Commons Attribution License (CC BY). The use, distribution or reproduction in other forums is permitted, provided the original author(s) and the copyright owner(s) are credited and that the original publication in this journal is cited, in accordance with accepted academic practice. No use, distribution or reproduction is permitted which does not comply with these terms.



Multi-Omics Integration Analysis Identifies Lipid Disorder of a Non-Alcoholic Fatty Liver Disease (NAFLD) Mouse Model Improved by Zexie–Baizhu Decoction

OPEN ACCESS

Edited by:

Xijun Wang,
Heilongjiang University of Chinese
Medicine, China

Reviewed by:

Hyeong-Geug Kim,
Indiana University, Purdue University
Indianapolis, United States
Aihua Zhang,
Heilongjiang University of Chinese
Medicine, China

*Correspondence:

Likun Gong
lkong@simm.ac.cn
Wanying Wu
wanyingwu@simm.ac.cn
Jing Chen
jingchen@simm.ac.cn
Jinjun Hou
jinjun_hou@simm.ac.cn

[†]These authors have contributed
equally to this work and share first
authorship

Specialty section:

This article was submitted to
Ethnopharmacology,
a section of the journal
Frontiers in Pharmacology

Received: 20 January 2022

Accepted: 25 April 2022

Published: 20 June 2022

Citation:

Cao Y, Shi J, Song L, Xu J, Lu H, Sun J,
Hou J, Chen J, Wu W and Gong L
(2022) Multi-Omics Integration
Analysis Identifies Lipid Disorder of a
Non-Alcoholic Fatty Liver Disease
(NAFLD) Mouse Model Improved by
Zexie–Baizhu Decoction.
Front. Pharmacol. 13:858795.
doi: 10.3389/fphar.2022.858795

Yuhan Cao^{1,2†}, Jingying Shi^{2,3†}, Luyao Song^{1,2}, Junjiu Xu⁴, Henglei Lu¹, Jianhua Sun¹,
Jinjun Hou^{3*}, Jing Chen^{1,2*}, Wanying Wu^{2,3*} and Likun Gong^{1,2,4*}

¹State Key Laboratory of Drug Research, Shanghai Institute of Materia Medica, Chinese Academy of Sciences, Shanghai, China,

²University of Chinese Academy of Sciences, Beijing, China, ³National Engineering Research Center of TCM Standardization
Technology, Shanghai Institute of Materia Medica, Chinese Academy of Sciences, Shanghai, China, ⁴School of Chinese Materia
Medica, Nanjing University of Chinese Medicine, Nanjing, China

Non-alcoholic fatty liver disease (NAFLD) is an increasingly epidemic metabolic disease with complex pathogenesis. Multi-target therapy may be an effective strategy for NAFLD treatment, and traditional Chinese medicine (TCM) characterized by multi-ingredients and multi-targets has unique advantages in long-term clinical practice. Zexie–Baizhu (ZXBZ) decoction is a Chinese classical formula to treat body fluid disorders initially. Although many bioactive monomers from Zexie and Baizhu had been discovered to improve lipid disorders, limited research studies were focused on the aqueous decoction of ZXBZ, the original clinical formulation. In the current study, we identified 94% chemical composition of ZXBZ decoction and first discovered its hepatoprotective effect in a gubra-amylin NASH (GAN) diet-induced NAFLD mouse model. Based on metabolomics and transcriptomics analyses, we speculated that lipid and glucose metabolisms might be regulated by ZXBZ decoction, which was further confirmed by improved dyslipidemia and hepatic steatosis in ZXBZ groups. Consistently with cross-omics analysis, we discovered ZXBZ decoction could influence two energy sensors, Sirt1 and AMPK, and subsequently affect related proteins involved in lipid biosynthesis, catabolism, and transport. In conclusion, ZXBZ decoction regulated energy sensors, consequently impeded lipogenesis, and promoted fatty acid oxidation (FAO) to alleviate lipid disorders and protect the liver in NAFLD models, which suggested ZXBZ decoction might be a promising treatment for NAFLD.

Keywords: NAFLD, metabolomics, transcriptomics, lipid metabolism, traditional Chinese medicine

INTRODUCTION

Non-alcoholic fatty liver disease (NAFLD) is an emerging global health problem, especially in economically developed areas (Stefan et al., 2019). However, there are few officially approved drugs for NAFLD due to the extremely complicated pathogenesis (Konerman et al., 2018; Mullard, 2020). The most widely accepted hypotheses of NAFLD are the “two-hit hypothesis” and “multiple parallel hits hypothesis” (Day and James, 1998; Tilg and Moschen, 2010), and the consensus of these

assumptions is that excessive hepatic lipid accumulation forms the first hit for the development of NAFLD (Lomonaco et al., 2012; Hirsova et al., 2016). As reported, the excessive lipid accrual in the liver leads to lipotoxicity, subsequently causing many adverse changes in hepatocytes, such as endoplasmic reticulum (ER) stress (Fu et al., 2012), mitochondria and lysosomal dysfunction (Manne et al., 2018), and impaired autophagy (Li et al., 2008). In addition, lipotoxicity can exacerbate glucose dysmetabolism (Ahmed et al., 2021), inflammation, and intestinal microbiota dysfunction (Bastin and Andreelli, 2020). These risk factors become the second hits to NAFLD, based on the excessive hepatic lipid accumulation as the first hit. Therefore, improving lipid metabolism is a fundamental therapeutic strategy for NAFLD.

Because of the tangled network of glucose and lipid disorders causing the complicated pathogenesis, there were limitations that single-target drugs might end up in adverse effects and compensatory feedbacks from other pathways, resulting in the lack of safe and effective drugs for NAFLD. In this case, seeking multi-target drugs which improve NAFLD phenotypically has unique advantages. Nowadays, traditional Chinese medicine (TCM) has garnered more interest in offering plentiful candidates for NAFLD treatment, with its effectiveness proved in long-term clinic use. Not only many bioactive monomers, such as silymarin and berberine are under phase four clinical trials (Yan et al., 2020), but also numbers of classical formulas have been proven to alleviate NAFLD (Dai et al., 2021; Yang, Sun, Wang, Zhang, Zhang, Gao et al.). Zexie–Baizhu (ZXBZ) decoction is a classical traditional Chinese medicine formula, which was initially written in *Synopsis of Prescriptions of the Golden Chamber* (Jingui Yaolue, AD. ~ 220) in the Han dynasty to treat metabolism disorders of the body fluid, especially in the liver or stomach (abdomen). ZXBZ decoction is prepared with water in a ratio of 5:2 of Zexie (*Alismatis Rhizoma*, the rhizome of *Alisma plantago-aquatica* subsp. *orientale* (Sam.) Sam.) and Baizhu (*Atractylodis macrocephalae Rhizoma*, the rhizome of *Atractylodes macrocephala* Koidz.). Many extracts and some bioactive monomers of zexie and baizhu have been discovered to ameliorate metabolic diseases, especially lipid metabolism disorders. For instance, alisol A/alisol B/alisol-2,3-C from Zexie and atractylenolides (I, II, and III) from Baizhu can improve lipid metabolism via activating PI3K/Akt, AMPK, and JAK-STAT pathways (Chen et al., 2020; Wang et al., 2020; Yu et al., 2020; Sun et al., 2021a; Deng et al., 2021; Luan et al., 2021). Several kinds of alcohol extracts of zexie were also reported to benefit the lipid metabolism and relieve inflammation (Park et al., 2014; Jang et al., 2015; Zhang et al., 2017; Liu et al., 2019), and several TCM formulas containing Zexie and Baizhu are effective for NAFLD in previous studies (Fang et al., 2017; Feng et al., 2019a; Cheng et al., 2019; Tang et al., 2020). However, limited studies were performed on ZXBZ aqueous decoction itself. Since ZXBZ decoction is the most original prescription with effects proven by wide clinical applications since ancient China, we are determined to verify its efficacy in the NAFLD mouse model and investigate the underlying mechanisms for the further development and exploration of ZXBZ decoction.

In the current study, we first discovered the protective effects of ZXBZ decoction on the liver in the gubra-amylin NASH (GAN) diet-induced NAFLD model. Then, the multi-omics integration analyses including metabolomics and transcriptomics revealed the potential mechanisms of the lipid metabolism improved by ZXBZ decoction. Finally, the related genes including Sirt1, AMPK, and their downstream genes were detected by WB, RT-PCR, and IF, in which we found that ZXBZ decoction could protect the liver and balance lipid disorders in the NAFLD model via influencing AMPK and Sirt1. In addition, we have also observed similar pharmacological actions *in vitro*. Altogether, these results shed a light on the effects and mechanisms of ZXBZ decoction and propose further development of TCM toward NAFLD treatment.

MATERIALS AND METHODS

Preparation and Verification of ZXBZ Decoction

Zexie pieces (*Alismatis Rhizoma*, the rhizome of *Alisma plantago-aquatica* subsp. *orientale* (Sam.) Sam., origin from Fujian, China) was obtained from Kangmei Pharmaceutical Co., Ltd., while Baizhu pieces (*Atractylodis macrocephalae Rhizoma*, the rhizome of *Atractylodes macrocephala* Koidz., origin from Anhui, China) was purchased from Shanghai Leiyunshang Co., Ltd. Dr. JJ Hou had authorized the two herbs of ZXBZ decoction based on Chinese Pharmacopoeia (2020 edition, Volume I). According to the “Synopsis of Prescriptions of the Golden Chamber,” the ratio of Zexie to Baizhu is 5:2 (w/w). Thus, zexie pieces (600.0 g) and Baizhu pieces (240.0 g) in ZXBZ decoction were soaked with water (16.0 L) for half an hour. Then, they were slightly boiled for 2 h. The filtrates were concentrated by reducing pressure at 45°C, and freeze-dried into the water extract, in which the yield was 30.0%. The powder of water extract was stored at –20°C. Before gavage administration in mice, the water extract (75 and 150 mg/ml) was dissolved in 0.5% sodium carboxymethyl cellulose (CMC-Na).

Animal Handling and Grouping

Six weeks old male C57/BL6 mice were purchased from Shanghai Laboratory Animal Co. (Shanghai, China) and fed in specific pathogen-free (SPF)-grade according to requirements of the Institutional Ethics Committee of Shanghai Institute of Materia Medica. The relative humidity was 30%–70%, the light/dark cycle was 12/12 h, and diet and drinking water were provided *ad libitum*. After 1-week adaptation and a 5-week gubra-amylin NASH (GAN) diet induction (rodent diets with 40 kcal% fat) (Primex or Palm Oil, Research Diets, United States) (Boland et al., 2019), the mice were distributed evenly into four groups according to body weights and ALT, besides normal control diet (NOD) mice were fed with regular diet and water ($n = 10$). Then the four GAN diet-induced groups were given vehicle (i.g.), obeticholic acid (30 mg/kg, i.g.), and ZXBZ decoction (750 and 1,500 mg/kg, i.g.) every day, respectively. After a feeding period of 17 weeks along with drug treatment

of 12 weeks, the mice were sacrificed, and the liver and serum were collected for subsequent analysis.

Serum Biochemistry Analysis

Blood was collected every 4 weeks via the tail veins of mice since drug or vehicle treatment began when mice had been fed on GAN diet for 5 weeks. The levels of serum ALT, AST, TC, TG, and LDL-C were measured using an automatic Roche biochemical analyzer with Roche kits (ALT, AST, TC, TG, and LDL-C).

Fasting Blood Glucose, Oral Glucose Tolerance Test, Insulin Tolerance Test, and HOMA-IR

Fasting blood glucoses were determined after 6 hours of fasting using the OneTouch Select Simple[®] glucose meter (Johnson & Johnson, United States). As for the oral glucose tolerance test (OGTT) and insulin tolerance test (ITT), the mice were fasted for 16 and 6 h, respectively, at the 11th and 13th week of GAN diet induction with the treatment of 1 g/kg glucose (i.g.) or 0.75 U/kg insulin (i.p.). The glucose baseline levels were measured at 0, 15, 30, 45, 60, 90, and 120 min and calculated by the area under the curve (AUC). The homeostasis model assessment of the insulin resistance (HOMA-IR) level was performed at the 12th week of GAN diet induction and evaluated according to the formula $HOMA-IR = [fasting\ plasma\ glucose\ (mmol/L) \times fasting\ plasma\ insulin\ (ng/ml)] / 22.5$. The insulin levels were examined using the ELISA kit (Beijing Solarbio Science & Technology Co., Ltd., Beijing, China).

Histopathological Analysis

The livers were removed after a 12-week drug or vehicle treatment when HFD induction lasted for 17 weeks and fixed in 10% neutral buffered formalin to dehydrate for 3 days and embedded in paraffin. Serial transverse sections of 3–4 μ m were stained with hematoxylin and eosin. To evaluate the degree of NAFLD quantitatively, the liver lesions were observed under low-power microscopy and examined following the NAFLD activity score (Kleiner et al., 2005).

The left lobes of livers were embedded by optimal cutting temperature compound (OCT) and frozen in liquid nitrogen immediately, then, the frozen tissues were cut into lesions and laid flat on glass slides. After staying at room temperature for 5 min, the samples were washed with distilled water and 60% isopropanol twice. Then, the samples were dyed with oil red O working solution for 5 min and terminated with distilled water and redyed with hematoxylin. The samples were observed and screened under a low-power microscope.

Untargeted Urine Metabolomics Analysis

At 1, 5, and 9 weeks, urine was collected over 24 h through metabolic cages. The acquired urine samples were stored at -80°C pending sample preparation (Khamis et al., 2017; Feng et al., 2019b). The urine samples were thawed at room temperature before the measurement. The supernatant was diluted with water. The dilution factor was determined by the creatinine level measured in the urine sample by the HPLC

procedure according to the Ministry of Health of the People's Republic of China (People's Republic of China, 1996). The diluted samples were centrifuged at 14,000 rpm for 10 min at 4°C for the UPLC–MS analysis. The exact UPLC–MS method has been reported before (Feng et al., 2019b). In brief, an LTQ-Orbitrap Velos Pro hybrid mass spectrometer (Thermo Fisher Scientific Corp.) linked to an Ultimate 3000 UHPLC system was used to produce high-resolution mass spectra for metabolomic investigation. A Waters ACQUITY UPLC HSS T3 column (1.8 μ m, 2.1 mm \times 100 mm) with an online filter was used to separate the samples. The mobile phase consisted of solvent A [100% H_2O (0.1% formic acid)] and solvent B [100% acetonitrile (0.1% formic acid)]. The elution procedure is as follows: 0–1 min, 99% A; 1–3 min, 99%–85% A; 3–6 min, 85%–50% A; 6–9 min, 50%–5% A; and 9–10 min, 5% A. The flow rate remained constant at 0.5 ml/min. The autosampler and column were held at 4 and 40°C , respectively. The injection volume was fixed at 5 μ l for all samples. The quality control (QC) sample was made up of an equal volume (10 μ l) of each urine sample, and used to evaluate the peak intensity stability of metabolomics analysis. The QC sample was injected each after five samples.

In Vitro Assay

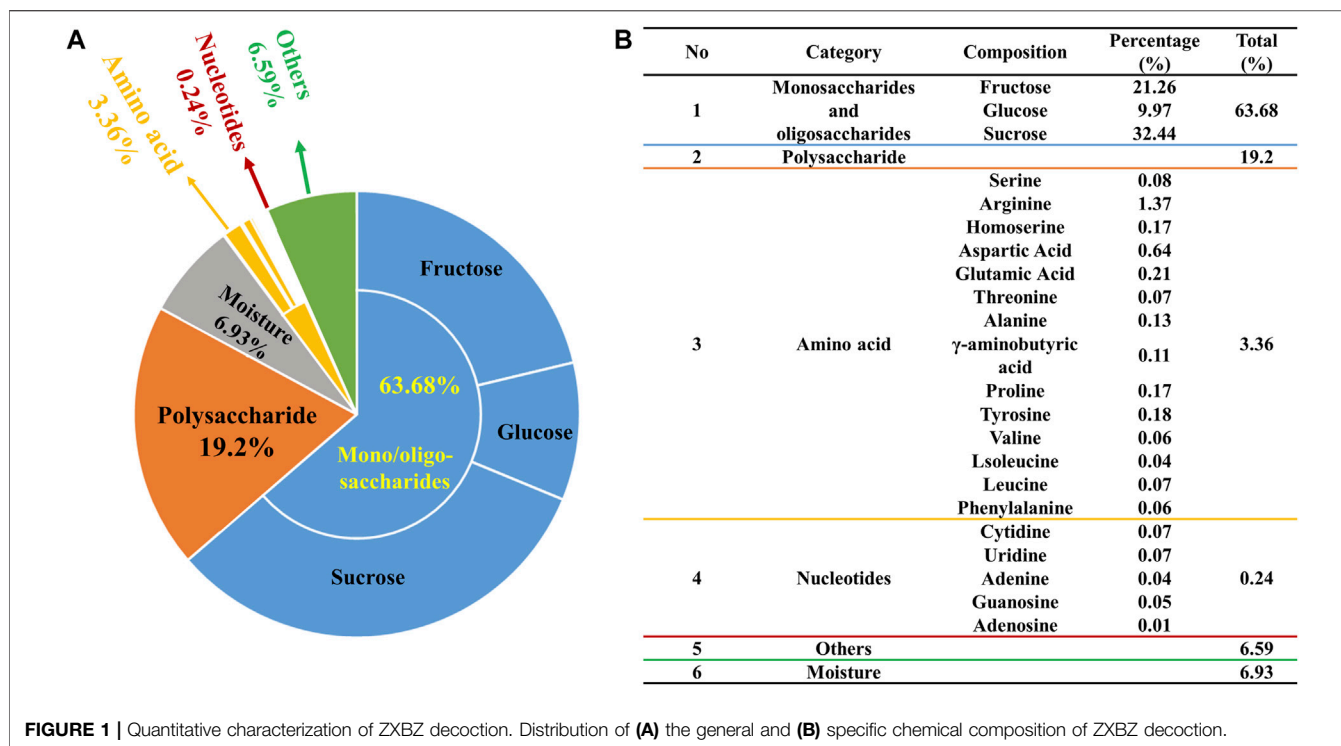
HepG2 cells were plated in 6-well plates at a density of 1×10^5 cells/ml and incubated in a humidified incubator at 37°C with 5% CO_2 . After the confluence reached 80%–90%, the culture medium was changed to the serum-free medium and the cells were starved for 12 h before treatment. Then, the medium was replaced by 1 mM oleic acid (OA)-palmitic acid (PA) = 2:1 or 500 μ M PA medium. The ZXBZ decoction was filtered through a 0.22 μ m membrane, and diluted into different concentrations. The negative control was 0.2% BSA and (0.1% DMSO or 0.1% ddH₂O) containing medium, and the 10 μ M Compound C and EX-527 were used to pre-treat the cells 1 h before ZXBZ intervention. After being co-incubated under different conditions for 24 h, the cells were lysed using 1% TritonX-100 or RIPA with 1% PMSF for the TG content assay or WB experiment, respectively.

RNA Isolation and qRT-PCR Analysis of mRNA Expression

Total RNA was isolated using the TRIzol reagent (Yeastar Biotechnology (Shanghai) Co., Ltd.) and a UNIQ10 RNA extraction column kit (Sangon Biotech, Shanghai, China). cDNA was reverse transcribed using the PrimeScript[™] RT Master Mix (Takara, Shiga, Japan), and qRT-PCR was analyzed on an ABI 7500 Fast system (ABI, CA, United States) using the Hieff[®] qPCR SYBR Green Master Mix (Yeastar, Shanghai, China). All results were normalized to the RPS18 expression and calculated using the $2^{-\Delta\Delta\text{Ct}}$ method and the primers of qRT-PCR are provided in Table 1.

Western Blotting

Mouse livers (20 mg) were lysed using RIPA lysis buffer (Beyotime, China) containing 1% cock-tail (Sigma-Aldrich, St Louis, MO, United States). Total protein lysates were separated on 10% SDS-PAGE gels and then transferred to PVDF



membranes (Millipore, United States), and then were incubated overnight at 4°C with antibodies against sirtuin 1 (Sirt1), histone 3, phospho-AMPK α (Thr172), and AMPK α (Cell Signaling Technology, United States), PGC-1 α , phospho-ACC1-S79, ACC, phospho-mTOR-S2448, SREBP-1c, PPAR α (ABclonal Technology Co., Ltd., Wuhan, China), β -actin, and β -tubulin (Abcam, MA, United States). The membranes were washed and incubated with HRP-conjugated secondary antibodies (Jackson ImmunoResearch Laboratories, Inc., United States) and then detected using an ECL Plus immunoblot detection system (Clinx, Shanghai, China).

Data Processing and Statistical Analysis

SIMCA-P software (version 14.1, Umetrics AB) was employed for multivariate analysis. Principal component analysis (PCA) analysis was carried out to demonstrate the aggregation of QC samples. Bidirectional orthogonal projection to latent structures discriminant analysis (O2PLS-DA) analysis was performed to describe the different metabolic profiles of the NC, vehicle, ZXBZ-L, ZXBZ-H, and positive groups. Orthogonal partial least squares discriminant analysis (OPLS-DA) analysis was used to better investigate the metabolic difference between the NC group and the vehicle group. R² and Q² were calculated to evaluate the quality of the model, and 200 permutation tests were performed to test the model. Potential biomarkers were confirmed based on the $p < 0.05$ and VIP > 1 between the NC and vehicle groups.

The potential urine biomarkers were identified using the metabolite database HMDB (<http://www.hmdb.ca/>) based on the MS¹ and MS² information. The pathway analysis was performed using MetaboAnalyst (<http://www.metaboanalyst.ca/>).

GSEA analysis was performed on GSEA 4.2.0 (36, 37) using the Reactome database (<https://reactome.org/>). The results were visualized using the R code (version 4.0.2) developed by us in RStudio. Paths were sorted by NES (NES < -1 or NES > 1 was considered significantly enriched).

The data from animal experiments are presented as the mean \pm SEM, and *in vitro* experimental data are presented as the mean \pm SD. Student's *t*-tests were used to compare two groups. Comparisons among multiple groups were made with a one-way analysis of variance (ANOVA). A value of $p < 0.05$ was considered statistically significant.

RESULTS

Components of ZXBZ Decoction Are Identified by Multiple Analytical Methods

The 94% chemical composition of ZXBZ decoction (Batch 20191129) was identified with four assays (Figure 1A). First, the contents of monosaccharides and oligosaccharides were determined using the high-performance liquid chromatography-diode array detection (HPLC-DAD) method (Supplementary Material 1), in which fructose accounted for 21.26%, glucose for 9.97%, and sucrose for 32.44%. The total content of the three saccharides had reached 63.7% of the aqueous extracts. Second, the contents of polysaccharides were analyzed using the phenol-sulfuric acid method (Chen et al., 2019), in which their percentage in the aqueous extract composition was 19.2%. Third, the varieties and contents of amino acids were assayed using the AccQ•Tag pre-column derivation method (Boogers et al., 2008). Fourteen amino

TABLE 1 | Primers for qRT-PCR.

| Primer | Sequence |
|-------------------------|--------------------------------|
| RPS18 forward primer | 5'-CGCCGCCATGTCTCTAGT-3' |
| RPS18 reverse primer | 5'-CCCTCTTGGTGAGGTCGATG-3' |
| SREBP-1c forward primer | 5'-CTGCTAGCTAGATGACCCCTGC-3' |
| SREBP-1c reverse primer | 5'-TCTGGCTTTGATCCCGGAAG-3' |
| CHREBP forward primer | 5'-CTGGGGACCTAACAGGAGC-3' |
| CHREBP reverse primer | 5'-GAAGCCACCCTATAGCTCCC-3' |
| CPT1A forward primer | 5'-CATGTCAAGCCAGACGAAG-3' |
| CPT1A reverse primer | 5'-TGGTAGGAGAGCAGCACCT-3' |
| G6PC forward primer | 5'-TTACCAAGACTCCCAGGACTG-3' |
| G6PC reverse primer | 5'-GAGCTGTTGCTGTAGTAGTCG-3' |
| CYP7A1 forward primer | 5'-TGATCCTCTGGGCATCTCAAGCAA-3' |
| CYP7A1 reverse primer | 5'-AGCTCTTGGCCAGCACTCTGTAAT-3' |
| CYP27A1 forward primer | 5'-TTGCCTGGATAGGGCTCATAG-3' |
| CYP27A1 reverse primer | 5'-GTGGGGCACTAGCCAGATTC-3' |
| LXRA forward primer | 5'-GCCCTGCACGCCCTACGT-3' |
| LXRA reverse primer | 5'-TAGCATCCGTGGGAACATCA-3' |
| Creb-forward primer | 5'-GACGGAGGTTAAGTCGAGCC-3' |
| Creb-reverse primer | 5'-TCTTCCTCCGCACTCGTTTC-3' |
| LPL forward primer | 5'-CCAGCTGGGCCCTAATTTGA-3' |
| LPL reverse primer | 5'-AACTCAGGCAGAGCCCTTTC-3' |
| HMGCR forward primer | 5'-GCTACTGGGATGGTCGTAT-3' |
| HMGCR reverse primer | 5'-TTGAACATGTCCAGGGAGGC-3' |

acids were detected at a total content of 3.36%, among which the highest amino acid was arginine (1.37%). Fourth, a total of five nucleotides were quantified (**Supplementary Material 2**) using the HPLC-UV method and their total content was 0.24%. At last, the water content of ZXBZ aqueous extracts was determined using USP 40 <921> method III (rtf), in which the result was 6.93% (**Figure 1B**). The representative total ion chromatogram of ZXBZ was also characterized (**Supplementary Figure S1**) and 33 compounds were identified (**Supplementary Table S1**).

ZXBZ Decoction Impedes Liver Injury in the GAN Diet-Induced NAFLD Model

Given the regulatory role of ZXBZ decoction as a classical formula in the hepatic fluid metabolism disorder, we wondered whether it can modulate other metabolic pathways of the liver, especially glucose and lipid metabolism. Thus, the GAN diet-induced NAFLD mouse model was used, where C57 BL/6 mice were pre-fed with the GAN diet for 5 weeks and administered ZXBZ decoction by oral gavage daily for 12 weeks (**Figure 2A**). The GAN diet is a commonly used diet to induce NAFLD/NASH models, which shares similar characteristics with NAFLD/NASH patients in the respects of histopathology, transcription, and metabolism (Hansen et al., 2020; Radhakrishnan et al., 2020). In this experiment, we selected obeticholic acid (OCA), a candidate for NAFLD treatment in phase III clinical trials (Ratzin et al., 2016), as the positive control for the therapeutic effects. As shown in **Figure 2B**, the body weights of the vehicle group increased gradually with GAN diet feeding when compared with that of the NC group fed by the normal diet, while the body weights were obviously lowered no matter in the positive group or the low and high dosages of ZXBZ treated (ZXBZ-L and ZXBZ-H) groups than those in the vehicle

group. Moreover, the hepatosomatic indexes of OCA, ZXBZ-L, and ZXBZ-H groups and liver weights of OCA and ZXBZ high groups were also markedly lower than vehicles after 12 weeks of continuous administration (**Figure 2C**).

To assess the effects of ZXBZ decoction on the liver function, the serum biomarkers, aspartate aminotransferase (AST), and alanine aminotransferase (ALT), were detected. Compared to the vehicle group, the ZXBZ-L and ZXBZ-H groups both exhibited lower ALT and AST levels since the fourth week of drug treatment, which was continued until the end of the experiment (**Figures 2D,E**). Afterward, the pathological changes in liver tissues from different groups were observed by H&E staining and quantified by NAFLD activity score (NAS). The vehicle group with a NAS of 5 had significantly hepatic steatosis, ballooning, and lobular inflammation compared to NC and reached the threshold for the diagnosis of NASH (Brunt et al., 2011). The high dosage ZXBZ treatment could alleviate hepatic steatosis and ballooning of hepatocytes obviously and relieved the lobular inflammation slightly without significance (**Figures 2F,G**).

The aforementioned results showed that ZXBZ decoction could reduce the levels of ALT and AST, relieve hepatic steatosis, and ballooning degeneration significantly in the GAN diet-induced NAFLD model.

Metabolomics Reveals That ZXBZ Decoction Could Improve the β -Oxidation

To monitor the metabolic changes, the urine metabolites were collected monthly and studied. The PCA score plot showed good stability and feasibility of the detection method due to the aggregation of points in the QC group (**Supplementary Figure S2A**). As illustrated by the O2PLS-DA score plot (**Supplementary Figure S2B**), there was an excellent separation among the NC and vehicle groups, indicating that the urine metabolites in NAFLD mice were significantly changed. The ZXBZ-H and ZXBZ-L groups were close to each other and had similar metabolic phenotypes. In addition, the ZXBZ-H group could be separated from the vehicle group, showing the benefits of ZXBZ at the metabolic level.

An OPLS-DA model was established to search for potential biomarkers of NAFLD between the NC and vehicle groups (**Figure 3A** and **Supplementary Figures S2C,D**). In addition, the data were categorized according to different time points. The parameters of the model (the R^2Y and Q^2 values should be near to 1, indicating a good ability to forecast) were acceptable, indicating good prediction and reliability. Furthermore, the models were validated using permutation tests ($n = 200$). Variables with VIP values > 1 and p values < 0.05 were identified as significant endogenous biomarkers. The candidate ions were tentatively identified by searching the MS and MS/MS fragments using the online library (<http://www.hmdb.ca/>). Finally, 60 metabolites were identified as potential biomarkers in the NAFLD model. The results of the detailed identification information and shifting trends of biomarkers are shown in **Supplementary Table S1**. Overall, 30 metabolites were stably present in all three sampling occasions, and the reversal effect was

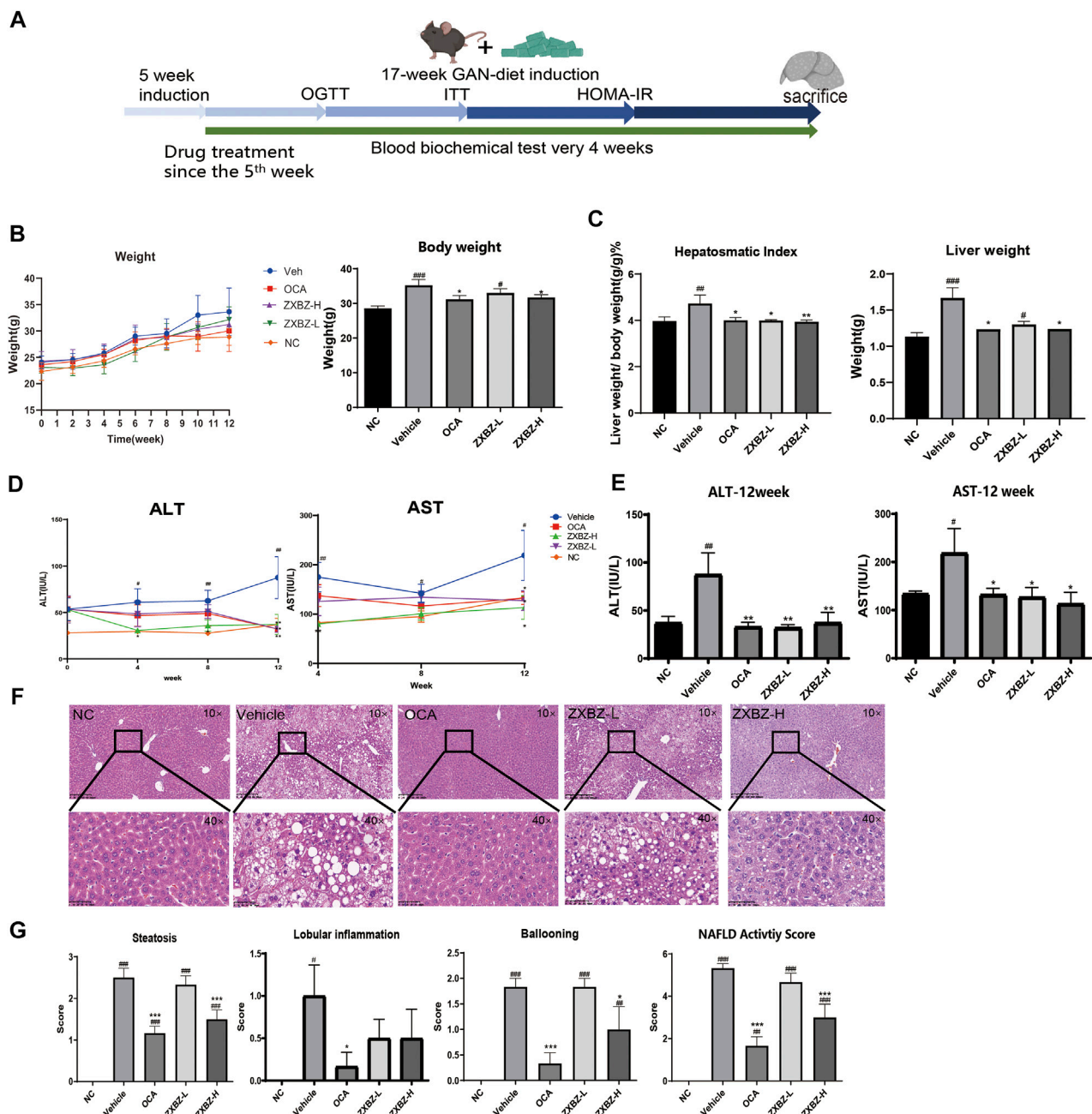
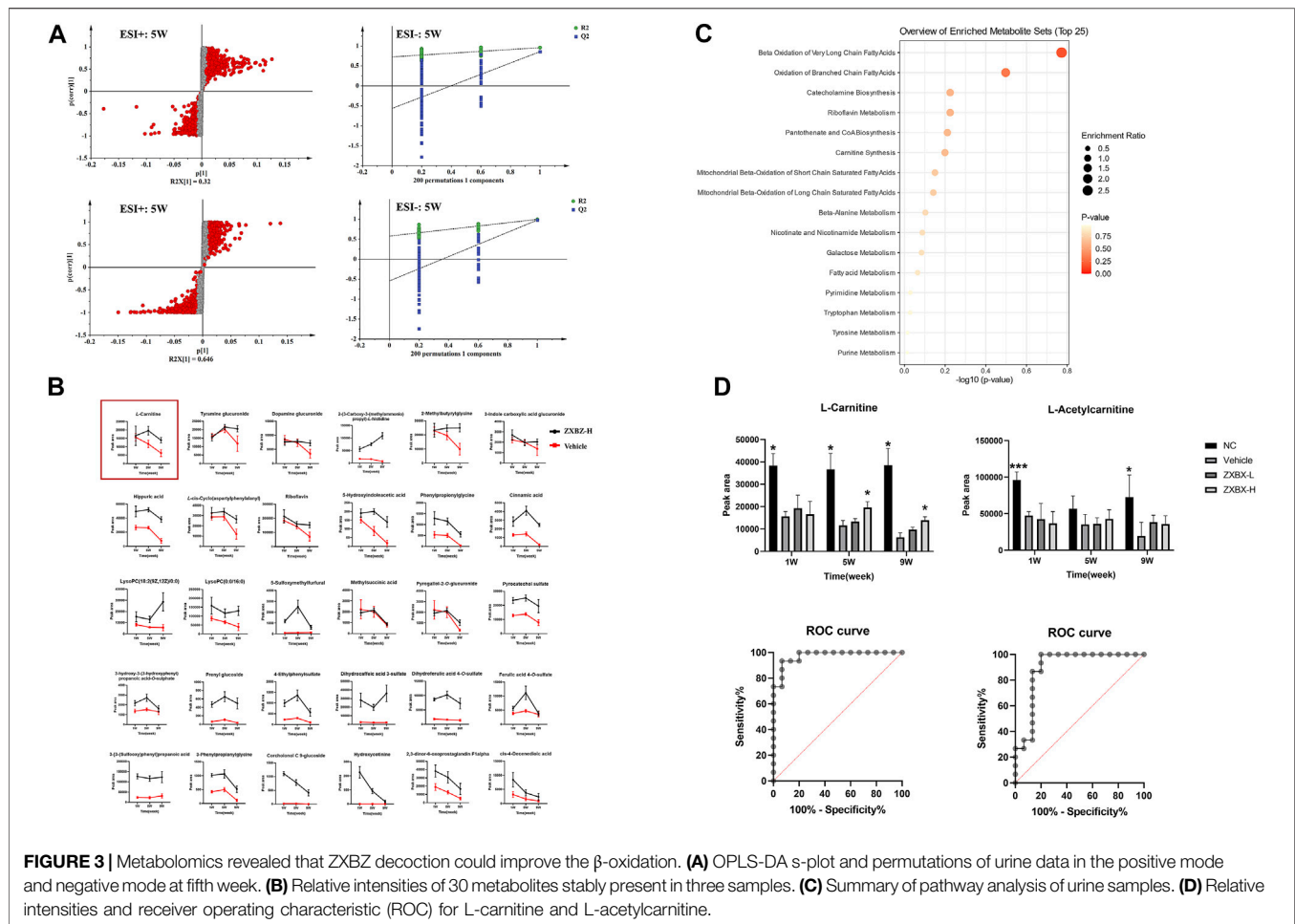


FIGURE 2 | Liver protective effect of ZXBZ decoction. **(A)** Design and timeline of animal experiments. **(B)** Body weight throughout the whole drug treatment process and the end point body weight. **(C)** Hepatosomatic index and the liver weight. **(D)** ALT and AST in the drug treatment process. **(E)** End point ALT and AST. **(F)** H&E staining of each group (10× and 40×). **(G)** NAFLD activity score. The histological NAS scores of necroinflammatory, ballooning, and macrovesicular steatosis were determined by a certified pathologist. The data are the mean ± SEM ($n = 8-10$ per group). # $p < 0.05$, ## $p < 0.01$, ### $p < 0.001$ compared to NC. * $p < 0.05$, ** $p < 0.01$, *** $p < 0.001$ compared to vehicle.

reflected in the ZXBZ administration groups (Figure 3B and Supplementary Figure S2E).

To further investigate the metabolic pathways disturbed in NAFLD, an online tool, MetaboAnalyst 5.0 software (www.metaboanalyst.ca/), was used and 16 related pathways were found to be affected (Figure 3C). Among them, beta-oxidation of very long-chain fatty acids and oxidation of branched-chain

fatty acids were the two most important pathways in the urine metabolite pathways, including L-carnitine and L-acetylcarnitine. As shown in Figure 3D, L-carnitine and L-acetylcarnitine decreased in the vehicle group and increased after ZXBZ treatment. Moreover, the AUC of the two metabolites were 0.9733 and 0.8978, both sensitive to being a biomarker, especially L-carnitine. Moreover, L-carnitine and



L-acetylcarnitine were identified using available standards (Supplementary Figure S3).

Transcriptomics Reveals That ZXBZ Decoction Could Improve Energy Metabolism

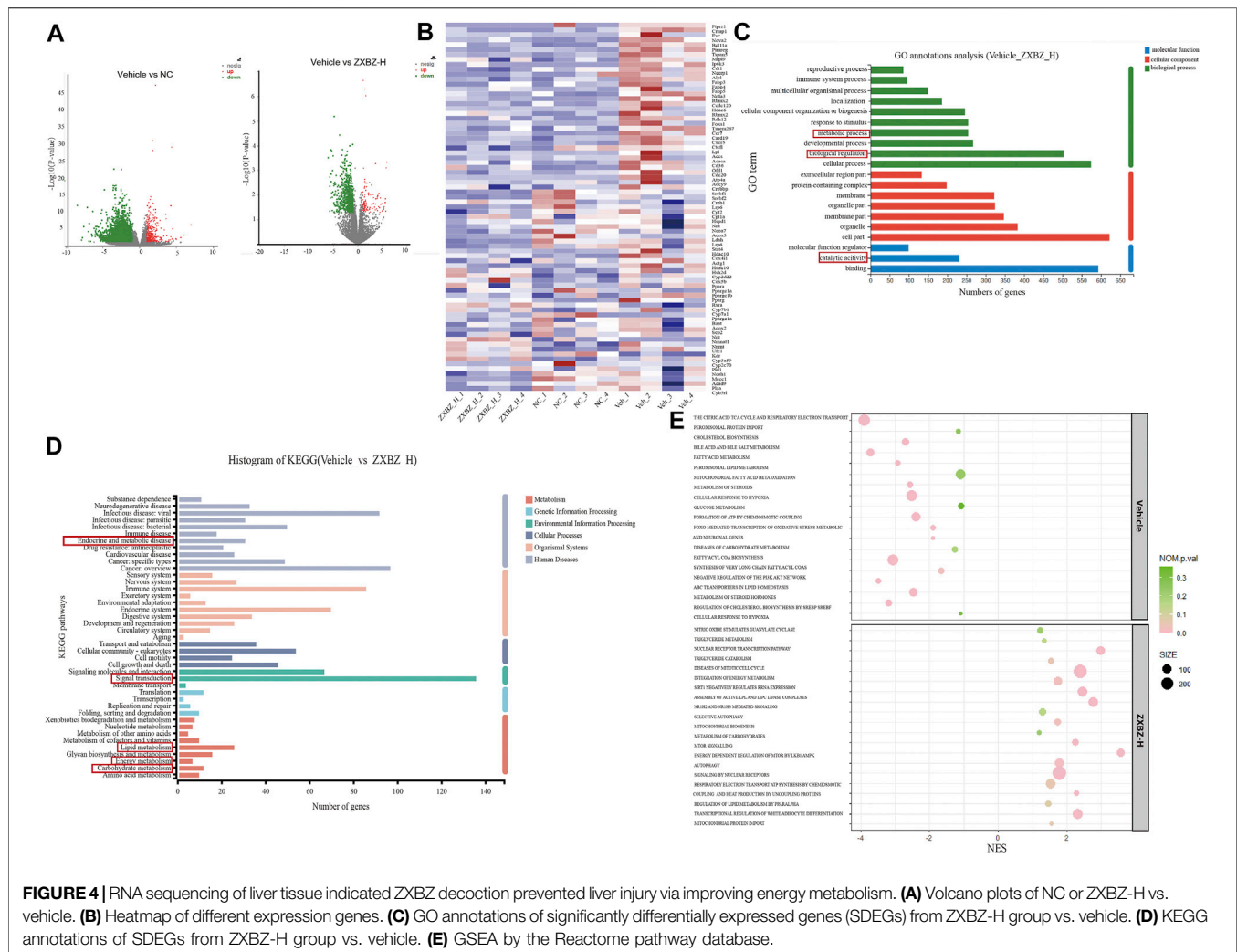
To study the underlying mechanisms of ZXBZ's hepatoprotective functions thoroughly, high-throughput RNA-seq technology was used to profile liver transcriptomes of vehicle, NC, and ZXBZ-H groups, respectively ($n = 4/\text{group}$), and the data were analyzed on the free online platform of the Majorbio Cloud Platform (<http://www.majorbio.com/>) and GSEA (<https://www.gsea-msigdb.org/gsea/>). The overall significantly differentially expressed genes (SDEGs) in NC and ZXBZ-H groups compared to the vehicle group were shown in the volcano chart (Figure 4A). The details of SDEGs related to NAFLD were shown in the cluster heatmap (Figure 4B), including the genes of lipid metabolism and transport such as *Lpl*, *Accs*, and *Cd36*, nuclear receptors such as *Ppara*, *Pparg*, and *Rxra*, electron transport chain, for instance, *Atp4*, *Cox4*, and *Nmant*, and bile acid metabolism-related genes, such as *Cyp7a1*. The SDEGs between ZXBZ-H and vehicle groups were further analyzed KEGG pathway and GO annotation, respectively, and the results demonstrated that ZXBZ decoction

mainly regulated lipid metabolism, glycan biosynthesis and metabolism, and carbohydrate metabolism (Figures 4C,D). The gene set enrichment analysis (GSEA) was also performed to reveal the potential pathways and biological processes influenced by ZXBZ decoction (Figure 4E), and the results indicated that ZXBZ decoction might balance cellular energy states. The lipogenesis (FAs, cholesterol, and sterols) and hypoxia were enhanced in the vehicle group, whereas the genes involved in the mitochondrial function including ATP synthesis and mitochondrial biogenesis, nitric oxide metabolism, and nuclear receptor (PPAR and LXR) pathways were enriched in the ZXBZ-H group. Interestingly, these pathways are regulated by Sirt1. In addition, autophagy and mTOR pathways indicated the activation of the AMPK/mTOR pathway.

The transcriptomic data suggested that ZXBZ decoction improved energy metabolism, especially lipid metabolism, by affecting energy sensing and regulatory pathways.

ZXBZ Decoction Alleviates Hepatic Steatosis and Dyslipidemia

Since the multi-omics results clued ZXBZ decoction might influence energy metabolism, particularly lipid metabolism, we assessed the lipid metabolism in NAFLD mice among different



groups. The total cholesterol (TC) and low-density lipoprotein cholesterol (LDLC) in serum were elevated in response to the nutritious diet stimulation, while the high dose of ZXBZ could decrease the TC and LDLC (**Figure 5A**). The parallel results also appeared in the ratio of white adipose tissue (WAT)/bodyweight and WAT weights (**Figure 5B**). The oil red O staining (**Figures 5C,D**) and lower hepatic steatosis score (**Figure 2E**) demonstrated the reduced hepatic lipid accumulation and steatosis intuitively from histology. In addition, the cholesterol and triglycerides (TGs) in liver tissue were reduced in OCA and ZXBZ-L and H groups compared to vehicle group (**Figure 5E**).

Taken together, we can conclude that ZXBZ decoction could ameliorate lipid disorders in the aspects of reducing circulating lipid levels and hepatic steatosis.

ZXBZ Decoction Regulates the Energy-Sensing Network to Improve Lipid Metabolism

We further confirmed the possible molecular mechanisms based on the remarkable phenotypic improvements in the lipid disorder

of NAFLD models and multi-omics analysis results. As shown in **Figure 6A**, both dosages of ZXBZ treatment increased Sirt1 and activated AMPK, two nutrient sensors responding to NAD⁺/NADH and AMP/ATP, respectively in mammalian cells (Fulco and Sartorelli, 2008; Wang et al., 2011). As reported, Sirt1 activation can suppress *de novo* lipogenesis by inhibiting SREBP-1c and *Chrebp*, and promote fatty acid oxidation (FAO) by increasing PPARα and PGC-1α expressions (Cantó and Auwerx, 2009). The corresponding changes in ZXBZ treatment on these genes were consistent with the previous research works. Similarly, the downstream genes of PPARα, such as *Cyp7a1*, *Cyp27a1*, and *Lxra* (Defour et al., 2012) were also increased under the condition of ZXBZ treatment, which indicated that ZXBZ might regulate bile acid metabolism, stimulate cholesterol clearance, and reverse cholesterol transport from peripheral tissues (Liang et al., 2021). Moreover, the activation of AMPK by ZXBZ consequently inactivated ACC and further reduced FASN (**Figure 6B**) and SREBP-1c, while increasing the *Cpt-1α* expression to reduce the fatty acid synthesis and promote the fully oxidation of long-chain and very long-chain FAs (Huang et al., 2017). We also found that

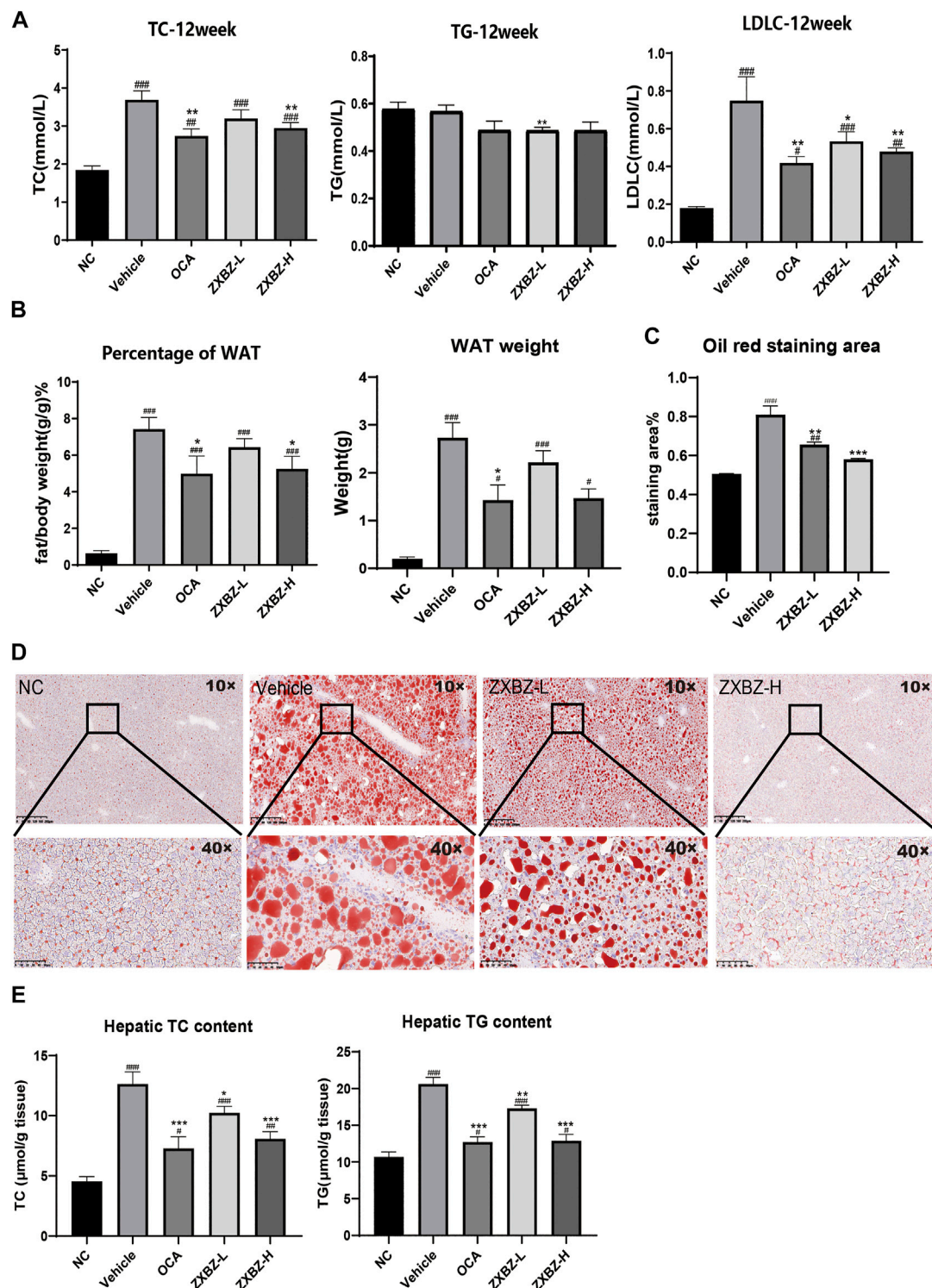
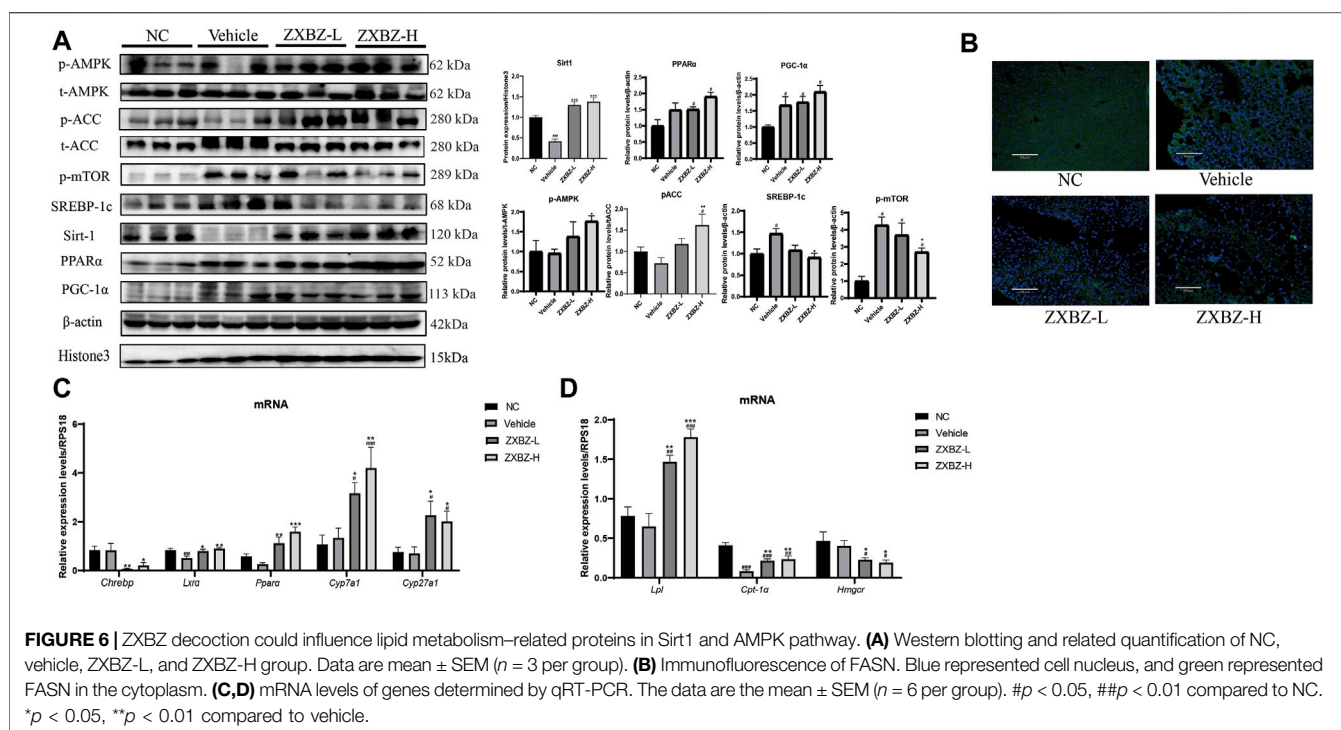


FIGURE 5 | ZXBZ decoction could improve the lipid metabolism in NAFLD mice. **(A)** Levels of TC, TG, and LDLC in serum after 12-week treatment. **(B)** Percentage of white adipose tissue and white adipose tissue weight of each group. **(C)** The oil red staining area of liver tissues. The positive areas were calculated using Image Pro plus 6.0. **(D)** Oil red O staining of livers and quantification in NC, vehicle, ZXBZ-L, and ZXBZ-H groups. **(E)** The TC and TG contents in mouse livers and normalized by tissue weight. The data are the mean \pm SEM ($n = 8-10$ per group). $\#p < 0.05$, $\##p < 0.01$, $\###p < 0.001$ compared to NC. $*p < 0.05$, $**p < 0.01$, $***p < 0.001$ compared to vehicle.



AMPK activation downregulated *Hmgcr* transcription, meanwhile increasing *Lpl* mRNA levels (Figure 6C), which might reduce cholesterol synthesis and accelerate TG decomposition (Figure 6D) (Day et al., 2021; Trefts and Shaw, 2021). Furthermore, the phosphorylation of mTOR was inhibited in ZXBZ groups, suggesting autophagy was prompted after ZXBZ treatment, which could protect hepatocytes (Kim and Guan, 2021).

Altogether, ZXBZ decoction mainly regulated the energy-sensing network by influencing the Sirt1 expression and AMPK activation to govern lipid metabolism-related protein expressions and activations, consequently inhibiting lipogenesis and boosting lipids utilization in GAN diet-induced NAFLD mice.

ZXBZ Decoction Has a Weak Effect on Glucose Metabolism in GAN Diet-Induced NAFLD Models

Since glucose metabolism is another important assessment indicator in NAFLD, the oral glucose tolerance test (OGTT), HOMA-IR, and the insulin tolerance test (ITT) were measured on the sixth, seventh, and eighth week. As shown in Supplementary Figure S4, insulin resistance was not evident in this model, because there was no change in HOMA-IR and only an 18.65% increase in the AUC of the ITT between NC and vehicle groups. For OGTT with the obvious change between the NC and vehicle groups, we found ZXBZ decoction showed obvious improvement (Figure 7A). In addition, the serum fructosamine levels, which reflected blood sugar levels in the last one to 3 weeks, were also measured at the end of the

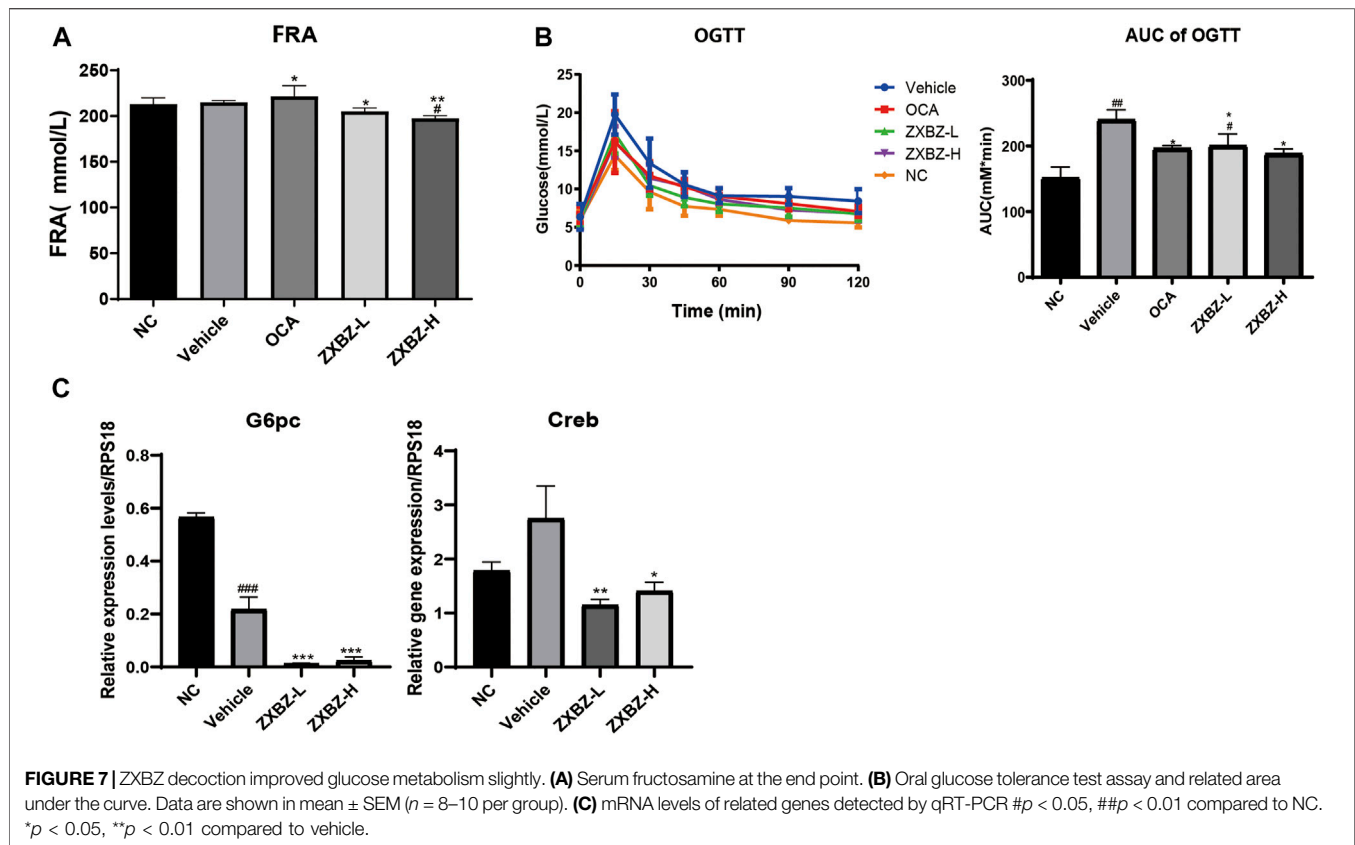
experiment. Although serum fructosamine level had a slight change under diet induction, the administrated ZXBZ groups showed a weak but statistically significant reduced fructosamine level (Figure 7B). Meanwhile, the expression of gluconeogenesis genes *G6pc* and *Creb* which can be upregulated by AMPK activation were significantly hindered by ZXBZ treatment, which indicated that ZXBZ decoction may have regulatory effects in glucose metabolism (Figure 7C).

To sum up, the 12 weeks of ZXBZ administration improved the glucose tolerance, decreased serum fructosamine, and reduced gluconeogenesis gene transcriptions in the GAN diet-induced NAFLD mice model.

DISCUSSION

Nowadays, obesity-related diseases, especially NAFLD, have become a heavy burden for the global society, but the economical and effective treatments are still badly unmet. Most studies believe that lipid disorder is not only the primary risk factor for NAFLD development but a key trigger for other metabolic diseases as well. However, clinical applications suggested single-target drugs have many drawbacks, as a result, classical TCM formulas, with the advantages of multi-ingredients, multi-targets, and multi-pathways, have drawn increasing interest as potential treatments for NAFLD.

ZXBZ decoction was a classical TCM formula serving as a treatment for metabolism disorders in the body fluid since ancient time, and the alcohol extracts and monomers of Zexie and Baizhu, had been proven to improve lipid metabolism in modern studies. In this study, we proved that the chemical

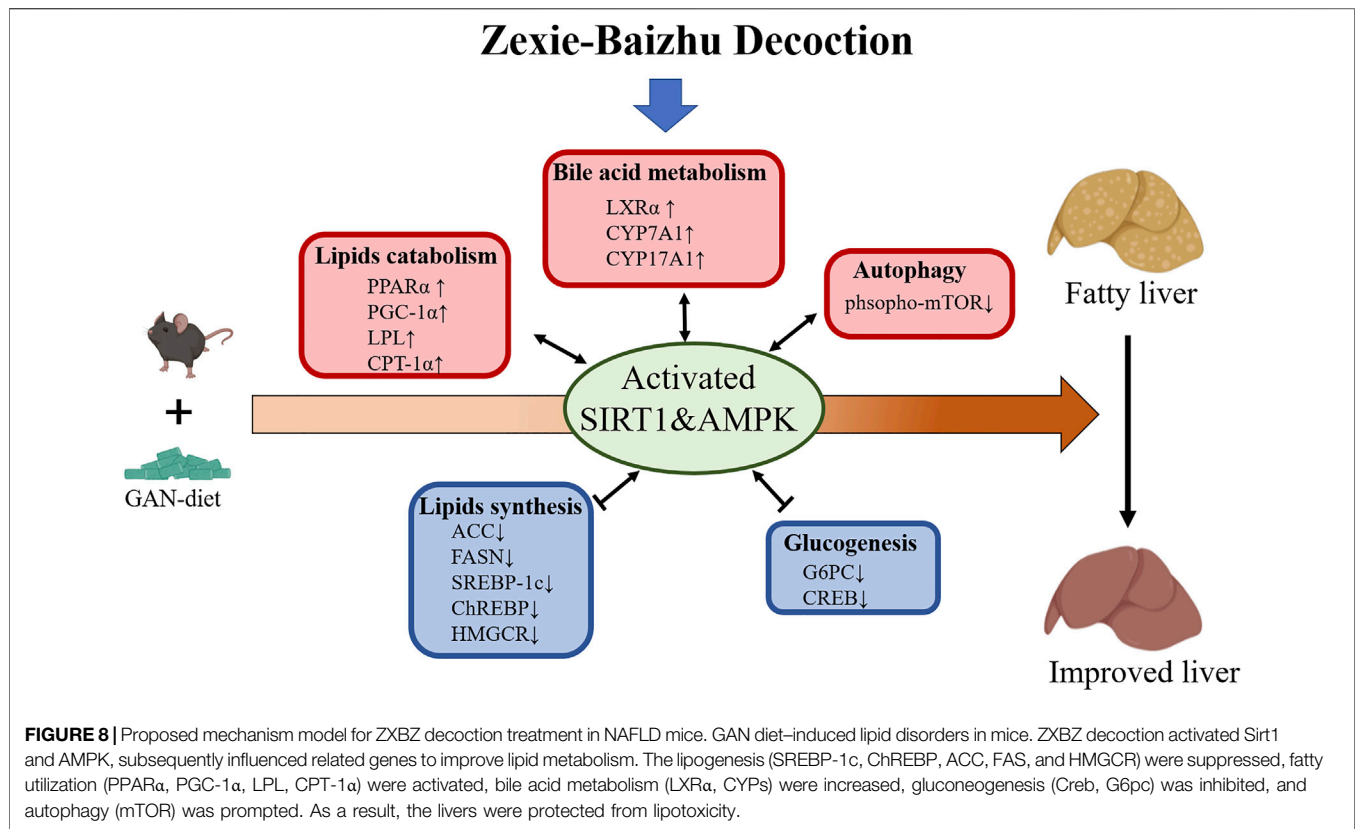


composition of ZXBZ decoction is dominated by polar glycoconjugates, especially polysaccharides, while the secondary metabolites are very low. This indicates that the presence of polysaccharide macromolecules in traditional Chinese medicine tonics cannot be ignored. The beneficial regulation of gut microbiota has been widely reported for polysaccharides, including providing energy for intestinal microorganisms, shaping the diversity of the gut microbiota, protecting bacteria from environmental, and host factors, including the host immune system, and so on (Porter and Martens, 2017; Hsieh and Allen, 2020; Sun et al., 2021b; Song et al., 2021). Thus, the polysaccharide in ZXBZ may be separated and tested further for understanding its pharmacological substances. Considering the ZXBZ decoction was the most original, convenient, and widely used formulation in folk, we aimed to verify the therapeutic effects of ZXBZ decoction in the NAFLD mice model and reveal the underlying mechanisms combining multi-omics analysis and molecular biological verification.

In our study, ZXBZ decoction alleviated liver injury in the GAN diet-induced NAFLD model featured by lower ALT, AST, hepatosomatic index, and NAFLD activity score. Metabolomics hinted ZXBZ decoction promoted lipid utilization and transcriptomics implied that energy metabolisms, especially lipid metabolism, were improved, which was confirmed by the alleviated hepatic steatosis and dyslipidemia with ZXBZ decoction treatment *in vivo*. In metabolomics studies, two

important potential biomarkers, L-carnitine and L-acetylcarnitine, were identified. Carnitine plays a key role in energy metabolism, transporting long-chain fatty acids into the mitochondria for oxidation and modulating the rise in the intramitochondrial acyl-CoA/CoA ratio (Tanphaichitr and Leelahagul, 1993). L-carnitine reduces fructose-mediated lipid accumulation by activating AMPK (Montesano et al., 2020), shown to be closely related to fatty acid β oxidation (Minokoshi et al., 2021). The mechanism of L-acetylcarnitine is also related to AMPK, inhibiting TNF- α -induced insulin resistance in skeletal muscle cells via the AMPK pathway (Zhang et al., 2009). Then, the interplays were uncovered in protein and mRNA levels. Two central energy sensors, Sirt1 and AMPK were activated, subsequently, lipogenesis-related proteins (SREBP-1c, ChREBP, ACC, FASN, and HMGCR) were suppressed, FAO involved genes (PPAR α , PGC-1 α , LPL, and CPT-1 α) were activated, and lipid transport regulated genes (LXR α and CYPs) were increased (Figure 8).

As reported, AMPK and Sirt1 pathways are intertwined in mammals, that is to say, AMPK and Sirt1 could activate and regulate each other, and they co-worked as an energy-sensing network sharing many common downstream targets (Ruderman et al., 2010; Cantó et al., 2009). AMPK can be activated in response to the change of the AMP/ATP ratio, and then the activated AMPK affects the NAD⁺/NADH ratio to activate Sirt1. At the same time, the activation of Sirt1 can also activate AMPK via LKB1 (Silvestre et al., 2014). However, the activation of



AMPK and Sirt1 could also be independent. In neurons, the activation of AMPK needs LKB1 but does not require Sirt1 (Dasgupta and Milbrandt, 2007). In HepG2 cells, resveratrol could activate AMPK in Sirt1-dependent or Sirt1-independent manners (Hou et al., 2008; Shin et al., 2009). Also, in Sirt1^{-/-} mice, the activation of AMPK increased to rescue the depletion of Sirt1 (Pillai et al., 2010; Lee et al., 2008). In epithelial cells, the phosphorylation or inhibition of AMPK did not affect the activation of Sirt1 (Zu et al., 2010). Taken together, the regulation and interplay of these two key sensors of energy state in mammalian cells vary under different conditions. In the current study, we discovered that ZXBZ decoction could inhibit TG accumulation in both *in vivo* (Figure 5) and *in vitro* experiments (Supplementary Figure S5A). ZXBZ decoction increased AMPK phosphorylation significantly under the stimulation of 1 mM OA/PA for 24 h (Supplementary Figure S5B), while the Sirt1 level also increased slightly. Since the presence of OA would promote the expression of Sirt1 (Lim et al., 2013), PA without OA was used to stimulate HepG2 cells to further detect the effect of ZXBZ decoction on Sirt1. As shown in Supplementary Figure S5C, ZXBZ decoction elevated Sirt1 obviously. All these results indicated that ZXBZ decoction could regulate AMPK and Sirt1, which was also consistent with the result *in vivo*. Moreover, we also investigated the interplay of AMPK and Sirt1 activated by ZXBZ decoction through co-incubated with Compound C (specific AMPK inhibitor) and EX-527 (specific Sirt1 inhibitor). Interestingly, we discovered that ZXBZ decoction could activate AMPK and

Sirt1 independently because the inhibition toward either AMPK or Sirt1 did not affect the activation of the other (Supplementary Figure S5D). It must be pointed out that TCM is characterized by multiple ingredients and targets; as a result, it was hard to determine the exact targets of ZXBZ decoction. Whether the activation of Sirt1 and AMPK was triggered by ZXBZ decoction directly, or derived from regulations of nuclear receptors, lipogenesis enzymes and lipid transporters, needs more experiments on transgenic mice.

As for glucose metabolism, ZXBZ decoction slightly reduced blood glucose, increased oral glucose tolerance, and decreased the expressions of glycogenesis-related genes (CREB and G6PC) along with the activation of Sirt1 and AMPK. Also, the inflammation was not severe in the 17-week GAN diet induction, since the severity of lobular inflammation (Figure 2G) was not serious, and the hepatic TNF- α and IL-6 were not increased significantly in the vehicle group (data not shown). The effects of ZXBZ decoction on glucose metabolism and inflammation need to be testified in another model.

Interestingly, the ZXBZ-L group exhibited lower hepatic enzyme levels but only slightly ameliorated hepatic lipid accumulation and dyslipidemia. There might be two reasons for this phenomenon: 1) the protective effects on hepatocytes might attribute to the increased level of PGC-1 α , which also protected mitochondria from oxidative stress (Figure 6A). 2) Since the standard of steatosis is according to the overall lipid droplet areas, the ZXBZ-L and vehicle groups had similar ranges of steatosis (33–66%) (Figure 2F). But, the ZXBZ-L group had

generally fewer large lipid droplets than the vehicle group (**Figure 2F**). Many previous studies demonstrated that the larger size of lipid droplets would make more serious hepatocyte injuries (Ferri et al., 2021; Mashek, 2021). Therefore, we speculated that the low dosage of ZXBZ decoction could protect livers by reducing the formation of large hepatic lipid droplets and increasing the PGC-1 α expression.

Noteworthy, the characteristics of hyperglycemia and insulin resistance in NAFLD did not exacerbate in the 17-week GAN diet-induced mouse model. As a result, the possible improvements in glucose metabolism could not be observed in this model. The insulin resistance was not evident in this model (**Supplementary Figures S4A,B**), since the PI3K-Akt pathway was activated in the vehicle group as the feedback toward a high-fructose diet. The inhibition of GSK3 β (S9 phosphorylation) was remarkable along with the activated Akt in the ZXBZ-L group (**Supplementary Figure S4C**). However, it was hard to get the conclusion that ZXBZ decoction could influence the PI3K/Akt pathway, as the activation was in three GAN diet groups compared to NC, which could be the feedback toward the GAN diet. Also, the transcription of G6PC was reduced in vehicle, ZXBZ-L, and H groups. It might be due to the fructose being the main sugar resource in the GAN diet, subsequently, leading to reduced gluconeogenesis in these groups. But ZXBZ groups still had significantly lower expressions of G6PC compared to vehicle, which also indicated the potential glucose metabolism regulatory ability of ZXBZ decoction. Also, whether ZXBZ decoction improved glucose metabolism needs further research based on STZ-induced or db/db mice.

Although there are several studies on the pharmacological effects of alcohol extracts of Zexie and Baizhu or monomers in the NAFLD treatment, the current study was focused on the initial-described and universal-used ZXBZ aqueous decoction for the first time. Moreover, the composition of active ingredients in aqueous decoction was first identified and discovered completely different compared to alcohol extracts. The combination of transcriptomics and metabolomics can demonstrate drug efficacies and mechanisms at multiple levels, especially fit in the research works of complex diseases and TCM with multiple ingredients and targets. Transcriptomics could reveal the expressions of related genes at overall levels, and metabolomics could reflect the holistic and real-time dynamic changes of endogenous metabolites after TCM intervention. The results emphasized the regulation of multiple targets and pathways and the whole energy sensing and regulatory network, highlighting the strength of TCM toward metabolic diseases. Of note, this study broadened the potential utilizations of ZXBZ decoction, helped understand the relationship between the mechanisms and functions of ZXBZ decoction and developed the natural herbs as complicated disease treatment candidates further.

DATA AVAILABILITY STATEMENT

The original contributions presented in the study are publicly available. This data can be found here: <https://submit.ncbi.nlm.nih.gov/subs/bioproject/SUB10918355/overview>, BioProject ID PRJNA795724.

ETHICS STATEMENT

The animal study was reviewed and approved by the Animal Ethical and Welfare Committee of Institutional Ethics Committee of Shanghai Institute of Materia Medica. From research proposal to publication of the manuscript, we abided by the ethics of the Committee on Publishing Ethics (COPE), and there is no potential improper behavior (IACUC: 2019-03-GLK-07).

AUTHOR CONTRIBUTIONS

Conceptualization, YC, WW, and LG; data curation, YC, JS, and HL; formal analysis, YC and JH; funding acquisition, JX and LG; investigation, YC and LS; methodology, JS and HL; project administration, YC; resources, JX and JS; supervision, JC, WW, and LG; validation, LS, HL and JH; visualization, YC and JS; writing—original draft, YC and JC; and writing—review and editing, YC, JC, WW, and LG.

FUNDING

This research was funded by grants from the National Natural Sciences Foundation of China (Grant No. 81973470), the Guangdong Province Science and Technology Plan Project (Grant No. 2019B020202003), the Innovation Team and Talents Cultivation Program of National Administration of Traditional Chinese Medicine (No: ZYYCXTD-D-202210), and the Foundation of Shanghai Science and Technology Committee (Grant No. 21DZ2291100).

ACKNOWLEDGMENTS

The authors are grateful to Jin Ren and Shouyan Wu for invaluable advice.

SUPPLEMENTARY MATERIAL

The Supplementary Material for this article can be found online at: <https://www.frontiersin.org/articles/10.3389/fphar.2022.858795/full#supplementary-material>

REFERENCES

- Ahmed, B., Sultana, R., and Greene, M. W. (2021). Adipose Tissue and Insulin Resistance in Obese. *Biomed. Pharmacother.* 137, 111315. doi:10.1016/j.biopha.2021.111315
- Bastin, M., and Andreelli, F. (2020). The Gut Microbiota and Diabetic Cardiomyopathy in Humans. *Diabetes Metab.* 46 (3), 197–202. doi:10.1016/j.diabet.2019.10.003
- Boland, M. L., Oró, D., Tølbøl, K. S., Thrane, S. T., Nielsen, J. C., Cohen, T. S., et al. (2019). Towards a Standard Diet-Induced and Biopsy-Confirmed Mouse Model of Non-alcoholic Steatohepatitis: Impact of Dietary Fat Source. *World J. Gastroenterol.* 25 (33), 4904–4920. doi:10.3748/wjg.v25.i33.4904
- Boogers, I., Plugge, W., Stokkermans, Y. Q., and Duchateau, A. L. (2008). Ultra-performance Liquid Chromatographic Analysis of Amino Acids in Protein Hydrolysates Using an Automated Pre-column Derivatisation Method. *J. Chromatogr. A* 1189 (1–2), 406–409. doi:10.1016/j.chroma.2007.11.052
- Brunt, E. M., Kleiner, D. E., Wilson, L. A., Belt, P., and Neuschwander-Tetri, B. A. (2011). Nonalcoholic Fatty Liver Disease (NAFLD) Activity Score and the Histopathologic Diagnosis in NAFLD: Distinct Clinicopathologic Meanings. *Hepatology* 53 (3), 810–820. doi:10.1002/hep.24127
- Cantó, C., and Auwerx, J. (2009). PGC-1 α , SIRT1 and AMPK, an Energy Sensing Network that Controls Energy Expenditure. *Curr. Opin. Lipidol.* 20 (2), 98–105. doi:10.1097/MOL.0b013e328328d0a4
- Cantó, C., Gerhart-Hines, Z., Feige, J. N., Lagouge, M., Noriega, L., Milne, J. C., et al. (2009). AMPK Regulates Energy Expenditure by Modulating NAD⁺ Metabolism and SIRT1 Activity. *Nature* 458 (7241), 1056–1060. doi:10.1038/nature07813
- Chen, F., Huang, G., Yang, Z., and Hou, Y. (2019). Antioxidant Activity of Momordica Charantia Polysaccharide and its Derivatives. *Int. J. Biol. Macromol.* 138, 673–680. doi:10.1016/j.ijbiomac.2019.07.129
- Chen, Q., Chao, Y., Zhang, W., Zhang, Y., Bi, Y., Fu, Y., et al. (2020). Activation of Estrogen Receptor α (ER α) Is Required for Alisol B23-Acetate to Prevent Postmenopausal Atherosclerosis and Reduced Lipid Accumulation. *Life Sci.* 258, 118030. doi:10.1016/j.lfs.2020.118030
- Cheng, S., Sun, H., Li, X., Yan, J., Peng, Z., You, Y., et al. (2019). Effects of Alismatis Rhizoma and Rhizoma Smilacis Glabrae Decoction on Hyperuricemia in Rats. *Evid. Based Complement. Altern. Med.* 2019, 4541609. doi:10.1155/2019/4541609
- Dai, X., Feng, J., Chen, Y., Huang, S., Shi, X., Liu, X., et al. (2021). Traditional Chinese Medicine in Nonalcoholic Fatty Liver Disease: Molecular Insights and Therapeutic Perspectives - PubMed [Internet]. *Chin. Med.* 16 (1). doi:10.1186/s13020-021-00469-4
- Dasgupta, B., and Milbrandt, J. (2007). Resveratrol Stimulates AMP Kinase Activity in Neurons. *Proc. Natl. Acad. Sci. U. S. A.* 104 (17), 7217–7222. doi:10.1073/pnas.0610068104
- Day, C. P., and James, O. F. (1998). Steatohepatitis: a Tale of Two "hits"? *Gastroenterology* 114 (4), 842–845. doi:10.1016/s0016-5085(98)70599-2
- Day, E. A., Ford, R. J., and Steinberg, G. R. AMPK as a Therapeutic Target for Treating Metabolic Diseases - ScienceDirect. *Trends Endocrinol. Metabolism* 28 (8), 545–560. doi:10.1016/j.tem.2017.05.004
- Defour, A., Dessalle, K., Castro Perez, A., Poyot, T., Castells, J., Gallot, Y. S., et al. (2012). Sirtuin 1 Regulates SREBP-1c Expression in a LXR-dependent Manner in Skeletal Muscle. *PLoS One* 7 (9), e43490. doi:10.1371/journal.pone.0043490
- Deng, M., Chen, H., Long, J., Song, J., Xie, L., and Li, X. (2021). Atractylenolides (I, II, and III): a Review of Their Pharmacology and Pharmacokinetics. *Arch. Pharm. Res.* 44 (7), 633–654. doi:10.1007/s12272-021-01342-6
- Fang, J., Sun, X., Xue, B., Fang, N., and Zhou, M. (2017). Dahuang Zexie Decoction Protects against High-Fat Diet-Induced NAFLD by Modulating Gut Microbiota-Mediated Toll-like Receptor 4 Signaling Activation and Loss of Intestinal Barrier. *Evidence-Based Complementary Altern. Med.* 2017, 1–13. doi:10.1155/2017/2945803
- Feng, Y., Chen, Y., Yang, B., Lan, Q., Wang, T., Cui, G., et al. (2019). Hepatoprotective Effect of Jianpi Huoxue Formula on Nonalcoholic Fatty Liver Disease Induced by Methionine-Choline-Deficient Diet in Rat. *Biomed. Res. Int.* 2019, 7465272. doi:10.1155/2019/7465272
- Feng, Z., Hou, J., Yu, Y., Wu, W., Deng, Y., Wang, X., et al. (2019). Dissecting the Metabolic Phenotype of the Antihypertensive Effects of Five Uncaria Species on Spontaneously Hypertensive Rats. *Front. Pharmacol.* 10, 845. doi:10.3389/fphar.2019.00845
- Ferri, F., Carotti, S., Carpino, G., Mischitelli, M., Cantafora, A., Molinaro, A., et al. (2021). The Propensity of the Human Liver to Form Large Lipid Droplets Is Associated with PNPLA3 Polymorphism, Reduced INSIG1 and NPC1L1 Expression and Increased Fibrogenetic Capacity. *Int. J. Mol. Sci.* 22 (11), 6100. doi:10.3390/ijms22116100
- Fu, S., Watkins, S. M., and Hotamisligil, G. S. (2012). The Role of Endoplasmic Reticulum in Hepatic Lipid Homeostasis and Stress Signaling. *Cell. Metab.* 15 (5), 623–634. doi:10.1016/j.cmet.2012.03.007
- Fulco, M., and Sartorelli, V. (2008). Comparing and Contrasting the Roles of AMPK and SIRT1 in Metabolic Tissues. *Cell. Cycle* 7 (23), 3669–3679. doi:10.4161/cc.7.23.7164
- Hansen, H. H., Ægidius, H. M., Oró, D., Evers, S. S., Heebøll, S., Eriksen, P. L., et al. (2020). Human Translatability of the GAN Diet-Induced Obese Mouse Model of Non-alcoholic Steatohepatitis. *BMC Gastroenterol.* 20 (1), 210. doi:10.1186/s12876-020-01356-2
- Hirsova, P., Ibrahim, S. H., Gores, G. J., and Malhi, H. (2016). Lipotoxic Lethal and Sublethal Stress Signaling in Hepatocytes: Relevance to NASH Pathogenesis. *J. Lipid Res.* 57 (10), 1758–1770. doi:10.1194/jlr.R066357
- Hou, X., Xu, S., Maitland-Toolan, K. A., Sato, K., Jiang, B., Ido, Y., et al. (2008). SIRT1 Regulates Hepatocyte Lipid Metabolism through Activating AMP-Activated Protein Kinase. *J. Biol. Chem.* 283 (29), 20015–20026. doi:10.1074/jbc.M802187200
- Hsieh, S. A., and Allen, P. M. (2020). Immunomodulatory Roles of Polysaccharide Capsules in the Intestine. *Front. Immunol.* 11, 690. doi:10.3389/fimmu.2020.00690
- Huang, T. Y., Zheng, D., Houmard, J. A., Brault, J. J., Hickner, R. C., and Cortright, R. N. (2017). Overexpression of PGC-1 α Increases Peroxisomal Activity and Mitochondrial Fatty Acid Oxidation in Human Primary Myotubes. *Am. J. Physiol. Endocrinol. Metab.* 312 (4), E253–E263. doi:10.1152/ajpendo.00331.2016
- Yang, J.-M., Sun, Y., Wang, M., Zhang, X.-L., Zhang, S.-J., Gao, Y.-S., et al. Regulatory Effect of a Chinese Herbal Medicine Formula on Non-alcoholic Fatty Liver disease, (2019), World Journal of Gastroenterology. 25(34):5105–5119. doi:10.3748/wjg.v25.i34.5105
- Jang, M. K., Han, Y. R., Nam, J. S., Han, C. W., Kim, B. J., Jeong, H. S., et al. (2015). Protective Effects of Alisma Orientale Extract against Hepatic Steatosis via Inhibition of Endoplasmic Reticulum Stress. *Int. J. Mol. Sci.* 16 (11), 26151–26165. doi:10.3390/ijms161125944
- Khamis, M. M., Adamko, D. J., and El-Aneel, A. (2017). Mass Spectrometric Based Approaches in Urine Metabolomics and Biomarker Discovery. *Mass Spectrom. Rev.* 36 (2), 115–134. doi:10.1002/mas.21455
- Kim, Y. C., and Guan, K.-L. mTOR: a Pharmacologic Target for Autophagy Regulation. *J. Clin. Investigation.* 125 (1), 25–32. doi:10.1172/jci73939
- Kleiner, D. E., Brunt, E. M., Van Natta, M., Behling, C., Contos, M. J., Cummings, O. W., et al. (2005). Design and Validation of a Histological Scoring System for Nonalcoholic Fatty Liver Disease. *Hepatology* 41 (6), 1313–1321. doi:10.1002/hep.20701
- Konerman, M. A., Jones, J. C., and Harrison, S. A. (2018). Pharmacotherapy for NASH: Current and Emerging. *J. Hepatology* 68 (2), 362–375. doi:10.1016/j.jhep.2017.10.015
- Lee, I. H., Cao, L., Mostoslavsky, R., Lombard, D. B., Liu, J., Bruns, N. E., et al. (2008). A Role for the NAD-dependent Deacetylase Sirt1 in the Regulation of Autophagy. *Proc. Natl. Acad. Sci. U. S. A.* 105 (9), 3374–3379. doi:10.1073/pnas.0712145105
- Li, Z., Berk, M., McIntyre, T. M., Gores, G. J., and Feldstein, A. E. (2008). The Lysosomal-Mitochondrial axis in Free Fatty Acid-Induced Hepatic Lipotoxicity. *Hepatology* 47 (5), 1495–1503. doi:10.1002/hep.22183
- Liang, Z., Chen, Y., Gu, T., She, J., Dai, F., Jiang, H., et al. (2021). LXR-mediated Regulation of Marine-Derived Piericidins Aggravates High-Cholesterol Diet-Induced Cholesterol Metabolism Disorder in Mice. *J. Med. Chem.* 64 (14), 9943–9959. doi:10.1021/acs.jmedchem.1c00175
- Lim, J. H., Gerhart-Hines, Z., Dominy, J. E., Lee, Y., Kim, S., Tabata, M., et al. (2013). Oleic Acid Stimulates Complete Oxidation of Fatty Acids through

- Protein Kinase A-dependent Activation of SIRT1-Pgc1 α Complex. *J. Biol. Chem.* 288 (10), 7117–7126. doi:10.1074/jbc.M112.415729
- Liu, S. S., Sheng, W. L., Li, Y., Zhang, S. S., Zhu, J. J., Gao, H. M., et al. (2019). Chemical Constituents from *Alismatis Rhizoma* and Their Anti-inflammatory Activities *In Vitro* and *In Vivo*. *Bioorg. Chem.* 92, 103226. doi:10.1016/j.bioorg.2019.103226
- Lomonaco, R., Ortiz-Lopez, C., Orsak, B., Webb, A., Hardies, J., Darland, C., et al. (2012). Effect of Adipose Tissue Insulin Resistance on Metabolic Parameters and Liver Histology in Obese Patients with Nonalcoholic Fatty Liver Disease. *Hepatology* 55 (5), 1389–1397. doi:10.1002/hep.25539
- Luan, Z.-L., Ming, W.-H., Sun, X.-W., Zhang, C., Zhou, Y., Zheng, F., et al. A Naturally Occurring FXR Agonist, Alisol B 23-acetate, Protects against Renal Ischemia-Reperfusion Injury. *Am. J. Physiology-Renal Physiology* 321 (5), F617–F628. doi:10.1152/ajprenal.00193.2021
- Manne, V., Handa, P., and Kowdley, K. V. (2018). Pathophysiology of Nonalcoholic Fatty Liver Disease/Nonalcoholic Steatohepatitis. *Clin. Liver Dis.* 22 (1), 23–37. doi:10.1016/j.cld.2017.08.007
- Mashek, D. G. (2021). Hepatic Lipid Droplets: A Balancing Act between Energy Storage and Metabolic Dysfunction in NAFLD. *Mol. Metab.* 50, 101115. doi:10.1016/j.molmet.2020.101115
- Minokoshi, Y., Kim, Y.-B., Peroni, O. D., Fryer, L. G. D., Müller, C., and Carling, D. Leptin Stimulates Fatty-Acid Oxidation by Activating AMP-Activated Protein Kinase. *Nature*. 415 (6869), 339–343. doi:10.1038/415339a
- Montesano, A., Senesi, P., Vacante, F., Mollica, G., Benedini, S., Mariotti, M., et al. (2020). L-carnitine Counteracts *In Vitro* Fructose-Induced Hepatic Steatosis through Targeting Oxidative Stress Markers. *J. Endocrinol. Investig.* 43 (4), 493–503. doi:10.1007/s40618-019-01134-2
- Mootha, V. K., Lindgren, C. M., Eriksson, K. F., Subramanian, A., Sihag, S., Lehar, J., et al. (2003). PGC-1 α -responsive Genes Involved in Oxidative Phosphorylation Are Coordinately Downregulated in Human Diabetes. *Nat. Genet.* 34 (3), 267–273. doi:10.1038/ng1180
- Mullard, A. (2020). FDA Rejects NASH Drug. *Nat. Rev. Drug Discov.* 19 (8), 501. doi:10.1038/d41573-020-00126-9
- rtf, My. End. Note. Library.
- Park, Y. J., Kim, M. S., Kim, H. R., Kim, J. M., Hwang, J. K., Yang, S. H., et al. (2014). Ethanol Extract of *Alismatis Rhizome* Inhibits Adipocyte Differentiation of OP9 Cells. *Evid. Based Complement. Altern. Med.* 2014, 415097. doi:10.1155/2014/415097
- People's Republic of China (1996). *Ministry of Health of the People's Republic of China*. Beijing: China Medical Science Press People's Republic of China Health Industry Standard.
- Pillai, V. B., Sundaresan, N. R., Kim, G., Gupta, M., Rajamohan, S. B., Pillai, J. B., et al. (2010). Exogenous NAD Blocks Cardiac Hypertrophic Response via Activation of the SIRT3-LKB1-AMP-Activated Kinase Pathway. *J. Biol. Chem.* 285 (5), 3133–3144. doi:10.1074/jbc.M109.077271
- Porter, N. T., and Martens, E. C. (2017). The Critical Roles of Polysaccharides in Gut Microbial Ecology and Physiology. *Annu. Rev. Microbiol.* 71, 349–369. doi:10.1146/annurev-micro-102215-095316
- Radhakrishnan, S., Ke, J. Y., and Pellizzon, M. A. (2020). Targeted Nutrient Modifications in Purified Diets Differentially Affect Nonalcoholic Fatty Liver Disease and Metabolic Disease Development in Rodent Models. *Curr. Dev. Nutr.* 4 (6), nzaa078. doi:10.1093/cdn/nzaa078
- Ratzliff, V., Sanyal, A. J., MacConell, L., Shringarpure, R., Marmon, T., Shapiro, D., et al. (2016). Intercept Pharmaceuticals. A Phase 3, Double-Blind, Randomized, Long-Term, Placebo-Controlled, Multicenter Study Evaluating the Safety and Efficacy of Obeticholic Acid in Subjects with Nonalcoholic Steatohepatitis. *J. Hepatology*. 64 (2), S294–S295. doi:10.1016/s0168-8278(16)00372-x
- Ruderman, N. B., Xu, X. J., Nelson, L., Cacicedo, J. M., Saha, A. K., Lan, F., et al. (2010). AMPK and SIRT1: a Long-Standing Partnership? *Am. J. Physiol. Endocrinol. Metab.* 298 (4), E751–E760. doi:10.1152/ajpendo.00745.2009
- Shin, S. M., Cho, I. J., and Kim, S. G. (2009). Resveratrol Protects Mitochondria against Oxidative Stress through AMP-Activated Protein Kinase-Mediated Glycogen Synthase Kinase-3 β Inhibition Downstream of poly(ADP-Ribose)polymerase-LKB1 Pathway. *Mol. Pharmacol.* 76 (4), 884–895. doi:10.1124/mol.109.058479
- Silvestre, M. F., Viollet, B., Caton, P. W., Leclerc, J., Sakakibara, I., Foretz, M., et al. (2014). The AMPK-SIRT Signaling Network Regulates Glucose Tolerance under Calorie Restriction Conditions. *Life Sci.* 100 (1), 55–60. doi:10.1016/j.lfs.2014.01.080
- Song, Q., Wang, Y., Huang, L., Shen, M., Yu, Y., Yu, Q., et al. (2021). Review of the Relationships Among Polysaccharides, Gut Microbiota, and Human Health. *Food Res. Int.* 140, 109858. doi:10.1016/j.foodres.2020.109858
- Stefan, N., Häring, H. U., and Cusi, K. (2019). Non-alcoholic Fatty Liver Disease: Causes, Diagnosis, Cardiometabolic Consequences, and Treatment Strategies. *Lancet Diabetes Endocrinol.* 7 (4), 313–324. doi:10.1016/S2213-8587(18)30154-2
- Subramanian, A., Tamayo, P., Mootha, V. K., Mukherjee, S., Ebert, B. L., Gillette, M. A., et al. (2005). Gene Set Enrichment Analysis: A Knowledge-Based Approach for Interpreting Genome-wide Expression Profiles. *Proc. Natl. Acad. Sci. U. S. A.* 102 (43), 15545–15550. doi:10.1073/pnas.0506580102
- Sun, Y., Long, J., Chen, W., Sun, Y., Zhou, L., Zhang, L., et al. (2021). Alisol B 23-acetate, a New Promoter for Cholesterol Efflux from Dendritic Cells, Alleviates Dyslipidemia and Inflammation in Advanced Atherosclerotic Mice. *Int. Immunopharmacol.* 99, 107956. doi:10.1016/j.intimp.2021.107956
- Sun, Y., Zhang, Z., Cheng, L., Zhang, X., Liu, Y., Zhang, R., et al. (2021). Polysaccharides Confer Benefits in Immune Regulation and Multiple Sclerosis by Interacting with Gut Microbiota. *Food Res. Int.* 149, 110675. doi:10.1016/j.foodres.2021.110675
- Tang, K., Deng, Y., Zheng, C., Nie, H., Pan, M., and Chen, R. (2020). Prevention of Nonalcoholic Hepatic Steatosis by Shenling Baizhu Powder: Involvement of Adiponectin-Induced Inhibition of Hepatic SREBP-1c. *Oxidative Med. Cell. Longev.* 2020, 1–13. doi:10.1155/2020/9701285
- Tanphaichitr, V., and Leelahagul, P. (1993). Carnitine Metabolism and Human Carnitine Deficiency. *Nutrition* 9 (3), 246–254.
- Tilg, H., and Moschen, A. R. (2010). Evolution of Inflammation in Nonalcoholic Fatty Liver Disease: the Multiple Parallel Hits Hypothesis. *Hepatology* 52 (5), 1836–1846. doi:10.1002/hep.24001
- Trefts, E., and Shaw, R. J. (2021). AMPK: Restoring Metabolic Homeostasis over Space and Time. *Mol. Cell.* 81 (18), 3677–3690. doi:10.1016/j.molcel.2021.08.015
- Wang, K., Zhang, B., Song, D., Xi, J., Hao, W., Yuan, J., et al. (2020). Alisol A Alleviates Arterial Plaque by Activating AMPK/SIRT1 Signaling Pathway in apoE-Deficient Mice. *Front. Pharmacol.* 11, 580073. doi:10.3389/fphar.2020.580073
- Wang, Y., Liang, Y., and Vanhoutte, P. M. (2011). SIRT1 and AMPK in Regulating Mammalian Senescence: a Critical Review and a Working Model. *FEBS Lett.* 585 (7), 986–994. doi:10.1016/j.febslet.2010.11.047
- Yan, T., Yan, N., Wang, P., Xia, Y., Hao, H., Wang, G., et al. (2020). Herbal Drug Discovery for the Treatment of Nonalcoholic Fatty Liver Disease. *Acta Pharm. Sin. B* 10 (1), 3–18. doi:10.1016/j.apsb.2019.11.017
- Yu, X.-C., Fu, Y., Bi, Y.-H., Zhang, W.-W., Li, J., and Ji, T. (2020). Alisol B 23-acetate Activates ABCG5/G8 in the Jejunum via the LXRA/CAT2 Pathway to Relieve Atherosclerosis in Ovariectomized ApoE $-/-$ Mice. *Aging (Albany NY)* 12 (24), 25744–25766. doi:10.18632/aging.104185
- Zhang, L.-L., Xu, W., Xu, Y.-L., Chen, X., Huang, M., and Lu, J.-J. (2017). Therapeutic Potential of *Rhizoma Alismatis*: a Review on Ethnomedicinal Application, Phytochemistry, Pharmacology, and Toxicology. *Ann. N. Y. Acad. Sci.* 1401 (1), 90–101. doi:10.1111/nyas.13381
- Zhang, Z., Zhao, M., Li, Q., Zhao, H., Wang, J., and Li, Y. (2009). Acetyl-L-carnitine Inhibits TNF- α -Induced Insulin Resistance via AMPK Pathway in Rat Skeletal Muscle Cells. *FEBS Lett.* 583 (2), 470–474. doi:10.1016/j.febslet.2008.12.053
- Zu, Y., Liu, L., Lee, M. Y., Xu, C., Liang, Y., Man, R. Y., et al. (2010). SIRT1 Promotes Proliferation and Prevents Senescence through Targeting LKB1 in Primary Porcine Aortic Endothelial Cells. *Circ. Res.* 106 (8), 1384–1393. doi:10.1161/CIRCRESAHA.109.215483

Conflict of Interest: The authors declare that the research was conducted in the absence of any commercial or financial relationships that could be construed as a potential conflict of interest.

Publisher's Note: All claims expressed in this article are solely those of the authors and do not necessarily represent those of their affiliated organizations, or those of the publisher, the editors, and the reviewers. Any product that may be evaluated in this article, or claim that may be made by its manufacturer, is not guaranteed or endorsed by the publisher.

Copyright © 2022 Cao, Shi, Song, Xu, Lu, Sun, Hou, Chen, Wu and Gong. This is an open-access article distributed under the terms of the Creative Commons Attribution License (CC BY). The use, distribution or reproduction in other forums is permitted, provided the original author(s) and the copyright owner(s) are credited and that the original publication in this journal is cited, in accordance with accepted academic practice. No use, distribution or reproduction is permitted which does not comply with these terms.



The Role and Mechanisms of Traditional Chinese Medicine for Airway Inflammation and Remodeling in Asthma: Overview and Progress

Bo-wen Zhou¹, Hua-man Liu² and Xin-hua Jia^{2*}

¹Shandong University of Traditional Chinese Medicine, Jinan, China, ²Affiliated Hospital of Shandong University of Traditional Chinese Medicine, Jinan, China

OPEN ACCESS

Edited by:

Xijun Wang,
Heilongjiang University of Chinese
Medicine, China

Reviewed by:

Geng Wenye,
Fudan University, China
Aihua Zhang,
Heilongjiang University of Chinese
Medicine, China

*Correspondence:

Xin-hua Jia
jiaxinhua_jn@163.com

Specialty section:

This article was submitted to
Ethnopharmacology,
a section of the journal
Frontiers in Pharmacology

Received: 11 April 2022

Accepted: 09 June 2022

Published: 15 July 2022

Citation:

Zhou B-w, Liu H-m and Jia X-h (2022)
The Role and Mechanisms of
Traditional Chinese Medicine for
Airway Inflammation and Remodeling
in Asthma: Overview and Progress.
Front. Pharmacol. 13:917256.
doi: 10.3389/fphar.2022.917256

Asthma as an individual disease has blighted human health for thousands of years and is still a vital global health challenge at present. Though getting much progress in the utilization of antibiotics, mucolytics, and especially the combination of inhaled corticosteroids (ICS) and long-acting β -agonists (LABA), we are confused about the management of asthmatic airway inflammation and remodeling, which directly threatens the quality of life for chronic patients. The blind addition of ICS will not benefit the remission of cough, wheeze, or sputum, but to increase the risk of side effects. Thus, it is necessary to explore an effective therapy to modulate asthmatic inflammation and airway remodeling. Traditional Chinese Medicine (TCM) has justified its anti-asthma effect in clinical practice but its underlying mechanism and specific role in asthma are still unknown. Some animal studies demonstrated that the classic formula, direct extracts, and natural compounds isolated from TCM could significantly alleviate airway structural alterations and exhibit the anti-inflammatory effects. By investigating these findings and data, we will discuss the possible pathomechanism underlined airway inflammation and remodeling in asthma and the unique role of TCM in the treatment of asthma through regulating different signaling pathways.

Keywords: asthma, TCM, airway inflammation, airway remodeling, autophagy

INTRODUCTION

Bronchial asthma, characterized by bronchoconstriction, is a common chronic respiratory disease that negatively influences the quality of life of patients worldwide and the population of patients doubles every 10 years without any definite reasons, especially in developing countries (Suk et al., 2016). In asthma, previous research focused more on big airways because of their obvious changes and easy access for biopsy. However, increasing evidence shows that small airway (<2 mm in diameter) dysfunction, which involves airway inflammation and remodeling, is a key relevant factor in the pathogenesis of asthma, which also represents a trademark of asthma persistence. Based on a large prospective study (Postma et al., 2019), the chronic soakage of inflammatory cells and its pathway was involved in almost all asthma severities and aggravated the abnormalities in airway function and structure. Compared with healthy lungs, mucus-secreting goblet cells in the epithelium have been frequently observed in the small airways of patients with severe asthma according to the flatter of inflammatory mediators (van den Bosch et al., 2021). Such structural changes are collectively termed “airway remodeling.” The cause(s) of airway remodeling is still unknown

though airway inflammation has long been considered the culprit. It is suggested that airway smooth muscle epigenetic changes (Kaczmarek et al., 2019), autophagy (Theofani and Xanthou, 2021), and immune cells (Guida and Riccio, 2019) are drivers of remodeling, which indicates that both airway inflammation and remodeling are independent factors of asthma fatal attacks.

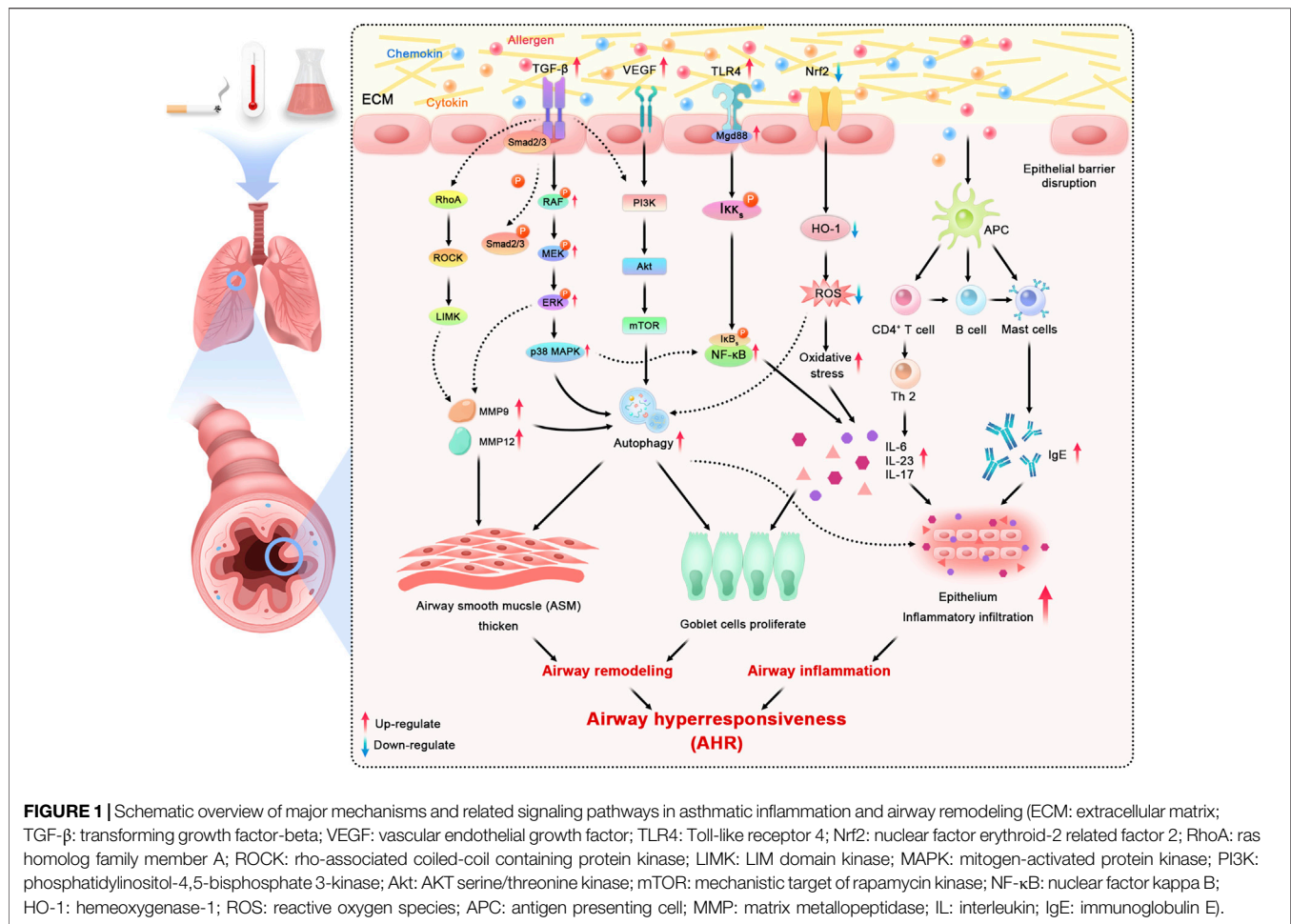
Currently, asthma endotypes have been defined and broadly regarded as type 2 (T2) high or T2 low based on the classical description of immediate or late allergic airway disorders. These two different types correspond to either eosinophilic asthma or non-eosinophilic phenotypes (Carr et al., 2018). The combined administration of β_2 adrenoceptor agonists and inhaled corticosteroids, as well as biological therapy (Costello and Cushen, 2020), has been widely applied in clinical circumstances for chronic airway inflammation and remodeling. However, not only these therapies above may cause severe side effects but also quite a few patients without the rise of eosinophilic granulocyte in blood have been observed to have airway inflammation and remodeling in the biopsy. Therefore, it is necessary to explore more therapies for asthma, aiming at alleviating continuous airway inflammation and remodeling. Traditional Chinese Medicine (TCM) has been applied to the clinical treatment of asthma for thousands of years in China. Intriguingly, recent reports have found that multiple bioactive components isolated from Chinese herbal and formulas based on TCM theories could exhibit anti-inflammatory and anti-remodeling effects, such as Formononetin (Yi et al., 2020). Such findings suggest a potential of TCM in airway inflammation and remodeling therapy via modulating the immune system or autophagy. In this review, we will briefly discuss the driver mechanisms underlying airway inflammation and remodeling in asthma. The TCM theories for treating the disease and moderating symptoms will be described. And, we also discuss the formulas, extracts, and active ingredients with potential in anti-inflammation, anti-remodeling, and their roles in asthma. Further discussion on TCM will focus on the outlooks for future research and the challenges of utilizing TCM to moderate airway symptoms of asthma, which intend to enlighten the new therapies or strategies on small airway dysfunction.

Airway Inflammation and Remodeling Factors

Asthma is a chronic heterogeneous disease that is usually characterized by airway inflammation, obstruction, and airway hyperresponsiveness (AHR). Research (Wang C. et al., 2018) demonstrated that the increased airway smooth muscle (ASM) thickness and allergy contribute independently and additively to AHR, which is the primary structural abnormality of asthma. Meanwhile, the changes in ASM are one of the most crucial pathological progresses in airway remodeling. Although it has been difficult to confirm, it (Grainge and Park, 2018) has been seen in some asthmatics that airway remodeling contributes to the development of fixed airway obstruction. The aggravation of airway inflammation and remodeling is associated with the rapid attack of fatal asthma but the mechanisms and driver factors of them are still unknown.

The pathogenesis of inflammation in asthma is influenced by multiple factors, with environmental factors such as smoking, temperature, chemical irritants, and body weight abnormalities being the key elements leading to asthma progression (Liu et al., 2021). These factors above may boost the release of cytokines, allergens, chemokines, and infectious agents, which will activate signaling pathways in epithelial cells in asthma (Aghasafari et al., 2019). The majority of asthma patients show atopic symptoms and have allergic airway inflammation extending from the trachea down to peripheral airways. In general, Toll-like receptors (TLRs), existing on the membrane surface (Tripathi and Aggarwal, 2006), recognize associated molecular patterns and activate inflammatory cells like nuclear factor kappa-light-chain-enhancer of activated B-cells (NF- κ B). Then, the resolution process starts where antigen-presenting cells (APCs) endocytose inhaled allergens, which indirectly participate in activating mast cells by crosslinking surface-bound immunoglobulin E (IgE) molecules to release several bronchoconstrictor mediators. Moreover, many known immune signaling pathways, such as mitogen-activated protein kinase (MAPK) and nuclear factor erythroid-2-related factor 2/heme oxygenase-1 (Nrf2/HO-1) are specifically associated with airway inflammation in response to various factors (Wang K. C. W. et al., 2018). Peter J. Barnes (2017) found that the increased release of mediators from inflammatory cells (particularly mast cells) may induce the attack of AHR in asthma. According to the existing research (Wang J. et al., 2021), the multiple active ingredients from Chinese medicinal plants are potential treatment strategies in controlling AHR by reducing Th2 cytokines, modulating Th1/Th2, and suppressing inflammatory pathways, which systemically confirmed the effectiveness of TCM on airway anti-inflammation.

Airway remodeling is characterized by structural alternatives, consisting of increased mucus-secreting goblet cells in the epithelium, thickening of the sub-epithelial collagen layer, angiogenesis, as well as the increase of ASM mass and volume (Grainge and Park, 2018). Within the classical description of the relationship between airway inflammation and remodeling, some of the known Th2 highly induced factors, such as eosinophils, neutrophils, cytokines, chemokines, mast cells, and growth factors, contribute to the thickness of the epithelium, the basement membrane (BM), the subepithelial layer, and ASM (Bergeron and Boulet, 2006). These structural changes have been found in both big and small airways, yet not easy to demonstrate. Further, in a recent review, Guida (Guida and Riccio, 2019) pointed out a complex rather than single relationship between airways remodeling and inflammation, which are not limited to Th2-induced inflammatory effects but also induced, suppressed, or regulated by different cellular and molecular pathways, especially the extracellular matrix (ECM). ECM plays a unique role in the structural stability of the airways wall being consisting of a network of collagenous and non-collagenous ECM protein surrounding cells in the airways. Meanwhile, the lung ECM remodeling starts from the ongoing deposition of proteins, basically because of the transforming growth factor-beta (TGF- β) signaling. Confirmed by *in vivo* and *in vitro* trials (Saito et al., 2018), TGF- β increases ASM proliferation by activated fibroblasts and has been promoted by uncontrolled bronchoconstriction in



asthma. Other factors such as matrix metalloprotein (MMP), especially MMP-9, MMP-12, or Rho-kinase (ROCK) proteins, contribute to the remodeling process as well by degrading the components of the ECM. Several studies (Bortolozzo et al., 2018; Righetti et al., 2014) using ovalbumin (OVA)-induced models of asthma have shown functional and structural alterations in the respiratory system associated with the high expression of TGF-β, MMP-9, MMP-12 positive cells, and Th2 cytokines: the increased deposition of actin and elastic fibers, and increased mucus production among big and small airways. The functional consequences of these alterations mostly result in the obstruction of small airways, airways narrowing, and the depressing of lung function due to sputum secretion (Ito et al., 2019). However, despite the widespread utilization of bronchodilators and corticosteroids to relieve the symptoms of asthma airways remodeling, there are no clinical medicines that have shown a significant efficacy to reverse all changes mentioned above. Fortunately, an increasing number of trials suggested the effective treatment of TCM therapies for airway anti-remodeling. Wieczfinska et al. (2020) have justified that the *Leonurus sibiricus* root extracts could significantly decrease airways remodeling marker expression via *in vivo* studies.

Among recent studies, the unbalance of autophagy has been widely demonstrated in allergic airway inflammation. As a vital regulator of fibrosis, autophagy can strongly enhance ECM production in ASM and mesenchymal cells, contributing to airway thickening and rigidity. Consistently, based on previous studies (Joan et al., 2017; Choi et al., 2018), the autophagy inhibition in pulmonary inflammation may help to preserve the maintenance of lung homeostasis and the control of fatal inflammatory responses by decreasing the exposure of immune factors, such as IL-17, IL-23, and TLR4. Similarly, the epithelial cells depleted autophagy-related 5 or autophagy-related 4 genes exerted a block in mucus generation with IL-13, which indicated that autophagy is critical for airway mucus generation and Th2 response in asthma (Dickinson et al., 2016). McAlinden et al. 2019) have shown that inhibition autophagy reduces airways remodeling and alleviates bronchoconstriction in a TGFβ1-dependant manner through building murine models. The potential pathological mechanism of airway alterations is also associated with the close relationship between abnormal autophagy and dysregulation of redox homeostasis (Ornatowski et al., 2020). The activation of oxidative stress results in increases in epithelial vascular permeability and ASM contraction (Kleniewska and Pawliczak, 2017). Overall, blocking and

moderating autophagy have been regarded as an attractive target to moderate airway remodeling and inflammation in asthma. All major mechanisms mentioned above in asthmatic airway inflammation and remodeling can be consulted in **Figure 1**.

As one of the main choices of complementary and alternative therapy for asthma, TCM has extensive prospects in reversing autophagy to control asthma serve attacks. The treatment of Shensuyin (Zhang H. et al., 2021), a traditional herbal formula, has been confirmed by its inhibition in the PI3K/Akt/mTOR signaling pathway, which is consistent with the induction of autophagy. A large number of single herbals from TCM show their potential possibilities as autophagy modulators providing a direct link from traditional therapies to modern treatment in asthma.

Theoretical Research in Inflammation and Remodeling of TCM

TCM, consisting of therapies and methods, has been widely applied in treating asthma in East and South Asia for a few thousand years as an effective medical system (Ou Yang and Gu, 1996). Unlike evidence-induced modern medicine (Chan and Ng, 2020), TCM is based on the clinical experience about the etiology of diseases, the diagnosis of disease syndromes, prevention, and treatments. In ancient theory, asthma was called wheezing disease for its pulmonary symptoms like cough, sputum, and wheezing sound. According to theoretical studies of TCM, it has been found that maintaining the lung function requires a relative balance between a smooth flow of energy (commonly called “Qi”) and blood. Only the smooth circulation of Qi and blood can ensure the respiratory function of the lung. Chinese Herbal medicine (CHM) believes that asthma is associated with the Qi deficiency in the lung, which directly leads to the disturbance of blood flow. The main courses of Qi deficiency could be attributed to congenital weakness or rapid chronic attack of illness. Meanwhile, when the lung is deficient, not blood but also other body fluids will hamper the body and become sputum blockage and blood stasis based on the TCM. It (Liu et al., 2021) is confident to be confirmed that these alterations are similar to chronic inflammatory progress and angiogenesis in airways remodeling.

In TCM theory, it was found that there is a close relationship between lungs and kidneys’ physiology. Once the kidney is deficient, the lung function will also be restrained. Thus, the major treatment therapeutic method of TCM aims to invigorate kidney function and strengthen the flow of Qi for asthma patients to relieve symptoms (Geng et al., 2016). Further, the TCM summarizes relative symptoms of airways inflammation as well as remodeling in asthma and has classified it as a stagnation of qi and blood stasis syndrome or phlegm-heat pattern. Thus, the aim of management of asthma is formulated by TCM therapy principles of removing blood stasis (quyu), benefiting the Qi (yiqi), clearing the heat (qingre), and eliminating sputum (qutan).

At present, the obvious advantages of TCM in asthma treatment and control have been given increasing attention and clinical proof. Several observational studies (Wang et al.,

2014) in China on more than 360 patients suggested that the addition of TCM to conventional therapy alleviated acute symptoms and reduced drug use. One meta-analysis (Song et al., 2016) over 20 RCTs involving 1,590 participants evaluated the safety and efficacy of CHM in treating childhood cough variant asthma (CVA) and demonstrated that there could be an additive benefit from CHM in terms of improving the induces among CVA patients. Normally, CVA patients present intractable cough and lung function alteration (mainly the forced expiratory volume in 1 second, FEV₁) along with the increase of LgC5 and IgE. The study has shown that the CHM group had a positive effect in improving FEV₁ and LgC5 as well as the falling total IgE level. There were also no major adverse effects to the treatment. However, there is still a long way to go in exploring specific mechanisms of TCM controlling asthma, especially anti-inflammation and anti-remodeling. The relevant content will be discussed in this review below.

The Herbal Medicine Formulae in Inhibiting Inflammation and Remodeling

As a mainstay therapeutic approach in TCM, Herbal therapy, or the Traditional Medicine Formulation, is the use of a mixture of herbal ingredients underlying different principles like one emperor, minister, or assistant. The emperor herb fulfills the main therapeutic purpose with the reminders of other herbs in the formulation modulating other effects.

Bu-Shen-Yi-Qi Fang

Bu-Shen-Yi-Qi Fang (BSYQF), a traditional medical formula, has been justified that could suppress chronic airway inflammation according to an *in vitro* study. The whole formulation consists of *Astragalus mongholicus* Bunge, *Rehmannia glutinosa* (Gaertn.) DC., and *Epimedium brevicornu* Maxim. A recent study (Huang M. et al., 2021) has reported that the modified BSYQF can alleviate airways inflammation, AHR, mucus hypersecretion, and collagen deposition via a decrease in the expression of the VIP-VPAC2 signaling pathway in the mouse model. BSYQF has more than 16 chemical constituents including acteoside, catalpol, and icariin. Some of these components have the effect of modulating oxidative stress and reactive oxygen species (ROS) signaling, which are involved in airways inflammation and remodeling in asthma (Chiou et al., 2004; Bi et al., 2008; Kleniewska and Pawliczak, 2017; Sahiner et al., 2018). Aiming to investigate whether BSYQF had an effect on airways remodeling, Cui et al. (2019) sensitized OVA-induced mice model with BSYQF orally. The results indicated that BSYQF treatment reduced airway remodeling including ASM thickening and peribronchial collagen deposition. In terms of oxidative stress, BSYQF treatment decreased the reactive oxygen species (ROS), malondialdehyde (MDA), NO, and restored mitochondrial ultrastructural changes of bronchial epithelia, which indicated the possibility of BSYQF playing an antioxidant role through mitochondrial pathway and eventually inhibited the airway remodeling. Further, after using the RNA-seq analysis to obtain the expressed genes, Cui et al. (2021) also found the expression of several coding genes that

had altered in asthmatic models. Based on the gene network by IPA, the study inferred that Adipoq, SPP1, and TNC may contribute to the regulation of BSYQF's anti-remodeling effect. Therefore, BSYQF is expected to become a hopeful preventive agent against airway inflammation and remodeling for asthma patients.

Gu-Ben-Fang-Xiao Decoction

Gu-Ben-Fang-Xiao decoction (GBFXD) is a well-known TCM formula derived from a combination of Yupingfeng San (YPFS), a classical formula widely used for treating respiratory diseases, and Erchen decoction. GBFXD has been clinically used in asthma for decades, and the collection of herbal plants can be traced back to Dan Xi Xin Fa, a famous TCM classic. Previous studies (Huang et al., 2016; Lu et al., 2016) have shown that GBFXD can not only downregulate the expression of asthmatic susceptibility genes orosomucoid 1-like protein 3 (ORMDL3) and ADAM33 but also inhibit endoplasmic reticulum stress (ERS), which attenuates chronic airway inflammation. A study (Liang et al., 2020) designed to explore if GBFXD offers inhibition against B cell activation in asthma has been conducted. The mice model of asthma was made by the intraperitoneal injection of OVA combined with the intranasal administration of respiratory syncytial virus (RSV). The eventual data showed that GBFXD reduced the level of inflammatory cytokines such as IL-6, IgE, tumor necrosis factor- α (TNF- α), and B cell-activating factor (BAFF), moderated the inflammatory alterations in lung tissues of asthmatic models, and decreased the proportion of BAFF + cell subsets in bronchoalveolar lavage fluid (BALF). In conclusion, the anti-inflammatory functions of GBFXD may be associated with the depression of B cell activation and the release of IgE. Xing et al. (2019), employed the label-free proteomic method to demonstrate the effect of GBFXD treatment in RSV-OVA-induced chronic persistent asthmatic mice and found that GBFXD may control the inflammatory response of asthma via regulating cholesterol transport and complement factor activation. As for structural abnormalities, GBFXD may avoid airway remodeling by possessing the function to repair damaged airway epithelium. According to another study (Liu et al., 2019) that evaluated the effect of GBFXD on asthmatic mice by the iTRAQ labeling technology, it was recorded that several mechanisms, such as improving Th1/Th2 balance, inhibiting alternatively activated macrophages, and suppressing mitochondrial function, are closely associated with the anti-remodeling of GBFXD in asthma.

Mahuang Decoction

Mahuang Decoction (MHD), a classical multi-herbal prescription from Treatise on Cold Pathogenic Disease (Shang Han Lun in Chinese), has been used for thousands of years to get spasmolysis, diffuse the lung to resolve phlegm, and relieve asthmatic symptoms. The ingredients of MHD (He et al., 2012) consist of *Ephedra sinica* Stapf, *Cinnamomum verum* J. Presl, *Prunus armeniaca* L., and *Glycyrrhiza glabra* L. In a recent study, Huang et al. (2020) determined seven components in MHD *in vivo* by the High-Performance Liquid Chromatography-Mass Spectrometry (HPLC-MS) method and found that amygdalin may play a more

vital role in modulating inflammatory cytokine levels of asthmatic mice models. However, the immune mechanism of MHD in asthma is still unknown. Through constructing asthma-related protein-protein interaction (PPI) network based on the DAVID database, Jiao et al. (2018) targeted 20 components in MHD at 32 kinds of proteins in the asthma network and verified it *in vivo*. The results suggested that the key compounds of MHD may regulate asthma via ERK, Fc ϵ RI, PI3K-Akt, TLRs, and JAK-STAT6 signaling pathways. Additionally, the mitigation of MHD in airway inflammation was proved in another study (He et al., 2018). MHD group significantly restrained the levels of MMP-9, ILs-(2,4,5), and Tissue Inhibitor of Metalloproteinase-1 (TIMP-1) in the rat serum and depressed the protein expression of IL-21, IL-21R, STAT3, and p-STAT3 in lung tissues, which indicate a close joint between the MHD inflammatory efficacy and its regulation of the IL-21/STAT3 signaling pathway in OVA-induced models. Meanwhile, given the monitoring role (Kim et al., 2013) of MMP and TIMP for regulating airway remodeling, the study also demonstrated the possibility of MHD that influences airway repair and remodeling by modulating ECM degradation, thereby inhibiting the thickness of airway walls.

Others

Apart from the mentioned formulas above, there are 11 decoctions that have been justified for the effect of anti-inflammation or anti-remodeling of asthmatic models *in vivo* or *in vitro*. The efficacy of YPFS is satisfactory in asthma, and YPFS can significantly downregulate the production of IgE. According to the addition and subtraction rules of TCM, Jia-Wei-Yu-Ping-Feng-San (JWYPFS) is improved from YPFS to clear the heat and reduce phlegm strongly and applied in OVA challenged mice. JWYPS (Xue et al., 2021) can control the type 2 response mediated by Group 2 innate lymphoid cells (ILC2s), accordingly restoring the expression of inflammatory cytokines IL-5 and IL-13. It is reported that the compound Maqin decoction (CMD) (Xie et al., 2016) and Fangxiao formula (FXT) (Ge et al., 2019) could inhibit the protein production level of Smad-3 in lung tissues, thereby resulting in the alleviated ASM thickness, which suggested the potential clinical effect of them in airway remodeling via TGF- β /Smad signaling pathway. Jin-Gui-Shen-Qi Wan (JGSQW), as a common formula originated from *Synopsis of Prescriptions of the Golden Chamber*, has been clinically utilized to treat various diseases belonging to kidney deficiency such as diabetes (Hu L. et al., 2021), allergic rhinitis (Feng et al., 2021) as well as asthma (Ji et al., 2018). Kao (Kao et al., 2018) surveyed the treatment of JGSQW on chronic asthma by suppressing the *Dermatophagoides pteronyssinus*-induced infiltration of inflammatory cells into airways. Moreover, the study investigated the modulating effect of JGSQW on the NF- κ B signaling pathway in epithelial cells and demonstrated that JGSQW could reverse abnormal lung functions by reducing the overexpression of NF- κ B-regulated genes (e.g., ICAM-1). Histopathological examinations justified that JGSQW alleviated the airway remodeling in mice models. Another decoction ameliorating Yang deficiency, Yanghe Pingchuan granules

TABLE 1 | Associated TCM formulae in inhibiting inflammation and remodeling.

| TCM Formulae | Form | Type of study | Animal | Inducer | Mechanism of action | Pathway | References |
|-----------------------------------|-----------|-----------------|--------------|---------|--|-------------------|-------------|
| Bu-Shen-Yi-Qi fang | Decoction | <i>In vivo</i> | BALB/c mice | OVA | AHR↓ | VIP-VPAC2 | Huang et al |
| | | <i>In vivo</i> | BALB/c mice | OVA | Mucus hypersecretion↓ collagen deposition↓ ASM thickness↓ Peribronchial collagen deposition↓ Oxidative stress↓ | Antioxidant | Cui et al |
| | | <i>In vivo</i> | BALB/c mice | OVA | Abnormal coding gene↓ | PI3K/AKT and MAPK | Cui et al |
| Gu-Ben-Fang-Xiao decoction | Decoction | <i>In vivo</i> | BALB/c mice | RSV | Susceptibility gene ↓ | ORMDL3 | Huang et al |
| | | <i>In vivo</i> | BALB/c mice | RSV | ERS↓ Chronic airway inflammation↓ | PERK and IRE1α | Lu et al |
| | | <i>In vivo</i> | BALB/c mice | RSV-OVA | Inflammatory cytokines↓ Asthmatic alterations↓ | B cell | Liang et al |
| | | <i>In vivo</i> | SPF mice | RSV-OVA | Regulate cholesterol transport and complement factor activation | RAF/MEK/ERK | Xing et al |
| Mahuang Decoction | Decoction | <i>In vivo</i> | BALB/c mice | OVA | Fit the pattern of an alternative M2 activation state, AHR↓ | M2 macrophage | Liu et al |
| | | <i>In vivo</i> | SD rats | OVA | Inflammatory cytokines↓ | | Huang et al |
| | | <i>In vivo</i> | BALB/c mice | OVA | Sensitization time↓ Abdominal breathing time↓ | TLR9 | Jiao et al |
| Jia-Wei-Yu-Ping-Feng-San (JWYPFS) | Powder | <i>In vivo</i> | SD rats | OVA | Related protein expression↓ | IL-21/STAT3 | He et al |
| Maqin decoction (CMD) | Decoction | <i>In vivo</i> | C57BL/6 mice | OVA | Inflammatory cytokines↓ | ILC2s | Xue et al |
| Fangxiao formula (FXT) | Decoction | <i>In vivo</i> | SD rats | OVA | Smad3↓ | TGF-β/Smad | Xie et al |
| Jin-Gui-Shen-Qi Wan (JGSQW) | Pilula | <i>In vivo</i> | SD rats | OVA | Smad3↓ | TGF-β/Smad | Ge et al |
| Yanghe Pingchuan granules (YPG) | Decoction | <i>In vivo</i> | BALB/c mice | Der p | Airway inflammatory infiltration↓ Reverse abnormal lung function | NF-κB | Kao et al |
| Modified Si-Jun-Zi Tang (MSZJT) | Decoction | <i>In vivo</i> | SD rats | OVA | ASMCs↓ | PI3K/PKB | Pan et al |
| Xiaochuanping powder (XP) | Powder | <i>In vivo</i> | BALB/c mice | OVA | AHR ↓ Inflammatory cytokine levels↓ | mTORC1 | Jin et al |
| Soufeng Yuchuan (SFYC) decoction | Decoction | <i>In vivo</i> | SD rats | OVA | Infiltration↓ Eosinophils↓ Recover the balance between the expression of MMP-9 and TIMP-1 | MMP/TIMP | Zhou et al |
| Qingfei oral liquid (QF) | Decoction | <i>In vivo</i> | SD rats | OVA | General condition↑ Lung damages↓ | VEGF/TGF-β1 | Yan et al |
| Yan-Hou-Qing (YHQ) formula | Decoction | <i>In vivo</i> | BALB/c mice | RSV | AHR↓ Mucus hypersecretion↓ | TRPV1 | Jing et al |
| Pingchunning Decoction | Decoction | <i>In vitro</i> | BALB/c mice | OVA | Asthmatic symptoms↓ | Th2 | Cheng et al |
| | Decoction | <i>In vitro</i> | SD rats | OVA | Pulmonary pathology↓ Autophagy↓ | PI3K/Akt/mTOR | Wang et al |

↑:increase; ↓:decrease; OVA: ovalbumin; AHR: airway hyperresponsiveness; ASM: airway smooth muscle; VIP- VPAC2: vasoactive intestinal polypeptide-type 2 VIP, receptor; Der p: Dermatophagoides pteronyssinus; PI3K/AKT: phosphatidylinositol 3-kinase and protein kinase B; MAPK: mitogen-activated protein kinase; RSV: respiratory syncytial virus; ORMDL3: orosomucoid 1-like protein 3; ERS: endoplasmic reticulum stress; PERK: protein kinase RNAlike ER, kinase; IRE1α: inositol-requiring enzyme 1α; TLR9: Toll-like receptor 9; IL-21: interleukin-21; STAT3: Signal Transducers and Activators of Transcription 3; TGF-β: transforming growth factor-beta; NF-κB: nuclear factor kappa-light-chain-enhancer of activated B-cells; mTORC1: Mechanistic Target of Rapamycin 1; MMP: matrix metalloprotein; TIMP: Tissue Inhibitor of Metalloproteinase; VEGF: vascular-endothelial-growth-factor; TRPV1: Transient-Receptor-Potential-Vanilloid-1.

(YPG), can restrain the abnormal proliferation of ASMCs (Pan et al., 2018) and control airway remodeling by blocking the PI3K/PKB pathway in asthmatic rats.

Several modified formulas have also been used to improve asthma symptoms clinically for decades in China. For asthma patients in remission, it is shown that the modified Si-Jun-Zi Tang (MSZJT), a multi-herbal decoction, can improve lung function and reduce AHR in asthma. As for the animal study (Jin et al., 2019), MSJZT effectively restrained the major characteristic features of asthma such as AHR, inflammatory cytokine, and especially T effector (Teff) cell levels, which occurred, fully or partly, through inhibiting the Mechanistic Target of Rapamycin 1 (mTORC1) signaling pathway in a

chronic murine model of asthma. Xiaochuanping powder (XP) is another TCM formula consisting of medical herbs with confirmed efficacy. Zhou et al. (2018) investigated the effect of XP on asthmatic rats and found that XP could suppress the infiltration as well as the activation of eosinophils, depress the mRNA production of MMP-9 and TIMP-1, and balance the expression between two factors, thereby moderating the inflammation and remodeling of the airways. Based on the TCM theory that “collaterals obstructed by Feng stasis and phlegm” as potential pathogenesis, Yan et al. (2020) verified the effect of Soufeng Yuchuan (SFYC) decoction against airway remodeling in asthmatic rat models. The results suggested that the early application of SFYC decoction in

asthma may ameliorate airway remodeling via downregulating the expression of vascular endothelial growth factor (VEGF) as well as TGF- β 1. Meanwhile, some patented drugs from TCM have been proved their anti-inflammation effect in asthma. It (Jing et al., 2020) was observed that Qingfei oral liquid (QF) inhibited the Transient Receptor Potential Vanilloid 1 (TRPV1) signal in RSV-infected models. Consequently, QF significantly alleviates asthmatic complications including AHR and mucus hypersecretion. Cheng explored the mechanism of the Yan-Hou-Qing (YHQ) formula in modulating asthmatic inflammation, utilizing the suppression of Th2 response in murine models (Cheng et al., 2019). An *in vitro* study (Wang C. et al., 2019) verified that Pingchunling Decoction plays a vital role in the anti-autophagy mechanism of asthma pathogenesis via activating the PI3K/Akt/mTOR signaling pathway. The whole mechanisms of different formulae are consulted in **Table 1**.

The Traditional Herbs in Inhibiting Airway Inflammation and Remodeling

As the most basic therapeutical unit in Chinese medical formulations, the herbs from TCM have been given great expectations for preventing or even treating a couple of diseases. But to find out the directed association between classical TCM therapies and pharmacodynamic evidence, an increasing number of molecular studies have focused on the individual herbs or herbal extracts. Specifically, it is investigated that several herbs are beneficial to alleviate asthmatic airway inflammation and remodeling in murine models.

Actaea cimicifuga L. is a common herbal remedy documented in editions of the pharmacopoeia of China. The dried roots of *cimicifuga*, known as *Cimicifuga heracleifolia* Kom., have been vastly utilized as the source of Chinese herbal medicine Sheng Ma in terms of its antipyretic, anti-inflammatory, and antioxidative effects (Niu et al., 2019). To evaluate the efficacy of *Cimicifuga Rhizoma* extract (CRE) on asthma, the mice (Lim et al., 2021; Pang et al., 2021) were administrated CRE orally at 30 and 100 mg/kg. The mice's inflammatory alterations, including the expression of pro-inflammatory cytokines and production of mucus, have been successfully attenuated at a dose of 100 mg/kg. In addition, CRE may upregulate the level of antioxidant proteins (e.g., HO-1, Nrf2) to protect against OVA-induced asthmatic inflammation and oxidate stress. Besides, Hu Z. et al. (2021) classified 110 chemical compounds from CRE and investigated their immunomodulatory activity evaluation through *in vivo* and *in vitro* studies as well. Based on the data of the study profile, it is proved that CRE could prevent neutrophil infiltration in the lung tissues against asthmatic chronic inflammation. In spite of that little research reported on the role of anti-airway remodeling induced by *cimicifuga*, the present findings still suggest that the treatment of *cimicifuga* might be a novel alternative therapy for asthmatic airway symptoms.

As a classic tonic for the deficiency of lung, the *Cordyceps*, including *Cordyceps sinensis* as well as its common substitute *Cordyceps militaris*, has been widely used for medicine in the

treatment of respiratory diseases. From previous research (Tan et al., 2020), one of the key compounds from *cordyceps*, *cordycepin*, has been prized against various inflammatory lung injuries owing to its multiple bioactivities such as accelerating the immunity and suppressing the cytokine storms. Moreover, the *in vivo* study (Chiou and Lin, 2012) indicated that the extract of *cordyceps* could remarkably modulate the airway inflammation in a murine model through downregulating the activity of NF- κ B. In terms of asthma, it (Wang et al., 2016) is reported that the administration of *Cordyceps sinensis* alleviated asthma symptoms, lung function, and especially accelerated the health-related quality of life of patients with moderate-to-severe persistent asthma in a clinical randomized controlled trial. Additionally, by restraining the activation of the TGF- β 1/Smad pathway, *Cordyceps polysaccharide*⁰ (Zheng et al., 2020) extracted from *Cordyceps militaris* could attenuate goblet cell hyperplasia and inflammatory cell infiltration so as to alleviate the OVA-induced AHR in a murine model. The present research cannot provide a direct proof that *Cordyceps* may alleviate airway remodeling in asthma, but *Cordyceps* (Yang et al., 2018) has been verified its potential efficacy in moderating the thickness of airway walls in rats with COPD, which indicated that the treatment of *Cordyceps* may become a useful approach for asthma patients.

With promising pharmacological findings meriting further experiments and clinical studies, an increasing number of Chinese herbal medicine have shown a unique bioactive effect in managing asthmatic small airway symptoms or alterations. Both ethanolic and water extract (Luo et al., 2019) from *Salvia miltiorrhiza* Bunge (*S. miltiorrhiza*) could significantly inhibit inflammatory cell infiltration, goblet cell hyperplasia, and restore the level of Th1/Th2 cytokines. Interestingly, the study indicated that *S. miltiorrhiza* water extract is more valid in alleviating airway remodeling and responsiveness. Wang Q. et al. (2021) investigated that the total flavonoids from *Qu zhi qiao*, known as the fruit of *Citrus aurantium* L., may regulate the Smad2/3 and MAPK signaling to improve the negative effect induced by airway structural alteration and remodeling. Simultaneously, the extracts from *Perilla frutescens* (L.) Britton (Zisu) (Yang H. et al., 2020), *Asparagus cochinchinensis* (Lour.) Merr (Tianmendong) (Sung et al., 2017), and *Leonurus japonicus* Houtt (Yimucao) (Wieczfinska et al., 2020) have also verified their possibilities as a suppressor in airway inflammation and remodeling in asthmatic murine models. The more detailed mechanisms of herbs' efficacy are consulted in **Table 2**.

The Function of Natural Compounds From TCM Against Airway Inflammation and Remodeling

The investigation of the mechanisms of the multi-target effect of TCM is extremely vital to developing anti-asthma new drugs. In recent years, multiple active ingredients from Chinese herbs have been recognized as the potential basis of TCM treatment with a diversity of pharmacological effects. To better explore and clarify the effectiveness of TCM in asthmatic inflammation and airway remodeling, researchers have tested the efficacy of herbal compounds *in vivo* or *in vitro*; thereby, the active ingredients

TABLE 2 | Major anti-airway inflammation and remodeling mechanisms of the traditional herbs.

| TCM herbs | Origin | Method of study | Animal or cell | Mechanism of action | References |
|---------------------|---|---|--------------------------------------|---|--|
| Shengma | <i>Actaea cimicifuga</i> L. | HPLC-DAD <i>In vitro</i> / <i>In vivo</i> | RAW264.7 cells/SD rats | Antipyretic, inflammation↓ oxidative effects↓ iNOS↓ Inflammatory activities↓ | Niu et al Pang et al |
| | | <i>In vivo</i> <i>In vitro</i> / <i>In vivo</i> | BALB/c mice BEAS-2B cells/SD rats | Nrf2/HO-1/NQO1↑ NF-κB↓ Neutrophil's infiltration↓ | Lim et al Hu et al |
| Dong Chongxiacao | <i>Cordyceps sinensis</i> and <i>Cordyceps militaris</i> | <i>In vitro</i> / <i>In vivo</i> <i>In vivo</i> RCT | A549 cell/SD rats BALB/c mice | Accelerate the immunity cytokine storms↓ Modulate the airway inflammation NF-κB↓ Alleviate asthma symptoms lung function↑ health-related quality of life↑ | Tan et al Chiou et al Wang et al |
| | | <i>In vivo</i> <i>In vivo</i> | BALB/c mice Wistar rats | Goblet cell hyperplasia↓ Inflammatory cells infiltration↓ The thickness of airway walls↓ | Zheng et al Yang et al |
| Danshen | <i>Salvia miltiorrhiza</i> Bunge | <i>In vivo</i> | BALB/c mice | Inflammatory cell infiltration↓ Goblet cell hyperplasia↓ Restore the level of Th1/Th2 cytokines | Luo et al |
| Qu zhi qiao | <i>Citrus aurantium</i> L. | <i>In vivo</i> | BALB/c mice | Smad2/3↓ MAPK↓ | Wang et al |
| Zisu | <i>Perilla frutescens</i> (L.) Britton | <i>In vivo</i> | BALB/c mice | Modulate airway inflammation Syk↑ | Yang et al |
| Tianmendong | <i>Asparagus cochinchinensis</i> (Lour.) Merr | <i>In vivo</i> | BALB/c mice | Recover histopathological structure inflammatory mediators↓ IgE↓ IL-4↓ IL-13↓ COX-2↓ | Sung et al |
| Yimucao | <i>Leonurus japonicus</i> Houtt | <i>In vivo</i> | WI-38 and HFL1 cells | Influence airway remodeling process MMP-9↓ TGF-β↓ | Wieczfinska et al |

↑:increase; ↓:decrease; HPLC-DAD: high-performance liquid chromatography coupled with diode array detection; iNOS: inducible nitric oxide synthase; Nrf2/HO-1/NQO1: Nuclear Transcription Factor 2/Heme Oxygenase 1/Recombinant NADH, dehydrogenase, Quinone 1; NF-κB: nuclear factor kappa-light-chain-enhancer of activated B-cells; RCT: randomized controlled trial; MAPK: mitogen-activated protein kinase; Syk: Spleen Tyrosine Kinase; IL-4: Interleukin-4; IL-13: Interleukin-13; COX-2: cyclooxygenase-2; MMP-9: matrix-metalloproteinase-9; TGF-β: transforming-growth-factor-beta; WI-38: Wistar-Institute-38; HFL1: human-fetal-lung-fibroblast.

are usually regarded as shooting stars in the study of new drugs. These ingredients are normally divided into different categories, including saponins, alkaloids, ketone, flavonoids, quinone, and others, which will be discussed separately below.

The Saponins

Glycyrrhizic acid (GA) is known as one of the most crucial signature bioactive constituents isolated from the traditional Chinese herb *Glycyrrhiza uralensis* Fisch. ex DC., where its anti-inflammatory activity has also been proved in a past study (Yang et al., 2017). GA (Yao and Fu, 2021) can significantly alleviate airway inflammation, inflammatory cell infiltration, and remodeling *in vitro* and markedly restore the thickness of ASM and airway walls *in vivo*, which is at least partly associated with the modulation of the TGF-β1/Smad signaling pathway. It is worth noting that the study was the first to investigate that GA may suppress chronic asthma symptoms. Similarly, the cycloastragenol (CAG), hydrolyzed from the roots of *Astragalus mongholicus* Bunge, has been widely utilized to exert an anti-inflammatory effect in clinical study. The asthmatic mice models⁰ were established by the immune of OVA and the study (Zhu et al., 2021) demonstrated that the CAG ameliorated AHR as well as the secretion of inflammatory cytokines *in vivo*. Furthermore, it is shown that both the autophagic flux and the expression level of autophagy-associated proteins reduced after the treatment of CAG, which suggested the relationship between CAG and the inhibition of autophagy in lung cells. The root of *Panax ginseng* is a classic herb in TCM for the treatment of asthma with lung-qi deficiency syndrome. Among the biologically active compounds extracted from *Panax ginseng*

C.A.Mey., Ginsenosides are believed as the main effective ones consisting of Rb1, Rb3, Rg1, Rc, Rh2, Rg2, and Rg3 (Kim, 2018). Ginsenoside Rg1 (Chen et al., 2015) can efficiently relieve AHR and airway inflammation through regulating Th2 activity in a mice model. Moreover, it (Guan et al., 2020) is reported that the administration of Rg1 inhibits inflammatory responses via modulating the TGF-β1/Smad3 signaling pathway, thereby improving lung function and against cigarette smoke-induced airway remodeling. In terms of reducing anti-oxidative stress, the present study (Huang W. C. et al., 2021) demonstrated that the application of Ginsenoside Rg3 has significantly positive potential as a regulator in asthmatic mice. It has notably restrained eosinophil infiltration and mucus hypersecretion in mice lung tissues and exerted its anti-inflammation effect by suppressing the expression of Th2 cytokine and eotaxin expressions.

The Alkaloid

As a symbolic bioactive compound, the alkaloid widely exists in Chinese herbal medicine. Some of which have been verified for their clinical efficacy after animal experiments. Cordycepin (Cor) is a commonly used ingredient for the treatment of asthma and originated from *Cordyceps militaris*, a traditional herbal mushroom, in Chinese medicine practice. In order to identify the target of Cor regulating airway remodeling, Fei et al. (2017) have compared the level of inflammatory cytokines in OVA-induced rats BALF between the Cor group, glucocorticoids group, and combination group. The result indicated that the treatment of Cor may up-regulate the transcription of A_{2A}AR mRNA as well as inhibit the generation of TGF-β1. Further, the data also revealed that the Cor exerts its anti-remodeling effect

primarily by suppressing the expression of the p38MAPK signaling pathways. It is reported that Sinomenine (Sin), a bioactive alkaloid isolated from the root of *Sinomenium acutum* (Thunb.) Rehder & E.H.Wilson, has an effective restrained effect on airway remodeling and inflammation in mice with asthma. Sin (He et al., 2021) not only hinders the expression of MMP7, MMP9, and vimentin *in vivo* but inhibits the EMT progress by modulating the IL-4 levels in the serum, which alleviates the airway inflammation in the mice lung. Meanwhile, the study has shown that the Sin decreases the synthesis of TGF- β 1 and Smad3 and attenuates subepithelial collagen deposition, which has a positive effect on relieving airway remodeling in asthmatic mice. In another study (Işık et al., 2018), the dose of 100 mg/kg Sin treatment has been investigated that provided effective improvement on all of the histopathological outcomes about airway remodeling compared to placebo ($p < 0.05$). The levels of cytokines in BALF, serum, or immunohistochemical scores have also markedly reduced in the 100 mg/kg Sin-induced group, which suggested that Sin efficacy may associate with its modulating effect on Th-2-derived cytokines and apoptosis of airway epithelial cells. Ligustrazine (LTZ) is extracted from a traditional medicinal herb *Ligusticum striatum* DC., which has been widely used in clinical practice to clear the heat and remove the stasis in blood. It (Liu et al., 2018) is reported that LTZ may play a positive role in alleviating asthmatic inflammatory symptoms by upregulating the secretion of suppressed factors IL-10 but downregulating promoting factors IL-17 in murine models of neutrophilic asthma. It has been suggested that imbalanced oxidative stress and antioxidant defense involve in the airway remodeling in asthma.

Additionally, several bioactive alkaloids, such as Piperlongumine (Lu et al., 2019), Matrine (Yu et al., 2019), and Oxysophocarpine (Li G. et al., 2020), have been adequately justified for their anti-inflammatory activities in murine models via inhibiting NF- κ B or MAPK signaling pathway. Apart from these, the alkaloid from TCM also displayed double-treated advantages both in airway inflammation and remodeling. Tetrandrine (Tet) isolated from the roots of *Stephania tetrandra* S. Moore can suppress alveolar inflammatory infiltration, airway remodeling, and the expression of CysLT1 and CysLTR1 in OVA-sensitive rats and inhibit the cell viability of ASM cells *in vitro* (Lin et al., 2019). Therefore, Tet may alleviate airway remodeling by affecting TGF- β 1/Nrf-2/HO-1 signaling cascades and become a novel drug candidate for patients with chronic asthma. In clinical practice, *Tetradium ruticarpum* (A.Juss.) T.G.Hartley, including its extractive Evodiamine, is a classic medicine in China for treating the deficiency of Yang, especially in the kidney. Considering the synergy between kidney and lung and bioactivities of Evodiamine, Wang S. et al. (2021) established the Al(OH)₃- and OVA-induced rat models to evaluate its potential protective effect against asthma. The study reported that the administration of Evodiamine can alert the level of IgE, reduce the expression of the HMGB1 gene, and the infiltration of inflammatory cells in rat lungs. Moreover, compared with the untreated group, the treatment of Evodiamine reduces mucus secretion, the thickness of both the airway wall and the smooth muscle layer, and collagen deposition in asthmatic rats, which profited from the knockdown

of HMGB1/NF- κ B/TLR-4. As a diterpenoid alkaloid extracted from *Aconitum carmichaeli* Debeaux plants, Bulleyaconitine A (BLA) is investigated that it (Liu L. et al., 2020) can suppress the excretion of IgE, IL-17A, and Th2 cytokines, but increase the excretion of Th1 cytokines to recover the Th1/Th2 balance in murine BALF and serum. These results eventually showed that BLA may have a positive role against AHR, lung inflammation, and airway remodeling. However, whether BLA has an anti-pain or bronchodilation activity should be evaluated in further study.

The Ketone

Icariin (ICA) is one of the most major active ingredients of the Chinese traditional herb *Epimedium brevicornum* Maxim and has been given special consideration in respect of its various bioactivities including enhancing humoral immunity, relieving asthmatic cough, anti-oxidant, and anti-allergic (Sze et al., 2010; Qiao et al., 2017). A couple of studies have been carried out to estimate the effects and mechanisms of ICA in airway inflammation and remodeling of asthma. ICA (Hu et al., 2019) can attenuate ASM proliferation and key factors of the MAPK/Erk pathway *in vitro* and downregulate the increase of IL-13 as well as endothelin-1 in serum and BALF of murine models exposed to OVA *in vivo*, which indicates a bright future that ICA as replacement therapy for asthmatic patients. On the other hand, Li Z. et al. (2020) investigated the underlying mechanism of ICA alleviating EMT in asthma *in vivo* and *in vitro*. The TGF- β induced the EMT progress including migration, and the up-regulation of N-cadherin and α -SMA in 16HBE cells has also been inhibited by ICA. The administration of ICA could restrain the phosphorylation of Smad-2, Smad-3, JAK, Erk, and p38 at the molecular level, thereby inhibiting the activation of the Smad and MAPK signaling pathway. Further, it (Tian et al., 2020) is demonstrated that icaraside II could moderate airway inflammation and remodeling induced by eosinophils *in vitro* and attenuate the cell proliferation and migration in ASMCs via NF- κ B and STAT3 signaling. These data reveal the exact reasons for the use of epimedium originated herbal medicine in TCM to gain ideal efficacy in treating asthma. Curcumin, one diketone compound, is well known for its anti-inflammatory potential in clinical. Kumari et al. (2019) treated the LPS- and OVA-exposed mice with curcumin through an intranasal way to evaluate its efficacy against airway structural alterations. The corresponding study indicates that intranasal curcumin may inhibit detrimental airway remodeling in lungs by means of regulating key signaling pathways and significantly suppressing inflammatory mediators as well as related proteins such as MMP-9 or TLR-4. In recent research (Zhang Y. et al., 2021), baicalin isolated from the roots of *Scutellaria baicalensis* Georgi has shown its protective effect on cigarette smoke-induced airway inflammation in COPD rats' models, which is partially through modulating the HDAC2/NF- κ B/PAI-1 signaling. Another animal study (Yuan et al., 2018) also suggested that the treatment of curcumin may have a positive effect on airway inflammation and remodeling in the COPD model, which is closely associated with the suppression of the BEAS-2B cell proliferation and the activation of NF- κ B and COX-2, whereas these findings figured out a possibility that

curcumin and baicalin are potential agents in the therapy of asthma.

In addition to modulating inflammatory signaling pathways, the ketone compounds still alleviate airway inflammation and remodeling in other ways. *Astragalus mongholicus* Bunge has been widely utilized in traditional Chinese medicine to benefit the flow of Qi and improve the deficiency of Qi, and formononetin (FMT) is the main isoflavone obtained from it. Yi et al. (2020) justified that the treatment of FMT remarkably subsided goblet cell hyperplasia and collagen deposition and simultaneously recovered the imbalance of oxidation and antioxidation as displayed by the inhibited reactive oxygen species (ROS) but stimulated the activity of superoxide dismutase (SOD). Similarly, to FMT, luteolin is a typical flavonoid compound that has been proved to its anti-inflammatory and immune regulating effects. Furthermore, luteolin (Wang W. et al., 2021) restrained the level of autophagy of lung tissues in OVA-induced mice models with the partial mechanism including activating the PI3K/Akt/mTOR signaling pathway and downregulating the beclin-1–PI3KC3 protein complex. In conclusion, the underlying mechanisms of the ketone compounds provide a solid basis for their clinical application in the treatment of asthmatic patients.

Others

The multiple natural compounds from TCM have gotten in the intervention of asthmatic airway inflammation and remodeling individually or jointly. It is approved that andrographolide (AG) plays a vital role in the anti-inflammation treatment of various pulmonary diseases such as cough and asthma. However, whether the related capacity of AG exerts by regulating the immunologic function is unknown. Thus, Yu et al. (2021) established the asthmatic mice model induced by OVA with AG treatment, and the conclusion is that AG could significantly attenuate the airway remodeling and the neutrophil infiltration of the lung tissue and block the activation of T17 cells. Interestingly, at the molecular level, another *in vivo* study (Xia et al., 2019) demonstrated that AG antagonizes CS-induced EMT progress as well as pulmonary dysfunction by restraining the IL-6/STAT3 pathway. Curcumin is a classic herbal monomer isolated from *Curcuma phaeocaulis* Valetton for its regulatory effects on pulmonary fibrosis and oxidative stress (Li L. et al., 2020). The present study (Jia et al., 2021) revealed that curcumin could obstruct the abnormal activation of the Wnt/ β -catenin pathway in turn to moderate the chronic lung inflammation and airway remodeling, which also explained the relief of symptoms in murine models.

Rheum palmatum, L. is used as an herbaceous plant for thousands of years in China, and it has been determined that anthraquinone derivatives are its main pharmacodynamic compounds such as emodin or chrysophanol. Most corresponding studies about emodin that have been published paid more attention on the anti-inflammatory effect on the asthmatic airway. An example of this is the study carried out by Hua et al. (2019) in which emodin decreased the expression of inflammatory cytokines (e.g., IL-5, IL-17) in BALF and serum of mice, which is partially related to the downregulation of the Notch pathway. However, aiming to explore the underlying

mechanism of emodin in ASMCs, the allergic mice models were established by OVA exposure. The findings (Liu Y. et al., 2020) eventually indicated that the intraperitoneal injection of emodin at 20 mg/kg moderated the thickness of ASM in lung tissues and AHR as well. Additionally, the emodin alleviated ASMC proliferation in a dose-dependent manner through blocking the PI3K/Akt pathway *in vivo* and *in vitro*. Similarly, another active constituent from Rheum, chrysophanol, has shown its potential effect on asthma-associated lung inflammation and airway remodeling *in vivo* and *in vitro*. Chrysophanol (Song et al., 2019) can improve the abnormal autophagy in the mice lung induced by OVA and inhibit the proliferation from the cell level via the NF- κ B signaling pathway. Both the anti-autophagy and antiproliferation effects of chrysophanol contribute to ameliorating asthmatic symptoms.

It has been revealed that cryptotanshinone (CTS) extracted from *Salvia miltiorrhiza* Bunge, a well-known Chinese medicine in terms of restoring the stasis of blood in the lung, could exert multiple bioactivities such as protecting LPS-induced lung injury in murine models (Tang et al., 2014). As for asthma, Li J. et al. (2020) found that the administration of CTS successfully alleviates the asthmatic airway inflammation in the way of recovering the secretion balance between Th1 and Th2 cytokines. Wang X. et al. (2019) investigated that CTS not only reduced the accumulation of inflammatory cells and the level of OVA-specific IgE in BALFs but also fulfilled a similar effect as a tumor necrosis factor-like weak inducer of apoptosis (TWEAK) inhibitor, which helps to relieve airway remodeling. Shikonin, a naphthoquinone, is isolated from the roots of *Arnebia euchroma* (Royle ex Benth.) I.M. Johnston, and its prohibitive effect (Wang et al., 2017) on the proliferation and migration of ASMCs was similar to the pyrrolidine dithiocarbamate (PDTTC), an inhibitor of the NF- κ B pathway, which may uncover the potential mechanism of shikonin treating airway inflammation and remodeling in asthma.

At present, aside from the discussed compounds above, there still occur various natural inhibitors from TCM with the potential efficacy against airway inflammation and remodeling in asthma. It is demonstrated in most cases that the active ingredients can markedly suppress the production of the inflammatory cells or cytokines and decreased the thickness of airway walls or smooth muscle, which at least partly makes a contribution to the alleviation of asthmatic inflammation and airway remodeling (e.g., resveratrol, osthole, and imperatorin) (Jiang et al., 2019; Yang Q. et al., 2020; Xian et al., 2020). Additionally, through OVA-induced murine models, Zeng et al. (2019) have justified the protective effect of polydatin (PD) for pulmonary injury in asthma by accelerating Nrf2-mediated antioxidation to recover the EMT progress of lung epithelial cells, in which PD treatment moderated the asthmatic reactive oxygen species (ROS) and airway remodeling. Chen et al. (2021) revealed that Schisandrin B (SB) could effectively block the activation of NLRP3 inflammasome and undermine pyroptosis from the molecular level, thereby improving the symptoms of asthmatic mice. The mechanism of components mentioned above is consulted in Table 3.

Thus, the cores of these *in vivo* and *in vitro* findings are the same, which highlight the potential mechanism of natural compounds

TABLE 3 | The active components from TCM against airway inflammation and remodeling.

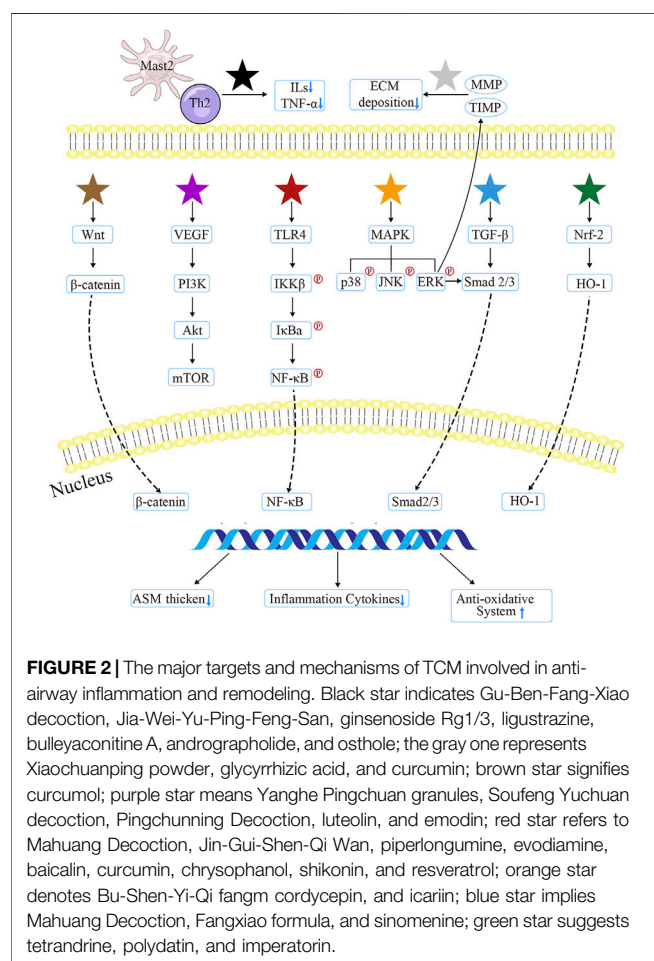
| Species | Components | Origin | Mechanism of action | Pathway | References |
|-------------------|-------------------|---|---|------------------------------------|---|
| Saponins | Glycyrrhizic acid | <i>Glycyrrhiza uralensis</i> Fisch. ex DC. | Exhibit its anti-inflammatory properties; the thickness of ASM↓. Airway walls↓ | TNF/MMP | Yang et al |
| | Cycloastragenol | <i>Astragalus mongholicus</i> Bunge | AHR↓ inflammatory cytokines↓ | Autophagy | Yao et al Zhu et al |
| | Ginsenoside Rg1 | <i>Panax ginseng</i> C.A.Mey | Autophagic flux↓ Autophagy-associated proteins↓ Relieve airway inflammation AHR↓ Th2 activity↓ Inflammatory responses↓ | Th2; TGF-β1/Smad3 | Chen et al Guan et al |
| | Ginsenoside Rg3 | <i>Panax ginseng</i> C.A.Mey | Th2 cytokine↓ Eotaxin expressions↓ | Th2 | Huang et al |
| Alkaloid | Cordycepin | <i>Cordyceps militaris</i> | A _{2A} ARmRNA↑ | TGF-β1/MAPK | Fei et al |
| | Sinomenine | <i>Sinomenium acutum</i> (Thunb.) Rehder & E.H.Wilson | Decrease the synthesis of related cytokines | MMP; TGF-β1/Smad3 | He et al |
| | | | EMT↓ Th2-derived cytokines↓ Apoptosis of airway epithelial cells↓ | | Işık et al |
| | Ligustrazine | <i>Ligusticum striatum</i> DC. | IL-10↑ IL-17↓ | IL | Liu et al |
| | Piperlongumine | <i>Piper longum</i> L | Inhibit TNF-α-induced inflammatory cytokine expression | NF-κB | Lu et al |
| | Matrine | <i>Sophora flavescens</i> Aiton | Neutrophil apoptosis↓ Cell apoptosis↓ | miR-155 | Yu et al.0 Li et al.0 |
| | Oxysophocarpine | <i>Sophora flavescens</i> Aiton | Inflammatory infiltration ↓ | | |
| | Tetrandrine | <i>Stephania tetrandra</i> S. Moore | ASM cells↓ CysLT1↓ CysLTR1↓ | TGF-β1/Nrf-2/HO-1 | Lin et al |
| Ketone | Evodiamine | <i>Tetradium ruticarpum</i> (A.Juss.) T.G.Hartley | Mucus secretion↓ the thickness of airway wall↓ the smooth muscle layers↓ Collagen deposition↓ | HMGB1/NF-κB/TLR-4 | Wang et al |
| | Bulleyaconitine A | <i>Aconitum camichaeli</i> Debeaux | Recover the Th1/Th2 balance | | Liu et al |
| | Icariin | <i>Epimedium brevicornum</i> Maxim | Exert anti-oxidant ability by active endogenous scavenging enzymes; PGD2↓ ASM↓ EMT↓ attenuate the cell proliferation and migration in ASMCs | CRTH2; MAPK/Erk; Smad; NF-κB/STAT3 | Sze et al Qiao et al Hu et al Li et al Tian et al |
| | Curcumin | <i>Curcuma longa</i> L | Regulate inflammatory mediators | MMP-9/TLR-4 | Kumari et al |
| | Baicalin | <i>Scutellaria baicalensis</i> Georgi | Protect lung tissues | HDAC2/NF-κB/PAI-1 | Zhang et al |
| | Curcumin | <i>Scutellaria baicalensis</i> Georgi | Cell's proliferation↓ | NF-κB | Yuan et al |
| | Formononetin | <i>Astragalus mongholicus</i> Bunge | Goblet cell hyperplasia↓ Collagen deposition↓ ROS↓ SOD↑ | | Yi et al |
| | Luteolin | <i>Lonicera japonica</i> Thunb | Autophagy↓ | | |
| Terpene | Andrographolide | <i>Andrographis paniculata</i> (Burm. F.) Nees | Attenuate neutrophil infiltration of lung tissue T17 cells↓ EMT progress↓ | PI3K/Akt/mTOR IL-6/STAT3 | Wang et al Yu et al |
| | Curcumol | <i>Curcuma phaeocaulis</i> Valetton | Obstruct the abnormal signaling Pulmonary fibrosis↓ oxidate stress↓ | Wnt/β-catenin | Xia et al Li et al |
| Anthraquinone | Emodin | <i>Rheum palmatum</i> L. | Inflammatory cytokines↓ The thickness of ASM↓ | Notch; PI3K/Akt | Jia et al Liu et al |
| Phenanthraquinone | Chrysophanol | <i>Rheum palmatum</i> L. | Abnormal autophagy↓ Proliferation↓ | NF-κB | Song et al |
| | Cryptotanshinone | <i>Salvia miltiorrhiza</i> Bunge | Protect lung injury; recover the secretion balance between Th1 and Th2 cytokines; IgE↓ | TWEAK | Tang et al |
| Naphthoquinone | Shikonin | <i>Arnebia euchroma</i> (Royle ex Benth.) I.M.Johnst | The proliferation and migration of ASMCs↓ | NF-κB | Li et al Wang et al Wang et al |
| Polyphenol | Resveratrol | <i>Reynoutria japonica</i> Hoult | Inflammatory cytokines↓ | HMGB1/TLR4/NF-κB | Jiang et al |
| | Polydatin | <i>Reynoutria japonica</i> Hoult | Recover the EMT progress | Nrf2 | Zeng et al |

(Continued on following page)

TABLE 3 | (Continued) The active components from TCM against airway inflammation and remodeling.

| Species | Components | Origin | Mechanism of action | Pathway | References |
|----------|------------------------|---|--|------------------------|--------------------------|
| Coumarin | Osthole Imperatorin | <i>Cnidium monnieri</i> (L.) Cusson <i>Kitagawia praeurptora</i> (Dunn) Pimenov | Restore the release of inflammatory cytokines Inflammatory cytokines↓ | IL-33/ST2 Nrf2/HO-1 | Yang et al Xian et al |
| Lignin | Schisandrin B | <i>Schisandra chinensis</i> (Turcz.) Baill | Pyroptosis↓ | NLRP3 | Chen et al |

↑:increase; ↓:decrease; TNF: tumor necrosis factor; MMP: matrix metalloproteinase; ASM: airway smooth muscle; AHR: airway hyperresponsiveness; TGF- β 1: transforming growth factor- β 1; MAPK: mitogen-activated protein kinase; EMT: Epithelial-Mesenchymal Transition; IL: interleukin; TNF- α : Tumor Necrosis Factor- α ; NF- κ B: nuclear factor kappa-light-chain-enhancer of activated B-cells; CysLTR1: Cysteinyl Leukotriene Receptor 1; Nrf-2/HO-1: Nuclear Transcription Factor 2/Heme Oxygenase 1; HMGB1: High Mobility Group Box 1; TLR-4: Toll-Like Receptor 4; CRTH2: known as prostaglandin D2 receptor 2; STAT3: Signal Transducer And Activator Of Transcription 3; HDAC2: Histone Deacetylase 2; ROS: reactive oxygen species; SOD: superoxide dismutase; PI3K: phosphatidylinositol-4, 5-bisphosphate 3-kinase; TWEAK: tumor necrosis factor-like weak inducer of apoptosis; NLRP3: NLR, Family Pyrin Domain Containing 3.



inhibiting airway inflammation as well as remodeling, and preferring novel insights for the treatment of asthma.

CONCLUSION AND OUTLOOK

Presently, bronchial inflammation and airway remodeling as the common pathologic basis shared by asthma have severely threatened the prognosis and life quality of chronic patients.

Specifically, small airway dysfunction including inflammatory cell infiltration and airway structural alteration is still the major difficulty in the treatment of asthmatic symptoms and depression of lung function. Current anti-asthma therapies consisting of ICS with LABA and updated monoclonal antibodies can only manage symptoms but do not alter sensitization or stabilize the milieu interne. However, as one of the major alternative and complementary medicines worldwide, TCM has multiple unique advantages against asthmatic inflammation and airway remodeling in clinic based on the *in vivo* and *in vitro* evidence.

After thoroughly reviewing these evidence, the major targets and pathways that formulae, herbs and natural compounds from TCM suppressing airway alterations can be classified into several types: Mast 2/Th2 cell type (e.g., BSYQF, ligustrazine, etc.) can alter the M2/Th2 activation state, thereby downregulating the cytokines' level; MMP/TIMP type (e.g., XP, glycyrrhizic acid, etc.) may reduce EMT deposition by regulating MMP or TIMP; Wnt/ β -catenin type (e.g., curcumol, etc.) would obstruct abnormal signaling pathway in order to alleviate pulmonary symptoms; VEGF/PI3K type (e.g., YPG, emodin, etc.) depresses inflammatory cytokines through blocking VEGF or PI3K pathways; TLR/NF- κ B type (e.g., JGSQW, evodiamine, etc.) may involve the most anti-inflammatory natural compounds that restore mucus secretion; MAPK type (e.g., BSYQF, icariin, etc.) could exert an anti-remodeling ability, which was also associated with EMT; TGF- β 1 type (e.g., CMD, sinomenine, etc.) inhibits the thickness of ASM and airway walls; and Nrf2/HO-1 type (e.g., tetrandrine, imperatorin, etc.) mainly improves the oxidative effects. The detailed mechanisms of TCM are consulted in **Figure 2**.

Above all, the mechanisms of how TCM alleviates bronchial inflammation and airway remodeling include but are not limited to blocking the activation of inflammatory cells, regulating various immune cytokines' level, reducing ECM progress in lung tissues, and AHR among big or small airways through different signaling pathways. From the molecular level, autophagy, as the core progress of cell self-renewal, has received increasing attention to participate in the regulation of several major human disorders (Klionsky et al., 2021) including diabetes, cancer, and pulmonary disorders. Accumulating

evidence suggest that autophagy activators from TCM (e.g., formula and bioactive extracts) are potential therapeutical candidates and promising strategies for asthmatic inflammation and airway remodeling treatment. Related research (Lambrecht and Hammad, 2012) has justified that the stress responses of airway epithelial cells are a major culprit in asthma and proved the benefit in the modulation of cytokines. Given the critical target cytokines that TCM altered mostly involved in the epithelium network, systematic TCM treatment may restore the innate epithelial response therapy to prevent airway remodeling and asthma exacerbations.

Although we have found that various decoctions, natural compounds, and extracts from TCM displayed anti-inflammation and anti-airway remodeling effects in different murine models, we are still far away from translating these TCM approaches into broad clinical applications for patients suffering from vital asthma. At present, the establishment of asthmatic animal models was normally induced by allergic factors such as OVA but not available for non-allergic factors, which also generate a wide range of airway inflammation and tissue structural changes (Fang et al., 2020). The property of asthma types should be taken into account, or which may weaken the efficacy of TCM in clinical application. Moreover, the above findings were mostly derived from *in vivo* or *in vitro* experiments, and the current clinical studies cannot provide valid support for the conclusion. Thus, not only large-scale randomized controlled tests or retrospective cohort studies but the deeper

pharmacological and theoretical research on TCM should be carried out to verify its safety, efficacy, and exact mechanisms in the future.

In conclusion, though there are still some issues that need to find the solution, it is still demonstrated from enumerated research that TCM has wide potential application and promising effect in managing small airway dysfunction in asthma. We believe that with further investigation focusing on Chinese traditional herbs and formulas, TCM will definitely offer more Eastern wisdom to cure human disorders.

AUTHOR CONTRIBUTIONS

BZ analyzed the data, wrote, edited, and revised the article; and X-J and H-L revised the article and participated in the preparation of the review. All the authors read carefully and participated in the article, contributing to the improvement of language and grammar.

FUNDING

The authors sincerely thank the National Natural Science Foundation of China (81804034) and the Natural Foundation of Shandong Province (Grants nos. ZR2020MH353) for their support.

REFERENCES

- Aghasafari, P., George, U., and Pidaparti, R. (2019). A Review of Inflammatory Mechanism in Airway Diseases. *Inflamm. Res.* 68 (1), 59–74. doi:10.1007/s00011-018-1191-2
- Barnes, P. J. (2017). Cellular and Molecular Mechanisms of Asthma and COPD. *Clin. Sci. (Lond)* 131 (13), 1541–1558. doi:10.1042/CS20160487
- Bergeron, C., and Boulet, L. P. (2006). Structural Changes in Airway Diseases: Characteristics, Mechanisms, Consequences, and Pharmacologic Modulation. *Chest* 129 (4), 1068–1087. doi:10.1378/chest.129.4.1068
- Bi, J., Jiang, B., Liu, J. H., Lei, C., Zhang, X. L., and An, L. J. (2008). Protective Effects of Catalpol against H₂O₂-Induced Oxidative Stress in Astrocytes Primary Cultures. *Neurosci. Lett.* 442 (3), 224–227. doi:10.1016/j.neulet.2008.07.029
- Bortolozzo, A. S. S., Rodrigues, A. P. D., Arantes-Costa, F. M., Saraiva-Romanholo, B. M., de Souza, F. C. R., Brüggemann, T. R., et al. (2018). The Plant Proteinase Inhibitor CrataBL Plays a Role in Controlling Asthma Response in Mice. *Biomed. Res. Int.* 2018, 9274817. doi:10.1155/2018/9274817
- Carr, T. F., Zeki, A. A., and Kraft, M. (2018). Eosinophilic and Noneosinophilic Asthma. *Am. J. Respir. Crit. Care Med.* 197, 22–37. doi:10.1164/rccm.201611-2232PP
- Chan, H. H. L., and Ng, T. (2020). Traditional Chinese Medicine (TCM) and Allergic Diseases. *Curr. Allergy Asthma Rep.* 20 (11), 67. doi:10.1007/s11882-020-00959-9
- Chen, T., Xiao, L., Zhu, L., Ma, S., Yan, T., and Ji, H. (2015). Anti-Asthmatic Effects of Ginsenoside Rb1 in a Mouse Model of Allergic Asthma through Relegating Th1/Th2. *Inflammation* 38 (5), 1814–1822. doi:10.1007/s10753-015-0159-4
- Chen, X., Xiao, Z., Jiang, Z., Jiang, Y., Li, W., and Wang, M. (2021). Schisandrin B Attenuates Airway Inflammation and Airway Remodeling in Asthma by Inhibiting NLRP3 Inflammasome Activation and Reducing Pyroptosis. *Inflammation* 44 (6), 2217–2231. doi:10.1007/s10753-021-01494-z
- Cheng, B. H., Hu, T. Y., Mo, L. H., Ma, L., Hu, W. H., Li, Y. S., et al. (2019). Yan-Hou-Qing Formula Attenuates Allergic Airway Inflammation via Up-Regulation of Treg and Suppressing Th2 Responses in Ovalbumin-Induced
- Asthmatic Mice. *J. Ethnopharmacol.* 231, 275–282. doi:10.1016/j.jep.2018.11.038
- Chiou, W. F., Lin, L. C., and Chen, C. F. (2004). Acteoside Protects Endothelial Cells against Free Radical-Induced Oxidative Stress. *J. Pharm. Pharmacol.* 56 (6), 743–748. doi:10.1211/0022357023501
- Chiou, Y. L., and Lin, C. Y. (2012). The Extract of Cordyceps Sinensis Inhibited Airway Inflammation by Blocking NF-Kb Activity. *Inflammation* 35 (3), 985–993. doi:10.1007/s10753-011-9402-9
- Choi, G. E., Yoon, S. Y., Kim, J. Y., Kang, D. Y., Jang, Y. J., and Kim, H. S. (2018). Autophagy Deficiency in Myeloid Cells Exacerbates Eosinophilic Inflammation in Chronic Rhinosinusitis. *J. Allergy Clin. Immunol.* 141 (3), 938–e12. doi:10.1016/j.jaci.2017.10.038
- Costello, R. W., and Cushen, B. (2020). Looking Back to Go Forward: Adherence to Inhaled Therapy before Biologic Therapy in Severe Asthma. *Eur. Respir. J.* 55 (5), 2000954. doi:10.1183/13993003.00954-2020
- Cui, J., Lv, Z., Teng, F., Yi, L., Tang, W., Wang, W., et al. (2021). RNA-seq Expression Analysis of Chronic Asthmatic Mice with Bu-Shen-Yi-Qi Formula Treatment and Prediction of Regulated Gene Targets of Anti-airway Remodeling. *Evid. Based Complement. Altern. Med.* 2021, 3524571. doi:10.1155/2021/3524571
- Cui, J., Xu, F., Tang, Z., Wang, W., Hu, L. L., Yan, C., et al. (2019). Bu-Shen-Yi-Qi Formula Ameliorates Airway Remodeling in Murine Chronic Asthma by Modulating Airway Inflammation and Oxidative Stress in the Lung. *Biomed. Pharmacother.* 112, 108694. doi:10.1016/j.biopha.2019.108694
- Dickinson, J. D., Alevy, Y., Malvin, N. P., Patel, K. K., Gunsten, S. P., Holtzman, M. J., et al. (2016). IL13 Activates Autophagy to Regulate Secretion in Airway Epithelial Cells. *Autophagy* 12 (2), 397–409. doi:10.1080/15548627.2015.1056967
- Fang, L., Sun, Q., and Roth, M. (2020). Immunologic and Non-immunologic Mechanisms Leading to Airway Remodeling in Asthma. *Int. J. Mol. Sci.* 21 (3), 757. doi:10.3390/ijms21030757
- Fei, X., Zhang, X., Zhang, G. Q., Bao, W. P., Zhang, Y. Y., Zhang, M., et al. (2017). Cordycepin Inhibits Airway Remodeling in a Rat Model of Chronic Asthma. *Biomed. Pharmacother.* 88, 335–341. doi:10.1016/j.biopha.2017.01.025

- Feng, L., Lin, L., Wang, S., Zhao, X., Dai, Q., Wang, L., et al. (2021). Clinical Practice Guidelines for the Treatment of Allergic Rhinitis in Children with Traditional Chinese Medicine. *Anat. Rec. Hob.* 304 (11), 2592–2604. doi:10.1002/ar.24718
- Ge, Y., Cheng, R., Sun, S., Zhang, S., Li, L., Jiang, J., et al. (2019). Fangxiao Formula Alleviates Airway Inflammation and Remodeling in Rats with Asthma via Suppression of Transforming Growth Factor- β /Smad3 Signaling Pathway. *Biomed. Pharmacother.* 119, 109429. doi:10.1016/j.biopha.2019.109429
- Geng, Y., Wang, W., Zhang, J., Bi, S., Li, H., and Lin, M. (2016). Effects of Traditional Chinese Medicine Herbs for Tonifying Qi and Kidney, and Replenishing Spleen on Intermittent Asthma in Children Aged 2 to 5 Years Old. *J. Tradit. Chin. Med.* 36 (1), 32–38. doi:10.1016/s0254-6272(16)30005-x
- Grainge, C., and Park, J. A. (2018). Inflammatory Insights into Airway Remodelling in Asthma. *Respirology* 23 (12), 1084–1085. doi:10.1111/resp.13390
- Guan, S., Yu, P., Cao, J., Xi, X., Zhang, Q., Zhu, C., et al. (2020). Ginsenoside Rg1 Protects against Cigarette Smoke-Induced Airway Remodeling by Suppressing the TGF- β /Smad3 Signaling Pathway. *Am. J. Transl. Res.* 12 (2), 493–506.
- Guida, G., and Riccio, A. M. (2019). Immune Induction of Airway Remodeling. *Semin. Immunol.* 46, 101346. doi:10.1016/j.smim.2019.101346
- He, H., Cao, L., Wang, Z., Wang, Z., Miao, J., Li, X.-M., et al. (2021). Sinomenine Relieves Airway Remodeling by Inhibiting Epithelial-Mesenchymal Transition through Downregulating TGF- β 1 and Smad3 Expression *In Vitro* and *In Vivo*. *Front. Immunol.* 12, 736479. doi:10.3389/fimmu.2021.736479
- He, Y., Gai, Y., Wu, X., and Wan, H. (2012). Quantitatively Analyze Composition Principle of Ma Huang Tang by Structural Equation Modeling. *J. Ethnopharmacol.* 143 (3), 851–858. doi:10.1016/j.jep.2012.08.010
- He, Y., Lou, X., Jin, Z., Yu, L., Deng, L., and Wan, H. (2018). Mahuang Decoction Mitigates Airway Inflammation and Regulates IL-21/STAT3 Signaling Pathway in Rat Asthma Model. *J. Ethnopharmacol.* 224, 373–380. doi:10.1016/j.jep.2018.06.011
- Hu, L., Li, L., Zhang, H., Li, Q., Jiang, S., Qiu, J., et al. (2019). Inhibition of Airway Remodeling and Inflammatory Response by Icarin in Asthma. *BMC Complement. Altern. Med.* 19 (1), 316. doi:10.1186/s12906-019-2743-x
- Hu, L., Song, X., Nagai, T., Yamamoto, M., Dai, Y., He, L., et al. (2021). Chemical Profile of Cimicifuga Heraclefolia Kom. And Immunomodulatory Effect of its Representative Bioavailable Component, Cimigenoside on Poly(I:C)-induced Airway Inflammation. *J. Ethnopharmacol.* 267, 113615. doi:10.1016/j.jep.2020.113615
- Hu, Z., Liu, X., and Yang, M. (2021). Evidence and Potential Mechanisms of Jin-Gui Shen-Qi Wan as a Treatment for Type 2 Diabetes Mellitus: A Systematic Review and Meta-Analysis. *Front. Pharmacol.* 12, 699932. doi:10.3389/fphar.2021.699932
- Hua, S., Liu, F., and Wang, M. (2019). Emodin Alleviates the Airway Inflammation of Cough Variant Asthma in Mice by Regulating the Notch Pathway. *Med. Sci. Monit.* 25, 5621–5629. doi:10.12659/MSM.915080
- Huang, M., Wu, J., and Dong, J. (2021). Modified BuShenYiQi Formula Alleviates Experimental Allergic Asthma in Mice by Negative Regulation of Type 2 Innate Lymphoid Cells and CD4+ Type 9 Helper T Cells and the VIP-VPAC2 Signalling Pathway. *Pharm. Biol.* 59 (1), 1216–1232. doi:10.1080/13880209.2021.1970198
- Huang, P., Tang, Y., Li, C., Zhou, H., Yu, L., Wan, H., et al. (2020). Correlation Study between the Pharmacokinetics of Seven Main Active Ingredients of Mahuang Decoction and its Pharmacodynamics in Asthmatic Rats. *J. Pharm. Biomed. Anal.* 183, 113144. doi:10.1016/j.jpba.2020.113144
- Huang, W. C., Huang, T. H., Yeh, K. W., Chen, Y. L., Shen, S. C., and Liou, C. J. (2021). Ginsenoside Rg3 Ameliorates Allergic Airway Inflammation and Oxidative Stress in Mice. *J. Ginseng Res.* 45 (6), 654–664. doi:10.1016/j.jgr.2021.03.002
- Huang, Z., Gao, L., Zhao, X., Ling, H., and Chen, W. (2016). Effect of Gubenfangxiao Decoction on Respiratory Syncytial Virus-Induced Asthma and Expression of Asthma Susceptibility Gene Orosomucoid 1-like Protein 3 in Mice. *J. Tradit. Chin. Med.* 36 (1), 101–106. doi:10.1016/s0254-6272(16)30015-2
- İşık, S., Karaman, M., Micili, S. Ç., Çağlayan-Sözmen, Ş., Bağryanık, H. A., Arıkan-Ayyıldız, Z., et al. (2018). Sinomenine Ameliorates the Airway Remodelling, Apoptosis of Airway Epithelial Cells, and Th2 Immune Response in a Murine Model of Chronic Asthma. *Allergol. Immunopathol. Madr.* 46 (1), 67–75. doi:10.1016/j.aller.2017.05.004
- Ito, J. T., Lourenço, J. D., Righetti, R. F., Tibério, I. F. L. C., Prado, C. M., and Lopes, F. D. T. Q. S. (2019). Extracellular Matrix Component Remodeling in Respiratory Diseases: What Has Been Found in Clinical and Experimental Studies? *Cells* 8 (4), 342. doi:10.3390/cells8040342
- Ji, B., Li, Y. Y., Yang, W. J., Zhang, L. Z., Fang, M. S., Fu, H. Y., et al. (2018). Jinkui Shenqi Pills Ameliorate Asthma with "Kidney Yang Deficiency" by Enhancing the Function of the Hypothalamic-Pituitary-Adrenal Axis to Regulate T Helper 1/2 Imbalance. *Evid. Based Complement. Altern. Med.* 2018, 7253240. doi:10.1155/2018/7253240
- Jia, S., Guo, P., Lu, J., Huang, X., Deng, L., Jin, Y., et al. (2021). Curcumin Ameliorates Lung Inflammation and Airway Remodeling via Inhibiting the Abnormal Activation of the Wnt/ β -Catenin Pathway in Chronic Asthmatic Mice. *Drug Des. Devel. Ther.* 15, 2641–2651. doi:10.2147/DDDT.S292642
- Jiang, H., Duan, J., Xu, K., and Zhang, W. (2019). Resveratrol Protects against Asthma-Induced Airway Inflammation and Remodeling by Inhibiting the HMGB1/TLR4/NF- κ B Pathway. *Exp. Ther. Med.* 18 (1), 459–466. doi:10.3892/etm.2019.7594
- Jiao, J., Wu, J., Wang, J., Guo, Y., Gao, L., Liang, H., et al. (2018). Ma Huang Tang Ameliorates Bronchial Asthma Symptoms through the TLR9 Pathway. *Pharm. Biol.* 56 (1), 580–593. doi:10.1080/13880209.2018.1517184
- Jin, H., Cai, C., Li, B., Jin, W., Xia, J., Wang, L., et al. (2019). Modified Si-Jun-Zi-Tang Attenuates Airway Inflammation in a Murine Model of Chronic Asthma by Inhibiting Teff Cells via the mTORC1 Pathway. *Front. Pharmacol.* 10, 161. doi:10.3389/fphar.2019.00161
- Jing, X., Yan, W., Zeng, H., and Cheng, W. (2020). Qingfei Oral Liquid Alleviates Airway Hyperresponsiveness and Mucus Hypersecretion via TRPV1 Signaling in RSV-Infected Asthmatic Mice. *Biomed. Pharmacother.* 128, 110340. doi:10.1016/j.biopha.2020.110340
- Joan, O., Hueber, A., Feller, F., Jirmo, A. C., Lochner, M., Dittrich, A. M., et al. (2017). Suppression of Th17-Polarized Airway Inflammation by Rapamycin. *Sci. Rep.* 7 (1), 15336. doi:10.1038/s41598-017-15750-6
- Kaczmarek, K. A., Clifford, R. L., and Knox, A. J. (2019). Epigenetic Changes in Airway Smooth Muscle as a Driver of Airway Inflammation and Remodeling in Asthma. *Chest* 155 (4), 816–824. doi:10.1016/j.chest.2018.10.038
- Kao, S. T., Wang, S. D., Lin, C. C., and Lin, L. J. (2018). Jin Gui Shen Qi Wan, a Traditional Chinese Medicine, Alleviated Allergic Airway Hypersensitivity and Inflammatory Cell Infiltration in a Chronic Asthma Mouse Model. *J. Ethnopharmacol.* 227, 181–190. doi:10.1016/j.jep.2018.08.028
- Kim, J. H. (2018). Pharmacological and Medical Applications of Panax Ginseng and Ginsenosides: a Review for Use in Cardiovascular Diseases. *J. Ginseng Res.* 42 (3), 264–269. doi:10.1016/j.jgr.2017.10.004
- Kim, J. S., Kang, J. Y., Ha, J. H., Lee, H. Y., Kim, S. J., Kim, S. C., et al. (2013). Expression of Nerve Growth Factor and Matrix Metalloproteinase-9/tissue Inhibitor of Metalloproteinase-1 in Asthmatic Patients. *J. Asthma* 50 (7), 712–717. doi:10.3109/02770903.2013.808664
- Kleniewska, P., and Pawliczak, R. (2017). The Participation of Oxidative Stress in the Pathogenesis of Bronchial Asthma. *Biomed. Pharmacother.* 94, 100–108. doi:10.1016/j.biopha.2017.07.066
- Klionsky, D. J., Petroni, G., Amaravadi, R. K., Baehrecke, E. H., Ballabio, A., Boya, P., et al. (2021). Autophagy in Major Human Diseases. *EMBO J.* 40 (19), e108863. doi:10.15252/embj.2021108863
- Kumari, A., Singh, D. K., Dash, D., and Singh, R. (2019). Intranasal Curcumin Protects against LPS-Induced Airway Remodeling by Modulating Toll-like Receptor-4 (TLR-4) and Matrixmetalloproteinase-9 (MMP-9) Expression via Affecting MAP Kinases in Mouse Model. *Inflammopharmacology* 27 (4), 731–748. doi:10.1007/s10787-018-0544-3
- Lambrecht, B. N., and Hammad, H. (2012). The Airway Epithelium in Asthma. *Nat. Med.* 18 (5), 684–692. doi:10.1038/nm.2737
- Li, G., Lin, J., and Peng, Y. (2020). Curcumin May Reverse Early and Advanced Liver Fibrogenesis through Downregulating the uPA/uPAR Pathway. *Phytother. Res.* 34 (6), 1421–1435. doi:10.1002/ptr.6616
- Li, J., Zheng, M., Wang, C., Jiang, J., Xu, C., Li, L., et al. (2020). Cryptotanshinone Attenuates Allergic Airway Inflammation through Negative Regulation of NF- κ B and P38 MAPK. *Biosci. Biotechnol. Biochem.* 84 (2), 268–278. doi:10.1080/09168451.2019.1687280
- Li, L., Shi, R., Shi, W., Zhang, R., and Wu, L. (2020). Oxyphocarpine Protects Airway Epithelial Cells against Inflammation and Apoptosis by Inhibiting miR-155 Expression. *Future Med. Chem.* 12 (16), 1475–1487. doi:10.4155/fmc-2020-0120

- Li, Z., Yuan, X., Wang, B., and Gao, F. (2020). Icariin Alleviates Transforming Growth Factor- β 1-Induced Epithelial-Mesenchymal Transition by Targeting Smad and MAPK Signaling Pathways. *Am. J. Transl. Res.* 12 (2), 343–360.
- Liang, Z. Q., Tu, P. C., Ji, J. J., Xing, Q. Q., and Zhao, X. (2020). Gu-Ben-Fang-Xiao Attenuates Allergic Airway Inflammation by Inhibiting BAFF-Mediated B Cell Activation. *Biomed. Pharmacother.* 132, 110801. doi:10.1016/j.biopha.2020.110801
- Lim, J. O., Song, K. H., Lee, I. S., Lee, S. J., Kim, W. I., Pak, S. W., et al. (2021). Cimicifugae Rhizoma Extract Attenuates Oxidative Stress and Airway Inflammation via the Upregulation of Nrf2/HO-1/NQO1 and Downregulation of NF-Kb Phosphorylation in Ovalbumin-Induced Asthma. *Antioxidants (Basel)* 10 (10), 1626. doi:10.3390/antiox10101626
- Lin, Y., Yao, J., Wu, M., Ying, X., Ding, M., Wei, Y., et al. (2019). Tetrandrine Ameliorates Airway Remodeling of Chronic Asthma by Interfering TGF- β 1/Nrf-2/ho-1 Signaling Pathway-Mediated Oxidative Stress. *Can. Respir. J.* 2019, 7930396. doi:10.1155/2019/7930396
- Liu, J. X., Zhang, Y., Yuan, H. Y., and Liang, J. (2021). The Treatment of Asthma Using the Chinese Materia Medica. *J. Ethnopharmacol.* 269, 113558. doi:10.1016/j.jep.2020.113558
- Liu, L. W., Xing, Q. Q., Zhao, X., Tan, M., Lu, Y., Dong, Y. M., et al. (2019). Proteomic Analysis Provides Insights into the Therapeutic Effect of GU-BEN-FANG-XIAO Decoction on a Persistent Asthmatic Mouse Model. *Front. Pharmacol.* 10, 441. doi:10.3389/fphar.2019.00441
- Liu, L., Wang, S., Xing, H., Sun, Y., Ding, J., and He, N. (2020). Bulleyaconitine A Inhibits the Lung Inflammation and Airway Remodeling through Restoring Th1/Th2 Balance in Asthmatic Model Mice. *Biosci. Biotechnol. Biochem.* 84 (7), 1409–1417. doi:10.1080/09168451.2020.1752140
- Liu, X. M., Wang, Y. B., Wu, Q., Bian, Z. R., and Che, X. W. (2018). Effects of Ligustrazine on Airway Inflammation in A Mouse Model of Neutrophilic Asthma. *Chin. J. Integr. Med.* 24 (5), 353–358. doi:10.1007/s11655-017-2830-0
- Liu, Y., Li, X., He, C., Chen, R., Wei, L., Meng, L., et al. (2020). Emodin Ameliorates Ovalbumin-Induced Airway Remodeling in Mice by Suppressing Airway Smooth Muscle Cells Proliferation. *Int. Immunopharmacol.* 88, 106855. doi:10.1016/j.intimp.2020.106855
- Lu, C., Zhang, B., Xu, T., Zhang, W., Bai, B., Xiao, Z., et al. (2019). Piperlongumine Reduces Ovalbumin-Induced Asthma and Airway Inflammation by Regulating Nuclear Factor-Kb Activation. *Int. J. Mol. Med.* 44 (5), 1855–1865. doi:10.3892/ijmm.2019.4322
- Lu, Y., Xu, J. Y., Zhang, X. H., and Zhao, X. (2016). Gu-Ben-Fang-Xiao Decoction Attenuates Sustained Airway Inflammation by Suppressing ER Stress Response in a Murine Asthma Remission Model of Respiratory Syncytial Virus Infection. *J. Ethnopharmacol.* 192, 496–509. doi:10.1016/j.jep.2016.09.039
- Luo, J., Zhang, L., Zhang, X., Long, Y., Zou, F., Yan, C., et al. (2019). Protective Effects and Active Ingredients of Salvia Miltiorrhiza Bunge Extracts on Airway Responsiveness, Inflammation and Remodeling in Mice with Ovalbumin-Induced Allergic Asthma. *Phytomedicine* 52, 168–177. doi:10.1016/j.phymed.2018.09.170
- McAlinden, K. D., Deshpande, D. A., Ghavami, S., Xenaki, D., Sohal, S. S., Oliver, B. G., et al. (2019). Autophagy Activation in Asthma Airways Remodeling. *Am. J. Respir. Cell. Mol. Biol.* 60 (5), 541–553. doi:10.1165/rcmb.2018-0169OC
- Niu, X., Qin, R., Zhao, Y., Han, L., Lu, J., and Lv, C. (2019). Simultaneous Determination of 19 Constituents in Cimicifugae Rhizoma by HPLC-DAD and Screening for Antioxidants through DPPH Free Radical Scavenging Assay. *Biomed. Chromatogr.* 33 (10), e4624. doi:10.1002/bmc.4624
- Ornatowski, W., Lu, Q., Yegambaram, M., Garcia, A. E., Zemskov, E. A., Maltepe, E., et al. (2020). Complex Interplay between Autophagy and Oxidative Stress in the Development of Pulmonary Disease. *Redox Biol.* 36, 101679. doi:10.1016/j.redox.2020.101679
- Ou Yang, B., and Gu, Z. (1996). *Essentials of Traditional Chinese Medicine*. Jinan, Shandong, China: Shandong Science and Technology Press.
- Pan, L. Y., Han, Y. Q., Wang, Y. Z., Chen, Q. Q., Wu, Y., and Sun, Y. (2018). Mechanism of Yanghe Pingchuan Granules Treatment for Airway Remodeling in Asthma. *Drug Des. Devel Ther.* 2712, 1941–1951. doi:10.2147/DDDT.S159428
- Pang, Q. Q., Li, T., Liu, L. X., Shi, D. F., Yao, X. S., Li, H. B., et al. (2021). Systematically Identifying the Anti-inflammatory Constituents of Cimicifuga Dahurica by UPLC-Q/TOF-MS Combined with Network Pharmacology Analysis. *Biomed. Chromatogr.* 35 (12), e5177. doi:10.1002/bmc.5177
- Postma, D. S., Brightling, C., Baldi, S., Van den Berge, M., Fabbri, L. M., Gagnatelli, A., et al. (2019). Exploring the Relevance and Extent of Small Airways Dysfunction in Asthma (ATLANTIS): Baseline Data from a Prospective Cohort Study. *Lancet Respir. Med.* 7, 402–416. doi:10.1016/S2213-2600(19)30049-9
- Qiao, J., Sun, S., Yuan, L., and Wang, J. (2017). Effects of Icariin on Asthma Mouse Model Are Associated with Regulation of Prostaglandin D2 Level. *Allergol. Immunopathol. Madr.* 45 (6), 567–572. doi:10.1016/j.aller.2017.02.007
- Righetti, R. F., Pigati, P. A., Possa, S. S., Habrum, F. C., Xisto, D. G., Antunes, M. A., et al. (2014). Effects of Rho-Kinase Inhibition in Lung Tissue with Chronic Inflammation. *Respir. Physiol. Neurobiol.* 192, 134–146. doi:10.1016/j.resp.2013.12.012
- Sahiner, U. M., Birben, E., Erzurum, S., Sackesen, C., and Kalayci, Ö. (2018). Oxidative Stress in Asthma: Part of the Puzzle. *Pediatr. Allergy Immunol.* 29 (8), 789–800. doi:10.1111/pai.12965
- Saito, A., Horie, M., and Nagase, T. (2018). TGF- β Signaling in Lung Health and Disease. *Int. J. Mol. Sci.* 19 (8), 2460. doi:10.3390/ijms19082460
- Song, G., Zhang, Y., Yu, S., Lv, W., Guan, Z., Sun, M., et al. (2019). Chrysophanol Attenuates Airway Inflammation and Remodeling through Nuclear Factor-Kappa B Signaling Pathway in Asthma. *Phytother. Res.* 33 (10), 2702–2713. doi:10.1002/ptr.6444
- Song, P., Zeng, L., Liang, Z., Wang, Q., and Ou, A. (2016). Clinical Efficacy and Safety of Chinese Herbal Medicine Auxiliary Therapy for Childhood Cough Variant Asthma: a Systematic Review and Meta-Analysis of 20 Randomized Controlled Trials. *Intern Med.* 55 (16), 2135–2143. doi:10.2169/internalmedicine.55.5546
- Suk, W. A., Ahanchian, H., Asante, K. A., Carpenter, D. O., Diaz-Barriga, F., Ha, E. A., et al. (2016). Environmental Pollution: An Under-recognized Threat to Children's Health, Especially in Low- and Middle-Income Countries. *Environ. Health Perspect.* 124 (3), A41–A45. doi:10.1289/ehp.1510517
- Sung, J. E., Lee, H. A., Kim, J. E., Yun, W. B., An, B. S., Yang, S. Y., et al. (2017). Saponin-enriched Extract of Asparagus Cochinchinensis Alleviates Airway Inflammation and Remodeling in Ovalbumin-Induced Asthma Model. *Int. J. Mol. Med.* 40 (5), 1365–1376. doi:10.3892/ijmm.2017.3147
- Sze, S. C., Tong, Y., Ng, T. B., Cheng, C. L., and Cheung, H. P. (2010). Herba Epimedii: Anti-oxidative Properties and its Medical Implications. *Molecules* 15 (11), 7861–7870. doi:10.3390/molecules15117861
- Tan, L., Song, X., Ren, Y., Wang, M., Guo, C., Guo, D., et al. (2020). Anti-inflammatory Effects of Cordycepin: A Review. *Phytother. Res.* 8. doi:10.1002/ptr.6890
- Tang, Y., Chen, Y., Chu, Z., Yan, B., and Xu, L. (2014). Protective Effect of Cryptotanshinone on Lipopolysaccharide-Induced Acute Lung Injury in Mice. *Eur. J. Pharmacol.* 723, 494–500. doi:10.1016/j.ejphar.2013.10.019
- Theofani, E., and Xanthou, G. (2021). Autophagy: A Friend or Foe in Allergic Asthma? *Int. J. Mol. Sci.* 22 (12), 6314. doi:10.3390/ijms22126314
- Tian, C., Gao, F., Li, X., and Li, Z. (2020). Icariside II Attenuates Eosinophils-Induced Airway Inflammation and Remodeling via Inactivation of NF-Kb and STAT3 in an Asthma Mouse Model. *Exp. Mol. Pathol.* 113, 104373. doi:10.1016/j.yexmp.2020.104373
- Tripathi, P., and Aggarwal, A. (2006). NF-kB Transcription Factor: a Key Player in the Generation of Immune Response. *Curr. Sci. Bangalore* 90 (4), 519.
- van den Bosch, W. B., James, A. L., and Tiddens, H. A. W. M. (2021). Structure and Function of Small Airways in Asthma Patients Revisited. *Eur. Respir. Rev.* 30 (159), 200186. doi:10.1183/16000617.0186-2020
- Wang, C., Choi, Y. H., Xian, Z., Zheng, M., Piao, H., and Yan, G. (2018). Alopentine Suppresses Allergic Airway Inflammation through NF-Kb, MAPK, and Nrf2/HO-1 Signaling Pathways in Mice. *Int. Immunopharmacol.* 65, 571–579. doi:10.1016/j.intimp.2018.11.003
- Wang, C., Zheng, M., Choi, Y., Jiang, J., Li, L., Li, J., et al. (2019). Cryptotanshinone Attenuates Airway Remodeling by Inhibiting Crosstalk between Tumor Necrosis Factor-like Weak Inducer of Apoptosis and Transforming Growth Factor Beta 1 Signaling Pathways in Asthma. *Front. Pharmacol.* 10, 1338. doi:10.3389/fphar.2019.01338
- Wang, J., Li, T., Cai, H., Jin, L., Li, R., Shan, L., et al. (2021). Protective Effects of Total Flavonoids from Qu Zhi Qiao (Fruit of Citrus Paradisi Cv. Changshanhuoyou) on OVA-Induced Allergic Airway Inflammation and Remodeling through MAPKs and Smad2/3 Signaling Pathway. *Biomed. Pharmacother.* 138, 111421. doi:10.1016/j.biopha.2021.111421
- Wang, K. C. W., Le Cras, T. D., Larcombe, A. N., Zosky, G. R., Elliot, J. G., James, A. L., et al. (2018). Independent and Combined Effects of Airway Remodelling and

- Allergy on Airway Responsiveness. *Clin. Sci. (Lond)* 132 (3), 327–338. doi:10.1042/CS20171386
- Wang, N., Li, J., Huang, X., Chen, W., and Chen, Y. (2016). Herbal Medicine Cordyceps Sinensis Improves Health-Related Quality of Life in Moderate-To-Severe Asthma. *Evid. Based Complement. Altern. Med.* 2016, 6134593. doi:10.1155/2016/6134593
- Wang, Q., Cui, Y., Wu, X., and Wang, J. (2021). Evodiamine Protects against Airway Remodelling and Inflammation in Asthmatic Rats by Modulating the HMGB1/NF-K β /I κ B Signaling Pathway. *Pharm. Biol.* 59 (1), 192–199. doi:10.1080/13880209.2020.1871374
- Wang, S. S., Wang, X. Y., Hui, C., and Zhou, J. (2014). Clinical Observation on Integration of Traditional Chinese and Western Medicine Treating 360 Cases of Acute Exacerbation of Asthma. *World Chin. Med. [shi jie zhong yi yao]* 9 (9), 1186–1189.
- Wang, S., Wuniquiemu, T., Tang, W., Teng, F., Bian, Q., Yi, L., et al. (2021). Luteolin Inhibits Autophagy in Allergic Asthma by Activating PI3K/Akt/mTOR Signaling and Inhibiting Beclin-1-Pi3kc3 Complex. *Int. Immunopharmacol.* 94, 107460. doi:10.1016/j.intimp.2021.107460
- Wang, T. Y., Zhou, Q. L., Li, M., and Shang, Y. X. (2017). Shikonin Alleviates Allergic Airway Remodeling by Inhibiting the ERK-NF-K β Signaling Pathway. *Int. Immunopharmacol.* 48, 169–179. doi:10.1016/j.intimp.2017.05.011
- Wang, W., Yao, Q., Teng, F., Cui, J., Dong, J., and Wei, Y. (2021). Active Ingredients from Chinese Medicine Plants as Therapeutic Strategies for Asthma: Overview and Challenges. *Biomed. Pharmacother.* 137, 111383. doi:10.1016/j.biopha.2021.111383
- Wang, X., Gao, Y., Yang, Q., Fang, X., and Li, Z. (2019). Pingchuanning Decoction Attenuates Airway Inflammation by Suppressing Autophagy via Phosphatidylinositol 3-kinase/protein Kinase B/mammalian Target of Rapamycin Signaling Pathway in Rat Models of Asthma. *J. Cell. Biochem.* 120 (3), 3833–3844. doi:10.1002/jcb.27665
- Wieczfinska, J., Sitarek, P., Kowalczyk, T., and Pawliczak, R. (2020). Leonurus Sibiricus Root Extracts Decrease Airway Remodeling Markers Expression in Fibroblasts. *Clin. Exp. Immunol.* 202 (1), 28–46. doi:10.1111/cei.13481
- Xia, H., Xue, J., Xu, H., Lin, M., Shi, M., Sun, Q., et al. (2019). Andrographolide Antagonizes the Cigarette Smoke-Induced Epithelial-Mesenchymal Transition and Pulmonary Dysfunction through Anti-inflammatory Inhibiting HOTAIR. *Toxicology* 422, 84–94. doi:10.1016/j.tox.2019.05.009
- Xian, Z., Choi, Y. H., Zheng, M., Jiang, J., Zhao, Y., Wang, C., et al. (2020). Imperatorin Alleviates ROS-Mediated Airway Remodeling by Targeting the Nrf2/HO-1 Signaling Pathway. *Biosci. Biotechnol. Biochem.* 84 (5), 898–910. doi:10.1080/09168451.2019.1710107
- Xie, Y. H., Li, X. P., Xu, Z. X., Qian, P., Li, X. L., and Wang, Y. Q. (2016). Effect of Compound Maqin Decoction on TGF- β 1/Smad Proteins and IL-10 and IL-17 Content in Lung Tissue of Asthmatic Rats. *Genet. Mol. Res.* 15 (3). doi:10.4238/gmr.15037539
- Xing, Q. Q., Liu, L. W., Zhao, X., Lu, Y., Dong, Y. M., and Liang, Z. Q. (2019). Serum Proteomics Analysis Based on Label-free Revealed the Protective Effect of Chinese Herbal Formula Gu-Ben-Fang-Xiao. *Biomed. Pharmacother.* 119, 109390. doi:10.1016/j.biopha.2019.109390
- Xue, L., Li, C., Ge, G., Zhang, S., Tian, L., Wang, Y., et al. (2021). Jia-Wei-Yu-Ping-Feng-San Attenuates Group 2 Innate Lymphoid Cell-Mediated Airway Inflammation in Allergic Asthma. *Front. Pharmacol.* 12, 703724. doi:10.3389/fphar.2021.703724
- Yan, Y., Liu, L., Dou, Z., Xu, Y., and Yan, X. (2020). Soufeng Yuchuan Decoction Mitigates the Ovalbumin-Induced Lung Damage in a Rat Model of Asthma. *Biomed. Pharmacother.* 125, 109933. doi:10.1016/j.biopha.2020.109933
- Yang, H., Sun, W., Ma, P., Yao, C., Fan, Y., Li, S., et al. (2020). Multiple Components Rapidly Screened from Perilla Leaves Attenuate Asthma Airway Inflammation by Synergistic Targeting on Syk. *J. Inflamm. Res.* 13, 897–911. doi:10.2147/JIR.S281393
- Yang, L., Jiao, X., Wu, J., Zhao, J., Liu, T., Xu, J., et al. (2018). Cordyceps Sinensis Inhibits Airway Remodeling in Rats with Chronic Obstructive Pulmonary Disease. *Exp. Ther. Med.* 15 (3), 2731–2738. doi:10.3892/etm.2018.5777
- Yang, Q., Kong, L., Huang, W., Mohammadtursun, N., Li, X., Wang, G., et al. (2020). Osthole Attenuates Ovalbumin-Induced Lung Inflammation via the Inhibition of IL-33/ST2 Signaling in Asthmatic Mice. *Int. J. Mol. Med.* 46 (4), 1389–1398. doi:10.3892/ijmm.2020.4682
- Yang, R., Yuan, B. C., Ma, Y. S., Zhou, S., and Liu, Y. (2017). The Anti-inflammatory Activity of Licorice, a Widely Used Chinese Herb. *Pharm. Biol.* 55 (1), 5–18. doi:10.1080/13880209.2016.1225775
- Yao, Z., and Fu, Y. (2021). Glycyrrhizic Acid Restrains Airway Inflammation and Remodeling in Asthma via the TGF- β 1/Smad Signaling Pathway. *Exp. Ther. Med.* 21 (5), 461. doi:10.3892/etm.2021.9892
- Yi, L., Cui, J., Wang, W., Tang, W., Teng, F., Zhu, X., et al. (2020). Formononetin Attenuates Airway Inflammation and Oxidative Stress in Murine Allergic Asthma. *Front. Pharmacol.* 11, 533841. doi:10.3389/fphar.2020.533841
- Yu, Q., Shi, Y., Shu, C., Ding, X., Zhu, S., Shen, Z., et al. (2021). Andrographolide Inhibition of Th17-Regulated Cytokines and JAK1/STAT3 Signaling in OVA-Stimulated Asthma in Mice. *Evid. Based Complement. Altern. Med.* 2021, 6862073. doi:10.1155/2021/6862073
- Yu, X., Seow, H. J., Wang, H., Anthony, D., Bozinovski, S., Lin, L., et al. (2019). Matrine Reduces Cigarette Smoke-Induced Airway Neutrophilic Inflammation by Enhancing Neutrophil Apoptosis. *Clin. Sci. (Lond)* 133 (4), 551–564. doi:10.1042/CS20180912
- Yuan, J., Liu, R., Ma, Y., Zhang, Z., and Xie, Z. (2018). Curcumin Attenuates Airway Inflammation and Airway Remodeling by Inhibiting NF-K β Signaling and COX-2 in Cigarette Smoke-Induced COPD Mice. *Inflammation* 41 (5), 1804–1814. doi:10.1007/s10753-018-0823-6
- Zeng, H., Wang, Y., Gu, Y., Wang, J., Zhang, H., Gao, H., et al. (2019). Polydatin Attenuates Reactive Oxygen Species-Induced Airway Remodeling by Promoting Nrf2-Mediated Antioxidant Signaling in Asthma Mouse Model. *Life Sci.* 218, 25–30. doi:10.1016/j.lfs.2018.08.013
- Zhang, H., Liu, B., Jiang, S., Wu, J. F., Qi, C. H., Mohammadtursun, N., et al. (2021). Baicalin Ameliorates Cigarette Smoke-Induced Airway Inflammation in Rats by Modulating HDAC2/NF-K β /pai-1 Signalling. *Pulm. Pharmacol. Ther.* 70, 102061. doi:10.1016/j.pupt.2021.102061
- Zhang, Y., Wang, X., Zhang, H., Tang, H., Hu, H., Wang, S., et al. (2021). Autophagy Modulators from Chinese Herbal Medicines: Mechanisms and Therapeutic Potentials for Asthma. *Front. Pharmacol.* 12, 710679. doi:10.3389/fphar.2021.710679
- Zheng, Y., Li, L., and Cai, T. (2020). Cordyceps Polysaccharide Ameliorates Airway Inflammation in an Ovalbumin-Induced Mouse Model of Asthma via TGF- β 1/Smad Signaling Pathway. *Respir. Physiol. Neurobiol.* 276, 103412. doi:10.1016/j.resp.2020.103412
- Zhou, T., Xu, S., Chen, X., Zhang, N., Hu, D., and Wang, W. (2018). Effect of Xiaochuanping Powder on the Inflammatory Response and Airway Remodeling in Asthmatic Rats. *J. Tradit. Chin. Med.* 38 (1), 61–66.
- Zhu, X., Cao, Y., Su, M., Chen, M., Li, C., Yi, L., et al. (2021). Cycloastragenol Alleviates Airway Inflammation in Asthmatic Mice by Inhibiting Autophagy. *Mol. Med. Rep.* 24 (5), 805. doi:10.3892/mmr.2021.12445

Conflict of Interest: The authors declare that the research was conducted in the absence of any commercial or financial relationships that could be construed as a potential conflict of interest.

Publisher's Note: All claims expressed in this article are solely those of the authors and do not necessarily represent those of their affiliated organizations, or those of the publisher, the editors, and the reviewers. Any product that may be evaluated in this article, or claim that may be made by its manufacturer, is not guaranteed or endorsed by the publisher.

Copyright © 2022 Zhou, Liu and Jia. This is an open-access article distributed under the terms of the Creative Commons Attribution License (CC BY). The use, distribution or reproduction in other forums is permitted, provided the original author(s) and the copyright owner(s) are credited and that the original publication in this journal is cited, in accordance with accepted academic practice. No use, distribution or reproduction is permitted which does not comply with these terms.



A UPLC-Q-TOF-MS-Based Metabolomics Approach to Screen out Active Components in Prepared Rhubarb for Its Activity on Noxious Heat Blood Stasis Syndrome

Hui Zhu^{1,2}, Yu Duan^{1,2}, Kunming Qin^{3,4}, Junjie Jin^{3,4}, Xiao Liu^{1,2*} and Baochang Cai^{1,2,3,4}

¹School of Pharmacy, Nanjing University of Chinese Medicine, Nanjing, China, ²Engineering Center of State Ministry of Education for Standardization of Chinese Medicine Processing, Nanjing University of Chinese Medicine, Nanjing, China, ³Nanjing Haichang Chinese Medicine Group Corporation, Nanjing, China, ⁴Nanjing Haiyuan Prepared Slices of Chinese Crude Drugs Co., Ltd., Nanjing, China

OPEN ACCESS

Edited by:

Xijun Wang,
Heilongjiang University of Chinese
Medicine, China

Reviewed by:

Jun-Song Wang,
Nanjing University of Science and
Technology, China
Aihua Zhang,
Heilongjiang University of Chinese
Medicine, China

*Correspondence:

Xiao Liu
300999@njucm.edu.cn

Specialty section:

This article was submitted to
Ethnopharmacology,
a section of the journal
Frontiers in Pharmacology

Received: 30 March 2022

Accepted: 22 June 2022

Published: 19 July 2022

Citation:

Zhu H, Duan Y, Qin K, Jin J, Liu X and
Cai B (2022) A UPLC-Q-TOF-MS-
Based Metabolomics Approach to
Screen out Active Components in
Prepared Rhubarb for Its Activity on
Noxious Heat Blood Stasis Syndrome.
Front. Pharmacol. 13:907831.
doi: 10.3389/fphar.2022.907831

Background: Prepared rhubarb was obtained by steaming raw rhubarb with wine. Different from raw rhubarb with a purgative effect, prepared rhubarb shows effects of promoting blood circulation and removing blood stasis. However, the mechanisms of its action through regulating endogenous metabolites remain unclear.

Purpose: The purpose of this study was to explore active chemical components in prepared rhubarb for its activity on noxious heat blood stasis syndrome (NHBS) by comprehensive metabolomics profiling.

Study design: Plant extracts usually show their activities in a synergistic way; therefore, integrated omics was developed as a rational way for a better understanding of their biological effects and potential active compounds.

Methods: The activities of prepared rhubarb were evaluated by biochemical and metabolomic analysis; meanwhile, serum chemical profiles were sought using UHPLC-Q-TOF-MS. Gray correlation analysis (GCA) was used for calculating the underlying correlations between them.

Results: The metabolomics profiles of rat plasma from model and control groups were significantly different, with 31 endogenous metabolites changed by NHBS. Then, after the administration of prepared rhubarb, 18 of them were regulated. Multiple metabolic pathways were disturbed after NHBS modeling and restored by prepared rhubarb, among which had a greater impact on sphingolipid metabolism. A total of 28 compounds from prepared rhubarb absorbed into the plasma were identified,

Abbreviations: APTT, activated partial thromboplastin time; CUR, curtain gas; DAVID, database for annotation, visualization, and integrated discovery; DBS, dynamic background subtraction; FIB, fibrinogen; GAS1, ion source gas 1; GAS2, ion source gas 2; GCA, gray correlation analysis; IDA, information dependent acquisition; IS, ion spray voltage; LPS, lipopolysaccharides; NHBS, noxious heat blood stasis syndrome; PCA, principal component analysis; PT, prothrombin time; TCM, traditional Chinese medicine; TEM, source temperature; TT, thrombin time; UPLC-Q-TOF-MS, ultra-performance liquid chromatography coupled with time of flight mass spectrometry.

including nine prototypes and 19 metabolites. Statistical results suggested that rhein and its metabolites accounted for half of the top 10 active compounds in prepared rhubarb for its biomedical activities.

Conclusion: This study presented evidence for the therapeutic effects and active chemicals of prepared rhubarb on NHBS in the way of metabolomics.

Keywords: prepared rhubarb, metabolomics, UHPLC-Q-TOF-MS, noxious heat blood stasis syndrome, gray correlation analysis

INTRODUCTION

Rhubarb is a classical botanical drug derived from the root and rhizome of three species of the *Polygonaceae* family, namely, *Rheum palmatum* L., *Rheum tanguticum* Maxim. ex Balf., and *Rheum officinale* Bail., which has a large range of processed products to satisfy various clinical medications (Chinese Pharmacopoeia Commission Pharmacopoeia of the People's Republic of China, 2020). Prepared rhubarb is obtained by steaming raw rhubarb with wine. This process can effectively relieve the original purgative effect of rhubarb and improve its efficacy in removing pathogenic heat and toxins from the organism, which could be applied for noxious heat blood stasis syndrome treatment. Noxious heat blood stasis syndrome (NHBS) is a common clinical complex syndrome caused by heat, and its pathogenesis is closely related to inflammation, fever, and blood stasis. Many inflammatory diseases and their complications such as viral hepatitis, cardiovascular disease, and systemic lupus erythematosus belong to the category of NHBS; the clinical treatment is mainly based on clearing heat and detoxifying, promoting blood circulation, and removing blood stasis (Zhang et al., 2019; Zhong et al., 2020; Xuan et al., 2022). Modern research showed that prepared rhubarb could cure diabetic bullae and infantile fester tonsillitis, which was in accordance with its characteristic of heat-clearing and detoxifying. In fact, whether it was applied singly or in combination with other kinds of botanical drugs for prescriptions, such as in Dahuang Zhechong Pill or Xiayuxue Decoction (Zhao et al., 2014; Dai et al., 2021; Li, 2021), prepared rhubarb exerted a good effect of promoting blood circulation. Because of the lowered purgative effect, the application of prepared rhubarb became much safer than raw rhubarb. So, prepared rhubarb was recorded in the list of "Functional Food Raw Materials" of China and could be given to children and old people for the treatment of diseases related to abnormal hemorheology in clinics (Wang et al., 2003; Wang et al., 2020; Zhao, 2020).

Spectrum-effect relationship analysis has become a classic method to explore the active compounds of traditional Chinese medicine (TCM) in recent years, by which the underlying correlation between chemical components and pharmacological functions of prepared rhubarb was explored in our previous study (Zhu et al., 2017). However, during the actual operation process, the acquisition of pharmacodynamics data was found to be quite difficult which showed strong uncontrollability. The detection of hemorheology and blood coagulation indicators could be easily affected by many factors including storage time, temperature, and so on. It was expected that all the samples could be

detected as soon as possible within 2 h after their collection (Goyal et al., 2015; Komiyama, 2015; Denessen et al., 2020). However, the reality was that this kind of test was time-consuming work which usually led to a large number of samples being overstocked. Hence, it was difficult to ensure that all the samples collected could be tested within the time limitation. The operators must be well trained and experienced, otherwise, the accuracy of the results is hard to guarantee, and this would influence the objectivity and authenticity of the subsequent correlation analysis. Metabolomics is a subject to study the metabolic processes occurring in cells, tissues, and organisms, to reveal the metabolite information changes after the organism was disturbed. These small endogenous metabolites (biomarkers) produced in response to the environmental stimulus can be used to monitor the change in pathophysiological status. Nowadays, accumulating evidence shows that the occurrence of diseases and the intervention of drugs or functional foods would cause changes in the body's metabolism (Xu et al., 2019; Bjerkhaug et al., 2021; Chen et al., 2021; Masoodi et al., 2021; Masutin et al., 2022). The advantage of omics analysis is that it provides a whole picture of the living organism, rather than focusing on a single known compound or compound group—"these analyses represent a more holistic approach as opposed to the investigation of a single protein or metabolite (Ulrich-Merzenich et al., 2007)." Compared to classical biochemical indexes, metabolomics biomarker information could be obtained using frozen plasma samples in storage; in addition, it could be detected by stable observation and quantization (Olivier, et al., 2019; Wörheide, et al., 2021). Therefore, in this study, biomarkers were introduced to replace the previous bio-effect indicators to improve the classic spectrum-effect correlation analysis, by which the controllability of data collection and the accuracy of subsequent analysis could be improved.

The liquid chromatography-mass spectrometry technique has been widely used in metabolomics at an exponentially increasing rate in recent years, owing to the following advantages: less consumption of analysis sample, high specificity, sensitivity, and accuracy of the instrument, and wide coverage of the metabolome (Zhao et al., 2018; Duan et al., 2020). As for the pharmacological activity of plant extracts, it may not be due to the effect of one or several major compounds; it usually may be a result of synergistic or antagonistic mechanisms. Even a low amount of phytochemical components may have an effect on this activity, but their identification and contribution are very difficult to ascertain. Here, an untargeted metabolomics study based on a UHPLC-Q-TOF-MS method was conducted to investigate the potential biomarkers of NHBS, and the modulating effects of prepared

rhubarb on these metabolites. Based on the UHPLC-Q-TOF-MS technique, the identification of these phytochemicals at low abundance in plant extracts is no longer difficult. In addition, using integrated metabolomics coupled with the gray correlation analysis (GCA), the underlying relationship between the endogenous metabolites and the drug relative metabolites was calculated objectively. Finally, the active chemical components in prepared rhubarb for its activity on noxious heat blood stasis syndrome were screened out.

MATERIALS AND METHODS

Materials and Reagents

Raw rhubarb was used as the material for the preparation of prepared rhubarb, which was purchased from Nanjing Haichang Chinese Medicine Group Corporation and authenticated by Prof. Jianwei Chen (School of Pharmacy, Nanjing University of Chinese Medicine). Raw rhubarb pieces of 100 kg were immersed for about 30 min in a mixed solution which comprised 30 kg glutinous rice wine and 30 kg water (10:3:3, *w/w/w*). After the liquid was absorbed exactly, the pieces were steamed for about 24 h until they turned black both inside and outside. Finally, they were naturally dried in a cool and dry condition. The decoction was prepared according to the classical literature, and the details were as follows: 180 g pieces of prepared rhubarb were immersed in water (1:10, *w/v*) for 30 min and boiled for 30 min, then the solution was filtrated through a four-layer mesh, after which the boiling process was repeated (1:8, *w/v*). Finally, the combined filtrate was concentrated to a density of 0.5 g/ml by rotary evaporation below 55°C for further experimental administration. The typical HPLC chromatogram of prepared rhubarb for chemical component profiling was provided as shown in **Supplementary Figure S1** and the content of main components in the prepared rhubarb decoction is shown in the **Supplementary Table S1**.

Lipopolysaccharides (LPS) were purchased from Biosharp (Beijing, China). Adrenaline hydrochloride injections were acquired from Tianjin KingYork Group Co., Ltd. (Tianjin, China). HPLC-grade methanol and acetonitrile were obtained from E. Merck (Merck, Darmstadt, Germany). Formic acid of HPLC grade (99.9%) was purchased from Anaqua Chemical Supply (ACS, Houston, United States). Ultra-pure water was generated by using a Milli-Q water purification system (Millipore Corporation, Bedford, MA, United States). The TT (thrombin time), PT (prothrombin time), APTT (activated partial thromboplastin time), and FIB (fibrinogen) test kits were purchased from Steellex Science Instrument Company (Beijing, China). All the other chemicals were of analytical grade and purchased from Nanjing Chemical Reagent Company (Nanjing, China).

Animals and Drug Administration

Male pathogen-free Sprague–Dawley rats, weighing 250 ± 20 g, were provided by the Slaccas Experiment Animal Company (Shanghai, China. Certificate No.: SCXK-2014-0001). All the rats were allowed to acclimate to the experimental environment (temperature of $22 \pm 2^\circ\text{C}$; relative humidity of 40–60%) for at least 7 days before the

experiment. Free access to food and water was allowed at all times except for fasting for 12 h before the experiment. All animal experiments conformed to the Guidelines for Animal Ethics Committee of the Nanjing University of Chinese Medicine.

The rats were randomly divided into three groups: control group, model group, and treatment group. The treatment group was further divided into six subgroups according to the point-in-time of blood collection ($n = 6$). The construction of the NHBS model of noxious heat blood stasis syndrome took 2 days: the rats were intraperitoneally injected with LPS (2 mg/kg) on day 1 and injected with 0.1% adrenaline hydrochloride (0.6 mg/kg) twice in a hypodermic way with a 4 h interval on day 2. The rats in the control group were injected with normal saline in the same manner. Also, the related evaluation indexes were detected to confirm the results of modeling. After successful modeling, rats in the treatment group were orally administrated with prepared rhubarb decoction (5 g/kg), whereas rats in the other groups were given the same volume of water instead. The abdominal aortic blood samples were collected at 0.5, 1, 2, 4, and 8 h after treatment on day 3 and 0.5 h after administration on day 4, and were recorded as group T1–T6. Blood samples were centrifuged at 3000 rpm/min for 10 min, and then the supernatant liquor of each sample was divided into two parts: one part was used for biochemical analysis; the other was transferred into 1.5 ml polypropylene tubes and stored under -80°C for further UPLC-Q-TOF-MS analysis.

Instruments and UHPLC-Q-TOF-MS Conditions

The analysis work was performed on a UHPLC-Q-TOF-MS system (Shimadzu, Kyoto, Japan), which has the following units: an LC-30A binary pump, an autosampler (Model SIL-20ACXR), an online degasser (DGU-20A5R), a column temperature controller compartment (CTO-30A), and a hybrid quadrupole time-of-flight tandem mass spectrometer (AB Sciex, Concord, ON, United States). An automatic coagulation analyzer (Beijing Zonic Technology Development Co., Ltd, China) was used to detect the plasma viscosity and the whole blood viscosity at four shear rates. An LG-PABER-1CH coagulation analyzer (Beijing Steellex Science Instrument Company, China) was used for the detection of TT, PT, APTT, and FIB.

The separation was achieved on an Extend C₁₈ column (Agilent, United States, 2.1 mm × 100 mm, 1.8 μm). The column temperature was maintained at 30°C. The mobile phase comprised 0.1% aqueous formic acid (A) and acetonitrile (B) at a constant flow rate of 0.3 ml/min. The gradient elution program was as follows: 0–3 min, 5–20% B; 3–7 min, 20–80% B; 7–30 min, 80–90% B; 30–32 min, 90–5% B. Then the column was reconditioned at 5% B for 3 min to prepare for the next injection. The samples were stored in an autosampler at 4°C before injection and the injection volume was 2 μl.

The MS instrument was equipped with an ESI ion source operating in both positive and negative ion modes. The optimized source temperature (TEM) and ion spray voltage (IS) were set at 550°C and –5500 V, respectively. The declustering potential was set at 60/–60 with a collision energy of 30/–30 V. The curtain gas (CUR), ion source gas 1 (GAS 1), and ion source gas 2 (GAS 2) were 35 psi, 55 psi, and 55 psi, respectively. The mass range was

scanned from 100 to 2000 Da in the TOF MS mode and 50 to 1000 in the TOF MS/MS mode, respectively. The experiments were run with 200 ms accumulation time for TOF MS and 80 ms accumulation time for TOF MS/MS. Automatic calibration was carried out at intervals of every six samples during the analytical run, to evaluate the stability and analytical repeatability of the instrument. Information-dependent acquisition (IDA) with dynamic background subtraction (DBS) was used to complete the data acquisition of low signal levels by reducing the influence of matrix interference.

Sample Pretreatment for UHPLC-Q-TOF-MS Analysis

All frozen plasma samples were thawed at 4°C. A total of 100 µl of the plasma sample was added with 300 µl of acetonitrile, then each mixture was vortexed for 3 min and centrifuged at 13,000 rpm/min for 5 min. The supernatant was transferred into an autosampler vial and stored at 4°C.

Data Acquisition and Processing

A total of 400 µl of blood or plasma was injected for the determination of whole blood viscosity or plasma viscosity, respectively. The levels of TT, PT, APTT, and FIB in rat serums were measured following the manufacturer's instruction, and all the results were expressed as mean ± SD. It is worth noting that the plasma and reagent need to be mixed and preheated for 3 min before APTT and FIB detection.

After using analyst software to control the equipment and collect raw data, the chromatographic peaks were processed by MarkerView software with the following parameters: retention time range within 1–30 min, mass scan range within 100–1000 Da, tolerance range of 0.01 Da and, peak intensity threshold of 100. The extracted ionic intensity was normalized by the total peak area method. Then, the normalized data were imported into SIMCA-P software for the PCA analysis (unsupervised pattern recognition) to have a preliminary understanding of the most realistic metabolic differences between the groups. OPLS-DA analysis (supervised mode) was further performed to distinguish the overall differences in metabolic profiles between groups, and cumulative R^2Y and Q^2 values were calculated to evaluate the fitness and predictive capability of constructed pattern recognition models. The variables differentially expressed between the groups were screened out and selected as candidate endogenous metabolites based on the variable importance in projection (VIP) of the OPLS-DA analysis and p -value ($VIP > 1$, $p < 0.05$). Afterward, corresponding structures were obtained by searching online public databases such as HMDB and KEGG. The potential endogenous metabolites were finally identified by checking the accurate molecular weight and secondary MS/MS spectrum. The contents of endogenous metabolites in plasma were expressed as the intensity to exhibit the variation trends among different groups. The generation of a heatmap and the analysis of the involved metabolic pathways were completed by the dedicated website MetaboAnalyst.

In our previous study, a database of chemical compounds in botanical drugs belonging to rheum and all varieties of

processed rhubarb has already been established, so compounds and structural characteristics in the prepared rhubarb decoction were thus identified. Based on this, the information of compounds and their possible metabolic pathways (including I phase and II phase metabolism) were imported into MetabolitePilot software, by which both prototypes and metabolic compounds were predicted by the functions of generic peak finding, predicted metabolites, isotope pattern, and mass defect. PeakView software could link the chemical structure to MS/MS spectrums (matching rate >75% and the m/z error within 10 ppm) to complete the final identification of these compounds based on their accurate molecular weights and the matching rates of the reasonable fragmentations. Ions in different samples that showed the same retention time (tolerance of 0.2 min) and the same m/z value could be defined as the same ions. The spectrum of the rat plasma in the model group was selected as the control to eliminate chromatographic peak interference coming from the endogenous compounds.

To guarantee the accuracy and reproducibility of the results, the compounds in plasma samples with an intensity below 100 were not taken into account. The intensity of compounds absorbed into rat plasma at different time points was the average value measured by data from six individuals.

Gray Correlation Analysis

The gray correlation analysis method can significantly reduce the bias caused by information asymmetry, hence, it was widely used to investigate the correlation degree between two sets of variations with a relatively simple calculation way (Hou et al., 2020; Ren, et al., 2020). The gray correlation degree was calculated by Excel functions and its data analysis tool. In detail, the dimensionless processed sequence is set as the feature sequence $X_0 = (x_0(1), x_0(2), \dots, x_0(n))$, then the sequence of associated factors is determined as follows: $X_1 = (x_1(1), x_1(2), \dots, x_1(n))$, $X_2 = (x_2(1), x_2(2), \dots, x_2(n))$, \dots , $X_i = (x_i(1), x_i(2), \dots, x_i(n))$, and the correlation coefficient could be calculated by the following formula:

$$\xi(x_0(k), x_i(k)) = \frac{\min_i \min_k |x_0(k) - x_i(k)| + \rho \max_i \max_k |x_0(k) - x_i(k)|}{|x_0(k) - x_i(k)| + \rho \max_i \max_k |x_0(k) - x_i(k)|}$$

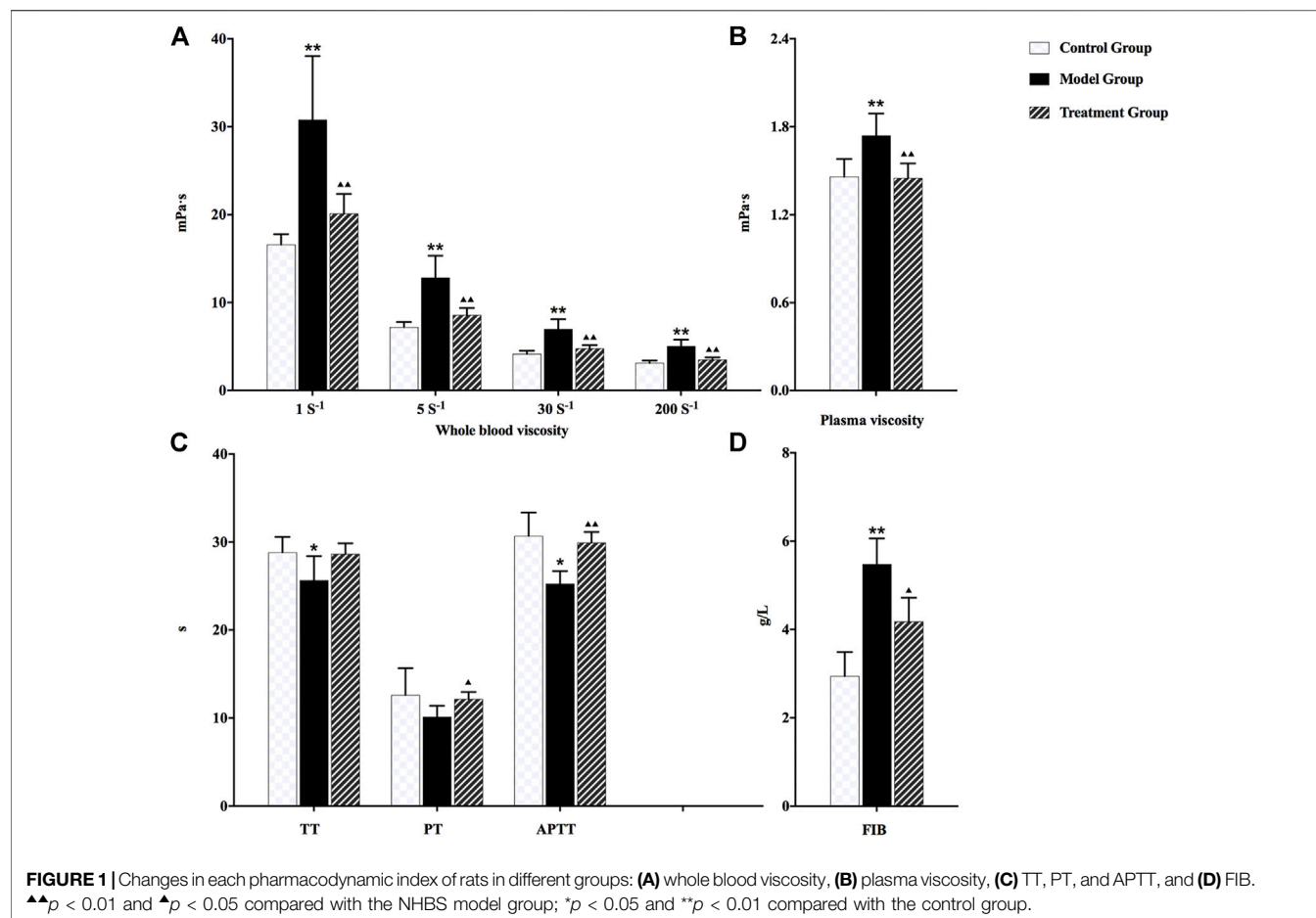
ρ is the distinctive coefficient lying between $0 < \rho < 1$, and it is usually set as 0.5.

The gray correlation grade could finally be obtained by averaging the correlation coefficient at different time points:

$$\xi(X_0, X_i) = \frac{1}{n} \sum_{k=1}^n \xi(x_0(k) - x_i(k))$$

Construction of a Compound-Target-Pathway-Disease Network

Based on the compounds screened out, related targets were found by searching the TCMSp database (<http://tcmspw.com/tcmsp>).



php), consulting the literature, education by the Swiss Target Prediction database (<http://www.swisstargetprediction.ch/>), and further inputting to UniProt (<https://www.uniprot.org/>) identifiers. The main pathways and associated diseases were extracted from the Integrated Discovery database (<https://david.ncifcrf.gov/>). The compound-target-pathway-disease network was finally constructed by using Cytoscape software.

RESULTS

Evaluation of Therapeutic Effects of Prepared Rhubarb

As shown in **Figure 1**, the whole blood viscosity, plasma viscosity, and content of plasma fibrinogen in the model group were significantly increased compared with rats in the control group. However, TT, PT, and APTT values were decreased. The obvious microcirculation disturbance and hemorheology abnormality were observed in rats after modeling, indicating that noxious heat blood stasis syndrome was constructed successfully. After the administration of prepared rhubarb, all the aforementioned pharmacodynamic indexes were reverse-regulated in varying degrees, suggesting an exact therapeutic effect on NHBS model rats.

Metabolic Spectrum Analysis

The plasma samples were analyzed by the UHPLC-Q-TOF-MS method in both positive and negative ion modes. The representative total ion chromatograms are shown in **Supplementary Figure S2**, and the extracted data were used for multivariate statistical analysis. PCA analysis was first taken into consideration to reflect the real differences between groups (**Supplementary Figure S3**). As shown in **Figures 2A,B**, a remarkable aggregation within the groups and an evident separation between model and control groups were observed, which indicated that the NHBS model was successfully constructed; meanwhile, the normal physiological metabolism of rats was affected after injection of LPS and adrenaline hydrochloride. To facilitate screening of candidate endogenous metabolites, OPLS-DA was further used to maximize the differences between the groups (**Supplementary Figure S4**). The candidate endogenous metabolites were excavated based on the criteria of a VIP value greater than 1 and p -value less than 0.05, and further identified according to practical and theoretical fragment ions provided by available databases. Consequently, a total of 31 endogenous metabolites in plasma were screened out by a comparison of the control group with the model group, including eight metabolites increased and 23 metabolites decreased, which could be used as potential biomarkers for noxious heat blood stasis syndrome indication. As listed in **Supplementary Table S2**, most of the metabolites detected

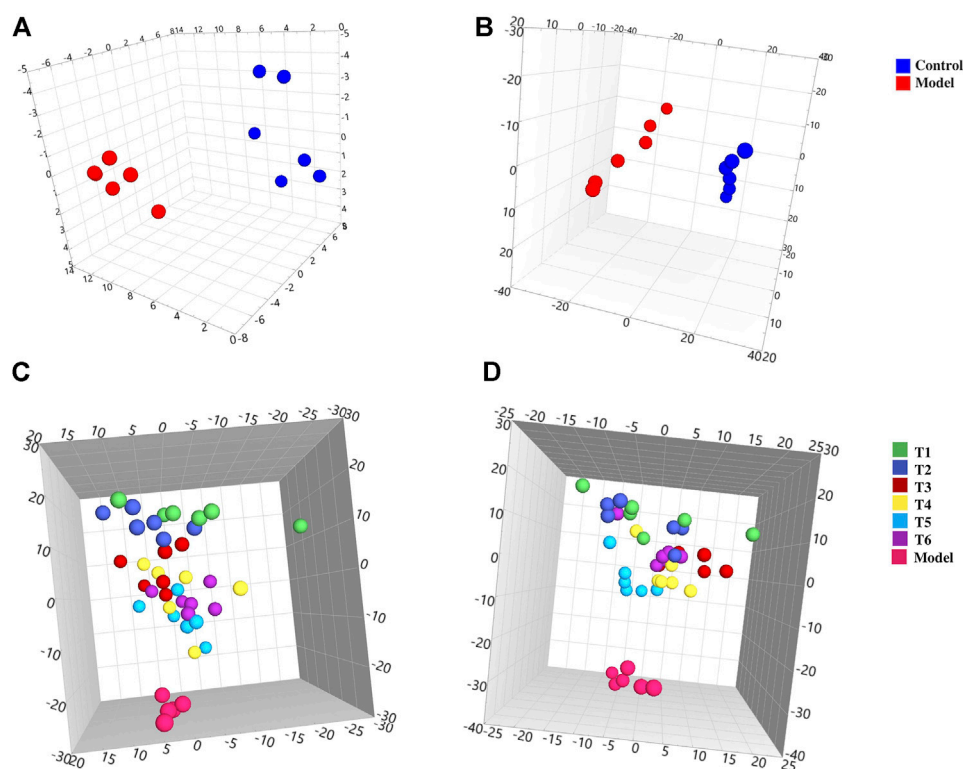


FIGURE 2 | 3D PCA score plots of the plasma samples from different groups. Control and model groups: **(A)** ESI⁺, $R^2X = 0.796$, $Q^2 = 0.754$ and **(B)** ESI⁻, $R^2X = 0.920$, $Q^2 = 0.838$; model and treatment groups: **(C)** ESI⁺, $R^2X = 0.730$, $Q^2 = 0.559$ and **(D)** ESI⁻, $R^2X = 0.752$, $Q^2 = 0.552$.

belonged to lysophosphatidylcholine ($n = 11$), lysophosphatidyl ethanolamine ($n = 4$), sphingolipids ($n = 3$), unsaturated fatty acids ($n = 3$), and amino acids ($n = 2$), suggesting that the occurrence of noxious heat blood stasis syndrome was mainly connected with multiple metabolic pathways including glycerophospholipid metabolism, sphingolipid metabolism, biosynthesis of unsaturated fatty acids, arachidonic acid metabolism, and aminoacyl-tRNA biosynthesis.

Similarly, the data of rat plasma from the control and model groups were subjected to both PCA (**Supplementary Figure S5**) and OPLS-DA (**Supplementary Figure S6**) analysis. **Figures 2C,D** show that scattered points representing rats in the model and different treatment groups were well separated, implying that prepared rhubarb had a certain intervention effect on the rat's metabolism. It could be seen that sports of the T1 group were the farthest from those of the model group. Then samples at subsequent time points were found gradually approaching the model group with obvious overlaps between subgroups, which, in accordance with our previous findings, was that prepared rhubarb works quickly after administration while its curative effect would gradually become weak over time. Also, the samples in the T6 group showed an obvious callback trend, suggesting that continuous administration of prepared rhubarb was necessary to consolidate its curative effect. Based on the established OPLS-DA model with good applicability and high predictability (**Supplementary Figure S7**), a total of 21 endogenous metabolites were screened out, comprised of 5 decreased and 16 increased. The

details and pathways involved are shown in **Supplementary Table S3**.

To further reveal the intervention effect of prepared rhubarb on NHBS rats from the perspective of the metabolic profile, pairwise analysis was performed by Venn diagrams. As shown in **Figure 3**, 18 endogenous metabolites were finally retained under positive and negative ion detective modes, which expressed significant differences after modeling but were reversely regulated after drug administration. They were L-isoleucine (leucine), L-phenylalanine, L-tryptophan, isovalerylcarnitine, sphinganine, phytosphingosine, eicosapentaenoic acid, sphingosine-1-phosphate (S1P), 11-octadecenylcarnitine, lysoPC (15:0), LysoPC (16:0), LysoPC (18:1), LysoPC (18:2), LysoPE (0:0/20:2), lysoPC (20:4), lysoPC (20:5), lysoPE (0:0/20:1), and lysoPE (0:0/22:4).

As a supplement to verification, heatmaps were presented according to the extracted peak intensity data to observe the variation trends of these metabolites in the samples from different groups directly (**Figure 4**). As shown, the clustering analysis grouped all of these samples into two major distinct clusters, which exactly conformed to the different physiological and pathological statuses of rats. In addition, the T1 and control groups were classified into the same cluster, which was consistent with the result of the PCA. After dosing, 13 declined endogenous metabolites exerted varying degrees of increase; meanwhile, the level of five elevated endogenous metabolites was decreased. Given all of the aforementioned data, these 18 variables could

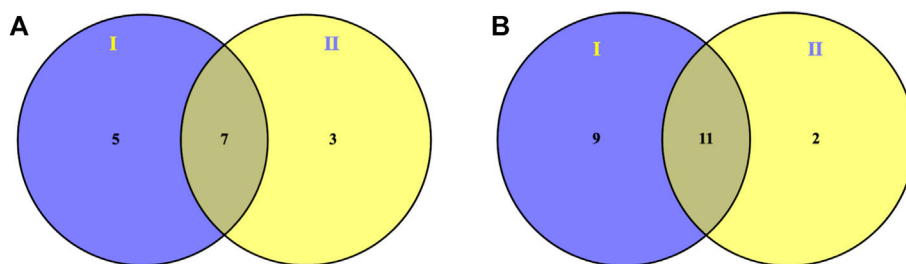


FIGURE 3 | Venn diagrams showing overlapped modulation of prepared rhubarb on endogenous metabolites of NHBS rats in both **(A)** ESI⁺ and **(B)** ESI⁻ mode by pairwise analysis: I (potential endogenous metabolites of NHBS) versus II (modulation of prepared rhubarb on endogenous metabolites of NHBS rats).

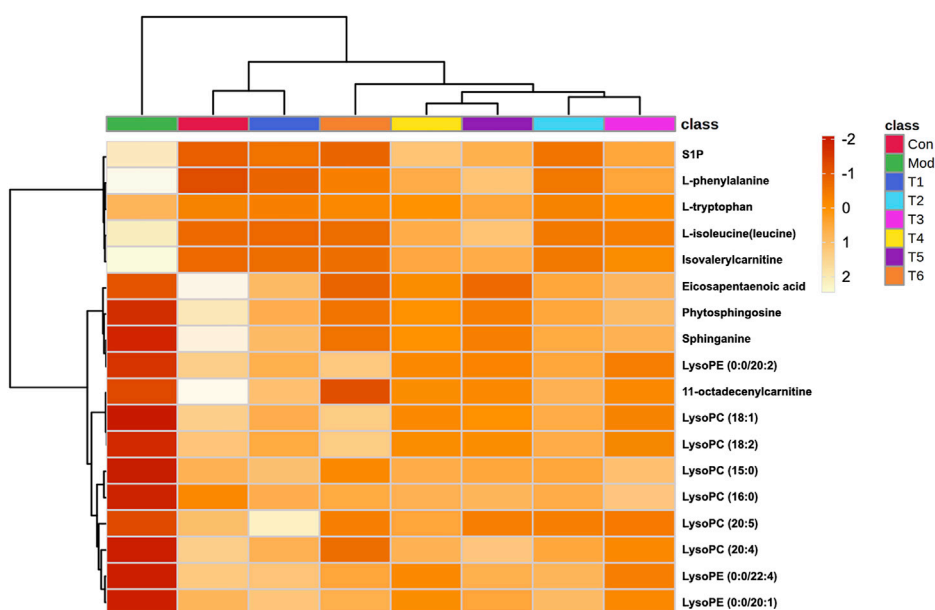


FIGURE 4 | Heatmap with hierarchical clustering analysis showed the change in the biomarkers between each group.

be chosen as the characteristic indexes for the subsequent GCA analysis.

Correspondingly, prepared rhubarb could regulate the following pathways disturbed by NHBS: aminoacyl-*t*-RNA biosynthesis; sphingolipid metabolism; valine, leucine, and isoleucine biosynthesis; valine, leucine, and isoleucine degradation; phenylalanine, tyrosine, and tryptophan biosynthesis; phenylalanine metabolism; biosynthesis of unsaturated fatty acids; glycerophospholipid metabolism; and tryptophan metabolism. These might lay a foundation for further exploration of drug action mechanisms.

Analysis and Identification of Prepared Rhubarb Relative Compounds in Rat Plasma

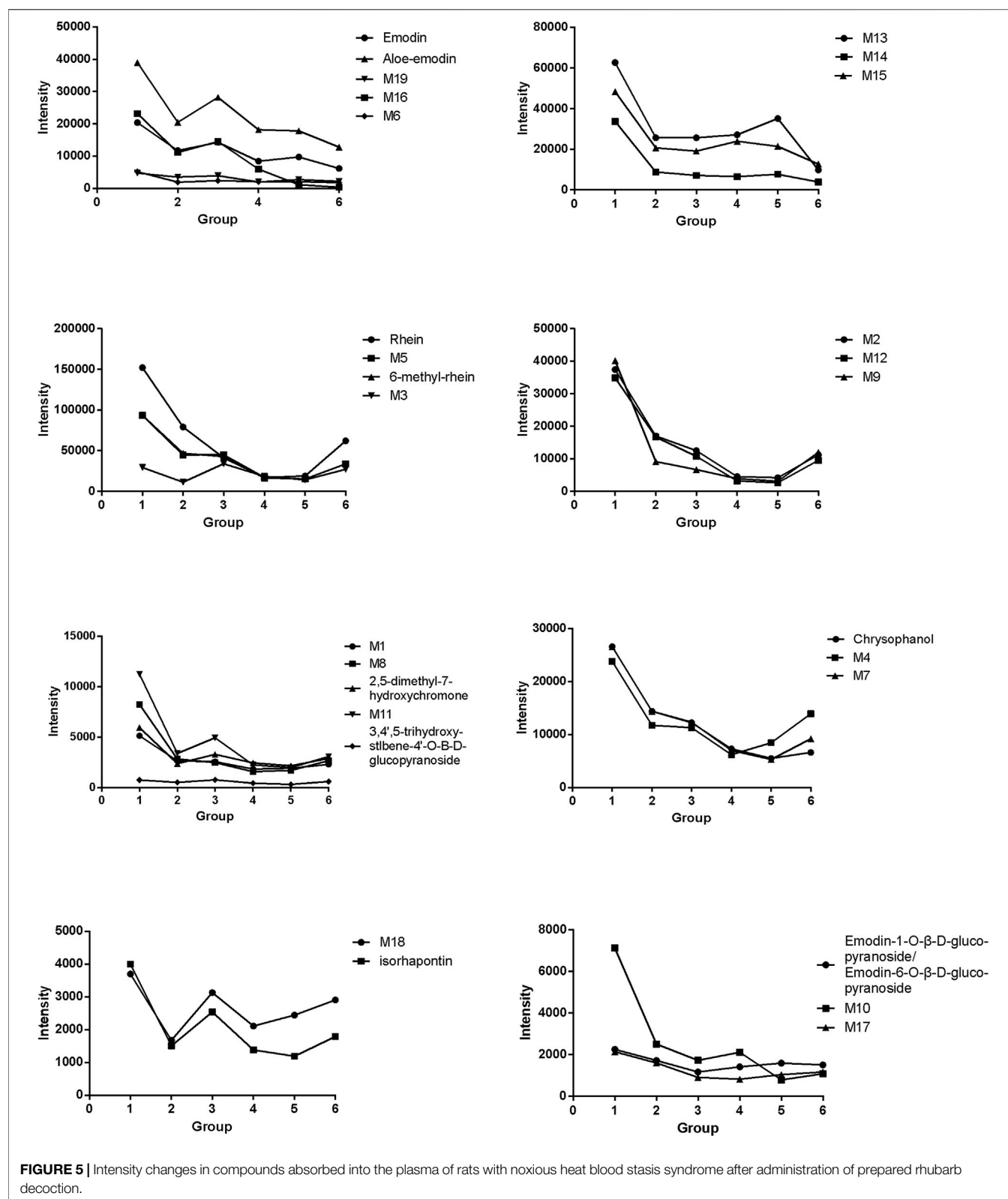
Finally, 28 compounds from prepared rhubarb in rat plasma were identified, including nine prototype compounds and

19 metabolites. The detailed information, including their specific molecular formula, molecular weight, retention time, mass deviation, fragmentation, and matching rate are shown in **Supplementary Table S4**. Specific metabolic pathways of the 19 metabolites were concluded as glucuronidation, sulfation, hydroxylation, methylation, oxidation, hydroxylation + sulfation, decarboxylation, decarbonylation, hydroxylation + glucuronidation, and hydrolyzation. The proposed metabolic pathways of rhein in NHBS rat plasma were illustrated as an example (**Supplementary Figure S8**).

The variation trend of each compound is presented as intensity-time curves in **Figure 5**. It could be found that although the absorption process of each compound *in vivo* was different, similar trends could still be found among them.

Gray Correlation Analysis Results

The results of the correlation between the intensity of each compound absorbed into rat plasma and the characteristic



endogenous metabolites screened out are shown in **Supplementary Table S5** (details listed in **Supplementary Table S6**). According to the score ranking, the top 10 potential

active compounds in prepared rhubarb for its activity on noxious heat blood stasis syndrome were found to be chrysophanol monosulfate (M14), hydroxy-emodin glucuronide (M11), rhein

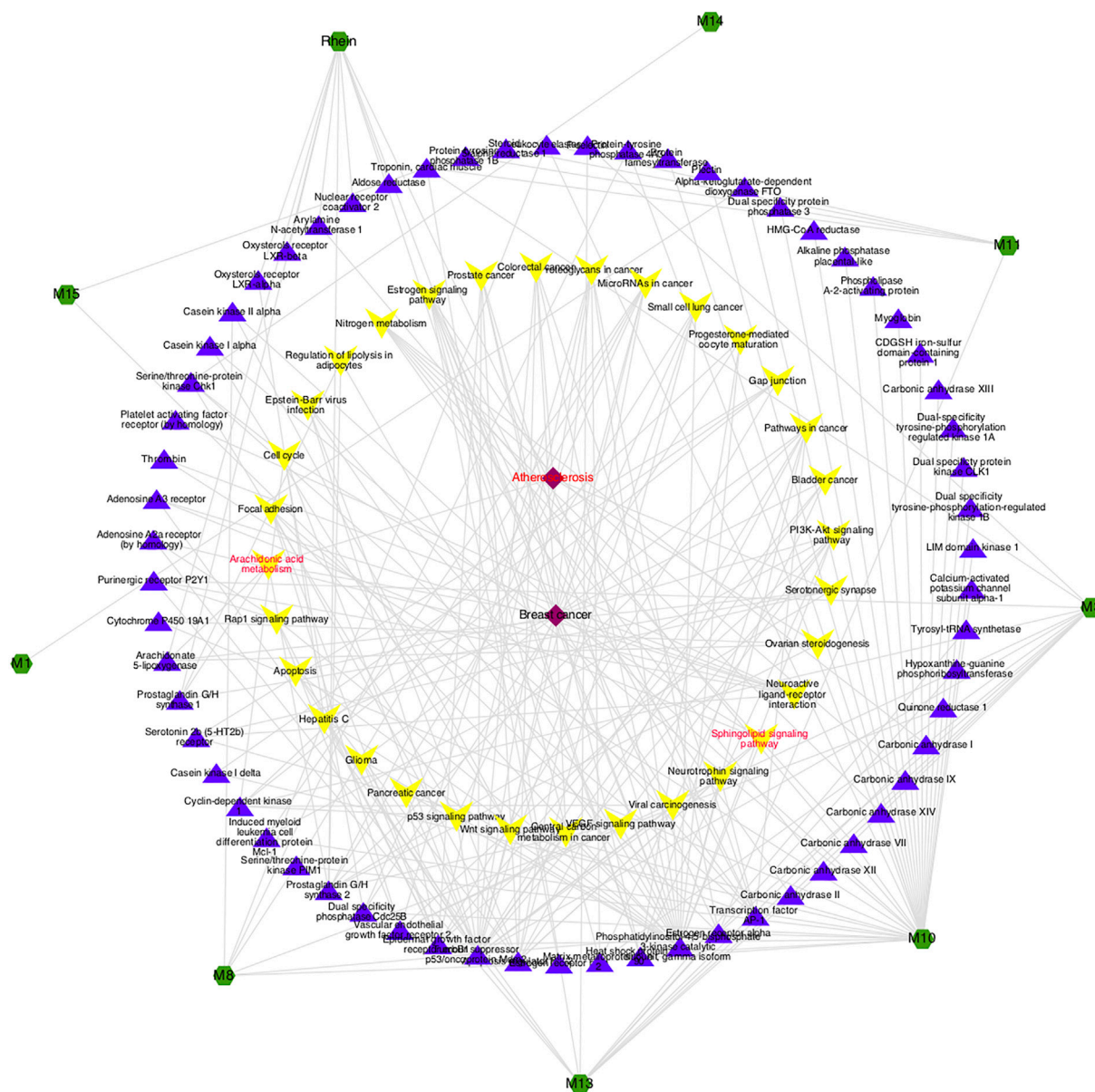


FIGURE 6 | Potential compound-target-pathway-disease network. The green nodes represent potential active components, purple nodes represent related targets, yellow nodes represent pathways, and red nodes represent predicted diseases.

glucuronide (M3), oxidative-rhein (M6), 1, 8-dihydroxy-anthraquinone (M10), aloe-emodin glucuronide (M13), hydroxy-emodin monosulfate (M8), hydroxy-rhein monosulfate (M1), emodin-1-*O*- β -D-glucopyranoside-desaturation (M15), and rhein. It is worth noting that rhein was the only prototype compound from prepared rhubarb among these 10 compounds, and the other nine were conjugate metabolites from chrysophanol, emodin, aloe-emodin, and rhein, which indicated that rhubarb anthraquinones were the main active compounds to exert the effects of prepared rhubarb in promoting blood circulation and removing blood stasis. Compared with our previous study, rhein glucuronide and hydroxy-emodin glucuronide still scored higher,

and the contribution of rhein and its metabolites during the treatment cannot be ignored (Zhu et al., 2017).

According to GCA results, the top 10 potential active compounds were selected for bioinformatics analysis as supplementary verification, also the compound-target-pathway-disease network was constructed. As shown in **Figure 6**, atherosclerosis is a common kind of cardiovascular and cerebrovascular disease in clinics, which belongs to the category of “blood stasis” in traditional Chinese medicine, and these compounds might exert a therapeutic effect by regulating various metabolic pathways including the sphingolipid signaling pathway and the arachidonic acid metabolism pathway. Part of

TABLE 1 | Molecular docking scores.

| Gene | P1 | M1 | M3 | M8 | M10 | M11 | M13 | M14 | M15 |
|-------|---------|----------|---------|---------|--------|---------|---------|----------|---------|
| TP53 | -76.02 | -85.18 | -105.66 | -86.23 | 0 | -100.14 | -92.89 | -74.50 | -85.34 |
| CASP3 | -108.10 | -112.634 | -134.44 | -110.67 | -92.22 | -128.38 | -143.27 | -108.22 | -135.93 |
| MAPK8 | -110.39 | -120.17 | -134.53 | -118.68 | -97.97 | -136.89 | -138.00 | -120.00 | -136.91 |
| MMP9 | -87.10 | -92.11 | -129.32 | -97.97 | -76.80 | -127.50 | -131.15 | -91.02 | -101.63 |
| EGFR | -95.17 | -111.64 | -138.76 | -107.21 | -85.17 | -142.38 | -136.43 | -100.67 | -128.05 |
| ESR1 | -96.48 | 0 | -84.18 | -105.97 | -82.29 | 0 | -107.17 | -100.207 | -110.59 |

The data represent the binding energy of the interaction (unit: kcal·mol⁻¹); the larger the absolute value, the stronger the affinity; 0 means no interaction.

the predictions were not only consistent with the results of the metabolomics but also in line with the efficacy and clinical application of prepared rhubarb (Liu et al., 2020; Guo et al., 2021), suggesting that the strategy based on metabolomics to find the active chemicals of TCM described in this study was quite feasible, giving reliable conclusions.

The pharmacological activity observed in functional plants was usually not due to a single compound. In most cases, plant extracts showed their activities based on synergistic or antagonistic effects. Therefore, the idea of a holistic approach described here was rational. Also, it was a remarkable fact that either the analysis of prototype components or these metabolites alone could not obtain the aforementioned ideal results, which prompted a synergistic work conducted by both prototype compounds and their metabolites. The verification of the efficacy of single or multiple potential active compounds and their precise mechanism of action still need to be further explored, especially the difficulty of obtaining metabolites and tracking their intracorporal process *in vivo*.

DISCUSSION

In this study, metabolomics was used to clarify that the metabolism profiles in noxious heat blood stasis syndrome rats changed significantly, and the disordered endogenous metabolites were excavated. Interestingly, most of the differential metabolites belonged to lipid molecules, the phenomenon of significant changes in lipid composition and expression in rats after modeling implied that the occurrence and development of noxious heat blood stasis syndrome were closely related to abnormal lipid metabolism, and the lipidomics method can be further applied to focus on the changes in lipid molecules of rats before and after the intervention of prepared rhubarb accurately.

Phytosphingosine, sphinganine, and sphingosine-1-phosphate are metabolites of sphingolipids, which are essential components of cell membranes and take part in many critical processes of signal transduction (Petersen et al., 2013; Tidhar et al., 2014; Drexler et al., 2021). Among them, phytosphingosine is the basic unit for the synthesis of various complex sphingolipid derivatives, which can protect the epidermal lipid barrier from external damage; sphinganine is involved in regulating the fluidity of lipid bilayer membranes, and both of them are closely related to changes in physiological and pathological states such as vascular growth, maturation, injury, and repair. After modeling, the level of phytosphingosine and sphinganine in noxious heat blood stasis

syndrome rats significantly decreased, which may be due to their increased consumption under the blood stasis state. In addition, studies have shown that emodin in rhubarb can significantly reduce the expression of phytosphingosine and sphinganine in the serum of chronic constriction injury model rats to inhibit neuroinflammation, suggesting that emodin may be the main component involved in the regulation of sphingosine metabolism (Chen et al., 2022). Sphingosine 1-phosphate is generated by the phosphorylation of sphingosine catalyzed by SPHK1/SPHK2 and expressed on endothelial cells, which are involved in mediating vascular maturation and maintaining vascular integrity. S1P is released by activated platelets and exposes fibrinogen receptors by binding to platelet surface receptors, increasing platelet reactivity and further stimulating platelet aggregation, thus resulting in blood stasis (Jung et al., 2012; Parham et al., 2015). However, highly expressed S1P and FIB in noxious heat blood stasis syndrome rats were significantly downregulated after the intervention treatment, implying that prepared rhubarb can regulate sphingolipid metabolism to improve blood stasis.

LysoPC and LysoPE are both lysophospholipids. The 15 differential lysophospholipids screened in this experiment can also be regarded as potential biomarkers for noxious heat blood stasis syndrome. Consistent with the results of our experiment, recent studies have shown that lysophospholipids are related to the occurrence of inflammatory reactions and the maintenance of vascular endothelial function, which can be used to predict the occurrence of cardiovascular diseases such as atherosclerosis and stroke with high accuracy (Liu et al., 2017; Paapstel et al., 2018; Wang et al., 2021).

Arachidonic acid is stored in cell membrane phospholipids and is enzymatically released from these phospholipids by the action of the PLA2 enzyme. PGH₂ catalyzed by cyclooxygenase is further catalyzed by specific prostaglandin synthase to obtain different forms of prostaglandins, which play an important role in the regulation of inflammation and oxidative stress. Among them, the synthesis and release of PGE₂ catalyzed by the PGES enzyme can cause an increase in body temperature. PGI₂ and TXA₂, which are catalyzed by the PGIS and TXS enzymes, have opposing roles in regulating blood vessel and platelet states, respectively. They are rapidly converted into metabolites TXB₂ and 6-keto-PGF_{1α} due to their extremely short half-lives. The broken dynamic balance between them leads to vasoconstriction and increased blood viscosity (Liu et al., 2019; Imig, 2020; Li et al., 2021). Similarly, the experimental results showed that prepared rhubarb can significantly reverse the level of arachidonic acid in noxious

heat blood stasis syndrome rats. Meanwhile, the previous research by our group proved that prepared rhubarb can effectively correct the ratio of TXB₂ and 6-keto-PGF_{1α} to normal in noxious heat blood stasis syndrome rats. It is indicated that prepared rhubarb plays the role of promoting blood circulation and removing blood stasis by regulating inflammatory response and improving blood rheology. In addition, studies have confirmed that a variety of prototype and derivative compounds in rhubarb are involved in the regulation of the synthesis and release of prostaglandins to exert corresponding pharmacological effects. For example, rhein can inhibit inflammatory factors such as IL-6, TNF-α, and PEG₂ to reduce fructose-induced inflammatory cell erosion (Dong, 2016); emodin can reduce the release of arachidonic acid metabolites such as TXB and PGs by inhibiting PLA2 and 5-LOX, thus exerting anti-inflammatory effects (Peng et al., 2017); and chrysophanol-8-O-glucoside can significantly inhibit platelet aggregation and TXA2 of rats *in vitro* (Seo et al., 2012); however, the regulatory effects of other potential active ingredients screened in this study on the arachidonic acid metabolic pathway remain to be further explored.

CONCLUSION

This was the first study in which the metabolomics profiles of NHBS were correlated with prototypes and metabolites from prepared rhubarb absorbed into rats' plasma. In this study, a UHPLC-Q-TOF-MS method coupled with the GCA analysis was developed, by which the contribution of all molecules to the functions of prepared rhubarb in promoting blood circulation and removing blood stasis was calculated. The biomarker-based method described was proved to be a simple and reproducible characterization approach, which could provide a reference leading to the discovery of new compounds with a specific activity in TCM.

REFERENCES

- Bjerkhaug, A. U., Granslo, H. N., and Klingenberg, C. (2021). Metabolic Responses in Neonatal Sepsis-A Systematic Review of Human Metabolomic Studies. *Acta Paediatr.* 110 (8), 2316–2325. doi:10.1111/apa.15874
- Chen, P., Wang, C., Luo, R. X., Wu, Z. B., and Xia, D. B. (2022). Mechanism of Emodin in Relieving Neuropathic Pain by Regulating Serum Metabolism. *Chin. J. Clin. Mater Med.* 47 (08), 2187–2194. doi:10.19540/j.cnki.cjcmm.20211027.402
- Chen, S., Wu, Q., Zhu, L., Zong, G., Li, H., Zheng, H., et al. (2021). Plasma Glycerophospholipid Profile, Erythrocyte N-3 PUFAs, and Metabolic Syndrome Incidence: a Prospective Study in Chinese Men and Women. *Am. J. Clin. Nutr.* 114, 143–153. doi:10.1093/ajcn/nqab050
- Chinese Pharmacopoeia Commission (2020). *Chinese Pharmacopoeia of the People's Republic of China*. 2020 edition, 1. Beijing: China Medical Science and Technology Press, 24–25.
- Dai, C. M., Jin, S., and Zhang, J. Z. (2021). Effect of Dahuang Zhechong Pills Combined with TACE on VEGF, MMP-2, TGF-B1 and Immune Function of Patients with Primary Liver Cancer (Blood Stasis and Collaterals Blocking Type). *Zhongguo Zhong Yao Za Zhi* 46 (3), 722–729. doi:10.19540/j.cnki.cjcmm.20200716.501
- Denessen, E. J. S., Jeurissen, M. L. J., Pereboom, R. M. T. A., Verhezen, P. W. M., and Henskens, Y. M. C. (2020). Determining the Maximal Storage Time of Centrifuged Citrated Samples for Performing Add-On Routine Coagulation Tests. *Thromb. Res.* 196, 54–62. doi:10.1016/j.thromres.2020.08.003
- Dong, X. Q. (2016). Protection of Rhein on Kidney Injury in Fructoseinduced Hyperuricaemia Rats. *Strait Pharm. J.* 28 (3), 42–44.
- Drexler, Y., Molina, J., Mitrofanova, A., Fornoni, A., and Merscher, S. (2021). Sphingosine-1-Phosphate Metabolism and Signaling in Kidney Diseases. *J. Am. Soc. Nephrol.* 32 (1), 9–31. doi:10.1681/ASN.2020050697
- Duan, X., Pan, L., Bao, Q., and Peng, D. (2020). UPLC-Q-TOF-MS Study of the Mechanism of THSWD for Breast Cancer Treatment. *Front. Pharmacol.* 10, 1625. doi:10.3389/fphar.2019.01625
- Goyal, V. K., Kakade, S., Pandey, S. K., Gothi, A. K., and Nirogi, R. (2015). Determining the Effect of Storage Conditions on Prothrombin Time, Activated Partial Thromboplastin Time and Fibrinogen Concentration in Rat Plasma Samples. *Lab. Anim.* 49 (4), 311–318. doi:10.1177/0023677215597137
- Guo, Y., Li, Q., Yu, X., and Liang, Y. (2021). Rhubarb Anthraquinone Glycosides Protect against Cerebral Ischemia-Reperfusion Injury in Rats by Regulating Brain-Gut Neurotransmitters. *Biomed. Chromatogr.* 35, e5058. doi:10.1002/bmc.5058
- Hou, A., Yang, L., Zhang, J., Wang, S., Man, W., Guo, X., et al. (2020). A Strategy for Qualitative and Quantitative Profiling of Angelicae Pubescentis Radix and

DATA AVAILABILITY STATEMENT

The datasets presented in this study can be found in online repositories. The names of the repository/repositories and accession number(s) can be found in the article/Supplementary Material.

ETHICS STATEMENT

The animal study was reviewed and approved by the Animal Ethics Committee of the Nanjing University of Chinese Medicine.

AUTHOR CONTRIBUTIONS

HZ wrote the paper draft. XL corrected the draft. XL and BC supervised the experiments. HZ, YD, KQ, and JJ performed the experiments together. All data were generated in-house, and no paper mill was used. All authors agreed to be accountable for all aspects of the work, ensuring integrity and accuracy.

FUNDING

This work was financially supported by the Key University Science Research Project of Jiangsu Province (17KJA360006 and 21KJA360008), the Science and Technology Support Program of Nanjing City (201812021), and the National Science Foundation of China (81873004).

SUPPLEMENTARY MATERIAL

The Supplementary Material for this article can be found online at: <https://www.frontiersin.org/articles/10.3389/fphar.2022.907831/full#supplementary-material>

- Detection of its Analgesic and Anti-inflammatory Components by Spectrum-Effect Relationship and Multivariate Statistical Analysis. *Biomed. Chromatogr.* 34, e4910. doi:10.1002/bmc.4910
- Imig, J. D. (2020). Eicosanoid Blood Vessel Regulation in Physiological and Pathological States. *Clin. Sci. (Lond)*. 134 (20), 2707–2727. doi:10.1042/CS20191209
- Jung, B., Obinata, H., Galvani, S., Mendelson, K., Ding, B. S., Skoura, A., et al. (2012). Flow-regulated Endothelial S1P Receptor-1 Signaling Sustains Vascular Development. *Dev. Cell*. 23 (3), 600–610. doi:10.1016/j.devcel.2012.07.015
- Komiyama, Y. (2015). Samples in Coagulation Test. *Rinsho. Byori*. 63 (12), 1397–1404.
- Li, L., Sluter, M. N., Yu, Y., and Jiang, J. (2021). Prostaglandin E Receptors as Targets for Ischemic Stroke: Novel Evidence and Molecular Mechanisms of Efficacy. *Pharmacol. Res.* 163, 105238. doi:10.1016/j.phrs.2020.105238
- Li, Z. C. (20212021). Curative Efficacy of Huoxue Zhuyu Qingdu Decoction on Patients with Acute Kidney Injury Induced by Sepsis and its Effect on Cardiovascular Event. *Shandong J. Tradit. Chin. Med.* 40 (3), 265–268. doi:10.16295/j.cnki.0257-358x.2021.03.009
- Liu, P., Li, R., Antonov, A. A., Wang, L., Li, W., Hua, Y., et al. (2017). Discovery of Metabolite Biomarkers for Acute Ischemic Stroke Progression. *J. Proteome Res.* 16 (2), 773–779. doi:10.1021/acs.jproteome.6b00779
- Liu, Q., Liang, X., Wang, Q., Wilson, E. N., Lam, R., Wang, J., et al. (2019). PGE2 Signaling via the Neuronal EP2 Receptor Increases Injury in a Model of Cerebral Ischemia. *Proc. Natl. Acad. Sci. U. S. A.* 116 (20), 10019–10024. doi:10.1073/pnas.1818544116
- Liu, X., Wu, J., Tian, R., Su, S., Deng, S., and Meng, X. (2020). Targeting Foam Cell Formation and Macrophage Polarization in Atherosclerosis: The Therapeutic Potential of Rhubarb. *Biomed. Pharmacother.* 129, 110433. doi:10.1016/j.biopha.2020.110433
- Masoodi, M., Gastaldelli, A., Hyötyläinen, T., Arretxe, E., Alonso, C., Gaggini, M., et al. (2021). Metabolomics and Lipidomics in NAFLD: Biomarkers and Non-invasive Diagnostic Tests. *Nat. Rev. Gastroenterol. Hepatol.* 18 (12), 835–856. doi:10.1038/s41575-021-00502-9
- Masutin, V., Kersch, C., and Schmitz-Spanke, S. (2022). A Systematic Review: Metabolomics-Based Identification of Altered Metabolites and Pathways in the Skin Caused by Internal and External Factors. *Exp. Dermatol.* doi:10.1111/exd.14529
- Olivier, M., Asmis, R., Hawkins, G. A., Howard, T. D., and Cox, L. A. (2019). The Need for Multi-Omics Biomarker Signatures in Precision Medicine. *Int. J. Mol. Sci.* 20 (19), 4781. doi:10.3390/ijms20194781
- Paapstel, K., Kals, J., Eha, J., Tootsi, K., Ottas, A., Piir, A., et al. (2018). Inverse Relations of Serum Phosphatidylcholines and Lysophosphatidylcholines with Vascular Damage and Heart Rate in Patients with Atherosclerosis. *Nutr. Metab. Cardiovasc. Dis.* 28 (1), 44–52. doi:10.1016/j.numecd.2017.07.011
- Parham, K. A., Zebol, J. R., Tooley, K. L., Sun, W. Y., Moldenhauer, L. M., Cockshell, M. P., et al. (2015). Sphingosine 1-phosphate Is a Ligand for Peroxisome Proliferator-Activated Receptor- γ that Regulates Neovascularization. *FASEB J.* 29 (9), 3638–3653. doi:10.1096/fj.14-261289
- Peng, F. F., Xu, Y. M., Tan, H. F., Luo, S., and Rong, X. F. (2017). The Inhibitory Effects of Emodin on the Proliferation and Metastasis of Synovial Cells Form Rheumatoid Arthritis. *Immunol. J.* 33 (01), 34–39.
- Petersen, N. H., Olsen, O. D., Groth-Pedersen, L., Ellegaard, A. M., Bilgin, M., Redmer, S., et al. (2013). Transformation-associated Changes in Sphingolipid Metabolism Sensitize Cells to Lysosomal Cell Death Induced by Inhibitors of Acid Sphingomyelinase. *Cancer Cell*. 24 (3), 379–393. doi:10.1016/j.ccr.2013.08.003
- Ren, Y., Ai, J., Liu, X., Liang, S., Zheng, Y., Deng, X., et al. (2020). Anticoagulant Active Ingredients Identification of Total Saponin Extraction of Different Panax Medicinal Plants Based on Grey Relational Analysis Combined with UPLC-MS and Molecular Docking. *J. Ethnopharmacol.* 260, 112955. doi:10.1016/j.jep.2020.112955
- Seo, E. J., Ngoc, T. M., Lee, S. M., Kim, Y. S., and Jung, Y. S. (2012). Chrysophanol-8-O-glucoside, an Anthraquinone Derivative in Rhubarb, Has Antiplatelet and Anticoagulant Activities. *J. Pharmacol. Sci.* 118 (2), 245–254. doi:10.1254/jphs.11123fp
- Tidhar, R., Sims, K., Rosenfeld-Gur, E., Shaw, W., and Futerman, A. H. (2014). A Rapid Ceramide Synthesis Activity Using NBD-Sphinganine and Solid Phase Extraction. *J. Lipid Res.* 56 (1), 193–199. doi:10.1194/jlr.D052001
- Ulrich-Merzenich, G., Zeitler, H., Jobst, D., Panek, D., Vetter, H., and Wagner, H. (2007). Application of the “-Omics” Technologies in Phytomedicine. *Phytomedicine* 14, 70–82. doi:10.1016/j.phymed.2006.11.011
- Wang, K., Guan, D., Zhao, X., Qiao, D., Yang, Y., and Cui, Y. (2020). Proteomics and Metabolomics of Raw Rhubarb and Wine-Processed Rhubarb in the Treatment of Rats with Intracerebral Hemorrhage. *Ann. Transl. Med.* 8 (24), 1670. doi:10.21037/atm-20-7831
- Wang, X., Zhang, L., Sun, W., Pei, L. L., Tian, M., Liang, J., et al. (2021). Changes of Metabolites in Acute Ischemic Stroke and its Subtypes. *Front. Neurosci.* 14, 580929. doi:10.3389/fnins.2020.580929
- Wang, Z. F., Shi, S. L., and Song, H. X. (2003). Effect of Prepared Rhubarb on Insulin Resistance in Patients with Pregnancy Induced Hypertension. *Chin. J. Integr. Med.* 9 (1), 35–38.
- Wörheide, M. A., Krumsiek, J., Kastenmüller, G., and Arnold, M. (2021). Multi-omics Integration in Biomedical Research - A Metabolomics-Centric Review. *Anal. Chim. Acta.* 1141, 144–162. doi:10.1016/j.aca.2020.10.038
- Xu, J., Li, X., Zhang, F., Tang, L., Wei, J., Lei, X., et al. (2019). Integrated UPLC-Q/TOF-MS Technique and MALDI-MS to Study of the Efficacy of YiXinshu Capsules against Heart Failure in a Rat Model. *Front. Pharmacol.* 10, 1474. doi:10.3389/fphar.2019.01474
- Xuan, Y. N., Qiu, F. J., Li, K. Q., Chen, X. L., Wang, J., Chen, E. S., et al. (2022). Clinical Efficacy of Lupus Prescription for Systemic Lupus Erythematosus with Heat-Induced Blood Stasis Type by Retrospective Analysis and Mechanism Exploration. *Guangdong Med. J.* 43 (04), 441–446. doi:10.13820/j.cnki.gdyx.20212539
- Zhang, M., Yang, Y., and Zhao, Q. (2019). Clinical Efficacy Observation of Qingzi Mixture Treating Henoch-Schönlein Purpura Children with Heat-Toxicity and Blood Stasis Syndrome. *Chin. J. Tradit. Chin. Med. Pharm.* 34 (4), 1822–1824.
- Zhao, G. H., Hou, X. L., Li, X. Y., Qu, M., Tong, C. Q., and Li, W. (2018). Metabolomics Analysis of Alloxan-Induced Diabetes in Mice Using UPLC-Q-TOF-MS after crassostrea Gigas Polysaccharide Treatment. *Int. J. Biol. Macromol.* 108, 550–557. doi:10.1016/j.ijbiomac.2017.12.057
- Zhao, J. (2020). *Clinical Study on Xuefu Zhuyu Decoction with Prepared Rhei Radix at Rhizoma with Wine in Treating Unstable Angina with Qi Stagnation and Blood Stasis Syndrome*. Jinan City: Shandong University of Traditional Chinese Medicine. [master's thesis]. [Shandong].
- Zhao, L., Hu, C. J., Pan, X. G., Geng, Y. Y., Wu, X. Q., Wu, W. H., et al. (2014). Effect of Raw/stewed Rhubarb in Xiayuxue Decoction on Vascular Endothelial Function and Microcirculation of Rats with Heat Accumulation of Blood Stasis. *Drug. Eval. Res.* 37 (05), 413–416.
- Zhong, X., Jiao, H. C., and Li, H. C. (2020). Research Progress on Application of Hot Toxin Theory in Cardiac Diseases. *J. Liaoning Univ. Tradit. Chin. Med.* 22 (06), 152–155. doi:10.13194/j.issn.1673-842x.2020.06.039
- Zhu, T. T., Wu, L., Wang, X. L., Zhu, H., Zhu, X. C., Zhou, Q. G., et al. (2017). Investigation on Relationships between Chemical Spectrum and Bioeffect of Prepared Rhubarb Decoction in Rats by UPLC-ESI-Q-TOF-MS Method Coupled with Gray Correlation Analysis. *J. Funct. Foods*. 31, 104–112. doi:10.1016/j.jff.2017.01.028

Conflict of Interest: The authors declare that the research was conducted in the absence of any commercial or financial relationships that could be construed as a potential conflict of interest.

Publisher's Note: All claims expressed in this article are solely those of the authors and do not necessarily represent those of their affiliated organizations, or those of the publisher, the editors, and the reviewers. Any product that may be evaluated in this article, or claim that may be made by its manufacturer, is not guaranteed or endorsed by the publisher.

Copyright © 2022 Zhu, Duan, Qin, Jin, Liu and Cai. This is an open-access article distributed under the terms of the Creative Commons Attribution License (CC BY). The use, distribution or reproduction in other forums is permitted, provided the original author(s) and the copyright owner(s) are credited and that the original publication in this journal is cited, in accordance with accepted academic practice. No use, distribution or reproduction is permitted which does not comply with these terms.



Proteomics and Metabolomics Unveil *Codonopsis pilosula* (Franch.) Nannf. Ameliorates Gastric Precancerous Lesions *via* Regulating Energy Metabolism

Rupu He^{1†}, Ruyun Ma^{1†}, Zheng Jin¹, Yanning Zhu¹, Fude Yang^{2*}, Fangdi Hu^{1*} and Jianye Dai^{1,3*}

OPEN ACCESS

Edited by:

Haitao Lu,
Shanghai Jiao Tong University, China

Reviewed by:

Tao Yi,
Hong Kong Baptist University, Hong
Kong SAR, China
Zhen-Yu Li,
Shanxi University, China
Weidong Cheng,
Southern Medical University, China

*Correspondence:

Fude Yang
gszyyfd@163.com
Fangdi Hu
hufd@lzu.edu.cn
Jianye Dai
daijy@lzu.edu.cn

[†]These authors have contributed
equally to this work and share first
authorship.

Specialty section:

This article was submitted to
Ethnopharmacology,
a section of the journal
Frontiers in Pharmacology

Received: 30 April 2022

Accepted: 17 June 2022

Published: 19 July 2022

Citation:

He R, Ma R, Jin Z, Zhu Y, Yang F, Hu F
and Dai J (2022) Proteomics and
Metabolomics Unveil *Codonopsis*
pilosula (Franch.) Nannf. Ameliorates
Gastric Precancerous Lesions *via*
Regulating Energy Metabolism.
Front. Pharmacol. 13:933096.
doi: 10.3389/fphar.2022.933096

¹School of Pharmacy, Lanzhou University, Lanzhou, China, ²School of Pharmacy, Gansu University of Chinese Medicine, Lanzhou, China, ³Collaborative Innovation Center for Northwestern Chinese Medicine, Lanzhou University, Lanzhou, China

Objective: This study aimed to systematically evaluate the efficacy of *Codonopsis pilosula* (Franch.) Nannf. (*Codonopsis Radix*, CR) and reveal the mechanism of its effects on suppressing Gastric Precancerous Lesions.

Methods: First, we established the GPL rat model which was induced by N-methyl-N'-nitro-N-nitrosoguanidine, a disordered diet, and 40% ethanol. The CR's anti-Gastric Precancerous Lesions effect was comprehensively evaluated by body weight, pathological section, and serum biochemical indexes. Then, quantitative proteomics and metabolomics were conducted to unveil the disturbed protein-network and pharmacodynamic mechanism. Furthermore, serum pharmacology was employed to confirm that CR's anti-gastritis and anti-cancer phenotype in cell models.

Results: In animal models, CR had been shown to control inflammation and ameliorate Gastric Precancerous Lesions. Considering the combination of proteomics and metabolomics, we found that CR could significantly reverse the biological pathways related to energy metabolism which were disturbed by the Gastric Precancerous Lesions model. Furthermore, the results of serum pharmacology indicated that the *Codonopsis Radix* containing serum could ameliorate gastritis injury and selectively inhibit the proliferation of gastric cancer cells rather than normal cells, which was closely related to ATP production in the above mentioned cells.

Conclusion: In summary, CR exerted anti-Gastric Precancerous Lesions effects by ameliorating gastritis injury and selectively inhibiting the proliferation of gastric cancer cells rather than normal cells. Proteomics and metabolomics unveiled that its efficacy was closely related to its regulation of the energy-metabolism pathway. This research not only provided new ideas for exploring the mechanism of complex systems such as Chinese

Abbreviations: CR, *Codonopsis pilosula* (Franch.) Nannf; GPL, Gastric Precancerous Lesions; CRCS, *Codonopsis pilosula* (Franch.) Nannf. containing serum; MNNG, N-methyl-N'-nitro-N-nitrosoguanidine; KEGG, Kyoto Encyclopedia of Genes and Genomes; GO, Gene Ontology.

herbals but also benefited the treatment strategy of Gastric Precancerous Lesions via regulating energy metabolism.

Keywords: proteomics, metabolomics, gastric precancerous lesions, energy metabolism, *Codonopsis Radix*

INTRODUCTION

The 2020 World Health Organization (WHO) Cancer Report shows that gastric cancer is one of the most common cancers in the world, with the fifth highest morbidity rate and the fourth highest mortality rate in malignant tumors (<https://www.who.int/data/gho/publications/world-health-statistics>). Surgery and chemotherapy currently are the main treatments for gastric cancer. However, the 5-year survival rate of these patients is still less than 30% even after surgical intervention, due to the high possibility of recurrence and metastasis (Zong et al., 2016). Commonly chemotherapy for gastric cancer includes fluorouracil, doxorubicin, and platinum compounds (Kolarić et al., 1986; Al-Batran et al., 2016; Patel et al., 2021). Yet, due to their inevitable drug resistance and toxic side effects, patients have poor compliance and prognosis.

According to the Correa model (Correa et al., 1975), the occurrence of gastric cancer often goes through the following process: normal gastric mucosa, inflammation, atrophy, metaplasia, dysplasia, and gastric cancer. Among them, atrophy, intestinal metaplasia, and dysplasia have been classified as precancerous lesions. Chronic inflammation is a crucial factor in this process (Maeda et al., 2001; Wang et al., 2014; Deswaerte et al., 2018; Duarte et al., 2018). However, it is often difficult for patients to cooperate because of mild symptoms. And it is too late to block “tumor deterioration”. Therefore, it is most feasible to block or reverse the “inflammation-cancer transformation” process. Through the “preventive treatment” strategy, the goal of reducing the incidence rate and the mortality rate of gastric cancer is expected to be achieved.

In fact, “preventive treatment” is one of the core concepts of traditional Chinese medicine. In clinical practice, many traditional prescriptions have been applied, such as the Sijunzi decoction (Zhong et al., 1997; Cai et al., 2008), Xiangshaliujunzi decoction (Lv et al., 2017; Hong et al., 2020), etc. Among these decoctions, *Codonopsis pilosula* (Franch.) Nannf. [Campanulaceae] (*Codonopsis Radix*, *Codonopsis pilosula*, Dangshen in Chinese, CR) is the principal herbal. It has been found that the polysaccharide of CR has anti-ulcer and anti-tumor pharmacological effects (Yang and Zhou, 2022). In addition, lobetyolin of CR, a polyacetylene compound, has a good protective effect on gastric mucosal damage caused by ethanol and has obvious anti-ulcer effects (Song et al., 2008; Bailly, 2021). Modern pharmacology has proved that CR and its active ingredients can treat stomach diseases (Sui et al., 2005; Xu et al., 2008; Li et al., 2017; Bailly, 2021) by ameliorating gastrointestinal motility (Wang et al., 1997; Wang et al., 2015) and regulating oxidase levels (Ma et al., 2014; Li et al., 2017). However, the detailed molecular mechanism is still unclear.

Therefore, we aim to systematically evaluate the pharmacodynamic effects of CR in GPL animal models. Furthermore, the potential mechanism and targeted pathways will be explained by proteomics and metabolomics. Finally, we will confirm our hypothesis via cellular models. It is expected to provide new revelations for the treatment of GPL and explore the mechanism of *Codonopsis pilosula* (Franch.) Nannf., a tonifying-spleen herbal.

MATERIALS AND METHODS

Materials and Reagents

Codonopsis pilosula (Franch.) Nannf. collected from Weiyuan County (Gansu Province, China), which was identified as *Codonopsis pilosula* (Franch.) Nannf. by Prof. Xicang Yang from the Affiliated Hospital of the Gansu University of Chinese Medicine. The main components of CR are polysaccharides (40–50%) and oligosaccharides (10–20%), and their extraction and component analysis have been reported previously (Chunxia et al., 2013; Bai et al., 2020). Vitacoenzyme was purchased from Deshengtang Pharmacy (Lanzhou, China). N-methyl-N'-nitro-N-nitrosoguanidine (M105583) was purchased from Aladdin (Shanghai, China). Ethyl ether (2020061501) was purchased from Kelong (Tianjin, China). CCK8 kit (M4839) was purchased from Abmole (TX, United States). Triton X-100 (T8787), Triethylammonium bicarbonate buffer (18597, TEAB), Urea (U5378), DL-Dithiothreitol (43815, DTT), Iodoacetamide (I1149, IAA), CH₂O (F1635), CD₂O (492620), ¹³CD₂O (596388), NaBH₃CN (42077), NaBD₃CN (190020), ammonium hydroxide solution (221228), formic acid (F0507) were purchased from Sigma (MI, United States). BCA protein assay kit (23225), Methanol (A456-4), Acetonitrile (A955-4), Isopropanol (A461-4) were purchased from Thermo Fisher Scientific (MA, United States). Trypsin (V5280) was purchased from Promega (WI, United States). ATP Test Kit (ADS-W-A001-96) was purchased from Kexing (Shanghai, China). Anti-Caspase three antibody (ER30804) and Anti-Caspase 12 antibody (ER62907) were purchased from HUABIO (Hangzhou, China). An anti-NF-κB antibody (8242 S) was purchased from CST (BSN, United States). Anti-β-actin antibody (SA00001-1) was purchased from Proteintech (CHI, United States). All metabolite standards were purchased from Sigma (MI, United States), Steraloids (Beijing, China), and TRC Chemicals (YTO, Canada). Human gastric mucosal cells (GES-1 cells) and Human gastric carcinoma cells (AGS cells) were purchased from China Center for Type Culture Collection (Wuhan, China).

To prepare the water extract, 3 kg CR were soaked in 24L water for 30 min and boiled for 1 h at 100°C. Then, the first extract was

TABLE 1 | Isotope label grouping table.

| Group | CH ₂ O | NaBH ₃ CN |
|------------------------|---------------------------------|----------------------|
| Health group-light | CH ₂ O | NaBH ₃ CN |
| Model group-middle | CD ₂ O | NaBH ₃ CN |
| CR-treated group-heavy | ¹³ CD ₂ O | NaBD ₃ CN |

filtrated, and then 12 L water was added to decoct for the second extract. After the combination, the extracts were concentrated at 0.36 kg/L.

Animal Experiments and Sample Collection

Male Wistar rats (6 weeks old, average weight 220 g) were purchased from Changsheng Biotechnology of Liaoning province in China (SCXK- 2015-0001), raised in the Animal Experiment Center of Gansu University of Chinese Medicine (50–70% humidity, 23–25°C, 12–12 h light/dark cycle). After 7 days of acclimatization, rats were randomly divided into seven groups, including Control group ($n = 12$, Control), Control group treated with high-dose of CR ($n = 6$, Control + CR(H)), GPL Model group ($n = 12$, Model), low-dose of CR group ($n = 6$, CR(L)), middle-dose of CR group ($n = 6$, CR(M)), high-dose of CR group ($n = 6$, CR(H)), and positive control group ($n = 6$, P-Control).

According to the reported protocol (Kim et al., 1999), a high-concentration of MNNG (0.2 g/kg/15 days) was given by gavage, combined with a disordered diet (1 time/3 days) and alcohol drinking (40% ethanol gavage, 1 ml/3 days), to establish GPL model. Saline was given to the control group and model group. Vitacoenzyme (Zhang and Wang, 2019; Xia et al., 2021) was given to the positive group at 0.28 g/kg/d. And intragastric administration was respectively performed with 0.6, 1.2, and 2.4 g/kg/d intragastrically, once a day for 16 weeks as the low, medium, and high dose of CR groups. All administered dosages were converted according to the clinically effective dose. When all animals were euthanized, blood and gastric tissues were collected. Gastric tissues from the control group, model group, and medium-dose of CR group were used for proteomic and metabolomic experiments.

Histopathology and Biochemical Index Test

The gastric tissues were fixed in 10% formalin. After dehydrating, the biopsies embedded in wax were sectioned at 3 μ m, and stained with hematoxylin and eosin for histopathological examination by light microscopy. Serum biochemical indicators were detected by an automatic biochemical analyzer.

Stable Isotope Dimethyl Labeling

Trypsin digestion: The rat gastric tissue was rinsed in ice-cold saline to remove the blood, then weighed 200 mg. The tissue was ground for 90 s with a tissue grinder, and the supernatant was collected after centrifuging (21500g, 4°C, 5 min). The protein was diluted to 3 mg/ml after quantification. Ten μ L protein diluent was reacted with 30 μ L urea (8M, TEAB) and 2 μ L DTT (200mM, H₂O) for 15min incubating at 65 °C in darkness. After the tube cooled to 35°C, 2 μ L IAA (400mM, H₂O) was added for 30 min at

35°C. Then 2 μ L DTT (200mM, H₂O) was added for 15 min incubating at 65°C in darkness. In the end, 100 μ L TEAB and 2 μ L trypsin (0.2 μ g/ μ L) were added to incubate overnight at 37°C.

Isotope dimethyl labeling: After digestion, the peptides were reacted with 6 μ L of CH₂O (4%) and 6 μ L of NaBH₃CN (0.6M) according to Table 1, and incubated with a constant temperature shaker (800rpm, 22°C) for 1 h. It was stopped by adding 24 μ L ammonia solution (1%, v/v) and 12 μ L formic acid. Finally, the light, middle, and heavy groups were mixed.

Desalting: Operating according to the instructions of Pierce™ C18 Tips (Thermo Scientific, 87782).

LC-MS/MS and Data Analysis

The isotope-labeled quantitative proteomics biological mass spectrometry detection and analysis were based on the published technical scheme (Boersema et al., 2009), and were carried out by the Q-Exactive Orbitrap mass spectrometer coupled to the Ultimate 3000 LC system. In short, the flow rate was set to 0.3 μ L/min, and the applied remote spray voltage was set to 2.8 kV. Labeled peptide samples were loaded onto a 100 μ m fused silica column packed with 15 cm \times 3 μ m C18 resin. A full scan (350–1,800 MW) was used, followed by data-dependent MS2 scans that enabled dynamic exclusion of the 20 most abundant ions for MS2 data collection. ProLuCID software was used to analyze the LC-MS/MS data. The parameter settings included static modification of cysteine residues (+57.0215 Da) and variable oxidation of methionine residues (+15.9949 Da). The data was further filtered through DTASelect 2.0.4769, and the peptides were restricted to those that were completely digested by trypsin, with a false discovery rate of 1%. According to the published technical scheme (Benjamin et al., 2012), the internal software CIMAGE is used to quantify the ratio of quantitative whole proteomics experiments. Proteins with an average ratio of greater than 1.5 or less than 0.66 in all samples were selected for KEGG pathway analysis and GO analysis by DAVID (<https://david.ncifcrf.gov/>). The selected proteins were imported into the STRING (<http://stringdb.org/>) database to construct the protein-protein interaction (PPI) network.

The mass spectrometry proteomics data have been deposited to the ProteomeXchange Consortium via the PRIDE (Perez-Riverol et al., 2022) partner repository with the dataset identifier PXD032714.

Quantitative Metabonomic Analysis

A total of 10 mg of gastric tissue was homogenized by 20 μ L of deionized water. Then, the derivation process was performed as in the previous reports (Xie et al., 2021). Ultra-performance liquid chromatography coupled to a tandem mass spectrometry (UPLC-MS/MS) system was used to quantitate all targeted metabolites in this project. The ultra-performance liquid chromatography coupled to tandem mass spectrometry (UPLC-MS/MS) system (ACQUITY UPLC-Xevo TQ-S, Waters Corp., Milford, MA, United States) was used to quantitate all targeted metabolites in this project. The column in the metabolomics analysis was ACQUITY UPLC BEH C18 1.7 μ m VanGuard pre-column (2.1 \times 5 mm). The UPLC-MS/MS operating condition was adapted from previous reports (Xie

et al., 2021). To diminish analytical bias within the entire analytical process, the samples were analyzed in the group but the groups were analyzed randomly. The raw data files generated by UP LC-MS/MS were processed using the MassLynx 4.1 software to perform peak integration, calibration, and quantitation for each metabolite. The different metabolites of each group were imported into KEGG (<https://www.kegg.jp/>) and MBRol 2.0 (<http://csbg.cnb.csic.es/mbrole2/>) to obtain the relevant metabolic pathways.

Preparation of Drug-Containing Serum

The blood of rats in each group was collected after intragastric administration according to the dose, centrifuged in a high-speed centrifuge for 10 min (4°C, 12000r/min), the supernatant was taken, and 4 times the volume of absolute ethanol was added to the serum to precipitate the protein. The protein suspension was centrifuged for 10 min (4°C, 15000r/min) to take the supernatant and spin dry (45°C, 1600r/min, 300min) in a vacuum spin dryer.

Cell Culture

GES-1 cells were cultured in Dulbecco's modified Eagle medium with 10% FBS and 1% penicillin-streptomycin at 37°C and 5% CO₂. The cells were inoculated into 96-well plates at 5×10³ cells per well and waited for 12 h to adhere. Then the cells were treated with drug-containing serum for 24 h. The culture methods and conditions of AGS cells were the same as that of GES-1 cells.

CCK8 Assay

The cell viability was tested via a CCK8 kit. After the cells were treated for 20 h, 10 µL of CCK8 reagent was added to each well and incubated for 4 h. The optical density (OD) was detected at 450 nm to measure the cell viability.

ATP Assay

The cells were collected and disrupted by ultrasonic waves on ice. Then, the samples were centrifuged (12,000 rpm, 4°C) for 10 min, and the supernatant was collected for testing. Ten µL sample was added to the 96-well plates. The chromogenic reagents were added to react with the sample for 5 min at 25°C. The optical density (OD) at 350 nm was measured by a microplate reader and calculated. The concentrations of proteins were detected by the BCA kit.

Western Blotting

The proteins were separated by electrophoresis in 10% sodium dodecyl sulfate-polyacrylamide gel, and then the separated proteins were transferred to the polyvinylidene fluoride (PVDF) membrane. The PVDF membranes were combined with anti-Caspase three antibody, anti-Caspase 12 antibody, anti-NF-κB antibody, anti-IL-17A antibody, or anti-β-actin antibody incubated overnight at 4 °C, then shaken with secondary antibody at room temperature for 1 h. Exposure was taken in a TANON gel imager.

Statistical Analysis

Differences between experimental and control groups were determined by unpaired *t*-test or by two-way ANOVA analysis

where more than two groups of data were compared. *p* values <0.05 were considered statistically significant. Graphs were prepared in Prism software (GraphPad, La Jolla, CA).

RESULTS

Codonopsis pilosula (Franch.) Nannf. Could Significantly Ameliorate Gastric Precancerous Lesions in the MNNG-Induced Animal Model

On the premise of clinical effectiveness, to further determine the therapeutic effects of CR, we adapted N-methyl-N'-nitro-N-nitrosoguanidine (MNNG)-induced GPL model, combined with a disordered diet and alcohol drinking (Kim et al., 1999). As the recorded body weight for 16 weeks, three doses of CR was higher than the model group after the fourth week. Among them, the high-dose group was always higher than the other dose groups, indicating that the state of the rats in the high-dose group might be better than in other models (Figure 1A). Then, the histological results evaluated the improvement of GPL. We observed that inflammatory cell infiltration and increased mast cells were seen in the muscle layer in the model group, which was significantly reduced after administration of CR (Figure 1B). The gastric glands in the model group were loosely arranged and a large number of intestinal metaplasia goblet cells were seen, while that was effectively recovered in the CR group (Figure 1B). Moreover, we found that the biomarkers, LDH and CK, were significantly reduced in CR groups, especially the high-dose group (Figure 1C). And CR presents mild pharmacodynamic effects in SOD and MDA. Supplementary Figure S1C). In addition, the results of healthy rats after administration of CR illustrated that it had few side effects (Supplementary Figures S1A–C). All the above evidence supported that CR was effective and low-toxicity for GPL treatment with long-term administration.

Quantitative Proteomics Revealed the Pharmacodynamic Network and Mechanism of *Codonopsis pilosula* (Franch.) Nannf.

We next employed quantitative proteomics based on stable isotope dimethyl labeling to simultaneously compare the protein networks in three groups (Healthy, model, and CR-treatment) (Figure 2A). After applying a cutoff of the ratio greater than 1.5 or less than 0.66 in all of the model and CR-treated groups, we collectively identified 110 up-regulated proteins in the model group and 183 down-regulated proteins in the CR-treated group as key targets (Figure 2B). According to KEGG and GO analysis, the results showed that the pathways intervened by modeling (Figures 2C,D) were reversed by CR-treatment (Figures 2E, F). Moreover, energy metabolism, such as the citrate cycle and glycolysis process, attracted our attention. In addition, we constructed the

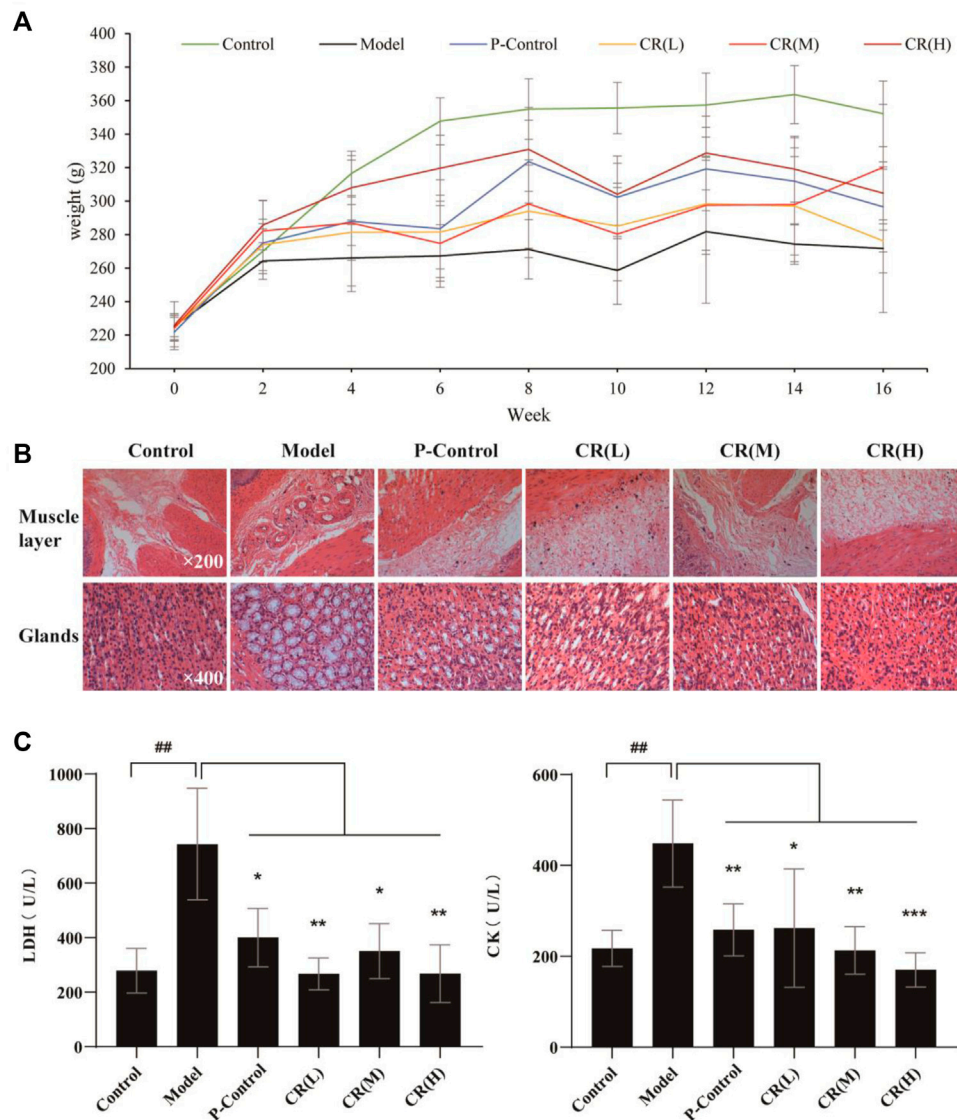


FIGURE 1 | The pharmacodynamic results of CR in the treatment of GPL rats. **(A)** Weight diversity curve of animal experiments. **(B)** HE stained pathological section of gastric tissue in different group. **(C)** The contents of LDH (Lactate Dehydrogenase) and CK (Creatine Kinase) in serum of different group. The graphs show the mean \pm SD of at five independent experiments ($n = 5$). $^{##}p < 0.01$ vs Control. $^{*}p < 0.05$, $^{**}p < 0.01$ and $^{***}p < 0.001$ vs. Model.

protein-protein interaction (PPI) network (**Supplementary Figures S2A, B**), which indicated that most of the proteins with high degree values were related to the glycolysis process and citrate cycle. Taken together, we hypothesized that CR suppressed the GPL mainly by regulating the pathways of energy metabolism.

Quantitative Metabolomics Verified That Energy Metabolism Was Critical for the Pharmacodynamic Effect of *Codonopsis pilosula* (Franch.) Nannf.

To verify whether energy metabolism was critical for the pharmacodynamic effect of CR, quantitative metabolomics

was employed to unveil the intervened metabolites after CR treatment. We identified and quantified 221 metabolites in these three groups, of which fatty acids, amino acids, and bile acids were the main metabolites (**Figure 3A**). Furthermore, PLS-DA analysis was performed on the overall gastric tissue metabolic profile of the healthy group, modeling group, and CR-treated group (**Figure 3B**). According to the results, the three groups could be well distinguished, and there was a tendency to return to health after CR administration in GPL modeling.

Based on the results of proteomics, we presumed that CR's efficiency may be derived from the regulation of energy metabolism. Further metabolic analysis could provide evidence for this hypothesis. KEGG analyses revealed the

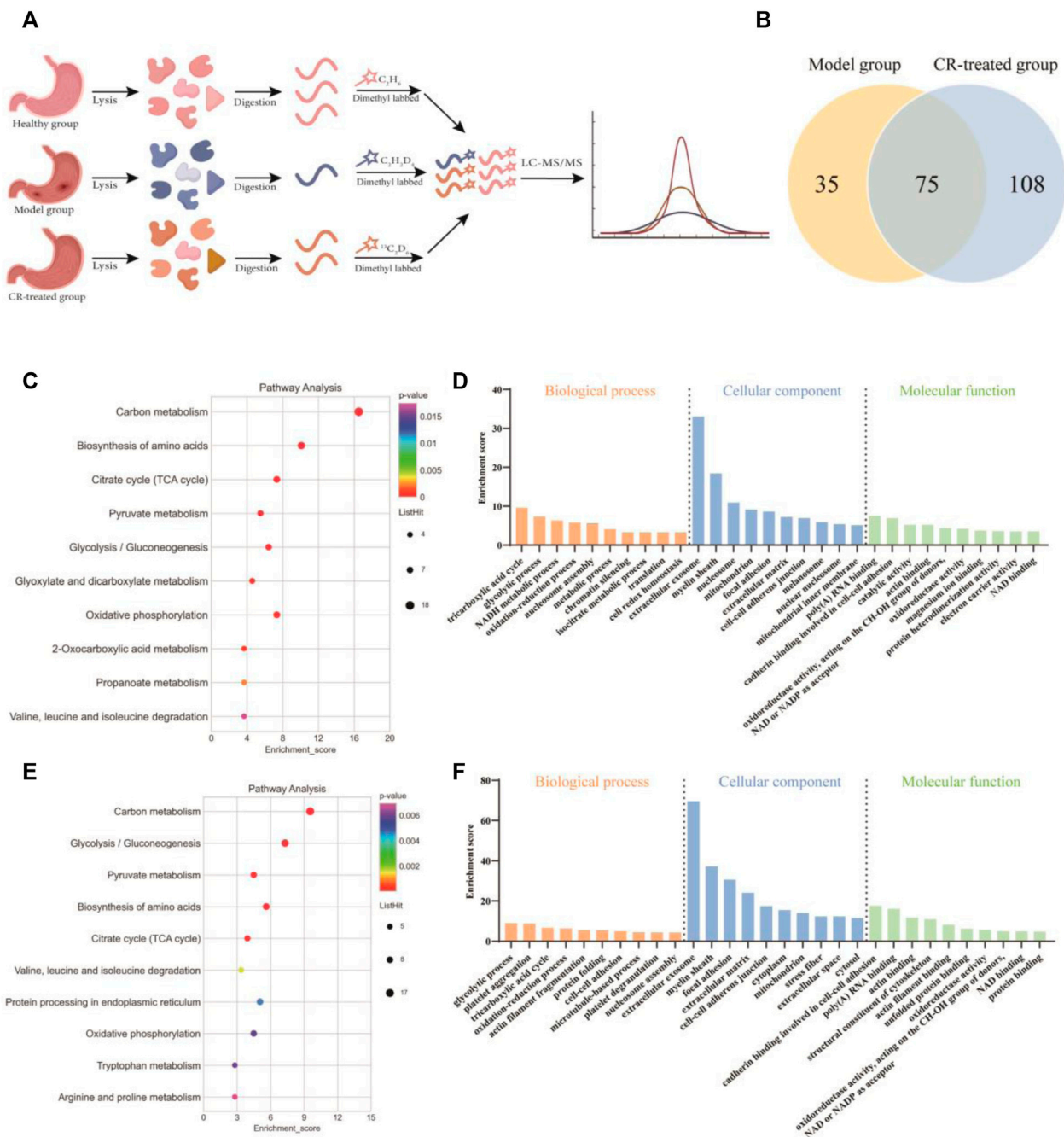


FIGURE 2 | Quantitative proteomics analysis of CR. **(A)** Schematic diagram of quantitative proteomics experiments. **(B)** Venn diagram showing the number of intervened proteins in the model group and CR-treated group. **(C,D)** Analysis of KEGG pathway and biological function (model group vs. healthy group) based on quantitative proteomics. **(E,F)** Analysis of KEGG pathway and biological function (CR-treated group vs. model group) based on quantitative proteomics.

top ten pathways. The metabolic pathway up-regulated in the model group which almost was down-regulated by CR, such as glycine, serine, and threonine metabolism, valine, leucine, and isoleucine biosynthesis, etc. (**Figures 3C–E**). After sorting out these metabolic pathways, we found that they are mainly some

metabolism and synthesis pathways of amino acids, which were highly related to glycolysis/gluconeogenesis and the citrate cycle. In summary, we believed that these amino acids were involved in the carcinogenesis of gastric epithelial cells as the material basis of energy metabolism.

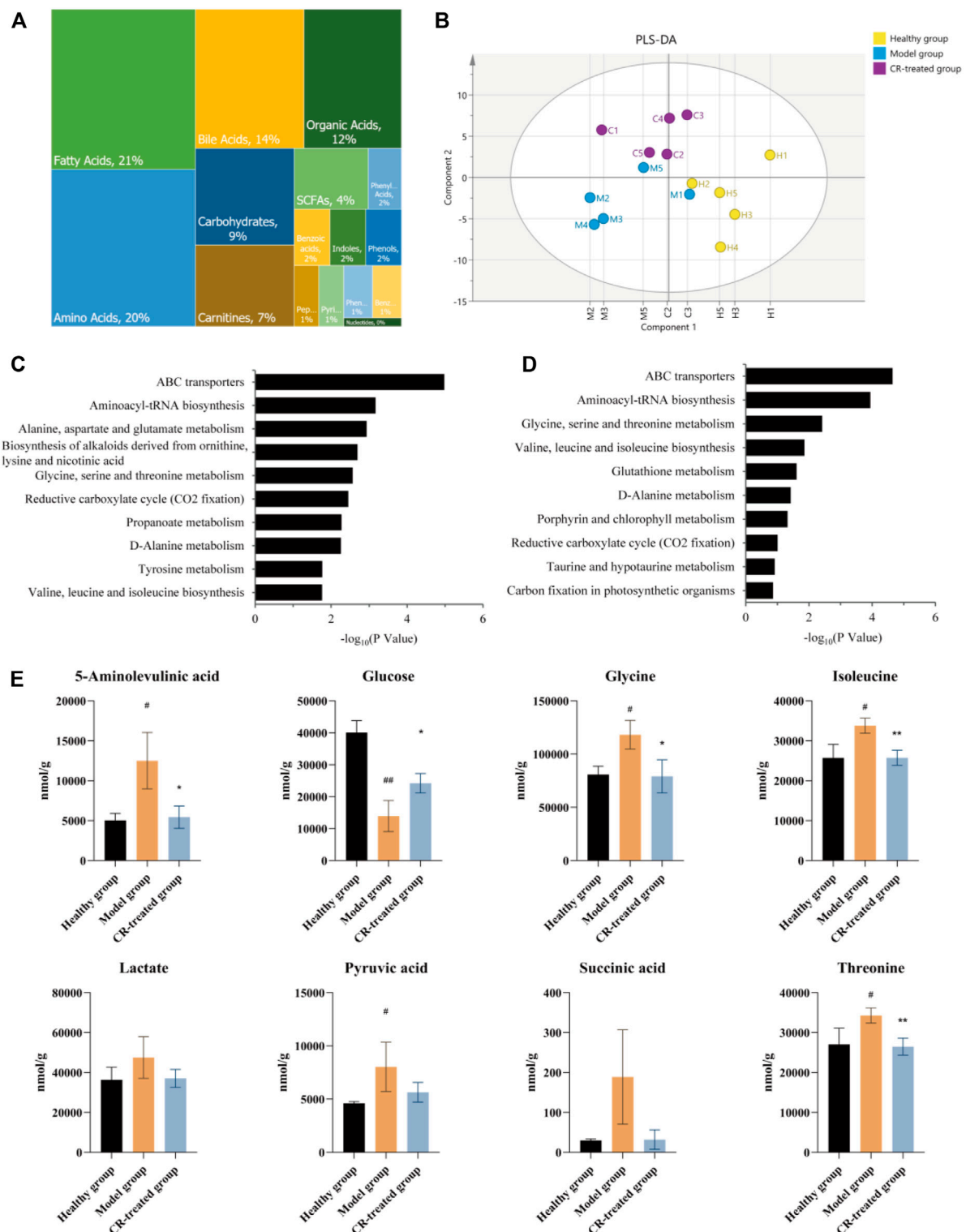


FIGURE 3 | Quantitative metabolomics analysis of CR. **(A)** Relative abundance of each metabolite class in 221 metabolites. **(B)** PLS-DA analysis in healthy group, model group and CR-treated group ($n = 5$). **(C)** Analysis of KEGG pathway (model group vs. healthy group) based on quantitative metabolomics. **(D)** Analysis of KEGG pathway (CR-treated group vs. model group) based on quantitative metabolomics. **(E)** CR intervention reverses the disturbed biomarkers of glycolysis and citrate cycle in GPL animal model. The graphs show the mean \pm SD in three independent experiments ($n = 5$). # $p < 0.05$ vs Healthy group. ## $p < 0.01$ vs Healthy group. * $p < 0.05$ and ** $p < 0.01$ vs Model group.

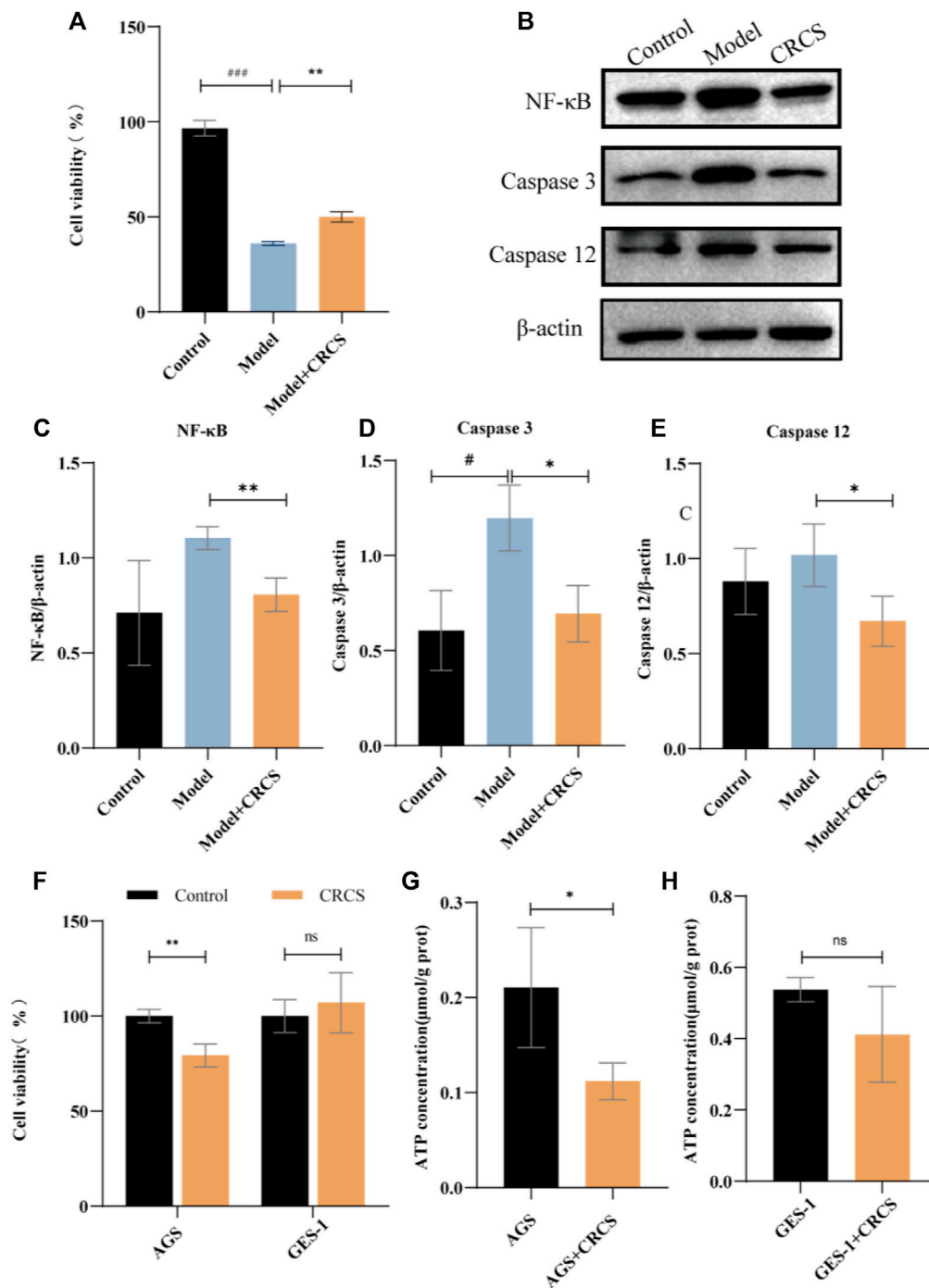


FIGURE 4 | CRCS's anti-inflammatory and anti-gastric-cancer effect on MNNG-induced GES-1 cells and AGS cells. **(A)** MTS assay of CRCS on MNNG-induced inflammatory GES-1 cells. **(B)** Western blots of inflammatory factors (NF-κB) and apoptosis factors (Caspase three and Caspase 12) in GES-1 cells (Control) and inflammatory GES-1 cells induced by MNNG (Model). **(C)** Western blotting analysis of NF-κB in inflammatory GES-1 cells treated with CRCS. **(D)** Western blotting analysis of Caspase three in inflammatory GES-1 cells treated with CRCS. **(E)** Western blotting analysis of Caspase nine in inflammatory GES-1 cells treated with CRCS. **(F)** MTS assay of CRCS's effects on AGS and GES-1 cells. **(G)** ATP contents in AGS cells treated with CRCS or not. **(H)** ATP contents in GES-1 cells treated with CRCS or not. β-actin served as the internal control in all Western blots. Data are presented as the mean ± SD, * $p < 0.05$, ** $p < 0.01$, *** $p < 0.001$, $n = 3$ per group.

Serum Pharmacology Confirmed That *Codonopsis pilosula* (Franch.) Nannf. Exerted Significant Anti-Inflammatory and Anti-Gastric-Cancer Effects in Inflammatory and Gastric Cancer Cell Lines

In order to further verify our hypothesis, we conducted gastritis cell models by MNNG-induced normal gastric epithelial cells (GES-1 cells) and gastric cancer cells (AGS) to simulate the possible anti-inflammatory and anti-cancer processes. And serum pharmacology was employed to illustrate CR's cellular phenotype. Our hypothesis was that the active ingredients of CR need to enter the blood to be effective, and CR-containing serum (CRCS) could act directly on relevant gastric cells. The results showed that CRCS had a protective effect on MNNG-induced inflammatory GES-1 cells (**Figure 4A**). Then western blot experiments were performed on MNNG-induced inflammatory GES-1 cells and the administration group (**Figure 4B**). As shown in quantification analysis, it could be seen that higher expression of NF- κ B protein in the model group could remarkably reduce after administration of CRCS (**Figure 4C**). Moreover, the intracellular apoptotic proteins in the model group were increased, such as Caspase-3 and Caspase-12, while those in the administration group were significantly decreased. (**Figures 4D,E**). In addition, CRCS presented inhibiting effect on gastric cancer cells (AGS cells), yet it was mild for normal gastric epithelial cells (GES-1 cells) (**Figure 4F**). So, we found the selective inhibiting effect of CRCS, which was consistent with animal experiments.

To further verify our hypothesis that CR could block the transformation of gastric cancer by reducing energy metabolism, we assayed ATP contents before and after administration of CRCS. The results showed that CRCS significantly reduced the energy in AGS cells but had little effect on GES-1 cells (**Figures 4G,H**). The above results are consistent with our results obtained by proteomics and metabolomics, indicating that regulating energy metabolism is an important way to prevent GPL.

DISCUSSION

Gastric cancer is the most important gastrointestinal cancer, and its high morbidity and mortality rate seriously endanger human health. At present, the main treatments for gastric cancer still present some shortcomings (Zong et al., 2016). Through an overview of the occurrence process of gastric cancer, we believe that blocking GPL may reduce the incidence and mortality of gastric cancer. Modern pharmacological research has shown that the pharmacological effects of *Codonopsis pilosula* (Franch.) Nannf. cover all stages of gastric cancer and precancerous lesions (Sui et al., 2005; Xu et al., 2008; Li et al., 2017; Bailly, 2021).

In this study, we employed traditional pharmacodynamics and serum pharmacology to evaluate the anti-GPL effects of CR. And quantitative proteomics and metabolomics were conducted to illustrate the mechanisms. First, we established a GPL rat model by MNNG combined with a disordered diet and alcohol drinking.

The results of pathological analyses proved that CR could significantly block the progress of GPL. Interestingly, in this study, the aggregation of a small number of mast cells was observed through HE-stained sections, and the number decreased after treatment with CR. Mast cells have been thought to be closely related to allergic reactions since they were discovered by Paul Ehrlich in 1878 (da Silva et al., 2014). Studies have shown that mast cells are related to the release of VEGF, FGF-2, TGF- β , IL-8, and Ang-1 (Crivellato et al., 2004). These angiogenesis-related factors could play a role in all stages of angiogenesis, including degradation of extracellular matrix, migration and proliferation of endothelial cells, and formation and distribution of new blood vessels (Patricia and Robert, 1987). Reducing mast cell aggregation might inhibit angiogenesis in tumors and chronic inflammation, which may be the potential pharmacological process.

According to the results of serum biochemical indicators, CR significantly regulated lactate dehydrogenase (LDH) and creatine kinase (CK). LDH is one of the rate-limiting enzymes in the carbohydrate metabolism pathway. LDH converts pyruvate into lactic acid during glycolysis, which is secreted out of the body by cells, and its increased content helps cancer cells obtain nutrients for growth and division through aerobic glycolysis (Koppenol et al., 2011; Xu et al., 2015). Based on the experimental results, we speculated that CR may reduce the content of LDH to promote the pyruvate of gastric cancer cells and other rapidly proliferating cells to enter the citrate cycle and reduce the production of lactic acid to increase the PH in the tumor microenvironment, which is not conducive to tumor cell invasion. Since CK mainly exists in the cytoplasm and mitochondria, it can affect the cell cycle process by regulating intracellular energy metabolism, which is closely related to the ATP homeostasis of cells (Zhou et al., 2016). However, the energy metabolism in GPL rats was in a compensatory active state, and the CK level is significantly increased. CR might regulate energy metabolism by inhibiting the aerobic glycolysis pathway of gastric cancer cells and fast-proliferating cells related to precancerous lesions. Therefore, we speculated that CR's anti-GPL efficacy was mainly related to the regulation of energy metabolism.

Protein is the carrier of cell or body function which reflects the process of function change. Metabolite is the final product of body function which reflects the result of function change. Proteomics and metabolomics have been widely used in the study of the pharmacodynamic mechanism by observing the changes in overall protein profile and metabolic profile at the system level and understanding the process and results of functional changes in organisms. To verify our hypothesis, quantitative proteomics and metabolomics were conducted to illustrate that GPL down-regulated energy metabolism, which might in turn affect the synthesis and metabolism of a variety of amino acids (**Figure 2F**; **Figure 3D**; **Supplementary Figure S3**). In addition, with serum pharmacology, we further verified that CR inhibited the proliferation of cancer cells via regulating energy metabolism (**Figures 4F–H**).

The proliferation of cancerous cells are closely related to glutamine and three other amino acids (glycine, serine, and methionine). Some studies have shown that glutamine intake is increased in many cancers such as pancreatic cancer, ovarian cancer, and breast cancer (Fan et al., 2013; Yang et al., 2014; van

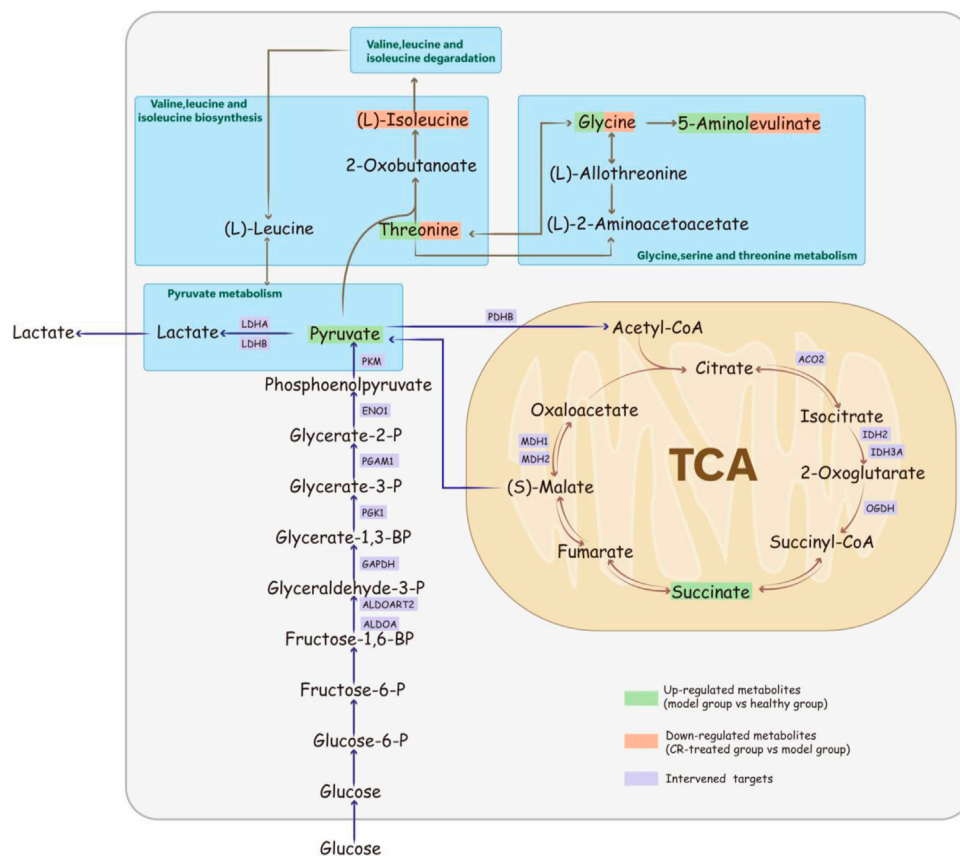


FIGURE 5 | Schematic diagram of *Codonopsis pilosula* (Franch.) Nannf. 's mechanism for suppressing GPL via the energy-related pathway.

Geldermalsen et al., 2016). This was also confirmed in clinical that plasma glutamine concentration of patients with different tumors is significantly lower than that of healthy subjects (Hamberger et al., 1991; Bode and Souba, 1999). Glycine and serine are involved in the synthesis and the conversion of one-carbon units. The one-carbon unit produces nucleotides, proteins, and lipids through the cycle of folate and methionine, which is an important source of substances for tumor cell growth (Locasale, 2013). In our metabolomic results, a variety of amino acid metabolism and synthesis pathways in the model group were up-regulated, including the synthesis materials of glutamine such as glutamic acid and isoleucine, the metabolism products of glutamine such as glutamic acid, aspartic acid, and pyruvate, the source of the one-carbon unit such as glycine and serine. It revealed that the metabolic cycle of glutamine and the formation of the one-carbon unit were closely related to the GPL model rats. In addition, it could also be seen in the proteomics results that CR had a certain regulatory effect on the synthesis and decomposition of various amino acids (Figures 2E, F). Therefore, we speculated that CR could inhibit the metabolic cycle of glutamine and the formation of the one-carbon unit, which reduces the growth of tumor cells.

Through the proteomics and metabolomics research on gastric tissue, we believe that the cancerous cells have changed the energy

metabolism-related pathways in order to grow and invade rapidly, preferring aerobic glycolysis to obtain the required energy and substances, resulting in the up-regulation of multiple amino acid metabolism and synthesis. CR down-regulates the related pathways of these amino acids and reduces their content, which may relate with treat GPL through energy metabolism.

CONCLUSION

In this study, we conducted a rat model to evaluate the anti-GPL effects of CR. Combining the proteomic and metabolomic analysis, we claimed that CR mainly through the regulation of glycolysis and tricarboxylic acid cycle and other processes, thereby affecting the energy metabolism of cancer cells to block the transformation of gastric cancer (Figure 5). In addition, we directly verified CR's anti-inflammatory and select tumor-inhibiting effects, which were closely related to cellular ATP. Thus, we claimed that CR could ameliorate inflammation and apoptosis via regulating energy metabolism pathways. This observation showed the pharmacodynamic mechanism of CR in suppressing GPL, which may provide a new perspective for exploring the mechanism of herbal medicine, especially traditional Chinese medicine. Regulating energy metabolism can provide a new strategy for early intervention of gastric cancer.

DATA AVAILABILITY STATEMENT

The original contributions presented in the study are included in the article/**Supplementary Material**; further inquiries can be directed to the corresponding authors.

ETHICS STATEMENT

The animal study was reviewed and approved by the ethics committee of Lanzhou University.

AUTHOR CONTRIBUTIONS

JD, FH, and FY designed the research; RH and RM performed experiments, analyzed data, wrote the manuscript, and critically edited the manuscript. ZJ and YZ performed partial experiments and analyzed data. JD supervised the research work. All authors read and approved the final manuscript.

REFERENCES

- Al-Batran, S. E., Hofheinz, R. D., Pauligk, C., Kopp, H. G., Haag, G. M., Luley, K. B., et al. (2016). Histopathological Regression after Neoadjuvant Docetaxel, Oxaliplatin, Fluorouracil, and Leucovorin versus Epirubicin, Cisplatin, and Fluorouracil or Capecitabine in Patients with Resectable Gastric or Gastro-Oesophageal Junction Adenocarcinoma (FLOT4-AIO): Results from the Phase 2 Part of a Multicentre, Open-Label, Randomised Phase 2/3 Trial. *Lancet Oncol.* 17 (12), 1697–1708. doi:10.1016/s1473-2045(16)30531-9
- Bai, R., Zhang, Y., Jia, X., Fan, J., Hou, X., Wang, Y., et al. (2020). Isolation, Characterization and Immunomodulatory Activity of Oligosaccharides from *Codonopsis Pilosula*. *J. Funct. Foods* 72, 104070. doi:10.1016/j.jff.2020.104070
- Bailly, C. (2021). Anticancer Properties of Lobetyolin, an Essential Component of *Radix Codonopsis* (Dangshen). *Nat. Prod. Bioprospect* 11 (2), 143–153. doi:10.1007/s13659-020-00283-9
- Benjamin, D. I., Cravatt, B. F., and Nomura, D. K. (2012). Global Profiling Strategies for Mapping Dysregulated Metabolic Pathways in Cancer. *Cell Metab.* 16 (5), 565–577. doi:10.1016/j.cmet.2012.09.013
- Bode, B. P., and Souba, W. W. (1999). Glutamine Transport and Human Hepatocellular Transformation. *JPEN J. Parenter. Enter. Nutr.* 23 (5 Suppl. 1), S33–S37. doi:10.1177/014860719902300509
- Boerema, P. J., Raijmakers, R., Lemeer, S., Mohammed, S., and Heck, A. J. (2009). Multiplex Peptide Stable Isotope Dimethyl Labeling for Quantitative Proteomics. *Nat. Protoc.* 4 (4), 484–494. doi:10.1038/nprot.2009.21
- Cai, J., Wang, H., Zhou, S., Wu, B., Song, H. R., and Xuan, Z. R. (2008). Effect of Sijunzi Decoction and Enteral Nutrition on T-Cell Subsets and Nutritional Status in Patients with Gastric Cancer after Operation: a Randomized Controlled Trial. *Zhong Xi Yi Jie He Xue Bao.* 6(1), 37–40. doi:10.3736/jcim20080108
- Chunxia, Y., Yuqiang, G., Chen, J., An, J., Chen, W., and Hu, F. (2013). Structural Characterization and Antitumor Activity of a Pectic Polysaccharide from *Codonopsis Pilosula*. *Carbohydr. Polym.* 98 (1), 886–895. doi:10.1016/j.carbpol.2013.06.079
- Correa, P., Haenszel, W., Cuello, C., Tannenbaum, S., and Archer, M. (1975). A Model for Gastric Cancer Epidemiology. *Lancet* 2 (7924), 58–60. doi:10.1016/s0140-6736(75)90498-5
- Crivellato, E., Beltrami, C. A., Mallardi, F., and Ribatti, D. (2004). The Mast Cell: an Active Participant or an Innocent Bystander? *Histol. Histopathol.* 19 (1), 259–270. doi:10.14670/hh-19.259

FUNDING

This work was financially supported by the National Key Research and Development Program of China (2018YFC1706300 and 2018YFC17063005), the Science and Technology Planning Project of Gansu Province (20JR10RA586), the Fundamental Research Funds for the Central Universities (lzujbky-2021-kb40), and the Project for Longyuan Youth Innovation and Entrepreneurship Talent.

ACKNOWLEDGMENTS

The authors thank Metabo-Profile Inc. for their service in Quantitative Metabolomics.

SUPPLEMENTARY MATERIAL

The Supplementary Material for this article can be found online at: <https://www.frontiersin.org/articles/10.3389/fphar.2022.933096/full#supplementary-material>

- da Silva, E. Z., Jamur, M. C., and Oliver, C. (2014). Mast Cell Function: a New Vision of an Old Cell. *J. Histochem Cytochem* 62 (10), 698–738. doi:10.1369/0022155414545334
- Deswaerte, V., Nguyen, P., West, A., Browning, A. F., Yu, L., Ruwanpura, S. M., et al. (2018). Inflammasome Adaptor ASC Suppresses Apoptosis of Gastric Cancer Cells by an IL18-Mediated Inflammation-independent Mechanism. *Cancer Res.* 78 (5), 1293–1307. doi:10.1158/0008-5472.CAN-17-1887
- Duarte, H. O., Gomes, J., Machado, J. C., and Reis, C. A. (2018). Gastric Cancer: Basic Aspects. *Helicobacter* 23 Suppl 1 (Suppl. 1), e12523. doi:10.1111/hel.12523
- Fan, J., Kamphorst, J. J., Mathew, R., Chung, M. K., White, E., Shlomi, T., et al. (2013). Glutamine-driven Oxidative Phosphorylation Is a Major ATP Source in Transformed Mammalian Cells in Both Normoxia and Hypoxia. *Mol. Syst. Biol.* 9, 712. doi:10.1038/msb.2013.65
- Hamberger, A., Nyström, B., Larsson, S., Silfvenius, H., and Nordborg, C. (1991). Amino Acids in the Neuronal Microenvironment of Focal Human Epileptic Lesions. *Epilepsy Res.* 9 (1), 32–43. doi:10.1016/0920-1211(91)90044-g
- Hong, X. C., Liang, Q. L., Luo, X. B., Hu, K. H., Yang, H. X., Ou, W. T., et al. (2020). Clinical Study of XiangShaLiuJunZi Decoction Combined with S-1 as Maintenance Therapy for Stage III or IV Gastric Carcinoma and Colorectal Carcinoma. *Med. Baltim.* 99 (19), e20081. doi:10.1097/md.00000000000020081
- Kim, D. J., Park, C. B., Lee, J. S., Tsuda, H., and Furihata, C. (1999). Enhanced Quinone Reductase (QR) Activity Correlates with Promotion Potential of Diethyl Maleate (DEM) in Rat Forestomach and Glandular Stomach Carcinogenesis Initiated with N-Methyl-N'-Nitrosoguanidine (MNNG). *Cancer Lett.* 137 (2), 193–200. doi:10.1016/s0304-3835(98)00358-9
- Kolaric, K., Potrebica, V., and Stanovnik, M. (1986). Controlled Phase III Clinical Study of 4-Epi-Doxorubicin + 5-fluorouracil versus 5-fluorouracil Alone in Metastatic Gastric and Rectosigmoid Cancer. *Oncology* 43 (2), 73–77. doi:10.1159/000226337
- Koppenol, W. H., Bounds, P. L., and Dang, C. V. (2011). Otto Warburg's Contributions to Current Concepts of Cancer Metabolism. *Nat. Rev. Cancer* 11 (5), 325–337. doi:10.1038/nrc3038
- Li, J., Wang, T., Zhu, Z., Yang, F., Cao, L., and Gao, J. (2017). Structure Features and Anti-gastric Ulcer Effects of Inulin-type Fructan CP-A from the Roots of *Codonopsis Pilosula* (Franch.) Nannf. *Molecules* 22 (12), 2258. doi:10.3390/molecules22122258
- Locasale, J. W. (2013). Serine, glycine and One-Carbon Units: Cancer Metabolism in Full Circle. *Nat. Rev. Cancer* 13 (8), 572–583. doi:10.1038/nrc3557
- Lv, L., Wang, F. Y., Ma, X. X., Li, Z. H., Huang, S. P., Shi, Z. H., et al. (2017). Efficacy and Safety of Xiangsha Liujunzi Granules for Functional Dyspepsia: A Multi-

- Center Randomized Double-Blind Placebo-Controlled Clinical Study. *World J. Gastroenterol.* 23 (30), 5589–5601. doi:10.3748/wjg.v23.i30.5589
- Ma, F. L., Shen, X. M., and Shi, J. (2014). Effect of Codonopsis Polysaccharide on Gastrointestinal Tract of Experimental Rats and Mice. *Anhui Med. Pharm. J.* 18 (09), 1626–1630. doi:10.3969/j.issn.1009-6469.2014.09.005
- Maeda, S., Akanuma, M., Mitsuno, Y., Hirata, Y., Ogura, K., Yoshida, H., et al. (2001). Distinct Mechanism of Helicobacter Pylori-Mediated NF-Kappa B Activation between Gastric Cancer Cells and Monocytic Cells. *J. Biol. Chem.* 276 (48), 44856–44864. doi:10.1074/jbc.M105381200
- Patel, J. N., Jiang, C., Owzar, K., Mulkey, F., Luzum, J. A., Mamon, H. J., et al. (2021). Pharmacogenetic Study in Gastric Cancer Patients Treated with Adjuvant Fluorouracil/leucovorin or Epirubicin/cisplatin/fluorouracil before and after Chemoradiation on CALGB 80101 (Alliance). *Pharmacogenet Genomics* 31 (9), 215–220. doi:10.1097/fpc.0000000000000442
- Patricia, A., and Robert, W. (1987). Mechanisms of Angiogenesis. *Ann. Rev. Physiol.* 49 (4), 53–64. doi:10.1146/annurev.ph.49.030187.002321
- Perez-Riverol, Y., Bai, J., Bandla, C., García-Seisdedos, D., Hewapathirana, S., Kamatchinathan, S., et al. (2022). The PRIDE Database Resources in 2022: a Hub for Mass Spectrometry-Based Proteomics Evidences. *Nucleic Acids Res.* 50 (D1), D543–d552. doi:10.1093/nar/gkab1038
- Song, D., Wang, Z. T., Li, L. Y., and Zhong, G. Y. (2008). Protective Effect of Lobetyolin on Gastric Mucosa of Experimental Gastric Ulcer in Rats. *JETCM* 07, 963–964+986.
- Sui, F., Wang, R., Wang, J., Li, Y., Du, Q., and Wu, Y. (2005). Effects of Dangshen Root Extract Serum on Intracellular Free Calcium in Gastric Parietal Cells of Dissociated Rats. *Zhong Yao Cai* 28 (10), 900–903.
- van Geldermalsen, M., Wang, Q., Nagarajah, R., Marshall, A. D., Thoeng, A., Gao, D., et al. (2016). ASCT2/SLC1A5 Controls Glutamine Uptake and Tumour Growth in Triple-Negative Basal-like Breast Cancer. *Oncogene* 35 (24), 3201–3208. doi:10.1038/onc.2015.381
- Wang, J., Ni, Z., Duan, Z., Wang, G., and Li, F. (2014). Altered Expression of Hypoxia-Inducible Factor-1 α (HIF-1 α) and its Regulatory Genes in Gastric Cancer Tissues. *PLoS One* 9 (6), e99835. doi:10.1371/journal.pone.0099835
- Wang, T., Ge, R., yang, F., and Gao, J. P. (2015). Protection of the Extract of Codonopsis Pilosula on Rat Gastric Mucosal Injury. *Pharmacol. Clin. Chin. Materia Medica* 31 (04), 138–141. doi:10.13412/j.cnki.zyyl.2015.04.043
- Wang, Z. T., Du, Q., Xu, G. J., Wang, R. J., Fu, D. Z., and Ng, T. B. (1997). Investigations on the Protective Action of Condonopsis Pilosula (Dangshen) Extract on Experimentally-Induced Gastric Ulcer in Rats. *Gen. Pharmacol.* 28 (3), 469–473. doi:10.1016/s0306-3623(96)00047-x
- Xia, P., He, H., Ma, R., Feng, X. M., and Wei, B. (2021). Effects of Shenqi Xiaopi Decoction on the Repair of Gastric Mucosa and the Mechanism of Angiogenesis in the Prophase of Chronic Atrophic Gastritis and the Related Effects of Serum P53, MDA and GSH-Px. *Chin. J. Integr. Trad. West Med. Dig.* 29 (01), 19–23.
- Xie, G., Wang, L., Chen, T., Zhou, K., Zhang, Z., Li, J., et al. (2021). A Metabolite Array Technology for Precision Medicine. *Anal. Chem.* 93 (14), 5709–5717. doi:10.1021/acs.analchem.0c04686
- Xu, L. P., Wang, H., and Yuan, Z. (2008). Triterpenoid Saponins with Anti-inflammatory Activity from Codonopsis Lanceolata. *Planta Med.* 74 (11), 1412–1415. doi:10.1055/s-2008-1081318
- Xu, X. D., Shao, S. X., Jiang, H. P., Cao, Y. W., Wang, Y. H., Yang, X. C., et al. (2015). Warburg Effect or Reverse Warburg Effect? A Review of Cancer Metabolism. *Oncol. Res. Treat.* 38 (3), 117–122. doi:10.1159/000375435
- Yang, L., Moss, T., Mangala, L. S., Marini, J., Zhao, H., Wahlig, S., et al. (2014). Metabolic Shifts toward Glutamine Regulate Tumor Growth, Invasion and Bioenergetics in Ovarian Cancer. *Mol. Syst. Biol.* 10, 728. doi:10.1002/msb.20134892
- Yang, Z. H., and Zhou, H. L. (2022). Effects of Codonopsis Pilosum Polysaccharide on the Proliferation, apoptosis and Expression of Inflammatory Factors in Gastric Cancer Cells AGS by Regulating miR-361-5p/TLR4/NF-Kb Pathway. *Immunol. J.* 38 (04), 347–353. doi:10.13431/j.cnki.immunol.j.20220048
- Zhang, J., and Wang, H. (2019). Morroniside Protects against Chronic Atrophic Gastritis in Rat via Inhibiting Inflammation and Apoptosis. *Am. J. Transl. Res.* 11 (9), 6016–6023.
- Zhong, W. R., Huang, Y. X., and Cui, J. P. (1997). Clinical Study on Modified Sijunzi Decoction in Treating Intestinal Metaplasia of Gastric Mucosa. *Zhongguo Zhong Xi Yi Jie He Za Zhi* 17 (8), 462–464.
- Zhou, D. Q., Gong, L., and Qian, Z. Y. (2016). Physiological Function of Creatine Kinase and Sport. *J. Anqing Teach. Coll. Nat. Sci. Ed.* 22 (03), 113–118. doi:10.1016/S0140-6736(16)32226-7
- Zong, L., Abe, M., Seto, Y., and Ji, J. (2016). The Challenge of Screening for Early Gastric Cancer in China. *Lancet* 388 (10060), 2606. doi:10.1016/s0140-6736(16)32226-7

Conflict of Interest: The authors declare that the research was conducted in the absence of any commercial or financial relationships that could be construed as a potential conflict of interest.

Publisher's Note: All claims expressed in this article are solely those of the authors and do not necessarily represent those of their affiliated organizations, or those of the publisher, the editors, and the reviewers. Any product that may be evaluated in this article, or claim that may be made by its manufacturer, is not guaranteed or endorsed by the publisher.

Copyright © 2022 He, Ma, Jin, Zhu, Yang, Hu and Dai. This is an open-access article distributed under the terms of the Creative Commons Attribution License (CC BY). The use, distribution or reproduction in other forums is permitted, provided the original author(s) and the copyright owner(s) are credited and that the original publication in this journal is cited, in accordance with accepted academic practice. No use, distribution or reproduction is permitted which does not comply with these terms.



OPEN ACCESS

EDITED BY

Haitao Lu,
Shanghai Jiao Tong University, China

REVIEWED BY

Jian-Bo Wan,
University of Macau, China
Xiaohui Fan,
Zhejiang University, China
Zhisheng Wu,
Beijing University of Chinese Medicine,
China

*CORRESPONDENCE

Wei Zhou,
zhouweisyl802@163.com
Yue Gao,
gaoyue@bmi.ac.cn

[†]These authors have contributed equally to this work

SPECIALTY SECTION

This article was submitted to
Ethnopharmacology,
a section of the journal
Frontiers in Pharmacology

RECEIVED 25 February 2022

ACCEPTED 27 June 2022

PUBLISHED 15 August 2022

CITATION

Wang N-n, Zhang X-x, Shen P,
Huang C-s, Deng H-f, Zhou L, Yue L-x,
Shen B-y, Zhou W and Gao Y (2022),
Pinelliae rhizoma alleviated acute lung
injury induced by lipopolysaccharide via
suppressing endoplasmic reticulum
stress-mediated NLRP3 inflammasome.
Front. Pharmacol. 13:883865.
doi: 10.3389/fphar.2022.883865

COPYRIGHT

© 2022 Wang, Zhang, Shen, Huang,
Deng, Zhou, Yue, Shen, Zhou and Gao.
This is an open-access article
distributed under the terms of the
[Creative Commons Attribution License](#)
(CC BY). The use, distribution or
reproduction in other forums is
permitted, provided the original
author(s) and the copyright owner(s) are
credited and that the original
publication in this journal is cited, in
accordance with accepted academic
practice. No use, distribution or
reproduction is permitted which does
not comply with these terms.

Pinelliae rhizoma alleviated acute lung injury induced by lipopolysaccharide via suppressing endoplasmic reticulum stress-mediated NLRP3 inflammasome

Ning-ning Wang^{1,2†}, Xian-xie Zhang^{2†}, Pan Shen^{2†},
Cong-shu Huang^{1,2}, Hui-fang Deng², Lei Zhou^{2,3}, Lan-xin Yue²,
Bao-ying Shen^{2,3}, Wei Zhou^{2*} and Yue Gao^{1,2*}

¹Tianjin University of Traditional Chinese Medicine, Tianjin, China, ²Department of Pharmaceutical Sciences, Beijing Institute of Radiation Medicine, Beijing, China, ³Guangdong Pharmaceutical University, Guangzhou, China

Pinelliae rhizoma (PR), one kind of commonly-used Chinese herbs, is generally prescribed to treat various respiratory diseases, including acute lung injury (ALI). However, the accurate bioactive ingredients of PR and the underlying pharmacological mechanism have both not been fully elucidated. Therefore, this study aimed to identify the bioactive ingredients that could alleviate lipopolysaccharide (LPS)-induced ALI and explore the possible mechanism involved. Our results confirmed that LPS infection indeed caused acute inflammatory damage in mice lung, accompanying with the enhancement of IL-1 β contents and the activation of the NLRP3 inflammasome in lung tissue and macrophagocyte, all of which were remarkably ameliorated by PR treatment. Next, mechanistically, LPS was found to trigger endoplasmic reticulum (ER) stress and downstream cellular calcium ions (Ca²⁺) release via activating Bip/ATF4/CHOP signaling pathway. Like PR, 4-PBA (a specific inhibitor of ER stress) not only obviously reversed Bip/ATF4/CHOP-mediated ER stress, but also significantly attenuated LPS-induced activation of the NLRP3 inflammasome. Furthermore, the bioactive ingredients of PR, which generated the anti-inflammatory effects, were screened by metabolomics and network pharmacology. *In vitro* experiments showed that chrysin, dihydrocapsaicin, and 7,8-dihydroxyflavone (7,8-DHF) notably suppressed LPS-induced ER

Abbreviations: 2-APB, 2-aminoethyl diphenylborinate; 4-PBA, sodium 4-phenylbutyrate; 7,8-DHF, 7,8-dihydroxyflavone; ALI, acute lung injury; ARDS, acute respiratory distress syndrome; ATF4, activating transcription factor (ATF)-4; Ca²⁺, calcium ions; CHOP, C/EBP homologous protein; COVID-19, coronavirus disease 2019; DHC, dihydrocapsaicin; ER, endoplasmic reticulum; GRP78, glucoseregulated protein 78; IL-1 β , interleukin-1 β ; IRE α , inositol-requiring enzyme 1 α ; LPS, lipopolysaccharide; NF- κ B, nuclear factor kappa-B; NLRP3, nucleotide-binding domain, leucine-rich repeat-containing receptor, pyrin domain-containing 3; PERK, protein kinase (PKR)-like ER kinase; PR, *Pinelliae rhizoma*; SARS-CoV-2, severe acute respiratory syndrome coronavirus 2; TCM, traditional Chinese medicine; UPR, unfolded protein response.

stress and following NLRP3 inflammasome activation. In conclusion, our findings suggested that PR alleviated LPS-induced ALI by inhibiting ER stress-mediated NLRP3 inflammasome activation, which is mainly relevant with these three bioactive ingredients. This study provided a theoretical basis for the clinical application of PR to treat ALI, and these bioactive ingredients of PR would be promising therapeutic drugs for the treatment of ALI.

KEYWORDS

Pinelliae rhizoma, acute lung injury, NLRP3 inflammasome, metabolomics, endoplasmic reticulum stress

Introduction

The global pandemic of severe acute respiratory syndrome coronavirus 2 (SARS-CoV-2) causes numerous severe pneumonia (named coronavirus disease 2019, COVID-19) and death, both of which are associated with SARS-CoV-2 induced acute lung injury (ALI) or its wilder form, acute respiratory distress syndrome (ARDS) (Habashi et al., 2021). Several Traditional Chinese Medicine (TCM) formulas have been reported to perform well against progressing to severe or critical COVID-19, largely because these prescriptions generated immune regulatory effects to prevent ALI or further ARDS (Huang et al., 2021). Of these TCM formulas used for the treatment of COVID-19, five kinds of herbs were documented as clinical commonly-used Chinese medicinal materials to treat and prevent various pulmonary diseases, including *Glycyrrhiza uralensis* Fisch ex DC. [Fabaceae], *Scutellaria baicalensis* Georgi [Lamiaceae], *Pinellia ternata* (Thunb.) Makino [Araceae], *Forsythia suspensa* (Thunb.) Vahl [Oleaceae], and *Semen Armeniacae Amarum* [Rosaceae] (Xiong et al., 2020; Luo et al., 2022). In particular, for its excellent efficacy in the therapy of chronic obstructive pulmonary disease (COPD), asthma, and respiratory tract infections, *Pinelliae rhizoma* (PR) has been widely used in many East Asian countries (Du et al., 2016; Hu et al., 2019). Growing studies are paying attention to the material basis and mechanism involved in the treatment of ALI using PR.

In general, ALI is considered to be an adverse outcome of immunological responses to bacterial or viral agents' infection, in addition to the key event in deciding deterioration of diseases (Mokra, 2020). Next, pathologically, ALI is characterized by elevated alveolar permeability and protein-rich edema, both of which are always caused by hyper-activated pro-inflammatory responses and following tissue damage (Kumar, 2020). Hence, it's not difficult to spot that controlling inflammatory injury would be the crux of ALI therapy. Previous studies found that PR exerts protective effects *via* attenuating allergic airway inflammation and mucus excessive secretion in asthma murine models and also relieves chronic airway inflammation in rats with COPD (Lee et al., 2013; Lyu et al., 2020). Moreover, Tang X et al. reported that the combination of PR or its bioactive ingredient (β -sitosterol) with another herb indeed decreased the

contents of inflammatory factors and ameliorated lung injury in lipopolysaccharide (LPS)-infected rat (Tang et al., 2018). However, the molecular mechanisms underlying PR-generated anti-inflammatory effects during the therapy of ALI are not fully elucidated. Besides, accumulating evidence demonstrated that PR contains plenty of bioactive ingredients, for example, alkaloids, anthraquinone glycosides, and their derivatives (Mao and He, 2020). Therefore, an urgent need also exists to identify the bioactive ingredients of PR that are associated with ALI treatment.

NF- κ B signaling and the downstream nucleotide-binding oligomerization domain, leucine-rich repeat, and pyrin domain-containing 3 (NLRP3) inflammasome act as the core modulators that mediate the outbursts of pro-inflammatory cytokines, including IL-1 β , TNF- α , and IL-18, and subsequent cell death during the over-activated inflammatory process of ALI (He et al., 2016). In recent times, endoplasmic reticulum (ER) stress, a cellular response to ensure proteins fold correctly, was initiated upon sensing LPS or virus infection to participate in the occurrence and development of ALI by regulating immunological recognition, macrophage activation, and alveolar endothelial function (Hrincius et al., 2015; Zhang et al., 2018; Zhao et al., 2020). Next, typically, the activation of ER stress triggers unfolded protein response (UPR) to restore cellular homeostasis (Kim et al., 2015) and programmed apoptosis *via* C/EBP homologous protein (CHOP) once protein misfolding occurs beyond repair capacity (Delbrel et al., 2018). Besides, over-activation of ER stress causes the cytoplasmic release of calcium ions from ER, resulting in the activation of the NLRP3 inflammasome and mitochondrial dependent death (Li et al., 2020; Mishra et al., 2021). Latest studies also showed that the cross-talk between ER stress and IKK β /NF- κ B signaling cascade was relevant to many pathological events, for instance, energy imbalance, autophagy, and apoptosis (Zhu et al., 2017; Lee et al., 2021). Thus, the interplay among ER stress and these pro-inflammatory signals would promote and exacerbate ALI. However, whether ER stress is targeted by bioactive ingredients of PR during ALI treatment remains unknown.

Here, we speculate that PR may alleviate lung injury *via* inhibiting ER stress-mediated pro-inflammatory responses. In this study, we confirmed that PR treatment alleviated LPS-

induced ALI *in vivo* and *in vitro*, and we also identified the relevant bioactive ingredients by metabolomics. Next, mechanistically, PR and these bioactive ingredients provided relief from acute inflammatory injuries mainly by inhibiting ER stress-mediated NLRP3 inflammasome, which could be a novel therapeutic target for ALI. The flow chart of the research process is shown in [Figure 1](#).

Materials and methods

Chemicals and reagents

LPS (L8880, HPLC \geq 99%, China), 7,8-dihydroxyflavone (7,8-DHF, CAS: 38183038, HPLC \geq 98%), and dihydrocapsaicin (DHC, CAS:19408845, HPLC \geq 98%) were obtained from Beijing Solarbio Science & Technology Co. Ltd. Chrysin (CAS: 480400, HPLC \geq 98%), 2-aminoethoxydiphenyl borate (2-APB, #9754, HPLC \geq 97%), Phosphate Buffered Saline, and formic acid (LC-MS grade) were all purchased from Sigma-Aldrich (Merck, United States). Next, Sodium 4-phenylbutyrate (4-PBA, T1535, HPLC \geq 99%) was purchased from Topscience Co. Ltd. Sodium chloride injection was obtained from Shijiazhuang NO.4 Pharmaceutical Co. Ltd., (Shijiazhuang, China). Methanol (LC-MS grade) and acetonitrile (LC-MS grade) were obtained from CNW Technologies (Shanghai, China). 2-Chloro-L-phenylalanine (\geq 98%, HPLC) was purchased from Hengbai Co. Ltd. (Shanghai, China), and other reagents were HPLC grade.

Anti-IL-1 β (511369) and anti-Caspase-1 (342947) were purchased from Zen-bioscience Biotechnology Co. Ltd. (Chengdu, China). Anti-NLRP3 (ab263899) was obtained from Abcam (Cambridge, MA, United States). Anti-ASC/TMS1 (67824), anti-Bip (3177), anti-ATF4 (11815), anti-IKK β (8943), anti-phospho-I κ B α (14D4), anti-I κ B α (L35A5), anti-phospho-NF- κ B p65 (93H1), anti-NF- κ B p65 (8242), and anti-GAPDH (5174) were all obtained from Cell Signaling Technology (Beverly, MA, United States). Anti-ALOX12 (A02275) was purchased from Boster Biological Technology Co. Ltd. (Wuhan, China). Anti-CHOP (15204) and anti-TRPV1 (66983) were obtained from Proteintech (Wuhan, China).

Preparation of the *Pinelliae rhizoma* aqueous extract

PR used in this study was *Pinelliae rhizoma Praeparatum Cum Alumine*, the processed product of the dried rhizome of *Pinellia ternata* (Thunb.) Makino [Araceae], and it was purchased from Minghui-Hengtong Pharmaceutical Co. Ltd. (LOT NO.: 20030102, Beijing, China). Professor Yan Jin, National Resource Center for Chinese Materia Medica authenticated the PR according to the Pharmacopeia of the

People's Republic of China (2020, volume I). The extraction procedures of PR used for *in vivo* experiments are as follows: PR (50 g) was immersed in distilled water (1 L) for 30 min, followed by boiling and decocting twice for 30 min each time. All decoctions were combined, and the extracts were filtered through a Buchner funnel. For *in vivo* experiments, the filtrates were concentrated under reduced pressure to 500 mg/ml at 60–70°C and stored at –20°C. For *in vitro* experiments, the filtrates were freeze-dried to obtain a dry fluffy powder (the drug extract ratio based on the mass was 6.5 g: 50 g) and stored at –20°C. In addition, we also carried out quality control of PR extract samples and listed the peaks of major ingredients of PR. Researchers identified by mass spectrometry that the water extract of PR contains succinate, adenine, ferulic acid, baicalein, and coumarin. For detailed data, please refer to [Supplementary Data Sheet S1](#) and [Supplementary Table S3](#).

Instruments

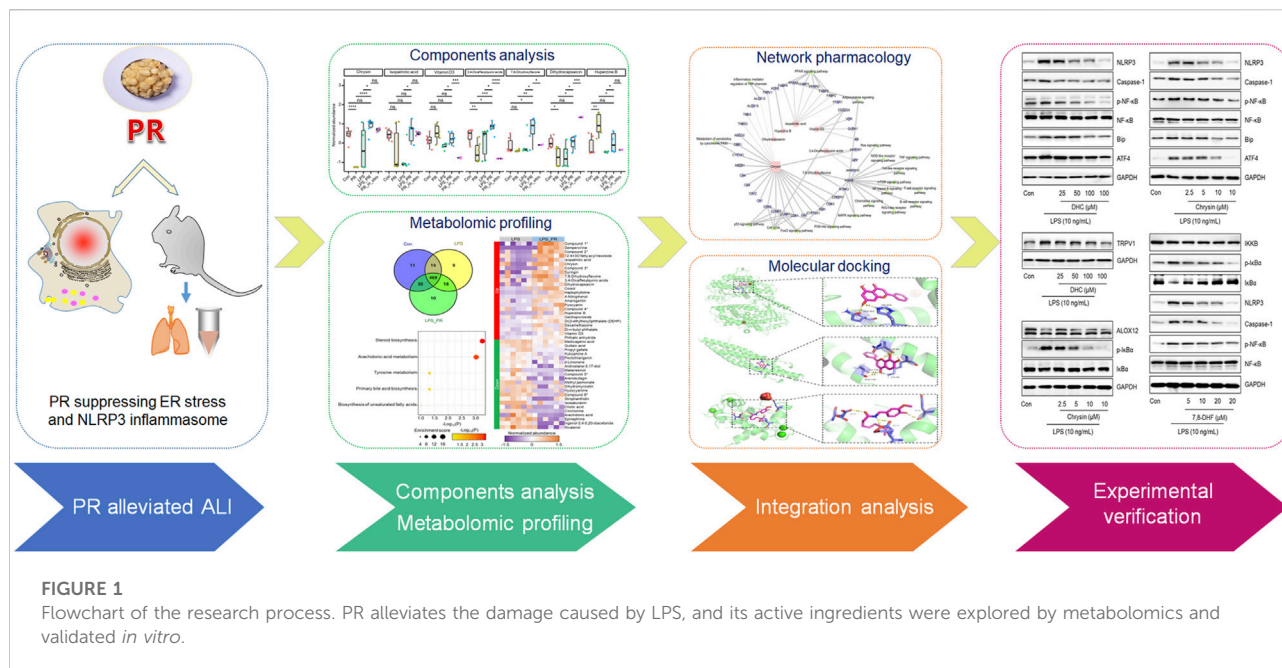
UHPLC system (Vanquish, Thermo Fisher Scientific, United States); Chromatographic column (ACQUITY UPLC BEH C18 (1.7 μ m 2.1*100 mm), Waters, United States); High resolution mass spectrum (Orbitrap Exploris 120, Thermo Fisher Scientific, United States); Analytical Balance (Mettler Toledo, Swiss); High-throughput tissue grinder (Shanghai, China); Pure water filter (Merck Millipore, United States); Ultrasonic cleaner (Fangao Co., Ltd., Shenzhen, China); CO₂ incubator (ThermoFisher, United States); Multifunctional enzyme marker (PerkinElmer, United States); Ultra low temperature refrigerator (Haier, China).

Cell culture and treatments

RAW264.7 cells were obtained from the National Infrastructure of Cell Line Resource. Cells were grown in DMEM medium (Gibco, ThermoFisher Scientific, United States) containing FBS (10%) and penicillin-streptomycin (1%). Next, RAW264.7 cells were cultured in a cell incubator at 37°C with 5% CO₂. When the cell density reached 80%, drug treatment was performed.

Animals and experimental design

C57BL/6 mice (8–10 weeks) were ordered from Beijing Vital River Laboratory Animal Technology (Beijing, China). Mice were kept in standard laboratory with unlimited access to standard diet and water. They were randomly divided into five groups ($n = 6$): control group, LPS-stimulated model group, PR-low dosage groups (1 g/kg/day), PR-medium dosage groups (2 g/kg/day), and PR-high dosage groups (4 g/kg/day). The Pharmacopeia of the People's



Republic of China (2020, volume I) stipulates that the maximum dose of PR is 9 g per person per day. According to the dose conversion guideline between mice and human stipulated by the FDA (Reagan-Shaw et al., 2008), the dose of PR administered in mice was 2 g/kg/d, so the low dose (1 g/kg/d) and high dose (4 g/kg/d) were 0.5 times and 2 times that of the middle dose group, respectively. The applied dose of this study demonstrates guiding significance for clinical medication. The mice model of ALI was established by intranasal inhalation of LPS at 5 mg/kg. Also, daily changes in weight and clinical signs were recorded during administration. Mice were killed by euthanasia at the end of administration, and the samples were saved for subsequent studies.

Hematoxylin-eosin staining of lung tissue

Mice were sacrificed after treatment, and lungs were collected and fixed in 10% neutral buffered formalin. Next, the fixed lungs were embedded in paraffin and cut into sections, followed by H&E staining to detect pathological damage in mouse lung tissue.

Western blot analysis

Group assignment and drug administration were performed according to the above method. Lung tissue and RAW264.7 cells were homogenized in ice-cold RIPA lysis buffer. Total proteins for each group were separated on PAGE gel by electrophoresis and then transferred onto PVDF membrane (Millipore, United States) using the Bio-Rad protein assay system (Bio-

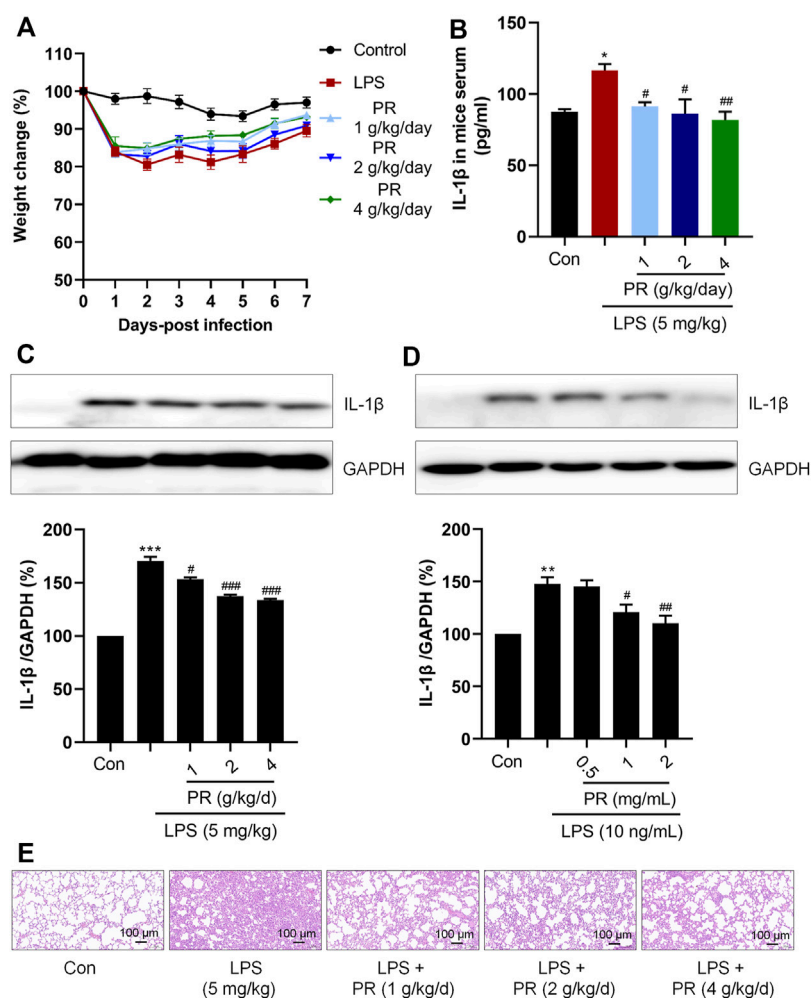
Rad, United States). The PVDF membranes were blocked with 5% BSA in TBST buffer for 3 h and then incubated with the corresponding primary antibody overnight at 4°C. The next day, PVDF membranes were washed with TBST and incubated with secondary antibody for 1 h. After thorough washing with TBST, the immunoreactive protein was visualized with an enhanced chemiluminescence assay and captured on ImageQuant™ LAS 500 (Healthcare BioSciences AB, United States). Data were standardized with the corresponding GAPDH. All experiments were repeated in triplicate.

Measurement of cytokine

Mice in each group were euthanized after 7 days treatment of PR, and their serum were harvested from the abdominal aorta using a syringe. The content of cytokine was measured using ELISA kits (IL-1β, MM-0040M1). The absorbency was examined at 540 nm. Next, each value was calculated and presented by deducting the background value.

Detection of the level of cytoplasmic calcium (Ca²⁺)

Fluo 4-AM (F312, Dojindo, Japan), a Ca²⁺-specific vital dye, was used to measure intracellular calcium levels. Dilute 1 mM Fluo 4-AM stock solution to 5 μM Fluo 4-AM working solution using HBSS buffer. The working solution (Fluo 4-AM) was incubated in cell incubator for 0.5 h. After washing the

**FIGURE 2**

PR exhibits anti-inflammatory efficacy in LPS stimulation. **(A)** body weight change of mice in 7 days during administration. **(B)** Serum IL-1 β levels were detected by Elisa kits ($n = 5-6$). **(C)** Immunoblot was employed to evaluate the expression of IL-1 β in lung tissue of mice. **(D)** RAW264.7 cells were treated with LPS or/and PR for 12 h, followed by Western blot analysis using IL-1 β antibody ($n = 3$). **(E)** Representative HE staining of lung tissue from ALI mice that were treated or untreated with PR ($n = 6$). Scale bar = 100 μ m * $p < 0.05$, ** $p < 0.01$, *** $p < 0.001$, **** $p < 0.0001$ vs. Control groups; # $p < 0.05$, ## $p < 0.01$, ### $p < 0.001$, #### $p < 0.0001$ vs. LPS-treated groups.

RAW264.7 cells three times with HBSS buffer, 1 ml of HBSS buffer was added to continue incubation for 30 min in a cell incubator. After the end, the content of calcium ions in each sample was detected according to the fluorescence intensity using a laser confocal microscope.

Metabolites extraction

Mice in each group were euthanized after 7 days treatment of PR, and their serum were harvested from the abdominal aorta using a syringe. The blood of the mice in the Con, LPS, and LPS_PR (2 g/kg/d) were centrifuged at 12,000 rpm for

15 min at 4°C. The serum was transferred to another new centrifuge tube, and the extract containing the internal standard solution was added. The samples were centrifuged at 4°C for 15 min, and the supernatant was filtered through a 0.22 μ m microporous membrane. 100 μ l from each sample was taken and mixed into QC samples. Next, hydrochloric acid (2 mol/L) was added to the serum sample, and it was allowed to stand at 4°C for 15 min. After repeating this for four times, acetonitrile was added. After centrifugation, the supernatant was aspirated to dry with nitrogen. Dried samples were dissolved in 80% methanol, vortexed and centrifuged, and the supernatants were taken for LC/MS detection.

LC-MS/MS conditions

LC-MS/MS analysis was carried out on a UHPLC system coupled with a Waters UPLC BEH C18 column. During the analysis, the injection speed and volume were 0.4 ml/min and 5 μ l, respectively. The mobile phase was a combination of 0.1% formic acid in water (A) and 0.1% formic acid in acetonitrile (B). After linear elution, MS and MS/MS data were harvested in IDA acquisition form using an Orbitrap Exploris 120 mass spectrometer.

Metabolome data processing and analysis

The raw data were processed by Progenesis Q1. The area-under-the-curve of each peak was quantified as peak intensity. Peaks with missing values in more than 1/4 of the samples were removed. For filtered peaks, missing values were replaced by 1/5 of the minimum positive value for each variable. To improve the power of subsequent results (Hackstadt and Hess, 2009), further peak filtering was based on interquartile range by R package MetaboAnalystR (version 3.2.0) (Pang et al., 2020). To conclude, the quantile normalized, and log transformed peak intensities were scaling by mean centering. Metabolites were identified by automated comparison using CAMERA (Kuhl et al., 2012). Next, partial least squares-discriminant analysis (PLS-DA) was applied for visualizing group separation and finding significantly changed metabolites by MetaboAnalystR. Welch's *t*-test was performed for comparing the expression differences of metabolites between each two groups. Metabolites with $p < 0.05$ and variable importance in projection (VIP, a weighted sum of squares of the PLS loadings taking into account the amount of explained Y-variation in each dimension) in component 1 > 1.0 were considered as potential biomarkers (Pang et al., 2020).

Network pharmacology analysis

The targets of PR were forecasted by the webtool SwissTargetPrediction (Daina et al., 2019) with probability > 0.5 in *Homo sapiens*. Also, the ALI-related targets in *Homo sapiens* were obtained from GeneCards (Safran et al., 2010) and OMIM (online mendelian inheritance in man) (Amberger et al., 2015; Amberger et al., 2019). The intersection between the two target sets were the final PR targets for ALI. The PR-target-pathway network was constructed by Cytoscape (version 3.4.0) (Shannon et al., 2003).

Metabolic pathway and function enrichment analysis

The metabolic pathway analysis was performed via the webtool MetaboAnalyst 5.0 (Pang et al., 2021). The R package

ClusterProfiler (version 4.2.1) (Wu et al., 2021) was used for gene function enrichment analysis. Each *p* value was corrected by the Benjamini-Hochberg method.

Molecular docking

The protein structures of ALOX12 (ID: 3d3l), IKKB (ID: 3brt) and TRPV1 (ID: 3sui) were downloaded from RCSB PDB. The ligands and solvent molecules in protein structures were removed via AutoDockTools (v 1.5.6). 7,8-DHF (ID: 1880) were download from <https://pubchem.ncbi.nlm.nih.gov>. The corresponding metabolite structures of chrysin (ID: MOL002560) and DHC (ID: MOL008698) were download from TCSMP. AutoGrid4 in Autodock Vina (v 1.2.2) was used for molecular docking of the proteins (as receptors) and metabolites (as ligands). Default input parameters were used in all computations. Binding energy between each ligand and receptor was calculated by Autodock Vina.

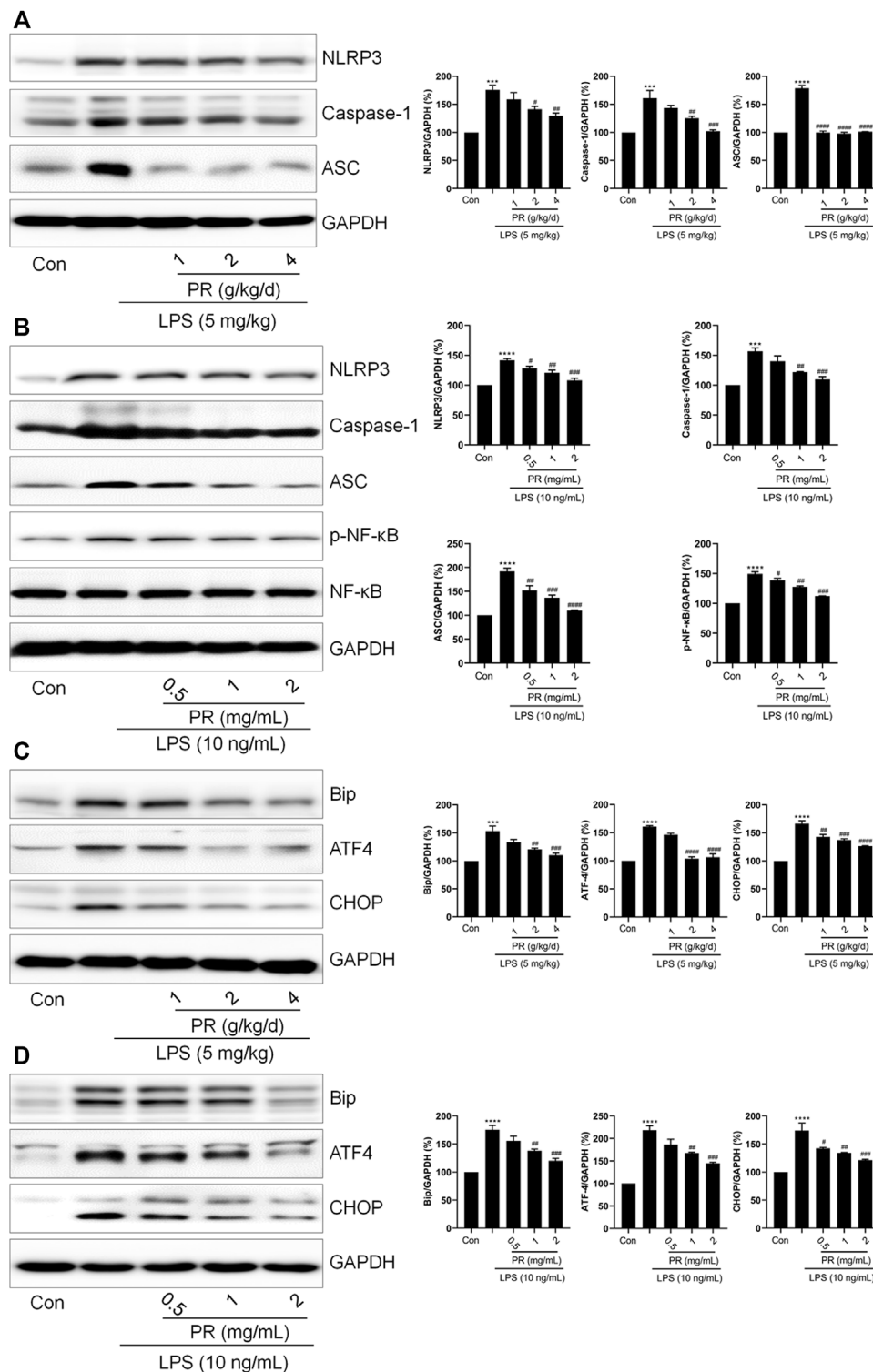
Statistical analysis

All values were expressed as mean \pm SEM, and statistical analyses were implemented using GraphPad Prism 8. A one-way ANOVA followed by Tukey's test was conducted to analyze the data for significant differences. *N* represents the number of mice in each group and the number of independent experiments. $p < 0.05$ indicated statistically significant.

Results

Pinelliae rhizoma exhibited anti-inflammatory efficacy in lipopolysaccharide-induced acute lung injury

LPS-induced ALI mice model was treated with PR for 7 days. The weight changes of the mice were recorded daily, and the results showed that LPS reduced the body weight of mice, and PR treatment alleviated the weight loss in ALI mice and recovered the body weight in the following 7 days gradually (Figure 2A). Pro-inflammatory cytokine IL-1 β is known to mediate the initiation of the immune response, which promotes the release of other pro-inflammatory cytokines and disrupts immune homeostasis (Kandasamy et al., 2019). Therefore, suppressing excessive IL-1 β will help to attenuate the inflammation response. IL-1 β is a secretory protein released by macrophages, so the effects of PR on the level of IL-1 β were examined in serum and lung tissue in ALI mice. As expected, PR not only effectively reduced the concentration of IL-1 β in serum (Figure 2B), but it also inhibited the expression of IL-1 β in lung tissue (Figure 2C).

**FIGURE 3**

PR inhibits LPS-induced ER stress and NLRP3 inflammasome activation. (A) The expressions of IL-1 β , NLRP3, Caspase-1, and ASC in the lung tissue of mice were determined by Western blot ($n = 3$). (B) RAW264.7 cells were challenged with LPS and treated with PR for 12 h. The expressions of IL-1 β , NLRP3, Caspase-1, and ASC in RAW264.7 cells were examined by Western blot. ($n = 3$). (C) The expression levels of ATF4, Bip, and CHOP in lung tissue were detected by Western blot. (D) RAW264.7 cells were challenged with LPS and treated with PR for 12 h. The expressions of ATF4, Bip, and CHOP in RAW264.7 cells were detected by Western blot ($n = 3$). (E) Intracellular Ca²⁺ content was detected with Fluo 4-AM. Scale bar = 100 μ m. (F) After 12 h LPS treatment with/without 4-PBA co-treatment, the expressions of Bip, ATF4, and NLRP3 were detected by Western blot ($n = 3$). * $p < 0.05$, ** $p < 0.01$, *** $p < 0.001$, **** $p < 0.0001$ vs. Control groups; # $p < 0.05$, ## $p < 0.01$, ### $p < 0.001$, #### $p < 0.0001$ vs. LPS-treated groups.

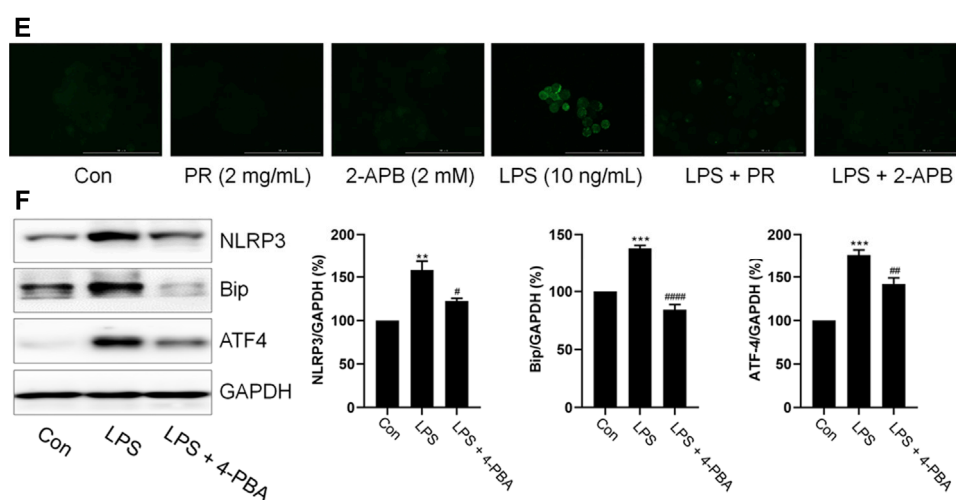


FIGURE 3

In this study, the dose of LPS was selected to be 10 ng/ml, and the dose of PR was in the range of 0.5 mg/ml to 2 mg/ml, according to the references and preliminary experiment (Zhang et al., 2015; Arikawa et al., 2016). Then, we detected the expression of IL-1 β in RAW264.7 cells after treatment with LPS and PR. As shown in Figure 2D, co-treatment with PR markedly reversed LPS-increased expression of IL-1 β *in vitro* and *in vivo*, suggesting that PR exerts an anti-inflammatory effect by acting on the upstream mediators of IL-1 β in response to LPS stimulation. Besides, histopathological examination of lung tissue was conducted by H&E staining. Researchers observed that severe infiltration of inflammatory cells and neutrophils in the alveolar space, diffuse edema in alveolar spaces and interstitium, and the alveolar walls were congested and thickened in LPS-induced ALI. The PR treatment group showed clearly ameliorated lesions in lung tissue with increased alveolar air space and reduced infiltration of inflammatory cells (Figure 2E).

Pinelliae rhizoma inhibited the activation of endoplasmic reticulum stress and NLRP3 inflammasome

Given that ER stress and NLRP3 are critical in LPS-induced ALI, we investigated relevant protein expressions *via* immunoblotting. As shown in Figures 3A,B, LPS stimulation elevates NLRP3, Caspase-1, and ASC levels in RAW264.7 cells and lung tissue. Next, interestingly, PR co-treatment decreased the levels of NLRP3, Caspase-1, and ASC in LPS-treated RAW264.7 cells and lung tissue (Figures 3A,B). Meanwhile, another significant inflammation-related signaling pathway known as the NF- κ B was stimulated by LPS, while PR treatment efficiently reduced its phosphorylation (Figure 3B).

Also, co-treatment with PR significantly reversed LPS-increased the expressions of ATF4, CHOP, and Bip (Figures 3C,D). Further, collectively, these data demonstrated that PR demonstrates a significant inhibitory effect on ER stress and NLRP3 activation *in vitro* and *in vivo*. In addition, RAW264.7 cells were stained with Fluo-4 AM to detect changes in intracellular Ca²⁺ levels after LPS and PR treatments. Our results showed that the cytoplasmic Ca²⁺ loading in the LPS-treated group was significantly enhanced, while the cytoplasmic Ca²⁺ content in the PR and 2-APB (the inhibitor of calcium ion) treated groups decreased (Figure 3E). To investigate whether ER stress regulates NLRP3 inflammasome activation, we used 4-PBA (the inhibitor of ER stress) to inhibit ER stress and examined the expression of ER stress and NLRP3-related proteins. Our data showed that 4-PBA inhibited the expression of Bip and ATF4, while down-regulating the expression of NLRP3 (Figure 3F). These results displayed that inhibition of ER stress suppressed NLRP3 inflammasome activation, that is, NLRP3 activation is closely related to ER stress.

Effects of *Pinelliae rhizoma* on serum metabolites of lipopolysaccharide-induced acute lung injury model

Serum metabolome is a new approach that combined TCM theory with advanced systematic pharmacology technology to study the TCM. In order to consider whether some bioactive ingredients were found in PR, which play the anti-inflammatory roles in the regulation of ER stress and NLRP3 inflammasome, serum metabolome can be used to overcome the difficulty of multi-ingredients and multi-targets in the research of PR. After quality control and data processing, the PLS-DA result showed

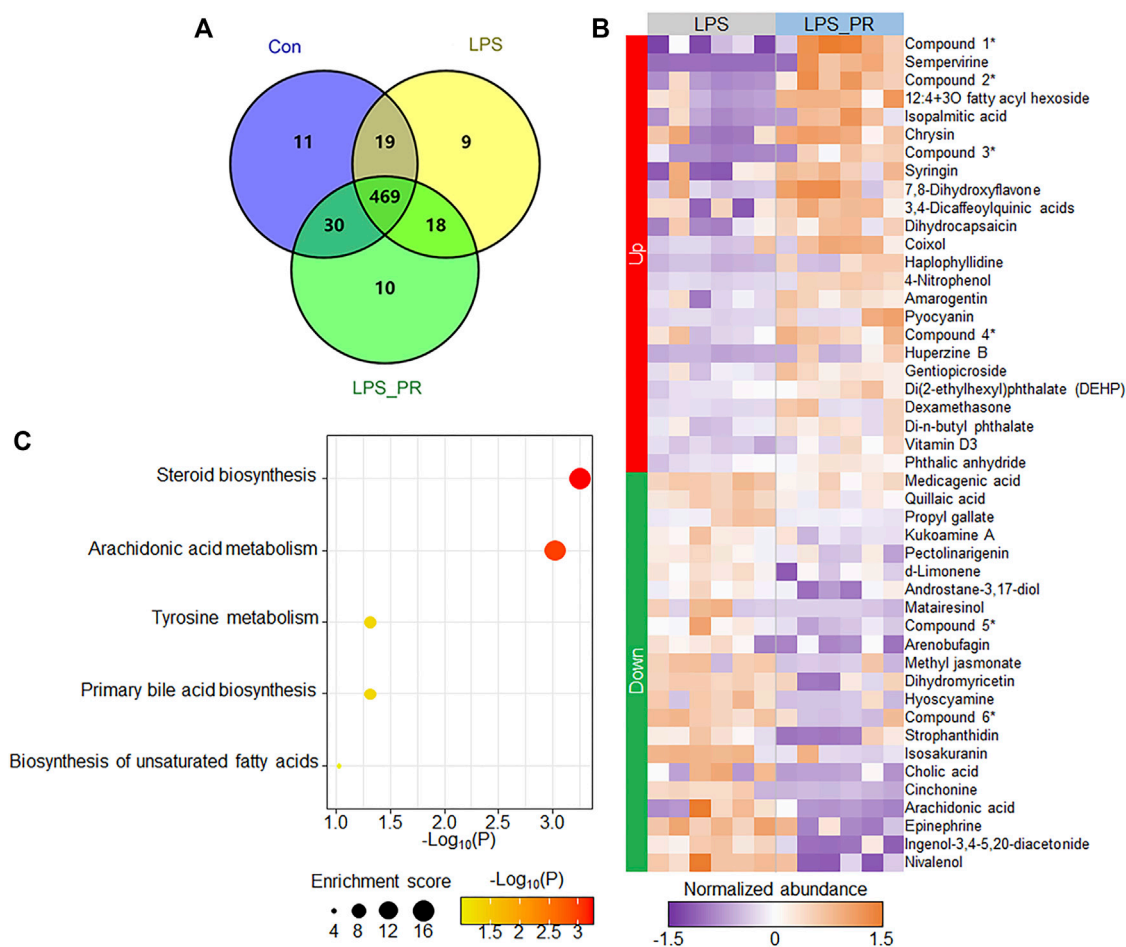


FIGURE 4

PR changed the serum metabolites of LPS-stimulated mouse. (A) Number of identified metabolites in the three types of experimental samples. (B) Heatmap of 46 differentially expressed metabolites in LPS and LPS_PR. Purple represents low expression and orange represents high expression. Due to the long names of some ingredients, abbreviations are used for display (indicated by asterisks on the right side of the heat map). Compound 1: [(1S,6S,7R)-6-acetyloxy-1-(3-methylbutanoyloxy)spiro[4a,5,6,7a-tetrahydro-1H-cyclopenta[c]pyran-7,2'-oxirane]-4-yl)methyl 3-methylbutanoate; Compound 2: Pyrrolo[1,2-*a*]pyrazine-1,4-dione, hexahydro-3-(1-methylethyl)-; Compound 3: (1S,2R,4aS,6aR,6bR,10S,12aR,14bS)-1,2,6b,9,9,12a-hexamethyl-10-[(2R,3R,4S,5S,6R)-3,4,5-trihydroxy-6-methyloxan-2-yl]oxy-2,3,4,5,6,6a,7,8,8a,10,11,12,13,14b-tetradecahydro-1H-picene-4a,6a-dicarboxylic acid; Compound 4: (2S,3S,4S,5R,6S)-3,4,5-trihydroxy-6-(5-hydroxy-4-oxo-2-phenylchromen-7-yl)oxyoxane-2-carboxylic acid; Compound 5: 2,4,6-trihydroxy-5-[1-(4-hydroxy-1,1,4,7-tetramethyl-1a,2,3,4a,5,6,7a,7b-octahydrocyclopropa[h]azulen-7-yl)-3-methylbutyl]benzene-1,3-dicarbaldehyde; Compound 6: (1S,4aR,6aS,6bR,10R,11R,12aR,14bS)-1,10,11-trihydroxy-2,2,6a,6b,9,9,12a-heptamethyl-1,3,4,5,6,6a,7,8,8a,10,11,12,13,14b-tetradecahydricene-4a-carboxylic acid. (C) Pathway enrichment results of differentially expressed metabolites. The darker the color, the more significant the *p* value.

that samples in the same group were clustered together, and the three groups were clearly distinguished (Supplementary Figure S1A), indicating that high-confidence metabolomes were obtained which could be used for downstream analysis. A total of 98,067 peaks were detected in the three types of experimental samples, 566 metabolites were identified (Figure 4A and Supplementary Table S1), and most (82.9%, 469/566) metabolites were co-identified in three groups. Next, subsequently, we focused on the expression changes of metabolites in the LPS model before and after PR administration. Significant differences were found between

the LPS and LPS_PR groups (Supplementary Figure S1B). The differential analysis identified a total of 46 differentially expressed metabolites ($p < 0.05$ and VIP > 1), of which 24 were up-regulated and 22 were down-regulated (Figure 4B and Supplementary Table S1), suggesting that PR alters mouse serum metabolome in the presence of ALI. These differentially expressed metabolites tend to be involved in steroid biosynthesis and arachidonic acid metabolism pathways (Figure 4C), which are closely related to inflammation (Riad et al., 2002; Mariotto et al., 2007; Wang et al., 2019).

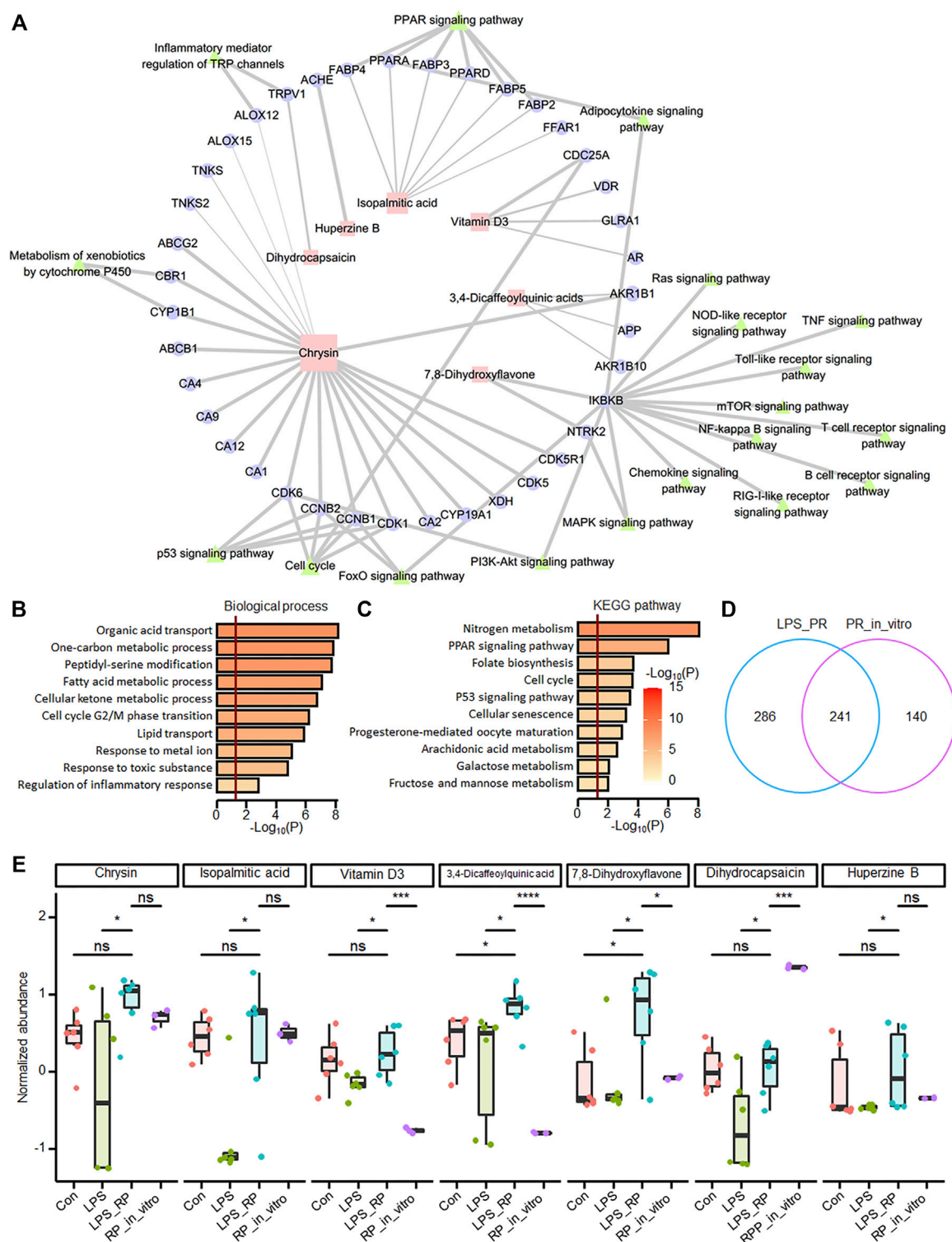


FIGURE 5

Network pharmacological analysis showed that potential anti-inflammatory ingredients are found in PR. (A) PR network pharmacology. 39 targets of seven metabolites and KEGG pathways closely related to inflammation were displayed in the network. Squares represent metabolites, circles represent potential targets, and triangles represent KEGG pathways. The size of the shape is positively correlated with the degree, and the thickness of the line is positively correlated with probability. (B) Functional enrichment results of targets of differentially expressed metabolites. The darker the color, the more significant the *p* value. The red vertical bar indicates that *p* value is 0.05. (D) overlap of identified metabolites in LPS_PR and PR *in vitro*. (E) Abundance of seven metabolites in four groups in Con, LPS, LPS_PR and PR *in vitro*. Welch's *t*-test was performed for compare the expression differences of metabolites between each two groups. **p* < 0.05, ***p* < 0.01, ****p* < 0.001, *****p* < 0.0001.

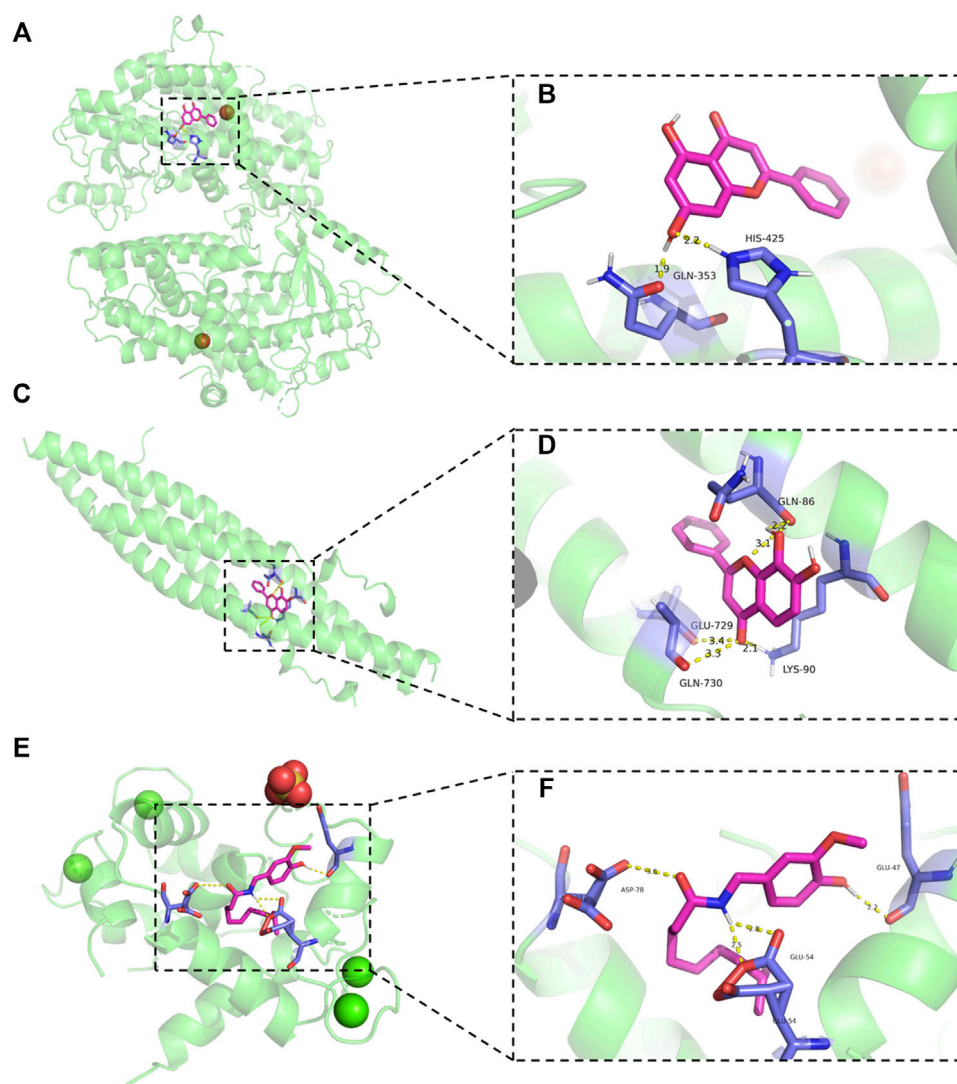


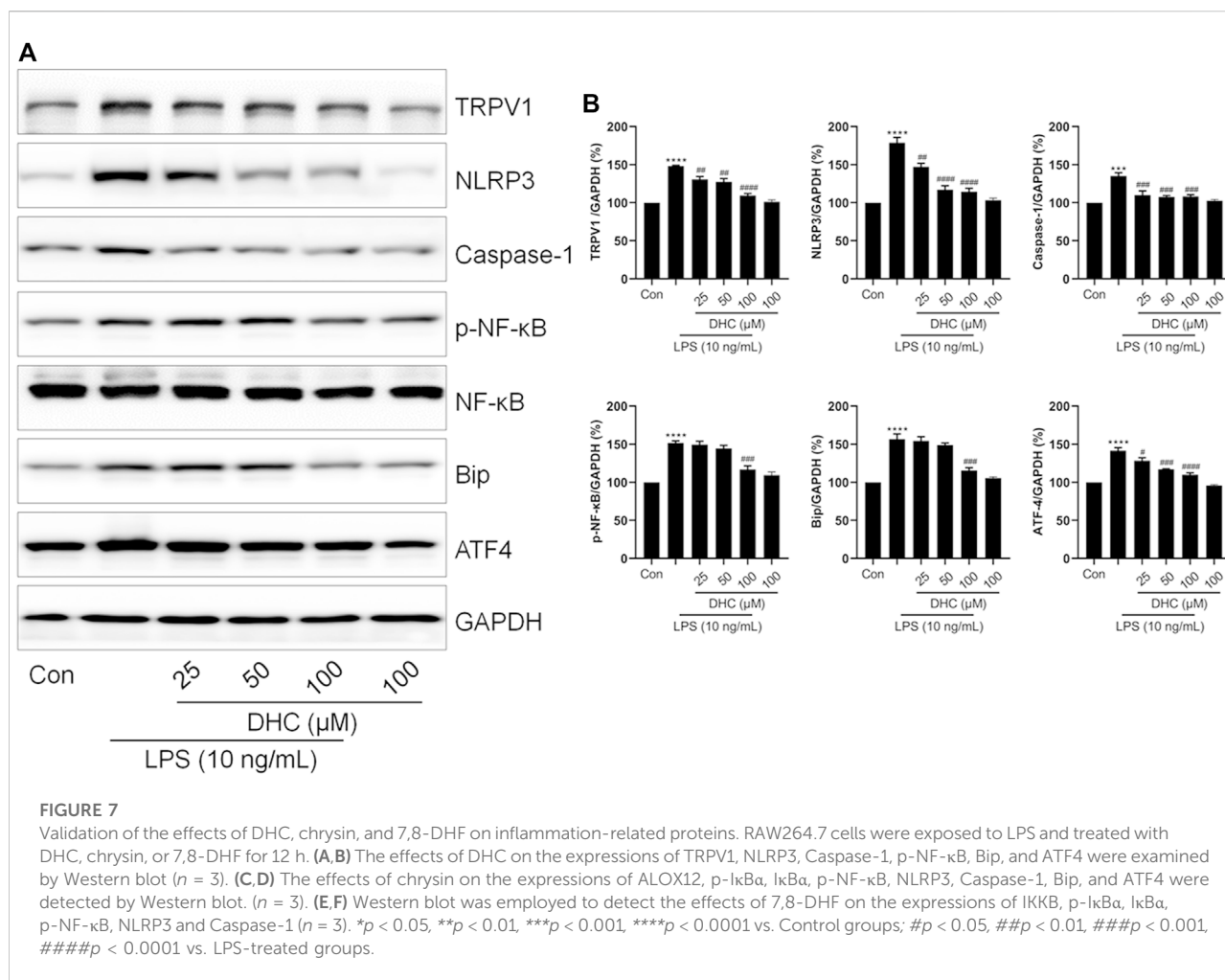
FIGURE 6

Molecular docking results. (A,B) Schematic diagram of the binding mode of chrysin to ALOX12 protein (left panels) and details of the binding pose (right panels). (C,D) Schematic diagram of the binding mode of 7,8-DHF to IKKB protein (left panels) and details of the binding pose (right panels). (E,F) Schematic diagram of the binding mode of DHC to TRPV1 protein (left panels) and details of the binding pose (right panels).

Network pharmacology revealed important bioactive ingredients in *Pinelliae rhizoma* and their possible targets

In order to explore the PR regulatory network, through network pharmacological analysis (see [methods](#)), we found that seven of the 24 up-regulated metabolites in LPS_PR regulate a total of 39 ALI-related targets, of which chrysin, isopalmitic acid, and vitamin D3 demonstrate the most targets, 22, 7, and 4, respectively (Figure 5A and [Supplementary Table S2](#)). Functional enrichment analysis showed that these 39 targets tend to be involved in the functions closely related to lipid and energy metabolism and

transport, cell cycle, response to stimulation and regulation of inflammatory response (Figure 5B), and tend to participate in metabolic pathway, PPAR signaling pathway, cell cycle, and p53 signaling pathway (Figure 5C). To explore which of these seven metabolites ([Supplementary Data Sheet S2](#)) are ingredients in PR, we identified all ingredients in PR using UHPLC-QE MS. 381 ingredients are found in PR, including 97 terpenoids, 65 alkaloids, 38 flavonoids, 26 phenylpropanoids, 23 phenols, 21 amino acid derivatives, and 111 other components ([Supplementary Table S3](#)). 241 metabolites were identified in both LPS_PR and PR_in_vitro (Figure 5D). Among them, chrysin, isopalmitic acid, DHC, and 7,8-DHF demonstrate relatively high expression levels in PR in vitro (Figure 5E),



suggesting that these ingredients in PR may regulate and treat inflammation through the above corresponding pathways. Since 7,8-DHF and chrysin demonstrate very similar chemical results, we speculated that the high abundance of 7,8-DHF in LPS_PR may be derived from the metabolism of chrysin in PR. These results suggested that these ingredients in PR may regulate and treat inflammation through the above corresponding pathways.

To further explore whether genes closely related to inflammation could be bound by ingredients and potential metabolic outcomes from PR, we carried out molecular docking on chrysin with ALOX12, 7,8-DHF with IKKB, and DHC with TRPV1. Binding energies between chrysin and ALOX12, 7,8-DHF with IKKB, and DHC with TRPV1 are -6.45 , -6.37 , and -5.91 kcal/mol, respectively. Chrysin binds to ALOX12 in the pocket between the one chain (Figure 6A). Hydroxyl groups of chrysin form hydrogen bonds with GLN-353 and HIS9425 in ALOX12 (Figure 6B). 7,8-DHF binds to IKKB in the pocket between the two chains (Figure 6C). Carbonyl group of 7,8-DHF form hydrogen bonds with GLU-729 and GLN-730 in chain A (Figure 6D).

Hydroxyl groups of 7,8-DHF form hydrogen bonds with GLN-86, and carbonyl group of 7,8-DHF form hydrogen bonds with LYS-90 in chain B (Figure 6D). DHC binds to TRPV1 in the pocket between the two chains (Figure 6E). Hydroxyl group of DHC form hydrogen bonds with GLU-47, and amino groups of DHC form hydrogen bonds with GLU-54 in chain A (Figure 6F). Carbonyl group of DHC form hydrogen bonds with ASP-78 in chain B (Figure 6F).

Bioactive ingredients of *Pinelliae rhizoma* suppressed endoplasmic reticulum stress and NLRP3 inflammasome

Next, we continued to investigate the effects of chrysin, DHC and 7,8-DHF on ER stress, respectively. LPS induced ER stress and NLRP3 inflammasome activation in cells, while both DHC (Figures 7A,B) and chrysin (Figures 7C,D) significantly down-regulated the expression of NLRP3, Caspase-1, Bip and ATF4. Also, co-treatment with DHC significantly reversed LPS-increased the expressions of

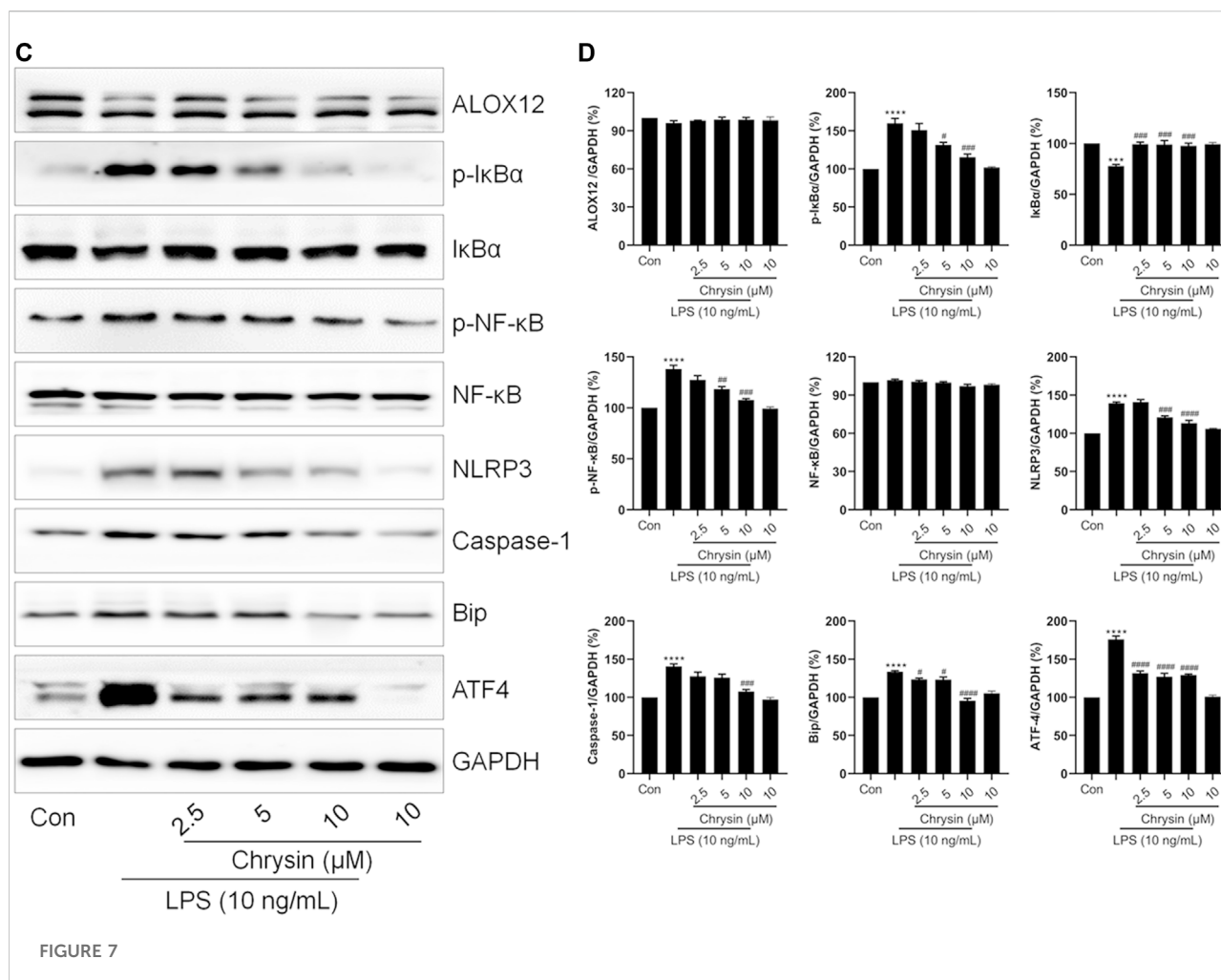


FIGURE 7

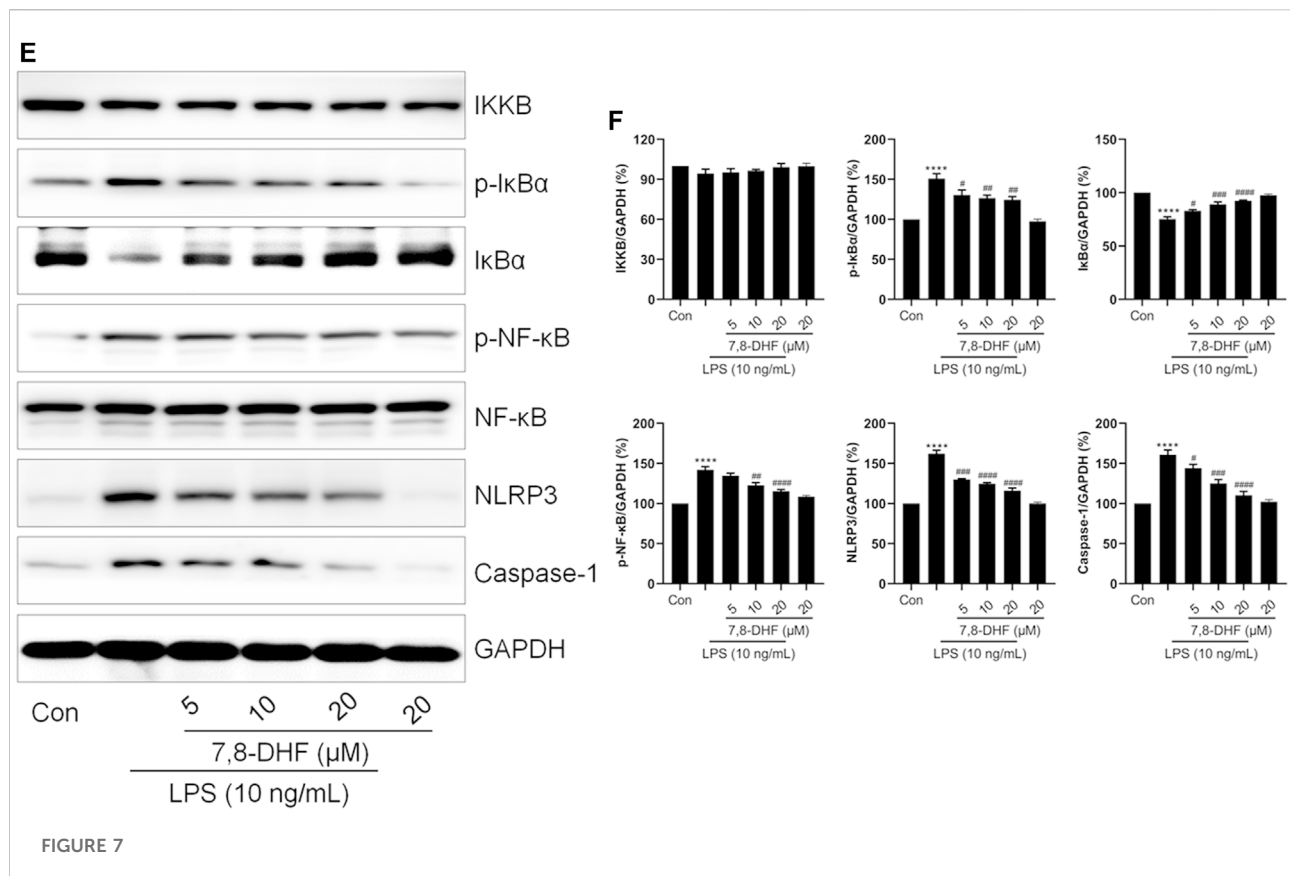
TRPV1 and p-NF-κB (Figures 7A,B). As shown in Figures 7C,D, compared with the LPS group, the expressions of p-IκBα and p-NF-κB were distinctly decreased, but that of IκBα was obviously increased in the chrysin-treated group. Also, no changes were found in ALOX12 expression between the Control, LPS-treated, and the chrysin-treated group (Figures 7C,D). Moreover, compared with the LPS group, the expressions of p-IκBα, p-NF-κB, NLRP3, and Caspase-1 were significantly decreased, and the expression of IκBα was increased in the 7,8-DHF-treated group (Figures 7E,F). Also, no changes were found in IKKB expression among the LPS-treated group and the 7,8-DHF treated group (Figures 7E,F). Taken together, these results indicated that chrysin, DHC, and 7,8-DHF are the effective ingredients of PR regulating inflammation-related signaling pathways and ion channels.

Discussion

ALI is one of the most common critical diseases in clinics, with rapid onset and high mortality (He et al., 2021). Severe ALI or

improper treatment could lead to further ARDS. Previous studies showed that TCM demonstrates its unique advantage in the treatment of lung injury, which is mainly reflected in the regulation of immune function (Ding et al., 2020). PR has been used to treat lung diseases for thousands of years, and it effectively suppressed pro-inflammatory cytokines and relieved airway inflammation (Du et al., 2016; Hu et al., 2019). This study identified that LPS triggered ER stress and increased cytoplasmic Ca^{2+} content *via* activating Bip/ATF4/CHOP signaling pathway. Also, PR effectively relieves ALI induced by LPS, mainly *via* suppressing ER stress-mediated NLRP3 inflammasome and excessive expression of IL-1β. In addition, the bioactive ingredients of PR exerting anti-inflammatory effects were screened. Among them, chrysin, DHC, and 7,8-DHF significantly inhibited LPS-induced ER stress and NLRP3 inflammasome activation.

The infiltration of inflammatory cells and excessive release of pro-inflammatory cytokines are key events that trigger ALI (Belchamber and Donnelly, 2017). With the pathogenic microorganisms invading the lungs, cytokines were released to repair lung injury; however, overwhelming cytokines are



destructive and cause serious injury (Parekh et al., 2011). Therefore, inhibition of cytokine release is necessary to alleviate lung injury. Consistent with previous reports and our hypothesis, this study confirmed that PR alleviated LPS-induced lung pathological injury and inhibited the excessive expression of cytokine IL-1 β . Besides, NLRP3 mediates the outbursts of pro-inflammatory cytokines and PR down-regulated the expression of NLRP3 in lung tissue and RAW264.7 cells, indicating that PR limited the activation of NLRP3 inflammasome caused by LPS. Also, importantly, ER stress-mediated NLRP3 inflammasome also participates in cytokine release (Talty et al., 2019). The ER is a reservoir of Ca²⁺, and a large amount of Ca²⁺ flow from the ER into mitochondria and cytoplasm during ER stress, resulting in mitochondrial Ca²⁺ overload and damage (Liu et al., 2018). Next, subsequently, damaged mitochondria produce excess mtROS and mtDNA and cause cardiolipin damage, thus promoting the assembly and activation of the NLRP3 inflammasome to release cytokines (Lee et al., 2012). In addition, elevated Ca²⁺ levels of cytoplasmic also directly activate the NLRP3 inflammasome (Murakami et al., 2012). Hence, inhibition of the activity of ER stress-mediated NLRP3 inflammasome is a fresh target for the cure of ALI. Not surprisingly, PR significantly down-regulated Bip/ATF4/CHOP signaling pathways in LPS-treated cells and lung tissue, and it reduced cytoplasmic Ca²⁺ loading in LPS-stimulated cells. Together, these results proved the effect of PR

in abolishing inflammation mainly through inhibiting ER stress and suppressing the NLRP3 inflammasome.

Bioactive ingredients of TCM are presented in the form of prototype components or metabolites in the body (Shi et al., 2016). To observe whether bioactive ingredients in PR were absorbed by mice and entered the blood to exert potent anti-inflammatory effects after administration, we determined the metabolites in mouse serum before and after LPS stimulation, and the ingredients of PR. 46 differentially expressed metabolites were identified, which tend to participate in inflammation-related pathways, such as steroid biosynthesis and arachidonic acid metabolism pathways. Network pharmacology and molecular docking analysis screened three prototype and metabolic components of PR and their target proteins, chrysin and ALOX12, DHC and TRPV1, 7,8-DHF, and IKK β . Further *in vitro* experiments demonstrated that chrysin, DHC, and 7,8-DHF treatment suppress ER stress and the activation of NLRP3 inflammasome.

Chrysin, 7,8-DHF, and DHC demonstrate significant biological properties, including anti-inflammatory and immune modulation (Chen et al., 2011; Janyou et al., 2017; Byun et al., 2021). The latest research shows that chrysin improved LPS-induced ALI in mice by inhibiting ER stress and NLRP3 inflammasome activation (Chen et al., 2021). Meanwhile, 7,8-DHF can inhibit the LPS-induced release of inflammatory mediators in RAW264.7 cells (Park et al., 2012).

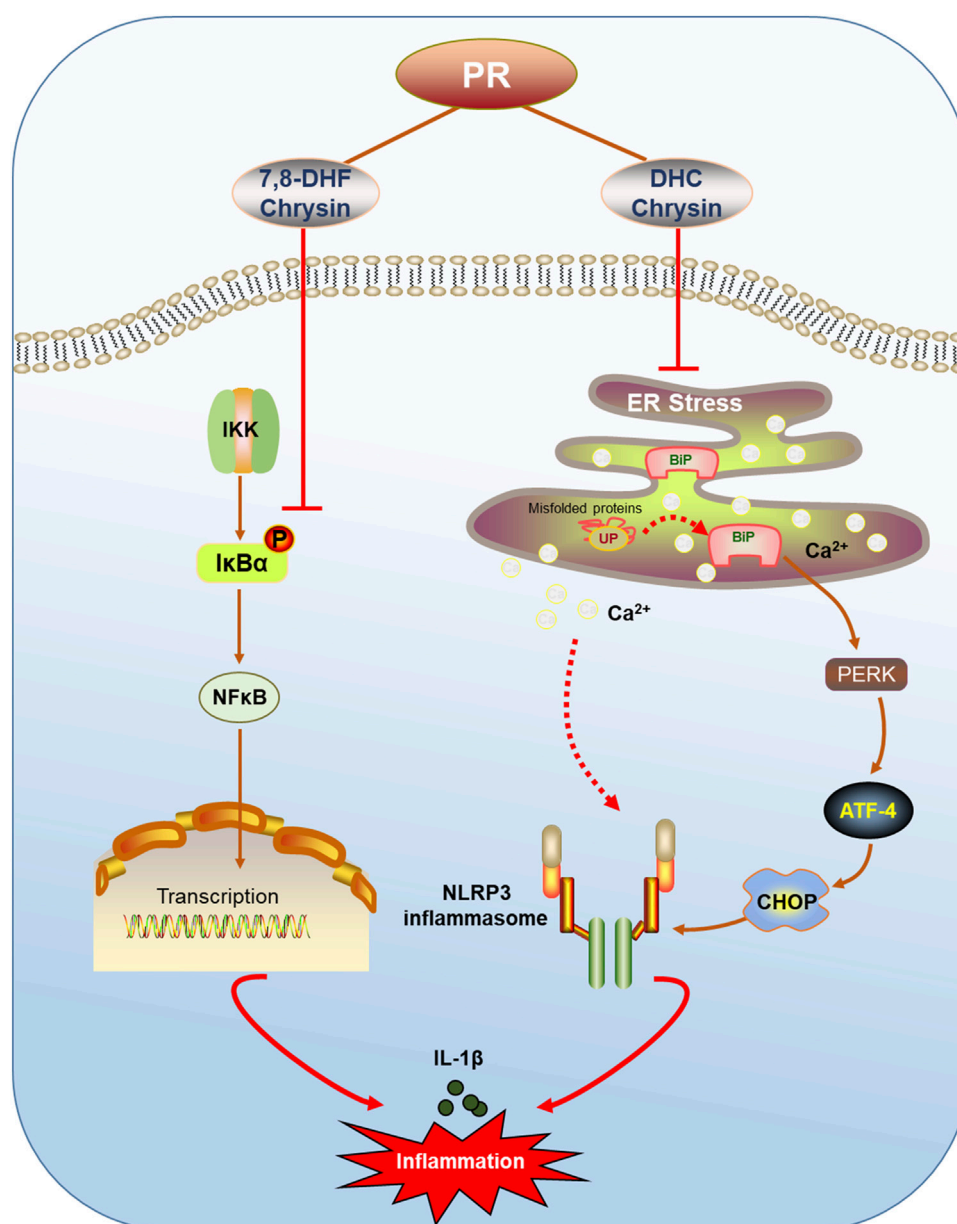


FIGURE 8

Schematic of PR relieving ALI by inhibiting ER stress. PR and its active ingredients alleviated inflammatory injury via regulating ER stress-mediated NLRP3 and NF-κB signaling pathways.

TRPV1 is a non-selective cation channel (Zhai et al., 2020). The activation of TRPV1 promotes Ca^{2+} influx, leads to intracellular calcium overload, and affects ER stress and a series of inflammatory responses (Stock et al., 2012; Stueber et al., 2017). From this, it seems that the suppression of ER stress by PR may benefit from the inhibition of TRPV1 activation by DHC. Next, interestingly, chrysin and 7,8-DHF demonstrated no effect on the expression of their target proteins ALOX12 and IKKB but inhibited the NF-κB signaling pathway. However, ALOX12 accelerates inflammatory responses and promotes

cytokine production through the p38 mitogen-activated protein kinase (MAPK) and NF-κB pathways (Funk and Cyrus, 2001; Nieves and Moreno, 2008). Also, accordingly, PR inhibition of NF-κB phosphorylation in RAW264.7 cells may be related to chrysin and 7,8-DHF.

Further, collectively, chrysin, DHC, and 7,8-DHF are the potential key bioactive ingredients of PR to regulate inflammatory response by inhibiting ER stress-mediated NLRP3 inflammasome activation, thereby conferring protection to the lungs and maintaining lung function and lung homeostasis.

Given that NLRP3 is one of the targets for the treatment of COVID-19 and inhibition of NLRP3 inflammasome activation could effectively alleviate infection-induced lung injury (Xian et al., 2021), this study not only elucidates the mechanism and components of PR in the treatment of ALI, but it will also contribute to the development of COVID-19 therapeutic drugs.

Conclusions

In summary, this study confirmed that LPS infection indeed caused acute inflammatory damage in mouse lung, and it is accompanied with the enhancement of IL-1 β contents and the activation of the NLRP3 inflammasome in lung tissue and macrophagocyte, all of which are remarkably ameliorated by PR treatment. PR not only obviously reversed Bip/ATF4/CHOP-mediated ER stress, but it also significantly attenuated LPS-induced activation of the NLRP3 inflammasome. Based on metabolome analysis and molecular docking, chrysin, 7,8-DHF, and DHC were found to notably suppress LPS-induced ER stress and NLRP3 inflammasome activation (Figure 8). Hence, this research provided a theoretical basis for the clinical application of PR to treat ALI, and these bioactive ingredients of PR would be promising therapeutic drugs for the treatment of ALI.

Data availability statement

The original contributions presented in the study are included in the article/Supplementary Material, and further inquiries can be directed to the corresponding authors.

Ethics statement

The animal study was reviewed and approved by Ethics Committee of Animal Experiments of the Beijing Institute of Radiation Medicine (Approval No.: IACUC-DWZX-2020-762).

References

- Amberger, J. S., Bocchini, C. A., Schiettecatte, F., Scott, A. F., and Hamosh, A. (2015). OMIM.org: Online Mendelian Inheritance in Man (OMIM®), an Online Catalog of Human Genes and Genetic Disorders. *Nucleic Acids Res.* 43, D789–D798. doi:10.1093/nar/gku1205
- Amberger, J. S., Bocchini, C. A., Scott, A. F., and Hamosh, A. (2019). OMIM.org: Leveraging Knowledge across Phenotype-Genotype Relationships. *Nucleic Acids Res.* 47, D1038–D1043. doi:10.1093/nar/gky1151
- Arikawa, M., Kakinuma, Y., Noguchi, T., Todaka, H., and Sato, T. (2016). Donepezil, an Acetylcholinesterase Inhibitor, Attenuates LPS-Induced Inflammatory Response in Murine Macrophage Cell Line RAW 264.7 through Inhibition of Nuclear Factor Kappa B Translocation. *Eur. J. Pharmacol.* 789, 17–26. doi:10.1016/j.ejphar.2016.06.053
- Belchamber, K. B. R., and Donnelly, L. E. (2017). Macrophage Dysfunction in Respiratory Disease. *Results Probl. Cell Differ.* 62, 299–313. doi:10.1007/978-3-319-54090-0_12
- Byun, E. B., Song, H. Y., Kim, W. S., Han, J. M., Seo, H. S., Park, W. Y., et al. (2021). Chrysin Derivative CM1 and Exhibited Anti-inflammatory Action by Upregulating Toll-Interacting Protein Expression in Lipopolysaccharide-Stimulated RAW264.7 Macrophage Cells. *Molecules* 26. doi:10.3390/molecules26061532
- Chen, J., Chua, K. W., Chua, C. C., Yu, H., Pei, A., Chua, B. H., et al. (2011). Antioxidant Activity of 7,8-dihydroxyflavone Provides Neuroprotection against Glutamate-Induced Toxicity. *Neurosci. Lett.* 499, 181–185. doi:10.1016/j.neulet.2011.05.054
- Chen, M., Li, J., Liu, X., Song, Z., Han, S., Shi, R., et al. (2021). Chrysin Prevents Lipopolysaccharide-Induced Acute Lung Injury in Mice by Suppressing the IRE1 α /TXNIP/NLRP3 Pathway. *Pulm. Pharmacol. Ther.* 68, 102018. doi:10.1016/j.pupt.2021.102018
- Daina, A., Michielin, O., and Zoete, V. (2019). SwissTargetPrediction: Updated Data and New Features for Efficient Prediction of Protein Targets of Small Molecules. *Nucleic Acids Res.* 47, W357–W364. doi:10.1093/nar/gkz382

Author contributions

YG and WZ were responsible for the conception of the study. N-nW, C-sH, H-fD, and LZ were responsible for data collection and analysis. L-xY and B-yS participated in processing the images. X-xZ and PS wrote the manuscript. All authors read and approved the final manuscript.

Funding

This work was supported by grants from the Young Elite Scientists Sponsorship Program by CAST (No. 2021-QNRC1-03) and the National Key research and Development Program of China (No. 2020YFC0845400).

Conflict of interest

The authors declare that the research was conducted in the absence of any commercial or financial relationships that could be construed as a potential conflict of interest.

Publisher's note

All claims expressed in this article are solely those of the authors and do not necessarily represent those of their affiliated organizations, or those of the publisher, the editors, and the reviewers. Any product that may be evaluated in this article, or claim that may be made by its manufacturer, is not guaranteed or endorsed by the publisher.

Supplementary material

The Supplementary Material for this article can be found online at: <https://www.frontiersin.org/articles/10.3389/fphar.2022.883865/full#supplementary-material>

- Delbrel, E., Soumare, A., Naguez, A., Label, R., Bernard, O., Bruhat, A., et al. (2018). HIF-1 α Triggers ER Stress and CHOP-Mediated Apoptosis in Alveolar Epithelial Cells, a Key Event in Pulmonary Fibrosis. *Sci. Rep.* 8, 17939. doi:10.1038/s41598-018-36063-2
- Ding, Z., Zhong, R., Xia, T., Yang, Y., Xing, N., Wang, W., et al. (2020). Advances in Research into the Mechanisms of Chinese Materia Medica against Acute Lung Injury. *Biomed. Pharmacother.* 122, 109706. doi:10.1016/j.biopha.2019.109706
- Du, W., Su, J., Ye, D., Wang, Y., Huang, Q., and Gong, X. (2016). Pinellia Ternata Attenuates Mucus Secretion and Airway Inflammation after Inhaled Corticosteroid Withdrawal in COPD Rats. *Am. J. Chin. Med.* 44, 1027–1041. doi:10.1142/S0192415X16500579
- Funk, C. D., and Cyrus, T. (2001). 12/15-lipoxygenase, Oxidative Modification of LDL and Atherogenesis. *Trends Cardiovasc Med.* 11, 116–124. doi:10.1016/s1050-1738(01)00096-2
- Habashi, N. M., Camporota, L., Gatto, L. A., and Nieman, G. (2021). Functional Pathophysiology of SARS-CoV-2-Induced Acute Lung Injury and Clinical Implications. *J. Appl. Physiol.* (1985) 130, 877–891. doi:10.1152/japplphysiol.00742.2020
- Hackstadt, A. J., and Hess, A. M. (2009). Filtering for Increased Power for Microarray Data Analysis. *BMC Bioinforma.* 10, 11. doi:10.1186/1471-2105-10-11
- He, Y., Hara, H., and Núñez, G. (2016). Mechanism and Regulation of NLRP3 Inflammasome Activation. *Trends Biochem. Sci.* 41, 1012–1021. doi:10.1016/j.tibs.2016.09.002
- He, Y. Q., Zhou, C. C., Yu, L. Y., Wang, L., Deng, J. L., Tao, Y. L., et al. (2021). Natural Product Derived Phytochemicals in Managing Acute Lung Injury by Multiple Mechanisms. *Pharmacol. Res.* 163, 105224. doi:10.1016/j.phrs.2020.105224
- Hrincius, E. R., Liedmann, S., Finkelstein, D., Vogel, P., Ganseboom, S., Samarasinghe, A. E., et al. (2015). Acute Lung Injury Results from Innate Sensing of Viruses by an ER Stress Pathway. *Cell Rep.* 11, 1591–1603. doi:10.1016/j.celrep.2015.05.012
- Hu, M., Liu, Y., Wang, L., Wang, J., Li, L., and Wu, C. (2019). Purification, Characterization of Two Polysaccharides from Pinelliae Rhizoma Praeparatum Cum Alumine and Their Anti-inflammatory Effects on Mucus Secretion of Airway Epithelium. *Int. J. Mol. Sci.* 20. doi:10.3390/ijms20143553
- Huang, K., Zhang, P., Zhang, Z., Youn, J. Y., Wang, C., Zhang, H., et al. (2021). Traditional Chinese Medicine (TCM) in the Treatment of COVID-19 and Other Viral Infections: Efficacies and Mechanisms. *Pharmacol. Ther.* 225, 107843. doi:10.1016/j.pharmthera.2021.107843
- Janyou, A., Wicha, P., Jittiwat, J., Suksamrarn, A., Tocharus, C., and Tocharus, J. (2017). Dihydrocapsaicin Attenuates Blood Brain Barrier and Cerebral Damage in Focal Cerebral Ischemia/Reperfusion via Oxidative Stress and Inflammation. *Sci. Rep.* 7, 10556. doi:10.1038/s41598-017-11181-5
- Kandasamy, M., Mak, K. K., Devados, T., Thanikachalam, P. V., Sakirrolla, R., Choudhury, H., et al. (2019). Construction of a Novel Quinoxaline as a New Class of Nrf2 Activator. *BMC Chem.* 13, 117. doi:10.1186/s13065-019-0633-4
- Kim, S. R., Kim, H. J., Kim, D. I., Lee, K. B., Park, H. J., Jeong, J. S., et al. (2015). Blockade of Interplay between IL-17A and Endoplasmic Reticulum Stress Attenuates LPS-Induced Lung Injury. *Theranostics* 5, 1343–1362. doi:10.7150/thno.11685
- Kuhl, C., Tautenhahn, R., Böttcher, C., Larson, T. R., and Neumann, S. (2012). CAMERA: an Integrated Strategy for Compound Spectra Extraction and Annotation of Liquid Chromatography/mass Spectrometry Data Sets. *Anal. Chem.* 84, 283–289. doi:10.1021/ac202450g
- Kumar, V. (2020). Pulmonary Innate Immune Response Determines the Outcome of Inflammation during Pneumonia and Sepsis-Associated Acute Lung Injury. *Front. Immunol.* 11, 1722. doi:10.3389/fimmu.2020.01722
- Lee, G. S., Subramanian, N., Kim, A. I., Aksentijevich, I., Goldbach-Mansky, R., Sacks, D. B., et al. (2012). The Calcium-Sensing Receptor Regulates the NLRP3 Inflammasome through Ca²⁺ and cAMP. *Nature* 492, 123–127. doi:10.1038/nature11588
- Lee, M. Y., Shin, I. S., Jeon, W. Y., Lim, H. S., Kim, J. H., and Ha, H. (2013). Pinellia Ternata Breitenbach Attenuates Ovalbumin-Induced Allergic Airway Inflammation and Mucus Secretion in a Murine Model of Asthma. *Immunopharmacol. Immunotoxicol.* 35, 410–418. doi:10.3109/08923973.2013.770522
- Lee, S. J., Lee, D. E., Choi, S. Y., and Kwon, O. S. (2021). OSMI-1 Enhances TRAIL-Induced Apoptosis through ER Stress and NF- κ B Signaling in Colon Cancer Cells. *Int. J. Mol. Sci.* 22. doi:10.3390/ijms222011073
- Li, W., Cao, T., Luo, C., Cai, J., Zhou, X., Xiao, X., et al. (2020). Crosstalk between ER Stress, NLRP3 Inflammasome, and Inflammation. *Appl. Microbiol. Biotechnol.* 104, 6129–6140. doi:10.1007/s00253-020-10614-y
- Liu, Q., Zhang, D., Hu, D., Zhou, X., and Zhou, Y. (2018). The Role of Mitochondria in NLRP3 Inflammasome Activation. *Mol. Immunol.* 103, 115–124. doi:10.1016/j.molimm.2018.09.010
- Luo, W., Ding, R., Guo, X., Zhan, T., Tang, T., Fan, R., et al. (2022). Clinical Data Mining Reveals Gancao-Banxia as a Potential Herbal Pair against Moderate COVID-19 by Dual Binding to IL-6/STAT3. *Comput. Biol. Med.* 145, 105457. doi:10.1016/j.combiomed.2022.105457
- Lyu, Y., Chen, X., Xia, Q., Zhang, S., and Yao, C. (2020). Network Pharmacology-Based Study on the Mechanism of Pinellia Ternata in Asthma Treatment. *Evid. Based Complement. Altern. Med.* 2020, 9732626. doi:10.1155/2020/9732626
- Mao, R., and He, Z. (2020). Pinellia Ternata (Thunb.) Breit: A Review of its Germplasm Resources, Genetic Diversity and Active Components. *J. Ethnopharmacol.* 263, 113252. doi:10.1016/j.jep.2020.113252
- Mariotto, S., Suzuki, Y., Persichini, T., Colasanti, M., Suzuki, H., and Cantoni, O. (2007). Cross-talk between NO and Arachidonic Acid in Inflammation. *Curr. Med. Chem.* 14, 1940–1944. doi:10.2174/092986707781368531
- Mishra, S. R., Mahapatra, K. K., Behera, B. P., Patra, S., Bhol, C. S., Panigrahi, D. P., et al. (2021). Mitochondrial Dysfunction as a Driver of NLRP3 Inflammasome Activation and its Modulation through Mitophagy for Potential Therapeutics. *Int. J. Biochem. Cell Biol.* 136, 106013. doi:10.1016/j.biocel.2021.106013
- Mokr , D. (2020). Acute Lung Injury - from Pathophysiology to Treatment. *Physiol. Res.* 69, S353–S366. doi:10.33549/physiolres.934602
- Murakami, T., Ockinger, J., Yu, J., Byles, V., Mccoll, A., Hofer, A. M., et al. (2012). Critical Role for Calcium Mobilization in Activation of the NLRP3 Inflammasome. *Proc. Natl. Acad. Sci. U. S. A.* 109, 11282–11287. doi:10.1073/pnas.1117765109
- Nieves, D., and Moreno, J. J. (2008). Enantioselective Effect of 12(S)-hydroxyicosatetraenoic Acid on 3T6 Fibroblast Growth through ERK 1/2 and P38 MAPK Pathways and Cyclin D1 Activation. *Biochem. Pharmacol.* 76, 654–661. doi:10.1016/j.bcp.2008.06.013
- Pang, Z., Chong, J., Li, S., and Xia, J. (2020). MetaboAnalystR 3.0: Toward an Optimized Workflow for Global Metabolomics. *Metabolites* 10. doi:10.3390/metabo10050186
- Pang, Z., Chong, J., Zhou, G., De Lima Morais, D. A., Chang, L., Barrette, M., et al. (2021). MetaboAnalyst 5.0: Narrowing the Gap between Raw Spectra and Functional Insights. *Nucleic Acids Res.* 49, W388–W396. doi:10.1093/nar/gkab382
- Parekh, D., Dancer, R. C., and Thickett, D. R. (2011). Acute Lung Injury. *Clin. Med. (Lond)* 11, 615–618. doi:10.7861/clinmedicine.11-6-615
- Park, H. Y., Kim, G. Y., Hyun, J. W., Hwang, H. J., Kim, N. D., Kim, B. W., et al. (2012). 7,8-Dihydroxyflavone Exhibits Anti-inflammatory Properties by Downregulating the NF- κ B and MAPK Signaling Pathways in Lipopolysaccharide-Treated RAW264.7 Cells. *Int. J. Mol. Med.* 29, 1146–1152. doi:10.3892/ijmm.2012.935
- Reagan-Shaw, S., Nihal, M., and Ahmad, N. (2008). Dose Translation from Animal to Human Studies Revisited. *FASEB J.* 22, 659–661. doi:10.1096/fj.07-9574LSF
- Riad, M., Mogos, M., Thangathurai, D., and Lumb, P. D. (2002). Steroids. *Curr. Opin. Crit. Care* 8, 281–284. doi:10.1097/00075198-200208000-00002
- Safraan, M., Dalah, I., Alexander, J., Rosen, N., Iny Stein, T., Shmoish, M., et al. (2010). GeneCards Version 3: the Human Gene Integrator. *Database* 2010, baq020. doi:10.1093/database/baq020
- Shannon, P., Markiel, A., Ozier, O., Baliga, N. S., Wang, J. T., Ramage, D., et al. (2003). Cytoscape: a Software Environment for Integrated Models of Biomolecular Interaction Networks. *Genome Res.* 13, 2498–2504. doi:10.1101/gr.1239303
- Shi, J., Cao, B., Wang, X. W., Aa, J. Y., Duan, J. A., Zhu, X. X., et al. (2016). Metabolomics and its Application to the Evaluation of the Efficacy and Toxicity of Traditional Chinese Herb Medicines. *J. Chromatogr. B Anal. Technol. Biomed. Life Sci.* 1026, 204–216. doi:10.1016/j.jchromb.2015.10.014
- Stock, K., Kumar, J., Synowitz, M., Petrosino, S., Imperatore, R., Smith, E. S., et al. (2012). Neural Precursor Cells Induce Cell Death of High-Grade Astrocytomas through Stimulation of TRPV1. *Nat. Med.* 18, 1232–1238. doi:10.1038/nm.2827
- Stueber, T., Eberhardt, M. J., Caspi, Y., Lev, S., Binshtok, A., and Leffler, A. (2017). Differential Cytotoxicity and Intracellular Calcium-Signalling Following Activation of the Calcium-Permeable Ion Channels TRPV1 and TRPA1. *Cell Calcium* 68, 34–44. doi:10.1016/j.cecc.2017.10.003
- Talty, A., Deegan, S., Ljubic, M., Mnich, K., Naicker, S. D., Quandt, D., et al. (2019). Inhibition of IRE1 α RNase Activity Reduces NLRP3 Inflammasome Assembly and Processing of pro-IL1 β . *Cell Death Dis.* 10, 622. doi:10.1038/s41419-019-1847-z
- Tang, X., Zhao, H., Jiang, W., Zhang, S., Guo, S., Gao, X., et al. (2018). Pharmacokinetics and Pharmacodynamics of Citrus Peel Extract in Lipopolysaccharide-Induced Acute Lung Injury Combined with Pinelliae Rhizoma Praeparatum. *Food Funct.* 9, 5880–5890. doi:10.1039/c8fo01337c

- Wang, T., Fu, X., Chen, Q., Patra, J. K., Wang, D., Wang, Z., et al. (2019). Arachidonic Acid Metabolism and Kidney Inflammation. *Int. J. Mol. Sci.* 20. doi:10.3390/ijms20153683
- Wu, T., Hu, E., Xu, S., Chen, M., Guo, P., Dai, Z., et al. (2021). clusterProfiler 4.0: A Universal Enrichment Tool for Interpreting Omics Data. *Innovation* 2, 100141. doi:10.1016/j.xinn.2021.100141
- Xian, H., Liu, Y., Rundberg Nilsson, A., Gatchalian, R., Crother, T. R., Tourtellotte, W. G., et al. (2021). Metformin Inhibition of Mitochondrial ATP and DNA Synthesis Abrogates NLRP3 Inflammasome Activation and Pulmonary Inflammation. *Immunity* 54, 1463–e11. e11. doi:10.1016/j.immuni.2021.05.004
- Xiong, X., Wang, P., Su, K., Cho, W. C., and Xing, Y. (2020). Chinese Herbal Medicine for Coronavirus Disease 2019: A Systematic Review and Meta-Analysis. *Pharmacol. Res.* 160, 105056. doi:10.1016/j.phrs.2020.105056
- Zhai, K., Liskova, A., Kubatka, P., and Büsselberg, D. (2020). Calcium Entry through TRPV1: A Potential Target for the Regulation of Proliferation and Apoptosis in Cancerous and Healthy Cells. *Int. J. Mol. Sci.* 21. doi:10.3390/ijms21114177
- Zhang, M., Gao, Y., Zhao, W., Yu, G., and Jin, F. (2018). ACE-2/ANG1-7 Ameliorates ER Stress-Induced Apoptosis in Seawater Aspiration-Induced Acute Lung Injury. *Am. J. Physiol. Lung Cell Mol. Physiol.* 315, L1015–L1027. doi:10.1152/ajplung.00163.2018
- Zhang, X., Cai, Y., Wang, L., Liu, H., and Wang, X. (2015). Optimization of Processing Technology of Rhizoma Pinelliae Praeparatum and its Anti-tumor Effect. *Afr. Health Sci.* 15, 101–106. doi:10.4314/ahs.v15i1.14
- Zhao, Y., Jiang, Y., Chen, L., Zheng, X., Zhu, J., Song, X., et al. (2020). Inhibition of the Endoplasmic Reticulum (ER) Stress-Associated IRE-1/XBP-1 Pathway Alleviates Acute Lung Injury via Modulation of Macrophage Activation. *J. Thorac. Dis.* 12, 284–295. doi:10.21037/jtd.2020.01.45
- Zhu, X., Huang, L., Gong, J., Shi, C., Wang, Z., Ye, B., et al. (2017). NF-κB Pathway Link with ER Stress-Induced Autophagy and Apoptosis in Cervical Tumor Cells. *Cell Death Discov.* 3, 17059. doi:10.1038/cddiscovery.2017.59



OPEN ACCESS

EDITED BY

Haitao Lu,
Prof., FRSC, Shanghai Jiao Tong
University, China

REVIEWED BY

Enilton A. Camargo,
Federal University of Sergipe, Brazil
Zhenzhou Jiang,
China Pharmaceutical University, China

*CORRESPONDENCE

Chengping Wen,
wengcp@163.com
Jia Zhou,
zhoujia@zcmu.edu.cn,
orcid.org/0000-0003-2182-8440

[†]These authors have contributed equally
to this work

SPECIALTY SECTION

This article was submitted to
Ethnopharmacology,
a section of the journal
Frontiers in Pharmacology

RECEIVED 08 May 2022

ACCEPTED 03 August 2022

PUBLISHED 29 August 2022

CITATION

Zhu Y, Zhang L, Zhang X, Wu D, Chen L,
Hu C, Wen C and Zhou J (2022),
Tripterygium wilfordii glycosides
ameliorates collagen-induced arthritis
and aberrant lipid metabolism in rats.
Front. Pharmacol. 13:938849.
doi: 10.3389/fphar.2022.938849

COPYRIGHT

© 2022 Zhu, Zhang, Zhang, Wu, Chen,
Hu, Wen and Zhou. This is an open-
access article distributed under the
terms of the [Creative Commons
Attribution License \(CC BY\)](https://creativecommons.org/licenses/by/4.0/). The use,
distribution or reproduction in other
forums is permitted, provided the
original author(s) and the copyright
owner(s) are credited and that the
original publication in this journal is
cited, in accordance with accepted
academic practice. No use, distribution
or reproduction is permitted which does
not comply with these terms.

Tripterygium wilfordii glycosides ameliorates collagen-induced arthritis and aberrant lipid metabolism in rats

Yitian Zhu^{1†}, Luyun Zhang^{2†}, Xiaofeng Zhang^{2†}, Dehong Wu³,
Leiming Chen⁴, Changfeng Hu², Chengping Wen^{2*} and
Jia Zhou¹ ^{2*}

¹The Second Clinical Medical College of Zhejiang Chinese Medical University, Hangzhou, China, ²Institute of Basic Research in Clinical Medicine, College of Basic Medical Science, Zhejiang Chinese Medical University, Hangzhou, China, ³The Second Affiliated Hospital of Zhejiang Chinese Medical University, Hangzhou, China, ⁴Department of Nephrology, Wenzhou Hospital of Integrated Traditional Chinese and Western Medicine, Wenzhou, China

Rheumatoid arthritis (RA) is a chronic inflammatory autoimmune disease, and the dysregulation of lipid metabolism has been found to play an important role in the pathogenesis of RA and is related to the severity and prognosis of patients. Tripterygium wilfordii glycosides (TWG) is extracted from the roots of Tripterygium wilfordii Hook F. with anti-inflammatory and immunosuppressive effects, and numerous clinical trials have supported its efficacy in the treatment of RA. Some evidence suggested that TWG can modulate the formation of lipid mediators in various innate immune cells; however whether it can improve RA-related lipid disorders has not been systematically studied. In the study, type II collagen-induced arthritis (CIA) model was used to investigate the efficacy of TWG in the treatment of RA and its effect on lipid metabolism. Paw volume, arthritis score, pathological changes of ankle joint, serum autoantibodies and inflammatory cytokines were detected to assess the therapeutic effect on arthritis in CIA rats. Then, shotgun lipidomics based on multi-dimensional mass spectrometry platform was performed to explore the alterations in serum lipidome caused by TWG. The study showed that TWG could effectively ameliorate arthritis in CIA rats, such as reducing paw volume and arthritis score, alleviating the pathological damages of joint, and preventing the production of anti-CII autoantibodies and IL-1 β cytokine. Significant increase in ceramide and decrease in lysophosphatidylcholine were observed in CIA rats, and were highly correlated with arthritis score and IL-1 β level. After TWG treatment, these lipid abnormalities can be corrected to a great extent. These data demonstrate that TWG exerts a beneficial therapeutic effect on aberrant lipid metabolism which may provide new insights for further exploring the role and mechanism of TWG in the treatment of RA.

KEYWORDS

rheumatoid arthritis, *Tripterygium wilfordii* glycosides, lipid metabolism, shotgun lipidomics, collagen-induced arthritis

1 Introduction

Rheumatoid arthritis (RA) is a chronic autoimmune disease affecting about 0.5–1% of the population worldwide (Symmons et al., 2002; Humphreys et al., 2013), with a high prevalence in women and a considerable disease and social burden including joint pain, disability, high incidence of comorbidities and long-term financial costs (Dougados et al., 2014). The true etiology of RA is complex, involving multiple factors such as pathogen infection, genetics, immunity, etc., and remains to be completely elucidated (McInnes and Schett, 2011; Croia et al., 2019; Jung et al., 2019; Karami et al., 2019). At present, the primary goal of RA treatment is to relieve symptoms and slow down the progress of the disease. A better understanding of disease mechanisms could lead to the development of effective preventive and therapeutic approaches to RA.

Numerous studies have demonstrated that lipids play an important role in the pathogenesis of RA. Some lipid species, like eicosanoids, sphingolipids and lipoxins, etc., are considered to be crucial for the development of arthritic diseases by tightly regulating inflammatory processes (Gerritsen et al., 1998; Serhan et al., 2008; McInnes and Schett, 2011). Peroxidation of membrane phospholipids produces biologically active aldehydes, such as malonaldehyde (MDA) and 4-hydroxynonenal (HNE), which damage the fluidity and permeability of the plasmatic membrane, eventually leading to destruction of cell structure and function (Phaniendra et al., 2015; Quiñonez-Flores et al., 2016). Studies have found that MDA level in RA patients was significantly elevated (Aryaeian et al., 2011; Hassan et al., 2011; Mishra et al., 2012), and positively associated with RA activity (Datta et al., 2014). In addition, alterations in a number of phosphatidylcholine (PC), lysophosphatidylcholine (LysoPC), phosphatidylethanolamine (PE), and sphingomyelin (SM) have been recognized to be correlated with disease activity in RA patients and reflect the therapeutic response to anti-rheumatic drugs (Kosinska et al., 2014; Koh et al., 2022). There are changes in the lipoprotein profiles in RA patients that may lead to increased morbidity and mortality (Toms et al., 2010). About 55–65% of RA patients developed dyslipidemia at an early stage (Curtis et al., 2012; Bag-Ozbek and Giles, 2015; Nowak et al., 2016; Phull et al., 2018), which may be accountable for the higher risk of comorbidities such as cardiovascular disease (CVD) in these patients (Myasoedova et al., 2010; Bag-Ozbek and Giles, 2015; Charles-Schoeman et al., 2015; Luczaj et al., 2016).

Tripterygium wilfordii Hook F. (TWHF), a traditional herbal medicine, was reported to be effective in the treatment of RA and other immune diseases (Tao and Lipsky, 2000; Jiang et al., 2015).

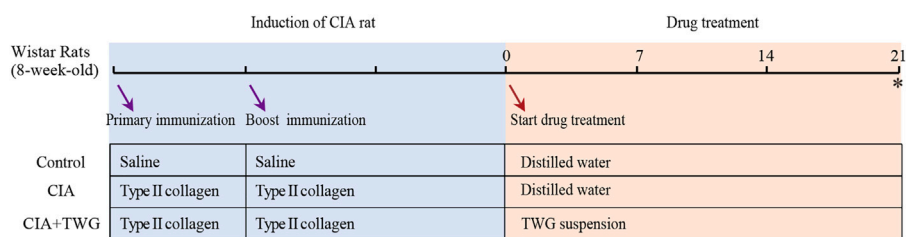
Tripterygium wilfordii glycosides (TWG) is extracted from the roots of TWHF and exhibits anti-inflammatory and immunosuppressive effects (Ma et al., 2007). Research in synovial fibroblasts of arthritis patients suggested that TWG has an effect on decreasing the activity of nuclear factor κ -B (NF- κ B), inhibiting gene expression of cyclooxygenase (COX)-2 and inducible nitric oxide synthase (iNOS), reducing the production of prostaglandin E2 (PGE2) and NO, and promoting caspase-3 expression (Yang et al., 2020). The dysregulation of lipid metabolism has been suggested to be involved in the pathogenesis of RA and is related to the severity and prognosis of patients. Improving lipid metabolism can help restore the metabolic homeostasis of RA patients, thereby alleviating the disease and reducing complications. Although TWG has been shown to exert a beneficial therapeutic effect in RA, whether it can improve RA-related lipid disorders has not been studied.

In the present study, type II collagen-induced arthritis (CIA) rat model, which has better similarity to human RA due to its chronic disease process (Holmdahl et al., 1992), was used to investigate the efficacy of TWG in the treatment of RA and its effect on lipid metabolism. The changes in paw volume, arthritis score, pathological changes of joint, serum autoantibodies and pro-inflammatory cytokines were detected to assess the efficacy of TWG on collagen-induced arthritis. Multi-dimensional mass spectrometry-based shotgun lipidomics (MDMS-SL) platform was employed to analyze the alterations of serum lipidome induced by TWG. Our results may provide further evidence of the role and mechanism of TWG in the treatment of RA.

2 Materials and methods

2.1 Reagents

Bovine type II collagen (CII) was purchased from Chondrex (Redmond, WA, United States), Freund's complete adjuvant (FCA) and Freund's incomplete adjuvant (FIA) were purchased from Sigma (St. Louis, MO, United States). Lipid standards were purchased from Avanti Polar lipids, Inc. (Alabaster, AL, United States). Chromatographic grade methanol and chloroform were purchased from Merck (Darmstadt, Germany). *Tripterygium wilfordii* glycosides tablets were purchased from Deende Pharmaceutical Co., Ltd. (Zhejiang, China. Lot: 1206101, 10 mg/tablet). The ELISA kit for rat IL-1 β was purchased from R&D systems (Minneapolis, MN, United States), and the anti-type II collagen antibodies (anti-CII) in serum were assayed by ELISA kit (Chondrex, Redmond, WA, United States).



* Rats sacrificed and sampled

FIGURE 1

Experimental flow chart for evaluating the effect of TWG on collagen-induced arthritis in Wistar rats.

2.2 Animal modeling and drug treatment

Female Wistar rats, 7 weeks old, weighing (160 ± 20) g, were provided by the Laboratory Animal Services Center of Zhejiang Chinese Medical University (Hangzhou, China). The animal experiment was approved by the Animal Ethics Committee of Zhejiang Chinese Medical University. After adaptive feeding for 1 week, rats were used to establish collagen-induced arthritis model according to a literature method (Rosloniec et al., 2010). The brief description is as follows: six rats were selected as control group, and the others were primarily immunized with CII emulsified in FCA. About 200 μ L of bovine CII emulsion (1.0 mg/ml) was injected intradermally at the base of the tail. 1 week after the primary immunization, a booster immunization was given with 150 μ L of CII emulsion in FIA (1.0 mg/ml). The control group was injected with an equal volume of normal saline.

21 days after primary immunization, the rats with induced arthritis (arthritis score > 6) were randomly divided into model group (CIA group, $n = 6$) and CIA + TWG group ($n = 6$). The CIA + TWG group was administrated with 6 mg/kg of TWG per day, equivalent to regular human dose of 1 mg/kg per day. The TWG suspension was prepared from tablet powder dissolved in distilled water. The CIA group and control group were given orally the same volume of distilled water. The rats were anesthetized with chloral hydrate (10%, w/v) and blood was collected from abdominal aorta after 21 days of intervention. The serum was separated by centrifugation for 10 min at 1,200 g and all samples were stored in refrigerator at -80°C . The detailed experimental process and grouping information are shown in Figure 1.

2.3 Evaluation of arthritis severity

After primary immunization, arthritis scores were measured every 7 days. Arthritis severity of each limb was graded on a 0–4 scale according to the modified method of (Wang et al.,

2021): no swelling (0 points); mild swelling of the little toe joints (1 point); swelling of the toe joints and foot plantar (2 points); swelling of the foot below the ankle (3 points); swelling of entire foot, including the ankle (4 points). The arthritis score of the rat was obtained by summing the scores of the four limbs, and a score equal to or greater than 6 points is considered to be successful modeling, with a maximum score of 16 points (4×4). In addition, at 0, 7, 14 and 21 days after drug treatment, the paw volume of the right hind limb was measured with a toe volume meter as the paw swelling index.

At the end of the animal experiment, ankle joints of rats were taken out. X-ray images (CARESTREAM Image Station System, Carestream Health, Inc., United States) were taken to observe the morphological changes of the joints. Furthermore, ankle joints were flushed with PBS, and fixed by 4% paraformaldehyde for 48 h. After decalcification, paraffin sections were made and stained with hematoxylin and eosin (H&E) to evaluate the histological changes of ankle joints.

2.4 Detection of IL-1 β and anti-CII antibodies levels

An aliquot (100 μ L) of serum samples from different groups or rats were collected to measure the levels of IL-1 β and anti-CII antibodies by ELISA kits according to the manufacturers' instructions.

2.5 Lipid extraction, analysis and data preprocessing

Serum lipids were extracted by the modified Bligh-Dye protocol (Bligh and Dyer, 1959) in the presence of internal standards as described in the reference (Yang et al., 2009). The chloroform phase containing lipids was collected. The extraction process was repeated twice, and the lipid extracts were combined and evaporated under a nitrogen stream. The dried lipid extracts were redissolved in 2 μ L of

chloroform/methanol (1:1, v/v), sealed with nitrogen, and stored at -20°C until analysis.

The analysis of serum lipids was carried out on a triple-quadrupole mass spectrometer (TSQ Quantiva, Thermo Scientific) connected to an automated nanospray ion source (NanoMate, Advion Bioscience) according to the reference (Han et al., 2005). Before lipid analysis, each lipid extract was further diluted with chloroform/methanol/isopropyl alcohol (1:2:4, v/v/v). Various species of lipids were characterized and quantified by MDMS-SL according to the reference (Yang, et al., 2009).

All the mass data were acquired through different sequence subroutines running by Xcalibur software. Data preprocessing, including baseline calibration, de-isotope peak, peak intensity calculation, etc., was carried out according to the published reference (Han, et al., 2005).

2.6 Statistical analysis

Principal component analysis (PCA) based on the phospholipid profiles was carried out by SIMCA-P 14.1 (Umetrics AB, Umea, Sweden) to generally observe the distribution of samples from the control, CIA and CIA + TWG groups after mean centering. Furthermore, orthogonal partial least squares discriminant analysis (OPLS-DA) was employed to distinguish groups and screen the discriminant serum lipids. Permutation test was used to verify whether the model was over-fitted. Lipids with a variable importance in projection (VIP) value of the OPLS-DA model greater than 1.0 were considered to play an important role in the classification of different groups. Both p values and VIP values were taken as criteria for screening potential differential lipids, and $\text{VIP} > 1.0$ and $p < 0.05$ were used as cutoff.

To investigate the statistical significance in the levels of the paw volume, arthritis scores, IL-1 β , anti-CII and lipids between control, CIA and CIA + TWG groups, ANOVA followed by a Bonferroni post hoc test for pairwise comparisons were performed using SPSS 18.0 (International Business Machines Corp., Armonk, United States). And $p < 0.05$ was considered statistically significant. In addition, Pearson's correlation between the arthritis score, IL-1 β , anti-CII and differential lipids were analyzed.

2.7 Role of the funding source

No funding source had any role in study design; in the collection, analysis, and interpretation of data; in the writing of the report; and in the decision to submit the paper for publication. The corresponding author had full access to all the data in the study and had final responsibility for the decision to submit for publication.

3 Results

3.1 Exploring the change of paw volume, arthritis score, IL-1 β and anti-CII after *Tripterygium wilfordii* glycosides treatment

During the experiment, we continued to observe the general condition of the rats. The rats in the control group were in good condition, with shiny fur and free movement. 5–7 days after the booster immunization with collagen, the CIA rats gradually developed polyarthritis, and showed fatigue, weight loss, swelling of foot joints, lameness and mobility impairment. After 21 days of treatment, the CIA + TWG group had smoother fur, significantly increased body weight ($p < 0.05$, Figure 2A), and improved mobility compared with the CIA group.

The severity of arthritis was measured by the paw volume and arthritis score, with greater paw volume and higher arthritis score indicating more severe disease. After modeling, the paw volume of the right hind foot and arthritis score in the CIA group were significantly higher than those in the control group ($p < 0.01$, $p < 0.01$); after 14 days of treatment, compared with the CIA group, the paw volume and arthritis score of CIA + TWG group began to decrease significantly ($p < 0.05$, $p < 0.01$); after 21 days of treatment, the paw volume and arthritis score in the CIA + TWG group continued to decrease ($p < 0.01$, $p < 0.01$), suggesting that the joint swelling was alleviated by TWG (Figures 2B,C).

Then, we investigated the change of pro-inflammatory cytokine in CIA rats. In the study, serum level of IL-1 β in CIA group was significantly increased; 21 days after TWG treatment, the IL-1 β level was remarkably decreased as compared with the CIA group ($p < 0.01$, Figure 2D), indicating that TWG could inhibit the production of IL-1 β to suppress the inflammatory response.

In addition, we examined the levels of anti-CII antibodies in the CIA and CIA + TWG groups after 21 days of treatment. Compared with the CIA group, the level of anti-CII antibodies was relatively lower after the treatment of TWG ($p < 0.01$, Figure 2E), indicating that TWG could prevent the antibody response mediated by collagen.

X-ray images showed that the CIA group developed severe joint swelling, joint deformity, joint space narrowing and other arthritis-related joint characteristics; after 21 days of treatment, the CIA + TWG group had mild joint space narrowing, joint swelling, joint deformity relief, etc., (Figures 3A–C). The H&E stained histological of ankle joint showed that there were narrowed joint space, significant proliferation of fibrous connective tissue and infiltration of inflammatory cells, and severe erosion of articular cartilage and bone in the CIA group. TWG could alleviate the pathological damages of joint

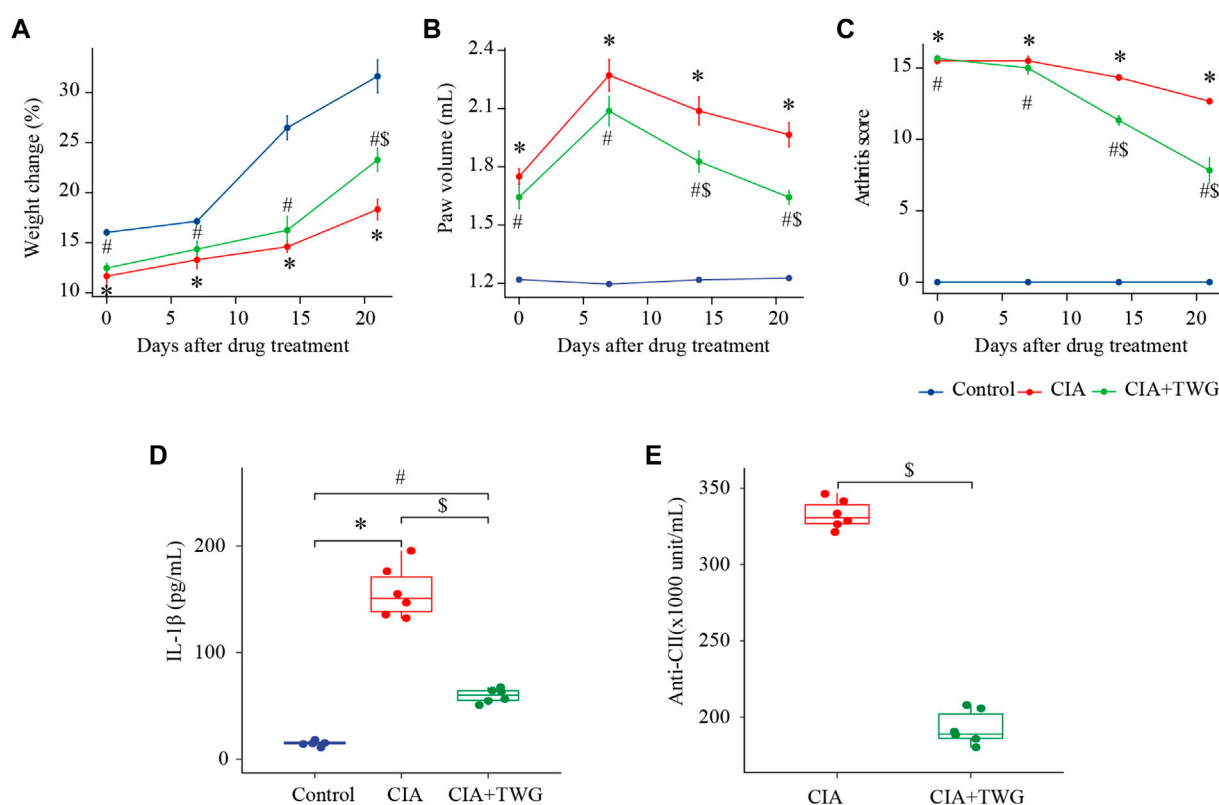


FIGURE 2

Comparison of percentage of weight change (A), paw volume (B), arthritis score (C), IL-1 β level (D), anti-CII level (E) in rats of the control, CIA and CIA + TWG groups. The percent change in weight was calculated as (weight after drug treatment-weight before immunization)/weight before immunization. * represents $p < 0.05$ between the control and CIA groups, # represents $p < 0.05$ between the control and CIA + TWG groups, and \$ represents $p < 0.05$ between the CIA and CIA + TWG groups.

tissues, including reducing inflammatory cell infiltration, and relieving articular cartilage and bone injury (Figures 3D,E).

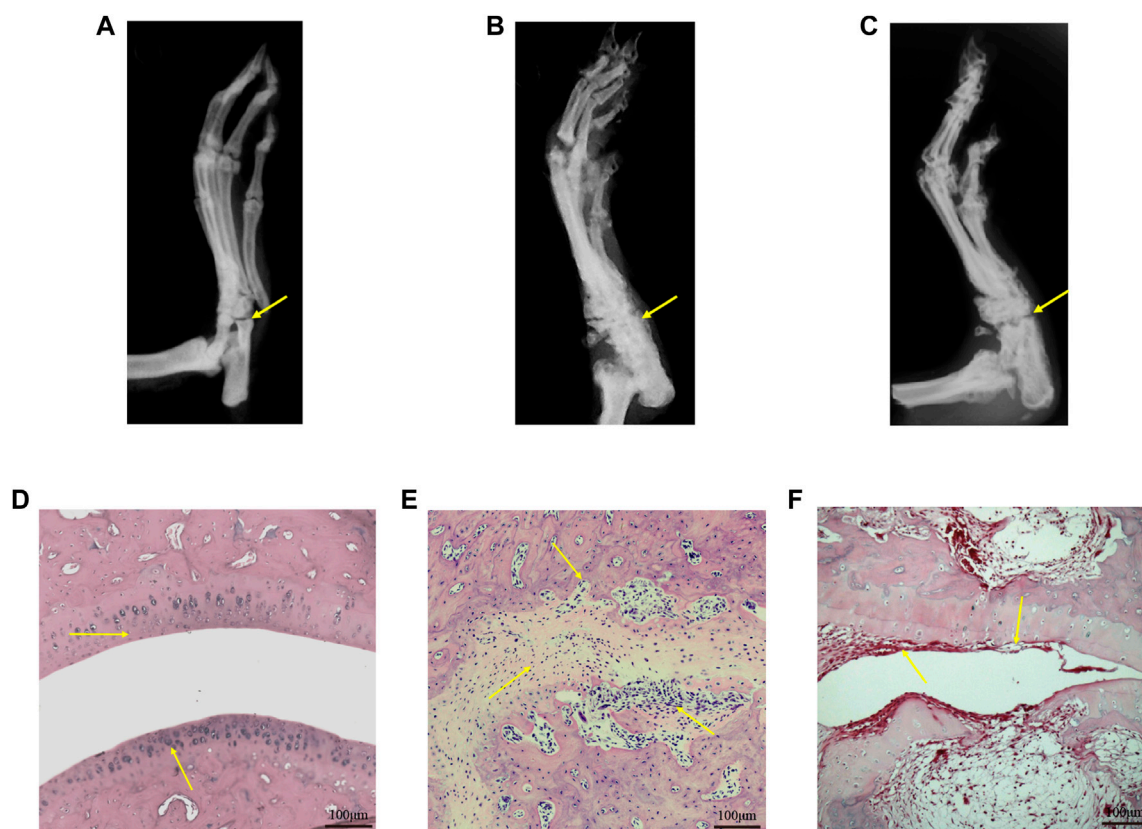
3.2 Alterations of total amounts of each lipid species after *Tripterygium wilfordii* glycosides treatment

Lipids in rat serum were analyzed by MDMS-SL. After data preprocessing such as baseline correction and peak intensity calculation, nearly 100 kinds of lipid molecules belonging to 6 lipid species with high response in mass spectrometry were quantified, including SM, PC, LysoPC, ceramide (Cer), phosphatidylinositol (PI) and phosphatidylglycerol (PG). The total amounts of each lipid species in different groups were calculated respectively. It was found that the most abundant phospholipids are PC and LysoPC among the 6 phospholipid species (Figure 4). As compared to the control group, the total SM level and Cer level was significantly up-regulated in the CIA group ($p < 0.05$), while the total LysoPC level was significantly down-regulated ($p < 0.05$). 21 days after

TWG treatment, the total LysoPC level was increased to that of the control group. In addition, TWG treatment reduced the total level of Cer (Figure 4).

3.3 Visualization of the difference of lipid profile after *Tripterygium wilfordii* glycosides treatment

In order to display the overall distribution and clustering of the samples from the control group, the CIA group and CIA + TWG group, the lipid data were subjected to PCA after mean centering. Principal components 1 and 2 explained 53.7% and 25.5% of the variance, respectively. The PCA score plot is shown in Figure 5A, it was observed that there is a clear separation in the lipid profiles between the CIA group and the control group, reflecting the significant changes in serum lipid metabolism in rats after the injection of collagen. The lipid profile of CIA + TWG group tends to be closer to that of the control group, but it is still different from that of the control group.

**FIGURE 3**

Representative X-ray images and H&E stained histological images of ankle joints in rats of the control [(A) and (D)], CIA [(B) and (E)] and CIA + TWG [(C) and (F)] groups.

3.4 Alterations of serum lipids associated with collagen immunization and/or *Tripterygium wilfordii* glycosides treatment

To reveal the lipid alterations caused by collagen immunization and TWG treatment, OPLS-DA was performed between the control group, CIA group and CIA + TWG groups. Permutation tests indicated good fitness of the OPLS-DA models in revealing the alterations in serum lipids. OPLS-DA score plots showed both collagen induction and TWG treatment led to changes in lipid profile (Figures 5B–D). Differential lipids were screened out based on the VIP values of OPLS-DA models ($VIP > 1$) and p values of significance tests ($p < 0.05$).

The collagen-induced abnormal lipids were selected by comparing the CIA group with the control group. Finally, 42 kinds of altered lipids were identified. There were significant decreases in 4 kinds of LysoPC (18:0, 20:4, 18:2 and 22:6) and 3 kinds of PC (D18:0–20:4, D18:2–22:6 and D18:0–22:6), increases in 3 kinds of Cer (N22:0, N23:0 and N24:0), 9 kinds of PI (16:0–18:2, 16:0–20:4, 18:1–18:2, 18:0–18:2, A18:0–20:4, 16:0–22:6, 18:0–22:6, 18:0–22:5 and 16:0–18:1), 13 kinds of SM (N15:0, N16:1, N16:0,

N17:0, N18:1, N23:0, N24:3, N24:2, N24:1, N24:0, N18:0, N20:0 and N22:1) and 10 kinds of PC (A16:0–16:0, D16:0–16:0, P16:0–18:1, P18:0–16:0, D16:0–18:2, D16:0–18:1, D18:1–18:2, P18:0–20:4, D18:0–20:2 and P16:0–16:0) in CIA rats (Figure 6).

The serum lipids related to TWG treatment were screened out by comparing the CIA group with the CIA + TWG group. It was found that 16 kinds of lipids were altered after the treatment of TWG. Among them, 5 kinds of sphingolipids were reduced after treatment, including 3 kinds of Cer (N22:0, N23:0 and N24:0) and 2 kinds of SM (N20:0 and N22:1); 11 kinds of glycerophospholipids were elevated, such as LysoPC (18:0, 20:4, 18:2, 14:0 and 18:1), PI (16:0–18:1 and 16:1–20:4), PC (D18:0–20:2, P16:0–16:0 and D16:1–18:2) and SM (N18:0) (Figure 6).

3.5 Effects of *Tripterygium wilfordii* glycosides treatment on the collagen-induced abnormal lipids

The effects of TWG on the collagen-induced abnormal lipids were also investigated (Figure 6). TWG treatment

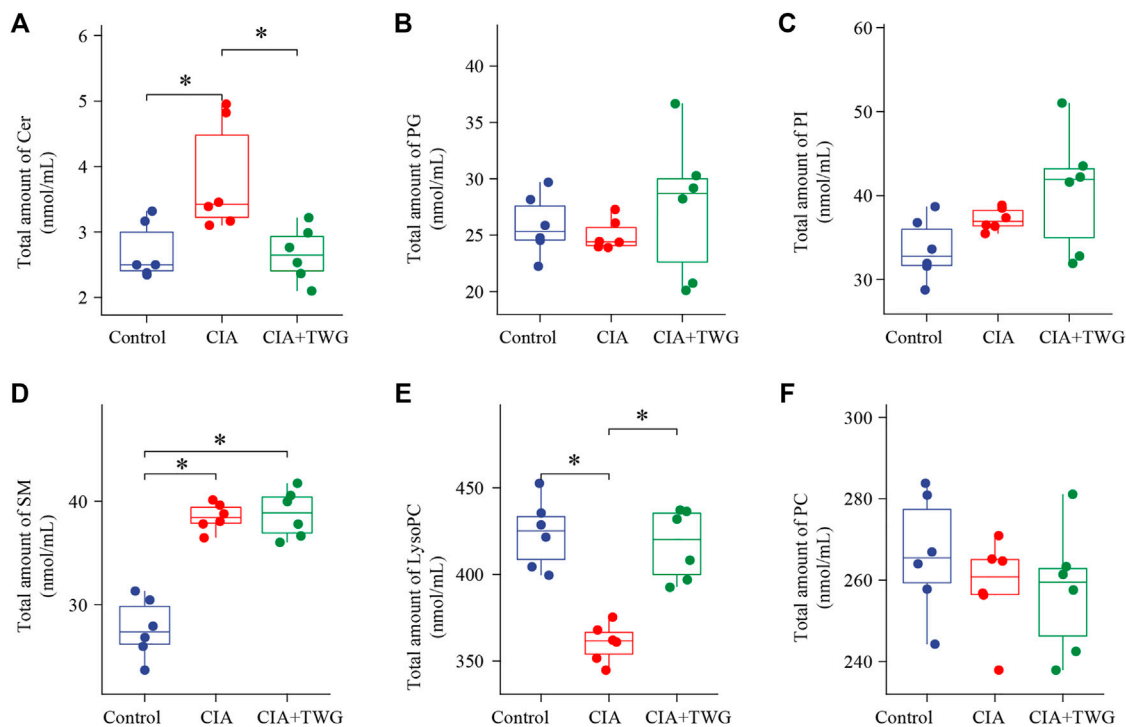


FIGURE 4
Comparison of the total amounts of individual Q18 lipid species in rats of the control, CIA and CIA + TWG groups. (A) Cer, (B) PG, (C) PI, (D) SM, (E) LysoPC, (F) PC. * $p < 0.05$.

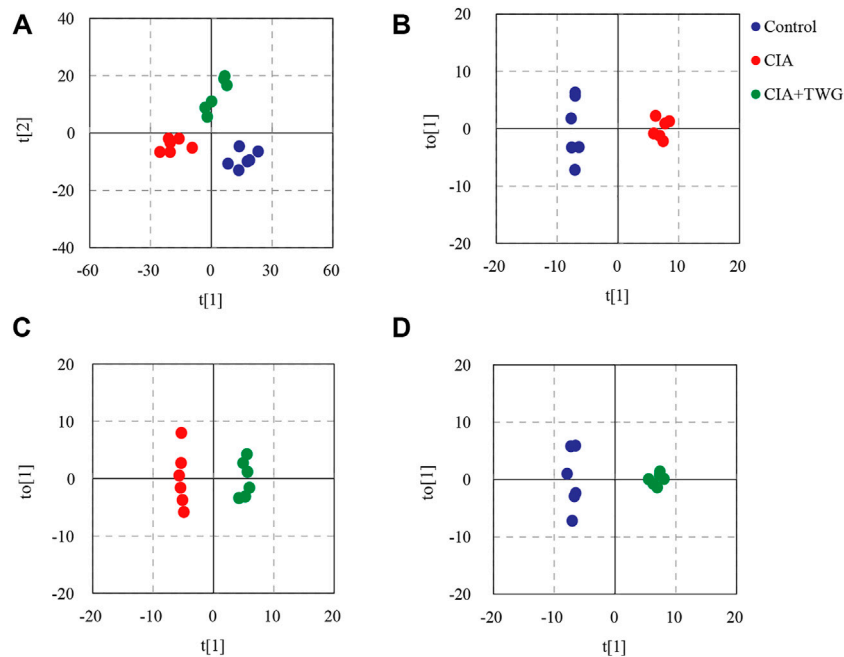
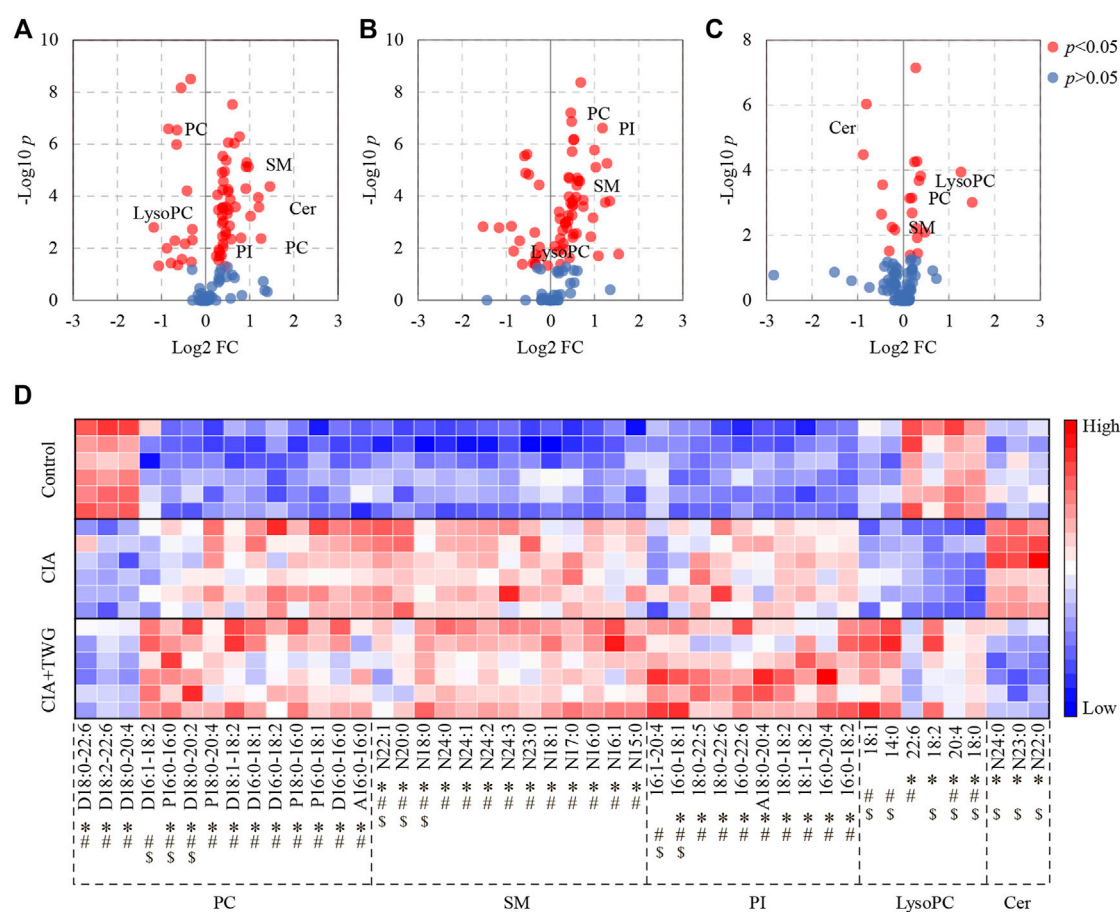


FIGURE 5
PCA and OPLS-DA based on the serum lipid profiles. (A) PCA score plot of the control, CIA and CIA + TWG groups, (B) OPLS-DA score plot of the control and CIA groups, (C) OPLS-DA score plot of the CIA and CIA + TWG groups, (D) OPLS-DA score plot of the control and CIA + TWG groups.

**FIGURE 6**

Significantly altered serum lipids related to collagen immunization and TWG treatment. Volcano plot showing the lipids with significant differences between the control and CIA groups (A), between the control and CIA + TWG groups (B), between the CIA and CIA + TWG groups (C), and heatmap showing the expression pattern of each differential lipid (D). Red color indicates high concentration of lipid and blue color indicates low concentration. * represents $p < 0.05$ between the control and CIA groups, # represents $p < 0.05$ between the control and CIA + TWG groups, and \$ represents $p < 0.05$ between the CIA and CIA + TWG groups.

adjusted the levels of 8 kinds of lipids closer to the normal level, including down-regulation of N22:0 Cer, N23:0 Cer, N24:0 Cer, N20:0 SM and N22:1 SM, up-regulation of 18:0 LysoPC, 20:4 LysoPC and 18:2 LysoPC; however, it caused the levels of 16:0–18:1 PI, N18:0 SM, D18:0–20:2 PC and P16:0–16:0 PC to be further away from the normal level. These results indicated that the abnormal lipid metabolism in CIA rats could be alleviated by TWG to a certain extent, especially Cer and LysoPC species.

3.6 Significant associations of arthritis score, IL-1 β , anti-CII antibodies with the levels of those differential lipids

In the study, we found there was a significant positive correlation between IL-1 β and arthritis score, which can reflect the severity of joint swelling. Among those screened lipids, the

levels of Cer (N24:0, N23:0 and N22:0), SM (N22:1 and N20:0) were positively correlated with IL-1 β level and arthritis score, as were the total amounts of SM species and Cer species; while LysoPC (20:4 and 18:0) and the total amount of LysoPC species were negatively correlated with IL-1 β and arthritis score. After collagen immunization, antibody response against CII was induced, and TWG treatment downregulated the level of anti-CII antibodies. There is an association between LysoPC, SM, Cer and anti-CII antibodies existed in CIA rats ($p < 0.05$, Figure 7).

4 Discussion

CIA is an extensively used animal model of autoimmune arthritis. The pathological manifestations of CIA models are progressive synovitis and synovial hyperplasia, inflammatory cell infiltration, cartilage destruction, and finally lead to joint injury and stiffness; these characteristics are more similar to

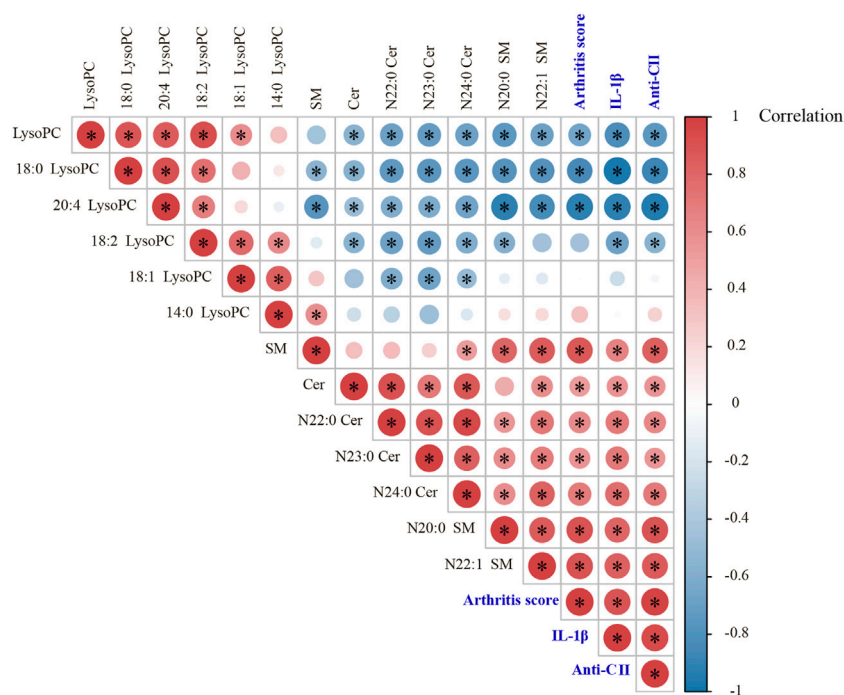


FIGURE 7

Pearson correlation analyses between arthritis score, IL-1 β , anti-CII antibodies and those significantly changed lipids in different groups of rats.

those of clinical RA (Holmdahl, et al., 1992). CIA model is established by immunizing genetically susceptible strains of mice/rats with CII. CII activates innate and adaptive immune responses, which have a primary role in the initiation and pathogenesis of RA in CIA model. Some studies found that anti-CII antibodies are present in the serum and synovial fluid of RA patients precede the onset of joint symptoms (Mullazehi et al., 2007; Whittingham et al., 2017). Patients with positive anti-CII antibodies exhibited higher disease activity and more severe symptoms (Mullazehi, et al., 2007). In the study, CIA rat model was used to investigate the efficacy of TWG. Anti-CII antibodies can be detected in CIA rats which implied that the immune response is induced by CII immunization. IL-1 β is the initiating factor of inflammation and regulates a variety of cytokines, cell adhesion molecules and inflammatory mediators. Previous studies have shown that the level of IL-1 in the circulation of RA patients is higher than that of other chronic inflammatory joint diseases (Kay and Calabrese, 2004), and is associated with bone erosion and cartilage destruction in RA (Guo et al., 2018). Our results demonstrated that TWG could alleviate the severity of the disease, including reducing joint swelling, repairing joint injury, decreasing the generation of serum autoantibodies (anti-CII) and the secretion of pro-inflammatory cytokines (IL-1 β).

As energy sources, structural constituents and signaling molecules, lipids participate in the regulation of many important biological processes, such as cell growth, proliferation,

differentiation, death, etc., (Wymann and Schneider, 2008; Han, 2016). The disorders of lipid metabolism may lead to abnormalities in signaling, inflammation and autoimmune responses (Wymann and Schneider, 2008). In this study, shotgun lipidomics revealed that the total amounts of Cer and SM species were increased in CIA rats, and were positively correlated with pro-inflammatory cytokine IL-1 β . SM is an important component of cell biofilms and plasma lipoproteins, and plays a pro-inflammatory role by enhancing the expression of COX-2 and encoding genes related to inflammatory cytokines (Miltnerberger-Miltner et al., 2020). SM can be hydrolyzed into Cer, which is involved in TNF α -mediated activation of NF- κ B and RANKL-mediated osteoclast differentiation to promote the development of RA (Qu et al., 2018). Recent studies have found that the levels of Cer and SM species in synovial fluid of patients with RA and osteoarthritis were increased as compared to the healthy controls, which is consistent with the role of Cer and SM in inflammation (Aletaha et al., 2010). The study showed that the treatment of TWG could totally reverse the elevation of Cer level, and greatly reduce the levels of some SM (N20:0 and N22:1) molecules, which may facilitate the amelioration of inflammation and joint swelling in CIA rats. Ceramidase is essential for converting Cer to sphingosine, and some evidence suggested that TWG can interact with ceramidase to regulate the level of Cer (Qian et al., 2022).

LysoPC is generated by phospholipase A2 (PLA2)-catalyzed degradation of membrane PC (Law et al., 2019),

and plays a chemotactic role at the inflammatory site, thus boosting inflammatory response. However, it was reported that low level of LysoPC was observed in active RA patients, which might be related to the decrease of PLA2 activity (Lourida et al., 2007; Koh, et al., 2022). Our study also showed that the total amount of LysoPC was significantly decreased in CIA rats, and accordingly, the levels of most PC molecules were elevated to some extent. LysoPC is a major component of oxidized low density lipoprotein (oxLDL), which has been proposed as a critical pathogenic factor of atherosclerosis (Law, et al., 2019). Evidence suggested that there was an inverse correlation between LysoPC and the risk of CVD (Lee et al., 2013; Stegemann et al., 2014), which has a high incidence in RA patients (Aviña-Zubieta et al., 2008). Intriguingly, the reduced level of LysoPC in CIA rats can be corrected after the treatment of TWG. Network pharmacology research has found that some absorbed components of TWG, such as hypoglaulide, triptotriterpenic acid A, Wilforlide A, can target PLA2G10, PLA2G2A and PLA2G1B, thereby interfering with glycerol phospholipid metabolism and ether lipid metabolism, which in turn led to changes in the level of lysoPC and PC (Qian, et al., 2022). Taken together, the observed lipid profiles suggest an ameliorative effect of TWG on lipid disorders associated with RA, but do not provide a mechanistic explanation for the finding. Whether this is a cause or a consequence of joint inflammation remains to be investigated further, which is one of the limitations of this study.

5 Conclusion

The present study showed that TWG could effectively relieve the joint swelling, repair joint injury, and prevent the production of anti-CII autoantibodies and the secretion of IL-1 β cytokine in CIA rats. Moreover, TWG could improve aberrant lipid metabolism caused by collagen immunization, including down-regulating Cer level and up-regulating LysoPC level. These results suggest that TWG exerts a beneficial therapeutic effect on lipid metabolism disorders, and further research is needed to better explain the biological mechanisms underlying these findings.

Data availability statement

The original contributions presented in the study are included in the article/supplementary material, further inquiries can be directed to the corresponding authors.

References

Aletaha, D., Neogi, T., Silman, A. J., Funovits, J., Felson, D. T., Bingham, C. O., et al. (2010). 2010 rheumatoid arthritis classification criteria: An American college

Ethics statement

The animal study was reviewed and approved by Experimental Animal Health Ethics Committee of Zhejiang Chinese Medical University.

Author contributions

Authors' contributions were as follows: experiment design (JZ and CW); animal experiment (LZ and LC); lipidomics study (LZ and CH); ELISA assay (YZ and DW); histological analysis (XZ); data analysis (JZ and DW); manuscript writing (YZ and JZ); and critical revisions (JZ and CW). All authors have read and approved the final manuscript.

Funding

This study has been supported by the National Key R&D Program of China (No. 2018YFC1705500), and the National Natural Science Foundation of China (No. 81403269).

Acknowledgments

We appreciate the technical support from the Public Platform of Medical Research Center, Academy of Chinese Medical Science, Zhejiang Chinese Medical University.

Conflict of interest

The authors declare that the research was conducted in the absence of any commercial or financial relationships that could be construed as a potential conflict of interest.

Publisher's note

All claims expressed in this article are solely those of the authors and do not necessarily represent those of their affiliated organizations, or those of the publisher, the editors and the reviewers. Any product that may be evaluated in this article, or claim that may be made by its manufacturer, is not guaranteed or endorsed by the publisher.

of rheumatology/European league against rheumatism collaborative initiative. *Arthritis Rheum.* 62 (9), 2569–2581. doi:10.1002/art.27584

- Aryaeian, N., Djalali, M., Shahram, F., Jazayeri, S., Chamari, M., and Nazari, S. (2011). Beta-carotene, vitamin E, MDA, glutathione reductase and arylesterase activity levels in patients with active rheumatoid arthritis. *Iran. J. Public Health* 40 (2), 102–109.
- Aviña-Zubieta, J. A., Choi, H. K., Sadatsafavi, M., Etminan, M., Esdaile, J. M., and Lacaille, D. (2008). Risk of cardiovascular mortality in patients with rheumatoid arthritis: A meta-analysis of observational studies. *Arthritis Rheum.* 59 (12), 1690–1697. doi:10.1002/art.24092
- Bag-Ozbek, A., and Giles, J. T. (2015). Inflammation, adiposity, and atherogenic dyslipidemia in rheumatoid arthritis: Is there a paradoxical relationship? *Curr. Allergy Asthma Rep.* 15 (2), 497. doi:10.1007/s11882-014-0497-6
- Bligh, E. G., and Dyer, W. J. (1959). A rapid method of total lipid extraction and purification. *Can. J. Biochem. Physiol.* 37 (8), 911–917. doi:10.1139/o59-099
- Charles-Schoeman, C., Fleischmann, R., Davignon, J., Schwartz, H., Turner, S. M., Beyens, C., et al. (2015). Potential mechanisms leading to the abnormal lipid profile in patients with rheumatoid arthritis versus healthy volunteers and reversal by tofacitinib. *Arthritis Rheumatol.* 67 (3), 616–625. doi:10.1002/art.38974
- Croia, C., Bursi, R., Suter, D., Petrelli, F., Alunno, A., and Puxeddu, I. (2019). One year in review 2019: Pathogenesis of rheumatoid arthritis. *Clin. Exp. Rheumatol.* 37 (3), 347–357.
- Curtis, J. R., John, A., and Baser, O. (2012). Dyslipidemia and changes in lipid profiles associated with rheumatoid arthritis and initiation of anti-tumor necrosis factor therapy. *Arthritis Care Res.* 64 (9), 1282–1291. doi:10.1002/acr.21693
- Datta, S., Kundu, S., Ghosh, P., De, S., Ghosh, A., and Chatterjee, M. (2014). Correlation of oxidant status with oxidative tissue damage in patients with rheumatoid arthritis. *Clin. Rheumatol.* 33 (11), 1557–1564. doi:10.1007/s10067-014-2597-z
- Dougados, M., Soubrier, M., Antunez, A., Balint, P., Balsa, A., Buch, M. H., et al. (2014). Prevalence of comorbidities in rheumatoid arthritis and evaluation of their monitoring: Results of an international, cross-sectional study (COMORA). *Ann. Rheum. Dis.* 73 (1), 62–68. doi:10.1136/annrheumdis-2013-204223
- Gerritsen, M. E., Shen, C. P., and Perry, C. A. (1998). Synovial fibroblasts and the sphingomyelinase pathway: Sphingomyelin turnover and ceramide generation are not signaling mechanisms for the actions of tumor necrosis factor- α . *Am. J. Pathol.* 152 (2), 505–512.
- Guo, Q., Wang, Y., Xu, D., Nossent, J., Pavlos, N. J., and Xu, J. (2018). Rheumatoid arthritis: Pathological mechanisms and modern pharmacologic therapies. *Bone Res.* 6, 15. doi:10.1038/s41413-018-0016-9
- Han, X. (2016). Lipidomics for studying metabolism. *Nat. Rev. Endocrinol.* 12 (11), 668–679. doi:10.1038/nrendo.2016.98
- Han, X., Yang, K., Cheng, H., Fikes, K. N., and Gross, R. W. (2005). Shotgun lipidomics of phosphoethanolamine-containing lipids in biological samples after one-step *in situ* derivatization. *J. Lipid Res.* 46 (7), 1548–1560. doi:10.1194/jlr.D500007-JLR200
- Hassan, S. Z., Gheita, T. A., Kenawy, S. A., Fahim, A. T., El-Sorougy, I. M., and Abdou, M. S. (2011). Oxidative stress in systemic lupus erythematosus and rheumatoid arthritis patients: Relationship to disease manifestations and activity. *Int. J. Rheum. Dis.* 14 (4), 325–331. doi:10.1111/j.1756-185X.2011.01630.x
- Holmdahl, R., Vingsbo, C., Hedrich, H., Karlsson, M., Kvick, C., Goldschmidt, T. J., et al. (1992). Homologous collagen-induced arthritis in rats and mice are associated with structurally different major histocompatibility complex DQ-like molecules. *Eur. J. Immunol.* 22 (2), 419–424. doi:10.1002/eji.1830220220
- Humphreys, J. H., Verstappen, S. M., Hyrich, K. L., Chipping, J. R., Marshall, T., and Symmons, D. P. (2013). The incidence of rheumatoid arthritis in the UK: Comparisons using the 2010 ACR/EULAR classification criteria and the 1987 ACR classification criteria. Results from the norfolk arthritis register. *Ann. Rheum. Dis.* 72 (8), 1315–1320. doi:10.1136/annrheumdis-2012-201960
- Jiang, M., Zha, Q., Zhang, C., Lu, C., Yan, X., Zhu, W., et al. (2015). Predicting and verifying outcome of Tripterygium wilfordii Hook F. Based therapy in rheumatoid arthritis: From open to double-blinded randomized trial. *Sci. Rep.* 5, 9700. doi:10.1038/srep09700
- Jung, N., Bueb, J. L., Tolle, F., and Bréhard, S. (2019). Regulation of neutrophil pro-inflammatory functions sheds new light on the pathogenesis of rheumatoid arthritis. *Biochem. Pharmacol.* 165, 170–180. doi:10.1016/j.bcp.2019.03.010
- Karami, J., Aslani, S., Jamshidi, A., Garshasbi, M., and Mahmoudi, M. (2019). Genetic implications in the pathogenesis of rheumatoid arthritis: an updated review. *Gene* 702, 8–16. doi:10.1016/j.gene.2019.03.033
- Kay, J., and Calabrese, L. (2004). The role of interleukin-1 in the pathogenesis of rheumatoid arthritis. *Rheumatol. Oxf. Engl.* 43 (3), iii2–iii9. doi:10.1093/rheumatology/keh201
- Koh, J. H., Yoon, S. J., Kim, M., Cho, S., Lim, J., Park, Y., et al. (2022). Lipidome profile predictive of disease evolution and activity in rheumatoid arthritis. *Exp. Mol. Med.* 54 (2), 143–155. doi:10.1038/s12276-022-00725-z
- Kosinska, M. K., Liebsch, G., Lochnit, G., Wilhelm, J., Klein, H., Kaesser, U., et al. (2014). Sphingolipids in human synovial fluid—a lipidomic study. *PLoS ONE* 9 (3), e91769. doi:10.1371/journal.pone.0091769
- Law, S. H., Chan, M. L., Marathe, G. K., Parveen, F., Chen, C. H., and Ke, L. Y. (2019). An updated review of lysophosphatidylcholine metabolism in human diseases. *Int. J. Mol. Sci.* 20 (5), E1149. doi:10.3390/ijms20051149
- Lee, Y. K., Lee, D. H., Kim, J. K., Park, M. J., Yan, J. J., Song, D. K., et al. (2013). Lysophosphatidylcholine, oxidized low-density lipoprotein and cardiovascular disease in Korean hemodialysis patients: Analysis at 5 years of follow-up. *J. Korean Med. Sci.* 28 (2), 268–273. doi:10.3346/jkms.2013.28.2.268
- Lourida, E. S., Georgiadis, A. N., Papavasiliou, E. C., Papathanasiou, A. I., Drosos, A. A., and Tselepis, A. D. (2007). Patients with early rheumatoid arthritis exhibit elevated autoantibody titers against mildly oxidized low-density lipoprotein and exhibit decreased activity of the lipoprotein-associated phospholipase A2. *Arthritis Res. Ther.* 9 (1), R19. doi:10.1186/ar2129
- Łuczaj, W., Gindzińska-Sieskiewicz, E., Jarocka-Karpowicz, I., Andrisic, L., Sierakowski, S., Zarkovic, N., et al. (2016). The onset of lipid peroxidation in rheumatoid arthritis: Consequences and monitoring. *Free Radic. Res.* 50 (3), 304–313. doi:10.3109/10715762.2015.1112901
- Ma, J., Dey, M., Yang, H., Poulev, A., Pouleva, R., Dorn, R., et al. (2007). Anti-inflammatory and immunosuppressive compounds from *Tripterygium wilfordii*. *Phytochemistry* 68 (8), 1172–1178. doi:10.1016/j.phytochem.2007.02.021
- McInnes, I. B., and Schett, G. (2011). The pathogenesis of rheumatoid arthritis. *N. Engl. J. Med.* 365 (23), 2205–2219. doi:10.1056/NEJMra1004965
- Miltenberger-Miltenyi, G., Cruz-Machado, A. R., Saville, J., Conceicao, V. A., Calado, A., Lopes, I., et al. (2020). Increased monohexosylceramide levels in the serum of established rheumatoid arthritis patients. *Rheumatol. Oxf. Engl.* 59 (8), 2085–2089. doi:10.1093/rheumatology/kez545
- Mishra, R., Singh, A., Chandra, V., Negi, M. P., Tripathy, B. C., Prakash, J., et al. (2012). A comparative analysis of serological parameters and oxidative stress in osteoarthritis and rheumatoid arthritis. *Rheumatol. Int.* 32 (8), 2377–2382. doi:10.1007/s00296-011-1964-1
- Mullazehi, M., Mathsson, L., Lampa, J., and Ronnelid, J. (2007). High anti-collagen type-II antibody levels and induction of proinflammatory cytokines by anti-collagen antibody-containing immune complexes *in vitro* characterise a distinct rheumatoid arthritis phenotype associated with acute inflammation at the time of disease onset. *Ann. Rheum. Dis.* 66 (4), 537–541. doi:10.1136/ard.2006.064782
- Myasoedova, E., Crowson, C. S., Kremers, H. M., Fitz-Gibbon, P. D., Thorneau, T. M., and Gabriel, S. E. (2010). Total cholesterol and LDL levels decrease before rheumatoid arthritis. *Ann. Rheum. Dis.* 69 (7), 1310–1314. doi:10.1136/ard.2009.123374
- Nowak, B., Madej, M., Łuczak, A., Malecki, R., and Wiland, P. (2016). Disease activity, oxidized-LDL fraction and anti-oxidized LDL antibodies influence cardiovascular risk in rheumatoid arthritis. *Adv. Clin. Exp. Med.* 25 (1), 43–50. doi:10.17219/acem/29847
- Phaniendra, A., Jestadi, D. B., and Periyasamy, L. (2015). Free radicals: Properties, sources, targets, and their implication in various diseases. *Indian J. Clin. biochem.* 30 (1), 11–26. doi:10.1007/s12291-014-0446-0
- Phull, A. R., Nasir, B., Haq, I. U., and Kim, S. J. (2018). Oxidative stress, consequences and ROS mediated cellular signaling in rheumatoid arthritis. *Chem. Biol. Interact.* 281, 121–136. doi:10.1016/j.cbi.2017.12.024
- Qian, Q., Gao, Y., Xun, G., Wang, X., Ge, J., Zhang, H., et al. (2022). Synchronous investigation of the mechanism and substance basis of *Tripterygium glycosides* tablets on anti-rheumatoid arthritis and hepatotoxicity. *Appl. Biochem. Biotechnol* in press. doi:10.1007/s12010-022-04011-6
- Qu, F., Zhang, H., Zhang, M., and Hu, P. (2018). Sphingolipidomic profiling of rat serum by UPLC-Q-TOF-MS: Application to rheumatoid arthritis study. *Molecules* 23 (6), E1324. doi:10.3390/molecules23061324
- Quiñonez-Flores, C. M., González-Chávez, S. A., Del Río Nájera, D., and Pacheco-Tena, C. (2016). Oxidative stress relevance in the pathogenesis of the rheumatoid arthritis: A systematic review. *Biomed. Res. Int.* 2016, 6097417. doi:10.1155/2016/6097417
- Rosloniec, E. F., Cremer, M., Kang, A. H., Myers, L. K., and Brand, D. D. (2010). Collagen-induced arthritis. *Curr. Protoc. Immunol.* 15, 1–25. doi:10.1002/0471142735.im1505s89
- Serhan, C. N., Chiang, N., and Van Dyke, T. E. (2008). Resolving inflammation: Dual anti-inflammatory and pro-resolution lipid mediators. *Nat. Rev. Immunol.* 8 (5), 349–361. doi:10.1038/nri2294
- Stegemann, C., Pechlaner, R., Willeit, P., Langley, S. R., Mangino, M., Mayr, U., et al. (2014). Lipidomics profiling and risk of cardiovascular disease in the prospective population-based Bruneck study. *Circulation* 129 (18), 1821–1831. doi:10.1161/CIRCULATIONAHA.113.002500

- Symmons, D., Turner, G., Webb, R., Asten, P., Barrett, E., Lunt, M., et al. (2002). The prevalence of rheumatoid arthritis in the United Kingdom: New estimates for a new century. *Rheumatol. Oxf. Engl.* 41 (7), 793–800. doi:10.1093/rheumatology/41.7.793
- Tao, X., and Lipsky, P. E. (2000). The Chinese anti-inflammatory and immunosuppressive herbal remedy *Tripterygium wilfordii* Hook F. *Rheum. Dis. Clin. North Am.* 26 (1), 29–50. doi:10.1016/s0889-857x(05)70118-6
- Toms, T. E., Symmons, D. P., and Kitas, G. D. (2010). Dyslipidaemia in rheumatoid arthritis: The role of inflammation, drugs, lifestyle and genetic factors. *Curr. Vasc. Pharmacol.* 8 (3), 301–326. doi:10.2174/157016110791112269
- Wang, M., Chen, J., Lin, X., Huang, L., Li, H., Wen, C., et al. (2021). High humidity aggravates the severity of arthritis in collagen-induced arthritis mice by upregulating xylitol and L-pyrogutamic acid. *Arthritis Res. Ther.* 23 (1), 292. doi:10.1186/s13075-021-02681-x
- Whittingham, S. F., Stockman, A., and Rowley, M. J. (2017). Collagen autoantibodies and their relationship to CCP antibodies and rheumatoid factor in the progression of early rheumatoid arthritis. *Antibodies (Basel)* 6 (2), 6. doi:10.3390/antib6020006
- Wymann, M. P., and Schneider, R. (2008). Lipid signalling in disease. *Nat. Rev. Mol. Cell Biol.* 9 (2), 162–176. doi:10.1038/nrm2335
- Yang, K., Cheng, H., Gross, R. W., and Han, X. (2009). Automated lipid identification and quantification by multidimensional mass spectrometry-based shotgun lipidomics. *Anal. Chem.* 81 (11), 4356–4368. doi:10.1021/ac900241u
- Yang, Y. J., Deng, Y., Liao, L. L., Peng, J., Peng, Q. H., and Qin, Y. H. (2020). Tripterygium glycosides combined with leflunomide for rheumatoid arthritis: A systematic review and meta-analysis. *Evidence-based Complementary Altern. Med. ECAM* 2020, 1230320. doi:10.1155/2020/1230320



OPEN ACCESS

EDITED BY

Xijun Wang,
Heilongjiang University of Chinese
Medicine, China

REVIEWED BY

Zhen-Yu Li,
Shanxi University, China
Feng-Qing Yang,
Chongqing University, China

*CORRESPONDENCE

Chunqin Mao,
mcq63@163.com
Tulin Lu,
ltl209@163.com

[†]These authors have contributed equally
to this work and share first authorship

SPECIALTY SECTION

This article was submitted to
Ethnopharmacology,
a section of the journal
Frontiers in Pharmacology

RECEIVED 22 April 2022

ACCEPTED 01 August 2022

PUBLISHED 13 September 2022

CITATION

Su L, Tong H, Zhang J, Hao M, Fei C, Ji D,
Gu W, Bian Z, Mao C and Lu T (2022),
Revealing the mechanism of raw and
vinegar-processed *Curcuma aromatica*
Salisb. [Zingiberaceae] regulates primary
dysmenorrhea in rats via
integrated metabolomics.
Front. Pharmacol. 13:926291.
doi: 10.3389/fphar.2022.926291

COPYRIGHT

© 2022 Su, Tong, Zhang, Hao, Fei, Ji, Gu,
Bian, Mao and Lu. This is an open-
access article distributed under the
terms of the [Creative Commons
Attribution License \(CC BY\)](#). The use,
distribution or reproduction in other
forums is permitted, provided the
original author(s) and the copyright
owner(s) are credited and that the
original publication in this journal is
cited, in accordance with accepted
academic practice. No use, distribution
or reproduction is permitted which does
not comply with these terms.

Revealing the mechanism of raw and vinegar-processed *Curcuma aromatica* Salisb. [Zingiberaceae] regulates primary dysmenorrhea in rats *via* integrated metabolomics

Lianlin Su^{1†}, Huangjin Tong^{2,3†}, Jiuba Zhang¹, Min Hao⁴,
Chenghao Fei¹, De Ji¹, Wei Gu¹, Zhenhua Bian⁵, Chunqin Mao^{1*}
and Tulin Lu^{1*}

¹College of Pharmacy, Nanjing University of Chinese Medicine, Nanjing, China, ²Affiliated Hospital of Integrated Traditional Chinese and Western Medicine, Nanjing University of Chinese Medicine, Nanjing, China, ³Jiangsu Province Academy of Traditional Chinese Medicine, Nanjing, China, ⁴College of Pharmacy, Zhejiang Chinese Medical University, Hangzhou, China, ⁵Wuxi TCM Hospital Affiliated to Nanjing University of Chinese Medicine, Wuxi, China

Primary dysmenorrhea (PDM) is a common disorder among women around the world. Two processed products of *Curcuma aromatica* Salisb. [Zingiberaceae] (CAS) are traditional Chinese medicine (TCM) that have long been used to treat gynecological blood stasis syndrome such as primary dysmenorrhea. The mechanisms and active substances of CAS are still largely unknown. The study aimed to establish a rat model of primary dysmenorrhea which investigates the differences between the pharmacodynamics and mechanisms of raw CAS (RCAS) and vinegar-processed CAS (VCAS). Histopathology, cytokinetics, and metabolomics were adopted to evaluate the anti-blood stasis effect of RCAS and VCAS. In metabolomics, endogenous differential metabolites in plasma, urine, and feces are the essential steps to evaluate the effect of RCAS and VCAS. In this study, the rat model of primary dysmenorrhea was successfully established. After RCAS and VCAS intervention, the uterine tissue morphology of dysmenorrhea model rats was improved, and gland hypertrophy and myometrial hyperplasia were reduced as well as neutrophil content. Compared with the RCAS group, the VCAS group had better uterine morphology, few inflammatory factors, and significantly improved amino acid and lipid metabolism. The aforementioned results support the conclusion that VCAS performed better than RCAS in primary dysmenorrhea and that vinegar processing increases the efficacy of CAS.

KEYWORDS

Curcuma aromatica Salisb. [Zingiberaceae], vinegar processing, primary dysmenorrhea, metabolomics, multivariate statistical analysis

1 Introduction

Primary dysmenorrhea (PDM) refers to the pain and distention of the lower abdomen before, during, and/or after menstruation caused by non-organic lesions of the reproductive organs. PDM is often accompanied by low back pain or other discomforts, all belonging to the category of “menstrual abdominal pain” (Chai et al., 2020). Epidemiological studies show that primary dysmenorrhea is the most common disease in gynecology, affecting 25–95% of women around the world, with 10% having serious symptoms. This is one of the most common and frequent causes for disruptions in women’s normal work and deterioration of their quality of life (De Sanctis et al., 2015; Nguyen et al., 2015; Sahin et al., 2018). According to TCM, dysmenorrhea is mainly caused by “pain when *Qi* and *Blood* are blocked” or “pain when the uterus is not well-nourished.” It is also often caused by damp heat accumulation, kidney qi deficiency, cold coagulation and blood stasis, qi stagnation and blood stasis, and *Qi* and *Blood* weakness.

According to modern research, the occurrence of primary dysmenorrhea is mainly related to increased proportion of prostaglandins (PGs), mainly PGF2 *a*/PGE2, in the endometrium during menstruation (Chan 1983; Maia et al., 2005). PGF2 *a* promotes contraction of the uterine smooth muscle and vasospasm, which can cause pain due to local ischemia and hypoxia, while PGE2 has the opposite reaction (Ju et al., 2014; Iacovides et al., 2015). In addition, related studies have shown that primary dysmenorrhea is also related to tumor necrosis factor (TNF - α), interleukin (IL), plasma thromboxane B2 (TXB2), 6-keto-PGF1 α , NO, Ca²⁺, and beta-endorphin (β - EP) (Dawood and Khan-Dawood, 2007a; Pu et al., 2014; Xie et al., 2014; Huang et al., 2016). At present, the treatment of primary dysmenorrhea in Western medicine is not yet satisfactory: non-steroidal anti-inflammatory drugs and oral contraceptives have limited clinical use due to their serious adverse reactions (Oladosu et al., 2018). TCM has many effective methods in the treatment of primary dysmenorrhea and has unique advantages in the improvement of dysmenorrhea symptoms and long-term curative effects (Xu et al., 2019). In the treatment of primary dysmenorrhea, ancient and modern doctors started with blood stasis, which is the main syndrome type. The main treatment methods revolve around promoting blood circulation and removing blood stasis. TCM treatments for promoting blood circulation and removing blood stasis can improve microcirculation, dilate blood vessels, and change hemorheology, all of which are significant and effective ways to relieve pain.

The dried rhizomes of CAS, a ginger plant, are spicy, bitter, and warm in nature. It promotes *Qi* and breaking blood, eliminating accumulation and relieving pain. It is used for treating syndromes such as lump, blood stasis and amenorrhea, chest arthralgia and heartache, food accumulation, and flatulence. According to the 2020 edition of

Chinese Pharmacopoeia (Chinese Pharmacopoeia, 2020), through different processing methods of steaming and vinegar, two processed products of CAS, RCAS, and VCAS, were prepared. Both RCAS and VCAS have the effect of removing blood stasis and pain, but their clinical applications have differences despite their similarity (Liu et al., 2017; Xie et al., 2020). CAS can relieve pain by promoting *Qi*, breaking blood, and removing blood stasis, and these effects are enhanced after vinegar processing. VCAS has a very high frequency in the clinical application of primary dysmenorrhea. For example, there are 18 prescriptions containing VCAS in the Chinese Pharmacopoeia 2020 edition, which mainly treat blood stasis-related diseases (Hao et al., 2018; Chinese Pharmacopoeia, 2020). In addition, *Fufang Ezhusan* uses VCAS as the principal medicine for treating dysmenorrhea of blood stasis type. Moreover, clinical and animal studies of formulae containing VCAS in the treatment of primary dysmenorrhea are also more common than those of RCAS (Gu et al., 2018; Hao et al., 2018). However, few reports can be found on the mechanism of enhancing stasis and relieving pain and relieving dysmenorrhea after vinegar processing. As a result, VCAS can enhance the treatment of primary dysmenorrhea which deserves further study.

Ultra-performance liquid chromatography–quadrupole–time-of-flight mass spectrometry (UHPLC-Q/TOF-MS) has the characteristics of high resolution, sensitivity, simplicity, and high-throughput. It has been used to successfully study metabolic changes caused by diseases and drug toxicity (Su et al., 2019). In this study, metabolomics technology based on UHPLC-Q/TOF-MS and multivariate statistics were used to screen out potential biomarkers in blood, urine, and fecal metabolites related to primary dysmenorrhea, analyze related metabolic pathways, and compare the efficacy and mechanism of RCAS and VCAS in the treatment of primary dysmenorrhea.

This study provides a basis for further research on the mechanism of VCAS in the treatment of primary dysmenorrhea. Through the in-depth analysis of dysmenorrhea-related pain factors, related metabolites, and metabolic pathways, it is found that metabolomics can comprehensively demonstrate the impact of the disease on the whole body, and the selected indicators can holistically reflect the state of the disease and provide a new approach for the study of mechanism, screening, or clinical drug treatment of diseases related to blood stasis syndrome.

2 Materials and methods

2.1 Preparation of RCAS and VCAS extracts

The fresh rhizome of CAS was purchased from Hebei Anguo juyatong Pharmaceutical Co., Ltd. (#1810003), Hebei, China in December 2018. The samples were identified as the rhizome of

Curcuma aromatica Salisb. [Zingiberaceae] by Professor Jianwei Cheng at Nanjing University of Chinese Medicine.

RCAS slices: RCAS was steamed for 2 h, cut into 3-mm thickness, and dried in the oven.

VCAS slices: RCAS was boiled with vinegar (per 100 kg samples with 20 kg vinegar and percentile of vinegar is 20% approximately), and dried in the oven at 40°C (Chinese Pharmacopoeia, 2020).

The RCAS and VCAS slices were refluxed for 1.5 h with 90% ethanol 15 times and extracted twice. The residues were extracted for 1.5 h with water 10 times. The aforementioned extracts of RCAS and VCAS were combined. After filtrating and concentrating, per 1 ml RCAS and VCAS extracts containing 1 g of raw medicines were prepared (Xie et al., 2020).

2.2 Chemicals and reagents

LC-MS-grade acetonitrile, LC-MS-grade methyl alcohol, HPLC-grade methanoic acid (Merck. Co. Inc., Darmstadt, Germany), and ultra-pure-grade water were obtained from a Milli-Q system (Millipore, Bedford, MA, United States). The other solvents were of analytical grade.

Epinephrine hydrochloride injection (#10180505) was purchased from Harvest Pharmaceutical Co., Ltd. (Shanghai, China). Estradiol benzoate (#20190301) injection was purchased from Jinke Pharmaceutical Co., Ltd. (Sichuan, China). Oxytocin injection (#190207) was purchased from Hongye Pharmaceutical Co., Ltd. (Anhui, China). *Tong Jing Bao Ke Li* (#181203) was purchased from Zhongjingwanxi Pharmaceutical Co., Ltd. (Henan, China). The ELISA kits of interleukin-6 (IL-6, #EK306-01), tumor necrosis factor- α (TNF- α , #EK382HS-01), 6-keto-prostaglandin F_{1a} (6-keto-PGF_{1a}, #E-EL-0054c), prostaglandin E₂ (PGE₂, #E-EL-0034c), prostaglandin F_{2 α} (PG F_{2 α} , #E-EL-R0795c), thromboxane B₂ (TXB₂, #E-EL-R0965c), and beta-endorphin (β -EP, #E-EL-R0105c) were purchased from Nanjing Kaiji Technology Co., Ltd., Nanjing, China. The colorimetric assay kits of calcium (Ca²⁺, #C004-2-1) and nitric oxide (NO, #A013-2-1) were provided by Jiangcheng Bioengineering Institute, Nanjing, China.

2.3 Chemical analysis of RCAS and VCAS extracts

RCAS and VCAS extracts were prepared with a reverse phase-solid phase extract column (RP-SPE) by gradient elution, and the analysis determination performance by UHPLC-Q/TOF-MS coupled with chemometric analysis according to literature and compared the differences in the chemical profiles of RCAS and VCAS (Hao et al., 2018). At the same time, the volatile oil content in RCAS and VCAS was analyzed by GC-MS. However, due to the thermal instability of

very few sesquiterpenoids, this part of the research was just a supplement to UHPLC-Q/TOF-MS (Yang et al., 2007). The results of the chemical composition analysis are detailed in the Supplementary Materials.

2.4 Animals and drug administration

A total of 70 specific pathogen-free (SPF) degree female Sprague–Dawley (SD) rats (180 \pm 20 g) were obtained from the animal breeding farm of Qinglong Mountain in Jiangning District, Nanjing, China (license approval number: SCXK (SU) 2019-0001). Before the experiment, the rats were fed in an environment-controlled breeding room. A 12-h light/dark cycle was set. Room temperature and relative humidity were regulated at 25 \pm 2°C and 60 \pm 5%, respectively. In this study, all experimental animals were allowed free access to food and tap water. All rats were adapted for 7 days before the experiment. The study protocol was in accordance with the Guide for the Care and Use of Laboratory Animals and was approved by the Animal Experimental Ethics Committee of the Nanjing University of Chinese Medicine.

A total of 40 rats were randomly divided into five groups with each group having eight rats. Five groups were set as below: the normal control group (NC), model group (M), RCAS, VCAS, and *Tong Jingbao* group (TJB, a Chinese patent medicine granule), which was the positive control group. TJB, RCAS, and VCAS were intragastrically administered to the TJB group (2.1 g/kg/day), RCAS group (3.8 g/kg/day), and VCAS group (3.8 g/kg/day), respectively, for the last 7 days. The dose of administration was changed according to the clinical equivalent dose of rats. NC and M groups were intragastrically administered normal saline. The models in M, TJB, RCAS, and VCAS groups were established on the 10th day after the dose according to the references: subcutaneous injected 0.1% adrenaline (0.9 mg/kg/d) for 10 days, and 4 h later, the rats were given comprehensive stimulation [A: sound stimulation (60 dB, (10 \pm 5) Hz) for 10 min; B: light stimulation [(2 \pm 1) Hz) for 10 min; C: binding for 10 min; D: nipping tail for 10 min; E: swimming in ice water (0–4°C) for 5 min]. The models were subcutaneously injected with 0.2% estradiol benzoate for 10 days, given a dose (2.5 mg/kg/d) on the 1st and 10th day, and another dose (1.25 mg/kg/d) from the 2nd to the 9th day. After the last estradiol benzoate injection, 1 h later, the rats were intraperitoneally injected with oxytocin (10 U/kg), while NC groups were intragastrically administered normal saline. After that, all rats were intraperitoneally injected with 1% pentobarbital sodium (50 mg/kg, i.p). Blood samples were collected by the abdominal aortic method.

2.5 Sample collection

The experiment continued for 10 days. At the end of treatment, the rats were euthanized, and blood samples were

collected by heparin sodium blood collection tubes. The samples were centrifuged at 3000 r/min for 10 min, and then the supernatants were stored at -80°C for related function detection. Urine and feces samples were collected in the 12 h after drug administration and stored at -80°C for UHPLC-Q/TOF-MS analysis.

2.6 Sample preparation

Before mass spectrometric detection, the urine and feces samples were unfrozen at ambient temperature. A total of 100-mg feces samples were added to 70% chromatographic pure methanol (2 ml). Eight times the volume of methanol was added to the 200- μl plasma or urine sample. The mixed samples were shaken violently for 30 s by a vortex mixer. Then, the mixture was centrifuged at 12,000 r/min at 4°C for 10 min. The supernate was prepared for mass detection.

2.7 Histopathology and writhing response

The uterus of rats was fixed in 10% formalin solution and processed routinely for paraffin embedding. Sections (5 μm thick) were deparaffinized and then stained with hematoxylin and eosin solutions (H&E). Then, the histopathology samples were examined under light microscopy (Leica, DFC-259, and Germany). According to the degree of endometrial hyperplasia, the morphological changes of all rats' uterus were graded as 0–4: 0 as no pathological phenomenon and 4 as the most serious pathological damage. The specific scoring criteria are as follows: 0: the uterine structure is clear, with a three-layer structure, including the endometrium, myometrium, and adventitia from inside to outside. The endometrial epithelial cells are complete, the distribution of glands in the lamina propria is normal, and the thickness of the endometrium and myometrium is normal. Four points: the uterine structure is disordered, the uterine cavity is not smooth, gland distribution in lamina propria is abnormal, gland hypertrophy, endometrial hyperplasia is obvious, myometrial hyperplasia is obvious, and inflammatory cell infiltration is obvious (Thaina et al., 2009).

On the 10th day of the experiment, after oxytocin was injected into the abdominal cavity of rats in each group, the writhing times and writhing latency of rats within 0–30 min were immediately observed: abdominal concave contraction, trunk and hind limb extension, and hip and one side limb internal rotation. Writhing latency: the time from the beginning of the intraperitoneal injection of oxytocin to the first writhing reaction in rats.

2.8 Biochemical assays

The rat uterine sample was washed with normal saline, dried, and weighed. Then, 10% of the tissue homogenate was prepared

with pre-cooled normal saline at a ratio of 1:9 (weight: volume). The homogenate was centrifuged at 3000 rpm for 5 min, and the supernatant was stored at -80°C for HYP detection, which was determined by ELISA or colorimetric assay method. PGF 2α , PGE 2 , β -EP, TXB 2 , 6-keto-PGF 1α , TNF- α , IL-6, NO, and Ca^{2+} were carried out in perfect accordance with the product's instructions (Hao et al., 2018).

2.9 Mass spectrum analysis and verification of methodology

The plasma, urine, and feces sample analysis was managed by Shimadzu UPLC (Kyoto, Japan) which consisted of an LC-30AD binary liquid pump, SIL-30SD auto sampler and DGU-20A5R on-line solvent degasser, a CTO-30 A column oven, an AB SCIEX Triple TOF 5600 $^{+}$ system, and an ESI source (Hao et al., 2018). Chromatographic conditions were as follows: Agilent C $_{18}$ reversed phase column (2.1 mm \times 100 mm, 1.8 μm , Palo Alto, CA, United States), mobile phase A (0.1% formic acid aqueous solution)-B (acetonitrile), gradient elution program: 0–1 min, 5–25% B; 1–3 min, 25–30% B; 3–13 min, 30–55% B; 13–15 min, 55–70% B; 15–25 min, 70–100% B; 25–28 min, 5–100% B; flow rate: 0.3 ml/min; column temperature: 35°C ; injection volume: 1 μl . Mass spectrometer condition: ESI source and data collection in positive and negative ion mode. The source parameters were set as follows: ion spray voltage floating: +4500/– 4500; declustering potential: +60/– 60 V; source temperature: 550°C ; the atomizing gas is N_2 , curtain gas: 35 psi; gas1 (nebulizer gas): 55 psi; gas 2 (heater gas): 55 psi; collision energy: +35/– 35e V; using MS/MS secondary mass spectrometry mode: the MS spectrometer ion scanning range was m/z 100–2000. The MS/MS spectrometer ion scanning range was m/z 50–1,000, and dynamic background subtraction was turned on. The quality control (QC) sample was obtained by even mixing of all groups of each kind of sample to ensure system suitability. Before the samples started testing, the QC sample was continuously detected six times. Moreover, system consistency was verified by QC samples after every five detected samples.

2.10 Multivariate statistical analysis

Analyst TF 1.6 software (AB Sciex, Boston, MA, United States) was used to extract the original metabolic fingerprint profiles. MarkerView1.2.1 (AB Sciex, United States) software was used for peak detection and calibration of the original samples of each group. The parameters were set as follows: retention time range: 0.5–30 min; quality range: 100–1,200 Da; retention time error limit: 0.01 min; mass error limit: 10 ppm; peak intensity threshold: 10; minimum peak width: 25 ppm; noise threshold:

100; retention time error range: 0.5 min. After the original map of each sample was calibrated and normalized by software, they were converted into a three-dimensional matrix containing the peak name (Rt-*m/z*) sample number and normalized peak area. The three-dimensional matrices of each group were imported into SIMCA-P 14.1 software (Umetrics AB, Sweden). The data were pretreated with Pareto-scaling, followed by PCA and OPLS-DA multivariate statistical analysis. The model predictors are R^2X (cum) and Q^2X (cum), with R^2X (cum) representing the ability of the variable to interpret the model and Q^2X (cum) signifying the ability to predict the model. The applicability of the model was good when R^2X (cum) and Q^2X (cum) both approached 1.0. In the OPLS-DA model, the ions with VIP values greater than 1.0 were identified as potential differential ions. At the same time, *t*-test single-dimensional statistical analysis was carried out on the three-dimensional matrices among different groups. $p < 0.05$ was determined as the ion with a significant difference. Potential differential ions with $VIP > 1.0$ and $p < 0.05$ were confirmed as the final differential ions after taking the intersection, whose structures were to be identified later (Yao et al., 2014).

2.11 Biomarker identification and metabolic pathway analysis

The online database One-Map (<http://www.5omics.com/>) was used for identification of the differential metabolites of plasma, urine, and feces. Excel data (including sample ID, mass/charge ratio/retention time, and ion strength) of all samples after the original chromatogram dimensionality reduction were imported into the One-MAP online cloud platform, and the differential metabolite search and metabolic pathway analysis were automatically carried out. According to the variable importance for the project (VIP) of the OPLS-DA model in each group, the differential ions were selected. Referring to the literature on metabolomics, this study set $VIP > 1$ as the differential ions between the two groups with independent sample *t*-test, excluding data with $p > 0.05$ (Xing et al., 2017; Su et al., 2019). Finally, the $p < 0.05$ differential ions were input into the HMDB database, the structure of the compounds according to the first-order mass spectrometry information was predicted, the predicted exogenous compounds were eliminated, and the final selected differential compounds for structure identification were obtained, which are compared with the HMDB database (<http://www.hmdb.ca/>), METLIN database (<https://www.sisweb.com/software/ms/wiley-metlin.htm>), and KEGG database (<http://www.genome.jp/kegg/>). The standard secondary mass spectrometry data and related literature were compared, and finally the endogenous differential metabolites were identified and the related metabolic pathways were analyzed.

3 Results and discussion

3.1 Histopathological and writhing response examination

The results are shown in Figure 1 and Table 1. As demonstrated in the NC group, the uterine tissue structure of rats in the blank control group was clear, including the endometrium, myometrium, and adventitia from inside to outside, arranged neatly and closely. Of note, the uterine wall became thinner, the structure was disordered, the endometrium was incomplete, the gland was hypertrophied, and the myometrium was obviously proliferated in the M group. There were a lot of inflammatory cells infiltrated, among which neutrophils were the main cells, and the pathological score had a significant difference ($p < 0.01$). In the TJB group, the uterine structure was clear, the endometrium was complete, and the myometrium hyperplasia was not obvious. There was a small amount of neutrophil infiltration, and the pathological score was significantly different ($p < 0.01$). Compared with the M group, the other groups had more regular uterine tissue morphology, less glandular hypertrophy and myometrial hyperplasia, and less neutrophil content ($p < 0.05$ and $p < 0.01$), especially the VCAS group. Moreover, there was no significant improvement in the dysmenorrhea uterus in the RCAS group ($p > 0.05$).

Compared with the model group, the TJB group can significantly prolong the latency of writhing and reduce the number of writhing in the primary dysmenorrhea model rats with qi stagnation and blood stasis ($p < 0.01$); the RCAS group had no statistical significance in writhing latency and writhing times; the VCAS group can significantly prolong the incubation period of writhing and reduce the number of writhing in rats with primary dysmenorrhea caused by qi stagnation and blood stasis ($p < 0.05$ and $p < 0.01$), that is, the effect of the VCAS group is significantly better than that of the RCAS group. The results are shown in Table 1.

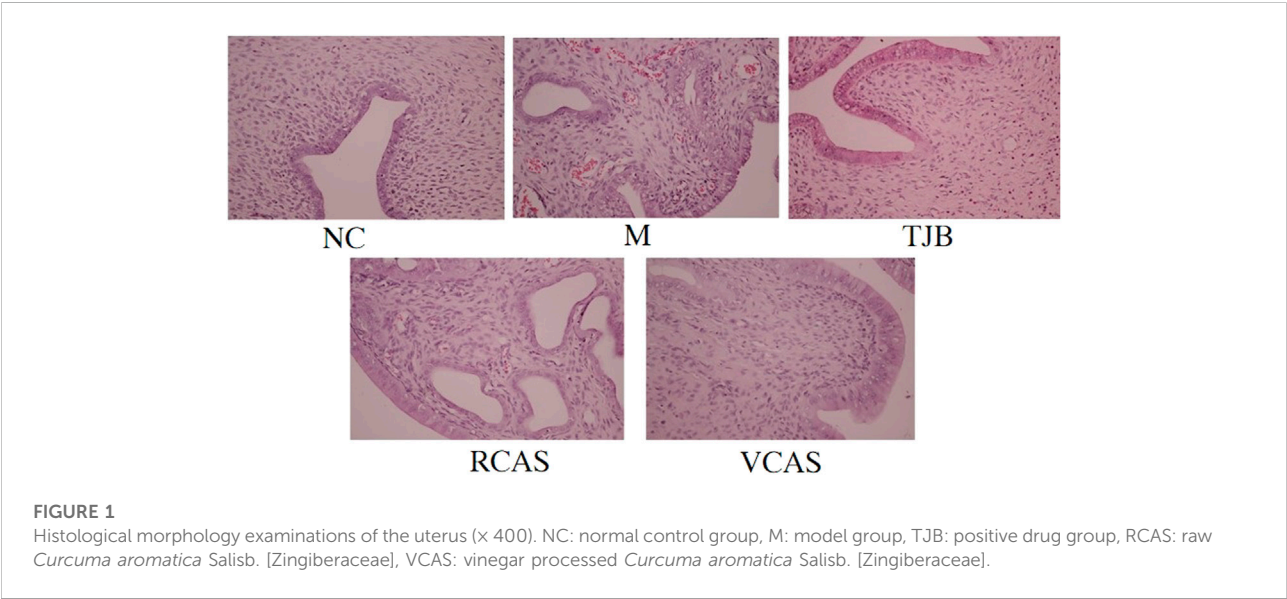
3.2 Cytokines examinations by ELISA

The results are shown in Figure 2; compared with the NC group, PGE2 and 6-Keto-PGF1 α (PG/ml) in the M group decreased significantly ($p < 0.01$), PGF2 α and TXB2 increased significantly ($p < 0.01$), and PGE2 and 6-Keto-PGF1 α (PG/mL) in the other administration groups were increased when compared with the M group, but PGF2 α and TXB2 decreased. Moreover, the most significant change was found in TJB and VCAS ($p < 0.01$). For the inflammatory factors TNF- α and IL-6, the M group increased significantly ($p < 0.01$) but decreased significantly after administration, and the anti-inflammatory effect in TJB and VCAS was significantly increased ($p < 0.01$). Although TNF- α and IL-6 decreased in RCAS, they were not evident and had no statistical significance. Compared with the NC group, the content of Ca²⁺ in the uterus tissue of the M group was significantly increased, and the content of NO was significantly decreased ($p < 0.01$). The Ca²⁺ in the

TABLE 1 Writhing response of each group during the experiment ($\bar{x} \pm s$, $n = 8$).

| Group | Dosage (g/kg) | Incubation (min) | Numbers of torsion spasm 30 min |
|-------|---------------|----------------------|---------------------------------|
| NC | — | — | 0 |
| M | — | $5.19 \pm 1.08^{**}$ | $10.88 \pm 2.53^{**}$ |
| TJB | 2.10 | $7.49 \pm 1.15^{**}$ | $6.63 \pm 1.60^{**}$ |
| RCAS | 3.80 | 6.43 ± 1.45 | 9.50 ± 3.16 |
| VCAS | 3.80 | $7.24 \pm 1.06^{**}$ | $7.25 \pm 1.49^{**}$ |

Compared with the NC group, $\#p < 0.0$ and $\#\#p < 0.01$; compared with the M group, $*p < 0.05$ and $**p < 0.01$.



administration group was decreased and NO was increased, especially in TJB and VCAS ($p < 0.01$). In the M group, β - EP significantly decreased, which plays an important role in the regulation of blood vessels. The decrease of β - EP concentration and activity will lead to vasoconstriction. The administration group can reduce the content of β - EP in brain tissue and increase the content of β - EP in plasma so as to inhibit vasoconstriction, while all groups of administration have an upward trend, in which the increase of TJB and VCAS is statistically significant. The VCAS group significantly increased the contents of PGE2, 6-Keto-PGF1a, and NO and significantly reduced TXB2, IL-6, and TNF- α content ($p < 0.05$). Of note, the VCAS group has a more significant role in regulating pain-related factors than the RCAS group.

3.3 Plasma metabolomics analysis

3.3.1 Multivariate statistical analysis

In order to deeply excavate the differential endogenous metabolites in plasma samples of each group, the original TIC

atlas under positive and negative ion mode was processed by using Marker view 1.2.1 software for dimension reduction, peak matching, and normalization, and further multivariate statistical analysis was carried out to screen the differential markers. The dimension-reduced Excel data (including sample ID, mass-charge ratio/retention time, and ionic strength) were imported into Simca-P 14.1 software for pattern recognition. First, principal component analysis (PCA) was used to summarize the dispersion degree of all samples. The modeling results of 3D-PCA under positive and negative ion modes are shown in Figures 3A,B. Any point in the figure represents a plasma sample. It can be seen from the figure that five groups of plasma samples can be roughly distinguished, but the boundaries are not obvious enough. Therefore, the orthogonal partial least squares method was further used to establish the 3D-PLS-DA model. The results are shown in Figures 3C,D. The grouping of the models modeled by the positive and negative ion modes was obvious, indicating that the endogenous metabolites in plasma samples were significantly different between the groups. Therefore, the OPLS-DA model was established by comparing

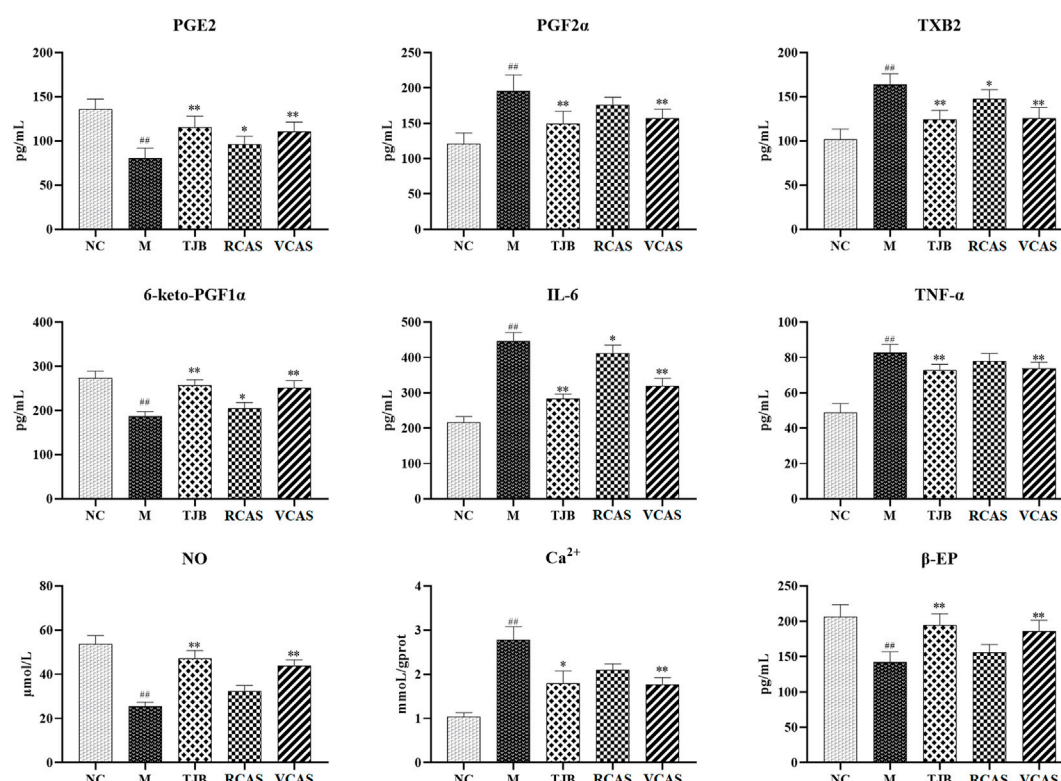


FIGURE 2

Effects of RCAS and VCAS on pain factors in rats with primary dysmenorrhea. ## and # represent the comparison with the NC group: $p < 0.01$, $p < 0.05$; ** and * represent the comparison with the M group: $p < 0.01$ and $p < 0.05$.

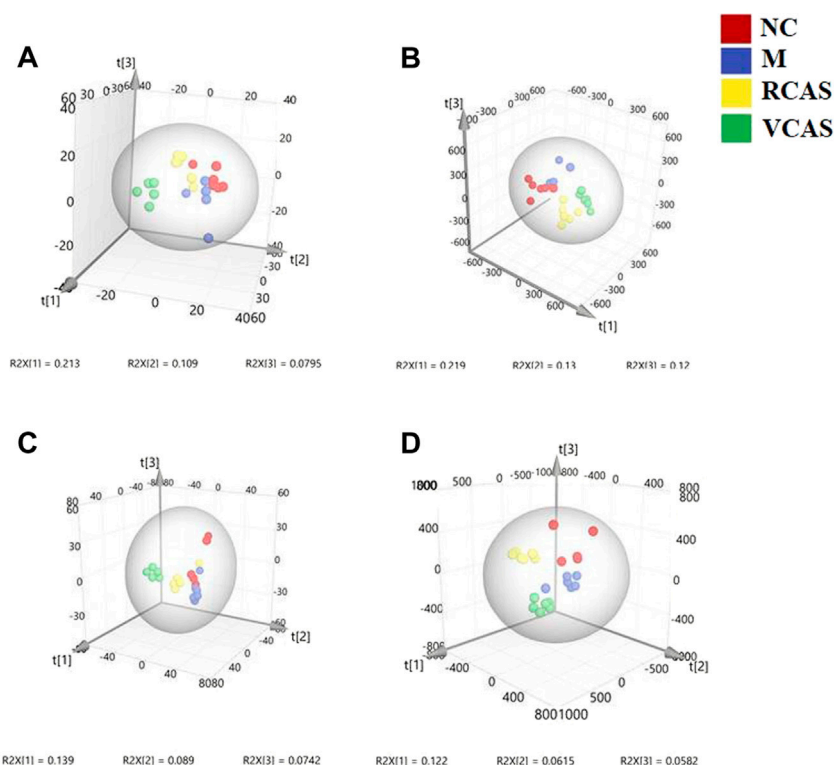
the NC, the RCAS, and the VCAS groups with the model group. The modeling parameters of each model are shown in [Supplementary Table S2](#). The data show that the modeling results are good. The S-plot graph was further drawn. Each point in the graph represents a “mass-charge ratio/retention time” pair (m/z -Rt). The closer the two ends of the “S” curve are, the greater the contribution of ions to the difference between groups. The S-plot plots of plasma samples in each group compared with the model group are shown in [Figure 4](#).

3.3.2 Identification of differential metabolites

In order to obtain the differential metabolites among the plasma samples of each group, the OPLS-DA model needs to be analyzed for the next step of data analysis. In order to improve experimental accuracy, the One-MAP cloud platform was utilized to identify the differential metabolites, the original spectra of all the initial samples after dimension reduction of Excel data (including sample ID, mass/charge ratio/retention time, and ionic strength) and the use of AB SCIEX secondary mass spectra of different substances extracted by the company’s supporting Pekview software were imported into the One-MAP online cloud platform, and differential metabolites were automatically searched and metabolic pathways were analyzed.

A variable important for the OPLS-DA model was projected according to each group. Projection, VIP screening of different ions, indicates that the greater the VIP value, the greater the contribution to the grouping. Referring to the literature on metabolomics, this study set a VIP value > 1 as the difference between the two groups. In this step, the number of differentiated ions obtained by screening is large, and there is some misjudgment. Therefore, the cloud platform automatically carries out an independent sample t -test for the differentiated ions obtained by preliminary screening and rejects the data with $p > 0.05$. Finally, the differential ions with $p < 0.05$ were input into the HMDB database, the structure of compounds was predicted based on the first-order mass spectrometry information, and the predicted exogenous compounds were eliminated to obtain the final selected differentials for structural identification. Each was compared with the standard second-order mass spectrometry data in the KEGG, HMDB, METLIN and other compound databases and relevant literature, and finally comprehensive analysis and identification were obtained. The differential metabolites of group samples are shown in [Supplementary Table S3](#).

Through analysis and identification of differential metabolites and matching with online databases such as

**FIGURE 3**

PCA and PLS-DA 3D-score scatter plot of UPLC-Q-TOF/MS data from plasma samples. (A) PCA 3D-score scatter plot in the positive ion mode; (B) PCA 3D-score scatter plot in the negative ion mode; (C) PLS-DA 3D-score scatter plot in the positive ion mode; (D) PLS-DA 3D-score scatter plot in negative ion mode.

HMDB and KEGG, the final 12 endogenous differential metabolites were identified in each group of plasma samples. These metabolites mainly include phenylalanine; phosphatidylcholine, also known as phosphatidylcholine (PC); lysophosphatidylcholine (LysoPC); tryptophan (L-tryptophan); and L-glutamic acid.

3.3.3 Analysis of metabolic pathways

The endogenous differential metabolites identified earlier were imported into the MetaboAnalyst 4.0 metabolomics online analysis platform (<https://www.metaboanalyst.ca/faces/home.xhtml>), the *Rattus norvegicus* (rat) pathway library was selected as the metabolic pathway database, the hypergeometric test as pathway enrichment analysis, relative-betweenness pathway topology was analyzed by centrality, and pathway enrichment was performed to screen out metabolic pathways with an impact value greater than 0.10. Pathway results of the blank group, each drug administration group, and the model group are shown in [Supplementary Table S4](#), and the pathway enrichment map is shown in [Figure 5](#). The results showed that the main metabolic pathways involved in the differential metabolites of plasma samples in each group included

pyrimidine metabolism, pyruvate metabolism, phenylalanine metabolism, and tyrosine metabolism. The abnormal metabolism of dysmenorrhea rats with blood stasis and the therapeutic effects of warm tulip on blood stasis syndrome were closely related to the aforementioned lipid metabolism pathways and amino acid metabolism pathways.

3.4 Urine metabolomics analysis

3.4.1 Multivariate statistical analysis

The modeling results of 3D-PCA under positive and negative ion modes are shown in [Figures 6A,B](#). Any point in the figure represents a urine sample. It can be seen from the figure that five groups of urine samples can be roughly distinguished, but the boundaries are not obvious enough. Therefore, the orthogonal partial least squares method was further used to establish the 3D-PLS-DA model. The results are shown in [Figures 6C,D](#). The grouping of the models modeled by the positive and negative ion modes was obvious, which indicated that the endogenous metabolites in urine samples were significantly different between the groups. Therefore, the OPLS-DA model was

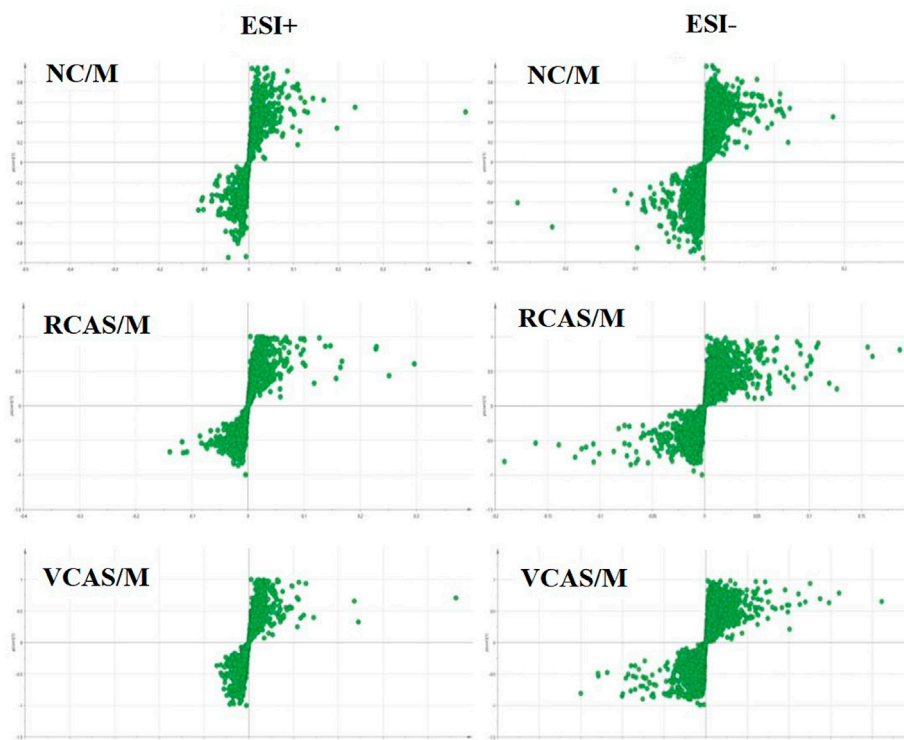


FIGURE 4
S-plot from plasma samples in the positive and negative ion mode.

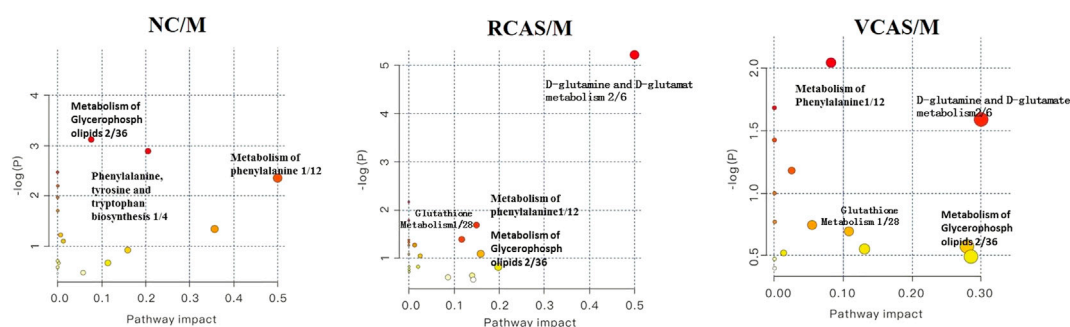


FIGURE 5
Enrichment results of metabolic pathways between plasma samples.

established by comparing the NC group, the RCAS group, and the VCAS group with the model group. The modeling parameters of each model are shown in [Supplementary Table S5](#). The data show that the modeling results are good. The S-plot graph was further drawn. Each point in the graph represents a “mass–charge ratio/retention time” pair (m/z -Rt). The closer the two ends of the “S” curve are, the greater the contribution of ions to the difference between groups. S-plot plots of urine samples in

each group compared with those of the model group are shown in [Figure 7](#).

3.4.2 Identification of different metabolites in urine samples of each group

The same method as mentioned earlier was used to obtain the comprehensive analysis and identification as shown in [Supplementary Table S6](#) for the results of differential

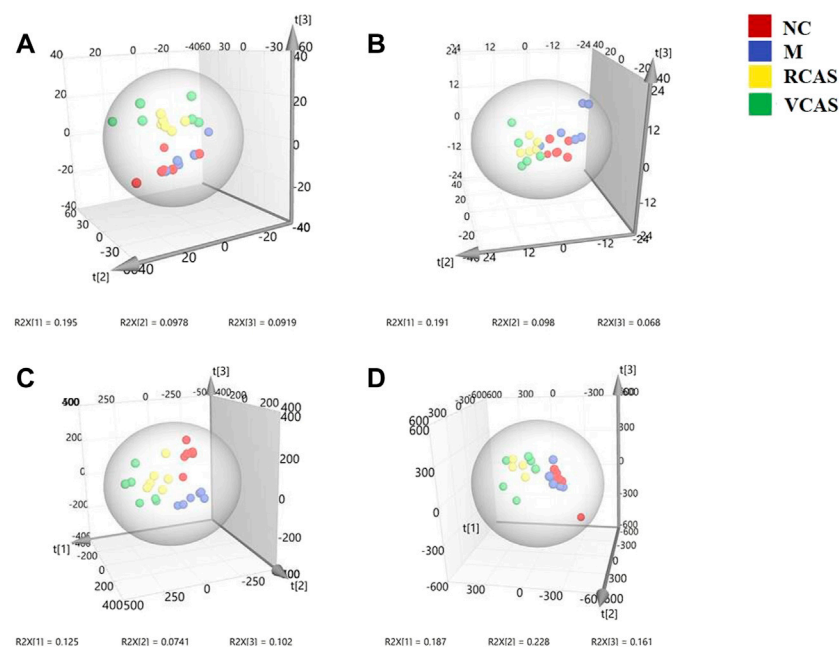


FIGURE 6 PCA and PLS-DA 3D-score scatter plot of UPLC-Q-TOF/MS data from urine samples. **(A)** PCA 3D-score scatter plot in the positive ion mode; **(B)** PCA 3D-score scatter plot in the negative ion mode; **(C)** PLS-DA 3D-score scatter plot in the positive ion mode; **(D)** PLS-DA 3D-score scatter plot in the negative ion mode.

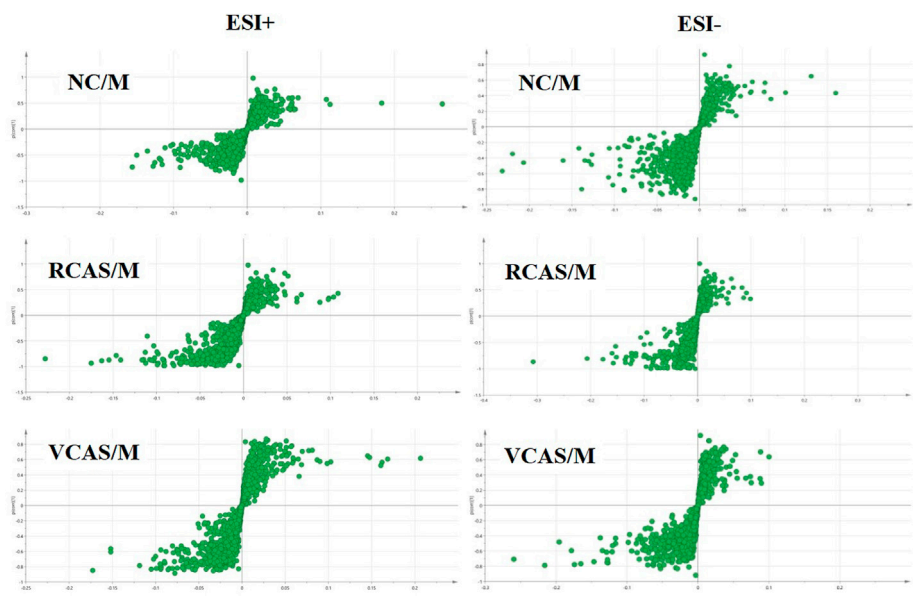


FIGURE 7 S-plot from urine samples in the positive and negative ion mode.

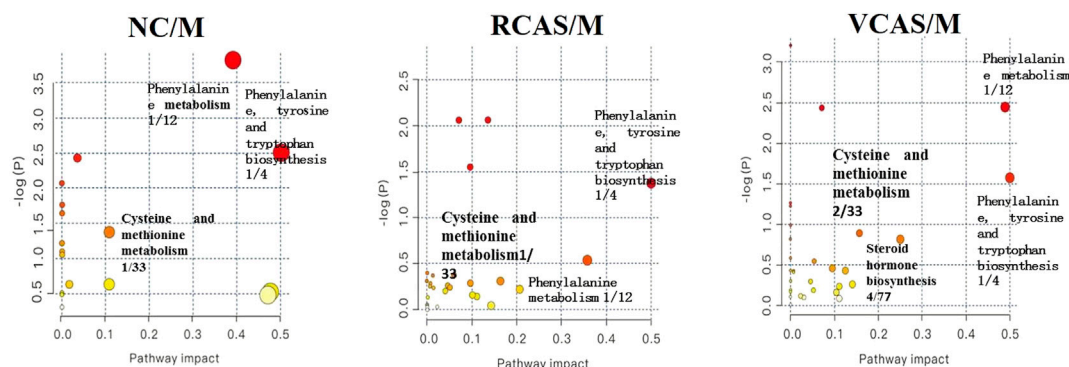


FIGURE 8
Enrichment results of metabolic pathways between urine samples.

metabolites. Through the analysis and identification of differential metabolites and matching with HMDB, KEGG, and other online databases, 19 endogenous differential metabolites were identified in each group of urine samples. These metabolites mainly include phenylalanine; phosphatidylcholine, also known as phosphatidylcholine (PC), lysophosphatidylcholine (lysoPC); and phosphatidic acid (PA) compounds, such as L-tyrosine, steroid hormones, and L-cysteine.

3.4.3 Analysis of metabolic pathways

The endogenous differential metabolites identified earlier were input into the MetaboAnalyst 4.0 metabolomics online analysis platform (<https://www.metaboanalyst.ca/faces/home.xhtml>). *R. norvegicus* (rat) was selected as the metabolic pathway database, and the hypergeometric test as the pathway enrichment analysis centrality analyzed the topological structure of the pathway, enriched the pathway, and screened out the metabolic pathway, with an impact value greater than 0.10. Pathway enrichment maps are shown in Figure 8. The results showed that the main metabolic pathways involved in the different metabolites of urine samples were pyrimidine metabolism, pyruvate metabolism, phenylalanine metabolism, and tyrosine metabolism. The metabolic abnormality of dysmenorrhea rats with blood stasis and the therapeutic effect of three processed products of VCAS on blood stasis syndrome were closely related to the aforementioned lipid metabolic pathway and amino acid metabolic pathway (Supplementary Table S7).

3.5 Fecal metabolomics analysis

3.5.1 Multivariate statistical analysis

The modeling results of 3D-PCA under positive and negative ion modes are shown in Figures 9A,B. Any point in the figure

represents a fecal sample. It can be seen from the figure that five groups of fecal samples can be roughly distinguished, but the boundaries are not obvious enough. Therefore, the orthogonal partial least squares method was further used to establish the 3D-OPLS-DA model, and the results are shown in Figures 9C,D. The grouping of the models modeled by the positive and negative ion modes was obvious, which indicated that the endogenous metabolites of the fecal samples were different among the groups to some extent. Therefore, the OPLS-DA model was established by comparing the NC group, RCAS group, and VCAS group with the M group. The modeling parameters of each model are shown in Supplementary Table S8. The results show that the modeling results are good. The S-plot graph was further drawn. Each point in the graph represents a “mass-charge ratio/retention time” pair (m/z -Rt). The closer the two ends of the “S” curve are, the greater the contribution of ions to the difference between groups. The S-plot of fecal samples in each group compared with that in the model group is shown in Figure 10.

3.5.2 Identification of different metabolites in fecal samples

The results of the differential metabolites are shown in Supplementary Table S9. Through differential metabolite analysis, identification, and matching with online databases such as HMDB and KEGG, 28 endogenous differential metabolites were identified in each group of fecal samples, which mainly included arachidonic acid, also known as leukotriene C4; phenylalanine; phosphatidylcholine, also referred as phosphatidylcholine (PC); sphingomyelin (SM); L-tyrosine; prostaglandin G2; and prostaglandin D2.

3.5.3 Analysis of metabolic pathways of fecal metabolites

The pathway results of group comparison are shown in Supplementary Table S10, and pathway enrichment maps are shown in Figure 11. The results showed that the metabolic

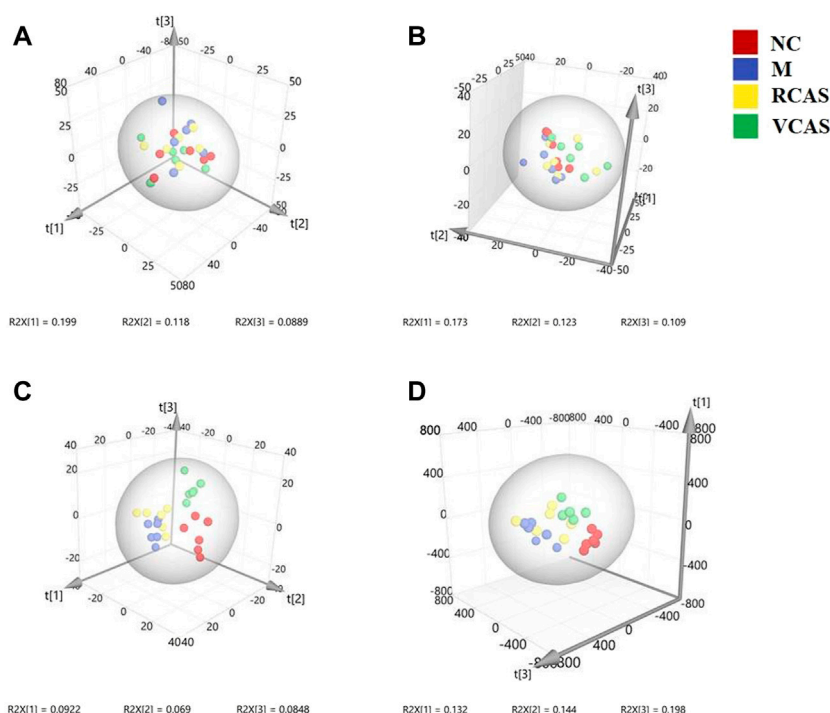


FIGURE 9

PCA and PLS-DA 3D-score scatter plot of UPLC-Q-TOF/MS data from feces samples. (A) PCA 3D-score scatter plot in the positive ion mode; (B) PCA 3D-score scatter plot in the negative ion mode; (C) PLS-DA 3D-score scatter lot in the positive ion mode; (D) PLS-DA 3D-score scatter plot in the negative ion mode.

pathways mainly involved in the differential metabolites of fecal samples in each group included glycerophospholipid metabolism, arachidonic acid metabolism, phenylalanine metabolism, and tyrosine metabolism, indicating that the abnormal metabolism of rats with blood stasis syndrome and the therapeutic effect of three processed products of warm tulip on blood stasis syndrome were closely related to the aforementioned lipid metabolism pathways and amino acid metabolism pathways.

4 Discussion

The endometrium is an important part of prostaglandin synthesis. It is generally believed that the occurrence of primary dysmenorrhea is mainly related to the increase of prostaglandin synthesis and release in the endometrium during menstruation. Prostaglandin (PG) can be converted into different *p*Gs in the body, such as PGF2 *a* (PGF2 α), PGE2 (PGE2), and TXA2 (thromboxane A2) (Guimarães and Pova, 2020). PGF2 *a* stimulates uterine contraction, increases uterine tension, and decreases blood flow; on the contrary, PGE2 inhibits uterine contraction, inhibits the spontaneous activity of smooth muscle, and relaxes the uterus (Ruoff and

Lema, 2003; Harel, 2004). Therefore, the concentration of PGF2 *a*/PGE2 in the endometrium and blood of dysmenorrhea patients 48 h before menstruation was significantly higher than that of normal people: the more severe the dysmenorrhea, the higher the level of PGF2 *a* (Richter et al., 2006; Dawood and Khan-Dawood, 2007a). In order to reduce the contractility of uterine smooth muscle and achieve the purpose of treating primary dysmenorrhea, it is necessary to inhibit the content of PGF2 *a* and increase the content of PGE2 (Dawood and Khan-Dawood, 2007b; Shi et al., 2011).

Thromboxane B 2 (TXB 2) and 6-keto-prostaglandin F 1 *a* (6-Keto-PGF 1 α) are relatively stable products transformed from two unstable bioactive substances, thromboxane A 2 (TXA 2) and prostacyclin I 2 (PGI 2) (Dawood and Khan-Dawood, 2007b). According to relevant research, TXA 2 is one of the most powerful vasoconstrictors reported *in vivo*, which can enhance platelet activation and aggregation, promote thrombosis, and cause Ca^{2+} influx, thus inducing dysmenorrhea (Das, 2008). Prostacyclin (PGI2) is mainly produced in vascular endothelial cells. By stimulating adenylate cyclooxygenase to increase the level of platelet endogenous camp, it can inhibit platelet aggregation and release induced by ADP, collagen, and AA (Kido et al.,

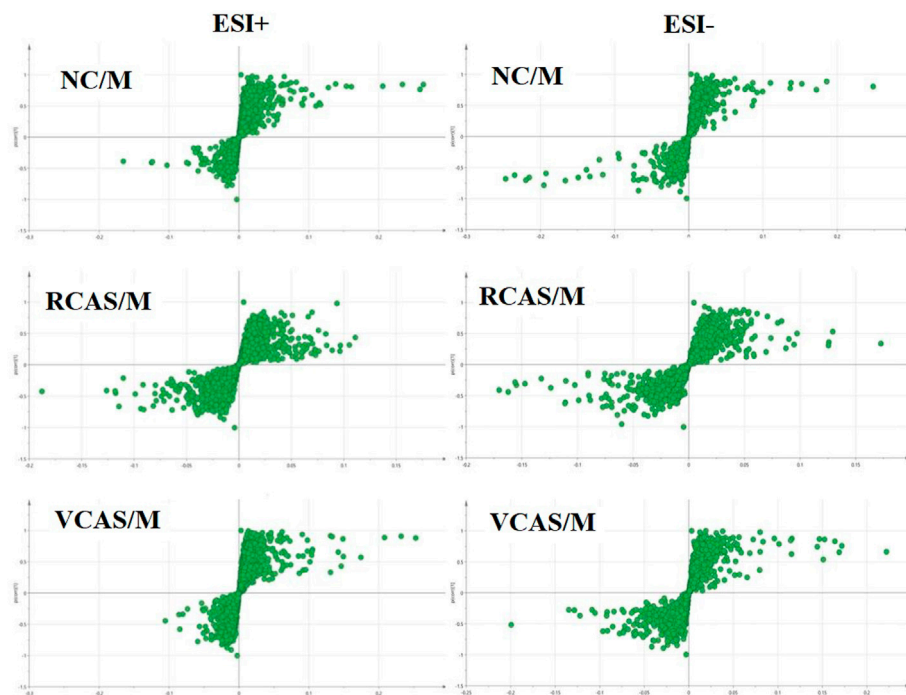


FIGURE 10
S-plot from feces samples in the positive and negative ion mode.

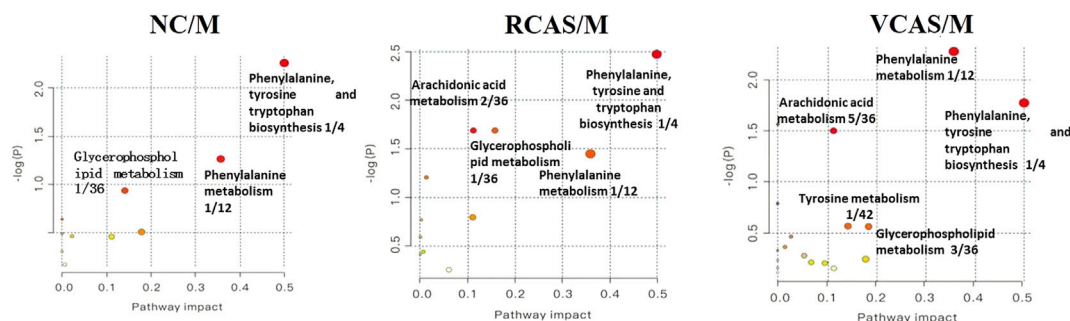


FIGURE 11
Enrichment results of metabolic pathways between feces samples.

2007), expand blood vessels, prevent platelet aggregation and thrombosis in local blood vessels, relieve dysmenorrhea symptoms, reduce the level of TXB₂ in plasma, increase the content of 6-k-PGF1 α , and reduce the ratio of TXB₂/6-k-PGF1 α so as to inhibit platelet aggregation, expand blood vessels, improve microcirculation, and restore the blood supply of the uterus by activating blood circulation and removing blood stasis so as to relieve dysmenorrhea (Shi et al., 2011).

The expression of TNF- α mRNA, protein, and its receptor in human endometrial decidua and trophoblast cells is regulated by estrogen and progesterone (Fluhr et al., 2007). TNF- α can inhibit endometrial hyperplasia, induce apoptosis, cause the loss of cadherin catenin actin complex, and promote the injury of endothelial cells. TNF- α , IL-6, and IL-4 can stimulate the AA metabolism of chorionic villi, the latter producing prostaglandins, thromboxane, and leukotrienes. The results showed that the serum levels of IL-6 and IL-10 in

dysmenorrhea women were significantly higher than those in non-dysmenorrhea women (Huang et al., 2016; Szebeni et al., 2019). NO is a vasoactive substance, which is the main component of the endothelium relaxing factor. It can dilate blood vessels, and it can reduce thrombosis by inhibiting platelet adhesion, aggregation, and TXB2 release. When the synthesis and release of endogenous NO decrease, the NO-mediated biological information transmission appears abnormal, and the regulation of vasoactive substances is maladjusted, which leads to dysfunction of endothelin function, thus causing pain. As a result, the blood supply of ischemic tissue is gradually restored, and the degree of pain is reduced (Jia et al., 2016).

According to modern medical research, the formation of primary dysmenorrhea may be related to the ischemia-reperfusion injury of the uterine muscle, which causes intracellular Ca^{2+} overload. On the one hand, it will aggravate the contraction of blood vessels and the myometrium and cause the blood supply of the endometrium to be insufficient; on the other hand, it will cause the imbalance of nuclear Ca^{2+} homeostasis, which will lead to depletion of cell energy and damage of the cell membrane, thus causing the production of dysmenorrhea. It can reduce the Ca^{2+} level in uterine smooth muscle cells and relax uterine smooth muscle (Hsia et al., 2008; Thaina et al., 2009; Xiong et al., 2019). β -EP is a class of neuropeptides with morphine-like activity, which is in the endometrial stroma, glandular epithelium, and muscle nerve fibers. It has an endogenous analgesic effect and participates in the regulation of reproductive endocrine. The content of β -EP in peripheral blood of patients with primary dysmenorrhea is significantly higher than that of the NC group (Jia et al., 2006).

VCAS can reduce the ratio of $\text{PGF}_2\text{a}/\text{PGE}_2$, $\text{TXB}_2/6\text{-k-PGF}_1\alpha$, $\text{TNF-}\alpha$, and IL-6 levels, promote the synthesis and release of endogenous NO, reduce the level of Ca^{2+} in uterine smooth muscle cells so as to inhibit platelet aggregation, dilate blood vessels, improve microcirculation, and restore the blood supply of the uterus by activating blood circulation and removing blood stasis so as to relieve dysmenorrhea. The effect of RCAS on $\text{PGF}_2\alpha$, $\text{TNF-}\alpha$, NO, Ca^{2+} , and β -EP was not obvious, so the therapeutic effect of RCAS on dysmenorrhea was weaker than that of VCAS.

The results of plasma metabolomics showed that the improvement of dysmenorrhea caused by blood stasis was mainly related to the metabolism of glycerin phospholipid, phenylalanine, glutathione, and tryptophan. The results of urine metabolomics showed that the improvement of dysmenorrhea caused by blood stasis was mainly related to the metabolism of glycerophosphatide, phenylalanine, steroid hormone, cysteine and methionine, arginine, and proline. The results of fecal metabolomics showed that the improvement of dysmenorrhea in blood stasis syndrome was mainly related to the glycerin phospholipid metabolic pathway, phenylalanine

metabolic pathway, tyrosine metabolic pathway, and arachidonic acid metabolic pathway.

LysoPCs are important metabolites of lipid metabolism and play an important role in dyslipidemia, diabetes, cancer, atherosclerosis, inflammation, and other diseases (Jackson et al., 2008; Jiang et al., 2013). LysoPC can inhibit transcription activity, tissue factor and NF- κ B during coagulation and participate in thrombosis by regulating the expression of tissue factors (Engelmann et al., 1999). Lysophosphatidic acid lysoPA (16:0/0:0) can promote the expression of cyclooxygenase-2 (Guimarães and Pova, 2020), and cyclooxygenase-2 is the key enzyme for the conversion of arachidonic acid to prostaglandins. Compared with the NC group, the contents of lysoPCs and lysoPA (16:0/0:0) in the M group were significantly increased. After the intervention, the RCAS and VCAS had a downregulation effect on the glycerophosphatidylcholine metabolites, especially the VCAS. The results showed that RCAS and VCAS could reduce the glycerol phospholipid metabolites and inhibit cyclooxygenase-2 by regulating the glycerophosphatidic metabolic pathway. The effect of VCAS on dysmenorrhea was more significant.

Arachidonic acid is a type of polyunsaturated fatty acid, which can mediate the production of inflammatory mediators such as $\text{TNF-}\alpha$ and IL-1, PGD_2 , TXA_2 , and leukotriene, which can induce platelet aggregation, promote blood coagulation, smooth muscle contraction, leukocyte chemotaxis, production of inflammatory cytokines, and immune function (Ma et al., 2013; Burns et al., 2018). The changes of PGG_2 and PGD_2 metabolites are closely related to the occurrence of primary dysmenorrhea. PGE_2 produced and released by the endometrium can inhibit the spontaneous activity of uterine smooth muscle, mediate the cAMP signal molecular transduction pathway, and regulate some neurotransmitters, thus leading to downstream pathway reactions (including reproduction and inflammation) (Iacovides et al., 2015; Guimarães and Pova, 2020). 12 (s)—HETE is one of the six monohydroperoxy fatty acids produced by non-enzymatic oxidation of arachidonic acid (leukotriene), which produces more stable hydroxyl fatty acid (+/-) 12-HETE through reduction reaction and then participates in host defense reaction and pathophysiological conditions, such as allergy and inflammation. Compared with the endogenous metabolite table, the contents of arachidonic acid, PGE_2 , PGD_2 and 12 (s)—HETE in the M group were significantly higher than those in the NC group. After the intervention of VCAS, the contents of arachidonic acid, PGE_2 , PGD_2 and 12 (s)—HETE in the M group were significantly higher than those in the NC group. Therefore, it is speculated that the pro-inflammatory effect of arachidonic acid may be a contributing factor to the formation of blood stasis syndrome. The arachidonic acid metabolic pathway is one of the important pathways for VCAS to remove blood stasis and relieve pain.

Through UHPLC-Q/TOF-MS and multivariate statistical pattern discrimination, the results showed that normal rats and model rats were discernibly divided into two groups. They exhibited clustering state, which indicated the successful replication of PDM rats from the perspective of metabolomics. In addition, uterine histopathology, the pain factors PGF2 *a*/PGE2 and TXB2 related to dysmenorrhea/6-keto-PGF1 α , IL-6, TNF - α , NO, Ca²⁺, β - EP, and other pharmacodynamic indexes changed before and after the establishment of the model. After RCAS and VCAS intervention, the uterine tissue morphology of dysmenorrhea model rats was improved, and gland hypertrophy and myometrial hyperplasia were reduced as well as neutrophil content. By regulating pain-related factors, the metabolism of glycerophospholipid, glutathione, steroid hormone biosynthesis, cysteine and arginine, and arachidonic acid was regulated, while the spasm of the uterine smooth muscles was relieved.

5 Conclusion

This study mainly carried out the metabonomics of plasma, urine, and feces of RCAS and VCAS decoction pieces to remove blood stasis and relieve pain and clarified the metabolic abnormalities of primary dysmenorrhea model rats with *Qi* stagnation and blood stasis, and the therapeutic effects of RCAS and VCAS on primary dysmenorrhea with *Qi* stagnation and blood stasis are closely related to lipid metabolism and amino acid metabolism. It effectively explains the similarities and differences in the clinical efficacy of RCAS and VCAS in removing blood stasis and relieving pain on the whole. RCAS can improve uterine ischemia and treat primary dysmenorrhea, and the effect of VCAS is even better. The related signal pathways and metabolic pathways of RCAS/VCAS in the treatment of primary dysmenorrhea are shown in [Supplementary Figure S4](#). This study provides a basis for further study on the mechanism of VCAS in the treatment of primary dysmenorrhea. Through in-depth analysis of dysmenorrhea-related pain factors, related metabolites, and metabolic pathways, it is found that metabolomics can comprehensively demonstrate the impact of the disease on the whole body, and the selected indicators can holistically reflect the state of the disease and provide a new approach for the study of mechanism, screening, or clinical drug treatment of diseases related to blood stasis syndrome.

Data availability statement

The original contributions presented in the study are included in the article/[Supplementary Material](#); further inquiries can be directed to the corresponding authors.

Ethics statement

The animal study was reviewed and approved by the Experimental animal center of Nanjing University of Chinese Medicine (license No. SYXK (Su) 2014-0001).

Author contributions

HT and LS: conceptualization, methodology, software, and roles/writing—original draft. TL and CM: data curation, funding acquisition, and formal analysis. JZ: visualization, investigation, and methodology. MH and WG: supervision and validation. ZB: software and resources. CF: data curation. TL and JZ: project administration, writing—review, and editing.

Funding

This research study was supported by the National Natural Science Foundation of China (Nos. 81673598 and 81973483) and Postgraduate Research and Practice Innovation Program of Jiangsu Province (No. KYCX20_1505).

Acknowledgments

The authors gratefully acknowledge the support of Hou Baoquan and interns Ji Yuxuan, Zuo Tongwen, Zhang Jingyi, Jiang Wangtao and thank Jiangsu Kaiji Biotechnology Co., Ltd. for providing kits.

Conflict of interest

The authors declare that the research was conducted in the absence of any commercial or financial relationships that could be construed as a potential conflict of interest.

Publisher's note

All claims expressed in this article are solely those of the authors and do not necessarily represent those of their affiliated organizations, or those of the publisher, the editors, and the reviewers. Any product that may be evaluated in this article, or claim that may be made by its manufacturer, is not guaranteed or endorsed by the publisher.

Supplementary material

The Supplementary Material for this article can be found online at: <https://www.frontiersin.org/articles/10.3389/fphar.2022.926291/full#supplementary-material>

References

- Burns, J. L., Nakamura, M. T., and Ma, D. W. L. (2018). Differentiating the biological effects of linoleic acid from arachidonic acid in health and disease. *Prostagl. Leukot. Essent. Fat. Acids* 135, 1–4. doi:10.1016/j.plfa.2018.05.004
- Chai, C., Hong, F., Yan, Y., Yang, L., Zong, H., Wang, C., et al. (2020). Effect of traditional Chinese medicine formula GeGen decoction on primary dysmenorrhea: A randomized controlled trial study. *J. Ethnopharmacol.* 261, 113053. doi:10.1016/j.jep.2020.113053
- Chan, W. Y. (1983). Prostaglandins and nonsteroidal antiinflammatory drugs in dysmenorrhea. *Annu. Rev. Pharmacol. Toxicol.* 23, 131–149. doi:10.1146/annurev.pa.23.040183.001023
- Chinese Pharmacopoeia (2020). *Chinese Pharmacopoeia 2015, part I*. Beijing: National Pharmacopoeia Committee, 274–275.
- Das, U. N. (2008). Essential fatty acids and their metabolites could function as endogenous HMG-CoA reductase and ACE enzyme inhibitors, anti-arrhythmic, anti-hypertensive, anti-atherosclerotic, anti-inflammatory, cytoprotective, and cardioprotective molecules. *Lipids Health Dis.* 7, 37. doi:10.1186/1476-511X-7-37
- Dawood, M. Y., and Khan-Dawood, F. S. (2007a). Clinical efficacy and differential inhibition of menstrual fluid prostaglandin F2alpha in a randomized, double-blind, crossover treatment with placebo, acetaminophen, and ibuprofen in primary dysmenorrhea. *Am. J. Obstet. Gynecol.* 196, 35 e1–5. doi:10.1016/j.ajog.2006.06.091
- Dawood, M. Y., and Khan-Dawood, F. S. (2007b). Differential suppression of menstrual fluid prostaglandin F2a, prostaglandin E2, 6-keto prostaglandin F1a and thromboxane B2 by suprofen in women with primary dysmenorrhea. *Prostagl. Other Lipid Mediat.* 83, 146–153. doi:10.1016/j.prostaglandins.2006.10.009
- De Sanctis, V., Soliman, A., Bernasconi, S., Bianchin, L., Bona, G., Bozzola, M., et al. (2015). Primary dysmenorrhea in adolescents: Prevalence, impact and recent knowledge. *Pediatr. Endocrinol. Rev.* 13, 512–520.
- Engelmann, B., Zieseniss, S., Brand, K., Page, S., Lentschat, A., Ulmer, A. J., et al. (1999). Tissue factor expression of human monocytes is suppressed by lysophosphatidylcholine. *Arterioscler. Thromb. Vasc. Biol.* 19, 47–53. doi:10.1161/01.atv.19.1.47
- Fluhr, H., Krenzer, S., Stein, G. M., Stork, B., Deperschmidt, M., Wallwiener, D., et al. (2007). Interferon-gamma and tumor necrosis factor-alpha sensitize primarily resistant human endometrial stromal cells to Fas-mediated apoptosis. *J. Cell Sci.* 120, 4126–4133. doi:10.1242/jcs.009761
- Gu, W., Mao, C., Zhang, J., Li, L., and Lu, T. (2018). Influence of processing process on the efficacy of Curcuma wenyujin Y.H.Chen et C.Ling for activating blood circulation and removing blood stasis. *Chin. Tradit. Pat. Med.* 40 (07), 1576–1580. doi:10.3969/j.issn.1001-1528.2018.07.027
- Guimarães, I., and Póvoa, A. M. (2020). Primary dysmenorrhea: Assessment and treatment. *Rev. Bras. Ginecol. Obstet.* 42, 501–507. doi:10.1055/s-0040-1712131
- Hao, M., JiLi, L., Su, L., Gu, W., Gu, L., Wang, Q., et al. (2018). Mechanism of Curcuma wenyujin rhizoma on acute blood stasis in rats based on a UPLC-Q/TOF-MS metabolomics and network approach. *Molecules* 24, E82. doi:10.3390/molecules24010082
- Harel, Z. (2004). Cyclooxygenase-2 specific inhibitors in the treatment of dysmenorrhea. *J. Pediatr. Adolesc. Gynecol.* 17, 75–79. doi:10.1016/j.jpaa.2004.01.002
- Hsia, S. M., Kuo, Y. H., Chiang, W., and Wang, P. S. (2008). Effects of arday hull extracts on uterine contraction and Ca2+ mobilization in the rat. *Am. J. Physiol. Endocrinol. Metab.* 295, E719–E726. doi:10.1152/ajpendo.90367.2008
- Huang, X., Su, S., Duan, J. A., Sha, X., Zhu, K. Y., Guo, J., et al. (2016). Effects and mechanisms of Shaofu-Zhuyu decoction and its major bioactive component for Cold - stagnation and Blood - stasis primary dysmenorrhea rats. *J. Ethnopharmacol.* 186, 234–243. doi:10.1016/j.jep.2016.03.067
- Iacovides, S., Avidon, I., and Baker, F. C. (2015). What we know about primary dysmenorrhea today: a critical review. *Hum. Reprod. Update* 21, 762–778. doi:10.1093/humupd/dmv039
- Jackson, S. K., Abate, W., and Tonks, A. J. (2008). Lysophospholipid acyltransferases: novel potential regulators of the inflammatory response and target for new drug discovery. *Pharmacol. Ther.* 119, 104–114. doi:10.1016/j.pharmthera.2008.04.001
- Jia, W., Wang, X., Xu, D., Zhao, A., and Zhang, Y. (2006). Common traditional Chinese medicinal herbs for dysmenorrhea. *Phytother. Res.* 20, 819–824. doi:10.1002/ptr.1905
- Jiang, C. Y., Yang, K. M., Yang, L., Miao, Z. X., Wang, Y. H., and Zhu, H. B. (2013). A (1)H NMR-based metabolomic investigation of time-related metabolic trajectories of the plasma, urine and liver extracts of hyperlipidemic hamsters. *PLoS One* 8, e66786. doi:10.1371/journal.pone.0066786
- Ju, H., Jones, M., and Mishra, G. (2014). The prevalence and risk factors of dysmenorrhea. *Epidemiol. Rev.* 36, 104–113. doi:10.1093/epirev/mxt009
- Kido, A., Togashi, K., Kataoka, M., Maetani, Y., Nakai, A., Kataoka, M. L., et al. (2007). The effect of oral contraceptives on uterine contractility and menstrual pain: an assessment with cine MR imaging. *Hum. Reprod.* 22, 2066–2071. doi:10.1093/humrep/dem122
- Liu, K., Song, Y., Liu, Y., Peng, M., Li, H., Li, X., et al. (2017). An integrated strategy using UPLC-QTOF-MS(E) and UPLC-QTOF-MRM (enhanced target) for pharmacokinetics study of wine processed Schisandra Chinensis fructus in rats. *J. Pharm. Biomed. Anal.* 139, 165–178. doi:10.1016/j.jpba.2017.02.043
- Ma, H., Hong, M., Duan, J., Liu, P., Fan, X., Shang, E., et al. (2013). Altered cytokine gene expression in peripheral blood monocytes across the menstrual cycle in primary dysmenorrhea: a case-control study. *PLoS One* 8, e55200. doi:10.1371/journal.pone.0055200
- Maia, H., Jr., Maltez, A., Studard, E., Zausner, B., Athayde, C., and Coutinho, E. (2005). Effect of the menstrual cycle and oral contraceptives on cyclooxygenase-2 expression in the endometrium. *Gynecol. Endocrinol.* 21, 57–61. doi:10.1080/09513590500099602
- Nguyen, A. M., Humphrey, L., Kitchen, H., Rehman, T., and Norquist, J. M. (2015). A qualitative study to develop a patient-reported outcome for dysmenorrhea. *Qual. Life Res.* 24, 181–191. doi:10.1007/s11136-014-0755-z
- Oladosu, F. A., Tu, F. F., and Hellman, K. M. (2018). Nonsteroidal antiinflammatory drug resistance in dysmenorrhea: epidemiology, causes, and treatment. *Am. J. Obstet. Gynecol.* 218, 390–400. doi:10.1016/j.ajog.2017.08.108
- Pu, B., Jiang, G., and Fang, I. (2014). Study on primary dysmenorrhea pain factor and its correlation. *Chin. J. Traditional Chin. Med.* 32, 1368–1370. doi:10.13193/j.issn.1673-7717.2014.06.037
- Richter, O. N., Bartz, C., Dowaji, J., Kupka, M., Reinsberg, J., Ulrich, U., et al. (2006). Contractile reactivity of human myometrium in isolated non-pregnant uteri. *Hum. Reprod.* 21, 36–45. doi:10.1093/humrep/dei295
- Ruoff, G., and Lema, M. (2003). Strategies in pain management: new and potential indications for COX-2 specific inhibitors. *J. Pain Symptom Manage.* 25, S21–S31. doi:10.1016/s0885-3924(02)00628-0
- Sahin, N., Kasap, B., Kirli, U., Yeniceri, N., and Topal, Y. (2018). Assessment of anxiety-depression levels and perceptions of quality of life in adolescents with dysmenorrhea. *Reprod. Health* 15, 13. doi:10.1186/s12978-018-0453-3
- Shi, G. X., Liu, C. Z., Zhu, J., Guan, L. P., Wang, D. J., and Wu, M. M. (2011). Effects of acupuncture at Sanyinjiao (SP6) on prostaglandin levels in primary dysmenorrhea patients. *Clin. J. Pain* 27, 258–261. doi:10.1097/AJP.0b013e3181fb27ae
- Su, L., Mao, J., Hao, M., Lu, T., Mao, C., JiTong, H., et al. (2019). Integrated plasma and bile metabolomics based on an UHPLC-Q/TOF-MS and network Pharmacology approach to explore the potential mechanism of schisandra chinensis-protection from acute alcoholic liver injury. *Front. Pharmacol.* 10, 1543. doi:10.3389/fphar.2019.01543
- Szebeni, G. J., Nagy, L. I., Berko, A., Hoffmann, A., Feher, L. Z., Bagyaszki, M., et al. (2019). The anti-inflammatory role of mannich curcuminoids; special focus on colitis. *Molecules* 24, E1546. doi:10.3390/molecules24081546
- Thaina, P., Tuncharoen, P., Wongnawa, M., Reanmongkol, W., and Subhadrirakul, S. (2009). Uterine relaxant effects of Curcuma aeruginosa Roxb. rhizome extracts. *J. Ethnopharmacol.* 121, 433–443. doi:10.1016/j.jep.2008.10.022
- Xie, D., Ju, M., Cao, P., Wang, D., and Yu, B. (2014). Research progress of correlation between inflammatory factors and primary dysmenorrhea. *Chin. Clin. Pharmacol. Ther.* 19, 346–350.
- Xie, H., Su, D., Zhang, J., JiMao, J., Hao, M., Wang, Q., et al. (2020). Raw and vinegar processed Curcuma wenyujin regulates hepatic fibrosis via blocking TGF-β/Smad signaling pathways and up-regulation of MMP-2/TIMP-1 ratio. *J. Ethnopharmacol.* 246, 111768. doi:10.1016/j.jep.2019.01.045
- Xing, J., Sun, H. M., Jia, J. P., Qin, X. M., and Li, Z. Y. (2017). Integrative hepatoprotective efficacy comparison of raw and vinegar-baked Radix Bupleuri using nuclear magnetic resonance-based metabolomics. *J. Pharm. Biomed. Anal.* 138, 215–222. doi:10.1016/j.jpba.2017.02.015
- Xiong, Z., Lang, L., Gao, X., Xiao, W., Wang, Z., and Zhao, L. (2019). An integrative urinary metabolomic study of the therapeutic effect of Guizhi Fuling capsule on primary dysmenorrheal rats based (1)H NMR and UPLC-MS. *J. Pharm. Biomed. Anal.* 164, 750–758. doi:10.1016/j.jpba.2018.11.039
- Xu, L., Xie, T., Shen, T., and Zhang, T. (2019). Effect of Chinese herbal medicine on primary dysmenorrhea: A protocol for a systematic review and meta-analysis. *Med. Baltim.* 98, e17191. doi:10.1097/MD.00000000000017191
- Yang, F. Q., Li, S. P., Zhao, J., Lao, S. C., and Wang, Y. T. (2007). Optimization of GC-MS conditions based on resolution and stability of analytes for simultaneous determination of nine sesquiterpenoids in three species of Curcuma rhizomes. *J. Pharm. Biomed. Anal.* 43, 73–82. doi:10.1016/j.jpba.2006.06.014
- Yao, W., Gu, H., Zhu, J., Barding, G., Cheng, H., Bao, B., et al. (2014). Integrated plasma and urine metabolomics coupled with HPLC/QTOF-MS and chemometric analysis on potential biomarkers in liver injury and hepatoprotective effects of Er-Zhi-Wan. *Anal. Bioanal. Chem.* 406, 7367–7378. doi:10.1007/s00216-014-8169-x



OPEN ACCESS

EDITED BY

Xijun Wang,
Heilongjiang University of Chinese
Medicine, China

REVIEWED BY

Aihua Zhang,
Heilongjiang University of Chinese
Medicine, China
Guang Hu,
Chongqing University of Technology,
China

*CORRESPONDENCE

Songsong Wang,
wangsongsong@sdfmu.edu.cn
Liwen Han,
hanliwen@sdfmu.edu.cn

*These authors have contributed equally
to this work

SPECIALTY SECTION

This article was submitted to
Ethnopharmacology,
a section of the journal
Frontiers in Pharmacology

RECEIVED 31 March 2022

ACCEPTED 20 September 2022

PUBLISHED 14 October 2022

CITATION

Dong R, Zhang Y, Chen S, Wang H, Hu K,
Zhao H, Tian Q, Zeng K, Wang S and
Han L (2022), Identification of key
pharmacodynamic markers of American
ginseng against heart failure based on
metabolomics and zebrafish model.
Front. Pharmacol. 13:909084.
doi: 10.3389/fphar.2022.909084

COPYRIGHT

© 2022 Dong, Zhang, Chen, Wang, Hu,
Zhao, Tian, Zeng, Wang and Han. This is
an open-access article distributed
under the terms of the [Creative
Commons Attribution License \(CC BY\)](#).
The use, distribution or reproduction in
other forums is permitted, provided the
original author(s) and the copyright
owner(s) are credited and that the
original publication in this journal is
cited, in accordance with accepted
academic practice. No use, distribution
or reproduction is permitted which does
not comply with these terms.

Identification of key pharmacodynamic markers of American ginseng against heart failure based on metabolomics and zebrafish model

Rong Dong^{1†}, Yougang Zhang^{1,2†}, Shanjun Chen¹, Huan Wang¹,
Kaiqing Hu¹, Huanxin Zhao¹, Qingping Tian², Kewu Zeng³,
Songsong Wang^{1*} and Liwen Han^{1*}

¹School of Pharmacy and Pharmaceutical Science, Shandong First Medical University and Shandong Academy of Medical Sciences, Jinan, China, ²School of Pharmaceutical Science of Shanxi Medical University, Taiyuan, China, ³School of Pharmaceutical Science of Peking University, Beijing, China

Background: American ginseng (*Panax quinquefolium* L., AG) is a traditional Chinese medicine with multiple cardiovascular protective properties. Many bioactive components have been discovered in AG over these years. However, the understanding of these key pharmacodynamic components of activity against heart failure is insufficient.

Methods: A heart failure model was established using AB line wild-type zebrafish (*Danio rerio*) to evaluate the anti-heart failure activity of AG. Untargeted metabolomics analysis based on ultra-high performance liquid chromatography-quadrupole electrostatic field orbitrap-mass spectrometry technology (UHPLC-QE-Orbitrap-MS) was performed to screen differential components from AG samples. The potential active components were verified using the zebrafish model. Simultaneously, network pharmacology and molecular docking techniques were used to predict the possible mechanism. Finally, the key targets of six key pharmacodynamic components were verified in zebrafish using quantitative real-time-polymerase chain reaction (Q-PCR) techniques.

Results: The heart failure model was successfully established in 48 h of post-fertilization (hpf) zebrafish larvae by treating with verapamil hydrochloride. The zebrafish assay showed that the anti-heart failure effects of AG varied with producing regions. The result of the herbal metabolomic analysis based on UHPLC-QE-Orbitrap-MS indicated that ginsenoside Rg3, ginsenoside Rg5, ginsenoside Rg6, malic acid, quinic acid, L-argininosuccinic acid, 3-methyl-3-butenyl-apinosyl (1→6) glucoside, pseudoginsenoside F11, and annonaine were differential components, which might be responsible for variation in efficacy. Further analysis using zebrafish models, network pharmacology, and Q-PCR techniques showed that ginsenoside Rg3, ginsenoside Rg5, ginsenoside Rg6, malic acid, quinic acid, and pseudoginsenoside F11 were the pharmacodynamic markers (P-markers) responsible for anti-heart failure.

Conclusion: We have rapidly identified the P-markers against heart failure in AG using the zebrafish model and metabolomics technology. These P-markers may provide new reference standards for quality control and new drug development of AG.

KEYWORDS

American ginseng (*Panax quinquefolius* L.), anti-heart failure, metabolomics, pharmacodynamic markers, zebrafish, network pharmacology

1 Introduction

Panax quinquefolius Radix, also known as American ginseng (AG), is the dry root of *Panax quinquefolium* L, belonging to the Araliaceae family (Huang et al., 2019). AG has been used in protecting cardiovascular lesions (Szczyka et al., 2019), glycemic control (Vuksan et al., 2019), delaying neurodegenerative diseases (Xie et al., 2018), regulating immune systems (Ghosh et al., 2020), and inhibiting tumor and infection (L. Qi et al., 2010; L. Wang et al., 2020) for a significant time. Ginsenosides were considered one major kind of active components in AG (Yuan et al., 2010). Many research studies have reported that ginsenosides increased ventricular myocyte viability, alleviated the early apoptosis of ventricular myocytes, and promoted energy production *via* the activation of AMP-activated protein kinase (AMPK) metabolic pathways (Yu et al., 2021). AG from North America was verified for its ability to attenuate β -adrenergic activation-induced heart failure *via* the prevention of protein kinase A activation and inhibition of cyclic AMP response element-binding protein phosphorylation (Tang et al., 2016). However, these known active compounds do not seem capable of explaining the anti-heart failure response of AG; hence, it is necessary to explore the more active components in AG.

Traditional Chinese medicine (TCM) is a relatively complex chemical composition system. Hence, exploring the relationship between active components and diseases is difficult (Zhang R et al., 2019). Metabolomics is a high-throughput, high-sensitivity, and unbiased approach (Rinschen et al., 2019), offering us a powerful technology for analysis of complex TCM. Over the years, metabolomics technology has been widely used for quality control of TCM (H. Xiong et al., 2020), pharmacodynamics analysis (Y. P. Shi et al., 2020), and toxicity evaluation (Duan et al., 2018). Especially, some innovative concepts based on metabolomics were proposed for exploring the scientific connotation of TCM, such as chinmedomics (Zhang A. H et al., 2019), functional metabolomics (T. Wang et al., 2021), and spatial metabolomics (Nakabayashi et al., 2021).

Zebrafish (*Danio rerio*) is an international recognized vertebrate model possessing various characteristics, such as fast reproduction, low consumption, and a short experimental period (MacRae and Peterson, 2015). The zebrafish genome is genetically similar to the human genome. Also, zebrafish has been used for high-throughput drug screening and drug toxicity evaluation (Horzmann and Freeman, 2018). Heart failure is

defined as the heart's inability to supply enough blood to meet the body's needs (Pfeffer et al., 2019). The heart structure, physiological functions, signal pathways, and ion channels of zebrafish are highly comparable with those of humans (X. Shi et al., 2018). In comparison with the mammalian models, heart failure models in zebrafish are simple, low-cost, and beneficial for mechanistic studies. Also, the embryonic cardiac function is easy to quantify and observe (Narumanchi et al., 2021). When injured, zebrafish can rapidly and effectively regenerate their hearts. Several zebrafish models of heart failure were established by genetic manipulation or by drug treatment. Many drugs, including isoproterenol (Wang J et al., 2019), aristolochic acid (X. Shi et al., 2017), and verapamil (X. Y. Zhu et al., 2018), could induce heart failure in zebrafish. Hence, zebrafish is an excellent animal model for studying heart-related diseases.

Therefore, in this study, we aimed to discover key anti-heart failure active components and pharmacodynamic markers (P-markers) in AG using metabolomics technology and the zebrafish model. Also, network prediction of the mechanism of AG against heart failure was achieved *via* network pharmacology, molecular docking techniques, and Q-PCR techniques. We hope these P-markers might play an important role in the qualitative evaluation of AG in the future.

2 Materials and methods

2.1 Chemicals, reagents, and instruments

Pronase E (Lot No. 41844523), tricaine, and N-phenylthiourea (Lot No. BCCC9256) were purchased from Sigma-Aldrich Trading Co., Ltd. (Shanghai, China). Dimethyl sulfoxide (DMSO, Lot No. K1723046), verapamil hydrochloride (Lot No. A2007039), and ammonium bicarbonate (analytical grade) were acquired from Aladdin Co. Digoxin (DIG, Lot No. XNPO-TP) was supplied by Tokyo Chemical Industry. Trichloromethane, propan-2-ol, ethanol, and analytical-grade formic acid was acquired from Sinopharm Chemical Reagent Co., Ltd. (Shanghai, China). HPLC-grade acetonitrile was purchased from Oceanpak (Goteborg, Sweden). HPLC-grade methanol was purchased from Fisher. Ultrapure water was supplied by Watsons Ltd., (Hong Kong, China). Reference standard ginsenoside Rg3 (G-Rg3, Lot No. AF8091509) was

TABLE 1 Collection information of AG samples.

| No. | Producing area | Collected time | No. | Producing area | Collected time |
|-----|---------------------|----------------|-----|--------------------------|----------------|
| S1 | Wendeng, Shandong | September 2020 | S11 | Jilin | August 2019 |
| S2 | Wendeng, Shandong | September 2020 | S12 | Liuba, Shanxi | January 2020 |
| S3 | Wendeng, Shandong | September 2020 | S13 | Xinbin, Liaoning | January 2020 |
| S4 | Wendeng, Shandong | September 2020 | S14 | Wisconsin, United States | November 2016 |
| S5 | Wendeng, Shandong | September 2020 | S15 | Canada | September 2019 |
| S6 | Wendeng, Shandong | September 2020 | S21 | Xinbin, Liaoning | November 2019 |
| S7 | Wendeng, Shandong | September 2019 | S22 | Xinbin, Liaoning | December 2019 |
| S8 | Beijing | January 2020 | S23 | Xinbin, Liaoning | January 2020 |
| S9 | Changbaishan, Jilin | September 2019 | S24 | Xinbin, Liaoning | November 2020 |
| S10 | Changbaishan, Jilin | September 2019 | | | |

purchased from Chengdu Alfa Biotechnology Co., Ltd. Ginsenoside Rg5 (G-Rg5, Lot No. B01SS11S122325), ginsenoside Rg6 (G-Rg6, Lot No. Y8D1H34968), malic acid (MA, Lot No. Z29O10H101559), quinic acid (QA, Lot No. A06N11L130218), and L-argininosuccinic acid (AS, Lot No. SLCC7592) were acquired from Sigma-Aldrich (Shanghai) Trading Co., Ltd. Pseudoginsenoside F11 (Lot No. KA0812CA14) was provided by Shanghai Yuanye Bio-Technology Co., Ltd. The purity of all chemicals was > 98%.

AG samples and their collection times are listed in Table 1. All AG samples were identified as the dry root of *Panacis quinquefolium* L. by Dr. Liwen Han. All samples were stored at the School of Pharmacy and Pharmaceutical Science, Shandong First Medical University.

2.2 Zebrafish husbandry and embryo collection

The wild AB line zebrafish were provided by the Zebrafish Research Center of the School of Pharmacy and Pharmaceutical Science, Shandong First Medical University and were cultivated in a professional breeding system (Shanghai Haisheng Biological Experimental Equipment Co., Ltd.). Adult zebrafish were reared in a semi-static system at 28°C under a 14-h light/10 h dark cycle (Progatzy et al., 2019) and fed with artemia twice a day. Before the night, adult male and female zebrafish were placed in a mating tank, at a ratio of 2:2. The next day, the zebrafish were stimulated by light to mate and spawn naturally. The embryos were collected within 1 h of spawning and washed with fish water. The clean embryos were transferred into the E3 medium (5 mM NaCl, 0.17 mM KCl, 0.4 mM CaCl₂, and 0.16 mM MgSO₄) (H. Sun et al., 2019) and placed in a light incubator at 28.5°C for subsequent experiments. After 24 h, 0.2 mM N-phenylthiourea was added to the E3 medium to prevent the embryos from forming melanin. The animal study was reviewed and approved by

the Ethics Committee of Shandong First Medical University and Shandong Academy of Medical Sciences.

2.3 Preparation of sample solutions

The dried AG was pulverized and sifted through a 50-mesh sieve. Then, 40 g of AG powder was extracted with 400 ml water twice by refluxing for 2 h. The two filtrates were combined and concentrated at 200 ml in a rotary evaporator. Then, four times the amount of ethanol was slowly added with constant stirring. After standing at 4°C for 24 h, the supernatant was collected via centrifugation and concentrated to a certain volume in a rotary evaporator. Finally, the sample was dried in a vacuum drying oven to obtain the AG extract. The tricine solution (1 mg mL⁻¹) was prepared with distilled water. Verapamil hydrochloride was made to 100 mg mL⁻¹ with dimethyl sulfoxide (DMSO). Digoxin was dissolved in DMSO to prepare a solution of 10 mg mL⁻¹. All AG samples were prepared into 100 mg mL⁻¹ stock solution with distilled water. Ginsenoside Rg3, ginsenoside Rg5, ginsenoside Rg6, malic acid, quinic acid, L-argininosuccinic acid, and pseudoginsenoside F11 were prepared into a stock solution of 40 mg mL⁻¹ with DMSO and diluted to the desired concentration before the experiment. AG samples (for UHPLC-MS analysis) were accurately weighed and dissolved in acetonitrile and methanol through a filter membrane to prepare solutions of 5 mg mL⁻¹ concentration before the experiment.

2.4 Biological activities of the American ginseng samples on the zebrafish

The 48 h of post fertilization (hpf) zebrafish, without the embryonic membrane, were placed in a 6-well plate at the rate of 20 larvae/well and divided into the control (Con), model, positive control (10 µg mL⁻¹ digoxin), and AG (100 µg mL⁻¹) groups. The positive control group and AG groups were pre-protected for 4 h.

Then, all the groups (excluding the control group) were treated with 200 μM verapamil hydrochloride (S. Li et al., 2021) for 1 h to induce heart failure (Figure S1). The heart of zebrafish larvae was then imaged with inverted microscopy (Olympus IX83, Japan) (Supplementary Figure S1). The pericardial area, the venous congestion area (Lu et al., 2020), and the distance between the sinus venosus and bulbus arteriosus (SV–BA) of the heart (Wan et al., 2021) were counted by Image Pro Plus5.1 software. The data were analyzed by one-way analysis of variance (ANOVA) using GraphPad Prism 6.01 software and expressed as the mean \pm standard error (SE). In order to evaluate the comprehensive anti-heart failure activity and prevent the incompatibility of statistical indicators, we proposed an integrated index, heart failure improvement rate, for comprehensively evaluating the activity of AG.

2.5 Untargeted metabolomics analysis and component identification of American ginseng

In total, 12 batches of AG samples collected from two regions with significantly different bioactivity (seven from Wendeng of Shandong province and five from Xinbin of Liaoning province) were used for untargeted metabolomics modeling analysis. Metabolomics analysis was performed using the Thermo Scientific™ Q Exactive™ Combination Quadrupole Orbitrap™ Mass Spectrometer under the following chromatographic conditions: an ACQUITY UHPLC BEH C18 column (1.7 μm , 2.1×100 mm, Waters) was used as the chromatographic column in the positive-ion mode. The column temperature was set to 50°C. The sample injection volume was 10 μL . The mobile phase was composed of water containing 0.1% formic acid (A) and acetonitrile containing 0.1% formic acid (B) at the flow rate of 0.35 ml/min. The gradient elution procedure was performed as follows: 0–1 min, 5% B; 1–24 min, 5–100% B; 24–27.5 min, 100% B; and 27.5–30 min, 5% B. The MS conditions were as follows: electrospray ion sources were used in the positive-ion mode; spray voltage (kV): +3.8; capillary temperature (°C): 320; aux gas heater temperature (°C): 350; sheath gas flow rate (Arb): 35; aux gas flow rate (Arb): 8; S-lens RF level: 50; mass range (m/z): 70–1050; full ms resolution: 70000; MS/MS resolution: 17500; TopN: 5; and NCE/stepped NCE: 20, 40. Except for the spray voltage (kV) -3.0, other conditions were identical in the negative-ion mode.

The raw data of 12 samples and the quality control (QC) samples were processed and converted by Xcalibur 2.2.0 software and ProteoWizard 3.0.21063 software, and then the processed data were uploaded to XCMSonline (Version 3.7.1) for analyses. Mathematical models such as principal component analysis (PCA) and orthogonal partial least squares-discriminant analysis (OPLS-DA) were constructed based on the component information of samples with large activity differences through a smart cloud platform for metabolite identification and biomarker discovery (One-MAP, Dalian ChemDataSolution Information Technology Co., Ltd.).

With the VIP (variables important in the projection) value >1.5 , $p < 0.05$ and the absolute value of the correlation coefficient $|\text{pcorr}| > 0.58$ as the screening conditions, the selected fragment ions were used for qualitative analysis to identify the potential differential components.

2.6 Activity validation and mechanism prediction of potential active components

The zebrafish heart failure model was also applied to verify whether those identified components in AG could be used as the pharmacodynamic substances. Accordingly, the heart failure model in zebrafish was basically the same as that described earlier. The zebrafish was divided into control, model, positive control, and ginsenoside Rg3 (25 $\mu\text{g mL}^{-1}$, 50 $\mu\text{g mL}^{-1}$, and 100 $\mu\text{g mL}^{-1}$), ginsenoside Rg5 (0.25 $\mu\text{g mL}^{-1}$, 0.5 $\mu\text{g mL}^{-1}$, and 1 $\mu\text{g mL}^{-1}$), ginsenoside Rg6 (25 $\mu\text{g mL}^{-1}$, 50 $\mu\text{g mL}^{-1}$, and 100 $\mu\text{g mL}^{-1}$), malic acid (10 $\mu\text{g mL}^{-1}$, 25 $\mu\text{g mL}^{-1}$, and 50 $\mu\text{g mL}^{-1}$), quinic acid (25 $\mu\text{g mL}^{-1}$, 50 $\mu\text{g mL}^{-1}$, and 100 $\mu\text{g mL}^{-1}$), L-argininosuccinic acid (25 $\mu\text{g mL}^{-1}$, 50 $\mu\text{g mL}^{-1}$, and 100 $\mu\text{g mL}^{-1}$), and pseudoginsenoside F11 (10 $\mu\text{g mL}^{-1}$, 25 $\mu\text{g mL}^{-1}$, and 50 $\mu\text{g mL}^{-1}$) groups. The concentration-tested groups are mentioned in the Results section.

The targets of the screened active compounds were found on the Traditional Chinese Medicine Systems Pharmacology Database and Analysis Platform (TCMSP, <http://tcmbspw.com/tcmssp.php>). Heart failure-related targets were searched in the GeneCard database (<http://www.genecards.org>). Their common targets served as core targets. Core targets were imported into the DAVID database (<https://david.ncicrf.gov/>) to obtain relevant pathways. The screened active compounds, core targets, and pathways were input into Cytoscape software 3.7.1 to obtain a “compound–target–pathway (C–T–P) network.” The targets with the top degree value in the “C–T–P” network were selected for further molecular docking validation. First, the compounds were structure-optimized with Chem3D software to minimize their energy. The water molecules were then removed from the inactive pocket, and OPLS_2005 force was added into the inactive pocket by Protein Preparation Wizard for energy minimization. Glide’s XP (extra precision) mode was selected for docking. The ligand supplied in the RCSB PDB database (<https://www.rcsb.org/>) served as the positive control. The position of the original ligand molecule was used as the active site. The size of the docking box and other settings were maintained as default parameters. After docking completion, the 2D mode of docking results was displayed.

2.7 Total RNA extraction and quantitative real-time polymerase chain reaction

According to the results of activity verification and target prediction, eight key targets, namely, FGF1, FGF2, VEGFA,

TABLE 2 Primer sequences for Q-PCR assay.

| Gene | Forward primer | Reverse primer |
|----------------|-----------------------------|--------------------------------|
| FGF1 | 5'-GCTCATGTCTGGTCTGGCTT-3' | 5'-CACATGCTTGAGGTATTTGGCA-3' |
| FGF2 | 5'-GTACCAACCGTTTCCTTGCC-3' | 5'-TACCAGTCGGGATACTTGCG-3' |
| VEGFA | 5'-GCTGTAATGATGAGGCGCTCG-3' | 5'-AAGGCTCACAGTGGTTTTCTTTCT-3' |
| BCL2L1 | 5'-GGGCTTGTTTGCTTGGTTGA-3' | 5'-AGAACACAGTGCACACCCTT-3' |
| MET | 5'-CGGTCGTGTTGTGAGTTCT-3' | 5'-TGAAGGGGCCAAATCCATGT-3' |
| CHRNA | 5'-CATCTCTACTCTGGCCCTGC-3' | 5'-CACAGAGTCAGATGTTGCCG-3' |
| STAT3 | 5'-GCTTCAGCAGAAGGTCTCGT-3' | 5'-GATGACAAGGGGTCGGTCAG-3' |
| PPARA | 5'-TCAGGACGAGTTACCTCCA-3' | 5'-GTCCGACGGAAGAAACCCTT-3' |
| β -Actin | 5'-TGCTCTGTATGGCGCATTGA-3' | 5'-AGGGGCCATCCACAGTCTTC-3' |

STAT3, BCL2L1, MET, PPARA, and CHRNA7 were verified in zebrafish. The groups with the best efficacy of each active component were selected for quantitative real-time polymerase chain reaction (Q-PCR). Zebrafish were divided into the control, model, and drug groups, and 50 zebrafish were included into each group. After removing water, the zebrafish were stored in a -80°C refrigerator for subsequent experiments. The total RNA was extracted using an ultrapure RNA extraction kit (Kangwei Century Biotechnology Co., Ltd. Jiangsu, China) according to the procedure provided by the manufacturer. The RNA concentration was determined and was quantified using an ultramicro-spectrophotometer (Thermo Fisher, United States). The reverse transcription process was performed on ice. The cDNA obtained by the reverse transcription process was directly subjected to Q-PCR analysis. The PCR mixtures contained 2 μL of the cDNA product, template, 10 μM Primer F and Primer R, ROX Reference Dye, and RNase free water in a total volume of 20 μL . Amplification was performed under the following conditions: initial denaturation at 95°C twice for 30 s, 40 cycles of denaturation at 95°C for 15 s, and annealing and extension at 60°C for 30 s three times. All data were determined by the $2^{-\Delta\Delta\text{Ct}}$ method and were normalized to the β -actin mRNA signals in each sample. The primer sequences for Q-PCR assay are listed in Table 2.

3 Results

3.1 Evaluation of the anti-heart failure effects of American ginseng samples from various regions

The pericardial area, venous congestion area, and SV–BA distance of the zebrafish heart in the model group were significantly increased compared with those of the control

group ($p < 0.01$), indicating the successful induction of heart failure in the zebrafish by verapamil hydrochloride treatment. The venous congestion area and SV–BA distance of the zebrafish heart were remarkably reversed after treatment with the positive drug digoxin ($p < 0.05$). Pericardial areas in the zebrafish were significantly reduced in the S6, S12, and S14 treatment groups than in the model group (Figure 1C). However, the pericardial area of the zebrafish in the S8, S13, and S15 treatment groups did not show a difference compared with that of the zebrafish in the model group. After the treatment, venous congestion in the zebrafish was relieved in the S6, S8, S10, S12, S14, and S15 treatment groups compared with the model group (Figure 1D). Our results showed that all AG samples, except S15, markedly decreased the SV–BA distance of the zebrafish heart in their respective groups than in the model group (Figure 1E). As shown in Figure 1F, the improvement rate of S13 for heart failure was the lowest, and the improvement rate of S6 and S10 was higher.

3.2 Screening of potential active components from American ginseng using untargeted metabolomics

The original data were preprocessed to obtain the superposition map of total ion chromatograms (Figures 2A,B). The calibration process was visualized using the calibration curve of retention time. Furthermore, the retention time of the peak should be within the ± 0.2 -min retention time window of the retention time observed in the available standard. As shown in Figures 2C,D, the peak of the AG sample met the standard. After preprocessing using XCMSonline software, a total of 4535 chromatographic peaks with $p < 0.01$ in the positive ion mode and 2668 chromatographic peaks in the negative ion mode were obtained.

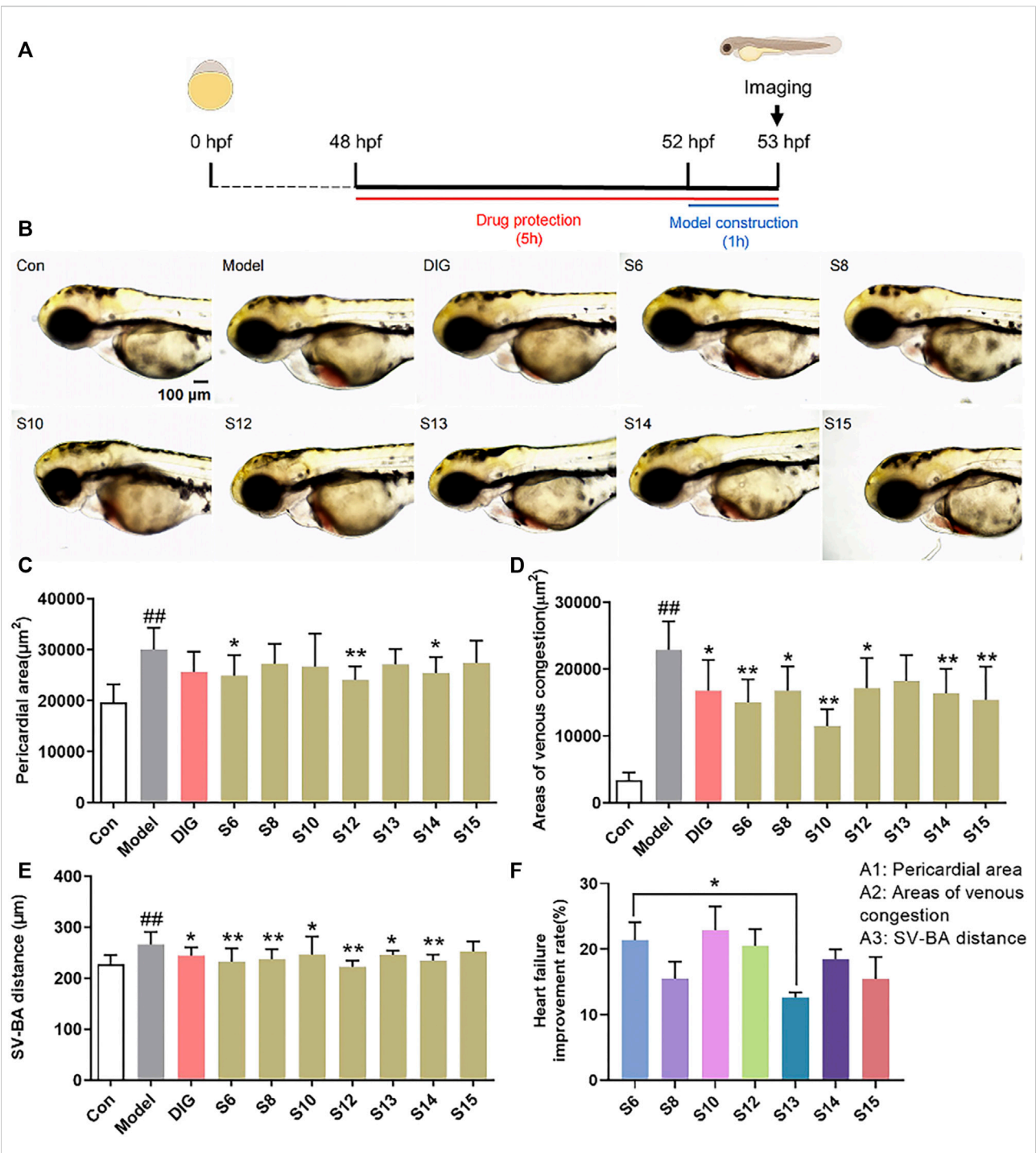


FIGURE 1
Comparison of the anti-heart failure activities of AG collected from different regions. (A) Diagram of drug treatment in the zebrafish heart failure experiment; (B) phenotypic micrograph of the zebrafish in the heart; (C) statistical results of the pericardial area of the zebrafish heart. $n = 10$; (D) statistical results of the venous congestion area of the heart in zebrafish. $n = 10$; (E) statistical results of SV-BA in the zebrafish hearts in all groups. $n = 10$; and (F) comparison of the improvement rate of heart failure of AG samples from different regions. Heart failure improvement rate = $(A1+A2+A3)/3$, $A = (\Phi - a)/\Phi \times 100\%$, Φ : Mean values of the model groups, (A) values of sample groups; ## $p < 0.01$ vs. the control group; * $p < 0.05$ and ** $p < 0.01$ vs. the model group.

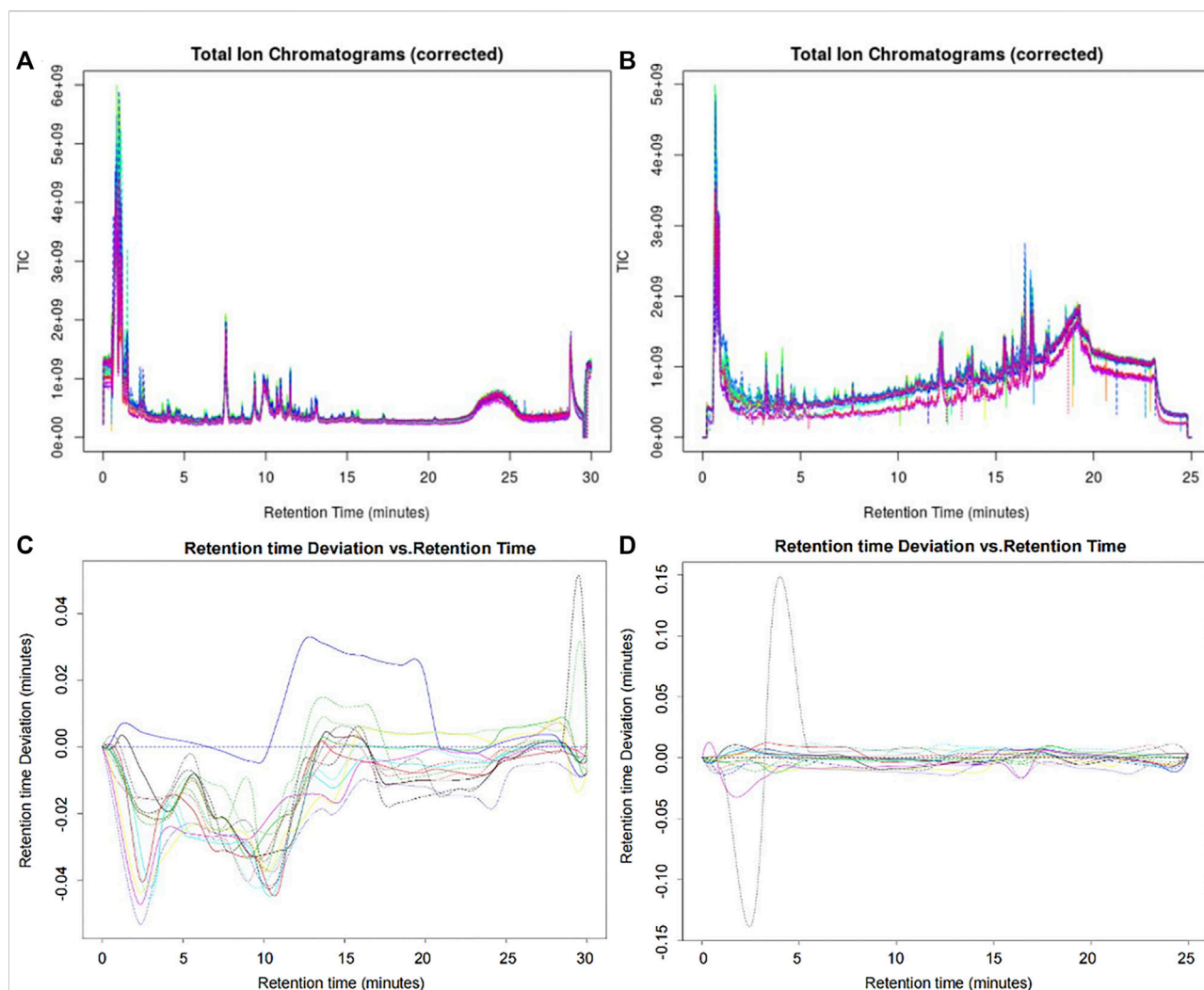


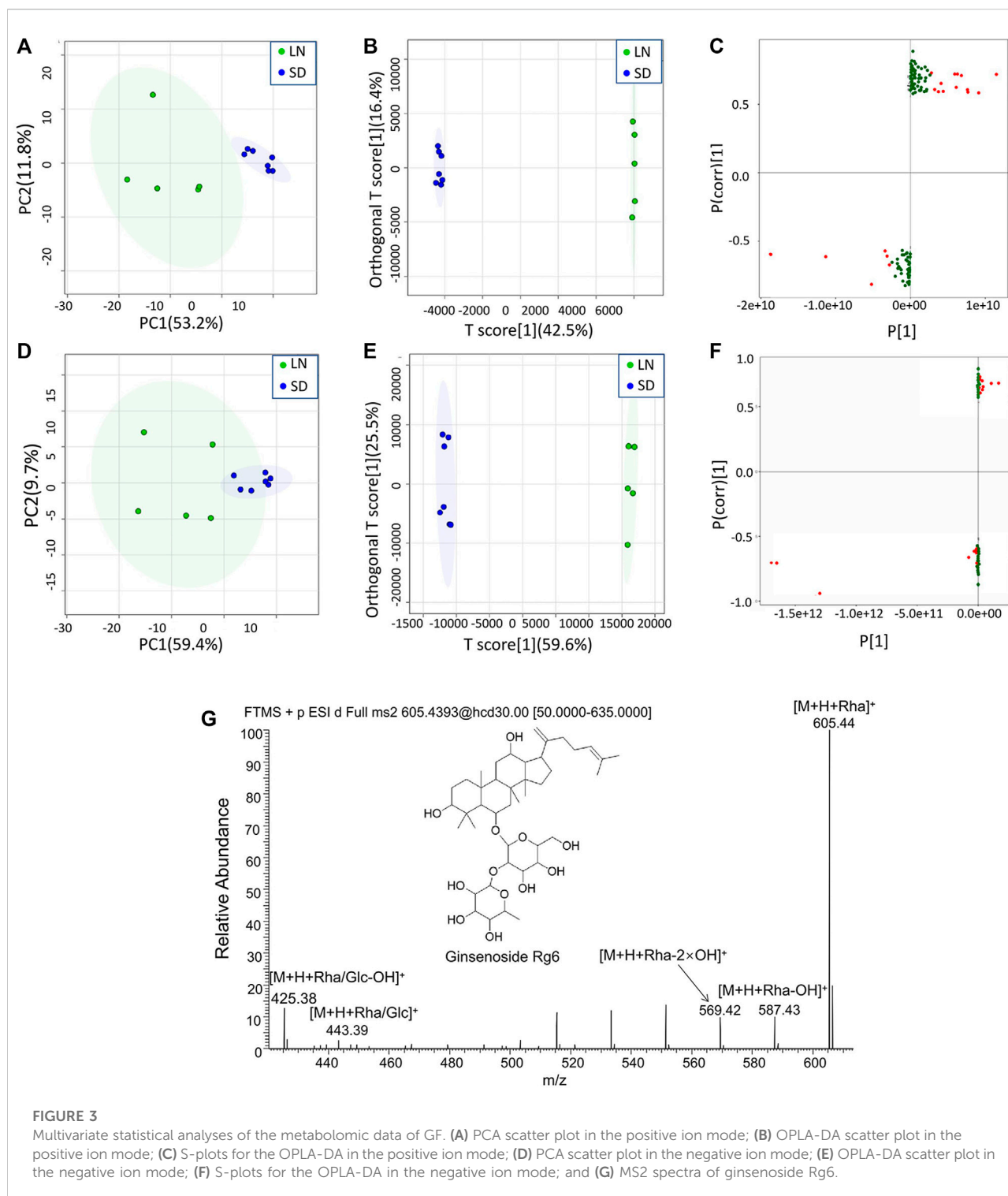
FIGURE 2

Superposition map of the total ion chromatograms of AG samples. (A) Corrected total ion chromatogram in the positive ion mode; (B) corrected total ion chromatogram in the negative ion mode; (C) retention time deviation diagram of the AG samples in the positive ion mode; and (D) retention time deviation diagram of the AG samples in the negative ion mode.

The MS data of 12 batches of AG were inputted into OneMap for principal component analysis. As shown in Figure 3A, the PCA scatter plot was constructed by the first principal component (53.2%) and the second principal component (11.8%) in the positive ion mode. It is observed that the AG samples obtained from two regions were clearly separated, indicating that some compounds of the two groups were different. The first and second principal components were 53.1% and 15.3% in the negative ion mode, respectively (Figure 3D). The AG samples were not completely separated from the scatter plot, and thus further modeling and analysis were required.

After the principal component analysis, the supervised OPLS-DA was used to further analyze the differences between these two groups. As shown in Figures 3B, E OPLS-DA

analysis could significantly distinguish the AG samples from two regions. The values of R^2Y (cum) and Q^2 (cum) in the positive and negative ion models were 0.98 and 0.85 and 0.92, and 0.84, respectively, indicating the good measurability and applicability of the OPLS-DA model. The permutation test validated whether the OPLS-DA model was overfitted. The results of the PT were $R^2 = (0.0, 0.21)$ and $Q^2 = (0.0, -0.51)$ and $R^2 = (0.0, 0.33)$ and $Q^2 = (0.0, -0.65)$. The intersection of the regression line of the Q^2 value with the ordinate was less than zero, and all Q^2 values on the left were less than the highest value on the right, indicating the usability of the model. VIP value > 1.5 , $p < 0.05$, and $|pcorr| > 0.58$ were used to screen the potentially important fragment ions (Table 3). The results were represented using S-plots of the OPLS-DA model (Figures 3C,F). The protective effects of



a total of nine potentially important components against heart failure were identified by standard substances or MS/MS data (Table 4). Compound 3 was an example of displaying the structure identification process of the compounds. Compound

3 gaged a quasi-molecular ion of m/z 767.4917 $[M+H]^+$; therefore, the calculated molecular formula was deduced as $C_{42}H_{70}O_{12}$ with an error of 3.7 ppm, which was consistent with that of ginsenoside Rg6. The MS/MS showed that obvious m/z 605.4393, 587.4288,

TABLE 3 Screening of the potentially active components of AG against heart failure.

| VarID | P (T-test) | VIP | Ion mode |
|--------|------------|-------------|----------|
| V20188 | 0.023302 | 1.56008179 | neg |
| V20301 | 0.014374 | 1.648690526 | neg |
| V33038 | 0.0030027 | 1.81109426 | pos |
| V18051 | 0.031844 | 1.526483347 | neg |
| V11178 | 0.033366 | 1.625269504 | neg |
| V6096 | 0.0083365 | 1.741859991 | neg |
| V2878 | 0.028691 | 1.515140861 | neg |
| V15698 | 0.0010554 | 1.922905341 | pos |
| V1259 | 0.010402 | 1.696352652 | neg |

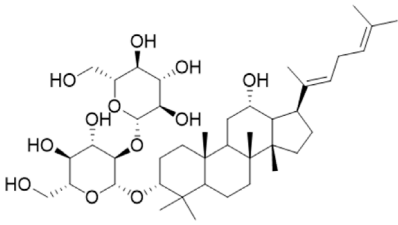
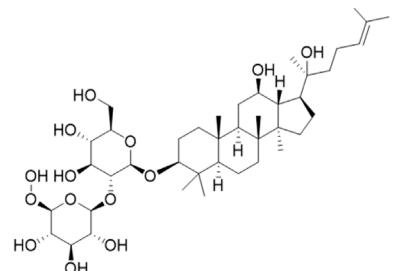
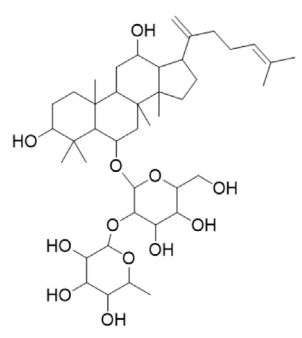
569.4183, 443.3870, and 425.3762 fragment ions were obtained compared with the literature data, and the fragment ion was deduced as m/z 605.4393 $[M + H-Rha]^+$; 587.4288 $[M + H-Rha-OH]^+$; 569.4183 $[M + H-Rha-2OH]^+$;

443.3870 $[M + H-Rha/Glc]^+$; and 425.3762 $[M + H-Rha/Glc-OH]^+$. Accordingly, compound 3 was speculated as ginsenoside Rg6 (Figure 3G).

3.3 Bioactivity evaluation of the identified bioactive compounds by the zebrafish model

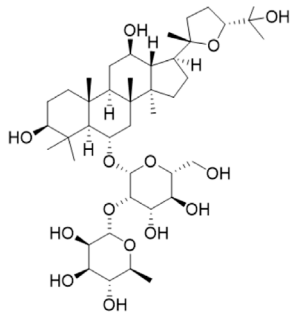
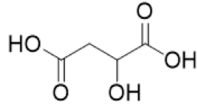
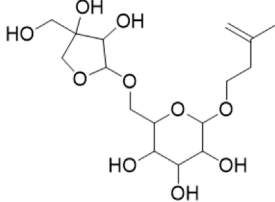
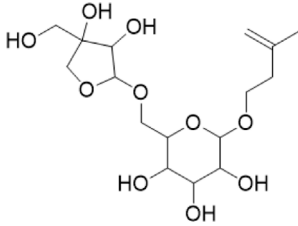
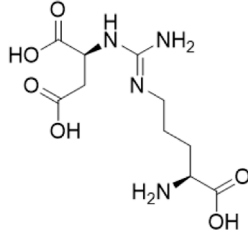
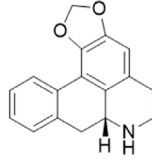
Potential differential components screened by metabolomics were validated using the zebrafish model. Among them, ginsenoside Rg3, ginsenoside Rg5, ginsenoside Rg6, malic acid, quinic acid, and pseudoginsenoside F11 could significantly improve heart failure caused by verapamil hydrochloride treatment in zebrafish. Ginsenoside Rg3, ginsenoside Rg6, quinic acid, and pseudoginsenoside F11 could improve the expansion of the pericardial area, venous congestion area, and SV-BA distance in zebrafish hearts. Ginsenoside Rg5 and malic acid only ameliorated venous congestion in zebrafish hearts.

TABLE 4 Identification of differential active components from AG using the UHPLC-QE-Orbitrap-MS.

| NO. | Rt | Measured m/z | Calculated m/z | ppm | MSE fragment ions | Compound identification | Chemical structure |
|-----|-------|----------------------------------|----------------|-------|--|------------------------------|---|
| 1 | 18.19 | 765.4783 [M-H] ⁻ | 765.4789 | -0.74 | 811.4829 [M + HCOO] ⁻ | Ginsenoside Rg5 ^a |  |
| 2 | 17.63 | 783.4889 [M-H] ⁻ | 783.4895 | -0.71 | 783.4895653.4199[M-H-Rha-H2O] ⁻ | Ginsenoside Rg3 ^b |  |
| 3 | 14.55 | 767.4917 [M + H] ⁺ | 767.4946 | -3.7 | 605.4393 [M + H-Rha] ⁺ ; 587.4288[M + H-Rha-OH] ⁺ ; 569.4183 [M + H-Rha-2OH] ⁺ ; 443.3870 [M + H-Rha/Glc] ⁺ ; 425.3762 [M + H-Rha/Glc-OH] ⁺ | Ginsenoside Rg6 ^b |  |

(Continued on following page)

TABLE 4 (Continued) Identification of differential active components from AG using the UHPLC-QE-Orbitrap-MS.

| NO. | Rt | Measured m/z | Calculated m/z | ppm | MSE fragment ions | Compound identification | Chemical structure |
|-----|-------|-----------------------------------|-------------------|-------|---|---|---|
| 4 | 10.72 | 799.4831 [M-H] ⁻ | 799.4829 | 2.3 | 653.4199[M-H-Rha-H ₂ O] ⁻ | Pseudoginsenoside F11 ^b |  |
| 5 | 3.68 | 191.0557 [M-H] ⁻ | 191.0556 | 0.58 | 145.0726[M + HCOO] ⁻ | Quinic acid ^b |  |
| 6 | 0.62 | 133.0139 [M-H] ⁻ | 133.0137 | 1.7 | 115.0325[M-H-H ₂ O] ⁻ | Malic acid ^b |  |
| 7 | 6.69 | 379.1602 [M-H] ⁻ | 379.1604 | -0.64 | 361.1384[M-H-H ₂ O] ⁻ | 3-methyl-3-butenyl- apinosyl (1→6) glucoside ^b |  |
| 8 | 0.77 | 291.1292 [M + H] ⁺ | 291.1305 | -4.4 | | L-argininosuccinic acid ^b |  |
| 9 | 4.86 | 264.1013722 [M-H] ⁻ | 264.1025 | -42 | | Annonaine ^b |  |

“a” refer to an identified component by standard substances; “b” refers to a speculated component; identification of active components according to MS data from reference (Huang et al., 2019; Y. Xia et al., 2018; Chen et al., 2017).

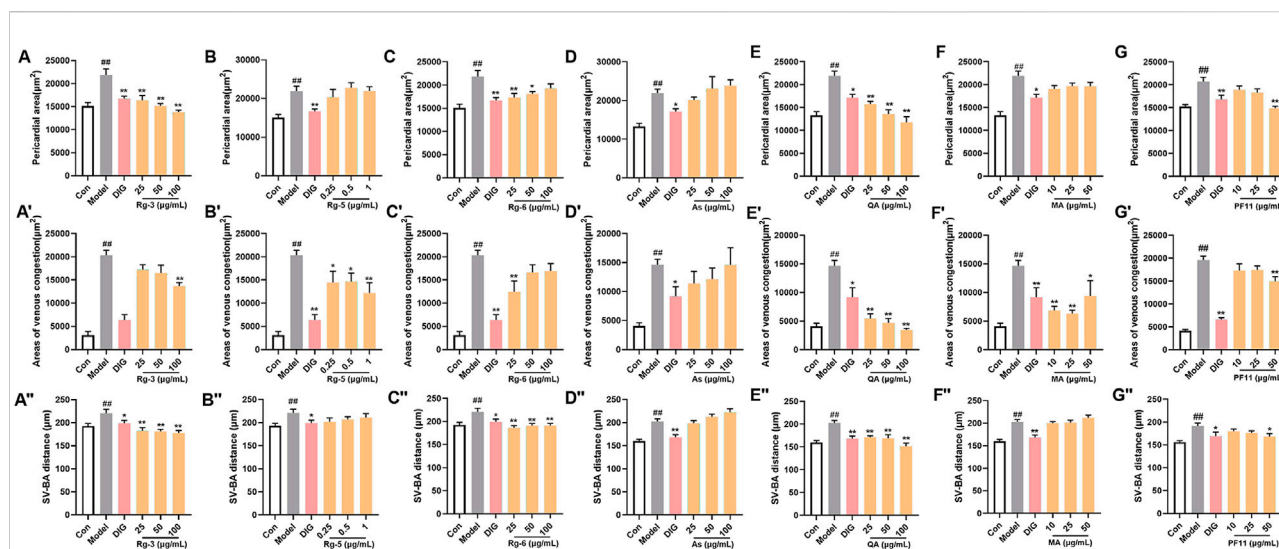


FIGURE 4

Validation of the anti-heart failure activity of ginsenoside Rg3, ginsenoside Rg5, ginsenoside Rg6, malic acid, L-argininosuccinic acid, quinic acid, and pseudoginsenoside F11. (A–G) Statistical results of the pericardial area of the zebrafish. $n = 10$; (A'–G') statistical results of the venous congestion area of the heart in zebrafish. $n = 10$; (A''–G'') statistical results of the SV–BA distance in zebrafish hearts. $n = 10$. ## $p < 0.01$ vs. the control group, * $p < 0.05$ and ** $p < 0.01$ vs. the model group.

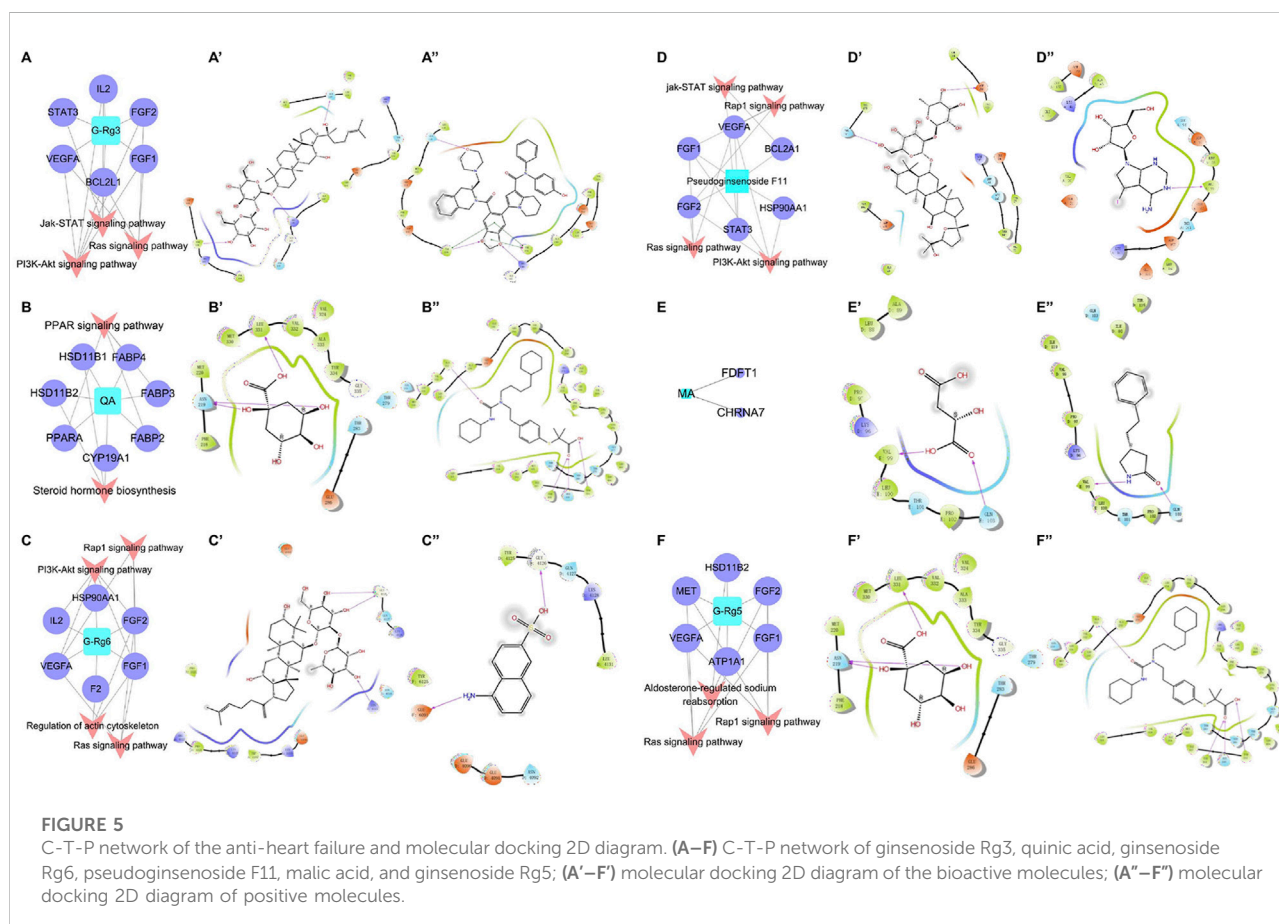


FIGURE 5

C-T-P network of the anti-heart failure and molecular docking 2D diagram. (A–F) C-T-P network of ginsenoside Rg3, quinic acid, ginsenoside Rg6, pseudoginsenoside F11, malic acid, and ginsenoside Rg5; (A'–F') molecular docking 2D diagram of the bioactive molecules; (A''–F'') molecular docking 2D diagram of positive molecules.

TABLE 5 Information of the compounds docking proteins.

| Compound | Target | PDB ID |
|------------------------------|--------|--------|
| Malic acid(MA) | CHRNA7 | 5AFN |
| Quinic acid(QA) | PPARA | 6KB3 |
| Ginsenoside Rg3(G-Rg3) | BCL2L1 | 6GL8 |
| Ginsenoside Rg5(G-Rg5) | MET | 4R1V |
| Ginsenoside Rg6(G-Rg6) | FGF1 | 1HKN |
| Pseudoginsenoside F11 (PF11) | STAT3 | 5AX3 |

L-argininosuccinic acid with different concentrations did not improve heart failure in zebrafish (Figure 4).

3.4 Network prediction of the action mechanism of bioactive compounds

The targets and regulatory pathways of ginsenoside Rg3, ginsenoside Rg5, ginsenoside Rg6, malic acid, quinic acid, and pseudoginsenoside F11 are shown in Figure 5A–5F. The results showed that these six compounds may, respectively, target alpha 7 nicotinic acetylcholine receptor (CHRNA7), peroxisome proliferator-activated receptor alpha (PPARA), B-cell lymphoma-2 like 1 (BCL2L1), hepatocyte growth factor receptor (MET), fibroblast growth factor 1 (FGF1), and signal transducer and activator of transcription 3 (STAT3) involved in multiple signaling pathways. Moreover, the results showed high binding energy in molecular docking. Malic acid targeted two targets, namely, farnesyl diphosphate farnesyl transferase 1 (FDFT1) and CHRNA7. Quinic acid targeted two pathways and seven targets, including PPARA, fatty acid-binding protein 2 (FABP2), and FABP3. In the network prediction analysis, ginsenoside Rg3 targeted BCL2L1, which was the key target in the signaling pathways. MET encoded a receptor tyrosine kinase c-MET for a hepatocyte growth factor (HGF) (Mo and Liu, 2017), which was an important target of ginsenoside Rg5 against heart failure. Ginsenoside Rg6 targeted six targets and four pathways, as performed by pseudoginsenoside F11.

The information on the predicted targets and related molecular docking is shown in Table 5. The action mode of the six pharmacodynamic compounds and their corresponding docking targets is displayed (Figure 5A'–5F' and 5A''–5F''). The binding energy of malic acid (–4.117 kcal/mol) was lower than that of the positive control molecule attached to the receptor. The carboxyl group formed hydrogen bonds with two amino acid residues in the active pockets of Val99 and GLN103. The binding energy of quinic acid to the PPARA target was –7.835 kcal/mol. Although the binding energy of quinic acid was lower than that of the molecule attached to the receptor, the binding energy of quinic acid was high as it involved the formation of three hydrogen bonds between the hydroxyl groups and two amino acid residues in the active pocket of ASN219 and LEU331. The

binding energy of ginsenoside Rg3 was slightly different from that of the positive control molecule attached to the receptor. The hydroxyl groups at carbon 20 and the glycoside part of ginsenoside Rg3 formed three hydrogen bonds with three amino acid residues (TYR108, ARG146, and GLN118) of the active pocket. Ginsenoside Rg5 formed five hydrogen bonds between the four amino-acid residues (ASP1164, GLU1082, LYS1161, and TYR1159) in the active pocket and the hydroxyl group on the glucose ring structure in the polar glycoside part. The binding energy of ginsenoside Rg6 was –5.438 kcal/mol, which was higher than that of the receptor FGF1 ligand. Ginsenoside Rg6 mainly formed three hydrogen bonds between the two amino acid residues (GLY4126 and LYS4113) in the active pocket and the hydroxyl groups on the glycoside in the polar part. Pseudoginsenoside F11 formed two hydrogen bonds with the amino acid residues.

3.5 Anti-heart failure-related gene expression of key compounds in American ginseng

To elucidate the mechanisms underlying the amelioration effect of key active compounds on heart failure in the zebrafish, the mRNA levels of genes involved in the regulation of heart failure were determined by Q-PCR analysis (Figure 6). In the verapamil-treated group, the mRNA levels of FGF2, VEGFA, and STAT3 were significantly increased ($p < 0.01$) compared with those of the control group. The mRNA expression of FGF1, PPARA, and CHRNA7 in the model group was moderately elevated compared with that of the control group. Treatment with ginsenoside Rg3 inhibited the mRNA expression levels of both FGF1 and STAT3 ($p < 0.05$). Ginsenoside Rg5 treatment significantly decreased the mRNA expression levels of FGF2 compared with the verapamil-treated zebrafish ($p < 0.05$), and the mRNA expression levels of VEGFA were not statistically significant in comparison with the model group. Ginsenoside Rg6 treatment obviously attenuated the mRNA expression levels of FGF2 and VEGFA in the model group ($p < 0.05$). The mRNA expression levels of FGF1, VEGFA, and FGF2 in the pseudoginsenosideF11-treated group were significantly lower than those in the model group ($p < 0.05$). Quinic acid and malic acid had no significant effect on the mRNA expression of PPARA and CHRNA7, but both these two components reduced the mRNA expression levels of PPARA and CHRNA7, respectively.

4 Discussion

As a traditional Chinese medicine for replenishing energy, American ginseng was reported to have a protective effect on the heart (L. Yang et al., 2020). Therefore, a zebrafish heart failure

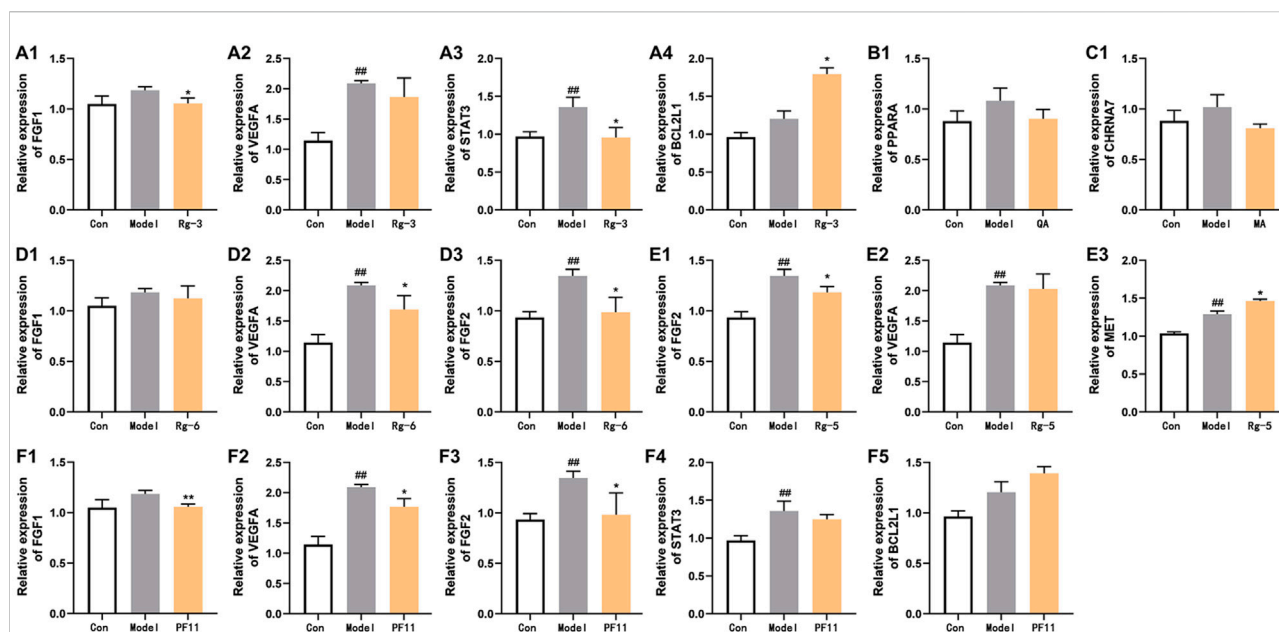


FIGURE 6

Effects of potential active compounds on heart failure-related gene expression. (A–F) Results of gene expression in zebrafish treated with ginsenoside Rg3, quinic acid, malic acid, ginsenoside Rg6, ginsenoside Rg5, and pseudoginsenoside F11, $^{*}p < 0.01$ vs. the control group, $^{*}p < 0.05$ and $^{**}p < 0.01$ vs. the model group.

model was established as a tool to evaluate the main activities of AG in this study. As a new vertebrate model organism between cells and mammals, zebrafish has been widely used in the screening of cardioprotective drugs in recent years (Da Silveira Cavalcante and Tessier, 2021). In this study, zebrafish was treated with verapamil hydrochloride, a calcium ion blocker, and established a fast drug screening model for heart failure. AG is widely distributed in low mountains near 37° north latitude, such as the Great Lakes region of North America, Northeast China, and North China. There are currently four producing areas in China: Northeast China, Shaanxi, Beijing, and Shandong. Studies had shown that the growth of AG was affected by climate, temperature, water, soil, and other environmental factors (J. Liang et al., 2019). Our study found that the anti-heart failure activities of AG in these four producing areas were different due to different growth environments.

Various case studies have reported that many components in AG had protective effects on the heart. Currently, the identified ginsenosides are the main secondary metabolites of *Panax L.* plants (W. Fan et al., 2020). Ginsenoside Re improves isoproterenol-induced heart failure in rats (Wang Q. W. et al., 2019). Ginsenoside Rh2 improves cardiac fibrosis in type 1-like diabetic rats (Lo et al., 2017). Ginsenoside Rb1 attenuates myocardial ischemia/reperfusion injury through inhibiting ROS production from mitochondrial complex I (L. Jiang et al., 2021). In this study, ginsenoside Rg3, ginsenoside Rg5,

ginsenoside Rg6, malic acid, quinic acid, and pseudoginsenoside F11 were screened as the P-markers of AG. Of note, the anti-heart failure activity of ginsenoside Rg6, pseudoginsenoside F11, and quinic acid has been reported for the first time.

Pharmacodynamic marker (P-marker) is a new concept proposed on the basis of quality marker (Q-marker) of TCM. P-markers are the key components of TCM to exert some or all of pharmacodynamic effects. The difference between the P-markers and Q-markers is that the latter are all markers reflecting the quality of TCM, while the former focuses on markers directly related to bioactive efficacy. This study integrated the advantages of the zebrafish model and metabolomics and established a new model of “component-activity” integrated research strategy, which can quickly discover markers related to specific activities. This strategy has been applied in the research on the pharmacodynamic components of *Gardenia Fructus* in our previous research (Y. P. Shi et al., 2020).

Network pharmacology is an emerging discipline integrating multi-directional pharmacology, bioinformatics, and physical chemistry. The emergence of network pharmacology provides a new method for multi-component and multi-target research of traditional Chinese medicine (Qu et al., 2021). Network pharmacology technology can realize multi-component target identification and can predict the target for known or new drug components. The

pharmacodynamic components found in this study are highly correlated with FGF1, FGF2, VEGFA, STAT3, BCL2L1, and other targets, and the prediction of network pharmacology provides a basis for subsequent in-depth verification.

The results of the phenotype and gene expression of zebrafish can partially reveal the potential mechanism of action of the P-markers discovered in this study. FGF1, FGF2 (Zhao et al., 2011), and VEGFA (Braile et al., 2020) are considered to be important factors in stimulating endothelial cell proliferation and in promoting angiogenesis. In addition, the structural activation of STAT3 can also promote angiogenesis (Hilfiker-Kleiner et al., 2005). In the current study, the increase of FGF1, FGF2, VEGFA, and STAT3 mRNA expression in verapamil-treated zebrafish suggested that they were likely response to initiate angiogenesis in cardiac injury. After pre-protection with ginsenoside Rg3, ginsenoside Rg5, ginsenoside Rg6, and pseudoginsenoside F11, the cardiac damage of zebrafish was alleviated, speculating that these components may protect the heart by participating in the regulation of cardiac angiogenesis and repairing itself in early-stage heart failure. PPARA is a key regulator of glucose transshipment. Heart failure activates PPARA to regulate fatty acid metabolism and provide energy for cardiomyocytes (Kaimoto et al., 2017). After pre-protection in zebrafish by quinic acid, low mRNA expression of PPARA was observed, suggesting that PPARA activation during heart failure improved myocardial function and energetics. Our data suggested that quinic acid against heart failure may be associated with regulating fatty acid metabolism to supply energy for cardiomyocytes. As a key regulator of apoptosis in the mitochondrial pathway, BCL2L1 is the common anti-apoptotic protein that promotes cell survival (Loo et al., 2020). MET is the tyrosine kinase receptor for HGF, which mainly activates prosurvival pathways, including prevention from apoptosis. The mRNA expression of BCL2L1 and MET was increased after ginsenoside Rg3, ginsenoside Rg5, and pseudoginsenoside F11 treatment, indicating that these three components may protect cardiomyocytes from damage by inhibiting apoptosis to improve heart failure. Acetylcholine binding to the CHRNA7 expressed on macrophages polarizes the pro-inflammatory into anti-inflammatory subtypes (Chung et al., 2020). STAT3 has an anti-inflammatory effect by restraining pro-inflammatory gene transcription, initiating efficient reparative mechanisms (Hillmer et al., 2016). After pre-protection by malic acid, ginsenoside Rg3, and pseudoginsenoside F11, the expressions of CHRNA7 and STAT3 mRNA were reduced, indicating that heart protection of malic acid, ginsenoside Rg3, and pseudoginsenoside F11 may be related with the activation of inflammatory response.

5 Conclusion

To summarize, six key P-markers of anti-heart failure in AG were identified using the zebrafish model and metabolomics technology. This study provided a new strategy for the discovery and identification of potentially active components of TCM, which had advantages over traditional research patterns. These results might contribute to evaluating the interior quality of AG.

Data availability statement

The original contributions presented in the study are included in the article/Supplementary Material; further inquiries can be directed to the corresponding authors.

Ethics statement

The animal study was reviewed and approved by the Ethics Committee of Shandong First Medical University and Shandong Academy of Medical Sciences.

Author contributions

RD and YZ performed the research, SC and HW analyzed the data, and RD wrote the manuscript. KH, HZ, QT, and KZ were supportive during the experiment. LH and SW designed and performed the study.

Funding

This work was financially supported by the Funding of the Key Project at Central Government Level: the ability establishment of sustainable use for valuable Chinese medicine resources (2060302), the Natural Science Foundation of Shandong Province (ZR2019MH037), and Academic Promotion Program of Shandong First Medical University (No. 2019LJ003).

Acknowledgments

The authors would like to thank all the reviewers who participated in the review and MJEditor (www.mjeditor.com) for its linguistic assistance during the preparation of this manuscript. We thank the Zebrafish Research Center of Shandong First Medical University and Shandong Academy of Medical Sciences which supplied the zebrafish line to us.

Conflict of interest

The authors declare that the research was conducted in the absence of any commercial or financial relationships that could be construed as a potential conflict of interest.

Publisher's note

All claims expressed in this article are solely those of the authors and do not necessarily represent those of their affiliated

organizations, or those of the publisher, the editors, and the reviewers. Any product that may be evaluated in this article, or claim that may be made by its manufacturer, is not guaranteed or endorsed by the publisher.

Supplementary material

The Supplementary Material for this article can be found online at: <https://www.frontiersin.org/articles/10.3389/fphar.2022.909084/full#supplementary-material>

References

- Braille, M., Marcella, S., Cristinziano, L., Galdiero, M. R., Modestino, L., Ferrara, A. L., et al. (2020). VEGF-A in cardiomyocytes and heart diseases. *Int. J. Mol. Sci.* 21 (15), 5294. doi:10.3390/ijms21155294
- Chen, Y., Zhao, Z., Chen, H., Brand, E., Yi, T., Qin, M., et al. (2017). Determination of ginsenosides in asian and American ginsengs by liquid chromatography-quadrupole/time-of-flight MS: Assessing variations based on morphological characteristics. *J. Ginseng Res.* 41 (1), 10–22. doi:10.1016/j.jgr.2015.12.004
- Chung, C. H., Bretherton, B., Zainalabidin, S., Deuchars, S. A., Deuchars, J., and Mahadi, M. K. (2020). Mediation of cardiac macrophage activity via auricular vagal nerve stimulation ameliorates cardiac ischemia/reperfusion injury. *Front. Neurosci.* 14, 906. doi:10.3389/fnins.2020.00906
- Da Silveira Cavalcante, L., and Tessier, S. N. (2021). Zebrafish as a new tool in heart preservation research. *J. Cardiovasc. Dev. Dis.* 8 (4), 39. doi:10.3390/jcdd8040039
- Duan, L., Guo, L., Wang, L., Yin, Q., Zhang, C. M., Zheng, Y. G., et al. (2018). Application of metabolomics in toxicity evaluation of traditional Chinese medicines. *Chin. Med.* 13, 60. doi:10.1186/s13020-018-0218-5
- Fan, W., Huang, Y., Zheng, H., Li, S., Li, Z., Yuan, L., et al. (2020). Ginsenosides for the treatment of metabolic syndrome and cardiovascular diseases: Pharmacology and mechanisms. *Biomed. Pharmacother.* 132, 110915. doi:10.1016/j.biopha.2020.110915
- Ghosh, R., Bryant, D. L., and Farone, A. L. (2020). Panax quinquefolius (north American ginseng) polysaccharides as immunomodulators: Current research status and future directions. *Molecules* 25 (24), E5854. doi:10.3390/molecules25245854
- Hilfiker-Kleiner, D., Hilfiker, A., and Drexler, H. (2005). Many good reasons to have STAT3 in the heart. *Pharmacol. Ther.* 107 (1), 131–137. doi:10.1016/j.pharmthera.2005.02.003
- Hillmer, E. J., Zhang, H., Li, H. S., and Watowich, S. S. (2016). STAT3 signaling in immunity. *Cytokine Growth Factor Rev.* 31, 1–15. doi:10.1016/j.cytogfr.2016.05.001
- Horzmann, K. A., and Freeman, J. L. (2018). Making Waves: New developments in toxicology with the zebrafish. *Toxicol. Sci.* 163 (1), 5–12. doi:10.1093/toxsci/kfy044
- Huang, X., Liu, Y., Zhang, Y., Li, S. P., Yue, H., Chen, C. B., et al. (2019). Multicomponent assessment and ginsenoside conversions of Panax quinquefolium L. roots before and after steaming by HPLC-MS(n). *J. Ginseng Res.* 43 (1), 27–37. doi:10.1016/j.jgr.2017.08.001
- Jiang, L., Yin, X., Chen, Y. H., Chen, Y., Jiang, W., Zheng, H., et al. (2021). Proteomic analysis reveals ginsenoside Rb1 attenuates myocardial ischemia/reperfusion injury through inhibiting ROS production from mitochondrial complex I. *Theranostics* 11 (4), 1703–1720. doi:10.7150/thno.43895
- Kaimoto, S., Hoshino, A., Ariyoshi, M., Okawa, Y., Tateishi, S., Ono, K., et al. (2017). Activation of PPAR- α in the early stage of heart failure maintained myocardial function and energetics in pressure-overload heart failure. *Am. J. Physiol. Heart Circ. Physiol.* 312 (2), H305–H313. doi:10.1152/ajpheart.00553.2016
- Li, S., Liu, H., Li, Y., Qin, X., Li, M., Shang, J., et al. (2021). Shen-Yuan-Dan capsule attenuates verapamil-induced zebrafish heart failure and exerts antiapoptotic and anti-inflammatory effects via reactive oxygen species-induced NF- κ B pathway. *Front. Pharmacol.* 12, 626515. doi:10.3389/fphar.2021.626515
- Liang, J., Chen, L., Guo, Y. H., Zhang, M., and Gao, Y. (2019). Simultaneous determination and analysis of major ginsenosides in wild American Ginseng grown in Tennessee. *Chem. Biodivers.* 16 (7), e1900203. doi:10.1002/cbdv.201900203
- Lo, S. H., Hsu, C. T., Niu, H. S., Niu, C. S., Cheng, J. T., and Chen, Z. C. (2017). Ginsenoside Rh2 improves cardiac fibrosis via PPAR δ -STAT3 signaling in type 1-like diabetic rats. *Int. J. Mol. Sci.* 18 (7), 1364. doi:10.3390/ijms18071364
- Loo, L. S. W., Soetedjo, A. A. P., Lau, H. H., Ng, N. H. J., Ghosh, S., Nguyen, L., et al. (2020). BCL-xL/BCL2L1 is a critical anti-apoptotic protein that promotes the survival of differentiating pancreatic cells from human pluripotent stem cells. *Cell Death Dis.* 11 (5), 378. doi:10.1038/s41419-020-2589-7
- Lu, S., Hu, M., Wang, Z., Liu, H., Kou, Y., Lyu, Z., et al. (2020). Generation and application of the zebrafish hegl1 mutant as a cardiovascular disease model. *Biomolecules* 10 (11), E1542. doi:10.3390/biom10111542
- MacRae, C. A., and Peterson, R. T. (2015). Zebrafish as tools for drug discovery. *Nat. Rev. Drug Discov.* 14 (10), 721–731. doi:10.1038/nrd4627
- Mo, H. N., and Liu, P. (2017). Targeting MET in cancer therapy. *Chronic Dis. Transl. Med.* 3 (3), 148–153. doi:10.1016/j.cdtm.2017.06.002
- Nakabayashi, R., Hashimoto, K., Mori, T., Toyooka, K., Sudo, H., and Saito, K. (2021). Spatial metabolomics using imaging mass spectrometry to identify the localization of asparagine A in *Asparagus officinalis*. *Plant Biotechnol.* 38 (3), 311–315. doi:10.5511/plantbiotechnology.21.0504b
- Narumanchi, S., Wang, H., Perttunen, S., Tikkanen, I., Lakkisto, P., and Paavola, J. (2021). Zebrafish heart failure models. *Front. Cell. Dev. Biol.* 9, 662583. doi:10.3389/fcell.2021.662583
- Pfeffer, M. A., Shah, A. M., and Borlaug, B. A. (2019). Heart failure with preserved ejection fraction in perspective. *Circ. Res.* 124 (11), 1598–1617. doi:10.1161/circresaha.119.313572
- Progatzy, F., Jha, A., Wane, M., Thwaites, R. S., Makris, S., Shattock, R. J., et al. (2019). Induction of innate cytokine responses by respiratory mucosal challenge with R848 in zebrafish, mice, and humans. *J. Allergy Clin. Immunol.* 144 (1), 342–345. e347. doi:10.1016/j.jaci.2019.04.003
- Qi, L. W., Wang, C. Z., and Yuan, C. S. (2010). American ginseng: Potential structure-function relationship in cancer chemoprevention. *Biochem. Pharmacol.* 80 (7), 947–954. doi:10.1016/j.bcp.2010.06.023
- Qu, S. Y., Li, X. Y., Heng, X., Qi, Y. Y., Ge, P. Y., Ni, S. J., et al. (2021). Analysis of antidepressant activity of Huang-Lian Jie-Du Decoction through network pharmacology and metabolomics. *Front. Pharmacol.* 12, 619288. doi:10.3389/fphar.2021.619288
- Rinschen, M. M., Ivanisevic, J., Giera, M., and Siuzdak, G. (2019). Identification of bioactive metabolites using activity metabolomics. *Nat. Rev. Mol. Cell. Biol.* 20 (6), 353–367. doi:10.1038/s41580-019-0108-4
- Shi, X., Chen, R., Zhang, Y., Yun, J., Brand-Arzamendi, K., Liu, X., et al. (2018). Zebrafish heart failure models: Opportunities and challenges. *Amino Acids* 50 (7), 787–798. doi:10.1007/s00726-018-2578-7
- Shi, X., Verma, S., Yun, J., Brand-Arzamendi, K., Singh, K. K., Liu, X., et al. (2017). Effect of empagliflozin on cardiac biomarkers in a zebrafish model of heart failure: Clues to the EMPA-REG OUTCOME trial? *Mol. Cell. Biochem.* 433 (1–2), 97–102. doi:10.1007/s11010-017-3018-9
- Shi, Y. P., Zhang, Y. G., Li, H. N., Kong, H. T., Zhang, S. S., Zhang, X. M., et al. (2020). Discovery and identification of antithrombotic chemical markers in

- Gardenia Fructus by herbal metabolomics and zebrafish model. *J. Ethnopharmacol.* 253, 112679. doi:10.1016/j.jep.2020.112679
- Sun, H. J., Zhang, Y., Zhang, J. Y., Lin, H., Chen, J., and Hong, H. (2019). The toxicity of 2, 6-dichlorobenzoquinone on the early life stage of zebrafish: A survey on the endpoints at developmental toxicity, oxidative stress, genotoxicity and cytotoxicity. *Environ. Pollut.* 245, 719–724. doi:10.1016/j.envpol.2018.11.051
- Szczuka, D., Nowak, A., Zaklos-Szyda, M., Kochan, E., Szymańska, G., Motyl, I., et al. (2019). American ginseng (*Panax quinquefolium* L.) as a source of bioactive phytochemicals with pro-health properties. *Nutrients* 11 (5), E1041. doi:10.3390/nu11051041
- Tang, X., Gan, X. T., Rajapurohitam, V., Huang, C. X., Xue, J., Lui, E. M., et al. (2016). North American ginseng (*Panax quinquefolius*) suppresses β -adrenergic-dependent signalling, hypertrophy, and cardiac dysfunction. *Can. J. Physiol. Pharmacol.* 94 (12), 1325–1335. doi:10.1139/cjpp-2016-0337
- Vuksan, V., Xu, Z. Z., Jovanovski, E., Jenkins, A. L., Beljan-Zdravkovic, U., Sievenpiper, J. L., et al. (2019). Efficacy and safety of American ginseng (*Panax quinquefolius* L.) extract on glycemic control and cardiovascular risk factors in individuals with type 2 diabetes: A double-blind, randomized, cross-over clinical trial. *Eur. J. Nutr.* 58 (3), 1237–1245. doi:10.1007/s00394-018-1642-0
- Wan, M., Huang, L., Liu, J., Liu, F., Chen, G., Ni, H., et al. (2021). Cyclosporine a induces cardiac developmental toxicity in zebrafish by up-regulation of wnt signaling and oxidative stress. *Front. Pharmacol.* 12, 747991. doi:10.3389/fphar.2021.747991
- Wang, L., Huang, Y., Yin, G., Wang, J., Wang, P., Chen, Z. Y., et al. (2020). Antimicrobial activities of Asian ginseng, American ginseng, and notoginseng. *Phytother. Res.* 34 (6), 1226–1236. doi:10.1002/ptr.6605
- Wang, Q. W., Yu, X. F., Xu, H. L., Zhao, X. Z., and Sui, D. Y. (2019). Ginsenoside Re improves isoproterenol-induced myocardial fibrosis and heart failure in rats. *Evid. Based. Complement. Altern. Med.* 2019, 3714508. doi:10.1155/2019/3714508
- Wang, T., Liu, J., Luo, X., Hu, L., and Lu, H. (2021). Functional metabolomics innovates therapeutic discovery of traditional Chinese medicine derived functional compounds. *Pharmacol. Ther.* 224, 107824. doi:10.1016/j.pharmthera.2021.107824
- Wang, J., Huertas-Vazquez, A., Wang, Y., and Lusis, A. J. (2019). Isoproterenol-induced cardiac diastolic dysfunction in mice: A systems genetics analysis. *Front. Cardiovasc. Med.* 6, 100. doi:10.3389/fcvm.2019.00100
- Xia, Y. G., Song, Y., Liang, J., Guo, X. D., Yang, B. Y., and Kuang, H. X. (2018). Quality analysis of American ginseng cultivated in Heilongjiang using UPLC-ESI-MRM-MS with chemometric methods. *Molecules* 23 (9), 2396. doi:10.3390/molecules23092396
- Xie, W., Zhou, P., Sun, Y., Meng, X., Dai, Z., Sun, G., et al. (2018). Protective effects and target network analysis of ginsenoside Rg1 in cerebral ischemia and reperfusion injury: A comprehensive overview of experimental studies. *Cells* 7 (12), E270. doi:10.3390/cells7120270
- Xiong, H., Zhang, A. H., Zhao, Q. Q., Yan, G. L., Sun, H., and Wang, X. J. (2020). Discovery of quality-marker ingredients of *Panax quinquefolius* driven by high-throughput chinmedomics approach. *Phytomedicine* 74, 152928. doi:10.1016/j.phymed.2019.152928
- Yang, L., Hou, A., Zhang, J., Wang, S., Man, W., Yu, H., et al. (2020). *Panax quinquefolii* Radix: A review of the botany, phytochemistry, quality control, pharmacology, toxicology and industrial applications research progress. *Front. Pharmacol.* 11, 602092. doi:10.3389/fphar.2020.602092
- Yu, Y. H., Zhang, P., Wang, C. L., Liu, J. G., Li, P., and Zhang, D. W. (2021). *Panax quinquefolium* saponin optimizes energy homeostasis by modulating AMPK-activated metabolic pathways in hypoxia-reperfusion induced cardiomyocytes. *Chin. J. Integr. Med.* 27 (8), 613–620. doi:10.1007/s11655-020-3194-4
- Yuan, C. S., Wang, C. Z., Wicks, S. M., and Qi, L. W. (2010). Chemical and pharmacological studies of saponins with a focus on American ginseng. *J. Ginseng Res.* 34 (3), 160–167. doi:10.5142/jgr.2010.34.3.160
- Zhang, A. H., Sun, H., Yan, G. L., Han, Y., Zhao, Q. Q., and Wang, X. J. (2019). Chinmedomics: A powerful approach integrating metabolomics with serum pharmacochemistry to evaluate the efficacy of traditional Chinese medicine. *Eng. (China)* 5 (1), 60–68. doi:10.1016/j.eng.2018.11.008
- Zhang, R., Zhu, X., Bai, H., and Ning, K. (2019). Network pharmacology databases for traditional Chinese medicine: Review and assessment. *Front. Pharmacol.* 10, 123. doi:10.3389/fphar.2019.00123
- Zhao, T., Zhao, W., Chen, Y., Ahokas, R. A., and Sun, Y. (2011). Acidic and basic fibroblast growth factors involved in cardiac angiogenesis following infarction. *Int. J. Cardiol.* 152 (3), 307–313. doi:10.1016/j.ijcard.2010.07.024
- Zhu, X. Y., Wu, S. Q., Guo, S. Y., Yang, H., Xia, B., Li, P., et al. (2018). A zebrafish heart failure model for assessing therapeutic agents. *zebrafish* 15 (3), 243–253. doi:10.1089/zeb.2017.1546

Frontiers in Pharmacology

Explores the interactions between chemicals and living beings

The most cited journal in its field, which advances access to pharmacological discoveries to prevent and treat human disease.

Discover the latest Research Topics

[See more →](#)

Frontiers

Avenue du Tribunal-Fédéral 34
1005 Lausanne, Switzerland
frontiersin.org

Contact us

+41 (0)21 510 17 00
frontiersin.org/about/contact



Frontiers in Pharmacology

